Faculty of Science and Engineering
School of Electrical Engineering, Computing and Mathematical Sciences

Reliable Long-Range and High Ambient Noise Underwater Communication

Nicholas Andronis

This thesis is presented for the Degree of
Doctor of Philosophy
of
Curtin University

March 2019

DECLARATION

To the best of my knowledge and belief this thesis contains no material previously published by any other person except where due acknowledgment has been made.

This thesis contains no material which has been accepted for the award of any other degree or diploma in any university.

L3 Oceania acknowledges that the candidate is the inventor of algorithms and associated software/hardware technologies described for the improvement of MCDSSS communication protocol and MCDSSS transceiver.

Signature: 

Date: 26 November 2018

ABSTRACT

Establishing a reliable wireless underwater communication link over a distance greater than 10 km is challenging due to the intrinsic properties of seawater and ocean conditions. Electromagnetic radiation of all practical frequencies is highly attenuated while travelling through the ocean. The 5 siemens/meter seawater conductivity absorbs radio frequency signals by 100 dB/km limiting the range of portable powered systems to a few tens of metres. The farthest penetrating blue-green light in the visible spectrum is absorbed at a rate of 90 dB/km and propagates less than 1 km in ideal clear-water conditions. In contrast, the comparatively low hydro-acoustic absorption of seawater, nominally 1 dB/km @ 10 kHz, enables sound waves to be used as long-range underwater information carriers beyond 10 km however reliability problems are encountered in harsh conditions. In the context of hydro-acoustic signals, 'harsh' ocean conditions are encountered in relatively shallow waters subject to interference induced by multipath reverberation, high ocean noise, biological noise (particularly snapping shrimp), shipping noise, sound velocity profile induced refraction attenuation and attenuation by sound-wave interactions with the rough surface and sea floor. Conventional long-range hydro-acoustic modems do not provide a reliable communication link in such conditions.

In this thesis a methodology has been explored and developed to establish a reliable hydro-acoustic link in harsh acoustic conditions. This thesis presents the theory, underlining technology, performance measurements and limitations of a novel hydro-acoustic communication protocol together with an analysis of deployed system sea-trials. The hydro-acoustic communication protocol analysed for this study is the L3 Oceania MASQ Multi Channel Direct Sequence Spread Spectrum (MCDSSS) commercial system. As the principal engineer for L3 Oceania (formerly NAUTRONIX) the candidate has focused the last 20 years on developing underwater digital communication protocols, including MASQ, used in mission-critical naval, industrial and oceanographic applications. L3 Oceania clients have sponsored many months of valuable vessel time for sea trials during the development of MCDSSS, and the data recorded during these trials has provided a solid foundation for the development and testing of the improved system presented in this thesis.

Although the MCDSSS underwater communication protocol normally provides better than 80% reliable communication over the design transmission range of up to 10 km, sea trial recordings in shallow Australian, Baltic and Singaporean waters have identified multiple sources of interference where the MCDSSS signal could not be decoded even though the signal to noise ratio was at least superficially favourable. This thesis details the whole-of-system algorithm and engineering optimisations developed in an attempt to increase the MCDSSS reliability to close to 100%. Alternative algorithms were developed and tested for transmit signal modulation, receive signal demodulation, non-linear multipath tracking control systems, and numerically efficient software defined radios. Engineering optimisations were identified for hydro-acoustic transducer design, broad-band matching networks, energy efficient low distortion power amplifiers, low noise floor electronics and low power consumption electronics.

There was no single subsystem optimisation resulting in a dramatic improvement in the covert communication message reliability. A combination of multiple interdependent control system optimisations were required with subsequent sea trials measuring an overall performance improvement of approximately 10 dB. The majority of the attempted non-linear control system algorithm, communication protocol, software and hardware interventions either failed, induced instability in other control systems or degraded performance in unrelated sea trial post processed message reliability. Only the algorithm and engineering optimisations with significant performance improvement are presented in this thesis.

An unexpected by-product of improving message reliability was an increase in the measurement accuracy of bit energy efficiency, which identified a non-linear relationship between the maximum baud rate and peak bit energy efficiency. This has significant implications for the reduction of hydro-acoustic noise pollution, lowering battery power consumption and the potential of ocean powered networked communication.

Long-range communication message reliability was increased from 80% to approximately 99% resulting in a reversal of deep/shallow water reliability. Long-range shallow water reverberating communication is now more reliable than deep water non-reverberating communication, at equivalent transmit source level, communication range and ambient noise level. The MCDSSS receiver control systems utilise shallow water multipath reverberation signals as an additional source of signal energy and the communication performance improvements can be used to either lower the minimum transmit source level by up to 10 dB, extend communication range by 50% or operate in environments with up to 10 dB louder ambient noise.

ACKNOWLEDGEMENTS

Principal supervision, electrical systems engineering– Professor Yue Rong.

Associate supervision, acoustic sub-systems – Dr Alec Duncan.

Associate supervision, L3 Oceania intellectual property auditor, conference paper co-author, sea trial acoustic analysis and technical questioning – Alessandro Ghiotto.

L3 Oceania, 108 Marine Terrace Fremantle, Western Australia.

Technical Staff:

Micro controller firmware support – Tim Wade.

Deep water sea trial data acquisition and spectrogram analysis – Rodney Thomson.

Sound velocity profile data processing – Chris Sorgiovanni.

Thesis grammar, spelling and format review – Dr Michael Caley.

Management:

Providing access to sea trial data and use of L3 Oceania facilities.

L3 Oceania clients:

Providing many months of accumulated vessel time for field trial measurements.

Family:

Jenny Andronis and Christina Andronis.

Thesis grammar and spelling review – Alexandros Andronis.

Table of Contents

List of Figures

List of Tables

Nomenclature and Abbreviations

A_N – MCDSSS transmitter **N**oise floor maximum **A**ttenuation [dB].

A_{NQ} – MCDSSS transmitter **Q**uiescent maximum **A**ttenuation [dB].

A_{TX} – MCDSSS **Transmitter A**ttenuation [dB].

BEE – **B**it **E**nergy **E**fficiency [bits/J @ 1 km].

BER – **B**it **E**rror **R**ate [ratio].

B_{CH} – Communication **Ch**annel **B**andwidth [Hz].

B_e – **B**andwidth **E**fficiency [bits/s/Hz].

B_M – **M**odulation **B**andwidth [Hz].

B_{PS} – **B**its **P**er **S**ymbol [number].

B_{PT} – **B**its **P**er **T**elemetry channel [number].

Br – Hydro-acoustic **B**aud **R**ate [bits/second].

Br_{BEE} – **H**ydro-acoustic **B**aud **R**ate where peak **BEE** occurs [bits/second].

Br_{MAX} – **Max** hydro-acoustic **B**aud **R**ate [bits/second].

Br_{MIN} – **Min** hydro-acoustic **B**aud **R**ate [bits/second].

Br_{PG} – Hydro-acoustic **B**aud **R**ate **P**rocessing **G**ain [dB].

B_{TX} – **B**and limited **Transmit** transducer 6 dB Bandwidth [Hz].

C – Encryption spread spectrum **C**ode [bipolar].

C_{FSK} – **FSK** time domain detector **C**omputational load [DFT operations/second].

C_{f} – **F**requency domain detector **C**omputational load [FFT operations/second].

C_{t} – **T**ime domain detector **C**omputational load [correlation operations/second].

c – Ocean speed of sound [$\mathrm{m.s^{-1}}$].

DI – Sonar equation **D**irectivity **I**ndex [dB] (narrow-band).

DT – Sonar equation **D**etection **T**hreshold [dB] (narrow-band).

D_{AIR} – **Air** Coupling Loss **D**irectivity Index [dB] (broad-band).

D_C – **C**ritical **D**oppler velocity [knots].

D_D – **D**oppler **D**etection threshold offset [dB].

$D_{DEFAULT}$ – **D**efault **D**oppler detection threshold offset [dB].

D_{FB} – **D**irectional hydrophone **F**ront to **B**ack ratio directivity index [dB].

D_M – **M**aximum **D**oppler velocity [±knots].

D_N – **D**oppler receivers [**N**umber].

D_{PWM} – Telemetry alert **PWM D**ata [Index] (broad-band).

D_R – **D**oppler search **R**esolution [knots].

D_{RX} – **Receiver** hydrophone **D**irectivity index [dB] (broad-band).

D_S – **D**oppler [**S**cale factor].

D_{TH} – Receiver **D**etection **Th**reshold [dB] (broad-band).

D_{TX} – **Transmitter** projector **D**irectivity index [dB].

E_{TX} – Hydro-acoustic **Transmit** symbol **E**nergy [Joules].

ε_C – RMS ocean speed of sound **E**stimate error [$\mathrm{m.s^{-1}}$].

ε_{PZT} – PZT transducer electrical to acoustic conversion efficiency [%].

ε_{TX} – Transmitter electrical efficiency [%].

FOM – Sonar equation **F**igure **O**f **M**erit [dB] (narrow-band).

$\mathcal{F}$ – **F**ourier Transform function.

$\mathcal{F}^{-1}$ – Inverse **F**ourier transform function.

$\mathbf{f}$ – **F**requency [Hz].

f_C – **C**arrier **F**requency [Hz].

f_e – Clock **F**requency **E**rror [seconds per second].

f_S – **S**ampling **F**requency [Hz].

f_T – **T**elemetry alert receiver sample rate [Hz].

ψ – Receiver correlation magnitude [volts].

G – **G**ain [dB].

G_M – **M**ultipath deconvolution **G**ain [dB].

G_{MAX} – **Max**imum fixed point arithmetic dynamic range [dB].

$h(\mathbf{t}, \boldsymbol{\tau})$ – Channel impulse response function.

H_{C1} – BPSK min/max **H**amming distance [normalised scale factor].

H_{C2} – QPSK normalise **H**amming distance [normalised scale factor].

H_{C3} – 8PSK normalised **H**amming distance [normalised scale factor].

H_{C5} – 32PSK normalised **H**amming distance [normalised scale factor].

I – MCDSSS **I**n phase reference channel spread spectrum code [bipolar].

LFB – **L**ower **F**requency 3 dB **B**and [Hz] (narrow-band).

LFB_{6dB} – PZT transducer **L**ower **F**requency **6 dB B**and [Hz] (broad-band).

L_A – Environmental **A**bsorption **L**oss [dB/km].

L_{C1} – MCDSSS BPSK (no telemetry channel) self-noise **L**oss [dB].

L_{C2} – MCDSSS QPSK inter-channel self-noise **L**oss [dB].

L_{C3} – MCDSSS 8PSK inter-channel self-noise **L**oss [dB].

L_{C5} – MCDSSS 32PSK inter-channel self-noise **L**oss [dB].

L_O – Physical **O**bstruction **L**oss [dB].

L_{OS} – MCDSSS transmit signal **O**ver **S**preading **L**oss [dB].

L_R – Sound velocity profile induced **R**efraction **L**oss [dB].

L_S – Spherical **S**preading **L**oss [dB].

L_T – **T**otal path **L**oss [dB].

M – PRN code [bipolar].

MAX – Signal **Max**imum function.

MIN – Signal **Min**imum function.

MOD – **Mod**ulo arithmetic function.

MR – **M**essage (frame) **R**eliability [%].

$M_{RELIABLE}$ – DSSS **Reliable** communication receive **M**argin [dB].

M_{RX} – DSSS **Receive M**argin equivalent to SNR [dB].

M_{TX} – DSSS **Transmit M**argin [dB].

M_1 – MCDSSS preferred pair **#1** encryption spread spectrum code [bipolar].

M_2 – MCDSSS preferred pair **#2** encryption spread spectrum code [bipolar].

m – Numerical index [integer].

NL – Sonar equation **N**oise **L**evel [dB Vrms / µPa @ 1 m] (narrow-band).

N_B – MCDSSS spread spectrum code **B**its [**N**umber].

N_C – MCDSSS **N**umber of **C**hannels [number].

N_{C1} – MCDSSS BPSK **N**umber of **C**hannels [number].

N_{C2} – MCDSSS QPSK **N**umber of **C**hannels [number].

N_{C3} – MCDSSS 8PSK **N**umber of **C**hannels [number].

N_{C5} – MCDSSS 32PSK **N**umber of **C**hannels [number].

N_{CFC} – **N**umber of **C**arrier **F**requency **C**ycles per modulation bandwidth [scale factor].

N_{DSP} – **N**umber of **D**igital **S**ignal **P**rocessing assembler function [number].

N_{FEC} – **N**umber of message symbols corrected by **F**orward **E**rror **C**orrection [**N**umber].

N_{FSK} – Telemetry alert **N**umber of **FSK** samples [number].

N_H – Network **H**eader symbols [**N**umber].

N_L – MASQ variable **L**ength **N**umber of symbols [number].

N_M – **N**umber of **M**ultipath signals [number].

N_{MATCH} – MCDSSS transmitter matching network total voltage step up [ratio].

N_P – Network **P**ayload data symbols [**N**umber].

N_{PING} – Telemetry alert signal **Ping** samples [**N**umber].

N_S – MCDSSS user **N**umber of payload **S**ymbols [number].

N_T – MCDSSS **T**elemetry channels [**N**umber].

N_{UT} – **N**umber of signal processing software module **U**nit **T**est functions [number].

N_Z – **Z**ero fill symbols [**N**umber].

n_A – **A**mbient **n**oise floor [Vrms].

n – Numerical integer [index].

OCV – Hydrophone **O**pen **C**ircuit **V**oltage response [dB Vrms / µPa @ 1 m].

PSD_A – Receiver **A**mbient noise RMS **P**ower **S**pectral **D**ensity [dB re 1 µPa/$\sqrt{\text{Hz}}$].

PSD_{ABS} – Receiver **Abs**olute RMS **P**ower **S**pectral **D**ensity [dB re 1 µPa/$\sqrt{\text{Hz}}$].

PSD_{DETECT}– Receiver signal **Detect** RMS **P**ower **S**pectral **D**ensity [dB re 1 µPa/$\sqrt{\text{Hz}}$].

PSD_M – **M**ultipath self noise RMS **P**ower **S**pectral **D**ensity [dB re 1 µPa/$\sqrt{\text{Hz}}$].

PSD_N – MCDSSS receiver **N**oise floor RMS **P**ower **S**pectral **D**ensity [dB re 1 µPa/$\sqrt{\text{Hz}}$].

PSD_Q – MCDSSS TX **Q**uiescent noise floor RMS **PSD** [dB re 1 µPa/$\sqrt{\text{Hz}}$ @ 1 m].

PSD_{REL} – Receiver **Rel**ative RMS **P**ower **S**pectral **D**ensity [dB].

$PSD_{SS\#}$ – **S**ea **S**tate **number** **P**ower **S**pectral **D**ensity across DSSS band [dB re 1 µPa/$\sqrt{\text{Hz}}$].

PSD_{RX} – MCDSSS **Receiver** absolute RMS **P**ower **S**pectral **D**ensity [dB re 1 µPa/$\sqrt{\text{Hz}}$].

PSD_{TX} – MCDSSS **Transmit** signal RMS **P**ower **S**pectral **D**ensity [dB re 1 µPa/$\sqrt{\text{Hz}}$].

P_C – Auto **C**orrelation RMS noise floor [dB].

P_F – **P**ower of the **F**ull bandwidth *sinc* function [watts].

P_G – MCDSSS **P**rocessing **G**ain [dB].

P_L – **P**ower of a 3 dB bandwidth **L**imited *sinc* function [watts].

P_N – Correlation RMS **N**oise floor [dB].

$P_{Q_{RX}}$ –MCDSSS **Transmitter** **Q**uiescent **P**ower [watts].

$P_{Q_{TA}}$ –FSK receiver **T**elemetry **A**lert **Q**uiescent **P**ower [watts].

$P_{Q_{TX}}$ –MCDSSS **Transmit** **Q**uiescent **P**ower [watts].

P_{RX} –**Receiver** electrical **P**ower consumption [watts].

P_{TX} –**Transmitter** electrical **P**ower consumption [watts].

P_{3dB} – Ratio of the bandwidth limited and full bandwidth *sinc* function [%].

Q_{1-4} – MCDSSS **Q**uadrature phase telemetry channels **1** to **4** codes [bipolar].

R – **R**esistance [ohms].

RL – **R**eceive **L**evel [dB re 1 µPa] (narrow-band).

RMS – **R**oot **M**ean **S**quare function.

R_{ABS} – Sound speed limited slant **R**ange **Abs**olute accuracy error [meters].

R_B – **B**ottom (sediment) ducting multipath hydro-acoustic slant **R**ange [meters].

R_D – **R**ange from the ocean surface to the bottom **D**epth [meters].

R_{DD} – **R**ange from the ocean surface to the **D**ucting **D**epth [meters].

R_H – **R**ange from the ocean surface to the **H**ydrophone or projector depth [meters].

R_M – **M**ultipath hydro-acoustic slant **R**ange [meters].

R_{MAX} – **M**aximum communication slant **R**ange [meters].

R_{REL} – RMS receiver detect time limited slant **R**ange **Rel**ative accuracy error [meters].

R_S – Line of sight hydro-acoustic **S**lant **R**ange [meters].

$\boldsymbol{R_T}$ – Surface ducting multipath hydro-acoustic slant **R**ange [meters].

SECOND – **Second** loudest correlation magnitude function.

$\boldsymbol{SL}$ – Sonar equation **S**ource **L**evel [dB Vrms / µPa @ 1 m] (narrow-band).

$\boldsymbol{SNR}$ – **S**ignal to **N**osie **R**atio equivalent to DSSS receive M_{RX} [dB] (narrow-band).

$\boldsymbol{SNR_{RX}}$ – MCDSSS **Receiver** correlator noise floor **S**ignal to **N**osie **R**atio [dB].

$\boldsymbol{SPL_{1W}}$ – **S**ound **P**ressure **L**evel to acoustic power conversion [dB re 1 µPa/W@ 1 m].

$\boldsymbol{SPL_{BEE}}$ – Minimum peak BEE transmit RMS **S**ound **P**ressure **L**evel [dB re 1 µPa @ 1 m].

$\boldsymbol{SPL_{MAX}}$ – **Max**imum transmit RMS **S**ound **P**ressure **L**evel [dB re 1 µPa @ 1 m].

$\boldsymbol{SPL_{MIN}}$ – Minimum transmit RMS **S**ound **P**ressure **L**evel [dB re 1 µPa @ 1 m].

$\boldsymbol{SPL_N}$ – SS transmitter quiescent **N**oise floor RMS **S**ound **P**ressure **L**evel [dB re 1 µPa @ 1 m].

$\boldsymbol{SPL_Q}$ – SS transmitter **Q**uiescent power RMS **S**ound **P**ressure **L**evel [dB re 1 µPa @ 1 m].

$\boldsymbol{SPL_{TX}}$ – Transmit signal RMS **S**ource **L**evel [dB re 1 µPa @ 1 m].

$\boldsymbol{SS\#}$ – Noise increase per IMO **S**ea **S**tate [**number**].

$\boldsymbol{SS_{\mathrm{dB}}}$ – Ambient noise or equivalent path loss increase per **S**ea **S**tate number [dB/$SS\#$].

$\boldsymbol{S_{CB}}$ – Encryption **S**pread spectrum **C**ode number of [**B**its].

$\boldsymbol{S_{CO}}$ – **S**pread spectrum **C**ode **O**rder [number].

$\boldsymbol{Sy}$ – MCDSSS **Sy**mbol unsigned code word [index].

$\boldsymbol{TL}$ – Sonar equation **T**ransmission **L**oss [dB] (narrow-band).

$\boldsymbol{TVR}$ – PZT transducer **T**ransmit **V**oltage **R**esponse [dB re 1 µPa /Vrms @ 1 m].

t – **T**ime [seconds].

$\boldsymbol{t_e}$ – Clock accuracy **T**ime **E**rror [seconds per second].

$\boldsymbol{t_f}$ – Hydro-acoustic **T**ime of **F**light [seconds].

$\boldsymbol{t_{GPS}}$ – **GPS T**ime [seconds].

$\boldsymbol{t_{FSK}}$ – Telemetry alert f_{FSK} receive **t**ime [seconds].

$\boldsymbol{t_M}$ – **M**ultipath signal flight **t**ime [seconds].

$\boldsymbol{t_S}$ – **S**lant range signal flight **t**ime [seconds].

τ – Period [seconds].

$\boldsymbol{\tau_{FSK}}$ – Telemetry alert **FSK** period [seconds].

τ_{ψ} – MCDSSS receiver correlator pulse compression period [seconds].

τ_{M} – **M**ultipath period [seconds].

τ_{MPE} – **M**ultipath reverberation **E**nvelope period [seconds].

τ_{PING} – Telemetry alert **P**ing period [seconds].

τ_{SY} – Spread spectrum **Sy**mbol period [second].

θ – Carrier frequency phase offset [degrees].

θ_{N} – Multipath induced carrier phase **N**oise [degrees].

θ_{RS} – MCDSSS **S**lant **R**ange induced carrier phase offset [degrees].

θ_{RX} – MCDSSS **Receiver** carrier phase offset [degrees].

θ_{TX} – MCDSSS **Transmitter** carrier phase offset [degrees].

UFB – **U**pper **F**requency 3 dB **B**and [Hz] (narrow-band).

UFB_{6dB} – PZT transducer **U**pper **F**requency **6 dB B**and [Hz] (broad-band).

$\mathbf{V}$ – **V**oltage [volts].

$\mathbf{V}_{A}$ – MCDSSS receiver **A**nalog front-end noise floor [**V**rms].

$\mathbf{V}_{ADC}$ – MCDSSS receiver **ADC** noise floor [**V**rms].

$\mathbf{V}_{D}$ – MCDSSS receiver **D**igital truncation noise floor [**V**rms].

$\mathbf{V}_{FSK_N}$ – MASQ telemetry alert **FSK** signal channel [**V**olts].

$\mathbf{V}_{I}$ – MCDSSS reference (I) spread spectrum code time domain signal [**V**olts].

$\mathbf{V}_{N}$ – MCDSSS receiver **N**oise floor [**V**rms].

$\mathbf{V}_{P}$ – MCDSSS receiver **P**ower supply noise [**V**rms].

$\mathbf{V}_{Q}$ – MCDSSS telemetry (Q) spread spectrum code time domain signal [**V**olts].

$\mathbf{V}_{RX}$ – MCDSSS **Receiver** signal [**V**olts].

$\mathbf{V}_{TX}$ – MCDSSS **Transmit** signal [**V**olts].

$\mathbf{v}$ – **V**elocity [$\mathrm{m.s^{-1}}$].

$\mathbf{v}_{WS}$ – Horizontal **W**ind **S**peed [knots].

Z_{PZT} – PZT transducer impedance [ohms].

Z^{T} – Delay line feedback **T**ap [number].

List of Acronyms and Abbreviations

ADC	- **A**nalog to **D**igital **C**onvertor.
AUSSNet	-L3 Oceania **A**utonomous **U**nderwater **S**urveillance **S**ensor **Net**work.
AUV	- **A**utonomous **U**nderwater **V**ehicle.
BGA	- **B**all **G**rid **A**rray electronics.
BPF	- **B**and **P**ass **F**ilter.
BW	- **B**and **W**idth.
CCITT-16	- **C**omite **C**onsultatif **I**nternational de **T**elegraphique et **T**elephonique 16 bit CRC.
CODEC	- ADC/DAC **Cod**er/**Enc**oder.
CRC	- **C**yclic **R**edundancy **C**heck.
CUUUWi	- **C**ommunication **U**sing **U**ltrasonic **U**nderwater **Wi**reless.
DAC	- **D**igital to **A**nalog **C**onvertor.
DFT	- **D**iscrete **F**ourier **T**ransform.
DP	- **D**ynamic **P**ositioning vessel.
DSP	- **D**igital **S**ignal **P**rocessor.
GPM300	- L3 Oceania ϕ80 mm internal diameter pressure housing hardware implementation of the hydro-acoustic **G**eneral **P**urpose **M**odem model number **300** with support for MASQ communication channel, HAIL, MK84 and UQC voice.
GPS	- **G**lobal **P**ositioning **S**ystem.
EMF	- **E**lectro **M**agnetic **F**orce.
FDR	- **F**alse **D**etect **R**ate.
FEC	- **F**orward **E**rror **C**orrection.
FFT	- **F**ast **F**ourier **T**ransform.
FIR	- **F**inite **I**mpulse **R**esponse.
FPGA	- **F**ield **P**rogrammable **G**ate **A**rray.
HAIL	- L3 Oceania **H**ydro **A**coustic **I**nformation **L**ink DSSS modulation.
ID	- **I**nner **D**iameter.
IFFT	- **I**nverse **F**ast **F**ourier **T**ransform.
IMO	- **I**nternational **M**artine **O**rganisation.
IP	- L3 Oceania **I**ntellectual **P**roperty audit.
ISI	- **I**nter **S**ymbol **I**nterference.
ISO	- **I**nternational **S**tandards **O**rganisation.
LDPC	- **L**ow **D**ensity **P**arity **C**ode error correction.

LFB - **L**ower **F**requency **B**and.

LNA - **L**ow **N**oise **A**mplifier.

LPI - **L**ow **P**robability of **I**ntercept.

LSB - **L**ower **S**ide **B**and.

MAC - **M**ultiply and **AC**cumulate.

MASQ - L3 Oceania third generation product acronym for a MCDSSS hydro-acoustic communication protocol (Commercial).

MATLAB™ - **Mat**rix **L**aboratory programming language.

MK84 - **M**ar**k 84** torpedo and vessel tracking DSSS modulation.

MPE - **M**ultipath reverberation **E**nvelope.

MRCS - **M**CDSSS **R**eceiver multipath tracking non-linear **C**ontrol **S**ystem.

MV - **M**erchant **V**estal.

NASNet™ - **N**AUTRONIX **A**coustic **S**ubsea **N**etwork [163].

NATO - **N**orth **A**tlantic **T**reaty **O**rganisation [158].

NMEA - **N**ational **E**lectrical **M**anufacturers **A**ssociation [157].

NO L3 IP - Diagram items containing **L3** Oceania **I**ntellectual **P**roperty have been removed.

OCV - PZT transducer **O**pen **C**ircuit **V**oltage response.

OD - **O**uter **D**iameter.

OLQ - **O**ptimise **L**ink **Q**uality NMEA command.

OSI - **O**pen **S**ystems **I**nterconnection.

PASOR - L3 Oceania **P**ortable **A**coustic **S**onobuoy **R**anging system.

PC - **P**ersonal **C**omputer.

PRN - **P**seudo **R**andom **N**umber sequence with good auto correlation correction properties.

PZT - Lead (**P**b) **Z**irconate **T**itanate piezoelectric ceramic transducer.

QA - **Q**uality **A**ssurance.

RF - **R**adio **F**requency.

RHIB - **R**igid **H**ulled **I**nflatable **B**oat.

RS - **R**eed **S**olomon forward error correction.

RX - **Receiver**.

SIMD - **S**ingle **I**nstruction **M**ultiple **D**ata signal processing hardware.

Slant Range - Line of sight distance between hydro-acoustic network modems. Distance reported in meters using a sound velocity estimate.

SOFAR - 1 km depth **So**und **F**ixing **A**nd **Ra**nging channel.

SVP - **S**ound **V**elocity **P**rofile.

STANAG - NATO a **Stan**dardization **Ag**reement.

STS - L3 Oceania **S**ubmarine **T**racking **S**ystem.

TBP - **T**ime **B**andwidth **P**roduct.

TCP/IP - **T**ransmission **C**ontrol **P**rotocol/**I**nternet **P**rotocol.

TONPIZ - Directional transducer (**Tonpiz** is German for tone mushroom).

TPC - **T**ransceiver **P**rocessor **C**ard.

Transpond - **Transpond** two-way time of flight measurement.

TWC - **T**hrough **W**ater **C**ommunications.

TX - **T**ransmitter.

UQC - NATO STANAG 1074 **U**nder water telephone **C**ommunications.

USB - **U**pper **S**ide **B**and

UT3000 - ELAC **U**nderwater **T**elephone model **3000** with support for a subset of **M**ASQ communication channel functions [151]

List of Modulation Acronyms

4DPSK - **4 D**ifferential **P**hase **S**hift **K**eying modulation (BW efficient).

8PSK - **8 P**hase **S**hift **K**eying modulation.

32PSK - **32 P**hase **S**hift **K**eying modulation.

32OFDM - **32 O**rthogonal **F**requency **D**ivision **M**odulation (BW efficient).

64OFDM - **64 O**rthogonal **F**requency **D**ivision **M**odulation (BW efficient).

128OFDM - **128 O**rthogonal **F**requency **D**ivision **M**odulation (BW efficient).

BFSK - **B**inary **F**requency **S**hift **K**eying modulation (BW efficient).

BPSK - **B**i-**P**hase **S**hift **K**eying modulation.

CDMA - **C**ode **D**ivision **M**ultiple **A**ccess modulation (BW efficient).

DPAM - **D**igital **P**ulse **A**mplitude **M**odulation.

DSSS - **D**igital **S**equence **S**pread **S**pectrum.

FDMA - **F**requency **D**ivision **M**ultiple **A**ccess modulation (BW efficient).

FM - **F**requency **M**odulation (BW efficient).

FSK - **F**requency **S**hift **K**eying modulation.

DSSS - **D**irect **S**equence **S**pread **S**pectrum.

MCDSSS - **M**ulti-**C**hannel **D**igital **S**equence **S**pread **S**pectrum.

MFSK - **M**ultiple **F**requency **S**hift **K**eying modulation (BW efficient).

PSK - **P**hase **S**hift **K**eying modulation.

QAM - **Q**uadrature **A**mplitude **M**odulation (BW efficient).

QPSK - **Q**uadrature **S**hift **K**eying modulation (BW efficient).

SS - **S**pread **S**pectrum modulation.

SSB - **S**ingle **S**ide **B**and modulation (BW efficient).

TDMA - **T**ime **D**ivision **M**ultiple **A**ccess modulation (BW efficient).

List of Efficient Channel Equalisation Acronyms

APF - Hydrophone **A**rray **P**rocessing **F**ilter equalisation.

BFC - **B**lind **F**eedback **C**hannel equalisation.

CRC - **C**yclic **R**edundancy **C**heck feedback estimation equalisation.

DFE - **D**ecision **F**eedback **E**qualisation.

FDE - **F**requency **D**omain **E**qualisation.

FTF - **F**ast **T**ransverse **F**iltering equalisation.

LMS - **L**east **M**ean **S**quare equalisation.

MCDEF - **M**ulti **C**hannel **D**ecision **F**eedback **E**qualisation.

RLS - **R**ecursive **L**east **S**quare equalisation.

1 INTRODUCTION

This thesis presents the theory, underlining technology and limitations of a novel hydro-acoustic communication protocol together with analysis of performance improvements validated via sea-trial measurements. The law of diminishing returns applies to the analysis of a communication system that was incrementally developed over many years to achieve near 100% non-convert communication reliability, so considerable effort was required to achieve the primary thesis requirement of increasing the covert communication reliability from 80% to near 100%.

In 1995 L3 Oceania [146] [147] (formerly NAUTRONIX) developed a medium-range underwater communication system for measuring one-way time of flight between an Australian submarine and hydrophones for the purpose of absolute sound pressure level measurements. Submarines equipped with Global Positioning Satellite (GPS) synchronised transmitters generate Direct Sequence Spread Spectrum (DSSS) signals which are detected below the ocean ambient noise floor by GPS synchronised hydrophones. Involvement with DSSS communication started when this candidate retrofitted a one-way telemetry channel to the Submarine Tracking System (STS). STS evolved into a two-way Hydro-Acoustic Information Link (HAIL) that provided communication range of up to 10 km. The hydro-acoustic performance measurements from STS and HAIL were used to develop a second-generation commercial underwater navigation system (NASNet™) which evolved into a third generation long-range and high ambient noise hydro-acoustic Multi Channel Direct Sequence Spread Spectrum (MCDSSS) communication system (MASQ), representing over 20 years of incremental performance improvements in under water communication technology (Table 1).

Gen	Initial	Protocol	Applications	Speed	Payload	Network	Range Measurement		Voice	Platform
#	Year	Name	Description	Baud	Max bits	Support	One way	Transpond	UQC	Hardware
1st	1995	STS	Covert submarine tracking	15/30	300	No	Yes	No	No	PC
	1998	HAIL	Covert submarine communication	48-96	720	No	Yes	No	No	DSP/PC
2nd	2000	NASNet™	Well head blow out protector	14	112	Yes	No	Yes	No	DSP/PC
			Underwater GPS				Yes	Yes	No	
			Deep water torpedo tracking				Yes	Yes	No	
			Shallow Water torpedo tracking				Yes	Yes	No	
3rd	2009	MASQ	All the above	10-1200	8192	Yes	Yes	Yes	Yes	DSP/PC
			Long range communication							
			Short range high ambient noise comms							
			High baud rate communication							

Table 1 L3 Oceania hydro-acoustic communication protocols

MASQ has been successfully deployed in mission critical applications across the globe in a wide variety of acoustic environments. An important objective of improving DSSS communication reliability is the lowering of acoustic power output, which has the benefit of reducing power consumption and anthropogenic noise, and minimising the impact on divers, marine mammals and ocean fauna. Operating hydro-acoustic modems at peak bit energy efficiency provides maximum covert performance and, in conjunction with network routing infrastructure, allows for the deployment of low power distributed underwater communication networks which can potentially be powered by ocean energy harvesting.

1.1 Performance Aims and Objectives

The primary objectives of the work described in this thesis were to achieve reliable long-range communication and reliable communication in high ambient environments by optimising subsystems associated with maximising message reliability and subsystems associated with maximising communication range as summarised below:

1. Maximising the communication message reliability (MR) requires:
    a. Provide tolerance to multipath reverberation (R_M);
    b. Provide tolerance to ocean induced interference (PSD_A);
    c. Maximising the receive margin (M_{RX});
    d. Maximising the transmission bandwidth (B_{TX});
    e. Maximising the processing gain (P_G);
    f. Resolving hardware and software reliability issues masked by P_G; and
    g. Optimising detector algorithms.
2. Maximising communication range (R_s) requires:
    a. Maximising the transmit source level (SPL_{MAX});
    b. Minimising the receiver noise floor (PSD_N);
    c. Minimising the detection threshold (D_{TH});
    d. Maximising the multipath gain (G_M);
    e. Maximising the transmit margin (M_{TX});
    f. Maximising transmit projector directivity (D_{TX}); and
    g. Maximising receiver hydrophone directivity (D_{RX}).

Improving message reliability can be achieved using hydrophone arrays or directional hydrophones however the increase in power consumption and the cost of deploying these solutions renders MCDSSS communication commercially unviable. Any MCDSSS performance improvement must not increase power consumption, manufacturing costs or deployment costs.

A viable long-range underwater communication system generally requires low power consumption modems that will most likely be battery powered, requiring a pressure-housing for a battery payload or alternatively could be powered by renewable energy. Electrical power consumption must be minimised because the manufacturing and deployment costs of pressure housings increase by approximately the square of the payload volume. A commercially viable long-range underwater communication modem has the following secondary performance objectives to minimise power consumption:

1. Maximising transmitter efficiency (ϵ_{TX});
2. Minimising receiver quiescent power consumption (P_{RX});
3. Minimising receive margin (M_{RX}) (i.e. covert signal receiver); and
4. Minimising the user data payload (N_S).

Acoustic communication systems may be deployed in environments that are shared by high conservation value noise-sensitive marine mammals or may require interoperability with other acoustic systems. Any performance improvement must minimise spectral pollution and minimise transmit source level.

1.2 Message Reliability Improvement Methodology

The methodology used to improve message reliability was as follows:

1. The L3 Oceania hydro-acoustic sea trial database was mined for failing MCDSSS communication signals.
2. The failure modes were analysed and alternative algorithms and/or engineering solutions were developed. The alternative algorithms and/or engineering solutions were tested to ensure that the navigation/range measurement accuracy was not degraded and power consumption not increased.
3. Software analysis tools were developed to measure algorithm performance improvements using the failing signal database and tests were carried out to verify that performance degradation did not occur in test signals with different multipath geometries.
4. Algorithm performance improvements were measured using a 0.2 m air test of baud rate min/max and transmit source level min/max in an environment that excludes multipath reverberation, frequency dependant path losses and MCDSSS receiver noise floor.
5. Algorithm performance improvements were measured using a 22 m air test of transmit source level min/max in a multipath reverberation bounded maximum baud rate environment that excludes MCDSSS transmitter noise floor, frequency dependant attenuation, ocean ambient noise.
6. Algorithm performance improvements were validated in the L3 hydro-acoustic tank across a 2 m communication channel of transmit source level min/max and bit energy efficiency in an extreme multipath interference environment and loud *SS*10 noise.
7. Algorithm performance improvements were validated with a 400 m range harbour test of baud rate min/max, transmit source level min/max and bit energy efficiency in and environment that exhibits loud *SS*2-4 out of band anthropogenic noise, high multipath interference, medium path loss, excludes frequency dependant attenuation and excludes sound velocity refraction,
8. When 100% message reliability was achieved for all the previous tests then ocean communication tests were carried out to ensure that the algorithm and engineering interventions had not been over-fitted to the failing signal database. Additional shallow and deep water sea trial data was acquired at communication range longer than 10 km and harsher environmental conditions, which required additional rounds of MR algorithm improvements.
9. A final performance test was required in a controlled ocean environment to accurately measure maximum baud rate and bit energy efficiency.

1.3 Original Contributions to Field

The primary contribution of the work described in this thesis to the field of underwater acoustic communications, is the improvement in the reliability of shallow-water and high ambient noise communication over distances of up to 15 km. This was achieved by addressing the following four areas:

1.3.1 MCDSSS Modulation Performance Improvements

The selection of MCDSSS transmitter modulation encryption spreading codes with good circular cross correlation properties and matching normalised MCDSSS receiver telemetry spreading codes provide a measurable MCDSSS receiver long-range communication performance improvement in the presence of high multipath and loud ambient noise.

1.3.2 Optimisation of Transmit Power Efficiency

A significant by-product of improving message reliability and subsequent precision environmental measurement of the relationship between peak bit energy efficiency and maximum baud rate demonstrates that maximum transmit power efficiency is achieved by operating at the most covert configuration and not the highest achievable baud rate using the lowest transmit source level. The approximate 10 dB improvement in MCDSSS transceiver performance opens up the potential of establishing semi-permanent networked communication links by powering MCDSSS transmitters using ocean energy harvesting when operated at peak bit energy efficiency.

1.3.3 MCDSSS Transmit Performance Improvements and Limitations

The maximisation of long-range communication requires the measurement of broad-band high power Lead (Pb) Zirconate Titanate (PZT) transducers performance requiring the de-rating of PZT transducer narrow-band power specifications, increasing the transmitter power efficiency and improving attenuation of hydro-acoustic side band pollution.

1.3.4 MCDSSS Receiver Performance Improvements

The approximate 10 dB improvement in MCDSSS receiver performance was achieved via performance improvements of multiple non-linear receiver control systems, Doppler processing and telemetry channel impulse response deconvolution. Numerically efficient software radio receiver algorithms were developed to reduce the receiver power consumption, which extends battery life and increases the communication range of energy limited MCDSSS receivers.

1.4 Overview of Thesis

Chapter 2 provides background information relating to SS communication and options available to improve reliability including a description of the narrow-band and broad-band sonar equations' constraints relevant to SS transceiver optimisations.

Chapter 3 literature review compares state of the art research and commercial high-medium baud rate modems with SS low baud rate modem communication bandwidth efficiency, time bandwidth product, bit error rate, message reliability and bit energy efficiency.

Chapter 4 provides an overview of MCDSSS communication.

Chapter 5 provides a summary of MCDSSS modulation, transmitter and receiver algorithm improvements and engineering optimisations applied to improve message reliability.

Chapter 6 presents performance improvement measurements for MCDSSS message reliability, BER, minimum transmit source level and maximum baud rate. Measurements of peak BEE are presented with the potential of establishing ocean energy powered under water communication network. The issue of peak BEE propagation modelling is discussed.

Chapter 7 discusses the conclusions and recommendations

Appendices B to P contain sea trial summaries and appendices Q to R contain technical data relevant to MCDSSS communication.

2 BACKGROUND

2.1 Introduction

This chapter provides background material required to understand the sources of interference and environmental limitations, which compromise hydro-acoustic communication reliability. Hydro-acoustic communication is subject to multiple sources of interference generated by self-noise from multipath propagation, environmental noise, bioacoustics noise, vessel propulsion noise and boat sonar noise. The reliability of a communication link is dependent on the ability of the receiver to tolerate multiple sources of interference. The robustness of a communication system can be improved by spreading the transmit symbol energy in frequency and time using Spread Spectrum (SS) modulation [37]. SS modulation involves the purposeful reduction of communication baud rate to improve resilience to temporal and tonal noise with an additional benefit of improving navigation/range accuracy. If the carrier frequency (f_C) is low enough then the carrier can be Directly Sequence modulated using a Pseudo Random (PRN) Spread Spectrum code (DSSS) without requiring intermediate modulation stages such as those used in Radio Frequency (RF) heterodyne transceivers. Additional communication channels can be added by modulating the Spread Spectrum code to generate multiple DSSS signals which are mixed with a carrier phase offset (θ_{TX}) to generate a single Multi Channel Direct Sequence Spread Spectrum (MCDSSS) signal as illustrated in Figure 1 to Figure 2 and detailed in Chapter 4.

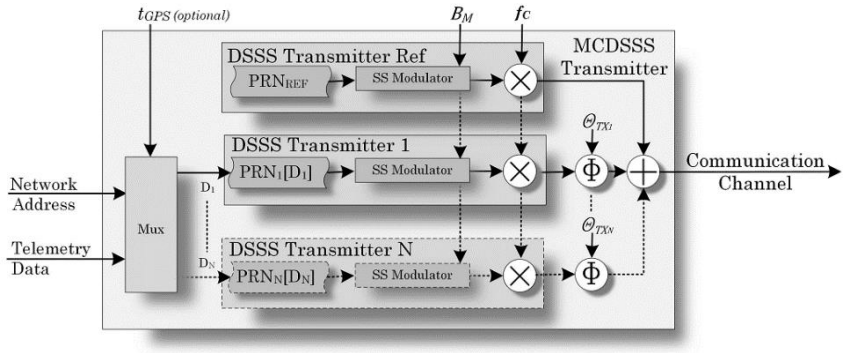

Figure 1 MCDSSS Transmitter

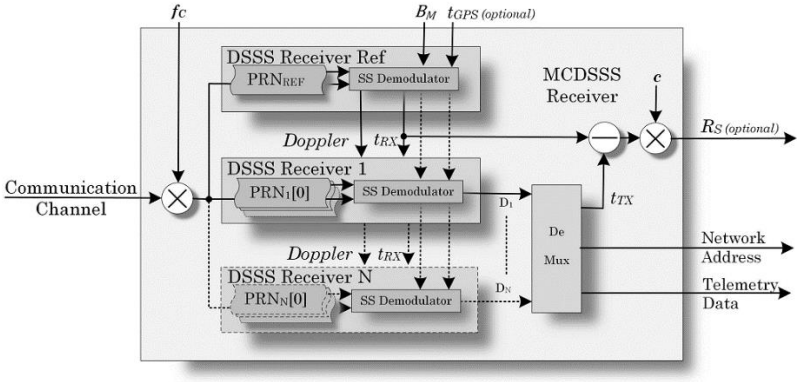

Figure 2 MCDSSS Receiver

2.2 Spread Spectrum Communication Reliability

The Multi-Channel Direct Sequence Spread Spectrum (MCDSSS) hydro-acoustic communication systems provide near 100% message reliability communication at signal-to-noise ratios greater than 0 dB above the ocean noise floor. The message reliability decreases to approximately 80% when the useful receive signal drops 0 dB to 15 dB below the ocean noise floor in the presence of multipath induced self-noise interference, loud environmental noise and/or anthropogenic noise. Figure 3 illustrates a transmitter located at the centre of the communication spheroid and a receiver located in the body of the spheroid. Non covert communication occurs when the receiver is close enough to the transmitter for the received signal to be louder than the ambient noise. Covert communication occurs when the receiver is far enough from the transmitter for the received signal receive margin to be below the ocean noise floor by less than the transmit margin. Shallow water truncates the top and the bottom of the communication spheroid with the ocean surface providing an efficient phase inverting reflector and the ocean bottom providing a less efficient variable phase reflector, which induces multipath interference. In the communication band of interest, the shallow water covert message reliability reduces to approximately 80% at communication ranges greater than 3 km. For communication range greater than 10 km (R_{MAX}) the message reliability decreases to less than 30%. At 15 km range the DSSS telemetry channels are no longer decodable. Beyond 15 km range the DSSS reference channel is no longer detectable.

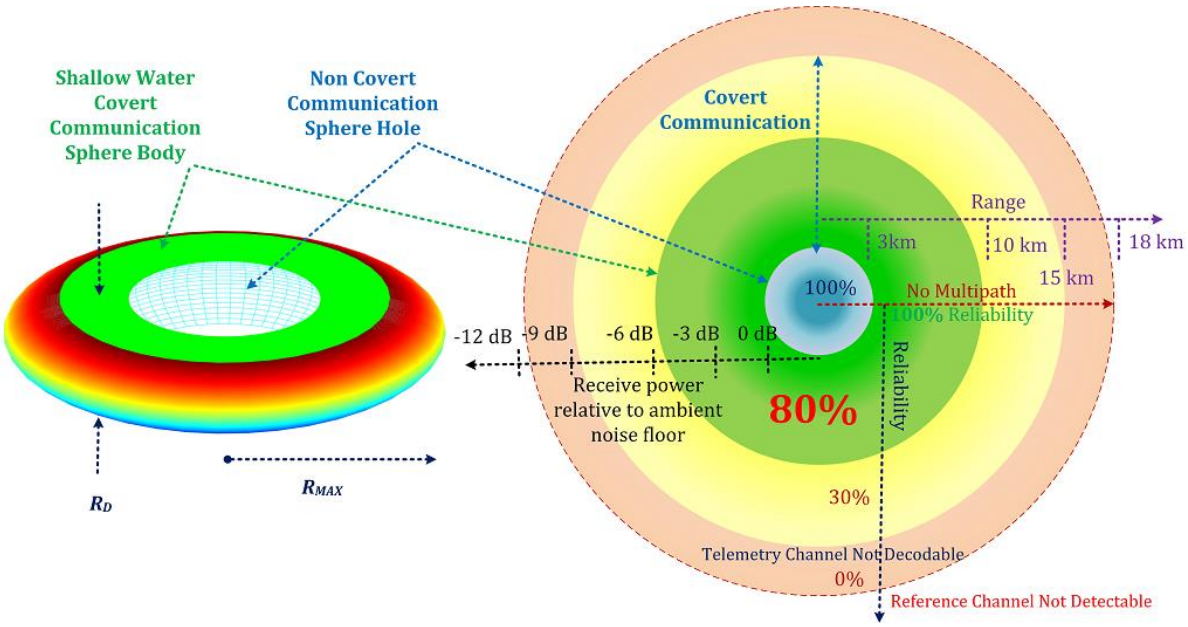

Figure 3 Conceptual hydro-acoustic communication reliability spheroid (firmware version 5.x)

2.3 Narrow-band Sonar Equation

The hydro-acoustic sonar equation states that a reliable communication link is established when the Received signal source Level (RL) is louder than the receiver Ambient Noise (AN) by at least the Detection Threshold (DT), this is also the case for RF and optical communication systems [129]. The received signal source level is also the difference between the transmit Source Level (SL) and Transmission Loss (TL). The

receiver ambient noise (AN) is the difference between the ambient Noise Level (NL) and the transceiver transducer Directivity Index gain (DI) Eq.(2-1).

$$RL = AN + DT = SL - TL = NL - DI + DT \tag{2-1}$$

If the received signal ($RL = SL - TL$) is louder than the received ambient noise ($AN = NL - DI$) by more than the Detection Threshold (DT) then the sonar equation is expressed in terms of the Figure Of Merit (FOM) which is a measure of the communication link reliability [129] Eq.(2-2).

$$FOM = RL - AN - DT = SL - TL - NL + DI - DT \tag{2-2}$$

2.4 Broad-band Sonar Equation

Equation (2-2) is applicable for narrow-band signalling applications such as echo sounders or voice communication where source level is expressed as the total in-band Sound Pressure Level (SPL) in dB referenced to 1 µPa at a distance of 1 m. Broad-band communication transmit signal strength can be expressed as Power Spectral Density (PSD_{TX}) in dB referenced to 1 µPa per $\sqrt{\text{Hz}}$ at a distance of 1 m. The narrow-band transmit source level (SL) becomes the Transmit Power Spectral Density (PSD_{TX}) which is a function of the Transmit Sound Pressure Level (SPL_{TX}) and Transmission Bandwidth (B_{TX}) [129] Eq.(2-3).

$$SL \equiv PSD_{TX} = SPL_{TX} - 10\log_{10}(B_{TX}) \tag{2-3}$$

The narrow-band sonar equation transmission loss is equivalent to the broad-band total Transmission Loss (L_T) which is the sum of spherical Spreading Loss (L_S), environmental Absorption Loss (L_A) and sound velocity induced Refraction Loss (L_R) Eq.(2-4).

$$TL \equiv L_T = L_S + L_A + L_R \tag{2-4}$$

Narrow-band multipath signals are received as coherent noise that increase the receive signal level (RL) (Figure 157). Broad-band Multipath signals are received as non-coherent interference that increase the self noise (Figure 159). The narrow-band noise level (NL) is equivalent to the broad-band receiver ambient noise Power Spectral Density (PSD_A) plus the in-band multipath interference (PSD_M) or self noise Eq.(2-5).

$$NL \equiv PSD_A + PSD_M \tag{2-5}$$

The directivity index (DI) is the sum of the Transmit projector Directivity index (D_{TX}) and the Receiver hydrophone Directivity index (D_{RX}) [129] Eq.(2-6).

$$DI \equiv D_{TX} + D_{RX} \tag{2-6}$$

The narrow-band sonar equation detection threshold (DT) is replaced with the broad-band transmit margin (M_{TX}) gain which is a function of the broad-band Processing Gain (P_G),

Multipath tracking Gain (G_M), broad-band symbol Detection Threshold loss (D_{TH}) and multi-channel interference self noise Loss (L_C) Eq.(2-7).

$$DT \equiv M_{TX} = P_G + G_M - D_{TH} - L_C \tag{2-7}$$

The narrow-band figure of merit (FOM) becomes the broad-band receive margin (M_{RX}) Eq.(2-17) which also describes covert communication performance when receive margin (M_{RX}) is less than the transmit margin (M_{TX}) Eq.(2-8). Broad-band receive margin is equivalent to narrow band SNR which must be greater than 3 dB to establish a communication link.

$$FOM \equiv M_{RX} > 3 \text{ dB} \quad (\text{SS communication is covert when } M_{RX} < M_{TX}) \tag{2-8}$$

2.4.1 Minimum Ambient Noise

Figure 4 illustrates the Australian shallow water ambient noise prediction curves [22]. The MASQ communication channel operates across the 6.5 kHz to 16.5 kHz frequency band (Appendix R Table 6).

For shallow water Sea State Zero (SSO), the ambient noise floor is approximately $PSD_{SS0} \approx$ 38 dB re 1 µPa/$\sqrt{\text{Hz}}$ across the MASQ frequency band. The SS receiver minimum noise floor (PSD_N) is bounded by and must be less than the shallow water sea state zero ambient noise floor (PSD_{SSO}) Eq.(2-9).

$$PSD_N < PSD_{SS0} \approx 38 \text{ dB re } 1 \text{ µPa}/\sqrt{\text{Hz}} \cong SSO \quad (\text{for MASQ}) \tag{2-9}$$

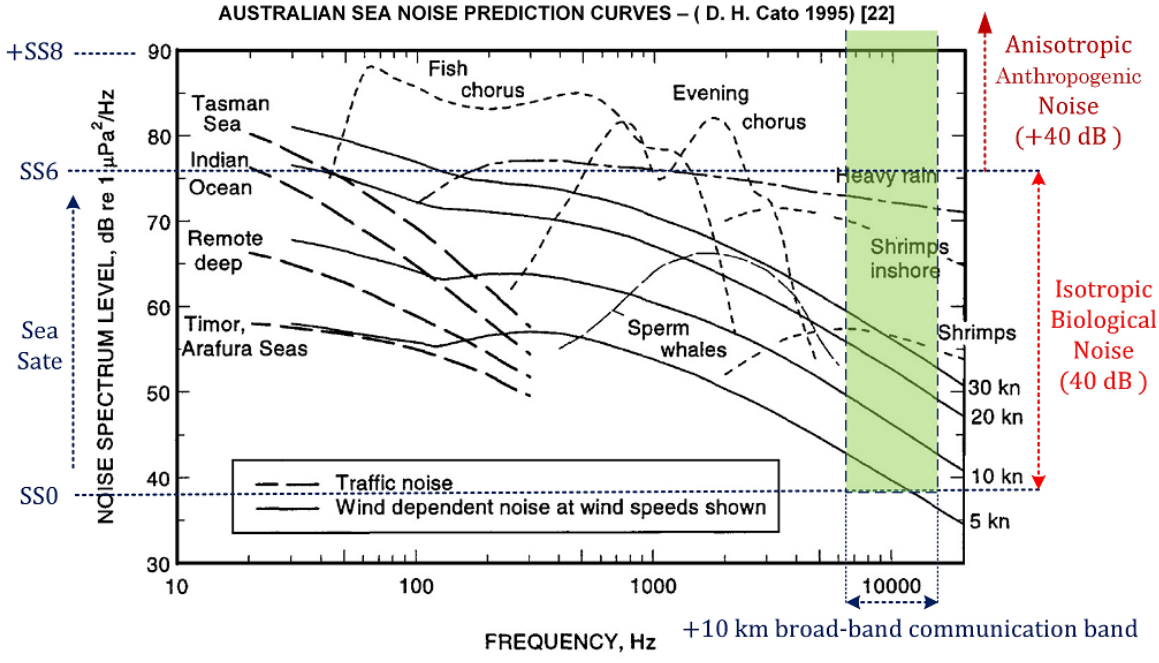

Figure 4 Shallow water ambient noise (MCDSSS 10 baud to 1,000 baud)

2.4.2 Maximum Transmit Source Level

From Table 6 Appendix R the maximum GPM300 PZT transducer transmission bandwidth is $B_{TX} < 10\text{ kHz} < 40\text{ dB re 1 Hz}$. The MASQ specified maximum Sound Pressure Level is $SPL_{MAX} = 190.5\text{ dB re 1 µPa @ 1 m}$ with a maximum transmit Power Spectral Density of $PSD_{MAX} \approx 155\text{ dB re 1 µPa}/\sqrt{\text{Hz}}\text{ @ 1 m}$ Eq.(2-10). Power spectral density measurement instruments such as Spectrum Analyser and Dynamic Signal analysers measure high impedance source voltage and low noise preamplifier and active hydrophone noise floor is also expressed as voltage spectral density. The PSD units convention used throughout this thesis is specified in voltage per square root of hertz to maintain consistence between instrument measurements and published noise figures.

$$PSD_{MAX} = SPL_{MAX} - 10\log_{10}(B_{TX}) \approx 190 - 35 \approx 155\text{ dB re 1 µPa}/\sqrt{\text{Hz}}\text{ @ 1 m} \quad (2\text{-}10)$$

2.4.3 Maximum Feasible Path Loss

In the assumed absence of sound velocity induced refraction ($L_R = 0$ dB) and also assuming no transmit margin ($M_{TX} = 0$ dB) the maximum communication range path loss ($L_T \approx 115$ dB), across the MASQ communication frequency band, is bounded by the maximum transmit source level (PSD_{MAX}) and the minimum receiver noise floor (PSD_{SSO}) Eq.(2-11).

$$L_T = PSD_{MAX} - PSD_{SS0} \approx 155 - 38 \approx 115\text{ dB} \quad \text{(for MASQ)} \quad (2\text{-}11)$$

2.4.4 Spherical/Cylindrical Spreading Path Loss

Deep water ($R_D > 100$ m) spherical spreading loss (L_S) is proportional to the square of Slant Range (R_S) as described by [129] Eq.(2-12).

$$L_S = 10\log_{10}(R_S^2) = 20\log_{10}(R_S) \quad (2\text{-}12)$$

The shallow water spreading loss varies from spherical spreading to cylindrical spreading as the depth approaches zero ($R_D \to 0$ m) as described by cylindrical spreading loss (L_S) [129] Eq.(2-13). Narrow-band multipath signals coherently sum to reduce the path loss by $10\log_{10}(1 + N_M) = 0\text{ dB} \to 6\text{ dB}$ as a function of number of multipath rays ($N_M = 0 \to 5$).

$$\begin{gathered} R_D \to 0\text{ m},\ N_M > 0 \\ L_S \to 10\log_{10}(R_S) \quad \text{(for narrow-band)} \end{gathered} \quad (2\text{-}13)$$

The candidate measured narrow-band spreading losses (L_S) at $17\log_{10}(R_S)$ to $14\log_{10}(R_S)$ in South Australian 40 m depth waters using multiple calibrated towed tone sources Eq.(2-14) with the estimated average number of multipath signals of $N_M \approx 1 - 10^{\frac{20\text{ dB} - (14\text{ dB to }17\text{ dB})}{10}} \approx 1$ to 3.

$$\begin{gathered} R_D \approx 40\text{ m} \\ L_S \approx 17\log_{10}(R_S)\text{ to }14\log_{10}(R_S) \end{gathered} \quad (2\text{-}14)$$

2.4.5 Frequency Dependent Path Loss

Figure 5 illustrates acoustic absorption (L_A) of seawater as a function of ocean frequency and temperature in the communication band of interest [129].

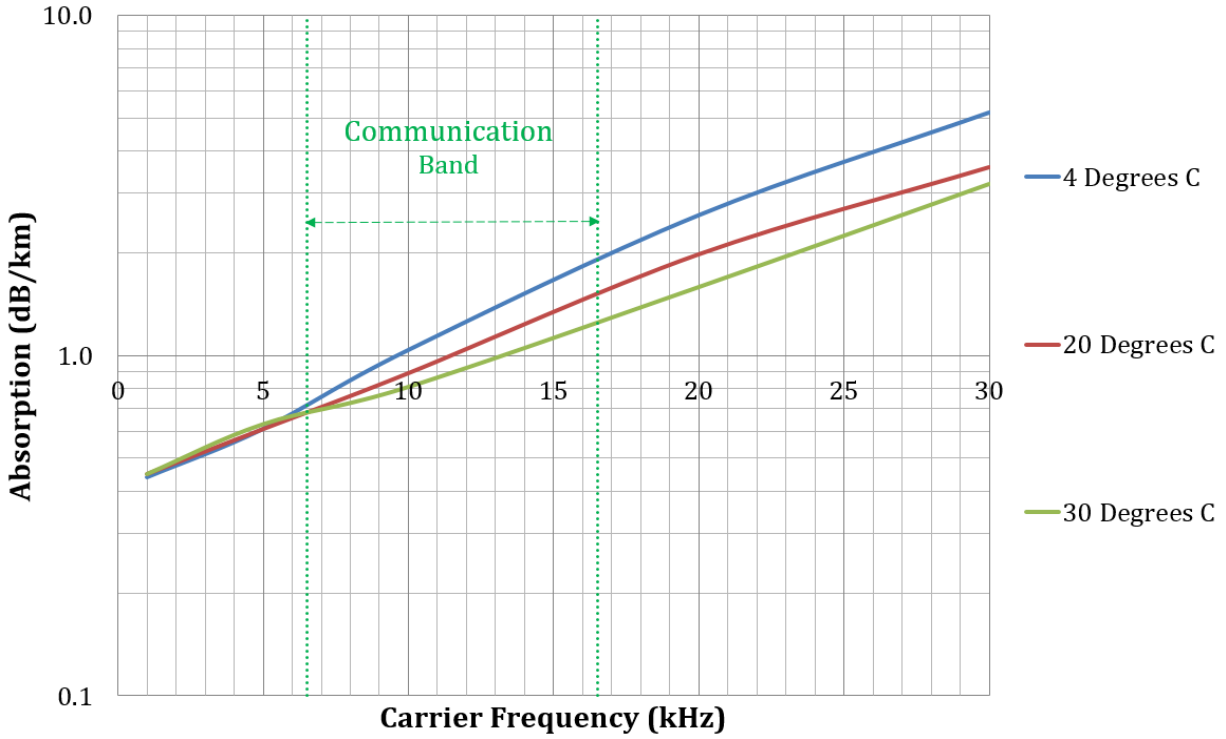

Figure 5 Acoustic absorption (MASQ communication band)

From Figure 5 the average environmental Absorption ($\bar{L}_A$), across the 6.5 kHz to 16.5 kHz MASQ communication band, is approximately 1 dB/km Eq.(2-15). High signal frequencies at 16.5 kHz are attenuated by approximately 1 dB/km more than low 6.5 kHz signal frequencies. The available communication channel bandwidth decreases with range which decreases the maximum baud rate.

$$\bar{L}_A \approx \frac{1.5\ \text{dB/km} + 0.7\ \text{dB/km}}{2} \approx 1\ \text{dB/km} \quad (\text{for MASQ 6.5 kHz to 16.5 kHz})$$
$$L_A = \frac{R_S}{1{,}000}\bar{L}_A \qquad (2\text{-}15)$$

2.4.6 Total Hydro-acoustic Path Loss

The total hydro-acoustic path loss (L_T), including sound velocity induced refraction (L_R), is the sum of spherical spreading loss (L_S) and environmental absorption loss (L_A) Eq.(2-16).

$$L_T = L_R + L_S + L_A \approx L_R + 20\log_{10}(R_S) + \frac{R_S}{1{,}000}\bar{L}_A \qquad (2\text{-}16)$$

In the absence of sound velocity induced refraction ($L_R = 0$) Figure 6 illustrates maximum path loss (L_T) versus range, DSSS hydro-acoustic communication baud rate (Br) and

transmission bandwidth (B_{TX}).Figure 6 green rectangle represents the thesis zone of performance improvement.

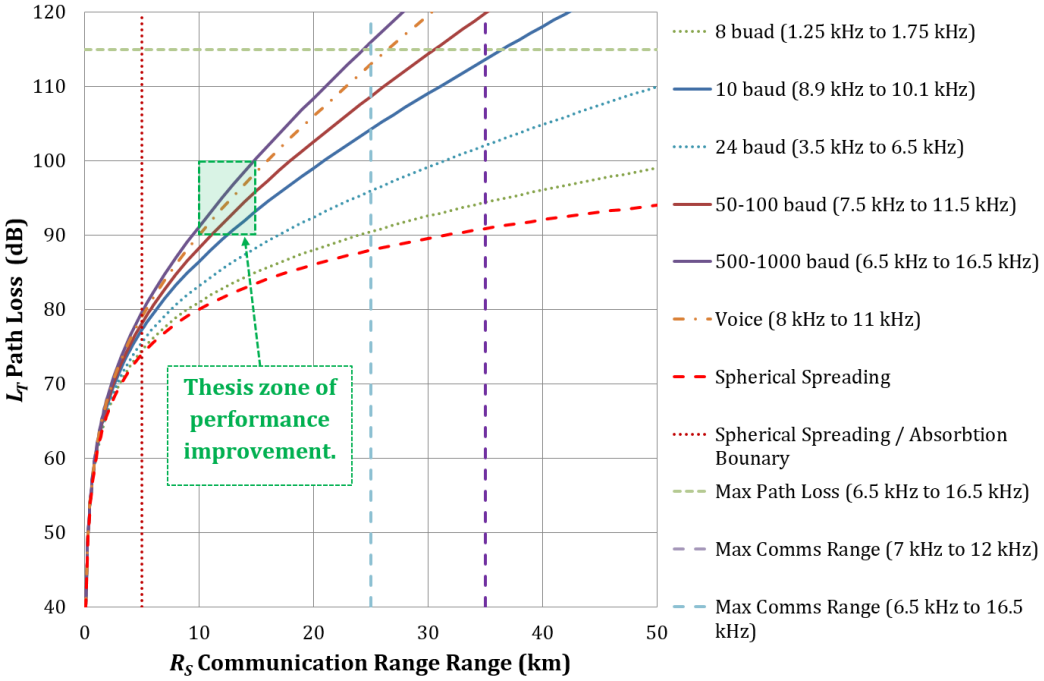

Figure 6 Maximum path loss versus range and hydro-acoustic baud rate

Spherical spreading dominates for ranges less than 5 km and frequency dependent environmental absorption dominates for ranges greater than 5 km which decreases the available communication channel bandwidth and limits the maximum baud rate. With a maximum path loss of 115 dB Eq.(2-11) the $SS0$ maximum SS communication range is between ($R_S \approx$ 25 km to 35 km). When multipath interference and sound velocity induced refraction ($L_R >$ 3 dB) is included the SS maximum communication range is reduced to approximately ($R_S \approx$ 10 km to 15 km). Maximising the SS communication range requires the lowest practical carrier frequency which requires a physically larger and higher cost hydro-acoustic projector. For example a low frequency 1.25 kHz to 1.75 kHz ($\bar{L}_A =$ 0.45 dB/km) hydro-acoustic projector could potentially establish a $R_S >$ 100 km communication link however the data transfer rate would be less than 10 baud, incur high power consumption and an order of magnitude increase in cost.

2.4.7 Spread Spectrum Communication Sonar Equation

Long-range (> 10 km) communication requires a high transmit source level and/or a low hydro-acoustic baud rate. Long-range performance can be traded for reliable high ambient noise short to medium range communication (i.e. maximising long-range performance also improves short-range high ambient noise performance). The maximum communication range is a function of the SS transmitter acoustic power, hydro-acoustic baud rate, the total acoustic channel propagation loss and the SS receiver sensitivity. Equation (2-17) and Figure 7 describes the hydro-acoustic broad-band communication receive margin (M_{TX}) sonar equation as a function of sea state (SS). Equation (2-7) incorporates multipath gain (G_M) into the transmit margin (M_{TX}). An estimate of the receiver ambient noise (PSD_A) can be calculated using wind speed or the International Martine

Organisation (IMO) sea sate number ($SS\#$) Eq.(7-25) and Table 5. For a given baud rate dependant transmission bandwidth (B_{TX}) equation (2-17) is used to predict the maximum communication range (R_S) which is proportional to the total path loss (L_T) and a function of sea state (SS) and transmit source level (SPL_{TX}) as illustrated in sea state versus communication diagrams such as Figure 191. Including the projector directivity (D_{TX}) to equation (2-3) provides a more accurate estimate of source level (PSD_{TX}). The difference between the transmit source level and receiver source level provides a measurement of total path loss which can be used to predict the maximum communication range using equation (2-16).

$$\begin{gathered} R_S \propto L_T = PSD_{TX} - PSD_{RX} \\ PSD_{TX} = SPL_{TX} - 10\log_{10}(B_{TX}) + D_{TX} \\ PSD_A \propto SS\# \\ M_{RX} = PSD_{RX} + M_{TX} - PSD_A + D_{RX} \end{gathered} \tag{2-17}$$

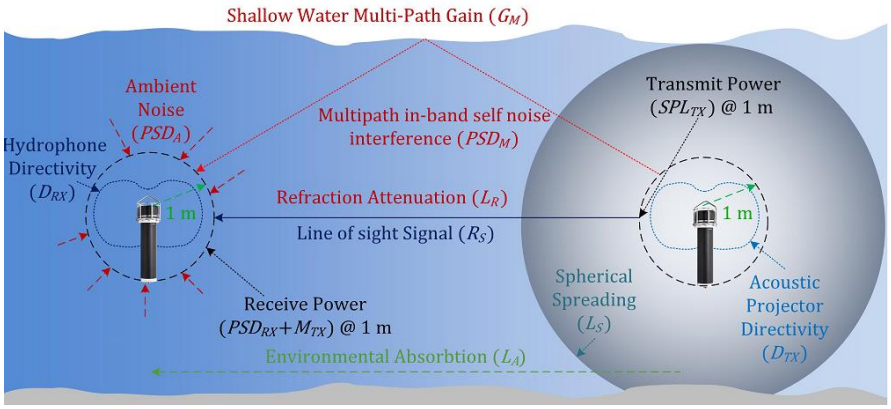

Figure 7 Spread spectrum communication sonar equation diagram (firmware V5.x)

2.5 High Ambient Noise

Reception of long-range signals is subject to isotropic biological and weather-induced ambient noise interference up to Sea State 6 [54] [57]. Anisotropic mechanically generated noise can induce interference louder than $SS6$ and up to the equivalent of $SS15$ (Appendix K) as illustrated in Figure 8 (spectrum) and Figure 9 (spectrogram).

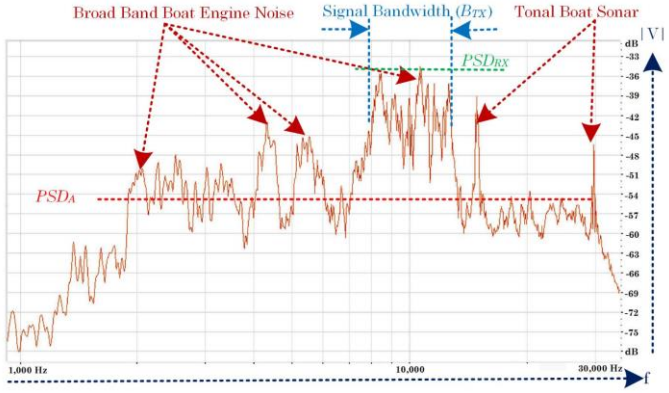

Figure 8 MCDSSS high ambient noise tolerance (receiver spectrum)

Tolerance to high ambient noise interference is provided by the MCDSSS modulator transmit margin (M_{TX}) Eq.(4-6) (Chapter 4.3.3).

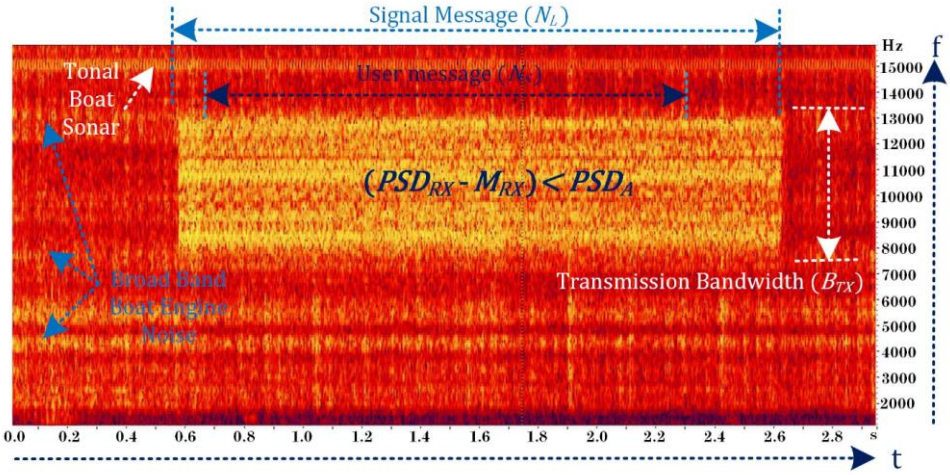

Figure 9 MCDSSS high ambient noise tolerance (receiver spectrogram)

2.6 Impulsive Noise

Loud impulsive biological and mechanical noise, especially propeller cavitation generated noise, can mask the detection of spread spectrum symbols, which may invalidate a user message (N_S). If a hydrophone signal is driven to the power supply rail or to ground by loud impulsive noise then the receiver is effectively deaf to incoming signals. Figure 10 illustrates a spectrogram of a spread spectrum signal in the presence of loud biological and mechanical noise. Snapping shrimp generate loud broad-band noise (spectrogram bright yellow vertical lines).

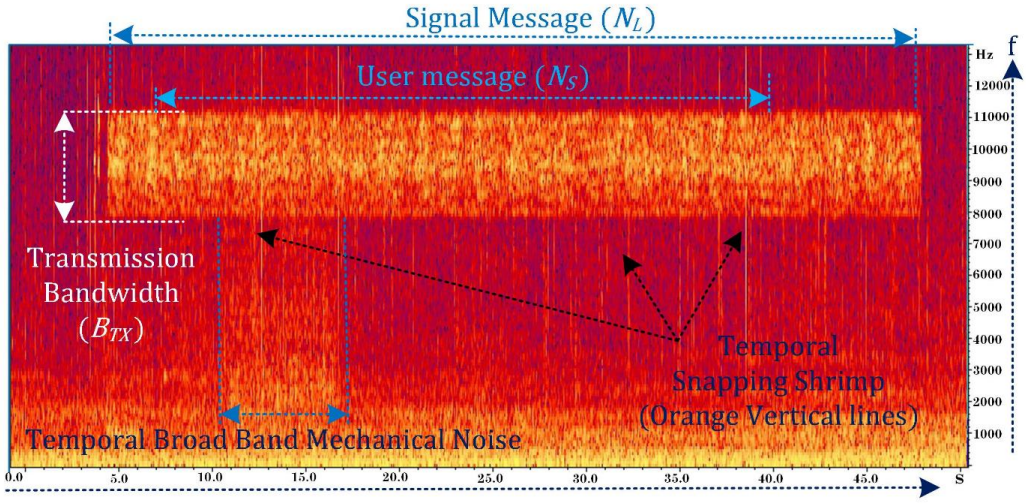

Figure 10 Impulsive biological noise (receiver spectrogram)

Tolerance to impulsive noise interference is provided by the MCDSSS modulator Forward Error Correction (FEC) and Cyclic Redundancy Check (CRC) which enables the MCDSSS receiver to correct corrupted MCDSSS symbols.

2.7 Low Probability of Intercept Covert Communication

MCDSSS provides processing gain (P_G) which allows the received signal to be detected below the ambient noise (i.e. low probability of intercept (LPI) covert communication). Figure 11 illustrates the spectrogram of a spread spectrum signal approximately 3 dB below ambient noise (faint horizontal orange stripes). MCDSSS signals that are more than 3 dB below the ambient noise are not generally visible on a spectrogram.

The MCDSSS modulator's 3 dB to 15 dB transmit margin allows the MCDSSS receiver to detect a signal up to 9 dB below the ambient noise (Chapter 4.3.3). The MCDSSS multipath tracking receiver provides additional processing gain of up to 5 dB which enables detection of signals approximately 12 dB below the ambient noise (Chapter 5.7.3.1).

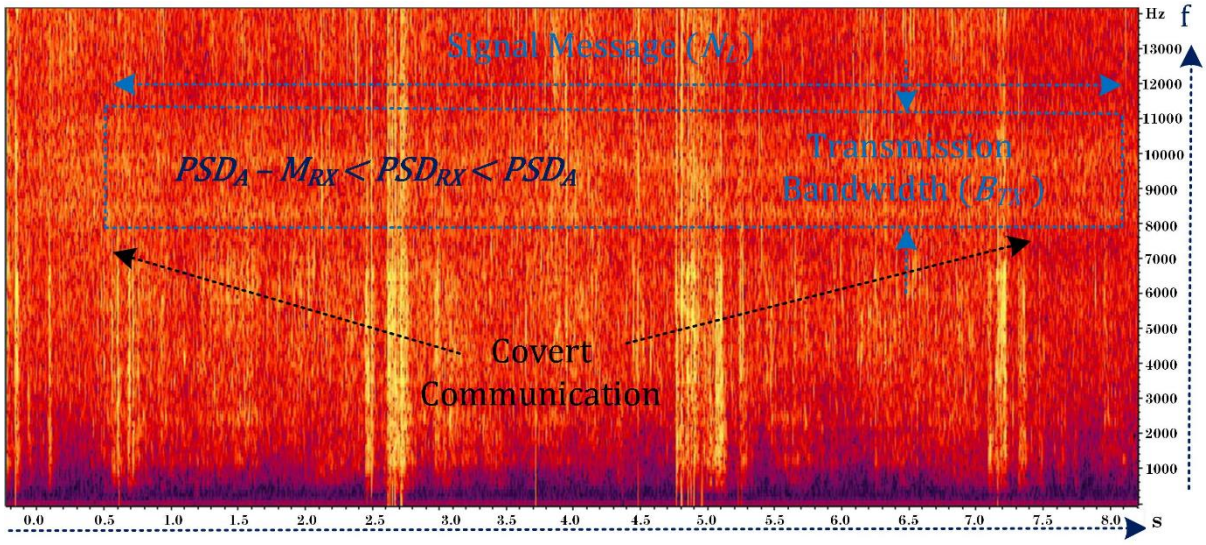

Figure 11 Low probability of intercept (spread spectrum signal)

2.8 Doppler

In the presence of motion between a transmitter, receiver or ocean currents the reception of signals is subject to an induced carrier frequency and Symbol period Doppler shift, which reduces receiver sensitivity. Vessel horizontal velocity elongates or compresses the symbol period (τ_{SY}) by a time varying Doppler scale factor (D_S) (Figure 12).

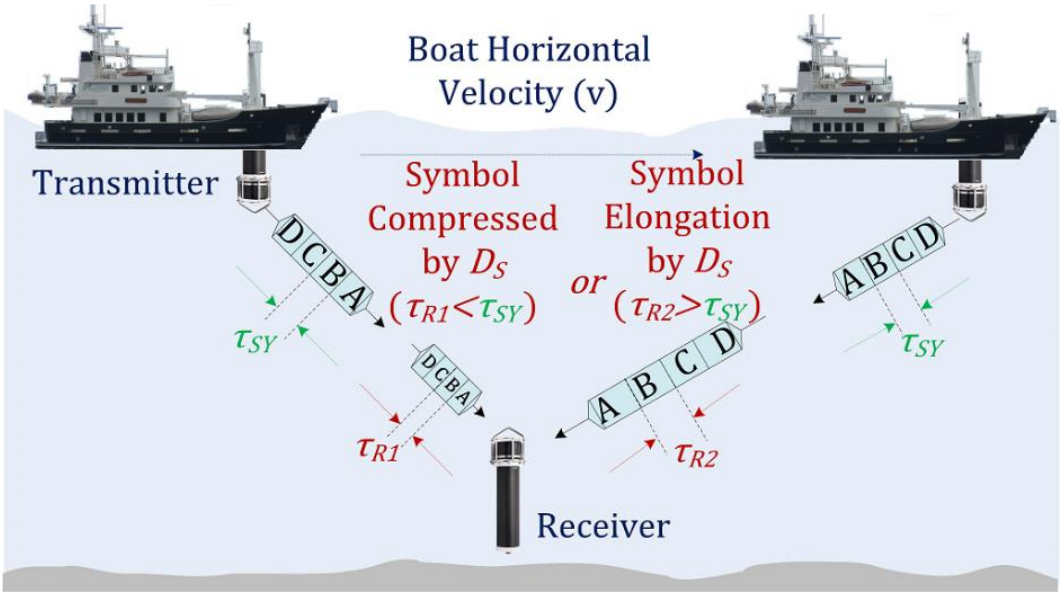

Figure 12 Receiver Doppler tolerance (horizontal motion)

Vessel vertical motion also elongates and compresses the symbol period by a time varying Doppler scale factor ($\frac{dD_S}{dt}$) (Figure 13). Tolerance to Doppler is provided by a control system which implements multiple MCDSSS receivers tuned to multiple Doppler shifted carrier frequencies, which maintains the MCDSSS receiver sensitivity (Chapter 5.7.2.1).

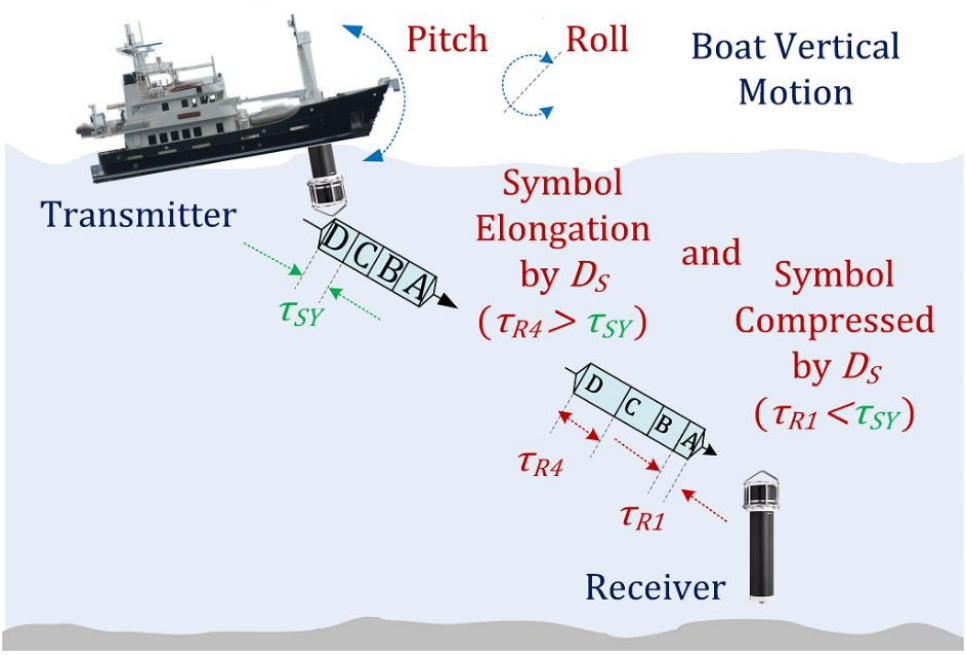

Figure 13 Receiver Doppler tolerance (vertical motion)

2.9 Shallow Water Multipath

Reception of a shallow water hydro-acoustic signal is subject to multipath interference which is normally characterised by a slant range (R_S) signal followed by Multipath signals (R_M) (Figure 14). The magnitude of multipath signals may be greater than the slant range signal for water Depths (R_D) less than 100 m.

Tolerance to shallow water multipath interference is provided by MCDSSS modulation and the MCDSSS receiver non-linear control system, which tracks the slant range signal and circumvents multipath interference (Chapter 5.7.1).

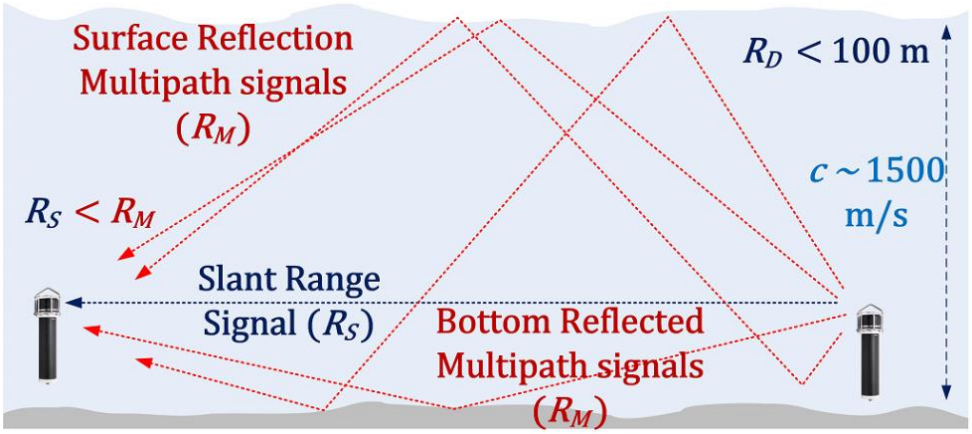

Figure 14 Shallow water multipath (propagation)

2.10 Bottom Ducting Multipath

Signal reception may be subject to bottom ducting interference which is characterised by a slant range signal (R_S) preceded by a multipath signal that propagates through sediment or hard Bottom (R_B) (Figure 15).

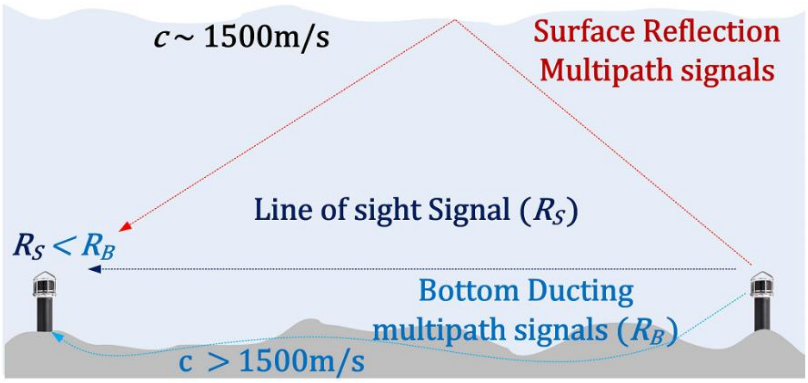

Figure 15 Bottom ducting multipath (propagation)

Figure 16 and Figure 143 illustrate environmental measurements of MCDSSS receiver detection of a bottom ducting multipath signal which is characterised by a slant range correlation pulse preceded by a weak bottom ducting multipath correlation pulse. The magnitude of the bottom ducting multipath signal is usually less than the slant range signal. The speed of sound through sediment or hard bottom is faster than the speed through water and the bottom ducting multipath signal arrives before the slant range signal which reduces message reliability and slant range measurement accuracy if the receiver locks onto the bottom ducting signal instead of the slant range signal.

Tolerance to bottom-ducting interference is provided by the MCDSSS demodulator which implements a MCDSSS receiver non-linear control system to track the slant range signal and circumvent bottom ducting interference (Chapter 5.7.1).

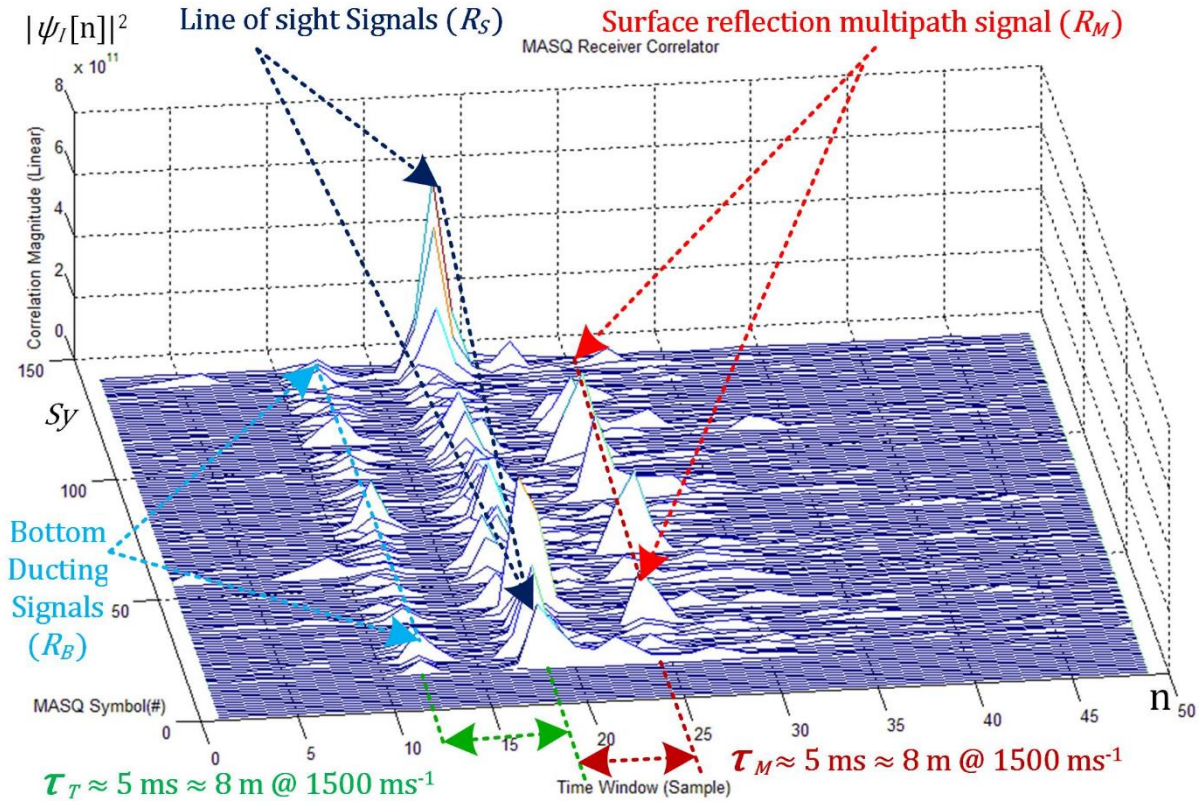

Figure 16 Bottom ducting (MCDSSS correlator water fall plot)

2.11 Sub Surface Ducting Multipath

Reception of a hydro-acoustic signal may be subject to Sound Velocity Profile (SVP) induced subsurface Ducting (R_{DD}) shadow zones which are characterised by a slant range signal (R_S) followed by surface ducting (R_T) multipath signals that propagates through a warm water surface mixed layer (Figure 17).

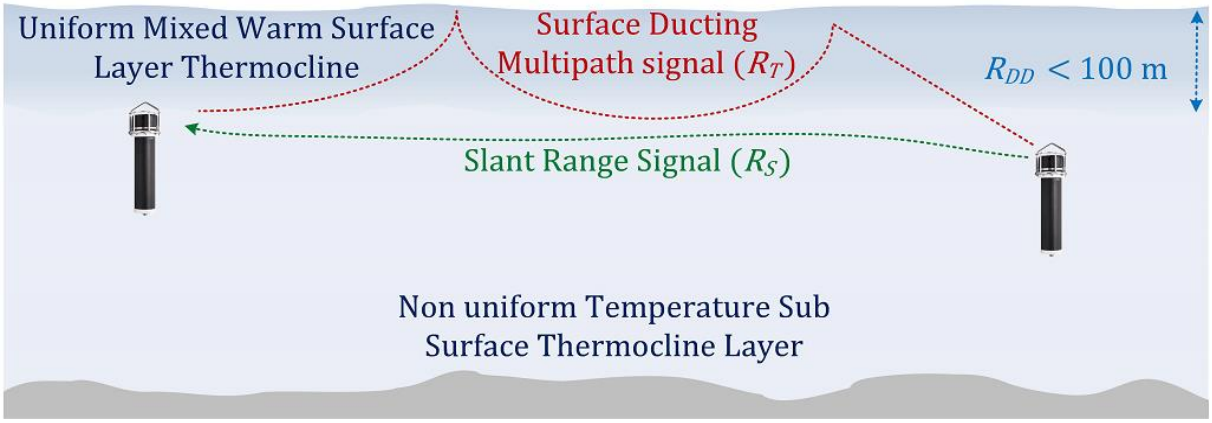

Figure 17 Sub-surface ducting multipath (propagation)

Figure 18 illustrates the MCDSSS receiver detection of a surface ducting multipath signal which is characterised by a slant range correlation pulse followed by one or more multipath correlation pulses. The MASQ 3 dB to 15 dB transmit margin provides tolerance to surface ducting attenuation as long as the surface ducting signal is no more than 15 dB louder than the slant range signal.

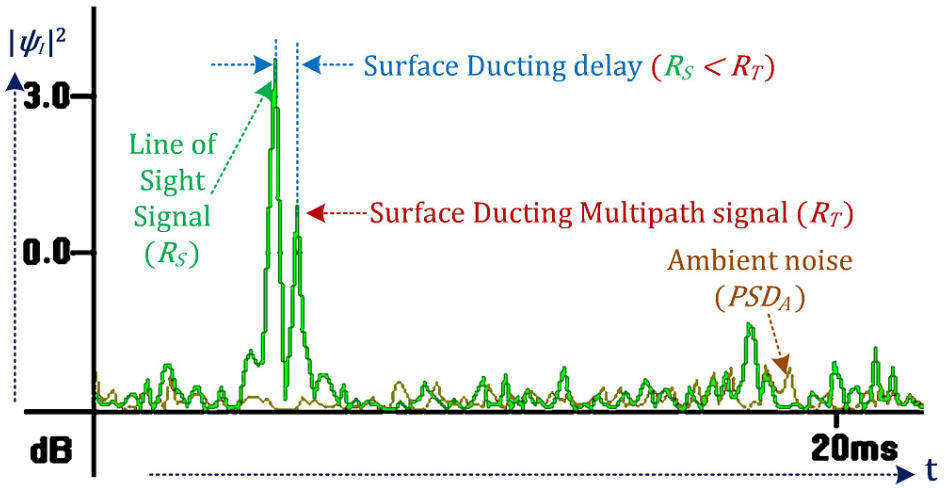

Figure 18 Sub-surface ducting (MCDSSS correlator)

Tolerance to surface ducting attenuation, for slant refraction losses (L_R) greater than 15 dB, is provided by the MASQ network routing which allows signals to be propagated via alternative paths as illustrated in Figure 19 multipath ray trace (Chapter 5.6.8).

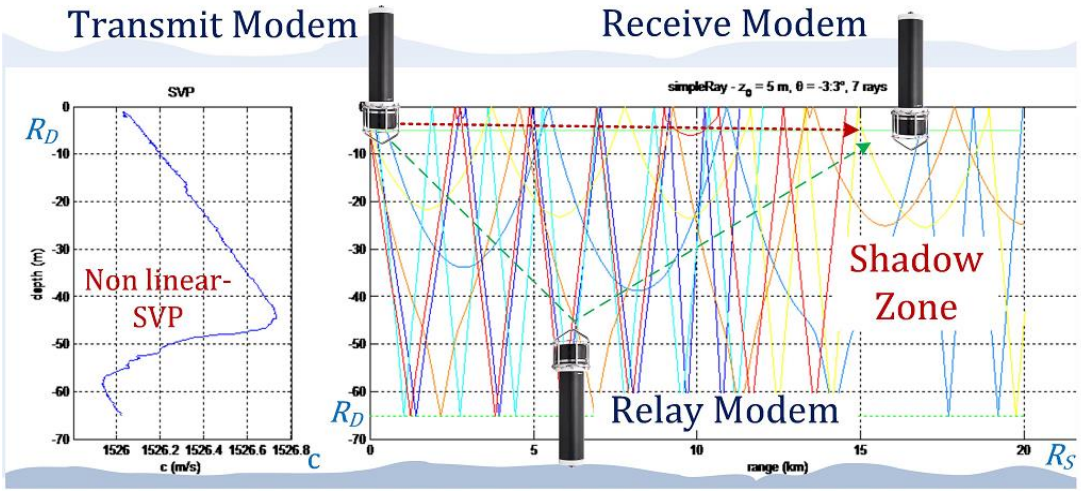

Figure 19 Sound velocity profile and multipath ray trace (65 m depth)

2.12 Sound Velocity Induced Refraction Shadow Zones

A downward refracting vertical sound velocity profile (SVP) will bend the path of a hydro-acoustic signal and may result in greater than 40 dB attenuation in shadow zones [129] (Figure 20). The MASQ communication protocol provides up to (0 dB → 34 dB) receive margin which is insufficient to overcome shadow zone refraction losses greater than 40 dB.

In this situation reliable communication is achieved using an intermediate transceiver to enable network routing via alternative paths. Multiple transceivers can be deployed at the surface, mid water or bottom to provide alternative acoustic paths (Chapter 5.6.8). When environmental conditions deteriorate, the communication link is re-establish by either increasing transmit source level, decreasing baud rate or re-routing the communication link, which requires dynamic transmit source level and baud rate modem transceiver infrastructure.

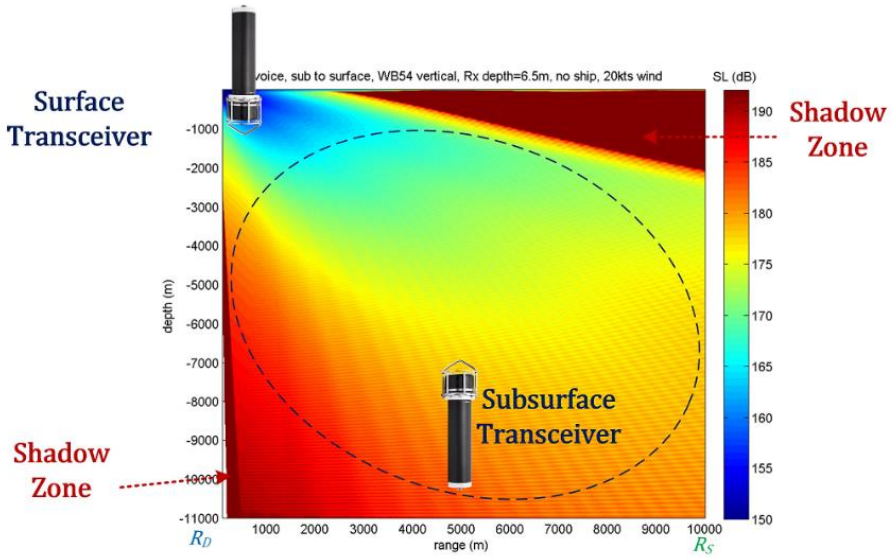

Figure 20 Sonar equation modelling for communications between submarine and surface

2.13 Dynamic Channel Equalisation

Figure 21 illustrates the hydro-acoustic spectrum of a 1,000 baud signal transmitter power spectral density (PSD_{TX}) as measured in the L3 hydro-acoustic tank with the characteristic band-limited (B_{TX}) flat in-band *sinc* function frequency response, excluding sinusoidal tank interference artefacts.

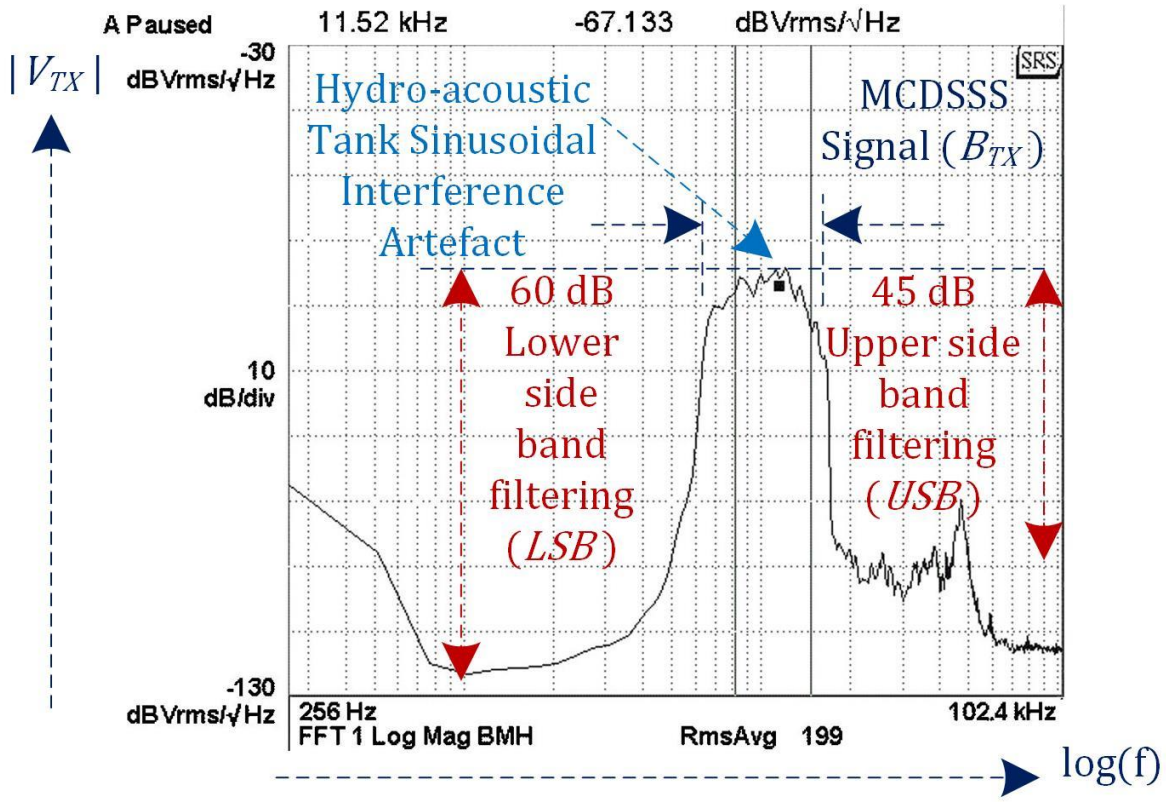

Figure 21 Transmit hydro-acoustic spectrum (MCDSSS 1,000 baud)

Reception of a broad-band signal $V_{RX}(\mathrm{t})$ is subject to Ambient Noise $n_A(\mathrm{t})$ interference and multipath induced non-uniform channel impulse response $h(\tau)$ interference [129] Eq.(2-18). Figure 22 illustrates the hydro-acoustic Receiver Power Spectral Density (PSD_{RX}) spectrum of a 100 baud signal as measured at an ocean deployed MCDSSS receiver. Although the in-band transmit signal frequency response is flat, the channel response induces non-uniform in-band interference which degrades the receiver performance by increasing the carrier Phase Noise (θ_N) Eq.(4-3)

$$V_{RX}(\mathrm{t}) \approx \int_{-\infty}^{\infty} V_{TX}(\mathrm{t}-\tau).h(\tau)\,\mathrm{d}\tau + n_A(\mathrm{t}) \tag{2-18}$$

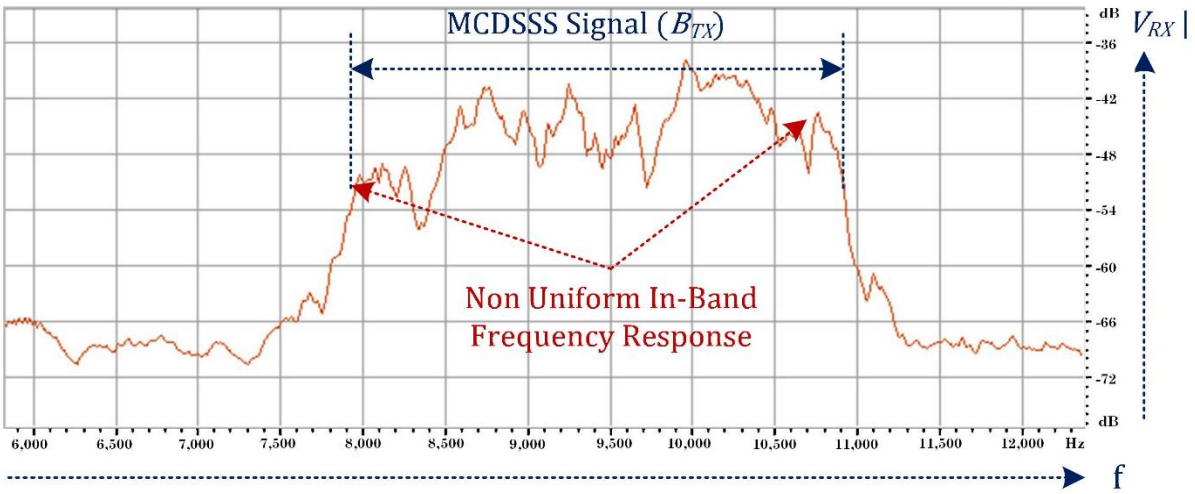

Figure 22 Non-uniform channel receiver frequency response (MCDSSS 100 baud)

Appendix L.6.1 and Figure 23 illustrate a channel in-band impulse response as measured by the MCDSSS 50 baud receiver where the third (R_{M3}) to fifth (R_{M5}) multipath signals are louder than the slant range signals, which is typical of long-range shallow water communication. The hydro-acoustic channel not only induces a non-uniform in-band frequency distortion but the distortion also changes with time denoted by $h(\mathrm{t},\tau)$ in Eq.(2-19).

$$V_{RX}(\mathrm{t}) \approx \int_{-\infty}^{\infty} V_{TX}(\mathrm{t}-\tau).h(\mathrm{t},\tau)\,\mathrm{d}\tau + n_A(\mathrm{t}) \tag{2-19}$$

Tolerance to the time varying channel response is provided by the DSSS modulator reference signal which allows a DSSS receiver to dynamically equalise telemetry channel multipath signals (Chapter 5.7.3.1).

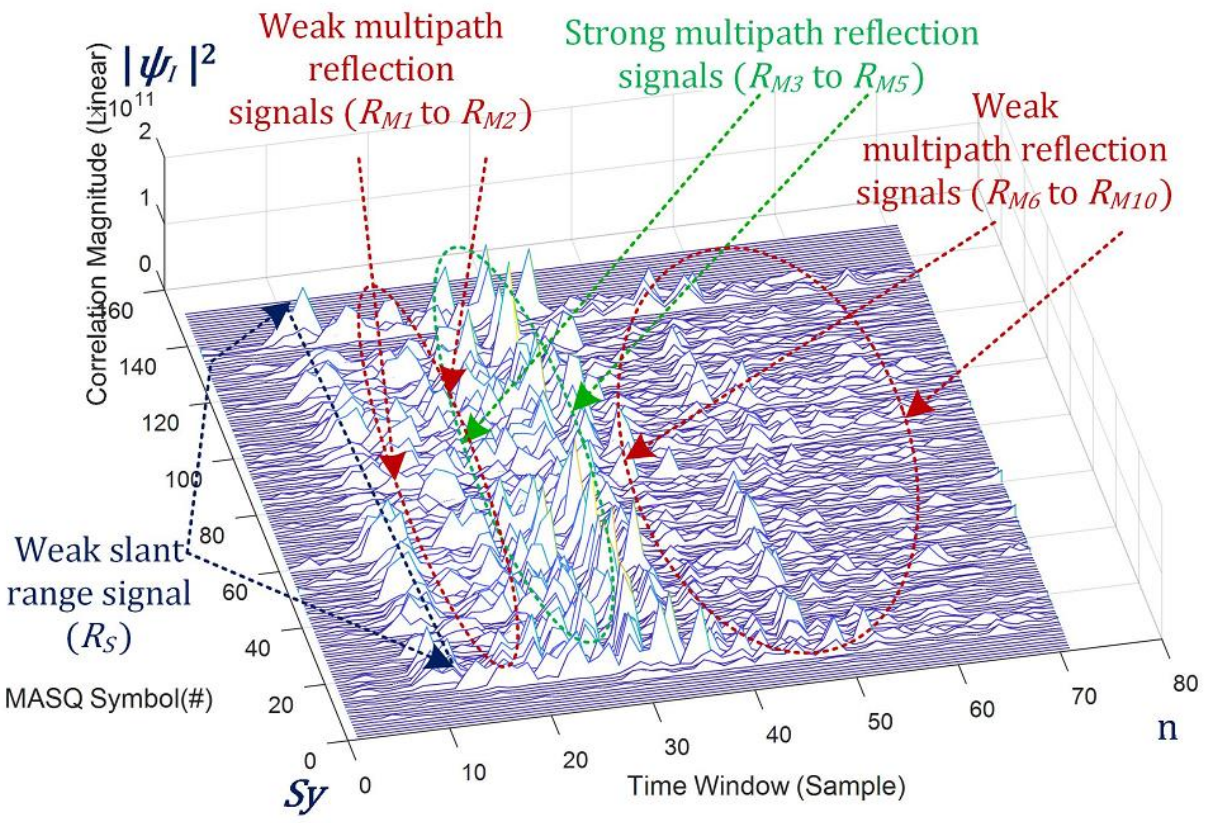

Figure 23 Time varining channel impulse response (DSSS Correlation)

2.14 Inter Symbol Interference

Inter-symbol interference (ISI) is a significant issue for high baud rate RF communication [52] and is also a serious issue for medium to high baud rate shallow water hydro-acoustic communication. Communication link tests in a reverberating hydro-acoustic tank (Appendix F), enclosed harbours (Appendix G) and shallow water (Appendix P) cannot be established for all MCDSSS baud rates when the multipath reverberation envelope period (τ_{MPE}) exceeds the MCDSSS symbol period (τ_{SY}). Inter-symbol interference occurs when multipath signals are received with a propagation delay difference greater than one symbol period ($\Delta t_M > \tau_{SY}$). Simultaneous reception of reference symbols via different propagation paths cannot be unambiguously separated by arrival time.

If the multipath receive signal power is 6 dB lower than the slant range signal then inter symbol interference is not an issue. If a multipath signal is received with a slant range signal and the propagation delay difference is less than one symbol period ($\Delta t_M < \tau_{SY}$) then ISI will not occur because the DSSS receiver can separate and track the multipath signals.

Figure 24 illustrates a MCDSSS 1,000 baud $R_D = 150$ m depth deployment for two modems with a slant range of $R_S = 2{,}000$ m and a surface multipath signal path length of $R_M = 2{,}022$ m. The slant range signal flight time is $t_S = 1.333$ s and the surface multipath flight time is $t_M = 1.348$ s. The flight time difference is $t_M - t_S = \Delta t_M = 15$ ms. A MCDSSS 1,000 baud signal with one telemetry channel ($N_T = 1$) has a symbol period of $\tau_{SY_1} = 8$ ms. If a message of "ABCD" is transmitted, then the first surface reflected multipath symbol

"A" will overlap with the slant range second symbol "B" and will induce ISI because τ_M = 15 ms is greater than τ_{SY_1} = 8 ms.

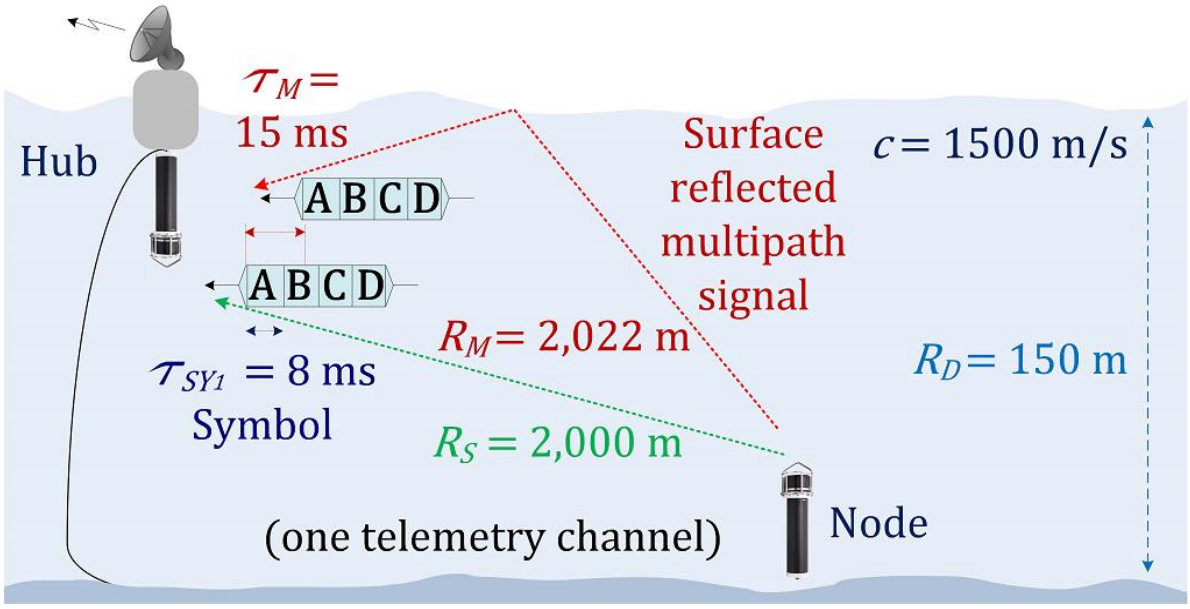

Figure 24 Inter-symbol interference (one data channel)

Figure 25 illustrates MCDSSS 1,000 baud configured with N_T = 4 telemetry channels with a symbol period of τ_{SY_4} = 32 ms. If the message "ABCD" is transmitted, then the first multipath symbol "ABCD" will overlap with the slant range first symbol "ABCD" and will not induce ISI because τ_M = 15 ms is less than τ_{SY_4} = 32 ms.

Susceptibility to inter-symbol interference can be reduced by increasing the symbol period using modulation schemes such as MCDSSS which uses multiple telemetry channels and multiple baud rates to extend the symbol period. A high speed and low transmit source level communication link can be established in a reverberating environment using a binary search of hydro-acoustic baud rates and transmit source levels as described in Chapter 4.3.1 and Appendix P.

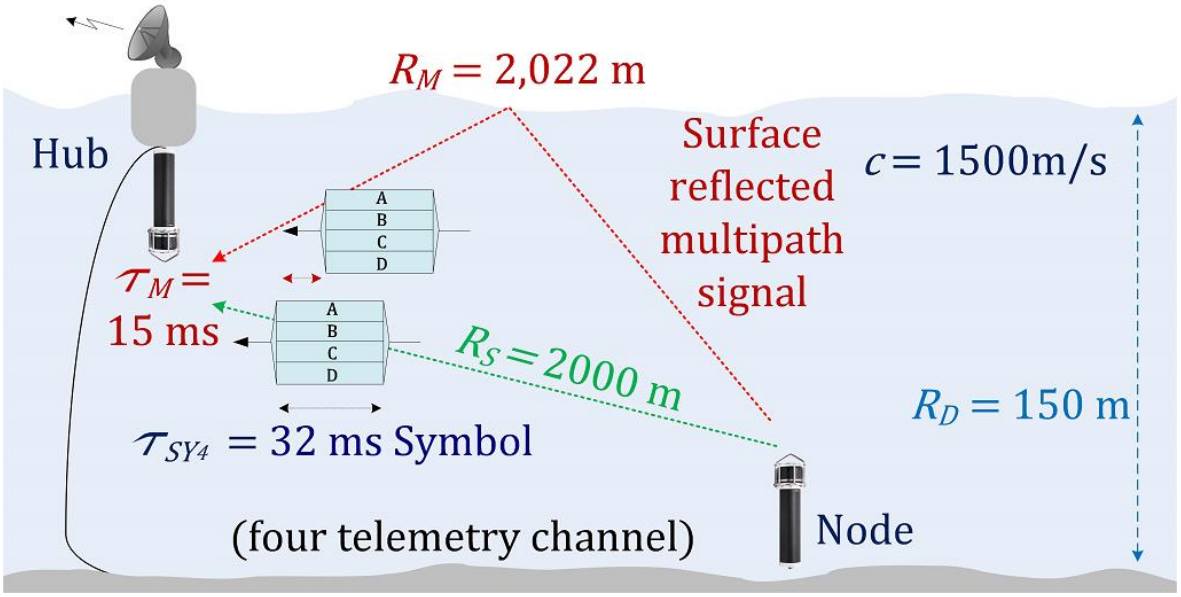

Figure 25 Inter-symbol interference (four data channels)

2.15 Summary

The maximum communication range at a given frequency is bounded by the physical laws governing fluid maximum cavitation pressure [100] at the transmitter and the ocean minimum ambient noise floor at the receiver, which cannot be circumvented. The key to reliable long-range underwater communication is the optimisation of the sonar equation variables SPL_{TX}, PSD_N, G_M, M_{RX}, M_{TX} using algorithm and engineering optimisations.

Battery powered SS communication requires low power signal processing to run numerically efficient algorithms to counter environmental effects such as Doppler, multipath, inter-symbol interference, isotropic environmental noise, anisotropic anthropogenic noise, channel equalisation and sound velocity induced refraction.

3 LITERATURE REVIEW

3.1 Introduction

This chapter examines the performance difference between low baud rate Spread Spectrum (SS) communication and medium to high baud rate communication. Underwater communication has been acknowledged as one of the most challenging communication channels for establishing a reliable communication link [89]. The last 30 years in underwater acoustic communication research has been focused on providing near real-time medium to high speed underwater wireless links for sonar, video, high volume environmental sensor and image data transfer, hydro-acoustic monitoring, digital voice communication, and underwater internet access (Figure 26 right blue zone). Low baud rate bandwidth inefficient SS communication [33] [71] [135] is used to provide a "Guarantee of Service" for precision navigation/range measurements and low to medium baud rate communication links for high value infrastructure such as divers, defence submarines, AUV's, wave gliders, mini-submarines, full ocean depth submarines, sonobuoy's, voice communication and high value sensor data access [46] (Figure 26 left green zone SS deployments).

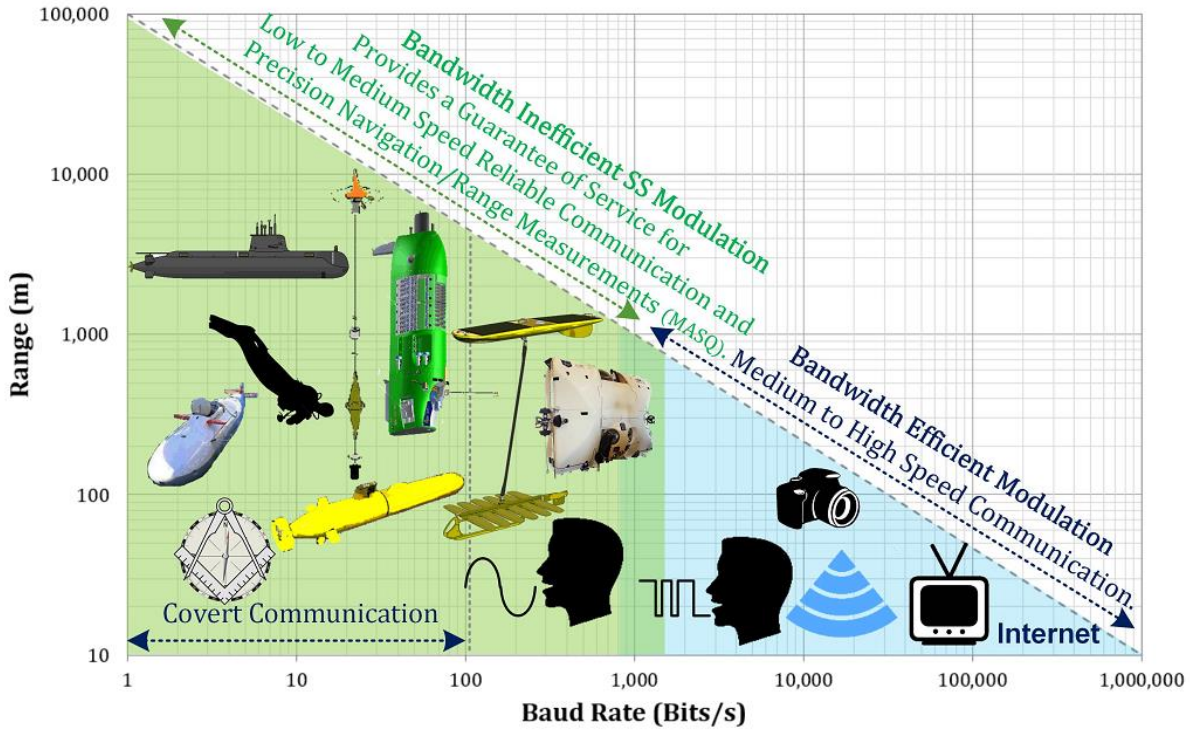

Figure 26 Hydro-acoustic application versue range and baud rate

3.2 Bandwidth Efficiency

Bandwidth efficiency (B_e bits/s/Hz) is a measure of how efficiently a modulation scheme maximises baud rate (Br) utilising the available channel transmission bandwidth (B_{TX}) [52] Eq.(3-1). SS baud rate is proportional to modulation bandwidth (B_M) and as the baud rate increases the modulation bandwidth will exceed the PZT transducers transmission bandwidth which will improve bandwidth efficiency and degrade covert performance.

$$B_e = \frac{Br}{B_{TX}} \tag{3-1}$$

SS modulation bandwidth efficiency (B_e) can be expressed as a function of the number of bits per telemetry channel (B_{PT}), the number of spreading code bit (S_{CB}) and modulation bandwidth (B_M). Eq.(3-2).

$$Br = \frac{B_{PT}}{\tau_{SY}} \quad \text{where} \quad \tau_{SY} = \frac{S_{CB}}{B_M} \quad \text{(SS symbol period in seconds)}$$
$$B_e = \frac{B_{PT}.B_M}{S_{CB}.B_{TX}} \tag{3-2}$$

The available short to medium-range underwater acoustic channel bandwidth is between 1 kHz and 100 kHz which limits hydro-acoustic baud rates from 100 baud [43], 1,000 baud [30] [43] [144], 3,000 baud [23] [39] [105] [117], 5,000 baud [62] [126] [136] to 10,000 baud [117] requiring hydro-acoustic modulation schemes operating near the Shannon limit [52], using bandwidth efficient modulation schemes listed on page (xxv) (16QAM [81], BFSK [93], CDMA [10], FSK [31], OFDM [120], QPSK [15] [114]). Some medium to high baud rate modulation schemes achieve reliable communication using 8 [6] [60] to 32 [138] element vertical hydrophone arrays providing less than 8 dB to 15 dB Directivity Index (DI) which reduces interference from isotropic noise, however hydrophone arrays are expensive to deploy and limited to fixed deployments. Very high 1 M bit/s acoustic baud rates have been achieved for distances less than 100 m, using directional transducers that provide ~10 dB DI but more significant +20 dB front to back isotropic noise isolation [65]. Directional transducers provide less than a 30° beamwidth requiring projectors and hydrophones to be mechanically aligned in depth, pitch and yaw which limits applications to either fixed installations or underwater vehicles docking close to hydro-acoustic access points. Faster communication links have been established using blue-green lasers and high power blue LED's [29].

High bandwidth efficiency medium to high-speed communication research modems are typically quoted between 10^{-1} bits/s/Hz [69] [91], 10^{0} bits/s/Hz [68] to 10^{1} bits/s/Hz [7] [14] [66]. SS bandwidth efficiency is two orders of magnitude worse than medium to high speed modems. SS modulation is the purposeful reduction of baud rate, with a resulting low 10^{-3} bits/s/Hz to 10^{-1} bits/s/Hz bandwidth efficiency, for high reliability communication in high multipath and high ambient noise environments (Figure 27, SS bottom left green trace).

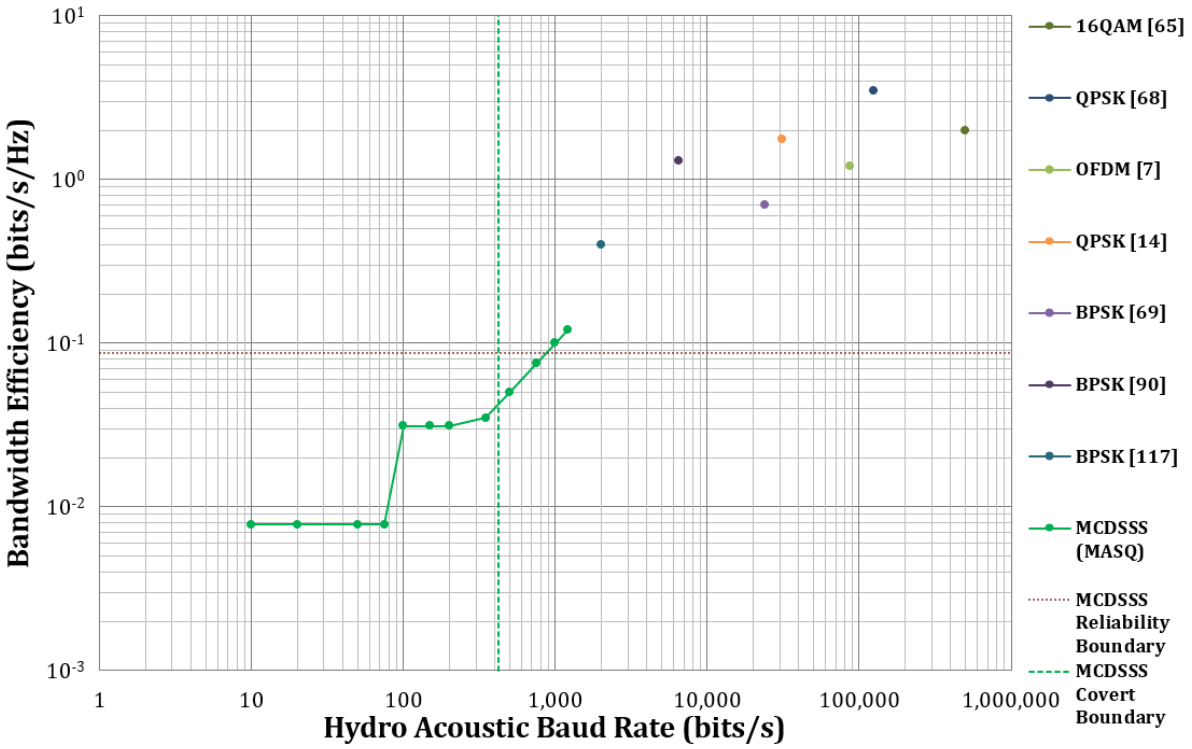

Figure 27 Modulation scheme bandwidth efficiency

3.3 Time Bandwidth Product

In the presence of noise, Time Bandwidth Product (TBP) is a measure of SS navigation range measurement accuracy and processing gain. A large TBP reduces the maximum baud rate, improves receiver sensitivity and improves receive time resolution of the detector correlation magnitude and phase. SS modulation TBP can be expressed as the number of Spreading Code Bits (S_{CB}) multiplied by the ratio of the transmission bandwidth (B_{TX}) and modulation bandwidth transmission (B_M). TBP is also proportional to processing gain (P_G) [52] Eq.(3-3).

$$\text{TBP} = \tau_{SY} \times B_{TX}$$

$$\text{TBP} = \frac{S_{CB} \times B_{TX}}{B_M} \quad \text{(for SS)} \tag{3-3}$$

$$P_G \propto 10\log_{10}(\text{TBP})$$

Medium to high speed communication does not have sufficient TBP available for precision navigation, continuous channel equalisation or to provide a robust modulation scheme to counter multipath interference, inter symbol interference, inter carrier interference, sound speed induced attenuation or extreme ocean noise (Figure 28).

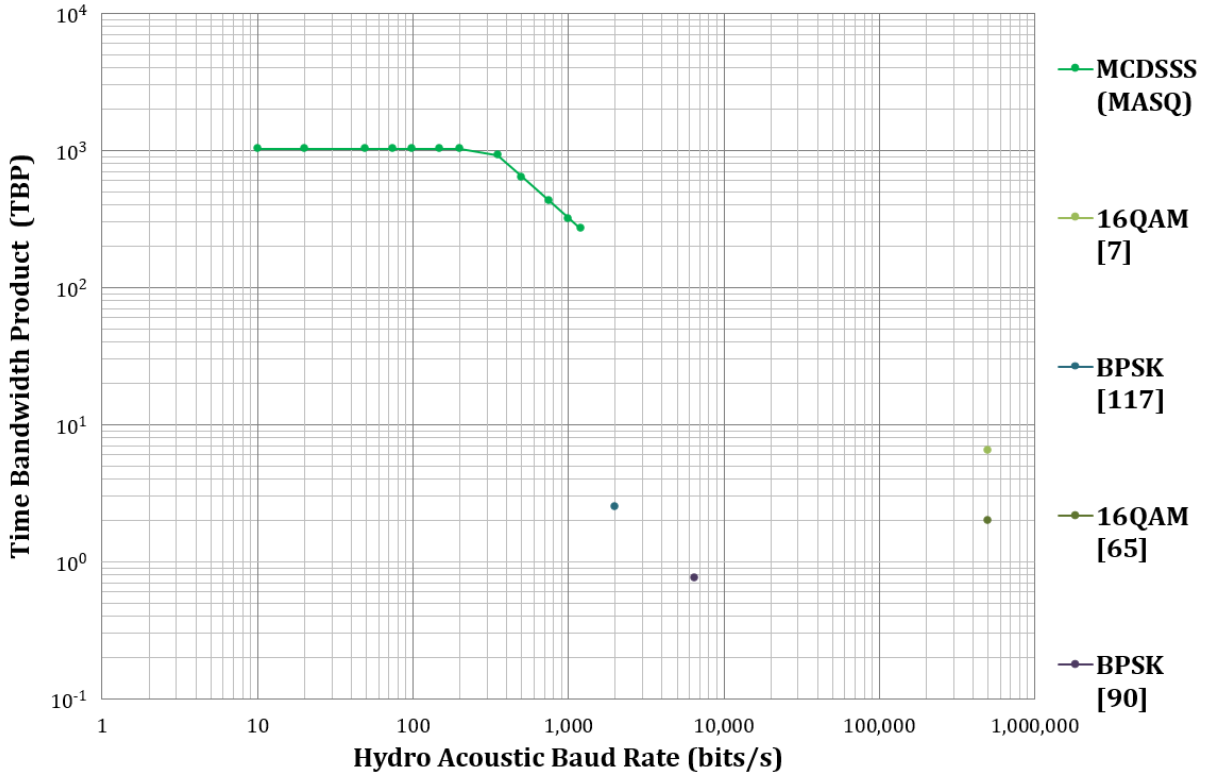

Figure 28 Time bandwidth product

To counter the lack of TBP a large proportion of underwater communication research is focused on medium to high speed channel equalisation [53] using advanced feedback control systems such as those listed on page (xxvi), requiring channel simulators to model multipath interference (forward scattering [35] [36] [98], Bellhop [18] [24] [38] [85] [86] [101] [142] [143] and wave propagation [40] [41]). Channel equalisation feedback control systems such as APF [48], BFC [32] [127], DFE [107] [109] [113] [130], FDE [51], FTF [103] [104], LMS [20] [53] [112] [122], MCDEF [58] [61], RLS [67] can be unstable in the presence of high multipath, high ambient noise, high Doppler and sound velocity induced refraction.

3.4 Bit Error Rate

Bit Error Rate (BER) is the primary performance metric for research and commercial modems. BER is the Number of altered symbols divided by the Number of message Symbols (N_S) streamed over a communication channel. BER can be statistically estimated for ideal conditions however if the message reliability is near 100% then the error correction system reported number of corrected symbols (N_{FEC}) can be used to measure the BER for a particular deployment environment [52] Eq.(3-4). BER cannot be measured in non-reverberating environments where the SS receive signal is louder than the ambient noise (non-covert), because very few error symbols occur ($N_{FEC} = 0$) and BER Eq.(3-4) is zero.

$$\text{BER} = \frac{N_{FEC}}{N_S},\ N_{FEC} = 0 \rightarrow \text{BER} = 0 \tag{3-4}$$

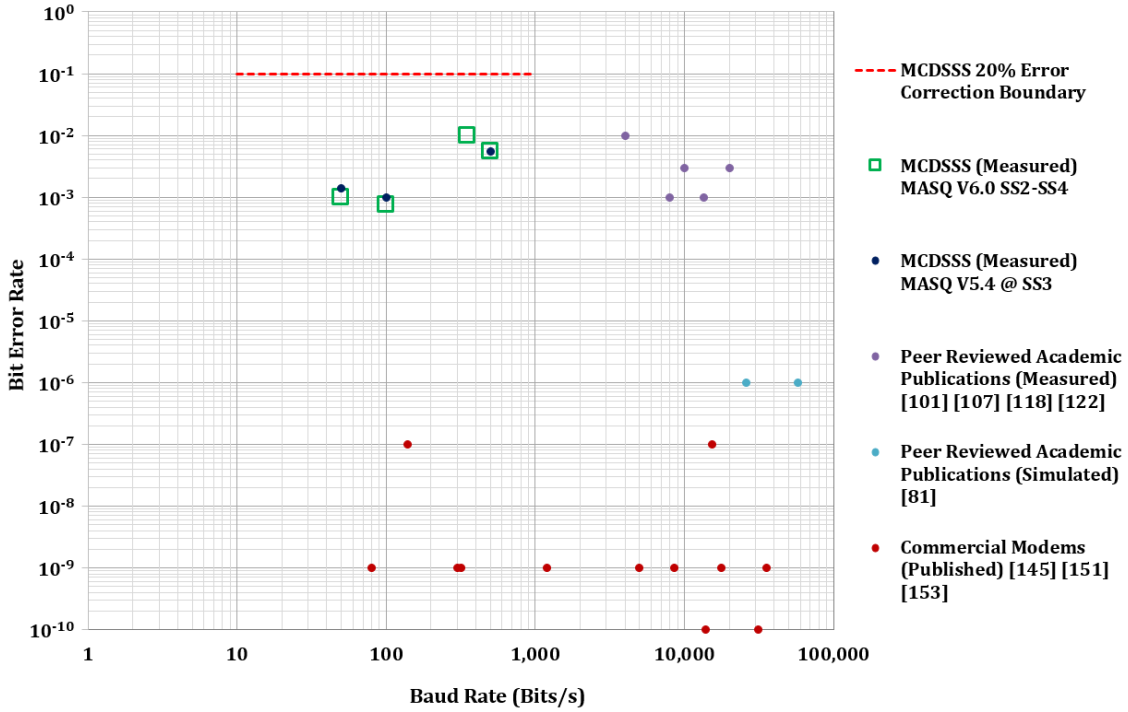

Figure 29 Bit error rates (measured and simulated)

Commercial hydro-acoustic modem data sheets quote theoretical bit error rates between 10^{-7} (99.99999% reliability) [151], 10^{-9} (99.9999999% reliability) [145], to 10^{-10} (99.99999999% reliability) [153]. Peer reviewed academic papers quote simulated high speed modem BERs at 10^{-6} (99.9999% reliability) [81] and medium to high speed modem BERs have been measured between 10^{-2} (99% reliability) [107], 10^{-3} (99.9% reliability) [28][119] [126], 10^{-4} (99.99% reliability) [32] [119] [137] however BER as a function of sea state is rarely stated. In comparison reliable SS communication BER has been measured at worse than 10^{-3} (<99.9% reliability) in a +SS4 harsh reverberating environment Figure 29, Figure 121, Figure 122. If a communication protocol implements error correction, then BER is no longer a useful measure of communication message reliability. SS communication typically implement 20% overhead error correction system that can correct 10% random errors as long as the BER is better than 10^{-1} (>90% reliability).

3.5 Message Reliability

A more useful measure of communication performance, other than BER, is the Message Reliability (MR) which is the percentage of successful received messages. MR is occasionally published and stated between 65% [72], 80% [78] to 99% [80] however MR is rarely quoted as a function of sea state or channel reverberation. The SS measured MR is between 80% to 99% at $+SS4$ Figure 30, Figure 118 and Figure 119. In a shallow water reverberating environment there is an approximate inverse linear relationship between hydro-acoustic baud rate and MR, where the lowest hydro-acoustic baud rate yields the best MR. The main focus of this study is performance improvement and validation measurements of MR.

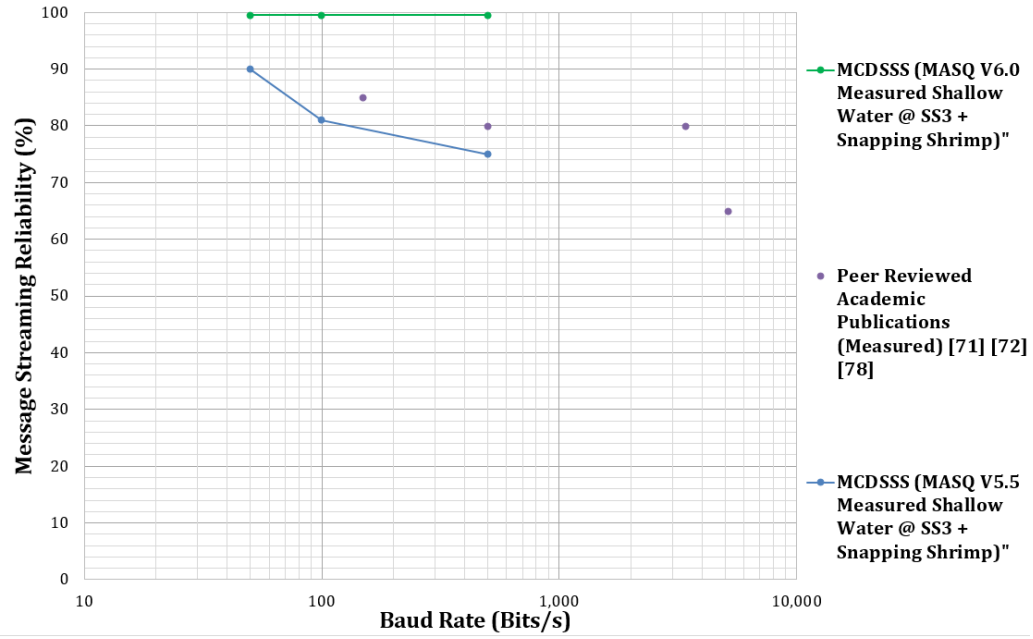

Figure 30 Hydro-acoustic message reliability (measured)

3.6 Bit Energy Efficiency

If a communication link is established with MR > 99% then a more useful measure of performance, for battery powered applications, is not the BER but the Bit Energy Efficiency (BEE) which is the number of bits that can be transmitted per 1 joule of electrical energy normalised to a 1 km range, as described by equation (3-5) derived from equation (2-12) and equation (2-16), where Br is the baud rate in bits per second, P_{TX} is the transmitter electrical power in watts, R_S is the slant range in meters, R_{REF} is the normalised range in meters and $\bar{L}_A$ is the frequency dependant absorption in dB/km.

$$\bar{R}_S = \left(\frac{R_S}{R_{REF}}\right)^2, \quad \Delta L_A = \frac{\bar{L}_A \times (R_S - R_{REF})}{R_{REF}} \text{ dB}$$

$$\text{BEE} = \frac{Br}{P_{TX}} \times \bar{R}_S \times 10^{\left(\frac{\Delta L_A}{20}\right)} \tag{3-5}$$

$$\text{BEE} = \frac{Br}{P_{TX}} \times \left(\frac{R_S}{R_{REF}}\right)^2 \times 10^{\left(\frac{\bar{L}_A \times (R_S - R_{REF})}{20 \times R_{REF}}\right)} \text{ Bits/J @ 1 km, } L_R \to 0 \text{ dB}$$

$$R_{REF} = 1{,}000 \text{ m}$$

Commercial modems do not publish BEE figures and refereed academic simulation studies are limited. Order of magnitude estimates of $10^3 \to 10^5$ bits/J @ 1 km for 1,000→100,000 baud are given in [34] but with no reference to sea state or channel reverberation. SS communication shallow water $+SS3$ bit energy efficiency is more than one order of magnitude worse than medium to high speed research modems and has been measured between 10^1 bits/J @ 1 km to 10^5 bits/J @ 1 km (Figure 31).

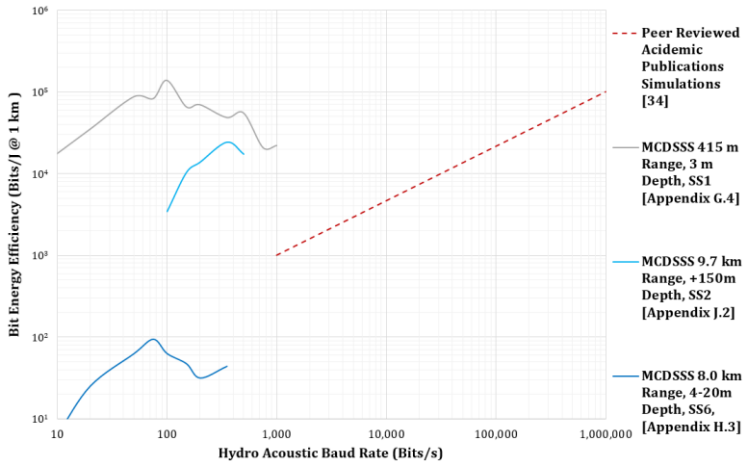

Figure 31 Hydro-acoustic bit energy efficiency (measured and simulated)

In a shallow water reverberating environment there is no established relationship between hydro-acoustic baud rate and bit energy efficiency, and the highest hydro-acoustic baud rate may not yield the best bit energy efficiency. In addition to frequency dependant environmental absorption loss and transmit projector transmission bandwidth, the reverberating environment generates high inter-symbol interference which compromises the performance of high hydro-acoustic baud rates that is a function of channel reverberation clear time. Higher hydro-acoustic baud rates require higher transmit source level to maintain the energy per bit however high transmit source level also increases in-band reverberation interference. Lower hydro-acoustic baud rates with lower transmit source level generate lower in-band reverberation interference which maximises the bit energy efficiency. Fully automatic shallow water SS transmit source level and hydro-acoustic baud rate optimisation may not be feasible because of the dynamic variability of ocean conditions and the non-linear relationship between hydro-acoustic baud rate and bit energy efficiency, which compromises the control system stability. BEE sea trial measurements are acquired in environments with different sea states (SS) and in order to compare performance measurements BEE must be normalised to sea state zero as described by equation (3-6), derived from equation (3-5) and equation (7-25).

$$\text{BEE} \approx \frac{Br}{\text{P}_{\text{TX}}} \times \left(\frac{R_S}{R_{REF}}\right)^2 \times 10^{\left(\frac{\bar{L}_A \times (R_S - R_{REF})}{20 \times R_{REF}}\right)} \times 10^{\left(\frac{SS\# \times SS_{\text{dB}}}{20}\right)} \text{ Bits/J @ 1 km re } SS0 \qquad (3\text{-}6)$$

$$SS_{\text{dB}} \approx 6 \text{ dB path loss increase per sea sate}$$

3.7 Summary

There has been sustained research interest in the technology developed for medium to high speed under water communication 1984 [5] [21], 1992 [42],1993 [29], 1994 [47] [56], 1995 [55], 2000 [66], 2008 [25] [26], 2009 [51], [87] 2002, 2012 [7], 2013 [74] [88], 2015 [96]. To date there are no low-cost commodity based mass-market hydro-acoustic modems that provide reliable high baud rate and long-range underwater communication. Medium to low baud rate and long communication range SS modems are relatively expensive and limited to a very small number of mission critical applications.

High speed research modems dominate the short to medium range hydro-acoustic communication operating across the $f_C \approx$10 kHz→1 MHz frequency band which is subject to high environmental absorption ($\bar{L}_A \approx 1 \rightarrow$100 dB/km). Transmit source level is typically less than 180 dB re 1 µPa @ 1 m, requiring approximately 30 W transmitter power, providing reliable communication range of $R_S \approx 0.1$ km $\rightarrow 10$ km under favourable conditions with bit error rates are measured between $10^{-2} \rightarrow 10^{-3}$. Some high-speed communication links improve reliability using a statically deployed hydrophone array receiver or directional transducers which cannot handle high Doppler or high seas. Many short to medium range high speed reliable communication links have been successfully established in favourable environments such as bays (15 m [3] [116] [140], 100m [4]) and fjords (10 m [132], 50 m [14] [133]) with no snapping shrimp [131] [134], open ocean with low reverberation [19], low sediment bottom ducting [89] or low surface ducting.

The commercial market is dominated by short to medium range hydro-acoustic modems operating across the $f_C \approx 15$ kHz $\rightarrow$ 40 kHz frequency band, which is subject to high environmental absorption ($\bar{L}_A \approx 12 \rightarrow$ 8 dB/km). Transmit source levels of up to $SPL_{TX} <$ 180 dB re 1 µPa @ 1 m provide reliable communication range of up to $R_S < 8$ km under favourable conditions [153]. Commercial modem data sheets quote bit error rates between $10^{-7} \rightarrow 10^{-10}$ [145] [151] [153] which does not translate to high MR communication when operated in shallow reverberating waters such as Australia (Appendix H; Appendix I; Appendix J), Baltic (Appendix B) or Singapore (Appendix C). Commercial hydro-acoustic modem baud rates vary from 1,200 to 38,400 baud requiring high bandwidth efficient modulation schemes such as MFSK and OFDM which does not provide adequate processing gain to circumvent multipath reverberation, high ambient noise or sound velocity induced refraction.

Very long communication range ($R_S >$ 100 km) sub 10 baud underwater communications applications, using the Sound Fixing And Ranging (SOFAR) channel, are limited to a small number of research organisations using large high powered and expensive Directional PZT transducer (TONPIZ) projectors [161] or low frequency ocean surface RF propagation [9] [50] [88].

Long-range ($R_S >$ 10 km) and low baud rate hydro-acoustic SS communication [16] [17] requires a modulation scheme with high processing gain, which in turn necessitates low bandwidth efficiency, low carrier frequency, high power transmitter Lead Zirconate Titanate (PZT) projectors and low noise receivers. The commercial and defence markets for reliable long-range under water SS communication are limited to a very small number of mission critical applications. Publicly available literature in this domain is sparse and much of it postdates the L3 Oceania commercial deployment of SS [84] [108]. A significant proportion of academic hydro communication publications are highly detailed simulation studies (BELLHOP [63], Sensor Networks [123], QAM [128], RF [83], 10,000 baud [110] [111] [121] [121], hydrophone array [102], short range modems [75] [141], wave propagation [124]). This thesis is focussed less towards simulation and more towards performance validation via sea trial measurements.

4 OVERVIEW OF MCDSSS COMMUNICATION

4.1 Introduction

This chapter provides an overview of Multi Channel Direct Sequence Spread Spectrum (MCDSSS) communication. The primary performance advantages of using MCDSSS modulation are to counter multipath interference, inter-symbol interference, communication channel bandwidth limits and transmission bandwidth limits. As the number of MCDSSS telemetry channels increases, the symbol period also increases which improves resilience to multi-path induced inter symbol interference. The modulation bandwidth also decreases with an increase in telemetry channels which improves the efficient utilisation of the limited channel bandwidth and maximises transmit margin cover performance.

4.2 DSSS Receiver Correlation Pulse Compression

Shallow water multipath signals propagation delays are approximately $\tau_M \approx 0 \rightarrow 20$ ms. Non DSSS detectors with low slant range resolution such as the MASQ telemetry alert ping Frequency Shift Key (FSK) receiver, with a correlation pulse width (τ_{FSK}) Figure 110 equal to the ping period of $\tau_{PING} = 7.8$ ms have insufficient correlation pulse resolution to track multipath signals. In comparison a DSSS receiver's correlation pulse width is inversely proportional to the modulation bandwidth and compresses the correlation pulse width with sufficient resolution to track multipath signals (Figure 32). High hydro-acoustic baud rates with modulation bandwidths (B_M) that exceed the transmission bandwidth (B_{TX}) of the acoustic projectors require the transmit signal to be band limited, which widens the correlation pulse width (τ_{ψ_I}) to a *sinc* function Eq.(4-1).

$$\begin{aligned} \tau_{FSK} &= \tau_{PING} \approx 7.8 \text{ ms} \quad \text{(for MASQ Telemetry Alert)} \\ \tau_{\psi_I} &= \frac{1}{B_{TX}} \approx \frac{1}{10 \text{ kHz}} \rightarrow \frac{1}{1.5 \text{ kHz}} \approx 100 \text{ µs} \rightarrow 650 \text{ µs} \quad \text{(for MASQ MCDSSS)} \end{aligned} \tag{4-1}$$

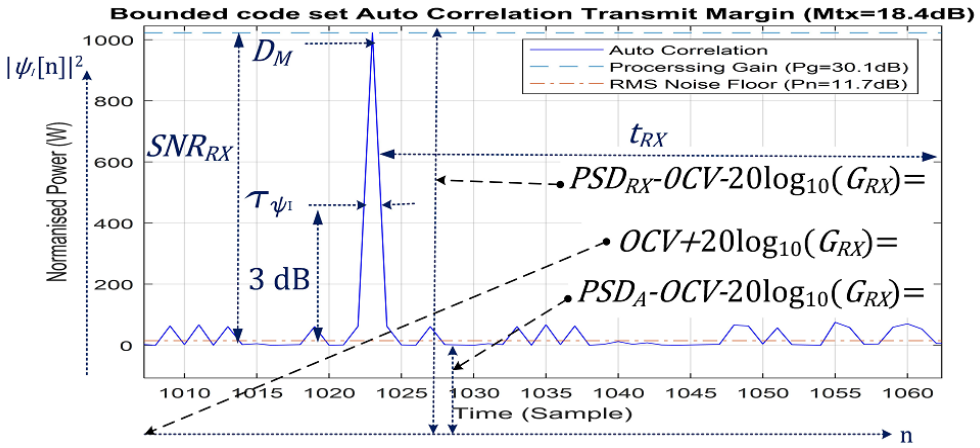

Figure 32 DSSS receiver correlation pulse compression

Navigation and range accuracy is a function of MCDSSS transmission bandwidth (B_{TX}). Relative range accuracy (R_{REL}) is proportional to transmission bandwidth and absolute range accuracy (R_{ABS}) is proportional to the speed of sound estimate error (ε_C) Eq.(4-2).

$$R_{REL} = c/B_{TX} \cong 0.25 \text{ m RMS} \quad \text{(for MASQ)}$$
$$R_{ABS} \propto \varepsilon_C < 1 \text{ m RMS} \tag{4-2}$$

4.3 MCDSSS Modulation

A DSSS signal is a bi-phase modulated sine wave carrier (f_C) (Figure 33). MCDSSS signals are generated by summing multiple DSSS signals with different encryption codes $C(\mathrm{t})$ and carrier phase offsets (θ_{TX}). The MCDSSS receive signal (V_{RX}) carrier phase (θ_{RX}) is the sum of the transmit carrier phase (θ_{TX}) rotated by the signal Slant Range propagation phase offset (θ_{RS}) and multipath induced phase noise (θ_N) Eq.(4-3).

$$V_{TX}(\mathrm{t}) = C(\mathrm{t}).\sin(2\pi f_C \mathrm{t} + \theta_{TX})$$
$$\theta_{RX} = \theta_{TX} + \theta_{RS} + \theta_N \tag{4-3}$$
$$V_{RX}(\mathrm{t}) = h(\mathrm{t},\tau) \otimes \big(C(\mathrm{t}).\sin(2\pi f_C \mathrm{t} + \theta_{RX})\big) + n_A(\mathrm{t})$$

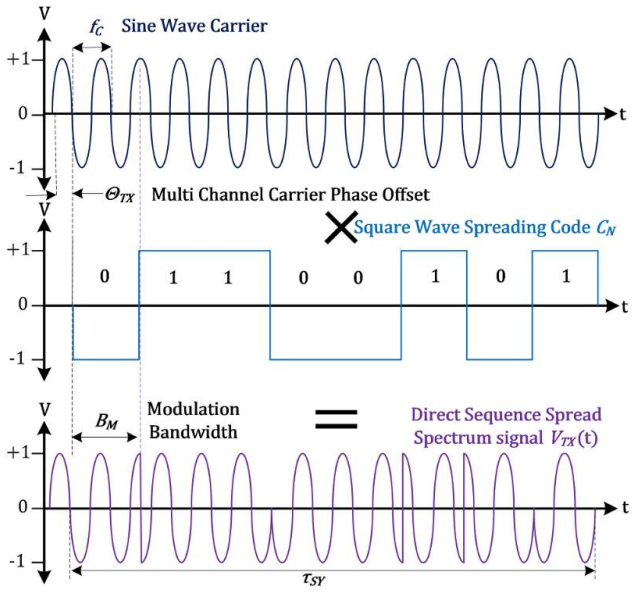

Figure 33 DSSS signal (time domain)

4.3.1 MCDSSS Telemetry Channel (Q) Self Noise

Multiple DSSS channels are derived from single orthogonal spreading code which are mixed to generate a MCDSSS signal containing a reference channel and multiple telemetry channels. The MCDSSS telemetry channels interfere with the reference channel receiver and induce in-band self noise which decrease the DSSS processing gain by the self noise loss (L_C) and is a function of the number of MCDSSS channels (N_C)

Eq.(4-4). **Note:** The reference channel self noise also interferes with the telemetry receivers.

$$L_C = 10\log_{10}(N_C) = 0 \text{ dB} \rightarrow 7 \text{ dB} \quad \text{(for MASQ)} \tag{4-4}$$

4.3.2 MCDSSS Hydro-acoustic Baud Rate Dependencies

The hydro-acoustic baud rate (Br) is proportional to modulation bandwidth (B_M) and is derived from the number of MCDSSS telemetry channels (N_T) Eq.(4-5).

$$\tau_{SY} = \frac{S_{CB}}{B_M} = \frac{1023}{B_M} = 27 \text{ ms} \rightarrow 800 \text{ ms} \quad \text{(for MASQ)}$$

$$N_T = N_C - 1$$

$$B_{PS} = 8 \text{ Bits per symbol} \quad \text{(for MASQ)} \tag{4-5}$$

$$B_{PT} = B_{PS} \times N_T = 8 \times N_T = 8 \text{ Bits} \rightarrow 32 \text{ Bits per telemetry channel} \quad \text{(for MASQ)}$$

$$Br = \frac{B_{PT}}{\tau_{SY}} = 10 \text{ Baud} \rightarrow 1{,}200 \text{ Baud} \propto B_M = 1.2 \text{ kHz} \rightarrow 48 \text{ kHz} \quad \text{(for MASQ)}$$

4.3.3 MCDSSS Transmit Margin

MCDSSS modulation spreads the transmitted hydro-acoustic symbol energy in frequency by the modulation bandwidth and in time by the spreading code. The length of spreading code provides processing gain which results in the ability to detect the MCDSSS signal below the ambient noise ($PSD_{RX} < PSD_A$) providing covert communication at the receiver. Covert performance is characterised by the receive margin which is the difference between the MCDSSS receiver signal power (PSD_{RX}) and the ambient noise (PSD_A) Eq.(2-17). The transmit margin (M_{TX}) is derived from the transmission bandwidth (B_{TX}), modulation bandwidth (B_M), over spreading loss (L_{OS}), number of telemetry channels (N_T) and detection threshold (D_{TH}) Eq.(4-6). The modulation bandwidth for MCDSSS baud rates greater than 500 baud exceed the transmission bandwidth resulting in a decrease in the transmit margin. If the transmit margin drops below 3 dB then using SS modulation for high speed data transmission is no longer effective and requires the use of bandwidth efficient modulation and channel equalisation communication.

$$\begin{gathered} L_{OS} = 10\log_{10}(B_M) - 10\log_{10}(B_{TX}) = 0 \text{ dB} \rightarrow 5 \text{ dB} \quad \text{(for MASQ)} \\ P_G = 10\log_{10}(S_{CB}) - L_C - L_{OS} = 18 \text{ dB} \rightarrow 27 \text{ dB} \quad \text{(for MASQ)} \\ D_{TH} \approx 14 \text{ dB} \quad \text{(for MASQ)} \\ M_{TX} = P_G - D_{TH} = 3 \text{ dB} \rightarrow 15 \text{ dB} \quad \text{(for MASQ)} \end{gathered} \tag{4-6}$$

Propagation through the ocean attenuates the transmit signal (PSD_{TX}) by spherical spreading loss (L_S) and sound velocity refraction (L_R). The received signal bandwidth (B_{TX}) is narrowed by the environmental absorption (L_A). The symbol period (τ_{SY}) is altered by the Doppler scale factor (D_S). The transmit margin (M_{TX}) remains constant

until the receive power (PSD_{RX}) is less than the ambient noise (PSD_A) and multipath interference (PSD_M) magnitude (Figure 34). The transmit margin (M_{TX}) is proportional to the symbols period (τ_{SY}) and as the baud rate decrease the transmit margin increases.

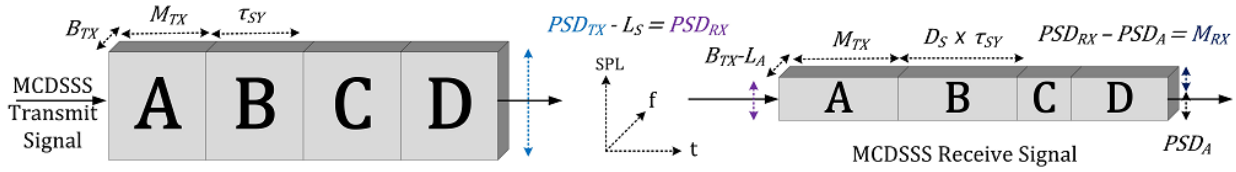

Figure 34 MCDSSS transmit margin to MCDSSS receive margin attenuation

4.3.4 MCDSSS Baud Rate and Transmit source level Equivalence

The MASQ modulation supports hydro-acoustic baud rates between 10 baud and 1,200 baud. Baud rate processing gain (Br_{PG}) is proportional to a change in the transmit source level (P_{TX}) Eq.(4-7).

$$\Delta P_{TX} \propto Br_{PG} = 10\log_{10}\left(\frac{Br_{MAX}}{Br_{MIN}}\right) = 10\log_{10}\left(\frac{1{,}200\ \text{Bits/s}}{10\ \text{Bits/s}}\right) \approx 20\ \text{dB} \tag{4-7}$$

In terms of transmit symbol energy (E_{TX}) injected into the environment, lowering the transmission baud rate is equivalent to increasing the transmit source level (SPL_{MAX}) Eq.(4-8) (Figure 35). When the effects of multipath ($N_M > 0$) and frequency dependent absorption ($R_S > 5$ km Figure 6) come into effect there is a non-linear relationship between transmit power (P_{TX}) and baud rate (Br_{PG}) because additional power is required to counter multipath self-noise to maintain receiver SNR which has a significant impact on BEE_{PEAK} (Chapter 6.6).

$$\epsilon_{TX} \approx 35\% \rightarrow 45\% \quad \text{Total electrical power to acoustic efficiency}$$

$$P_{TX} \approx \frac{10^{\left(\frac{SPL_{TX} - SPL_{1W}}{10}\right)}}{\epsilon_{TX}} \quad \text{for} \quad SPL_{1W} \approx 170.5\ \text{dB re 1 µPa/W @ 1 m} \tag{4-8}$$

$$E_{TX} = (4P_{TX}) \times \tau_{SY} = P_{TX} \times (4\tau_{SY}) \ \ (\text{for } N_M = 0 \text{ and } L_A = 0\ \text{dB})$$

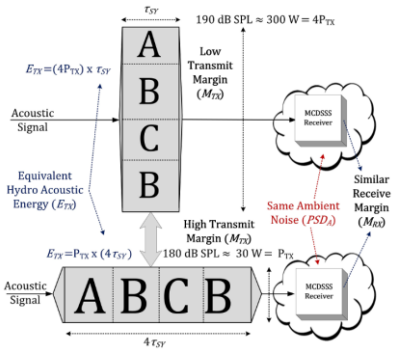

Figure 35 Hydro-acoustic baud rate versus transmit source level equivalence

The full 20 dB hydro-acoustic baud rate processing gain (Br_{PG}) cannot be realized because of the multi-channel (N_C) 3 dB to 7 dB self noise (L_C), and that the PZT transducer 6.5 kHz to 16.5 kHz = 10 kHz maximum transmission bandwidth (B_{TX}) limits the transmit margin (M_{TX}) to 3 dB → 15 dB (Figure 36), Eq.(4-6).

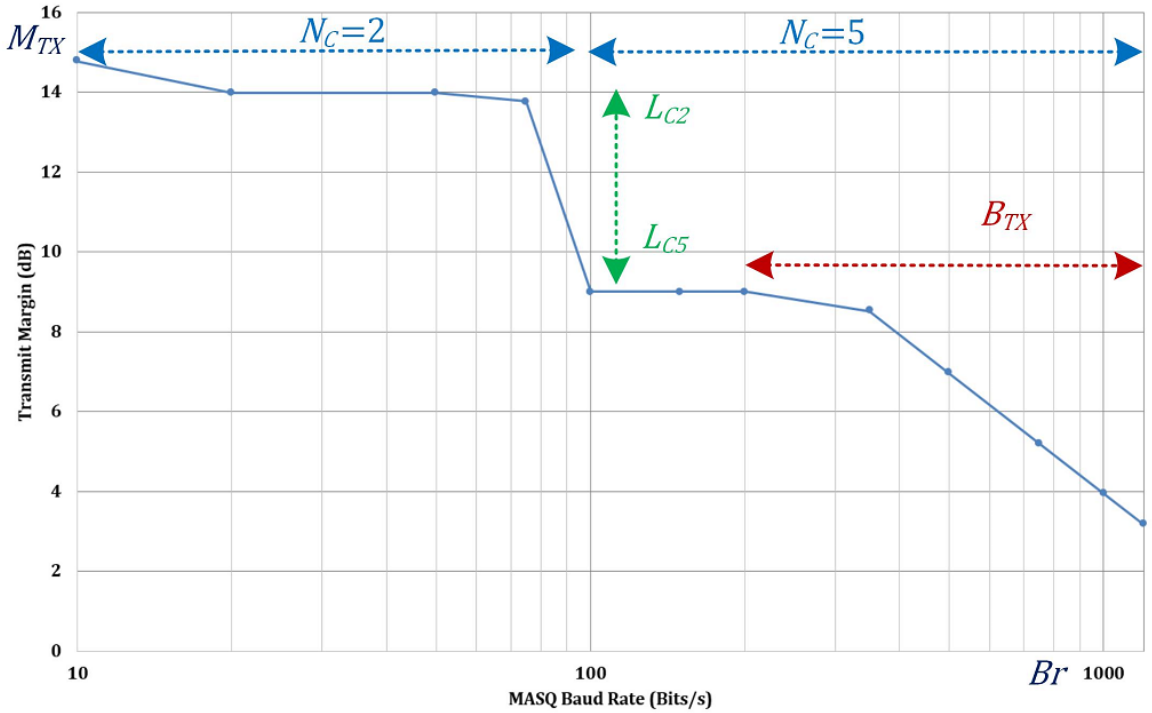

Figure 36 MASQ transmit margin versus hydro-acoustic baud rate

The ocean noise floor is highly variable and fluctuates by typically one sea state or ±3 dB during the reception of a MCDSSS message. In practice the full 3 dB to 15 dB transmit margin may not be realised because ocean noise fluctuations require a higher detection threshold to maintain the false detect rate.

4.3.5 MCDSSS Spread Spectrum Codes (C)

MCDSSS spread spectrum codes (C) must exhibit cross correlation properties (ψ_C) that minimise self-noise (P_N) and maximise the cross correlation transmit margin (M_{TX}) Eq.(4-9). The DSSS receiver detection threshold (D_{TH}) is nominally set to the minimise self-noise except when control system optimisations allow for fine tuning of the detection threshold.

$$\psi_C(\mathrm{t}) = C_x \otimes C_y = \int_{-\infty}^{\infty} C_x(\mathrm{t}).C_y(\mathrm{t}-\tau)\mathrm{d}\tau$$

$$\psi_C[\mathrm{n}] = \sum_{m=0}^{S_{CB}-1} C_x[\mathrm{n}] \times C_y[\mathrm{n}-\mathrm{m}] \qquad (4\text{-}9)$$

$$P_G = 10\log_{10}\big(\mathrm{MAX}(\psi_C)\big)$$

$$P_N = 10\log_{10}(\text{RMS}(\psi_C)) \approx D_{TH}$$

$$M_{TX} = P_G - P_N \approx P_G - D_{TH}$$

4.3.5.1 Spread Spectrum Code (*C*) Generation

Bounded code sets are good candidates for generating MCDSSS spread spectrum codes with excellent cross correlation properties. Bounded code sets are derived using base pairs of PRN codes as described by the generator polynomial Eq.(4-10).

$$M[\text{n}] = Z^{M_{S_{CB}}-1} + \cdots + Z^{M_0} + 1 \tag{4-10}$$

4.3.5.2 Spread Spectrum Code (*C*) Auto Correlation Self Noise

Figure 37 illustrates the auto correlation (ψ_{M1}) of the MCDSSS communication channel first preferred pair PRN M_1 with an auto correlation transmit margin of $M_{TX_{M_1}} = 21.2$ dB Eq.(4-11).

$$\begin{aligned} \psi_{M1} &= 10\log_{10}(|M_1 \otimes M_1|) \\ P_{G_{M_1}} &= \text{MAX}(\psi_{M1}) = \psi_{M1}(0) = \ 30.1 \text{ dB} \\ P_{N_{M_1}} &= 10\log_{10}\big(\text{RMS}(|M_1 \otimes M_1|)\big) = \ 8.9 \text{ dB} \\ M_{M1} &= P_{G_{M_1}} - P_{N_{M_1}} = \ 21.2 \text{ dB} \end{aligned} \tag{4-11}$$

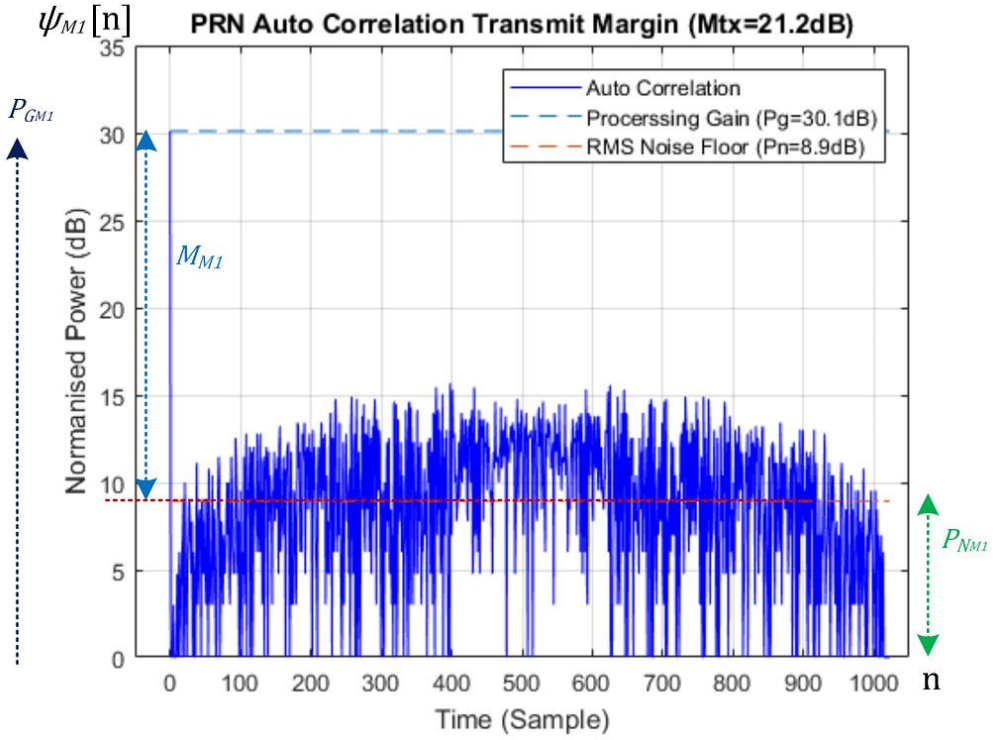

Figure 37 PRN auto correlation properties

Bounded code sets (C_m) are the dot product of code rotated preferred PRN pairs, which generates N_C unique codes (Figure 38) Eq.(4-12).

$$\begin{gathered} N_C = 2^{S_{CB}} - 1 \\ \mathrm{n} = 0 \text{ to } (N_C - 1) \\ \mathrm{m} = 0 \text{ to } (N_C - 1) \\ C_m[\mathrm{n}] = M_1[\mathrm{n}] \cdot M_2[\mathrm{MOD}(\mathrm{n} + \mathrm{m}, N_C)] \end{gathered} \tag{4-12}$$

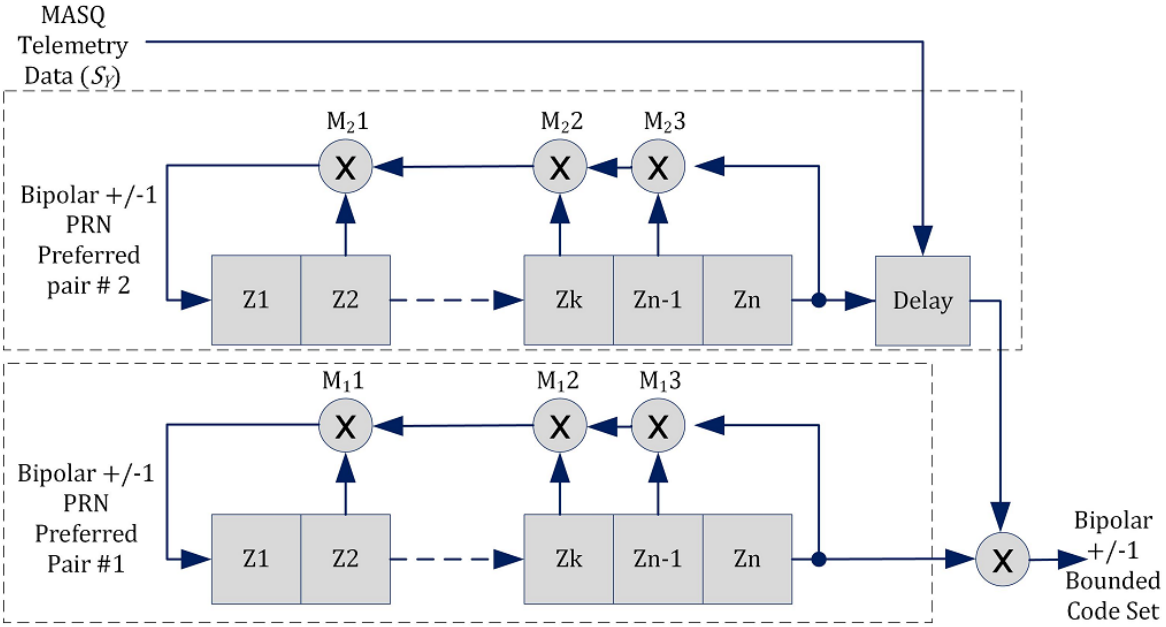

Figure 38 Example algorithm for bounded code set (*C*) generation

4.3.5.3 Reference Channel (*I*) Spread Spectrum Code Self Noise

Figure 39 illustrates the auto correlation (Ψ_I) of the MCDSSS communication reference (I) channel reference bounded code set C_I with a correlation margin (M_{G_I}) Eq.(4-13).

$$\begin{gathered} \psi_I = 10\log_{10}(|C_I \otimes C_I|) \\ P_{G_I} = \mathrm{MAX}(\psi_I) = \psi_I(0) = 30.1 \text{ dB} \\ P_{N_I} = 10\log_{10}\big(\mathrm{RMS}(|C_I \otimes C_I|)\big) = 11.7 \text{ dB} \\ M_{G_I} = P_{G_I} - P_{N_I} = 30.1 \text{ dB} - 11.7 \text{ dB} = 18.4 \text{ dB} \end{gathered} \tag{4-13}$$

Bounded code sets provide $N_C = 2^{S_{CB}} - 1$ number of spread spectrum codes with good cross correlation properties. The performance penalty for good cross correlation properties is that the cross correlation margin ($M_{G_I} = 18.4$ dB) for bounded code sets, is 3 dB lower than the auto correlation margin for PRN codes ($M_{M1} = 21.2$ dB).

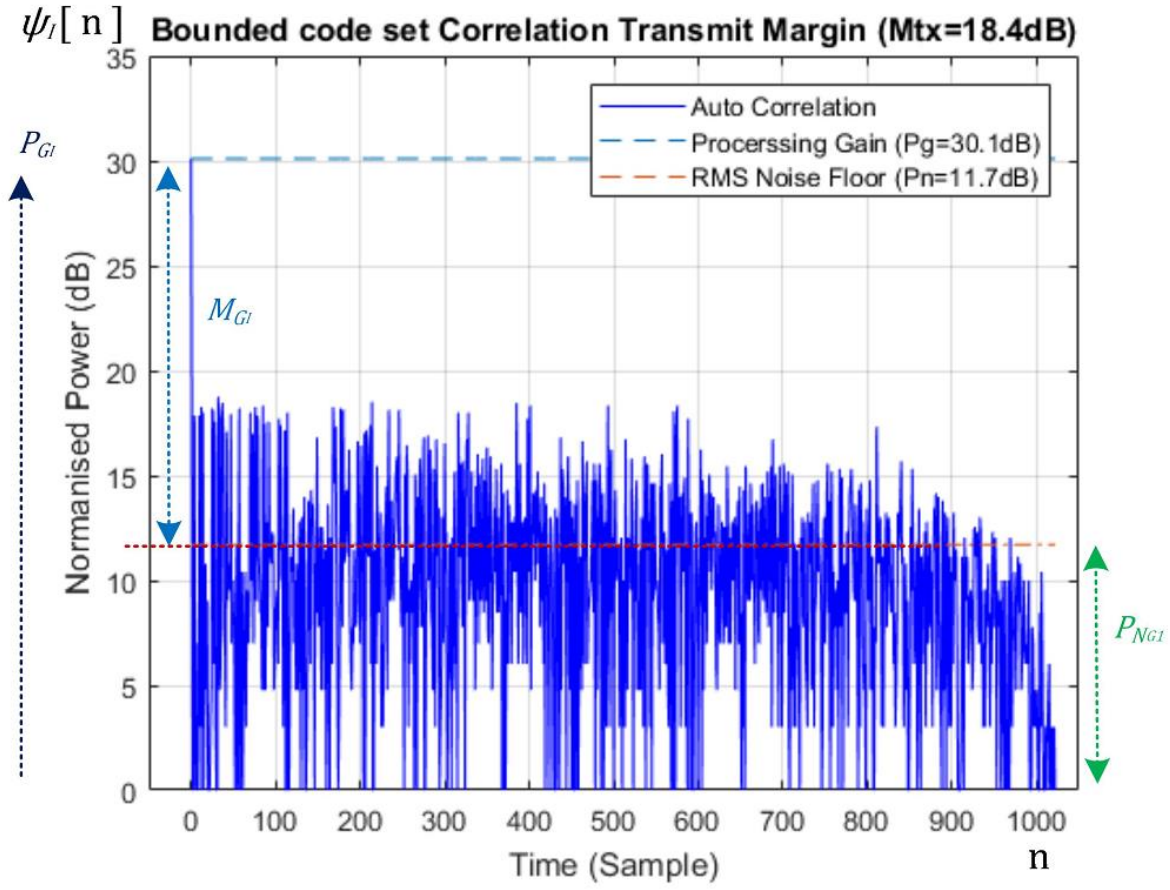

Figure 39 Bounded code set (*C*) auto correlation properties

4.3.5.4 Telemetry Channel (*Q*) Spread Spectrum Code Self Noise

Figure 40 illustrates the cross correlation (ψ_Q) of the MCDSSS communication telemetry (Q) channel bounded code set (C_{m}) noise floor (P_{N_G}) with a correlation margin of M_{Q} = 16.6 dB Eq.(4-14) (i.e. telemetry detection SNR is the difference between the loudest (P_{P_Q}) and second loudest (P_{N_Q}) correlation peak).

$$\psi_Q[\mathrm{n}] = \left|10\log_{10}\left(\mathrm{MAX}(|C_{\mathrm{m}} \otimes C_{\mathrm{n}}|)\right)\right|_{\mathrm{n}=1}^{S_{CB}}$$

$$P_{P_Q} = P_{G_I} = 30.1 \text{ dB}$$

$$P_{N_Q} = \left|10\log_{10}\left(\mathrm{SECOND}(|C_{\mathrm{m}} \otimes C_{\mathrm{n}}|)\right)\right|_{\mathrm{n}=1}^{S_{CB}} = 13.5 \text{ dB} \qquad (4\text{-}14)$$

$$M_{\mathrm{Q}} = P_{P_Q} - P_{N_Q} = 30.1 \text{ dB} - 13.5 \text{ dB} = 16.6 \text{ dB}$$

The telemetry cross correlation margin for bounded code sets (M_{Q} = 16.6 dB) is approximately 2 dB lower than the reference channel correlation margin (M_I = 18.4 dB) (i.e. the telemetry (Q) detector is 2 dB less sensitive than the reference (I) detector).

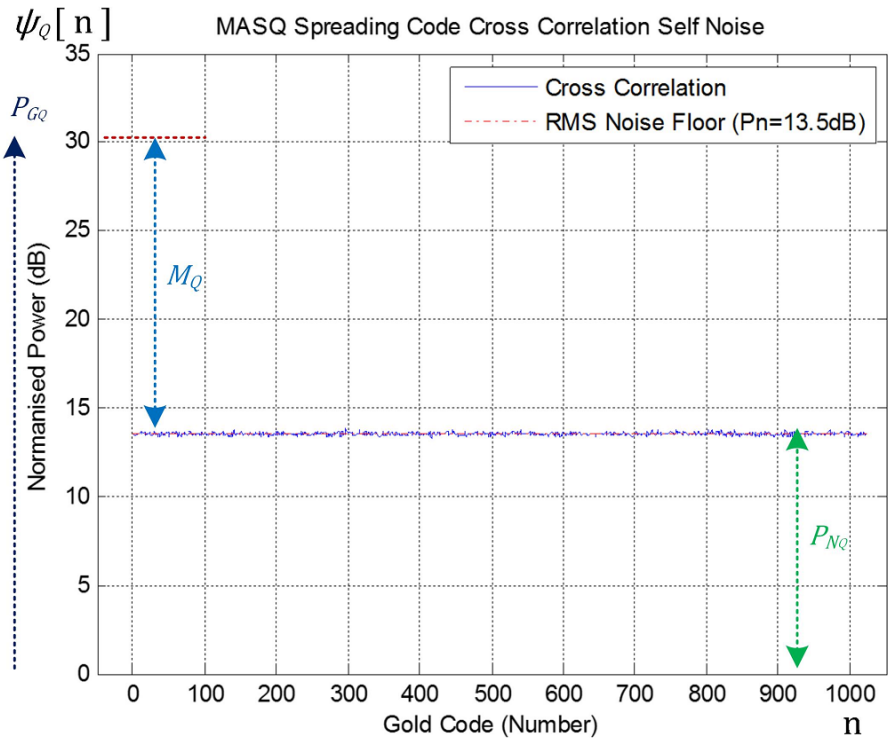

Figure 40 MCDSSS communication spread spectrum code (*C*) cross correlation

4.3.5.5 Two Channel Reference (*I*) Telemetry (*Q*) Spread Spectrum Codes

For low hydro-acoustic baud rate covert communication the MASQ communication channel uses a two channel MCDSSS signal to propagate 8-bit MCDSSS symbols. MASQ $N_C = 2$ channel MCDSSS modulation assigns the first bounded code (C_1) to the reference channel and the next C_2 *to* C_{258} bounded code sets to telemetry data Eq.(4-15).

$$\begin{gathered} \mathrm{n} = 0 \rightarrow (N_C - 1) \\ I[\mathrm{n}] = C_1[\mathrm{n}] = M_1[\mathrm{n}].M_2[\mathrm{n}] \\ \mathrm{m} = 0 \rightarrow (255 - 1) \\ Q[\mathrm{n}][\mathrm{m}] = C_{\mathrm{m}+2}[\mathrm{n}] \end{gathered} \tag{4-15}$$

4.3.5.6 Three Channel Telemetry (*Q*) Modulation Spread Spectrum Codes

MASQ three channel MCDSSS modulation assigns the first bounded code to the reference channel and the next 512 bounded code sets to the two 8-bit telemetry channels Eq.(4-16).

$$\begin{gathered} Q_1[\mathrm{n}][\mathrm{m}] = C_{\mathrm{m}+2}[\mathrm{n}] \\ Q_2[\mathrm{n}][\mathrm{m}] = C_{\mathrm{m}+258}[\mathrm{n}] \end{gathered} \tag{4-16}$$

4.3.5.7 Five Channel Telemetry (*Q*) Modulation Spread Spectrum Codes

For medium and high speed hydro-acoustic communication the MASQ communication channel uses a five channel MCDSSS signal to propagate 32-bit MCDSSS symbols. MASQ MCDSSS modulation assigns the first bounded code to the reference channel and next 256 bounded code sets for each 8 bits of telemetry data.

4.3.5.8 Spread Spectrum Carrier Modulation Signal (C)

The spread spectrum binary code sequence is converted to a bipolar square-wave which is used to phase modulate the MCDSSS carrier Eq.(4-17).

$$I(\mathrm{t}) = I[\mathrm{floor}(B_M.\mathrm{t})]$$
$$Q_N(\mathrm{t}) = Q_N[\mathrm{floor}(B_M.\mathrm{t})] \tag{4-17}$$

4.3.6 DSSS Hydro-acoustic Modulation Options

The MASQ telemetry modulation scheme evolved through 3 generations of L3 Oceania communication protocols (Table 1). L3 Oceania 1st generation communication protocols have been deployed on submarines and the L3 Oceania diver communication and navigation computer (MUCS) prototype. Figure 41 illustrates the sea trial used for L3 Oceania MUCS multipath reliability measurements (Figure 42).

Figure 41 L3 Oceania MUCS and 5 km communication test trial

The L3 Oceania 1st generation communication protocol uses a PRN (M_1) to encode the reference channel and a second PRN (M_2) to encode telemetry. Telemetry symbol data modulates the telemetry channel by code rotating PRN (M_2) in discrete course time domain bins Eq.(4-12) which can be detected using numerically efficient receivers. The width of the telemetry time modulation bin $\frac{N_C.\mathrm{Sy}}{N_B}$ is limited by the channel multipath reverberation period which also limits the maximum baud rate.

$$\mathrm{n} = 0 \text{ to } (N_C - 1)$$
$$\mathrm{Q[n]} = M_2\left[\mathrm{mod}\left(\mathrm{n} + \frac{N_C.\mathrm{Sy}}{N_B}, N_C\right)\right] \tag{4-18}$$

Both the demodulated reference (I) channel and telemetry (Q) channels encode carrier phase and both are subject to multipath interference. The telemetry channel (Figure 42 right) data bins are not time aligned with the reference channel (Figure 42 left) and measure a different channel multipath structure. The reference channel multipath measurement cannot be used to improve the telemetry multipath performance using de-convolution or cross correlation. MASQ uses the reference channel modulation from L3 Oceania 1st generation communication and time aligns telemetry (Q_N) bounded code sets using the telemetry modulation from L3 Oceania 2nd generation communication. The

telemetry channels no longer encode carrier phase because each data symbol uses a different modulation spreading code but the reference channel multipath channel probe measurement is used to de-convolve the telemetry channel's multipath interference. L3 Oceania 3rd generation communication (MASQ) uses MCDSSS to increase the symbol period which provides tolerance to inter-symbol interference.

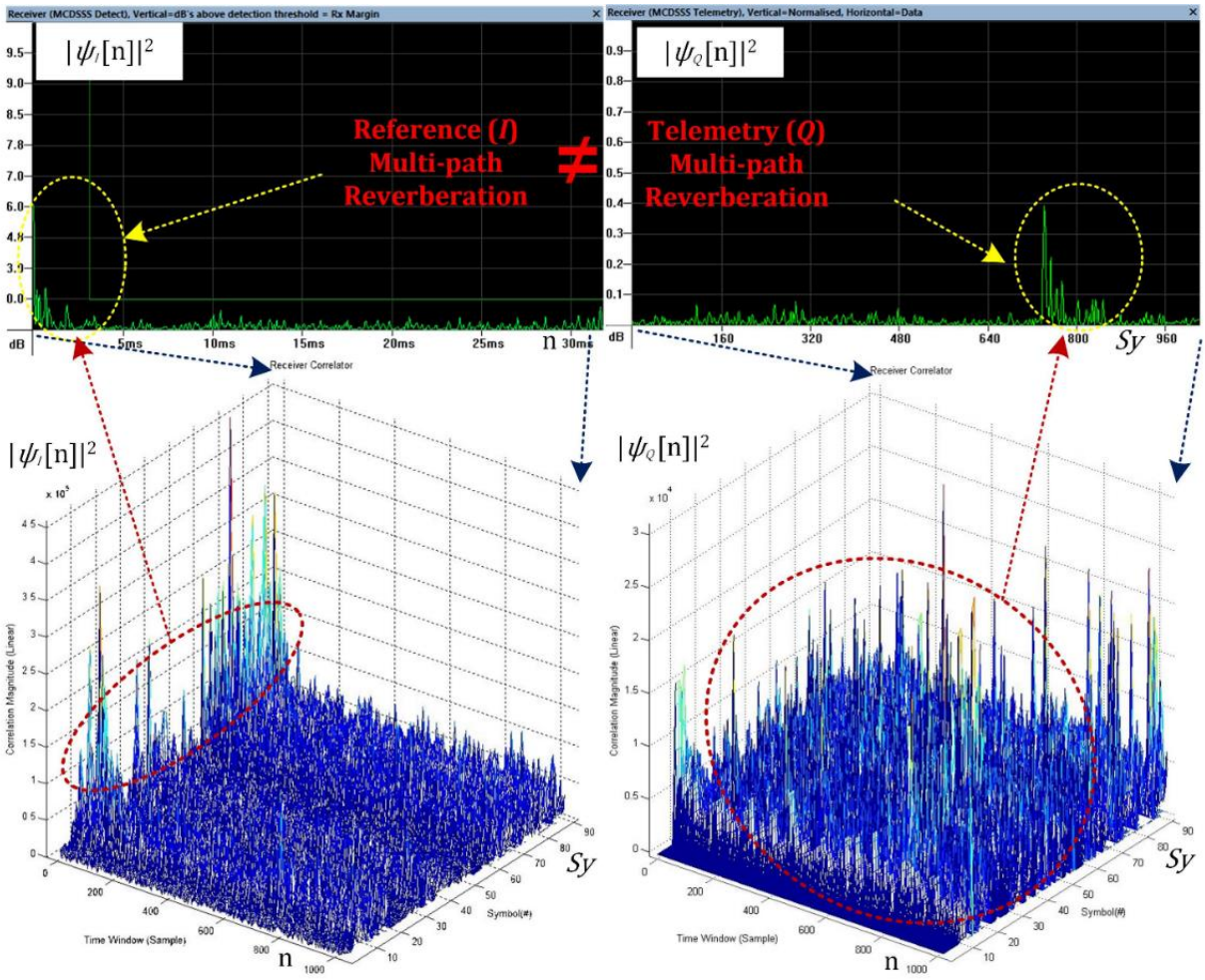

Figure 42 L3 Oceania MUCS reference I (left) telemetry Q (right) multipath

4.3.6.1 DSSS BPSK Modulation

MASQ uses BPSK modulation to generate a DSSS signal which is also commercially deployed on multiple telecommunication protocols [52]. Medium to high-speed bandwidth efficient modulation schemes such as DPAM, DPSK, FDMA, OFDM, QAM, and TDMA are not suitable for reliable long-range shallow water communication because of insufficient time bandwidth product (TBP) that is required to counter multipath and high environment noise.

4.3.6.2 MCDSSS QPSK, 8PSK and 32PSK Telemetry Modulation

MASQ encodes MCDSSS symbols using QPSK, 8PSK and 32PSK modulation to mix multiple DSSS channels. RF QPSK, 8PSK and 32PSK telemetry modulation uses the carrier phase to encode information whereas MASQ MCDSSS uses carrier phase modulation for multi-channel time and frequency domain symbol energy spreading.

4.3.7 Spread Spectrum Code (C) Generation Optimisation

Algorithm generated PRN sequences typically start with a Spreading Code Order (S_{CO}) number of ones, which degrades the cross correlation properties for example an 2^{10} order PRN sequence starts with 10 ones and cross correlating a random sequence with a string of ones degrades the cross correlation properties. PRN forward and reverse codes generate better cross correlation properties than two forward PRN generated bounded code sets. Mathematically derived or random generated spread spectrum codes, with good circular cross correlation properties, can be used for a spread spectrum code orders $S_{co} \geq 10$.

4.3.8 MCDSSS One Channel BPSK Modulation

A one channel MCDSSS signal is generated by Bi-Phase Shift Key (BPSK) modulating a sine wave carrier Eq.(4-19) (Figure 43) (Figure 46). BPSK modulation does not use a reference channel (I) but encodes a unique ID which is used by the MASQ Range Pulse (Q).

$$\theta_{BPSK} = 90$$
$$V_{TX1}(\mathrm{t}) = Q_1(\mathrm{t}).\sin(2\pi f_C \mathrm{t} + \theta_{BPSK}) \tag{4-19}$$

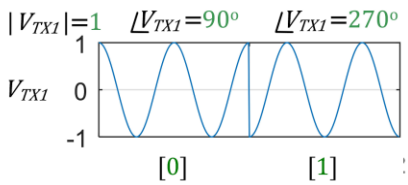

Figure 43 MCDSSS one channel BPSK (time domain)

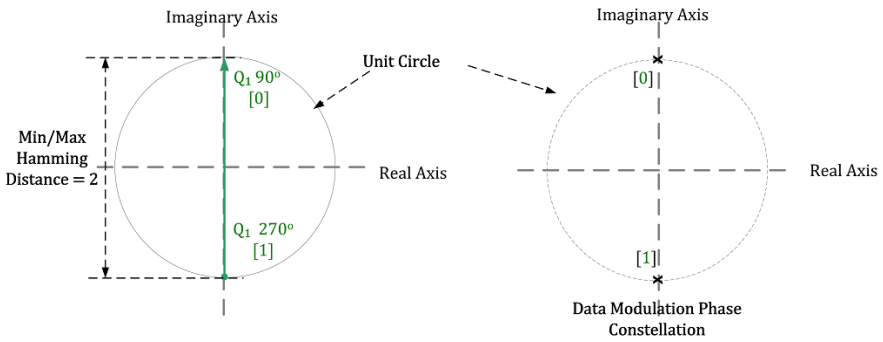

Figure 44 MCDSSS one channel BPSK (phasor diagram)

The BPSK self-noise $L_{C1} = 0$ dB and does not reduce the processing gain Eq.(4-20).

$$N_{C1} = 1$$
$$L_{C1} = 10\log_{10}(N_{C1}) = 0 \text{ dB} \tag{4-20}$$

The min/max hamming distance for BPSK is $H_{C1} = 2$ Eq.(4-21).

$$H_{C1} = 2\sin\left(\frac{\pi}{2N_{C1}}\right) = 2 \tag{4-21}$$

4.3.9 MCDSSS Two Channel QPSK Modulation

A two channel MCDSSS signal is generated by mixing two BPSK signals to generate a Quadrature Phase Shift Key (QPSK) modulating a sine wave carrier Eq.(4-22) (Figure 45) (Figure 46).

$$\begin{gathered} N_{C2} = 2 \\ \theta_{QPSK} = \frac{\pi}{N_{C2}} = \frac{\pi}{2} \\ V_I(\mathrm{t}) = I(\mathrm{t}).\,\mathrm{e}^{\mathrm{j}2\pi f_C \mathrm{t}} \\ V_{Q1}(\mathrm{t}) = Q_1(\mathrm{t}).\,\mathrm{e}^{\mathrm{j}(2\pi f_C \mathrm{t} + \theta_{QPSK})} \\ V_{IQ2}(\mathrm{t}) = V_I(\mathrm{t}) + V_{Q1}(\mathrm{t}) \\ V_{TX2}(\mathrm{t}) = \mathrm{Re}\left(V_{IQ2}(\mathrm{t})\right) + \mathrm{Im}\left(V_{IQ2}(\mathrm{t})\right) \end{gathered} \tag{4-22}$$

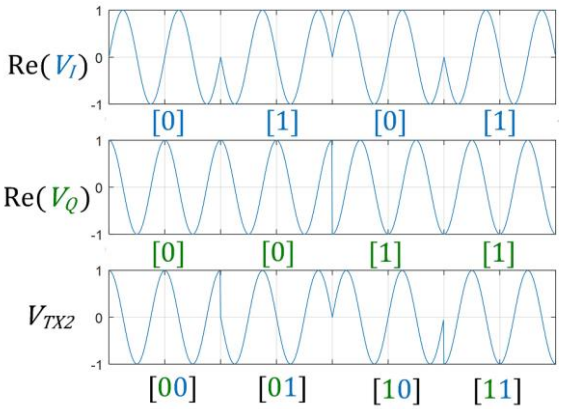

Figure 45 MCDSSS two channel QPSK mixing (time domain)

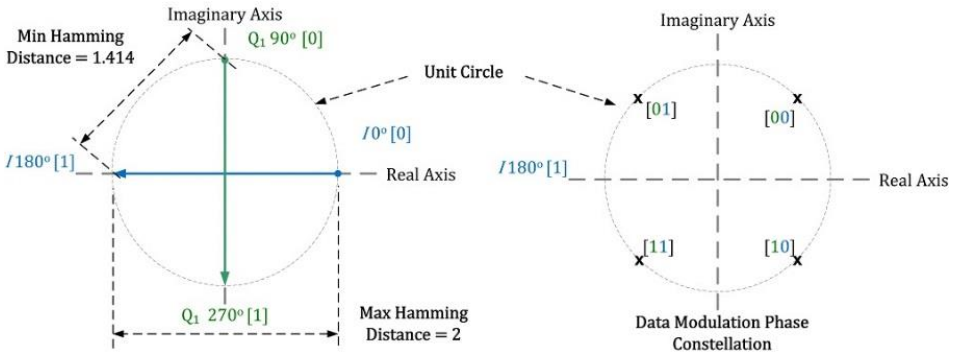

Figure 46 MCDSSS two channel QPSK mixing (phasor diagram)

The QPSK self-noise (L_{C2}) reduces the processing gain by 3 dB Eq.(4-23) (Figure 48) (Figure 47).

$$L_{C2} = 10\log_{10}(N_{C2}) = 3 \text{ dB} \tag{4-23}$$

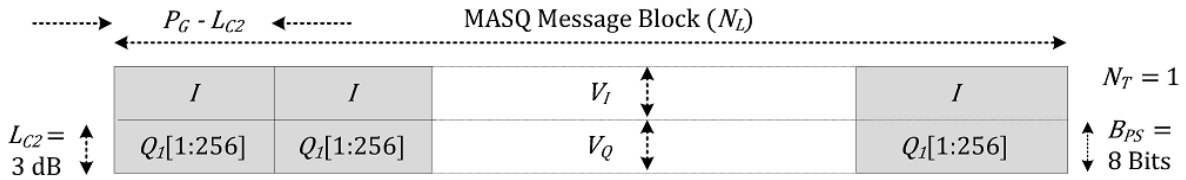

Figure 47 MCDSSS two channel QPSK inter channel interference loss

The normalised hamming distance for QPSK is $H_{C2} = 0.707$ Eq.(4-24).

$$H_{C2} = \frac{2\sin\left(\frac{\pi}{2N_{C2}}\right)}{H_{C1}} = \frac{\sqrt{2}}{2} = 0.707 \tag{4-24}$$

4.3.10 MCDSSS Three Channel 8PSK Modulation

A three channel MCDSSS signal is generated by mixing three phase shifted BPSK signals to generate a Phase Shift Key (8PSK) modulated sine wave carrier Eq.(4-25) (Figure 49). MCDSSS 8PSK modulation generates a crowded unit circle and duplicate codes at [010] and [101] which reduces the processing gain by $\log_{10}\left(\frac{7}{8}\right) = -0.6$ dB. The high baud rate sea trial (Appendix P) measured a lower performance for 8PSK compared to 32PSK.

$$N_{C3} = 3$$

$$\theta_{8PSK} = \frac{\pi}{N_{C3}} = \frac{\pi}{3}$$

$$V_I(\mathrm{t}) = I(\mathrm{t}).\, \mathrm{e}^{\mathrm{j}2\pi f_C \mathrm{t}}$$

$$V_{Q1}(\mathrm{t}) = Q_1(\mathrm{t}).\, \mathrm{e}^{\mathrm{j}(2\pi f_C \mathrm{t} + \theta_{8PSK})} \tag{4-25}$$

$$V_{Q2}(\mathrm{t}) = Q_2(\mathrm{t}).\, e^{\mathrm{j}(2\pi f_C \mathrm{t} + 2\theta_{8PSK})}$$

$$V_{IQ3}(\mathrm{t}) = V_I(\mathrm{t}) + V_{Q1}(\mathrm{t}) + V_{Q2}(\mathrm{t})$$

$$V_{TX3}(\mathrm{t}) = \mathrm{Re}\left(V_{IQ3}(\mathrm{t})\right) + \mathrm{Im}\left(V_{IQ3}(\mathrm{t})\right)$$

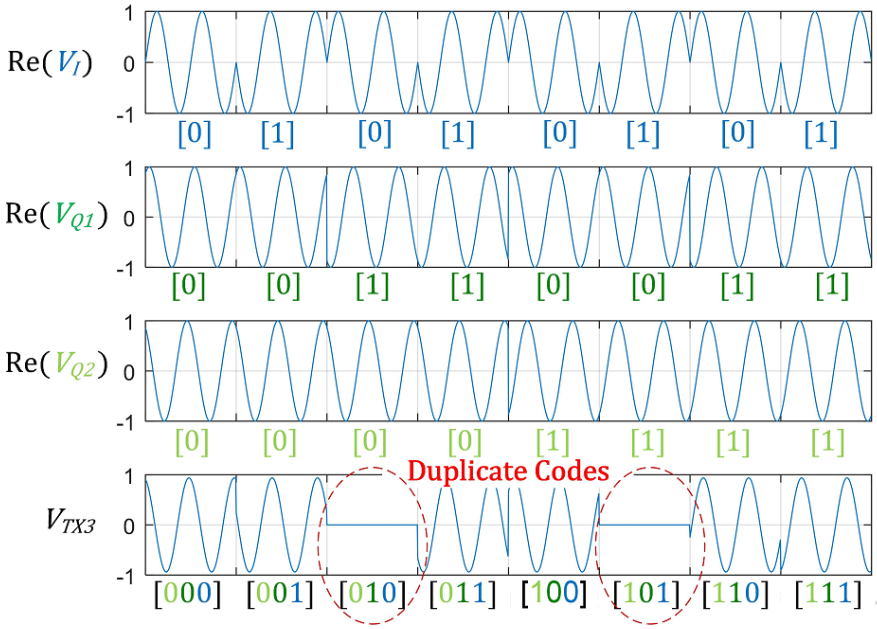

Figure 48 MCDSSS three channel 8PSK mixing (time domain)

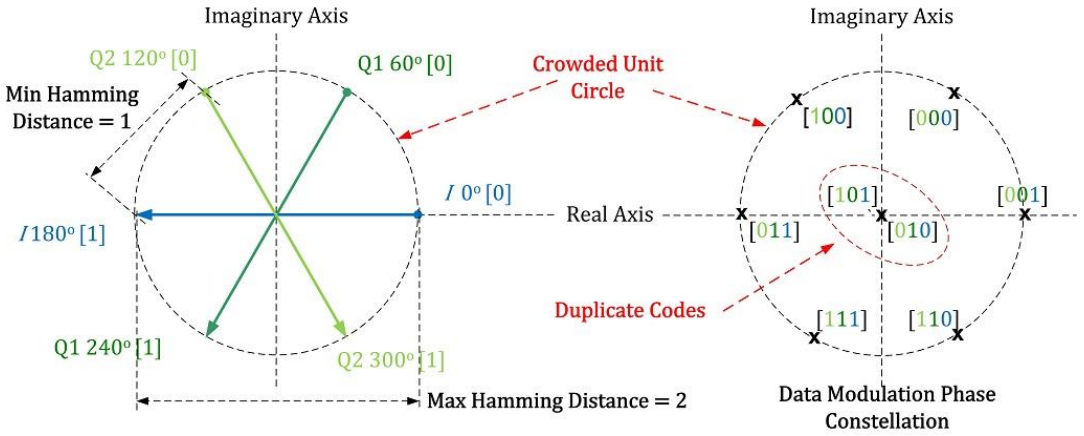

Figure 49 MCDSSS three channel 8PSK mixing (phasor diagram)

The 8PSK self-noise (L_{C3}) reduces the processing gain by 4.8 dB Eq.(4-26) (Figure 50).

$$L_{C3} = 10\log_{10}(N_{C3}) = 4.8 \text{ dB} \tag{4-26}$$

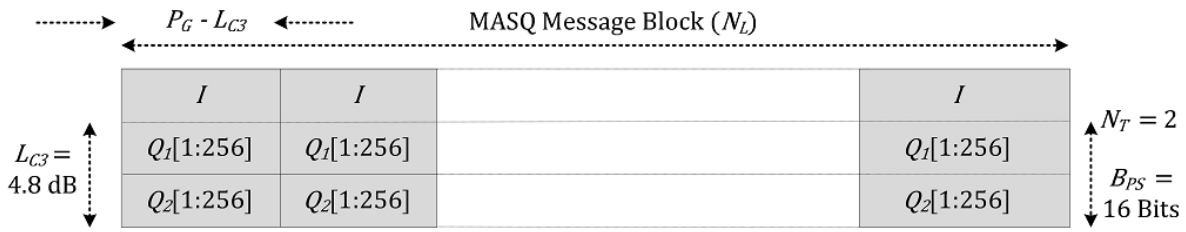

Figure 50 MCDSSS three channel 8PSK inter channel interference loss

The normalised hamming distance for 8PSK is $H_{C3} = 0.5$ Eq.(4-27).

$$H_{C3} = \frac{2\sin\left(\frac{\pi}{2N_{C3}}\right)}{H_{C1}} = 0.5 \tag{4-27}$$

4.3.11 MCDSSS Five Channel 32PSK Modulation

A five channel MCDSSS signal is generated by mixing five phase shifted BPSK signals to generate a 32 Phase Shift Key (32PSK) modulated sine wave carrier Eq.(4-28) (Figure 51) (Figure 52). MCDSSS 32PSK modulation generates a low crowded unit circle but generates duplicate codes at [01010] and [10101] which reduce the processing gain by $\log_{10}\left(\frac{30}{31}\right) = -0.1$ dB which is not significant compared to 8PSK.

$$N_{C5} = 5$$

$$\theta_{32PSK} = \frac{\pi}{N_{C5}} = \frac{\pi}{5}$$

$$V_I(t) = I(t).\,\mathrm{e}^{\mathrm{j}2\pi f_C t}$$

$$V_{Q1}(t) = Q_1(\mathrm{t}).\,\mathrm{e}^{\mathrm{j}(2\pi f_C \mathrm{t}+\theta_{32PSK})}$$

$$V_{Q2}(t) = Q_2(\mathrm{t}).\,\mathrm{e}^{\mathrm{j}(2\pi f_C \mathrm{t}+2\theta_{32PSK})} \tag{4-28}$$

$$V_{Q3}(t) = Q_3(\mathrm{t}).\,\mathrm{e}^{\mathrm{j}(2\pi f_C \mathrm{t}+3\theta_{32PSK})}$$

$$V_{Q4}(t) = Q_4(\mathrm{t}).\,\mathrm{e}^{\mathrm{j}(2\pi f_C \mathrm{t}+4\theta_{32PSK})}$$

$$V_{IQ5}(\mathrm{t}) = V_I(\mathrm{t}) + V_{Q1}(\mathrm{t}) + V_{Q2}(\mathrm{t}) + V_{Q3}(\mathrm{t}) + V_{Q4}(\mathrm{t})$$

$$V_{TX5}(\mathrm{t}) = \mathrm{Re}\left(V_{IQ5}(\mathrm{t})\right) + \mathrm{Im}\left(V_{IQ5}(\mathrm{t})\right)$$

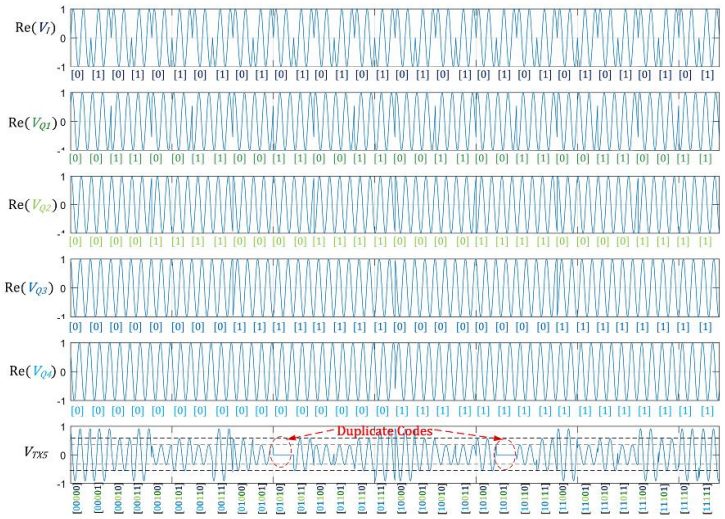

Figure 51 MCDSSS five channel 32PSK mixing (time domain)

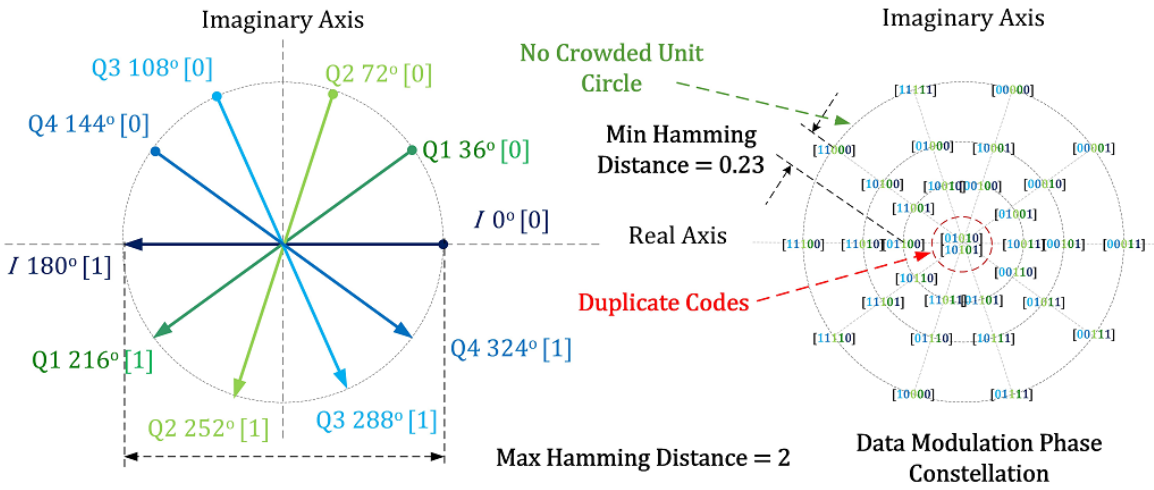

Figure 52 MCDSSS five channel 32PSK mixing (phasor diagram)

The 32PSK self-noise (L_{C5}) reduces the processing gain by 7.0 dB Eq.(4-29) (Figure 53).

$$L_{C5} = 10\log_{10}(N_{C5}) = 7.0 \text{ dB} \tag{4-29}$$

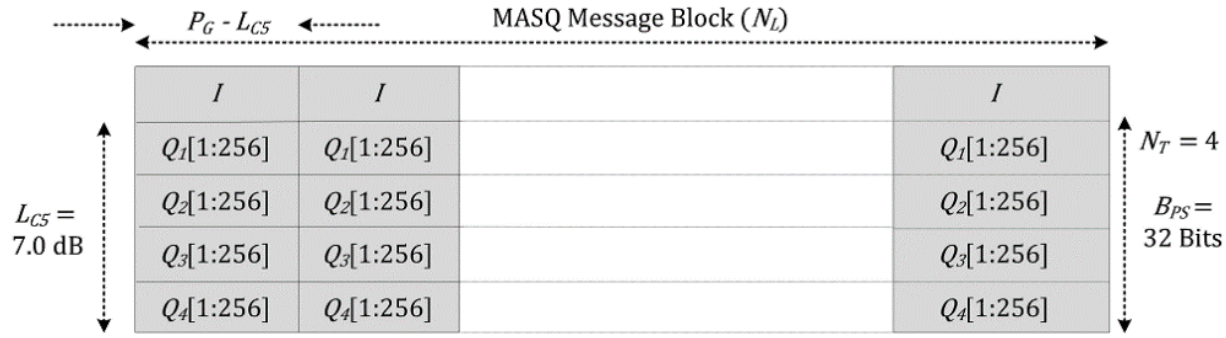

Figure 53 MCDSSS five channel 32PSK inter channel interference loss

The normalised hamming distance for 32PSK is $H_{C5} \approx 0.3$ Eq.(4-30).

$$H_{C5} \approx \frac{2\sin\left(\frac{\pi}{2N_{C5}}\right)}{H_{C1}} \approx 0.3 \tag{4-30}$$

4.3.12 MCDSSS Maximising Communication Range Optimisation

In the absence of processing gain ($P_G = 0$) the maximum communication range is independent of signal modulation such as MCDSSS, FSK, or Under Water Telephone (UQC) voice. Maximum communication range (R_{MAX}) is proportional to the maximum transmit source level (SPL_{MAX}) and minimum receiver noise floor (PSD_N) Eq.(4-31) (Figure 3). Maximising the transmitter communication range requires the maximising of the power amplifier SPL_{MAX} and acoustic projector directivity (D_{TX}). Maximising the receiver communication range requires the minimising of the hydrophone noise floor, maximising hydrophone directivity and maximising MCDSSS receiver sensitivity.

$$R_{MAX} \propto SPL_{MAX} + D_{TX} - PSD_N + D_{RX} - D_{TH} \tag{4-31}$$

4.4 MCDSSS Receiver

4.4.1 MCDSSS Receiver Reference (*I*) Channel Detector

Detection of a MCDSSS reference channel (ψ_I) is a function of the Doppler scale factor (D_S) and is the convolution of the receive signal (V_{RX}) with the reference signal (V_I) as described by equation (4-32).

$$V_I(\mathrm{t}) = I(\mathrm{t}).\, e^{-\mathrm{j}2\pi.f_C.D_S.\mathrm{t}} = I[\mathrm{floor}(B_M.D_S.\mathrm{t})].\, e^{-\mathrm{j}2\pi.f_C.D_S.\mathrm{t}}$$
$$\psi_I(\mathrm{t}) = V_{RX}(\mathrm{t}) \otimes V_I(\mathrm{t}) \equiv \left| \int_0^{\tau_{SY}} V_{RX}(\mathrm{t}) * V_I(\mathrm{t}-\tau)\mathrm{d}\tau \right| \tag{4-32}$$

4.4.2 MCDSSS Doppler Detector

The MCDSSS receive signal carrier and modulation bandwidth are subject to vessel and ocean induced Doppler shift. The MCDSSS Doppler detector consists of multiple MCDSSS receivers tuned to different Doppler shifted carrier frequencies ($f_{C_{DS}} = f_C.D_S$) and modulation bandwidths $\left(B_{M_{DS}} = B_M.D_S\right)$. The number of MCDSSS receivers (D_R) is a function of the min/max Doppler (D_M) and the Critical Doppler velocity (D_C) Eq.(4-33).

$$D_M = \pm 8 \text{ kn} \quad \text{(for MASQ Nominal)}$$
$$D_R = \frac{2D_M + 1}{D_C} \tag{4-33}$$

4.4.2.1 MCDSSS Doppler Scale Factor

MCDSSS signals are compressed or expanded in time in the presence of receiver, transmitter or ocean motion illustrated in Figure 24 and Figure 25. If the MCDSSS signal is compressed or expanded by more than the modulation bandwidth period ($\frac{1}{B_M}$) then the MCDSSS receiver will not detect the signal because of a misalignment of the spread spectrum code and the receive signal. Equation (4-34) describes the Doppler scale factor (D_S) as a function of the number of carrier frequency cycles (N_{CFC}) per modulation bandwidth period ($\frac{1}{B_M}$).

$$N_{CFC} = \frac{N_C.f_C}{B_M} \approx 1{,}200 \rightarrow 6{,}800$$
$$(N_C = 1023, f_C = 10 \text{ kHz}, B_M = 1.5 \text{ to } 48 \text{ kHz for MASQ})$$
$$D_S = \frac{N_{CFC}}{N_{CFC} \pm 1} \approx 0.9992 \rightarrow 1.0008 \quad \text{(for MASQ)} \tag{4-34}$$

4.4.2.2 MCDSSS Critical Doppler Velocity

The critical Doppler velocity (D_C) is the maximum acceleration or deceleration allowed per MCDSSS symbol period before the MCDSSS receiver can no longer detect a MCDSSS signal Eq.(4-35).

$$D_C = c(D_S - 1) \approx 0.6 \text{ ms}^{-1} \cong 1.2 \text{ kn} \quad \text{(for MASQ)} \tag{4-35}$$

4.4.3 MCDSSS Receiver Telemetry (Q) Channel Detector

Detection of a single channel MCDSSS telemetry data (Sy_C) is the time domain correlation of the signal received (V_{RX}) at time (t_{DETECT}) against 256 telemetry (Q_C) codes Eq.(4-36). The telemetry and reference symbols are time aligned and the telemetry receiver relies on the reference channel receiver to locate the telemetry signal in time and to correct for Doppler.

$$\psi_Q^2[\mathrm{n}] = \left| \int_0^{\tau_S} Q_{\mathrm{C}}(\tau, \mathrm{n}).\, \mathrm{e}^{-j(2\pi.f_C.\tau + C_Q.\theta_{TX})} * V_{RX}(t_{DETECT} - \tau) d\tau \right|^2$$
$$Sy_C = \left| \mathrm{MAX}\left(\psi_Q^2[\mathrm{n}]\right) \right|_{\mathrm{n}=0}^{256-1} \tag{4-36}$$

The quality of the telemetry signal SNR_Q is the ratio of the loudest correlation magnitude to the second loudest correlation and not to the RMS noise floor as used by the MCDSSS reference detector Eq.(4-37).

$$SNR_Q[\mathrm{n}] = 10 \log_{10} \left(\frac{\mathrm{MAX}\left(\psi_Q^2[\mathrm{n}]\right)}{\mathrm{SECOND}\left(\psi_Q^2[\mathrm{n}]\right)} \right) \tag{4-37}$$

In the absence of in-band interference ($N_M = 0$) the telemetry decoder SNR_Q is approximately 2 dB lower than the transmit margin Eq.(4-14). Figure 55 and Figure 54 illustrate the shallow water MCDSSS telemetry detector correlation for a 50 baud transmission of the ASCII alphabet with the measured $SNR_Q \approx 12$ dB which is 2 dB lower than the transmit margin ($M_{TX} = 14$ dB).

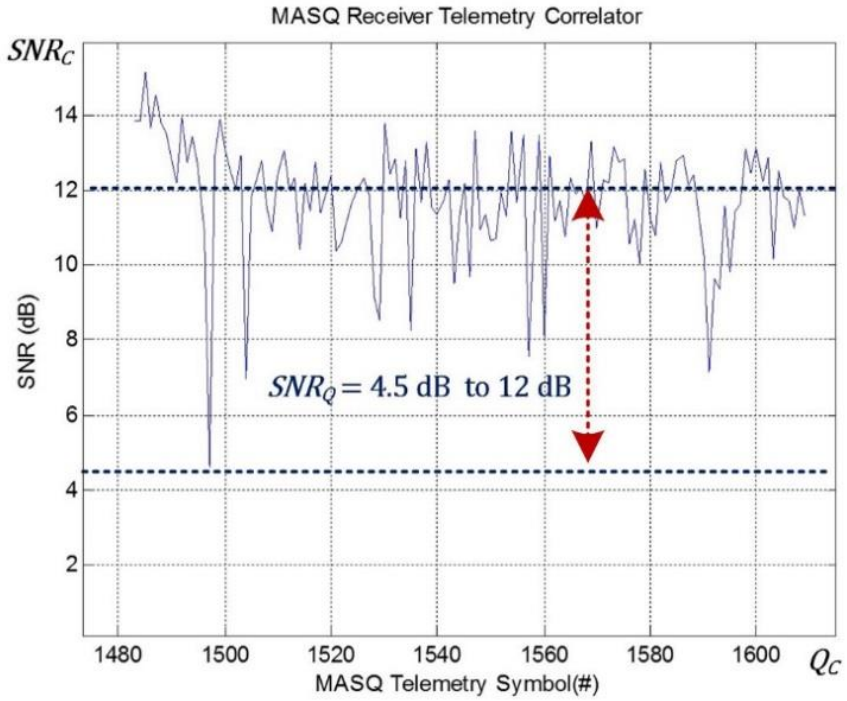

Figure 54 High SNR MCDSSS telemetry (Q) detector SNR

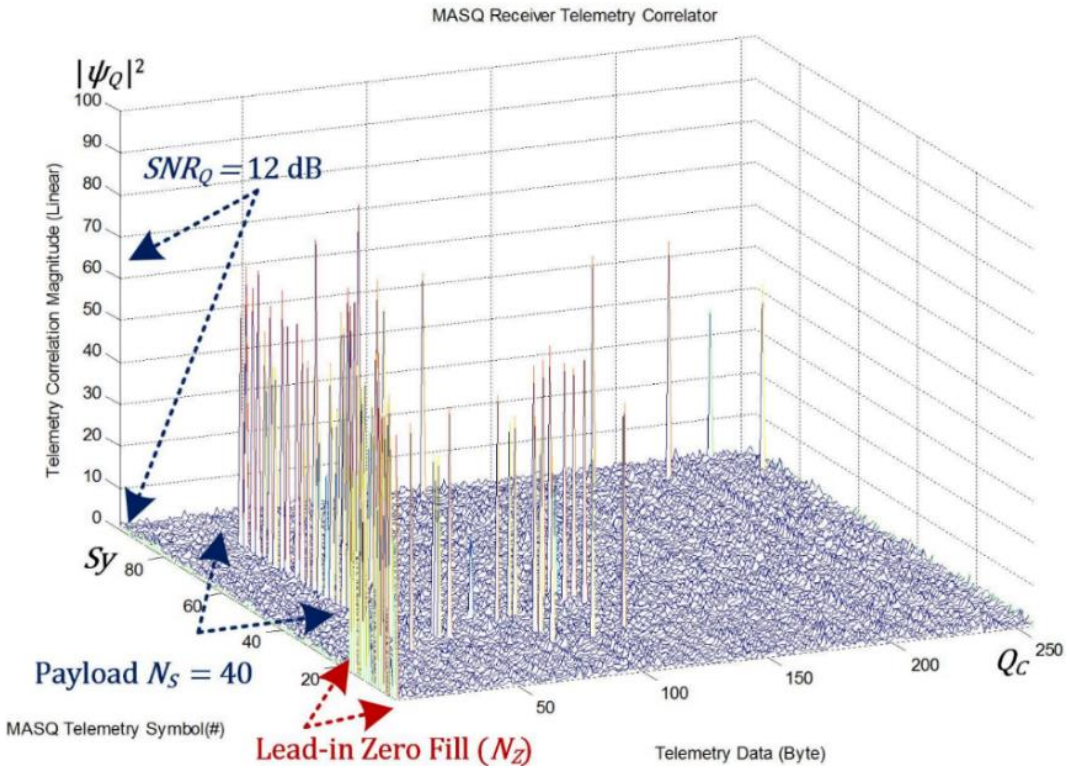

Figure 55 High SNR MCDSSS telemetry (*Q*) detector waterfall

4.4.4 Multipath Bounded BEE and Maximum Baud Rate

Figure 56 illustrates an example of a high ambient noise $N_L = 63$ symbol message MCDSSS receiver correlation waterfall plot which is characterised by a single strong slant range (R_S) correlation pulse per MCDSSS symbol followed by an intermittent and weak shallow water multipath signal (R_M). The multipath reverberation signal is not clearly defined for high ambient noise communication however the weak multipath signal is a significant driver of bit energy efficiency.

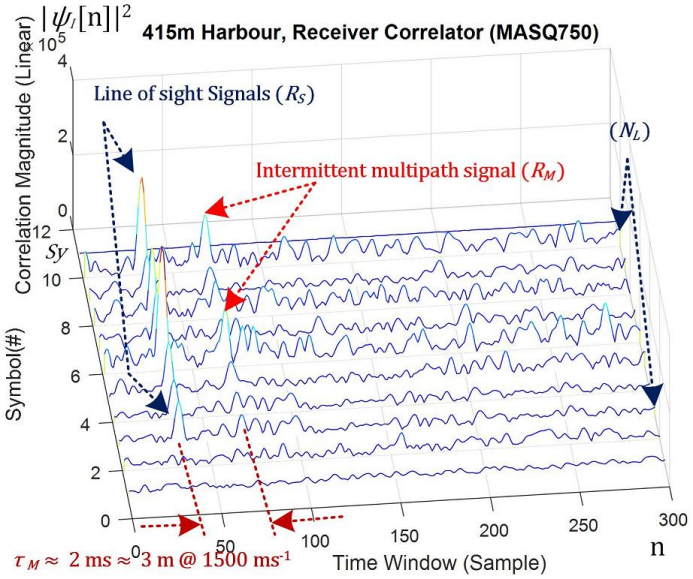

Figure 56 MCDSSS 750 baud reference (*I*) correlation (shallow water weak multipath)

Figure 57 illustrates a low ambient noise $N_L = 127$ symbol 200 baud message MCDSSS receiver correlation magnitude in the presence of strong shallow water multipath signals ($N_M > 0$), which are characterised by a multipath delay of $\tau_M = 6$ ms ≈ 9 m Eq.(4-38).

$$\Delta t_N = \mathrm{n_M} - \mathrm{n_S} \quad \text{(Correlation time window sample difference)}$$
$$\tau_M = \frac{\Delta t_N . \tau_{sy}}{S_{CB} + 1} \tag{4-38}$$

The MCDSSS receiver detects multipath signals as in-band noise (PSD_M) and reduces the processing gain by approximately the number of multipath signals (N_M) Eq.(4-39).

$$N_S = 1, \qquad N_M = 0 \rightarrow 4$$
$$PSD_M \approx 10\log_{10}(N_S + N_M) \approx 0 \text{ dB} \rightarrow 7 \text{ dB} \tag{4-39}$$

Compared to the high ambient noise signal (Figure 56) the low ambient noise (Figure 57) with a pronounced multipath signal (R_M) is not a significant driver of BEE, however loud multipath signals generate inter-symbol interference limits the maximum baud rate. Inter-symbol interference limited maximum baud rate is generally independent of transmit source level (SPL_{MIN} to SPL_{MAX}) because the multi-path interference is louder than the ambient noise.

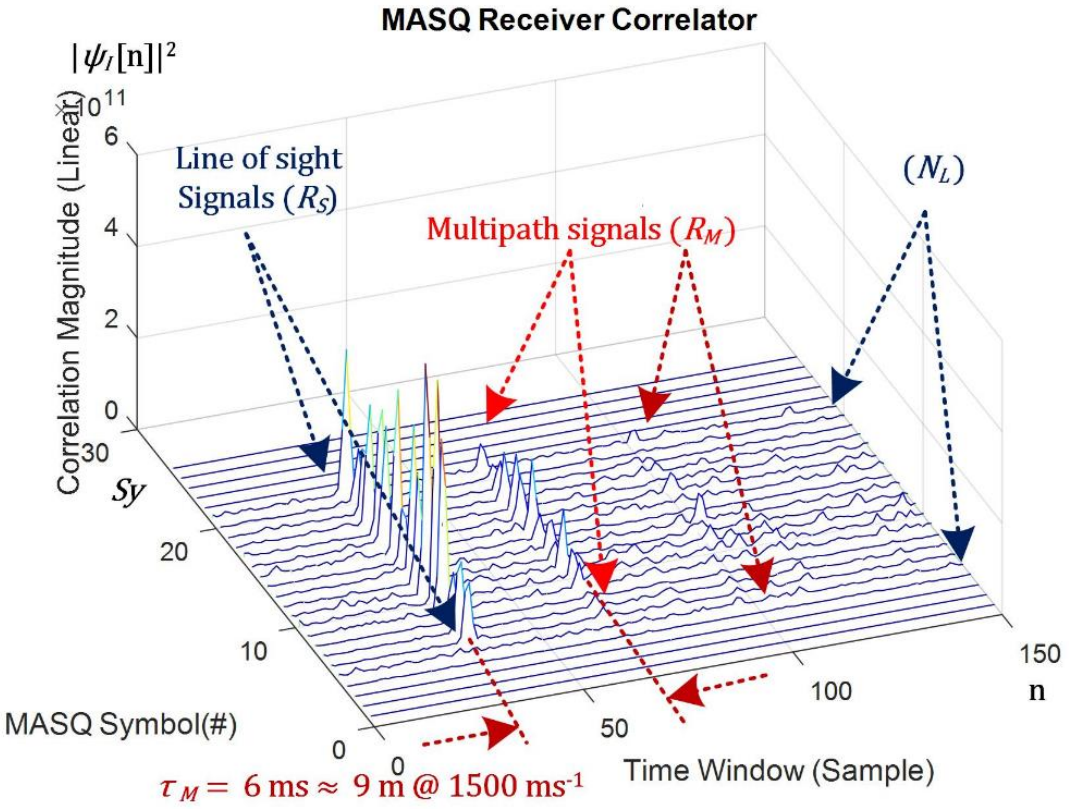

Figure 57 MCDSSS reference (*I*) correlation (shallow water with multipath)

4.4.5 Multipath Reverberation Envelope

A DSSS recevier will not detect multipath reverberation signals when the multipath magnitude drops below the ambient noise floor by more than the transmit margin ($\psi_M < PSD_A - M_{TX}$). The Multipath Reverberation Envelope (τ_{MPE}) period, excluding the bottom sediment multipath signal, is the time difference between the slant range signal and the last multipath signal above the detection threshold (D_{TH}) and is proportional to communication range (R_S) ocean ducting depth (R_{DD}) aspect ratio Eq.(4-40) (Figure 58).

$$\tau_{MPE} \propto \frac{R_S}{R_{DD}} \qquad (4\text{-}40)$$

$$\tau_{MPE} \cong \mathrm{MAX}(t_{RX}[\mathrm{n}] - t_{RX}[0]) \text{ for } \psi_M[\mathrm{n}] < D_{TH}$$

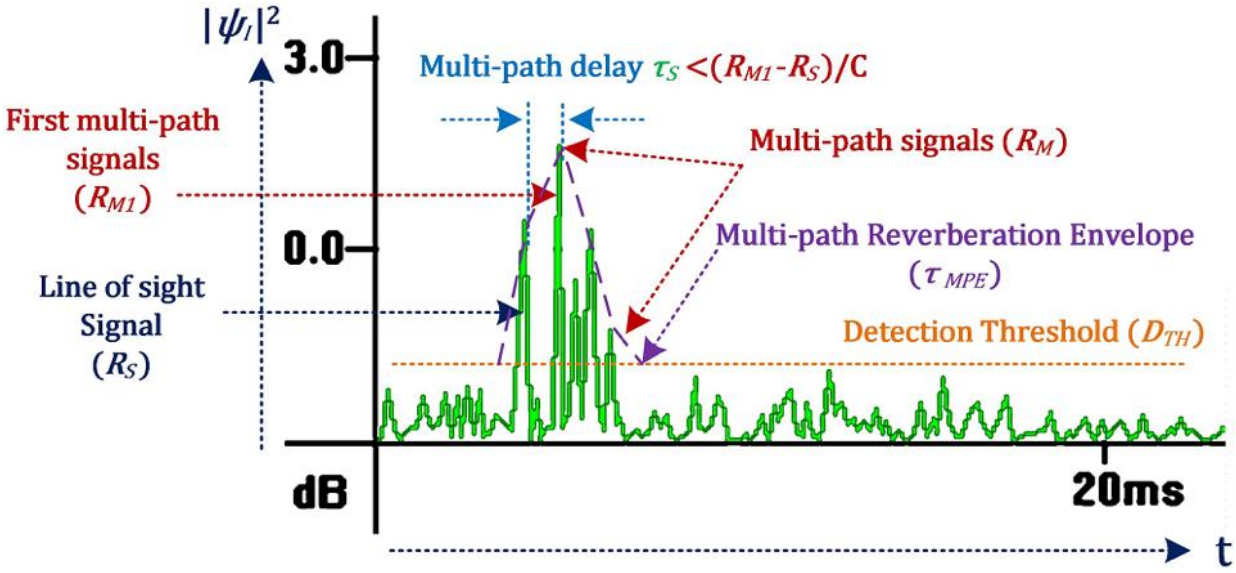

Figure 58 Multipath reverberation envelope

An estimate of the channel multipath reverberation envelope ($\overline{\psi_I^2[\mathrm{n}]}$) can be derived by summing the receiver correlation for all message symbols, Eq.(4-41), which can be used to determine the most covert baud rate as a function of BEE minimum transmit source level (SPL_{BEE}) Figure 169, Figure 186, Figure 219 and Figure 225.

$$\overline{\psi_I^2[\mathrm{n}]} \approx \sqrt{\sum_{\mathrm{m}=0}^{\mathrm{Sy}-1} |\psi_I^2[\mathrm{n},\mathrm{m}]|^2} \qquad (4\text{-}41)$$

4.4.5.1 Maximum Reverberation Envelope Bounded Baud Rate

A multipath reverberating environment limits the maximum hydro-acoustic baud rate (Br_{MAX}) when the multipath reverberation envelope period (τ_{MPE}) exceeds the symbol period (τ_{SY}), inducing inter-symbol interference Eq.(4-42).

$$Br_{MAX} \propto \tau_{MPE} < \tau_{SY} \qquad (4\text{-}42)$$

4.4.5.2 Minimum Reverberation Envelope Bounded Peak BEE

A multipath reverberating environment limits the peak bit energy efficiency (BEE_{PEAK}) to the acoustic baud rate (Br_{BEE}) with the lowest multipath reverberation envelope period (τ_{MPE}) Eq.(4-43).

$$\text{MIN}(\text{P}_{\text{TX}}) \propto Br_{BEE} \propto BEE_{PEAK} \propto \text{MAX}(BEE) \propto \text{MIN}(\tau_{MPE}) \tag{4-43}$$

4.4.6 Peak Bit Energy Efficiency

From nonlinear equation (3-5) and for fixed slant ranges BEE is proportional to baud rate (Br) or ($BEE \propto Br$). For SS modulation baud rate is proportional to modulation bandwidth (B_M) or ($Br \propto B_M$). As the modulation bandwidth increases, the effects of frequency dependant environmental absorption loss (L_A) will increase the total propagation loss ($L_T \approx L_S + L_A \approx 20\log_{10}(R_S) + L_A$) i.e. ($B_M \propto \frac{1}{L_A}$). As the communication range increases, linear environmental absorption losses will dominate the slant range spherical spreading losses. Therefore BEE is proportional to baud rate and inversely proportional to slant range. For SS modulation an increase in baud rate will increase the modulation bandwidth which will be hard limited by the transmit projector maximum transmission bandwidth and BEE will not uniformly increase as a function of the multipath bounded maximum baud rate. Therefore SS modulation BEE is not a linear function of slant range (R_S) as described by equation (4-44) derived from equation (3-5) with variables $\text{P}_{\text{TX}}, R_{REF}$ and $\bar{L}_A$ set as constants.

$$\text{BEE} \propto Br \times R_S^2 \times 10^{Rs} \tag{4-44}$$

4.4.7 Missing or Corruption Message Re-Transmission Optimisation

The speed of sound in the ocean is approximately $c = 1{,}500\ \text{m.s}^{-1}$ and a long-range ($R_S \rightarrow$ 10 km) underwater communication link imposes a 15 second propagation delay. For short messages ($N_L = 15$) of less than 1 second, the long propagation delay (t_S) can account for more than ten times ($10 \times N_L \times \tau_{SY} < t_S$) the communication transmission overhead. Bidirectional communication doubles the propagation delay overhead ($t_S = \frac{2R_S}{c}$) to 30 seconds. Bi-directional transaction communication protocols such as TCP/IP, which was used on the initial short range AUSSNet deployment (Appendix O), are not practical for long-range underwater communication because of the excessive turnaround delay. The firmware version 5.x MASQ communication protocol has deprecated TCP/IP and no longer use message transaction handshaking in the OSI transport layer 4. Acknowledgment of a successful transmission and reception of a MCDSSS messages is handled by the OSI application layer 7 low latency communication transaction (Figure 59). The source modem inserts a time stamp or sequence number in the user data payload, and the destination modem uses the time stamp and/or sequence number to detect a missing message and requests the missing message be re-transmitted. As missing or corruption message re-transmission modifications are handled by the user OSI application layer 7, no algorithm optimisations were applied to firmware version 6.0.

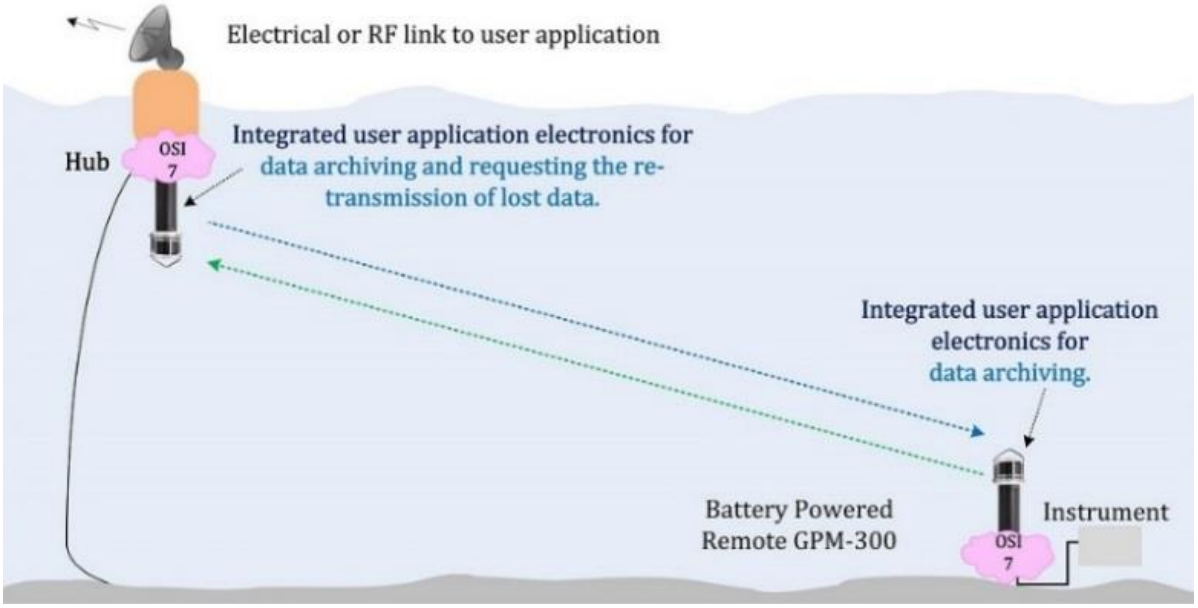

Figure 59 OSI 7 missing or corruption message re-transmission

4.5 Summary

DSSS modulation compresses the receiver correlation pulse with sufficient resolution to resolve multipath and improves navigation and range measurement accuracy. Multiple DSSS channels are combined to generate a single MCDSSS signal which increases the symbol period to counter inter-symbol interference. In the presence of loud multipath, the selection of MCDSSS spreading codes with good circular cross correlation properties is important for maximising transmit margin. The MCDSSS transmit margin provides resilience to multipath and inter-symbol interference with decreasing baud rate and increasing number of telemetry channels. The MCDSSS transmit margin also provides covert communication which improves with decreasing baud rate and decreasing number of telemetry channels. MCDSSS modulation incurs high receiver computational load for detection of the SS reference channel, decoding SS telemetry channels and countering Doppler.

5 MCDSSS COMMUNICATION OPTIMISATIONS

5.1 Introduction

This chapter provides a summary of the MCDSSS communication algorithm and engineering optimisations applied by the candidate to improve message reliability (MR).

5.2 Open Systems Interconnection Model

The seven layers of the International Standards Organisation (ISO) Open Systems Interconnection (OSI) model [155] are used to categorise communication hardware, software and algorithm optimisations. Figure 68 to Figure 112 software defined radio block diagram OSI layers have been colour coded as per Table 2.

Table 2 OSI model layers

OSI Level	Definition	MCDSSS Implementation
7	**Application** (User)	
6	**Presentation** (Encryption Data Compression / Decompression)	
5	**Session**	Public and Private Encryption codes (C) Communication Channels
4	**Transport**	Variable Length Message Data Exchange
3	**Network Layer**	Source to Destination Packet Routing
2	**Data Link**	Forward Error Correction, CRC, Block Format
1	**Physical**	MCDSSS

5.3 MCDSSS Transceiver Reliability Considerations

In the absence of power and mechanical design limitations, a reliable brute force MCDSSS transceiver can be implemented with +1,000 lines of Matrix Laboratory (MATLAB) code and an array of rack-mounted computer servers. The purpose of this chapter is to highlight the software and hardware complexities that are primarily driven by electrical, size and weight constraints. Maximising message reliability via algorithm optimisation exposed numerous subtle software and hardware bugs that were masked by the MCDSSS processing gain. Rigorous hardware and software testing was required to increase the message reliability to +99%. Algorithm performance improvements were measured using two (R_S = 0.2 m) air coupled L3 Oceania General Purpose Modems (GPM300) and tests were carried out from baud rate minimum to baud rate maximum, transmit source level

minimum to transmit source level maximum with performance compared against legacy firmware. The 0.2 m air coupling test excludes multipath reverberation, frequency dependant path losses and MCDSSS receiver noise floor in the presence of a $SS4$ equivalent MCDSSS transmitter Quiescent noise floor. Algorithm performance improvements were measured using a ($R_S = 22$ m) air corridor with two GPM300 modems. The 22 m air corridor excludes MCDSSS transmitter noise floor, frequency dependant attenuation and ocean ambient noise effects in the presence of a $SS0$ equivalent MCDSSS receiver noise floor. The 22 m air corridor tests measured multipath reverberation bounded maximum baud rate for all transmit source level levels (SPL_{MIN} to SPL_{MAX}). The performance measurements were compare against historical 22 m air corridor tests of GPM300 modems running legacy firmware. Algorithm performance improvements were validated in the L3 hydro-acoustic tank using two GPM300 modems across a 2 m communication range. The hydro-acoustic tank induces extreme multipath interference and the GPM300 modem generates loud $SS10$ transmitter induced self-noise. Hydro-acoustic tank tests measured multipath reverberation bounded maximum baud rate, channel geometry bounded peak bit energy efficiency and all transmit source levels (SPL_{MIN} to SPL_{MAX}). The performance measurements were compared against historical tank tests of a GPM300 running legacy firmware. Algorithm performance improvements were validated with a harbour test deployment in a short ($R_S \approx 400$ m) range and shallow water ($R_D \approx$ 3 m to 5 m) depth channel using multiple GPM300 modems. The short 400 m range shallow water harbour exhibits $SS2$-4 loud out of band anthropogenic noise, high multipath interference, medium path loss, excludes frequency dependant attenuation and excludes sound velocity refraction. The performance tests measured channel geometry bounded bit energy efficiency at all baud rates (Br_{MIN} to Br_{MAX}) and all transmit source level levels (SPL_{MIN} to SPL_{MAX}). The performance measurements were compared against historical harbour tests of GPM300 modems running legacy firmware. The final Br_{MAX} and BEE_{PEAK} performance tests required a carefully designed sea trial in a controlled environment with the following characteristics:

1. Approximately 10 km communication range to induce high path loss (L_S) and high frequency dependant attenuation (L_A).
2. Low wind and shallow 5 m to 20 m water depth to induce high multipath reverberation (R_M).
3. High shipping traffic and boat sonar operations to generate anisotropic anthropogenic noise (PSD_A).
4. Very high isotropic ambient noise (in-shore snapping shrimp) ($PSD_A > SS5$).
5. Modems deployed next to highly reflective surfaces such as hard concrete walls and cylindrical concreate pylons to induce additional multipath reverberation (R_M).

5.3.1 Software Defined Radio Reliability

Figure 62 to Figure 112 illustrates the internal structure of the MCDSSS transceiver software defined radio. Improving the message reliability required fine tuning of multiple control systems using a channel simulator and recordings of MCDSSS signals in extreme ocean conditions. Achieving acceptable software reliability consumed a significant proportion of this thesis analysis. Acceptable MCDSSS control system reliability was achieved by implementing a configurable MCDSSS generic transceiver and using test

data from multiple DSSS communication protocols (i.e. MASQ, HAIL, MK84). The MCDSSS generic transceiver software is deployed on the GPM300 modem, and on GPM300Windows running on an industrial PC and ELAC UT3000 underwater telephone [152]. The MCDSSS generic transceiver software is designed to run on a low power 16 bit fixed point DSP chip with limited hardware resources. Low power DSPs are not equipped with memory management units, operating systems or advanced software development tools that are available on PCs. DSPs provide single clock cycle complex arithmetic multiply and accumulate operations with simultaneous data and coefficient memory read/write. To harness the full DSP computational power, the signal processing algorithms are implemented using hand coded machine language assembler. DSPs achieve single clock cycle performance using deep pipelines, which must be manually pre-loaded and manually post-unloaded and can be a source of subtle software errors which compromise long-range message reliability.

To validate DSP assembler signal processing algorithms high-level C and C++ functional equivalent unit tests were required which had an additional benefit of being deployable on general purpose computers (PC). The MCDSSS generic transceiver software implements $N_{DSP} > 1{,}000$ signal processing functions, however unit testing single functions provides limited reliability validation as complex signal processing algorithms are constructed from multiple signal processing functions. The number of unit test functions increases by approximately the square of the number of aggregated functions and the number of unit tests ($N_{UT} \approx N_{DSP}^2 > 1{,}000{,}000$) and become impractical to implement.

Figure 60 illustrates the GPM300Windows transceiver, which was developed by the candidate and is deployed on PC hardware. The GPM300Windows transceiver was extensively upgraded for use as the primary analysis tool for this thesis to provide the following additional analysis functions:

1. Real time, full speed and event triggered hydro-acoustic file playback.
2. Time domain impulse response display.
3. Time domain deconvolution telemetry decoder display.
4. Telemetry alert detector display.
5. False colour spectrogram.
6. Signal to noise, receiver PSD, Doppler and receiver lock tracking display.
7. Functional equivalent and National Electrical Manufacturers Association (NMEA) compatibility with MCDSSS compatible platforms.
8. Real time low latency audio performance for communication with GPM300.

The GPM300Windows transceiver has the advantage of providing real-time waveform probing of the MCDSSS transceiver signal processing which is not available on the DSP platform.

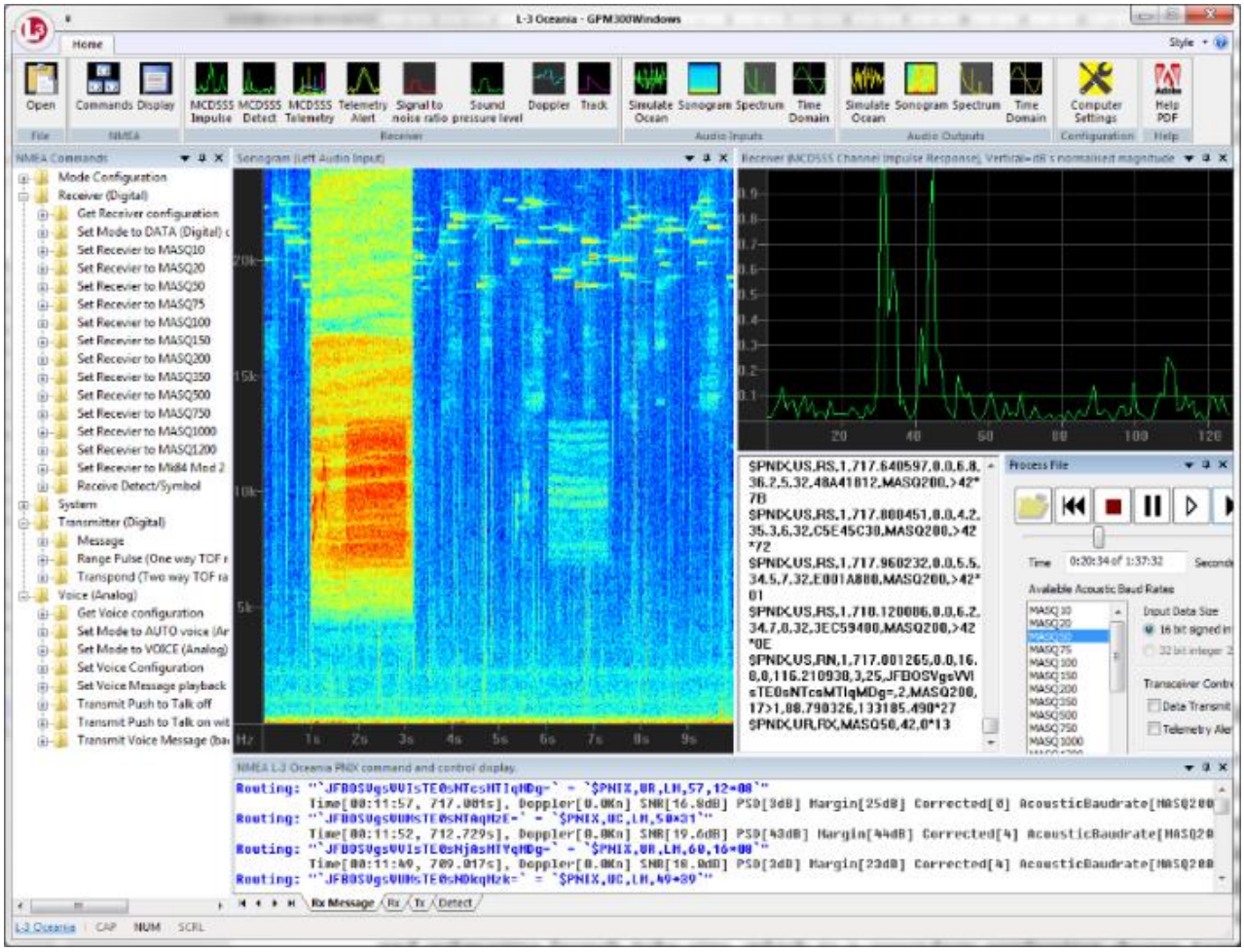

Figure 60 Thesis primary analysis tool L3 Oceania GPM300Windows (candidate coded)

The command line version of GPM300Windows provided a more robust automated software testing framework than unit testing and was extended to provide the following additional function for uses in this thesis:

1. Correlation waveform extraction for the MATLAB generation of 3D multipath plots.
2. Telemetry receiver waveform extraction for the MATLAB generation of 3D and 2D deconvolution plots.
3. Doppler domain waveform extraction for the MATLAB generation of 3D.
4. Batch testing performance metric to automatically detect failing control system optimisations.

Many hours of hydro-acoustic recordings, collected over 15 years, were batch processed to provide automated software stress tests of alternative control system algorithm candidates. Additional hydro-acoustic recordings were acquired from more extreme environments off the Western Australian coast to facilitate further message reliability stress testing (Appendix M and Appendix N) and to ensure that the algorithm optimisations had not been over fitted to the failing signal database.

5.3.2 Hardware Pressure Housing Constraints

The cost of machining pressure housing cylinders from solid rod is uneconomic. When designing hydro-acoustic modem hardware it is desirable to use ϕ90 mm (ϕ3.5 ") Internal Diameter (ID) standard titanium, aluminium or plastic tubes as illustrated by Figure 61. All electronics and electrical infrastructure Outer Diameters (OD) must have a nominal ϕ80 mm OD or less to provide a minimum 2.5 mm clearance when installed in a ϕ90 mm ID pressure housing. The ϕ80 mm OD electronic size limit is also imposed by the payload size of sonobuoy electronics, aircraft launch tube and submarine launch tube maximum size which is a secondary application design target. The ϕ80 mm OD limits the maximum size of the matching network and power amplifier which limits the transmit source level to approximately $P_{PA} \approx 300$ W and the PZT transducer to 100 W. The ϕ80 mm OD also limits the maximum size of the DSP, which requires the implementation of memory and power efficient software. The electronics stack maximum ϕ80mm OD is by far the most significant driver of hardware/software complexity which impacts the message reliability.

5.3.3 Message Reliability Dependant Hardware Issues

L3 Oceania hydro acoustic tank measurements of broad-band MCDSSS performance show less than $\epsilon_{PZT} < 50\%$ efficient radially polarized PZT transducers [139], less than $\epsilon_{MN} < 95\%$ efficient broad-band matching networks and $\epsilon_{TX} = 85\% \rightarrow 95\%$ 300 W efficiency power amplifiers. The total transmitter efficiency is $\epsilon_{TX} = \epsilon_{PZT} \times \epsilon_{MN} \times \epsilon_{TX} = 35\% \rightarrow 45\%$. When transmitting at the maximum source level of $SPL_{MAX} = 190$ dB re 1 µPA @ 1 m, requiring 300 W transmit power, 100 W of acoustic power is radiated into the ocean and the modem electronics stack is subject to 300 W − 100 W ≈ 200 W of heat, RF interference and mechanical vibration. The most common sources of high power SS modem electronics sub-system failure are electro-mechanical connections which are subjected to extreme mechanical vibration, electromagnetic radiation and heat associated with 190 dB re 1 µPa @ 1 m transmit source levels. The predecessor of the GPM300 was a ϕ150 mm OD, five circuit board electronic stack with five electrical interconnection harnesses. The GPM300 implements a three circuit board transceiver with a reliable 0.1" pitch digital and analog ribbon cable bus as illustrated in Figure 61. The prototype ϕ80 mm OD GPM300 transceiver used a commercial DSP mezzanine circuit board with fine pitch electrical connectors and multiple fine pitch ball grid array chips which proved to be unreliable when subjected to continuous hydro-acoustic induced vibration. The GPM300 transceiver was re-engineered to remove all fine pitch connectors and fine pitch Ball Grid Array (BGA) chips and use a single medium pitch BGA DSP. Subsequent long term BGA failure analyses required that the next generation of low power TPC design use a non BGA DSP. The prototype GPM300 electrical interconnection Field Programmable Gate Array (FPGA) was replaced with hardware/software and the number of electronic components minimised, which reduced manufacturing costs and improved reliability. Minimising the number of circuit boards and electrical connectors has provided a reliable hardware platform. In the presence of advanced algorithms, high technology software and complex electronics, the importance of using reliable low technology electrical connections cannot be overstated.

As firmware version 6.0 MR improved, more stress testing was applied which uncovered an obscure manufacture “control system instability” bug in the micro controller which required an external hardware fix (Figure 114 left green). As MCDSSS transceiver performance was improved by approximately 10 dB, two instances of high speed ADC clock signals capacitively coupling across marginal DSP BGA electrical connection were identified. The BGA failure had the effect of increasing the receiver phase noise that was previously masked by the MCDSSS processing gain, requiring the disposal of two Transceiver Processor Cards (TPC) that had previously passed factory Quality Assurance (QA) testing using legacy firmware version 5.5 but failed with higher receiver performance firmware version 6.0 (Figure 116 left green). The next generation TPC is in the process of being redesigned to replace all BGA parts with high reliability components where all circuit board components can be hand soldered to improve hardware related message reliability.

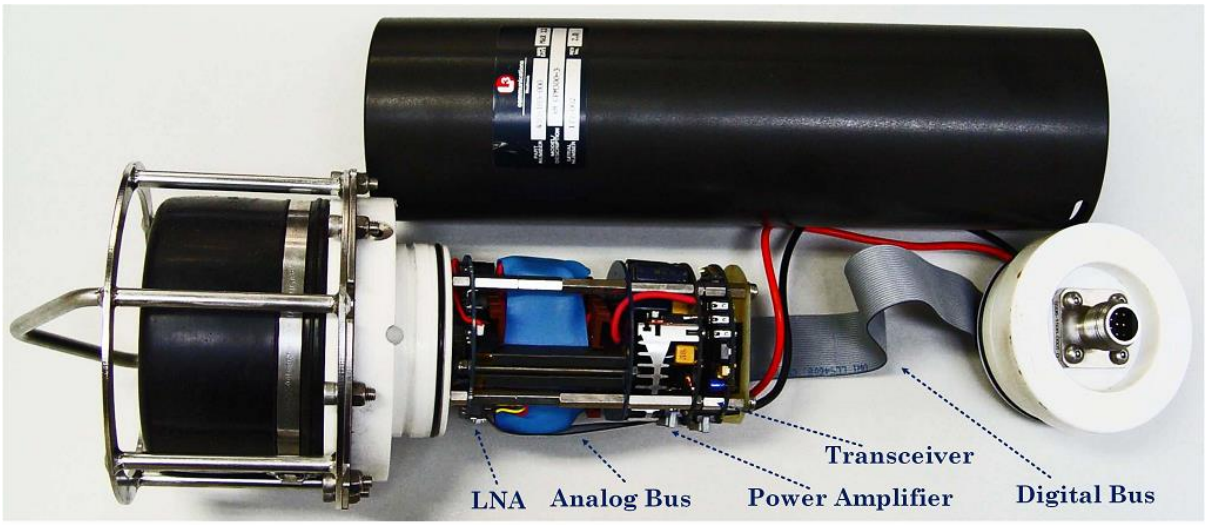

Figure 61 L3 Oceania GPM300 low tech reliable analog & digital bus (candidate design)

5.4 MCDSSS Communication Control System Optimisations

MCDSSS hydro-acoustic transceivers are implemented using multiple feedback control systems. In operation, the feedback control system stability can be compromised by external factors such as multipath reverberation, multipath self-noise, anisotropic anthropogenic noise, high ambient noise, isotropic wind / rain / biological noise and highly impulsive snapping shrimp noise emissions that are ubiquitous, particularly in shallow waters. The stability of a feedback control system can also be compromised by internal factors such as the electrical noise floor, saturation to ground, saturation to the power supply rails, or power supply interruptions (Figure 62). Subtle algorithm flaws, hardware faults and software bugs can be masked by the DSSS processing gain and only become evident during harsh or long-range communication.

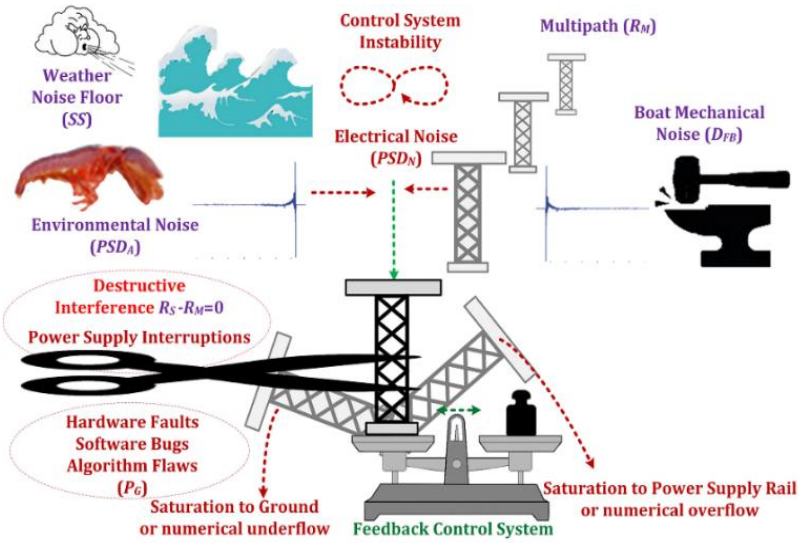

Figure 62 Feedback control system hydro-acoustic stability

The MCDSSS generic transceiver is implemented using interdependent control systems numbered ① to ⑩ (Figure 63). The MCDSSS sea trial measurements demonstrate that a MCDSSS performance improvement gain in one control system may result in a performance degradation in another control system when operated in environments with different noise signatures. The key to achieving near 100% message reliability is applying appropriate stabilisation algorithms to multiple feedback control systems.

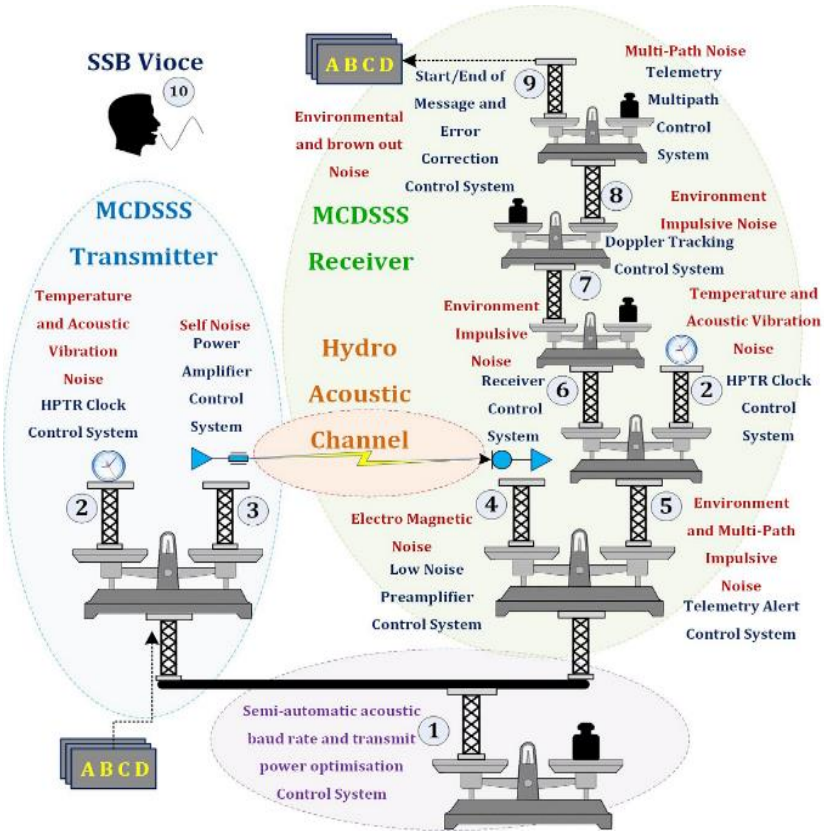

Figure 63 MCDSSS generic transceiver hierarchical control systems

Figure 64 illustrates the MCDSSS transceiver high level block diagram with one algorithm modification applied to the high level block diagram control system ①. Figure 67 illustrates the MCDSSS transmitter block diagram where algorithm and engineering optimisations were only applied to linear high speed signal processing control systems ③ and ⑩. Figure 79 illustrates the MCDSSS receiver block diagram where algorithm and engineering optimisations were applied to OSI layer control system ⑦, linear high speed processing control systems ⑧, ⑩ and non-linear control systems ⑥, ⑦, ⑧ and ⑨. Figure 104 illustrates the MASQ telemetry alert receiver block diagram where high level control system ④ and non-linear control system ⑤ were replaced. In summary the majority of the performance gains were applied in the non-linear control systems ⑤, ⑥, ⑦, ⑧ and ⑨. The majority of the non-linear control system algorithm, communication protocol, software and hardware interventions either failed, induced a performance degradation in other control systems or decreased the message reliability for sea trial data not targeted for performance improvement. Only the algorithm and engineering optimisations that resulted in significant performance improvements are presented in this chapter.

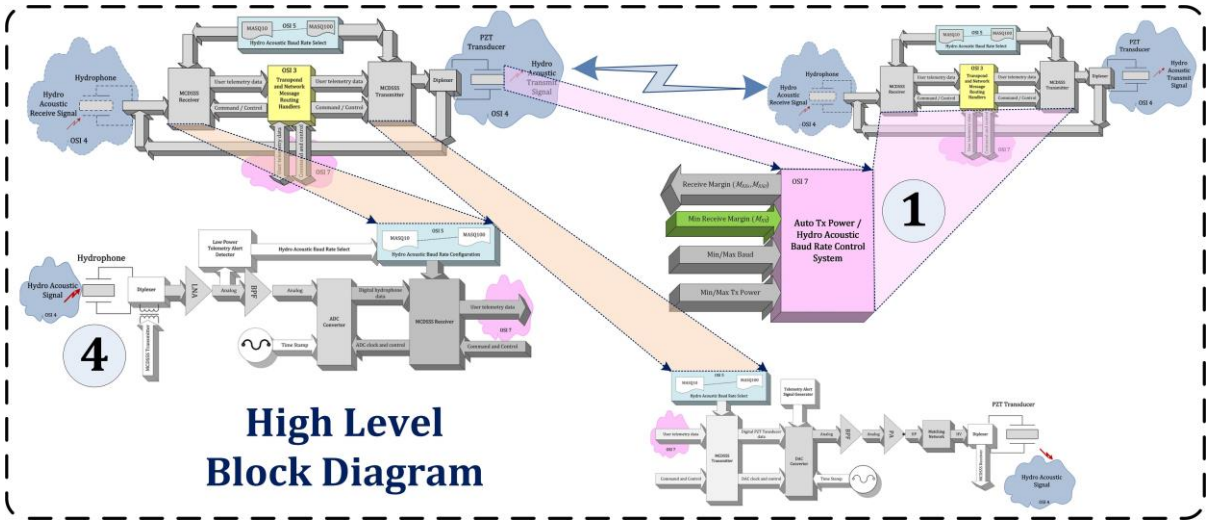

Figure 64 MCDSSS transceiver high level block diagram (optimisations green)

5.5 MCDSSS Modulation Optimisations

5.5.1 Telemetry (*Q*) Circular Cross Correlation Property Optimisation

Selecting spreading codes based on cross correlation properties described from chapter 4.3.5 to chapter 4.3.7 is not optimal in the presence of multipath reverberation because time delayed echoes may generate louder cross correlation magnitudes than the slant range signal (Figure 25). In the presence of loud multipath reverberation circular cross correlation properties provide a more robust selection of spreading codes Eq.(5-1).

$$\psi_X[\mathrm{n}] = \left|\left|10\log_{10}\left(\left|C_{\mathrm{m}} \otimes C_{\mathrm{n}}[\mathrm{MOD}(\mathrm{q}, N_C)]\right|\right)\right|_{\mathrm{n}=1}^{S_{CB}}\right|_{\mathrm{q}=1}^{N_C} \quad (5\text{-}1)$$

$$P_X = \text{MAX}(\psi_X) - \text{SECOND}(\psi_X) = 0 \rightarrow 6 \text{ dB}$$

Figure 65 illustrates the order $S_{CB} = 10$ PRN circular cross correlation properties. Of 7,000 PRN pairs, with good cross correlation properties, less than 3,000 pairs provide a circular cross correlation property greater than 5 dB. The MASQ PRN preferred pair 5.5 dB cross correlation property can be improved to 6 dB. A firmware version 6.x variant of MASQ MCDSSS is currently being deployed to support up to 300 communication channels with a 6 dB robust circular cross correlation property.

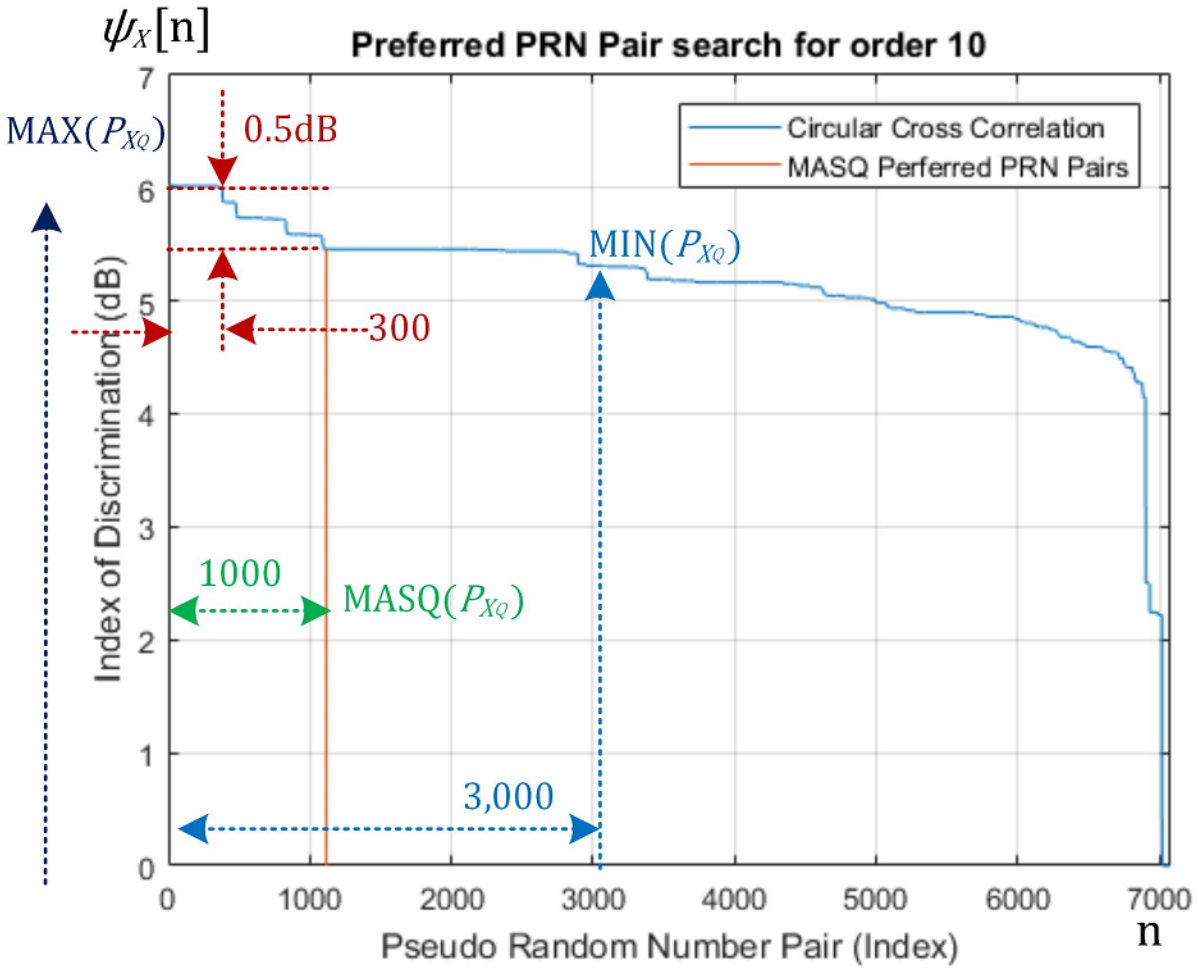

Figure 65 Telemetry (Q) circular cross correlation properties

5.5.2 MCDSSS Transceiver Time Synchronisation

MASQ transceivers support navigation, range and absolute receive power measurements using multi-user one way time of flight measurements using a clock with a low drift Time Error (t_e) rate of better than 10^{-9} second per second, low phase noise and a low power oscillator which translates to an absolute range accuracy drift rate of 0.25 m per 2 days Eq.(5-2). The absolute Frequency Error (f_e) accuracy of oven controlled oscillators are no better than 10^{-7} and require the frequency offset to be measured every 2 days, using the L3 Oceania hydro-acoustic time measurement protocol to lock the oscillator to GPS time.

$$R_{ABS} \geq R_S + c \times t_e \times \tau \geq 0.25 \text{ m for } \tau > 2 \text{ days} \qquad (5\text{-}2)$$

The L3 Oceania High Precision Timing Reference (HPTR) control system ② provides a minimum timing accuracy of less than $\varepsilon_{HPTR} < 1 \times 10^{-9}$ [149], typically less than $\varepsilon_{HPTR} < 5 \times 10^{-10}$, with a power consumption of less than $P_{HPTR} < 200$ mW (Figure 66). For a range accuracy of better than $\Delta R_S < 0.25$ m the HPTR must be re-synchronised to GPS every $\tau_{HPTR} \approx 4$ days Eq.(5-3).

$$\tau_{HPTR} = \frac{\Delta R_S}{3{,}600 \times c \times \varepsilon_{HPTR}} = \frac{0.25 \text{ m}}{3{,}600 \times 1{,}500 \text{ m/s} \times 5 \times 10^{-10}} < 90 \text{ Hours} < 4 \text{ Days} \qquad (5\text{-}3)$$

The HPTR can be GPS time re-synchronised via an electrical 1PPS signal or hydro-acoustic NMEA command which measures the time difference between GPS and HPTR.

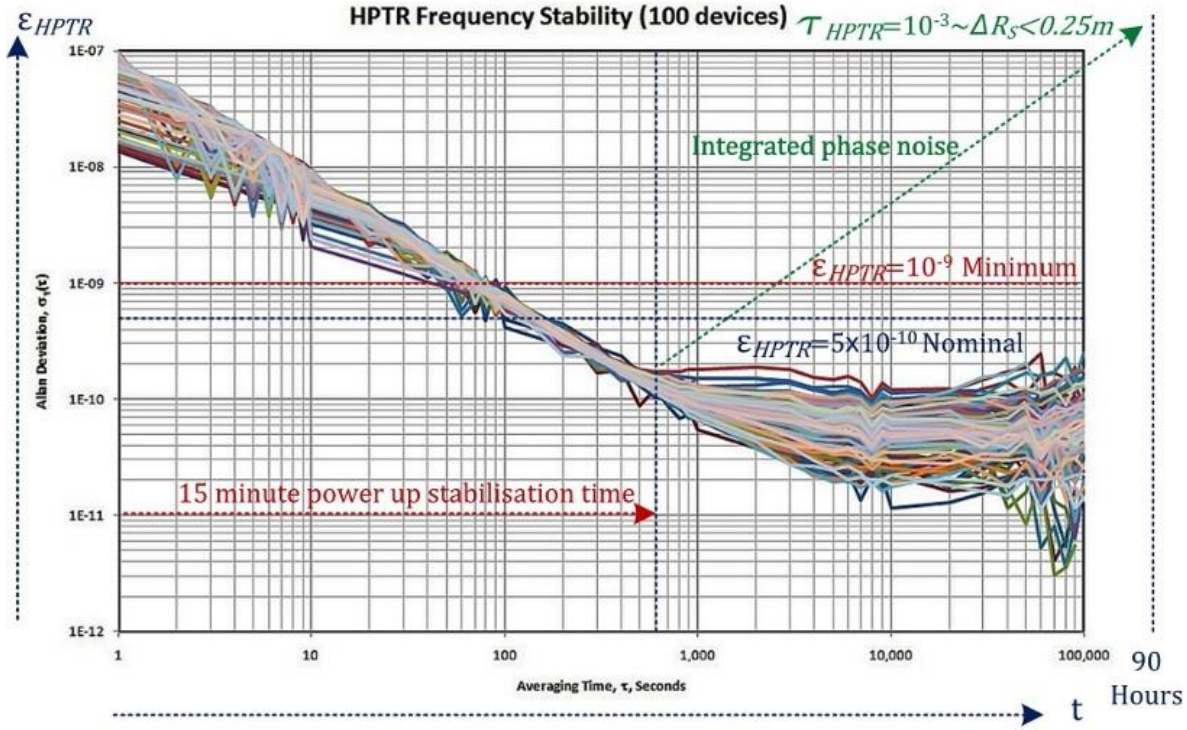

Figure 66 L3 Oceania HPTR frequency stability of 100 devices (candidate design)

Oven controlled low phase noise oscillators pre-date WW2. L3 Oceania have commercially deployed oven stabilized oscillators since the 2000's in the NASNet™ underwater GPS system [163]. The ocean thermal inertia in conjunction with a L3 Oceania non-linear control system ⑩ is used to improve the single oven stabilized oscillator phase noise which approaches the performance of a double oven stabilized oscillator but with lower power consumption and size.

Lower power consumption chip scale atomic clocks [156] with better absolute frequency accuracy $f_e < 10^{-9}$ are commercially available however the phase noise $t_e < 10^{-11}$ performance, in the presence of extreme acoustic vibration and strong electro-magnetic field, has not been validated. The frequency accuracy performance improvements of chip scale atomic clocks could potentially increase the GPS time re-synchronisation period from 2 days to +20 days which may open up a new class of underwater applications. Chip scale atomic clocks are not currently rated for extreme vibration and shock and as yet do not exhibit the reliability and performance repeatability

of a commodity product [44]. One way time of flight precision clocks are also subject to extreme shock, vibration and RF electromagnetic noise generated by the GPM300 PZT ceramic and 300 W power amplifier (Chapter 5.3.3) which could potentially disrupt the atomic clock 10 GHz RF control system.

5.6 MCDSSS Transmitter Optimisations

This chapter provides a summary of the MCDSSS transmitter algorithm and engineering optimisations applied to improve message reliability (MR) and reduce power consumption (P_{TX}). Figure 67 illustrates firmware version 6.0 MCDSSS transmitter block diagram algorithm optimisations and engineering modifications which are colour coded green.

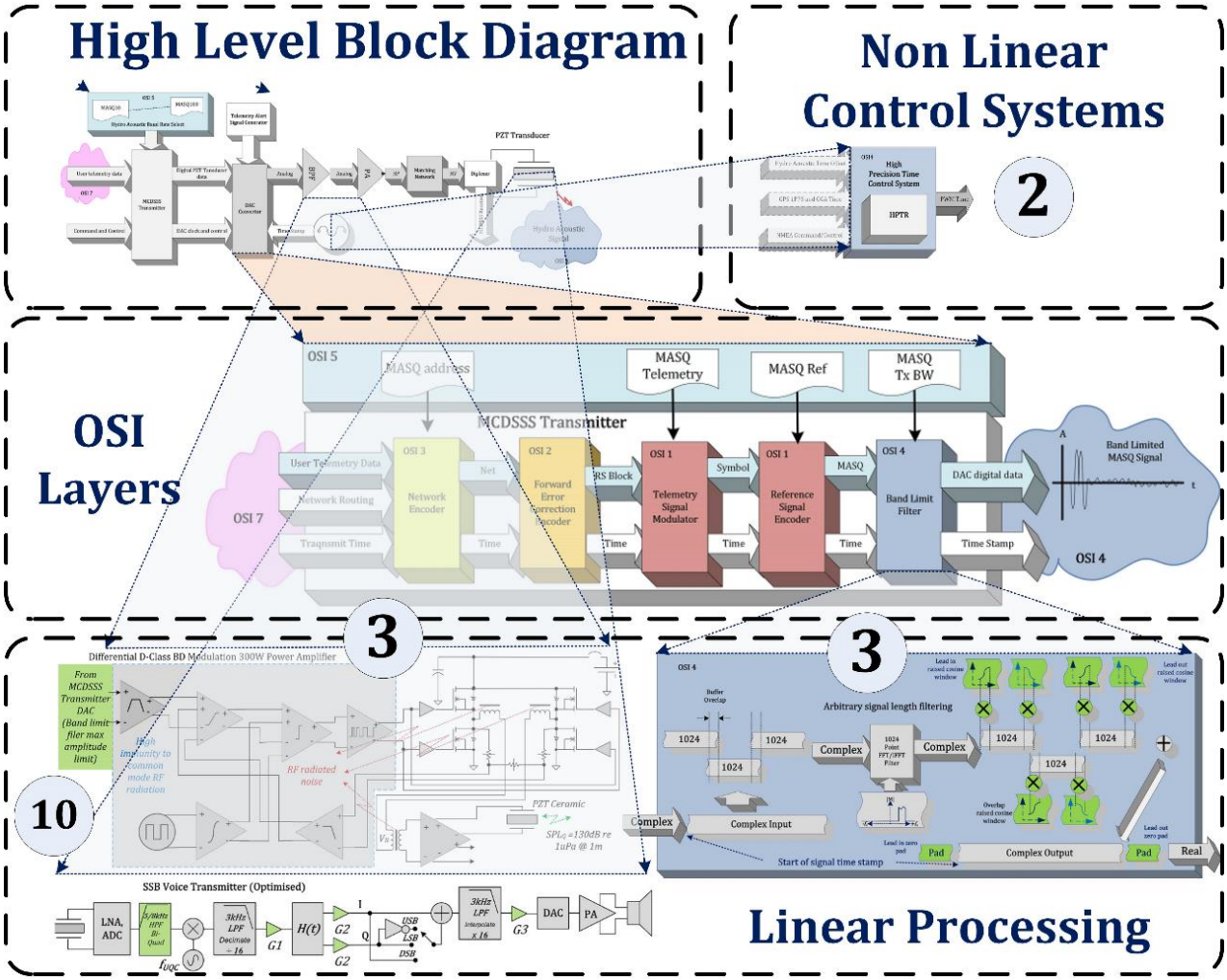

Figure 67 MCDSSS transmitter high level block diagram (optimisations green)

Figure 68 illustrates the MCDSSS Transmitter OSI block diagram. Performance optimisations of OSI 4 layer are detailed in chapter 5.6.3.

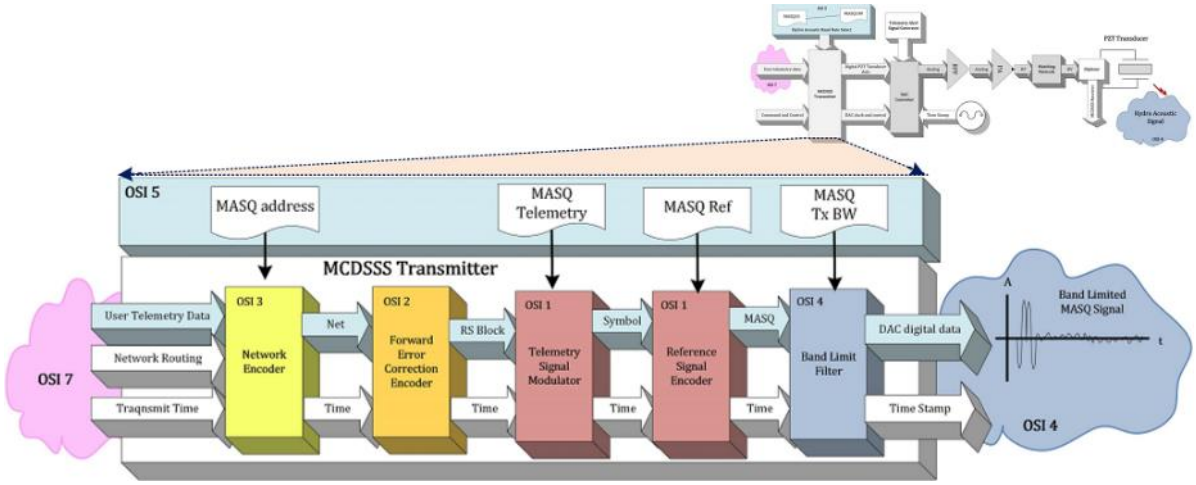

Figure 68 MCDSSS transmitter OSI block diagram (candidate design)

5.6.1 Hydro-acoustic Spectral Pollution Optimisation

One of the performance requirements for a hydro-acoustic modem deployment is that modems must not interfere with other hydro-acoustic systems. The L3 Oceania Australian Undersea Network (AUSSNet) deployment (Appendix O) required the modem Lower Side Band (LSB) noise to be less than $SS3$ below 1 kHz. The Singapore deployment (Appendix B) required the modem Upper Side Band (USB) noise not interfere with an acoustic backscatter Doppler profiler. Modem deployments may not or may not provide adequate interference specification which mandated that the acoustic modem sideband noise performance be maximised. Additional MCDSSS transmitter side band noise attenuation can be provided by physically separating the acoustic modem from other acoustic system to induce modem side band noise spherical spreading attenuation Eq.(2-12).

5.6.1.1 MCDSSS Transmitter Band Limiting Power Saving Optimisation

Equation (5-4) describes the frequency domain *sinc* function response of a DSSS transmitter signal (V_{TX}).

$$\begin{aligned} \mathrm{x} &= \frac{\pi}{4B_M}(\mathrm{f} - f_c) \\ V_{TX}(\mathrm{x}) &= \frac{sin(\mathrm{x})}{\mathrm{x}} = sinc(\mathrm{x}) \\ V_{TX}(\mathrm{f}) &= sinc\left(\frac{\pi}{4B_M}(\mathrm{f} - f_c)\right) \\ \mathrm{P} &= \frac{V^2}{R} \;\therefore \mathrm{P} \propto V^2 \\ P_{TX}(\mathrm{f}) \propto {V_{TX}}^2(\mathrm{f}) &\equiv sinc^2\left(\frac{\pi}{4B_M}(\mathrm{f} - f_c)\right) \end{aligned} \tag{5-4}$$

The 3 dB bandwidth of a DSSS signal resides in the centre 50% of a *sinc* function main lobe (Figure 69).

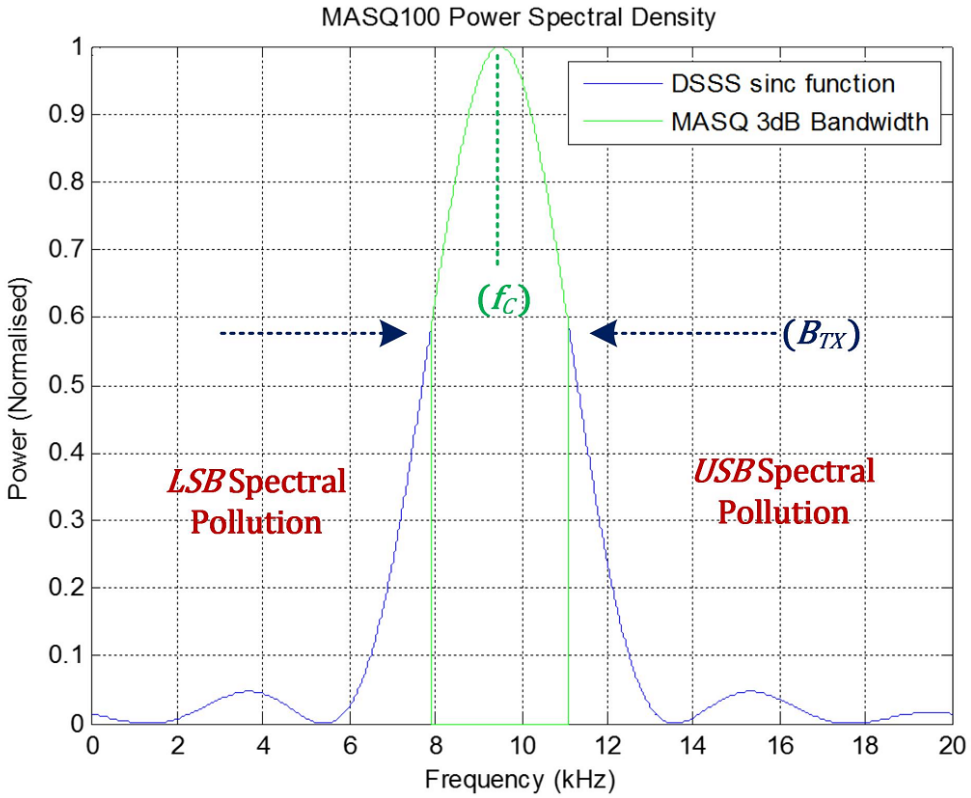

Figure 69 Transmitter PSD frequency domain (100 baud)

A characteristic of a *sinc* function is that 77% of the transmit power (P_{3dB}) resides in the centre 50% of the main lobe Eq.(5-5). The band limited power efficiency $\epsilon_{P_{3dB}}$ improvement is less than 1 dB however the linear power improvement is equivalent to a $100\% - P_{3dB} \approx 20\%$ decrease in the battery pack size, which is significant given the cost of manufacturing and deploying pressure housings is proportional to the square of the battery payload size. The firmware version 6.0 20% transmit band limiting power saving may be modest, but a 3 month battery powered modem deployment is extended from 90 to 110 days and this is significant given that the largest cost for deployment/recovery is vessel hire cost. This is high compared to the equipment capital cost and any small improvement in power consumption translates to long term operating cost savings.

$$
\begin{aligned}
P = \int_0^x \operatorname{sinc}^2(x)dx = Si(2x) - \frac{\sin^2(x)}{x} = \left(2x - \frac{(2x)^3}{3!\,3} + \frac{(2x)^5}{5!\,5} \ldots\right) - \frac{\sin^2(x)}{x} \\
P_f = \int_{f_c}^{\infty} \operatorname{sinc}^2\left(\frac{\pi}{4B_w}(f - f_c)\right) df \equiv \int_0^{\infty} \operatorname{sinc}^2(x)dx = \frac{\pi}{2} \\
P_{TX} = \int_{f_c}^{\frac{B_M}{2}} \operatorname{sinc}^2\left(\frac{\pi}{4B_w}(f - f_c)\right) df \equiv \int_0^{\frac{\pi}{4}} \operatorname{sinc}^2(x)dx \approx 1.2 \\
P_{3dB} = \frac{2P_{TX}}{2P_f} \approx \frac{2 \times 1.2 \times 100}{\pi} = 77\% \cong 20\% \text{ Power saving} \\
\epsilon_{P_{3dB}} = 10\log_{10}\left(\frac{100}{P_{3dB}}\right) \leq 1 \text{ dB}
\end{aligned}
\tag{5-5}
$$

Transmission of the out of band *sinc* function signal pollutes the side band spectrum and does not significantly increase the detectability of the received signal because the out of band transmit power is more efficiently utilised by band limiting and increasing the in band power. PZT transducers have less than one octave 6 dB bandwidth ($B_{TX} < f_C$) and if a PZT transducer is driven with a wide band signal then the out of band energy is dissipated as heat thus reducing the efficiency of battery powered MCDSSS transmitters. If the modulation bandwidth (B_M) is greater than the PZT transducer bandwidth (B_{PZT}) then the transmit signal bandwidth (B_{TX}) must be band limited as described by equation (5-6) and deployed on firmware version 6.0 transmitter.

$$\begin{gathered} B_{PZT} = UFB_{6dB} - LFB_{6dB} \\ \text{if } B_M > B_{PZT} \text{ then } B_{TX} = B_{PZT} \\ \text{if } B_M \leq B_{PZT} \text{ then } B_{TX} = B_M \end{gathered} \tag{5-6}$$

5.6.1.2 Maximizing Digital Filter Side Band Performance

The target signal processing platform for the MCDSSS transceiver is a low power 16-bit fixed point DSP. The dynamic range (G_{MAX}) for 16-bit arithmetic is approximately 90 dB Eq.(5-7). Digital filtering using 16-bit fixed point arithmetic can potentially provide up to ($G_{MAX} < 90$ dB) narrow-band attenuation.

$$G_{MAX} = 20\log_{10}\left(\frac{2^{Bits}}{\sqrt{2}}\right) \approx 90 \text{ dB} \quad \text{(for 16-bit arithmetic)} \tag{5-7}$$

Digital band pass filters can be implemented using a single Finite Impulse Response (FIR) filters. Stop band attenuation greater than 60 dB requires more than 32 FIR filter coefficients. To maximise dynamic range FIR filter coefficients are normalised (i.e. the sum of FIR filter coefficients is one). As the number of FIR filter coefficients increase the magnitude of the coefficients decrease and are subject to integer numerical round errors which limits the stop band performance. Wide band attenuation greater than 60 dB is not practical using a single wide-band 16-bit fixed point FIR filter.

Wide band attenuation greater than 60 dB , using 16-bit fixed point arithmetic, is achievable using frequency domain processing. A frequency domain filter is equivalent to multiple time domain narrow-band FIR filters which exhibit superior stop band performance than a single FIR wide band filter. The input signal is converted to the frequency domain using a FFT, multiplied by the window function and then converted back to the time domain via an Inverse Fast Fourier Transfer (IFFT) and the sum of the IFFT real and imaginary outputs drives the Digital to Analog Convertor (DAC) without incurring a numerically expensive square root magnitude operation. An advantage of frequency domain processing over time domain filtering is the support of arbitrary band pass equalisation which is used to correct of the non-linear frequency response of the PZT projector by multiplying the inverse of the PZT projector transfer function band pass window function and does not impose additional processing overhead. In firmware version 6.0 a band-limited window function was applied to the transmit signal.

Figure 21 illustrates measured 60 dB lower and 45 dB upper side band attenuation of a 6.5 kHz to 16.5 kHz MCDSSS signal. Numerical rounding errors can be minimised by

dynamic normalization of FFT butterfly iterations. Figure 70 illustrates a band limited spectrogram of firmware version 5.x which exhibits undesirable herring bone spectral leakage across the FFT boundary. Spectral leakage is minimised using overlapped FFT's. The spectral components are a consequence of the circular nature of FFT processing. The FFT assumes that the tail of the signal is connected to the head of the signal. When breaking up a very long signal into smaller 1024 FFT blocks a discontinuity is generated at the block boundaries. Any discontinuity or algorithmic artefacts generates undesirable spectral leakage products.

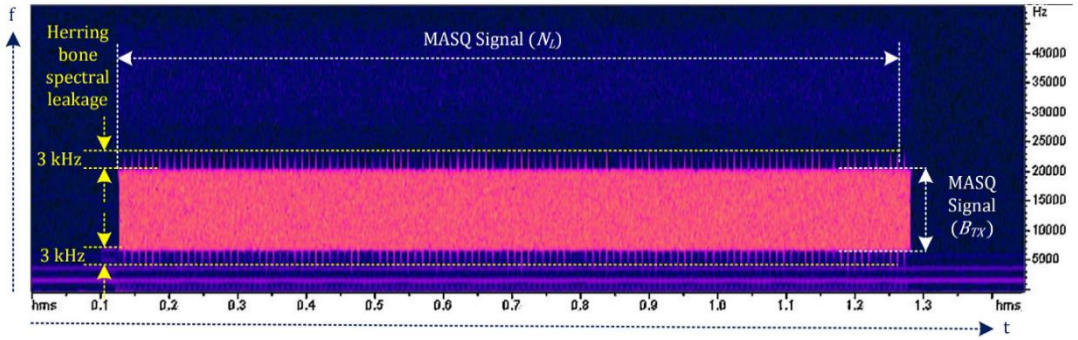

Figure 70 FFT side band filtering herring bone spectral leakage (spectrogram)

The multi-block output of the FFT filter are mixed together using an overlap window function. A raised cosine lead-out and lead-in window, derived from the FFT sine/cosine lookup table, is used to mix the multiple FFT blocks. Figure 71 (green) illustrates firmware version 6.0 FFT filtering topology which generates low spectral leakage at the FFT boundaries via the use of an overlap window cosine window.

Band limiting extends the signal length with an additional lead-in and lead-out samples appended to the input signal. The signal transmit time stamp requires adjusting for the addition of the lead in signal otherwise there will be a transpond or one way time of flight range measurement error. The firmware version 6.0 output signal is therefore time delayed and streamed to the DAC several samples before the start of the signal to guarantee that the signal is transmitted at the required time.

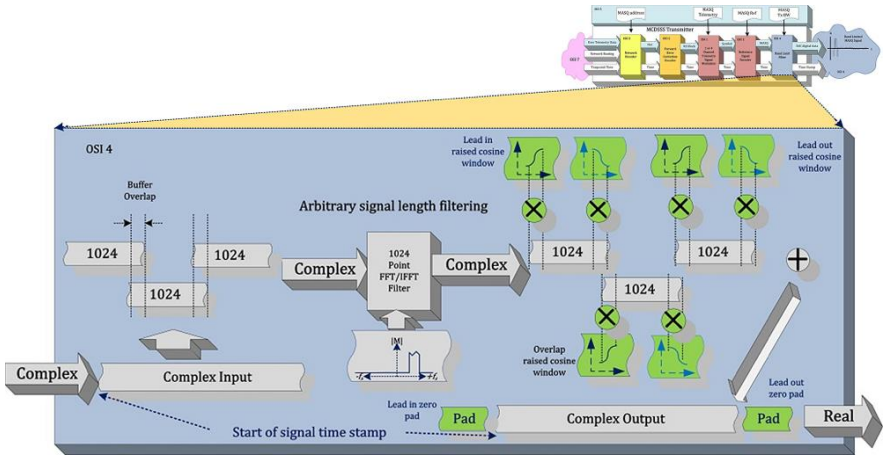

Figure 71 Arbitrary signal length FFT filtering (post process window function)

5.6.2 Alternative D-Class BD Modulation Power Amplifiers Options

The GPM300 transmitter uses a D-Class power amplifier as used in consumer products [162]. The high drive voltage requirements of a low cost PZT transducer and the 80 mm maximum internal diameter (ID) pressure housing limit mandated the custom design of an 85% → 95% efficiency power amplifier with low noise floor, low quiescent power, fast start-up time, fast shutdown time and low distortion. D-Class BD modulation was implemented to increase the drive voltage and reduce the large output RF filters. Commercial high-power amplifier replacement candidates for the GPM300 with equivalent or better performance are not currently available.

5.6.3 Power Amplifier Side Band Performance Optimisation

The efficiency of switch mode power amplifiers are in the order of 85% and for a 300 W power amplifier, 50 W will be dissipated as heat and RF radiation which is the largest source of transmitter electrical interference and as a result increases the side band noise floor. The design of a low distortion, compact OD = Φ80 mm low quiescent power, 300 W power amplifier is challenging however the recent introduction of +2 GHz rail-to-rail differential input-output operation amplifiers facilitated the design of a fully differential D-Class BD modulation power amplifier which minimises RF self noise interference.

Generating a 190 dB re 1 µPa @ 1 m band limited signal increases the peak to peak voltage (Chapter 5.6.1.1) and intermittently drives the power amplifier differential op-amps to the power supply rails or ground which compromises the RF common mode rejection and distorts the hydro-acoustic signal. A soft limiter was added to firmware version 6.0 power amplifier input which minimises hydro-acoustic signal distortion when transmitting at maximum power (Figure 72 green). Figure 228 illustrates that firmware version 6.0 achieved measured full power sideband attenuation of LSB > 60 dB and USB > 40 dB. Efficiency varies from 85% to 95% which is dependent on output power.

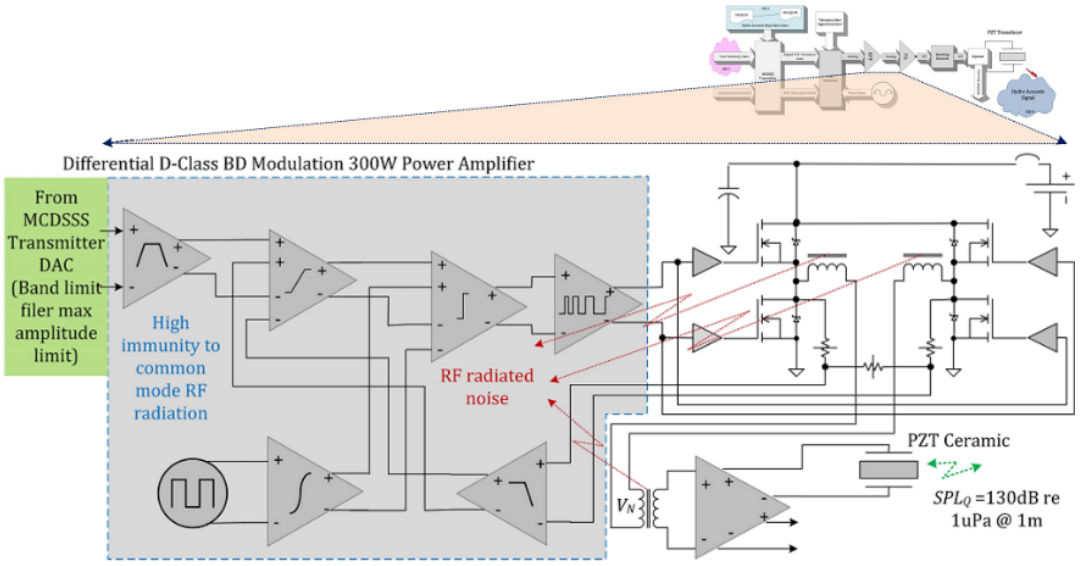

Figure 72 Differential D-class BD modulation power amplifier (NO L3 IP)

The GPM300 power amplifier output noise floor was measured at $V_N \approx 1$ mV RMS which generates audible acoustic noise (SPL_N) at the PZT projector equivalent to transmit

source level of $SPL_{TX} = 130$ dB re 1 µPa @ 1 m or an anisotropic noise source equivalent to $SS9$ @ 1 m Eq.(5-8) which imposes a minimum transmit source level attenuation (A_N) limit of 60 dB during covert communication optimisation (Chapter 5.6.7) (Appendix D).

$$SPL_N = 20\log_{10}(V_N \times N_{MATCH}) + TVR = 130 \text{ dB re 1 µPa @ 1 m}$$

$$PSD_N \equiv 90 \text{ dB re 1 µPa}/\sqrt{\text{Hz}} \text{ @ 1 m} \equiv SS9 \text{ @ 1 m} \quad (5\text{-}8)$$

$$A_N = SPL_{MAX} - SPL_N = 190 \text{ dB re 1 µPa @ 1 m} - 130 \text{ dB re 1 µPa @ 1 m} = 60 \text{ dB}$$

5.6.4 High Efficiency and Low Distortion Power Amplifier

The MCDSSS 500 and 1,000 baud sea trial (Appendix P) identified the requirement for a custom low distortion, high efficiency, compact 300 W power amplifier with 6 µA stand-by ultra-low quiescent current and fast start-up of less than 10 ms. The power amplifier's 3 W quiescent power consumption (P_Q) imposes a minimum transmit source level limit (A_Q) when optimising a communication link ① for peak BEE minimum power consumption Eq.(5-9) and (Chapter 5.6.7).

$$P_Q = 3 \text{ W for } SPL_{1W} = 170.5 \text{ dB re 1 µPa/W @ 1 m}$$

$$SPL_Q = 10\log_{10}(P_Q \times \epsilon_{PZT}) + SPL_{1W} \approx 170 \text{ dB re 1 µPa @ 1 m} \quad (5\text{-}9)$$

$$A_Q = SPL_{MAX} - SPL_Q \approx 20 \text{ dB}$$

The radially polarized PZT transducer high impedance ($Z_{PZT} \approx 3$ kΩ) is reflected from the $N_{MATCH} = 1:100$ transformer secondary to the primary by the turns ratio squared at $\frac{Z_{PZT}}{N_{MATCH}^2} = \frac{10 \text{ k}\Omega}{100^2} < 0.3\ \Omega$ which is two orders of magnitude lower than the 4 Ω load impedance of typical commercial power amplifiers. The design of a 0.05 Ω source impedance, low distortion 300 W power amplifier that fits inside a φ80 mm pressure housing payload is challenging (Figure 73). The efficiency of switch mode power amplifiers are in the order of 85% and for a $P_{PA} = 300$ W power amplifier, 50 W will be dissipated as heat inside the pressure housing.

The implementation of a D-Class BD modulation power amplifier doubles the drive voltage and removes the requirement for a common mode RF filter [161]. The capacitance of the PZT ceramic is reflected back to the power amplifier output by the square of the step up transformer turns ratio (N_{MATCH}) and is used to attenuate the RF modulation energy which is stored in the power supply back Electro Magnetic Force (EMF) capacitors and improves electrical efficiency. The use of a low volume custom built power amplifier, instead of a commercial commodity power amplifier, does not come without its problems because unintended interactions with other sub systems required additional hardware patches for firmware version 6.0 (Figure 73 right green).

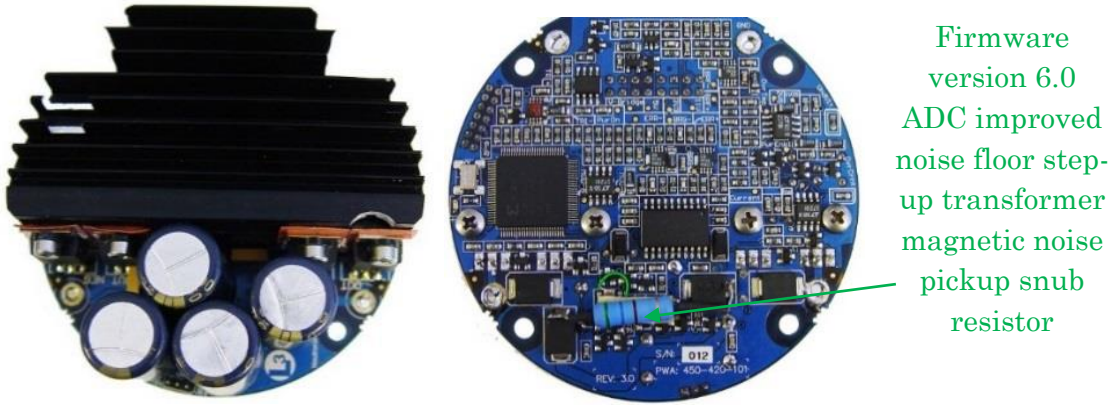

Figure 73 Φ80 mm OD 300 W D-Class BD modulation amplifier (candidate design)

5.6.5 Alternative PZT Transducer Options

The GPM300 uses conventional radially polarised PZT transducer technology which pre-dates WW2 [45]. High baud rate MCDSSS hydro-acoustic communication requires wide transmission bandwidth PZT transducers with more than one octave 6 dB bandwidth. Tests of commercial PZT transducers identified suitable candidates for high baud rate communication, however sea trial tests failed to replicate the published performance, requiring the design of a custom built wide bandwidth PZT transducer (Appendix P). The performance penalties of a low cost, lower efficiency PZT transducer requires higher drive voltage, efficient transmit electronics and lower noise floor receivers.

5.6.6 High Power PZT Ceramic Non Linear Distortion

Narrow-band communication shallow water cavitation pressure is approximately 200 dB re 1 µPa @ 1 m, requiring 3 kW of electrical power [100]. A lead filled ϕ100 mm OD spherical PZT transducer can deliver 200 dB re 1 µPa @ 1 m but provides less than one octave bandwidth and costs approximately $15,000 AU which is prohibitively expensive for use in commercial modems.

L3 Oceania has used high cost commercially available φ80 mm 2 kW 10 kHz broad-band 7.5 kHz to 17.5 kHz transducer in legacy products. The staved ring design [139] provides low Transmit Voltage Response (TVR) of 135 dB re 1 µPa/Vrms @ 1 m and a high Open Circuit Voltage (OCV) receive sensitivity of −175 dB Vrms / 1 µPa @ 1 m. Staved ring PZT transducers use multiple PZT ceramic blocks which are electrically coupled in parallel and mechanically bonded in series (Figure 74 right).

The TVR can be increased to 140 dB re 1 µPa/Vrms @ 1 m with a narrow-band matching network and a SPL_{MAX} of 190 dB re 1 µPa @ 1 m requires a low $SPL_{MAX} - TVR = 190$ dB − 140 dB = 50 dB Vrms ≈ 300 Vrms drive voltage. Staved ring PZT transducers are constructed using a multiple trapezoid PZT ceramics which are sandwiched between copper electrodes and held together with a pre-loaded fiberglass outer cylinder. The manufacturing and construction process is complex, as the PZT blocks must be individually cast and polished on all six sides and hand assembled into a ring. The unit cost is greater than $5,000 AU in production quantities but are too expensive for medium cost modems. Figure 74 left illustrates a low cost 36 stave 2 kW PZT transducer which is manufactured using a φ100 mm OD PZT tube which is sliced up into 36 trapezoid blocks

with approximately φ95 mm OD, with curved out and inner surfaces. The elimination of the polishing process halves the manufacturing cost to less than $2,500 AU.

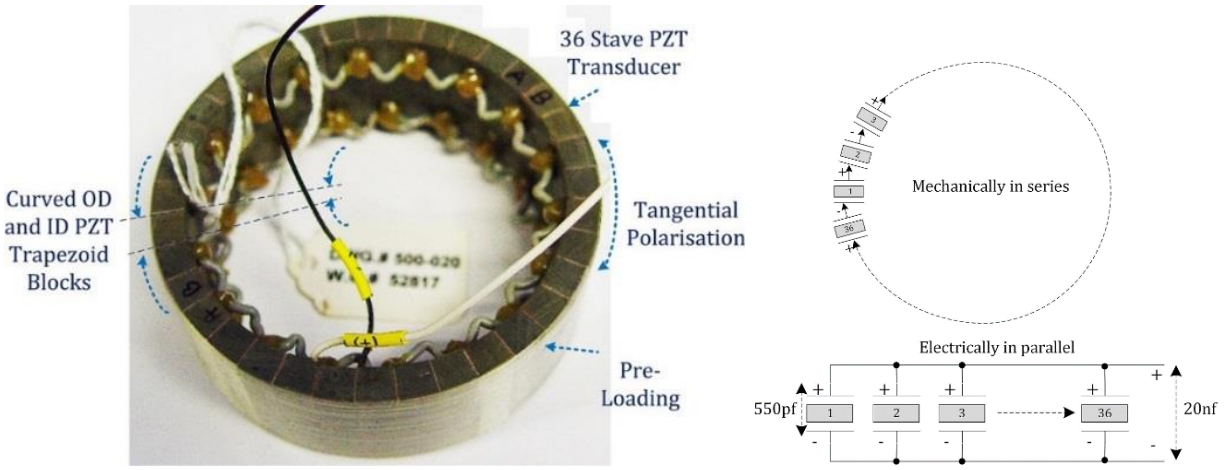

Figure 74 Φ80 mm OD 200 dB SPL low cost 36 stave ring PZT transducer (candidate design)

Many years of broad-band DSSS hydro-acoustic tank testing have encountered a power loss phenomenon for all high-powered oil filled PZT transducers, which the transducer manufactures could not explain as they only test ceramics using narrow-band low duty cycle signals. When driving any PZT oil filled transducer in shallow water with a high power DSSS broad-band 100% duty cycle signal the maximum transmit source level would be initially achieved, however several seconds later the low frequency band would attenuate and a drop in source level would follow. Immediate and subsequent transmissions would always generate lower source levels, however if there was a delay of several minutes between subsequent transmission then the maximum source level would be initially achieved followed by a source level drop. Staved ring PZT transducers are less than 60% efficient and approximately half the electrical power is dissipated as heat. It was assumed that the ceramics were overheating and the PZT transducers were being driven close to the de-polarisation sound level pressure. The source level loss phenomenon also occurred during the L3 Oceania 36 stave ring PZT transducer testing but at ¼ the maximum 2 kW power rating. This was a disappointing result as the candidate expected better shallow water source level performance from his transducer design. Figure 75 left illustrates the L3 Oceania 100 mm PZT transducer inside a butyl rubber transducer boot filled with de-gassed oil. The left image illustrates the transducer at time 17:33:09 and the right image illustrates the transducer 6 seconds later while being driven at an SPL_{MAX} of 190 dB re 1 µPa @ 1 m. At time 17:33:15 the PZT transducer is not overheating or de-polarising because the spherical artefacts at the centre of the PZT transducer (Figure 75 right) are oil cavitation bubbles. Although the ocean shallow water 1% duty cycle narrow-band cavitation pressure is greater than SPL of 198 dB re 1 µPa @ 1 m the 100% duty cycle broad-band transducer oil cavitation pressure is approximately 190 dB re 1 µPa @ 1 m. This phenomenon imposes a 6 dB de-rating for a 100% duty cycle broad-band PZT transducer shallow water maximum drive source level limit when complying with a full ocean depth and shallow water performance requirement. The design and manufacture of the low cost high power 36 stave ring transducer can at best be described as a false start because of the misdiagnosis of a physical phenomenon.

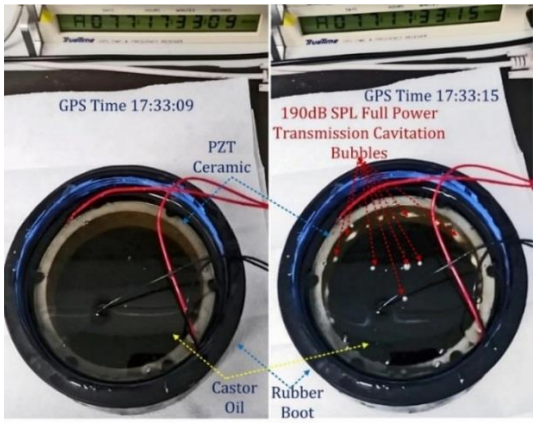

Figure 75 L3 Oceania oil filled PZT transducer shallow water cavitation

Shallow water oil cavitation limits the broad-band 100% duty cycle of the PZT transducer from a 198 dB re 1 µPa @ 1 m SPL (peak) source level to approximately 192 dB re 1 µPa @ 1 m , which can be met using conventional radially polarised PZT cylinders. Version 6.0 firmware protects the PTZ transducer from de-polarisation by limiting the source level to $SPL_{MAX} =$ 190 dB re 1 µPa @ 1 m (RMS).

5.6.7 Transmitter Power Consumption Minimisation

5.6.7.1 Auto Tx Power/Acoustic Baud Rate Control System Optimisation

Message reliability can be maximised by minimising message size and reducing power consumption which frees up battery energy that can be made available for high hydro-acoustic baud rate and/or higher transmit source level. For a fixed communication range the total path loss is bounded by the hydro-acoustic sonar equation and is a function of the maximum transmit acoustic power (SPL_{MAX}), acoustic baud rate dependent transmit margin (M_{TX}) and receive margin (M_{RX}). Minimum power consumption (P_{TX}) is achieved when the bit energy efficiency (BEE) is maximised Eq.(5-10).

$$\mathrm{MIN}(P_{TX}) \propto \mathrm{MAX}(BEE) \propto \mathrm{MIN}(M_{RX}) \propto \mathrm{MIN}\big((SPL_{MAX} - SPL_{MIN}) + M_{TX}\big) \qquad (5\text{-}10)$$

5.6.7.2 Semi-Automatic Communication link Control System Optimisation

The MASQ transceiver NMEA network infrastructure provides a control system ① to optimise a communication link for minimum covert ($M_{RX} < M_{TX}$) power consumption or maximum data transfer speed and is vital for measuring BEE_{PEAK} and establishing maximum covert communication. The firmware version 6.0 Optimise Link Quality (OLQ) control system was extended to retrieve the source and destination GPM300 modem ambient noise and receive power (Figure 76). The source transmit source level setting (PSD_{TX_S}) is transmitted to the destination modem and the destination modem measures the received signal ambient noise (PSD_{A_D}) and receive power (PSD_{RX_D}). The destination modem echoes the measurements using the source baud rate (Br_S) and transmit source level (PSD_{TX_S}). The source modem measures the reply received signal ambient noise (PSD_{A_S}) and receive power (PSD_{RX_S}).

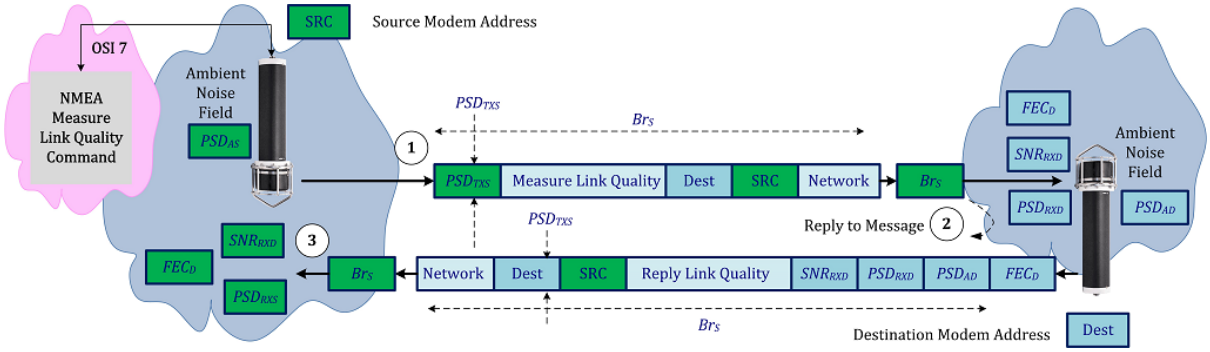

Figure 76 MCDSSS communication link quality measurement

The destination receive margin (M_{RX_D}) is the difference between the receive signal power (PSD_{RX_D}) and the destination ambient noise (PSD_{A_D}) Eq.(5-11).

$$M_{RX_D} = PSD_{RX_D} - PSD_{A_D} \tag{5-11}$$

The source receive margin (M_{RX_S}) is the difference between the reply signal power (PSD_{RX_S}) and the source ambient noise (PSD_{A_S}) Eq.(5-12).

$$M_{RX_S} = PSD_{RX_S} - PSD_{A_S} \tag{5-12}$$

The communication link quality (M_{RX}) is the lowest receive margin Eq.(5-13).

$$M_{RX} = \text{MIN}(M_{RX_S}, M_{RX_D}) \tag{5-13}$$

The OLQ control system ① provides a semi-automatic mechanism for optimising a communication using the specified min/max transmit source level and min/max hydro-acoustic baud rate. Incremental MCDSSS receiver MR improvements support reliable communication links using lower transmit source level. The firmware version 6.0 10 dB performance improvement required the auto transmit source level and hydro-acoustic baud rate control system (Figure 104) hard coded minimum receive margin $M_{RX} \geq$ 9 dB to be modified to support variable receive margins of $M_{RX} \geq$ 4 dB (SNR) as illustrated in Figure 77 (green).

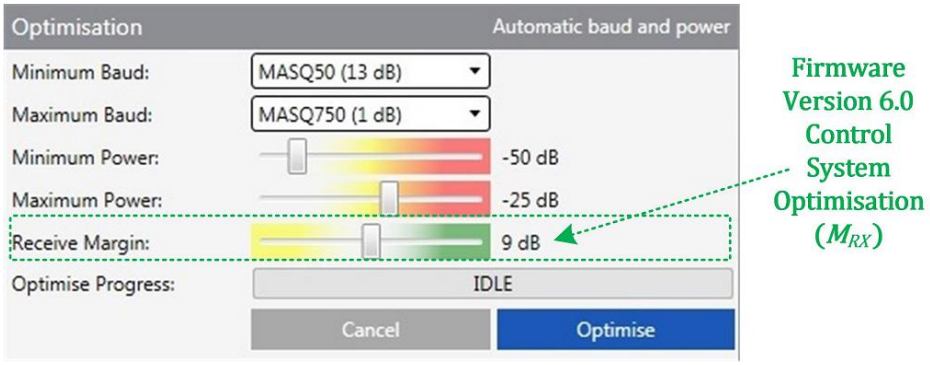

Figure 77 GPM300 configuration utility communication link optimise

The OLQ link quality algorithm conducts a binary search from the minimum hydro-acoustic baud rate to the maximum hydro-acoustic baud rate identifying the maximum baud rate for a reliable communication link. The OLQ algorithm then conducts a binary search of the maximum transmit source level ($A_{TX_{MAX}}$) to the minimum transmit source level ($A_{TX_{MIN}}$) identifying the minimum transmit source level required for a reliable communication link at the highest baud rate. Firmware version 6.0 adjustable receive margin facilitates covert communication link optimisation by setting the maximum baud rate (Br_{MAX}) to the median acoustic baud rate and the minimum transmit source level to the power amplifier noise floor ($A_N = 60$ dB) Eq.(5-8) minus the transmit margin Eq.(5-14).

$$SPL_{TX_{MIN}} \equiv A_{TX_{MIN}} = A_N - M_{TX} \approx 64 \text{ dB} \rightarrow 74 \text{ dB}$$
$$Br_{MAX} \leq 350 \text{ baud} \tag{5-14}$$

The communication link can be optimised for minimum power consumption by setting the maximum baud rate (Br_{MAX}) to the maximum acoustic baud rate and the minimum transmit source level to the power amplifier quiescent power ($A_Q = 20$ dB) Eq.(5-9) Eq.(5-15).

$$A_{TX_{MIN}} = A_Q \approx 20 \text{ dB}$$
$$Br_{MAX} \leq 1{,}200 \text{ baud} \tag{5-15}$$

Peak bit energy efficiency communication requires the OLQ measurement of minimum transmit source level (SPL_{BEE}) for every baud rate in order to calculate BEE_{PEAK} using equations (3-5) and (6-1).

5.6.7.3 Measuring Sound Velocity Refraction and Obstruction Loss

Sound velocity induced refraction attenuation can be estimated using sound velocity profile measurements which may not be available. Historic sound velocity measurements may not accurately represent the current environmental conditions. Physical obstruction induced attenuation is indistinguishable from the sound velocity induced refraction attenuation signal as measured by a receiver (Appendix I). Sound velocity induced refraction (L_R) and physical obstruction (L_O) attenuation can be measured as the difference between the measured path loss (L_T) and slant range (R_S) path loss Eq.(5-16).

$$L_R + L_O = L_T - 20\log_{10}(R_S) + \frac{R_S}{1{,}000}.\bar{L}_A \tag{5-16}$$

Slant range can be measured using the MCDSSS transmitter to MCDSSS receiver one-way time of flight or the MCDSSS transceiver transpond.

Path loss (L_T) can be measured using the known transmit source level (PSD_{TX}), measured receiver ambient (PSD_A) and the receive margin (M_{RX}), which is now reported in firmware version 6.0 OLQ. Equation (5-17) describes the total sound velocity induced refraction (L_R) and physical obstruction (L_O) attenuation. Appendix J shows that shallow water deployment with a sound velocity induced refraction of $L_R = 0$ was not significant and the physical obstruction attenuation was measured at $L_O \approx 10$ dB.

$$L_T = PSD_{TX} + D_{RX} + M_{TX} - M_{RX} - PSD_{A_D}$$

$$L_R + L_O = PSD_{TX} + D_{RX} + M_{TX} - M_{RX} - PSD_A - 20\log_{10}(R_S) + \frac{R_S}{1{,}000}.\bar{L}_A \quad (5\text{-}17)$$

5.6.8 Extended Communication via Network Routing Optimisation

A high reliability communication link in excess of $R_S > 10$ km can be established using the MASQ transceiver network routing for message store and forward (Figure 78).

The MASQ network message forwarding was extended with the following sequence:

1. Relay modem receives and buffers the MCDSSS message.
2. If the network index matches the number of destination addresses then the reply modem increments the network index, adjusts the transpond time for the relay delay and re-transmits the message.
3. If the network index is zero and the last destination address matches the modem address, then the messages is processed by the destination modem.
4. If the processed message generates a reply, then the network header is reversed and the replay is propagated back to the source modem using the same network routing path.

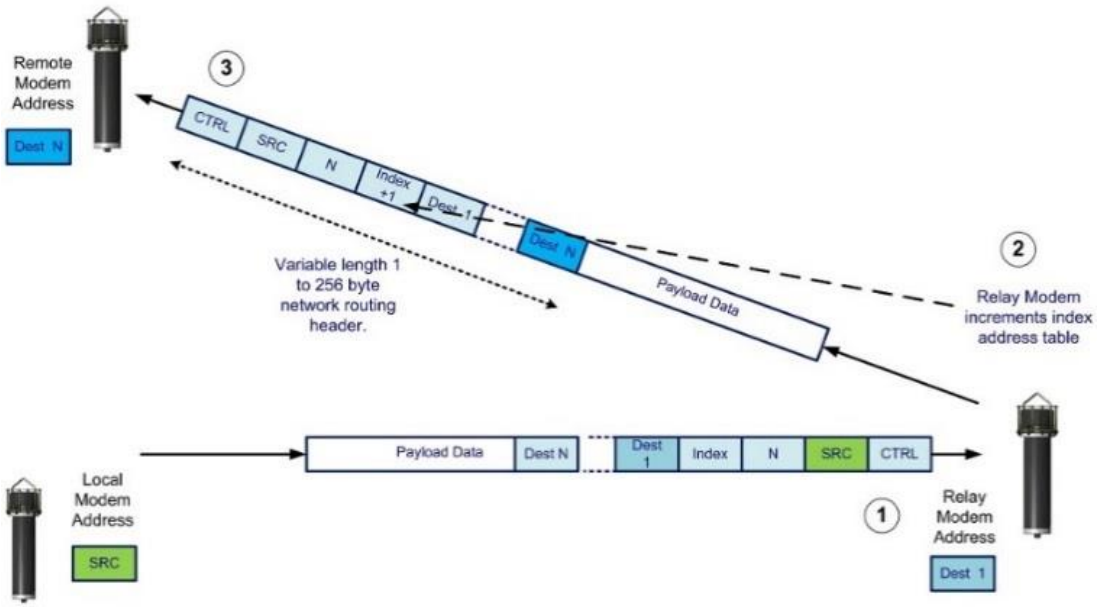

Figure 78 MASQ transceiver network routing handler block diagram

To improve communication reliability the Firmware version 6.0 network routing protocol uses the baud rate of the source modem instead of the local default baud rate.

5.7 MCDSSS Receiver Optimisations

This section provides a summary of the MCDSSS receiver algorithm and engineering optimisations applied to improve message reliability (MR) and reduce power consumption (P_{RX}). Figure 79 illustrates firmware version 6.0 MCDSSS' receiver block diagram with algorithm and engineering optimisations colour coded green.

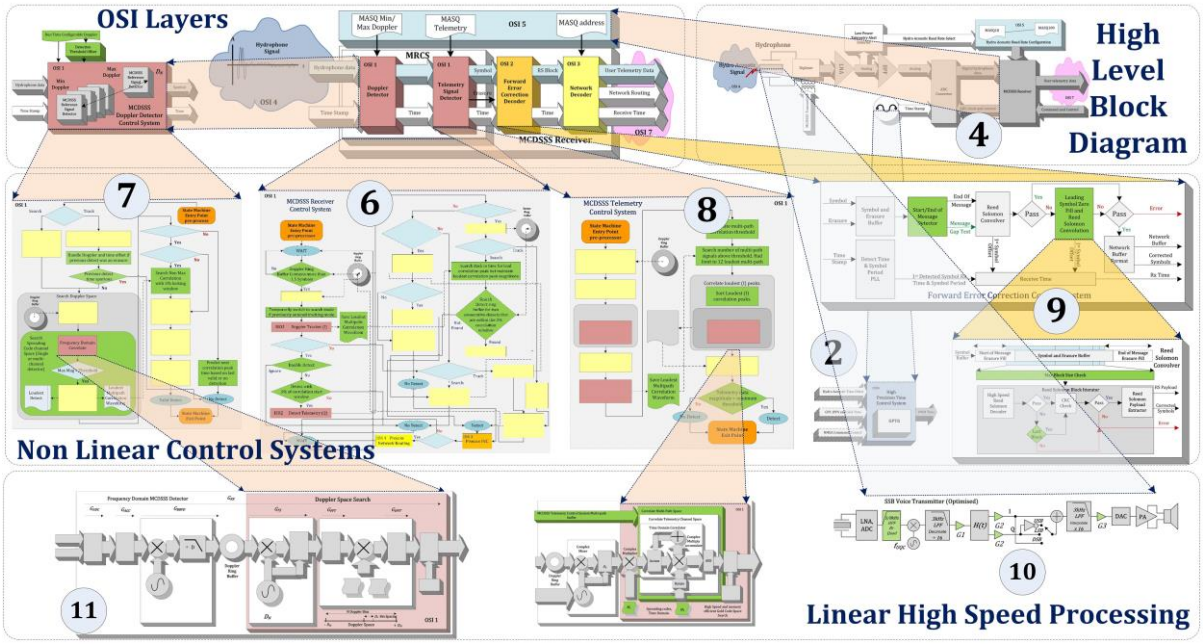

Figure 79 MCDSSS receiver high level block diagram (optimisations green)

Figure 80 illustrates the OSI block diagram for the run time configurable MCDSSS generic receiver. Performance optimisations of OSI 1 to OSI 3 are detailed from section 5.7.7.1 to chapter 5.7.7.4.

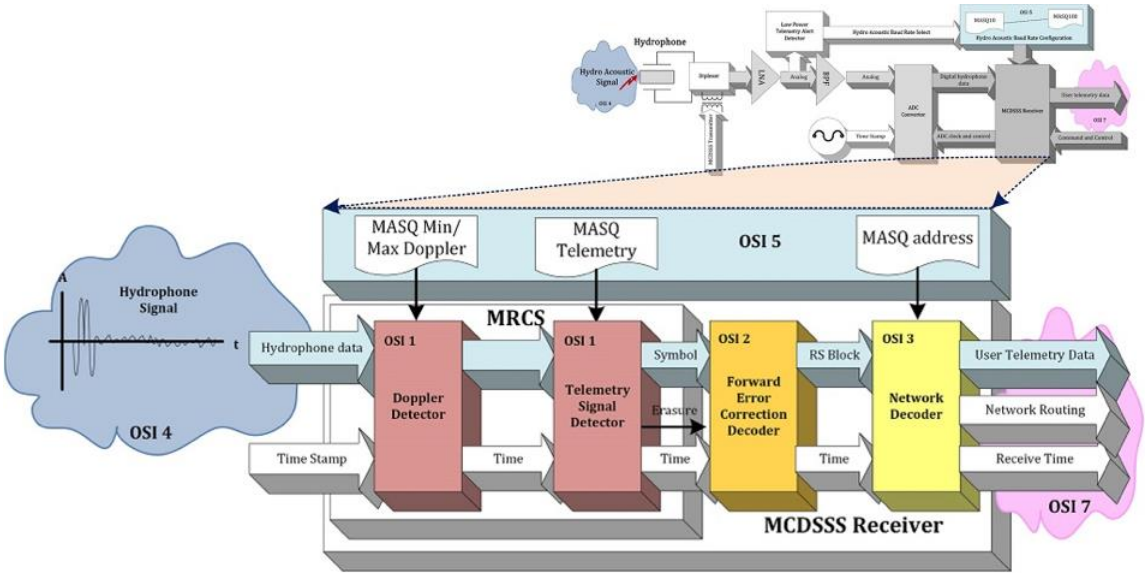

Figure 80 MCDSSS generic receiver OSI block diagram (candidate design)

5.7.1 MCDSSS Receiver Non-Linear Control System Optimisation

The MCDSSS Receiver multipath tracking non-linear Control System ⑥ (MRCS) provides tolerance to the following sources of interference:

1. High ambient noise floor (PSD_A).
2. Impulsive noise (PSD_A).
3. Multipath reverberation (R_M).
4. Surface ducting interference (R_T).

5. Bottom propagation interference (R_B).
6. Doppler tolerance (D_M).
7. Inter-symbol interference ($\Delta t_M > \tau_{SY}$).
8. Time varying channel response ($h(\mathrm{t},\tau)$).

Channel simulator data and sea trial recordings of hostile environments were used to optimise the MRCS control system and improve impulsive noise performance (Appendix B.2). Multiple performance optimisation iterations of firmware version 6.0 MRCS were required to maximise MR, with the most stable MRCS modification illustrated in Figure 81 (green). **NOTE**: Figure 81 items containing L3 Oceania IP have been removed.

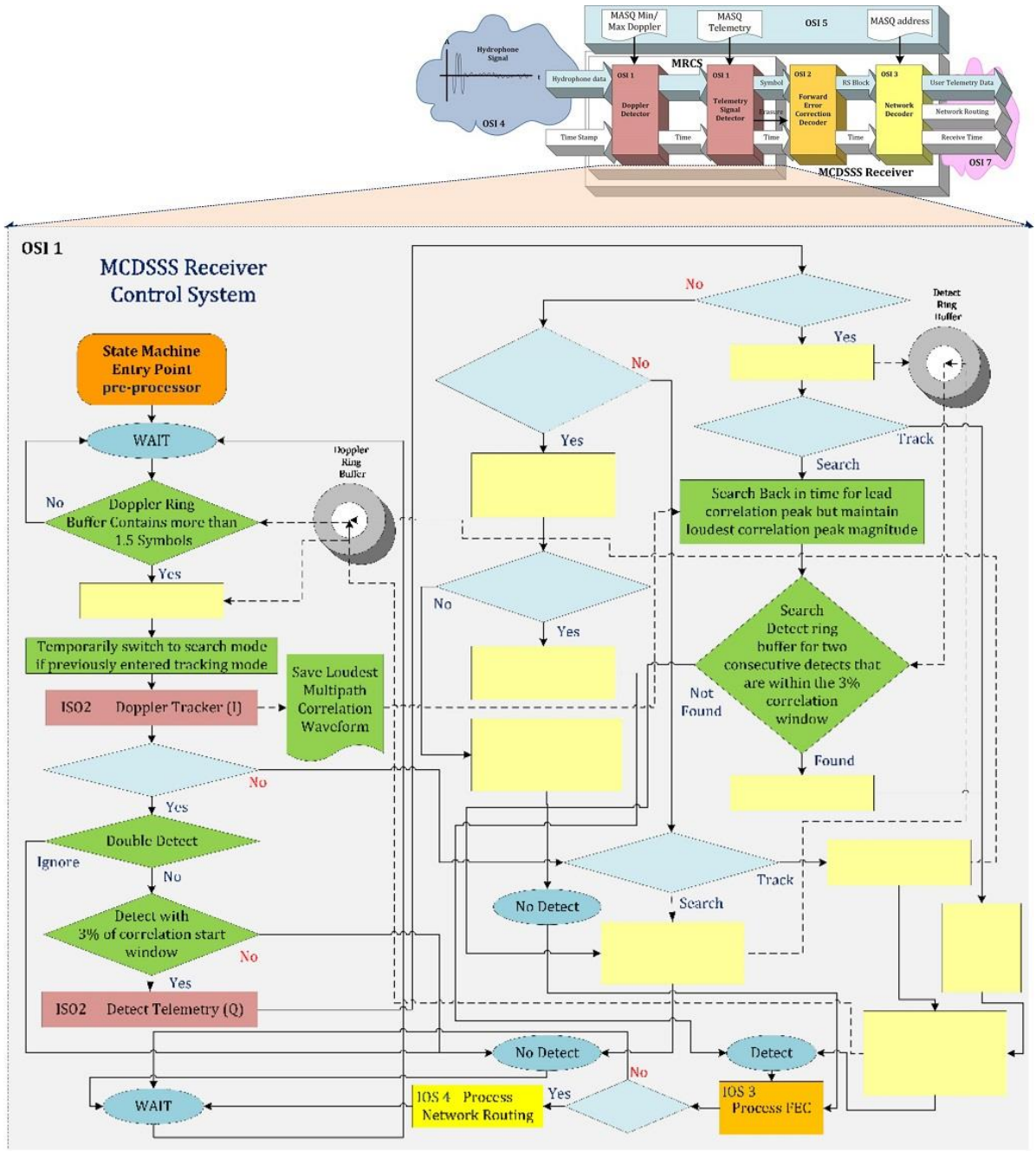

Figure 81 MCDSSS receiver multipath control system (NO L3 IP)

5.7.2 MCDSSS Doppler Detector Control System Optimisations

The firmware version 6.0 Doppler receiver was modified to support runtime configurable maximum Doppler and detection threshold Doppler which was required for the Doppler performance analysis optimisation (Figure 82 green).

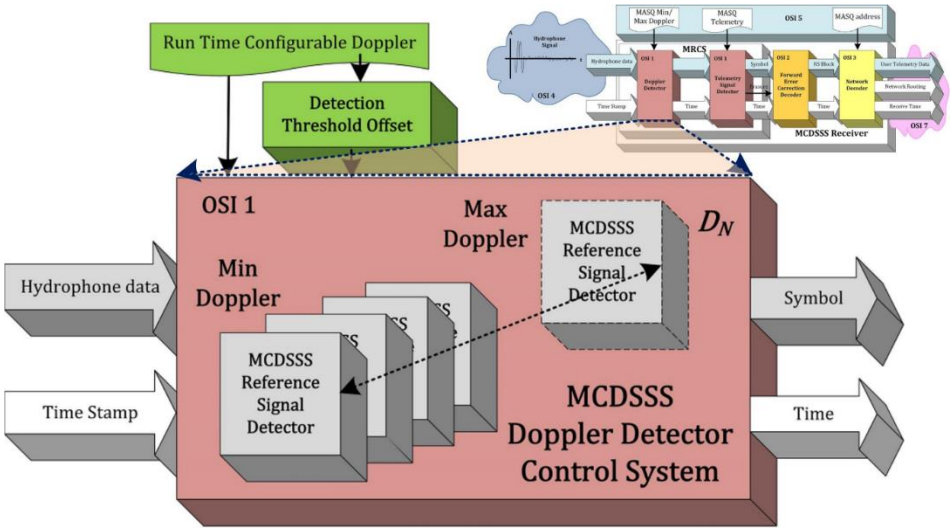

Figure 82 MCDSSS receiver doppler detector block diagram (optimisations green)

5.7.2.1 MCDSSS Doppler Receivers Optimisation

Over 80% of the MCDSSS receiver computational load is incurred by the MCDSSS Doppler detector. The MCDSSS receiver computational load (C_f) is proportional to the min/max Doppler (D_M) and the Critical Doppler velocity (D_C) ratio Eq.(5-18).

$$C_f \propto \frac{D_M}{D_C} \tag{5-18}$$

The MCDSSS receiver computational load and receiver power can be optimised by minimising the number of MCDSSS Doppler receivers. Increasing the Doppler search resolution improves the receiver sensitivity but also increases the false detect rate. Decreasing the Doppler search resolution reduces the processing load but decreases receiver sensitivity for Doppler shifted signal carrier frequencies ($f_C \times D_S$) residing between two Doppler receivers.

5.7.2.2 MCDSSS Doppler Detection Threshold Optimisation

The MCDSSS receiver detection threshold was set to generate a false detect rate of approximately 10^{-2} or less than one false detect per minute. The FDR is a function of the receiver noise floor and required the detection threshold to be manually tuned to better than ± 0.25 dB, for every communication protocol, every baud rate and for every maximum Doppler setting. Attempts to derive an optimal detection threshold algorithm failed to produce performance better than the tedious manual detection threshold optimisation procedure. As firmware version 6.0 message reliability was incrementally increased towards 100%, lower detection thresholds were possible and the detection thresholds required multiple rounds of manual fine adjustments to maximise communication range. The detection threshold requires fine tuning if the receiver control system has been

optimisation to handle a new type of interference. If the MCDSSS receiver control system is optimised to improve performance for a new environment then detection threshold may require another round of manual optimisation. If the maximum Doppler is halved then common sense would suggest then the FDR should also halve, allowing the detection threshold to be reduced by approximately 3 dB thus increasing communication range approximately 50%. This hypothesis is not supported by the measured MCDSSS FDR versus detection threshold (D_{TH}) , Doppler (D_{MAX}) and the default detection threshold ($D_{DEFAULT}$) Eq.(5-19) (Figure 83).

$$\Delta D_{TH} \approx 10\log_{10}\left(\frac{D_{MAX}}{D_{DEFAULT}}\right) \tag{5-19}$$

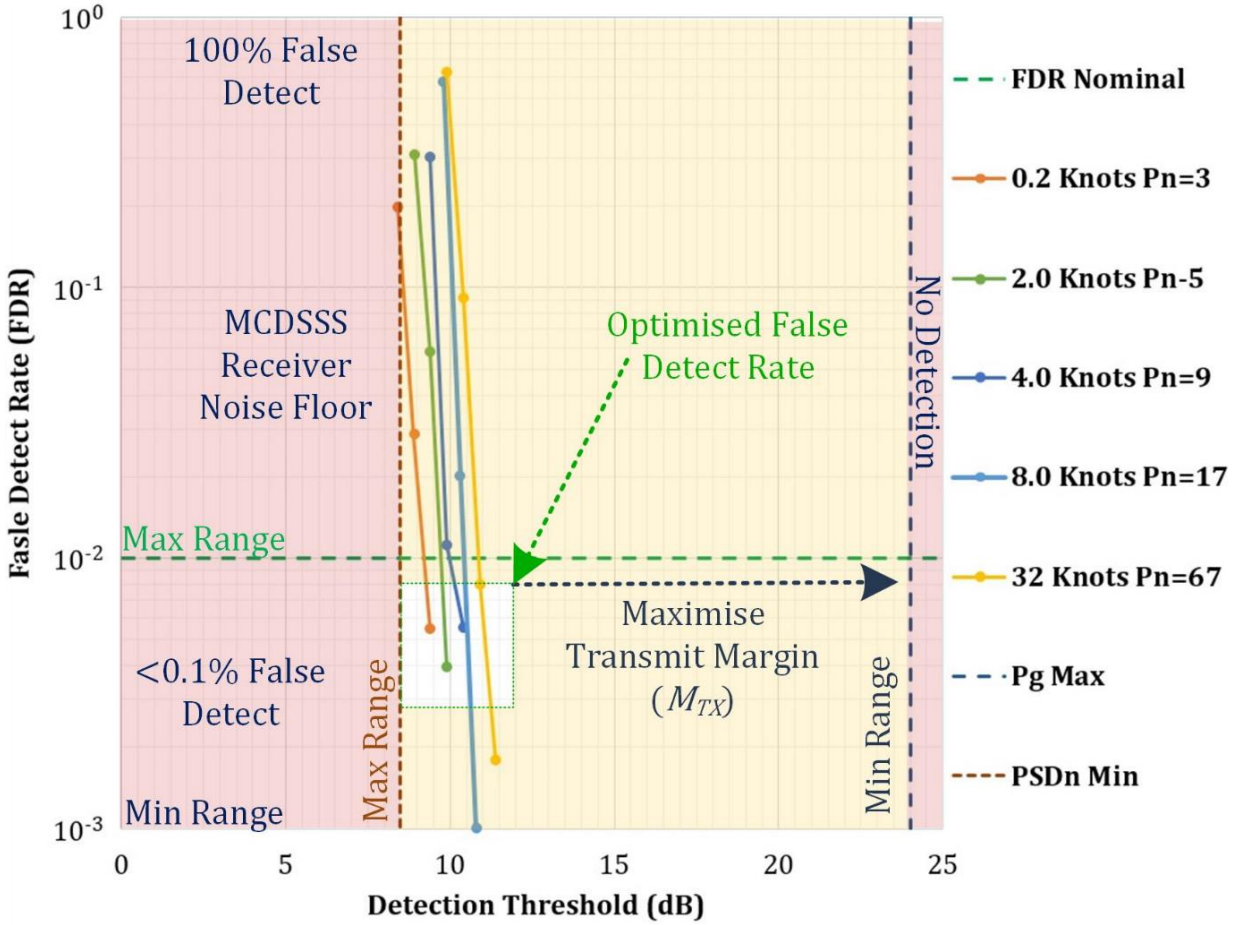

Figure 83 MCDSSS receiver measured false detect rate (50 baud)

Plots of the MCDSSS receiver FDR versus detection threshold (D_{TH}) with a logarithmic vertical scale were straight lines, implying that the two quantities are related by Eq.(5-20).

$$D_{TH} \propto -\log_{10}(\text{FDR}) \text{ dB} \tag{5-20}$$

The Doppler detectors are not independent receivers with independent probabilities of false detection. Each Doppler detector correlates a single received symbol against a frequency offset and temporal scaled reference. All the Doppler detectors have similar correlation peak signatures with adjacent Doppler receivers and have a common false

detect rate. Figure 85 illustrates a ±8 kn Doppler search where 11 of the 67 Doppler receivers detect a MCDSSS symbol from 5.5 kn to 5.1 kn above the detection threshold in a low ambient noise environment.

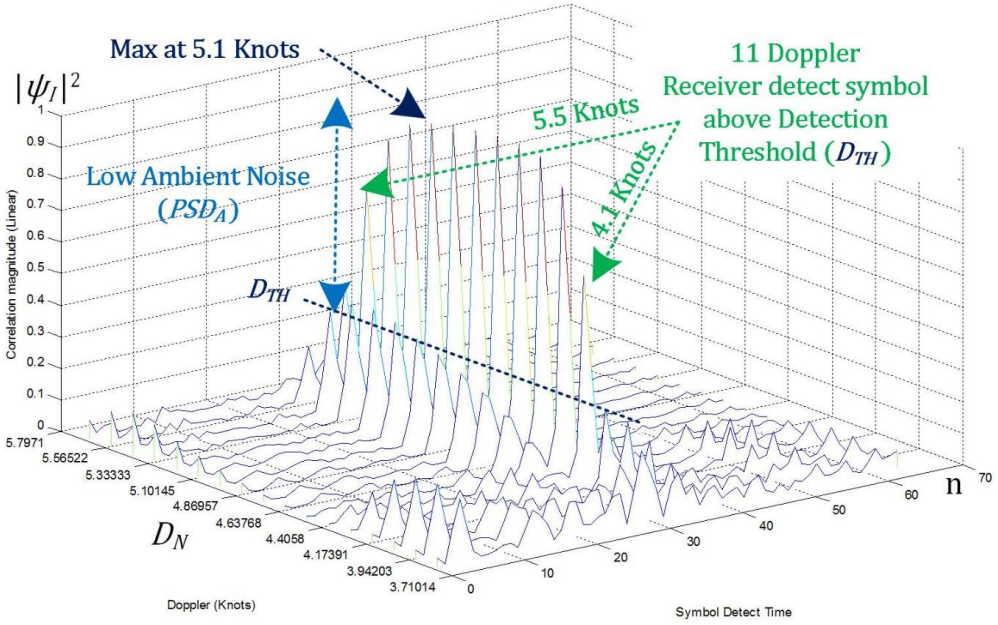

Figure 84 Correlation magnitude versus doppler (low ambient noise)

The primary function of the Doppler detector is to raise the correlation magnitude above the detection threshold for high ambient noise receptions. Figure 85 illustrates a high ambient noise environment ±8 kn Doppler search where 3 of the 67 Doppler receivers detect a MCDSSS symbol above the detection threshold from 3.7 kn to 4.1 kn.

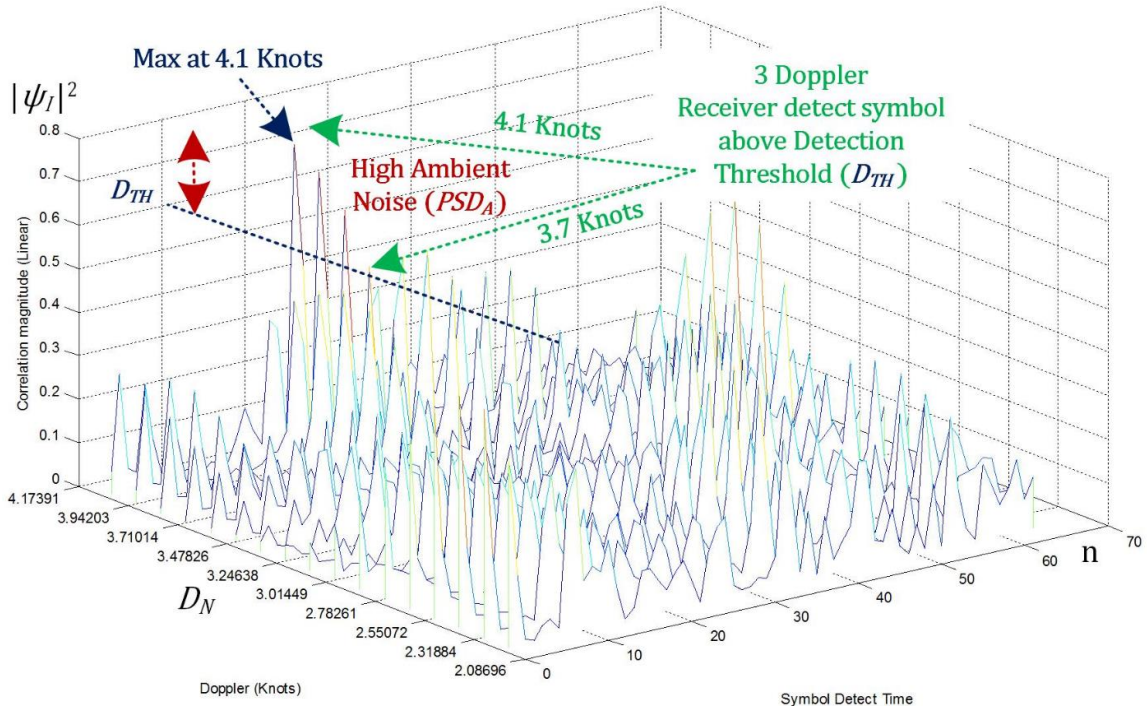

Figure 85 Correlation magnitude versus doppler (high ambient noise)

Even during a high ambient noise reception, neighbouring Doppler detectors have similar correlation peak signatures. From the MCDSSS receiver measured FDR, a nonlinear relationship between the detection threshold offset (ΔD_{TH}) and the maximum Doppler (D_{MAX}) can be estimated Eq.(5-21). When increasing the maximum Doppler the detection threshold (D_{TH}) must be increased by ΔD_{TH} otherwise the FDR increases and effectively disables the MCDSSS receiver because of continuous false detections.

$$\Delta D_{TH} \approx log_{10}\left(\frac{D_{MAX}}{D_{DEFAULT}}\right) \tag{5-21}$$

For static modem deployments reducing the maximum Doppler from 8 knots to 0 knots decreases the detection threshold by 1.5 dB which does not translate to a significant increase in the communication range. If the number of Doppler receivers is reduced from 17 to 3 there is a significant reduction of DSP computational load which firmware version 6.0 utilises to run the DSP at lower processor speed thus conserving receiver battery power.

5.7.2.3 MCDSSS Doppler Control System Optimisation

Extreme multipath environments, such as the shallow waters of Australia and Singapore, induce multipath signals that are intermittently louder than the slant range signal. The firmware version 5.x Doppler control system ⑦ would intermittently lock onto multipath signal, bottom ducting or surface ducting signals instead of the slant range signal which would eventually decay because of temporal fluctuations in destructive interference resulting in the message detection failure. Extreme multipath recordings (Appendix B) were used to optimise the firmware version 6.0 Doppler control system (Figure 86 green). **NOTE**: Figure 86 items containing L3 Oceania IP have been removed. Appendix M MCDSSS recordings of even more extreme environments were acquired to validate the firmware version 6.0 Doppler control system's robustness and that the algorithm optimisations had not been over fitted to the failing signal database.

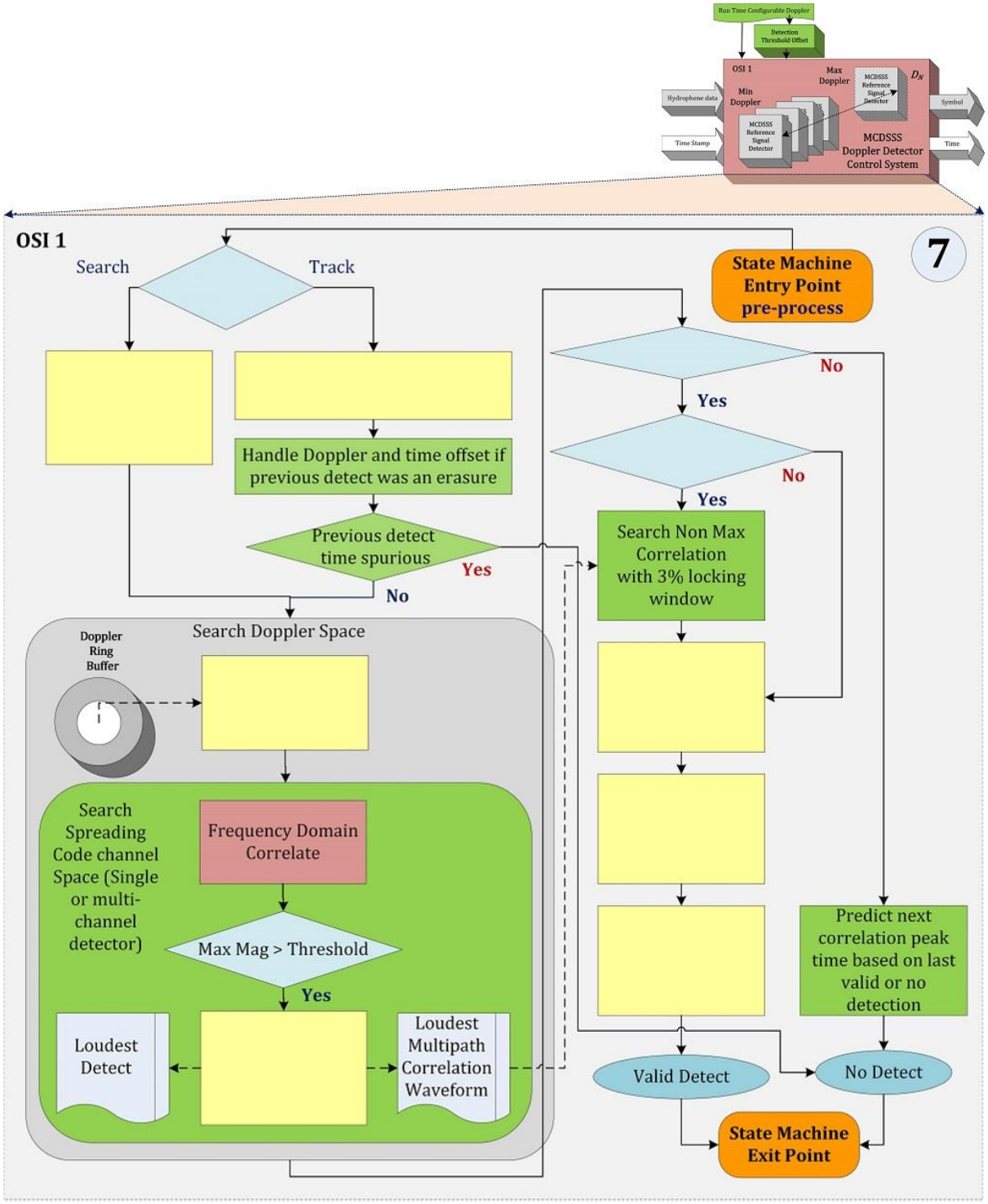

Figure 86 Doppler detector control system (NO L3 IP)

5.7.2.4 MCDSSS Reference (*I*) Detector Optimisation

Figure 87 illustrates the MCDSSS reference detector block diagram which correlates the receive signal with the reference signal. A MCDSSS signal detection occurs at time t_{DETECT} when the correlation magnitude is greater than the detection threshold.

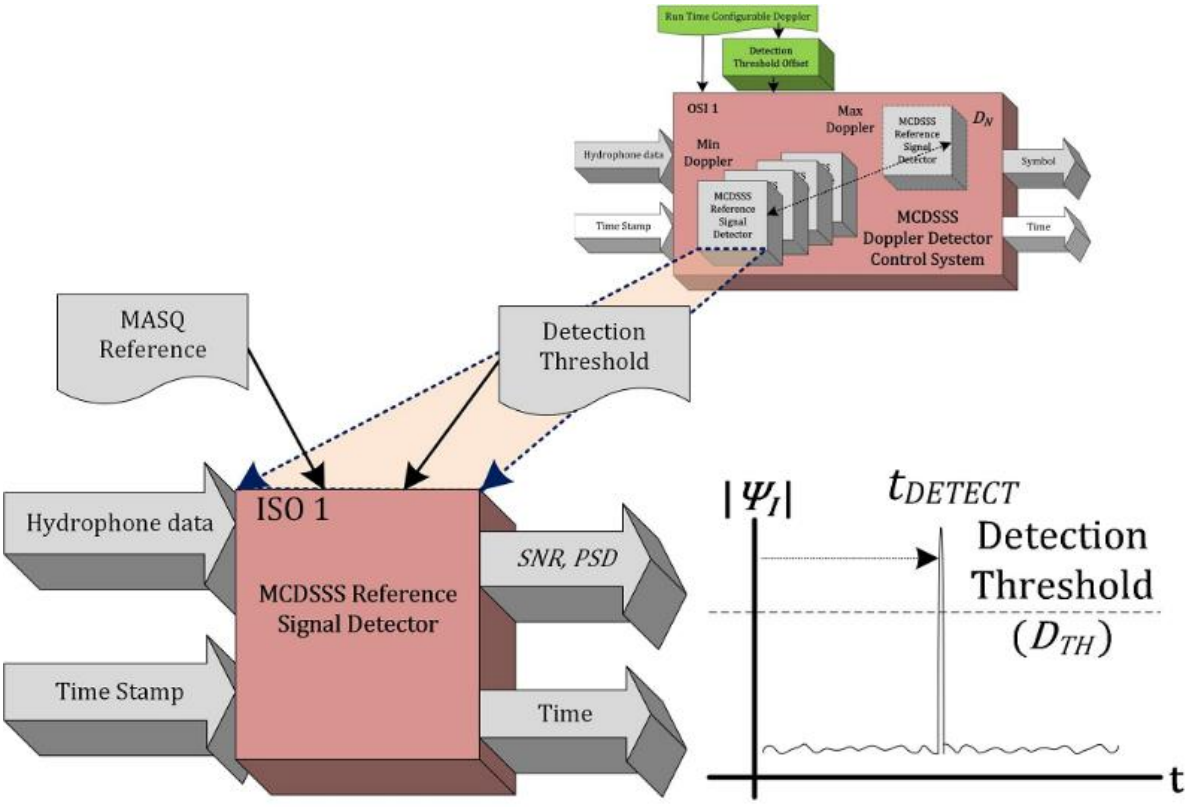

Figure 87 MCDSSS receiver reference (*I*) detector block diagram

5.7.2.5 MCDSSS Reference (*I*) Detector Hydro-acoustic Noise Floor

The MCDSSS receiver input noise floor must be less than the minimum ambient sea noise to maximise communication range. The MCDSSS receiver noise floor (V_N) is the vector sum of the receiver power supply induced noise (V_P), receiver analog noise floor (V_A), receiver ADC noise floor (V_{ADC}) and the receiver digital noise floor (V_D) Eq.(5-22). The GPM300 receiver noise floor is dominated by the loudest noise source which is the preamplifier noise floor.

$$V_N = \sqrt{V_P^2 + \frac{1}{G_A^2}\left(V_A^2 + \frac{1}{G_{ADC}^2}\left(V_{ADC}^2 + \frac{1}{G_D^2}V_D^2\right)\right)} \tag{5-22}$$

The gains of preceding signal processing blocks are applied to the noise voltage and reflected at hydrophone (V_N). All noise source voltages are measured relative to the hydrophone and converted to equivalent ocean PSD_N @ 1 m Eq.(5-23) (Figure 88). Engineering optimisations were applied to the power amplifier matching network (chapter 5.6.4) and hydrophone preamplifier (chapter 5.7.6.2) to reduce switch mode power supply noise pickup.

$$PSD_N = \mathrm{OCV} + 20\log_{10}(V_N) - 10\log_{10}(B_{TX})$$
$$PSD_N < PSD_{SS0} \tag{5-23}$$

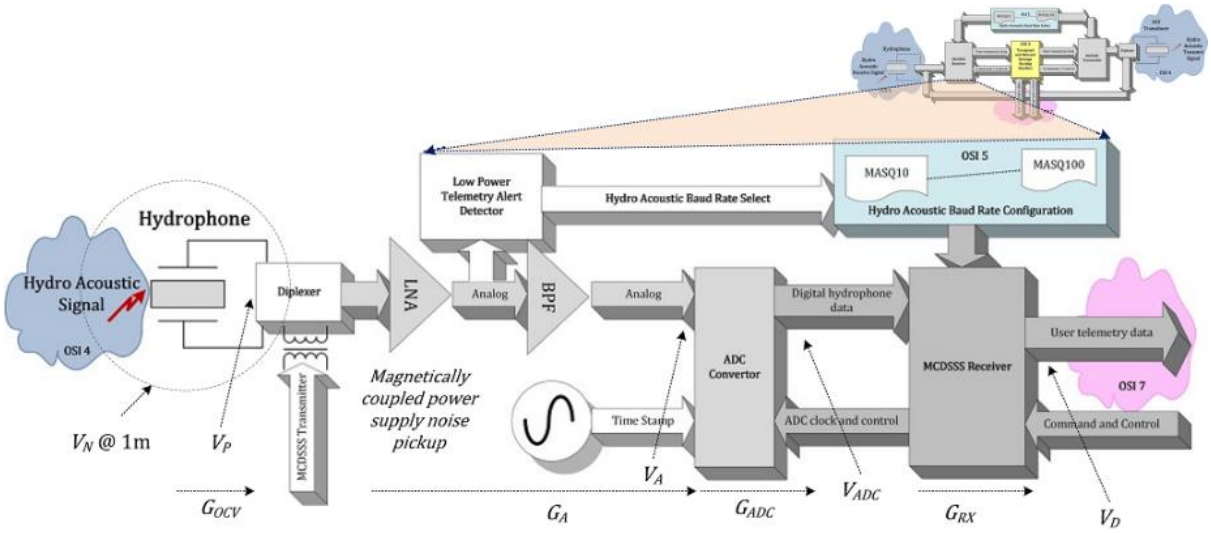

Figure 88 MCDSSS receiver self noise (candidate design)

For reliable MCDSSS signal detection the MCDSSS receiver detection threshold must be greater than the system noise floor (PSD_N) and less than the reference channel processing gain noise floor (P_{N_G}) Eq.(5-24). Firmware version 6.0 dynamic detection threshold, for a specific receiver noise floor and baud rate, was manually adjusted to ± 0.25 dB in order to generate no less than one MCDSSS symbol false detection per minute, which is a good compromise between maximising communication range and maximising message reliability.

$$P_{N_G} > D_{TH} > PSD_N \tag{5-24}$$

5.7.2.6 MCDSSS Reference (*I*) Detector SNR Optimisation

The MCDSSS receiver normalised correlation magnitude is used to calculate the receive Signal to Noise Ratio (SNR_{RX}) Eq.(5-25).

$$\begin{gathered} SNR_{RX} = 10\log_{10}\left(\frac{\mathrm{MAX}(\psi_I(\mathrm{t}))}{\mathrm{RMS}(\psi_I(\mathrm{t}))}\right) \\ t_{DETECT} = t \text{ when } SNR_{RX} \geq D_{TH} \\ P_{N_G} = SNR_{RX} \text{ when } SNR_{RX} < D_{TH} \end{gathered} \tag{5-25}$$

A MCDSSS signal is detected at time t_{DETECT} when SNR_{RX} is greater than or equal to the detection threshold. The SNR_{RX} measures the spread spectrum detector noise floor when SNR_{RX} is less than the detection threshold. SNR_{RX} is a non-linear measure of receive power and is not proportional to the path loss, as illustrated in Figure 90 (bottom blue trace). SNR_{RX} is the vector sum of receiver ambient noise (PSD_A), and spreading code self noise (P_{N_G}) and PSD_{RX}, which is dominated by P_{N_G} for non covert communication. SNR_{RX} remains constant at $SNR_{RX} \approx D_{TH} + M_{TX} - 3$ dB for path loss less than $(L_T - M_{TX})$ non covert communication and degrades exponentially when inside the covert spheroid body (Figure 3 left). The difference between the SNR_{RX} maximum and the detection threshold (D_{TH}) provides an estimate of the transmit margin (M_{TX}) Eq.(5-26).

$$M_{TX} \approx \text{MAX}(SNR_{RX}) - D_{TH} + 3 \text{ dB} \quad (5\text{-}26)$$

The SNR_{RX} can be graphed against time to provide a real-time indicator of a MCDSSS receive signal detection (Figure 89). The firmware version 6.0 real time SNR_{RX} display was implemented to facilitate the manual fine-tuning of the detection threshold to within ± 0.25 dB and optimise the false detect rate which maximises the communication range.

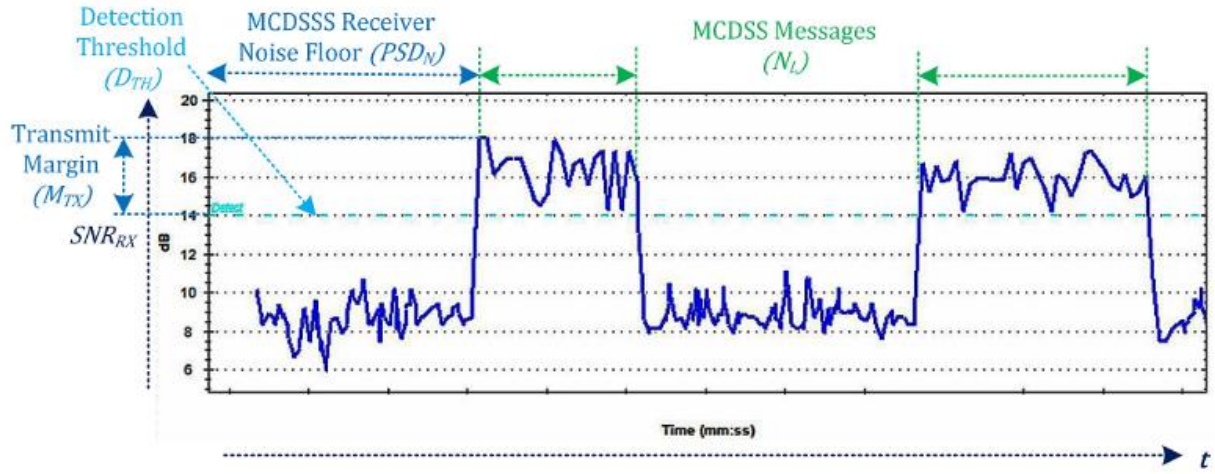

Figure 89 MCDSSS receiver reference (*I*) SNR

5.7.2.7 MCDSSS Reference (*I*) Detector PSD Measurement

The MCDSSS receive margin is equivalent to convention receiver SNR where the reliable communication link requires at least $M_{RX} \approx 6\,dB$ however reliable communications have been established in stable ambient noise environments with $M_{RX} > 3\,dB$. Therefore the quantification of the reliability of a communication link requires the measurement of the receive margin which is derived from the MCDSSS receiver PSD measurement. The firmware version 6.0 MCDSSS receiver was upgraded to provide a hydro acoustic tank (Appendix F) calibrated real-time ambient power spectral density (PSD) measurement of receive signal quality and used to predict the maximum communication range and optimise the communication link reliability.

The MCDSSS receiver absolute correlation magnitude (PSD_{ABS}) is used to measure the in-band ambient (PSD_A) and receive signal power (PSD_{RX}). The MCDSSS receive signal PSD_{RX} is inversely proportional to path loss (L_T) as illustrated in Figure 90 top red trace.

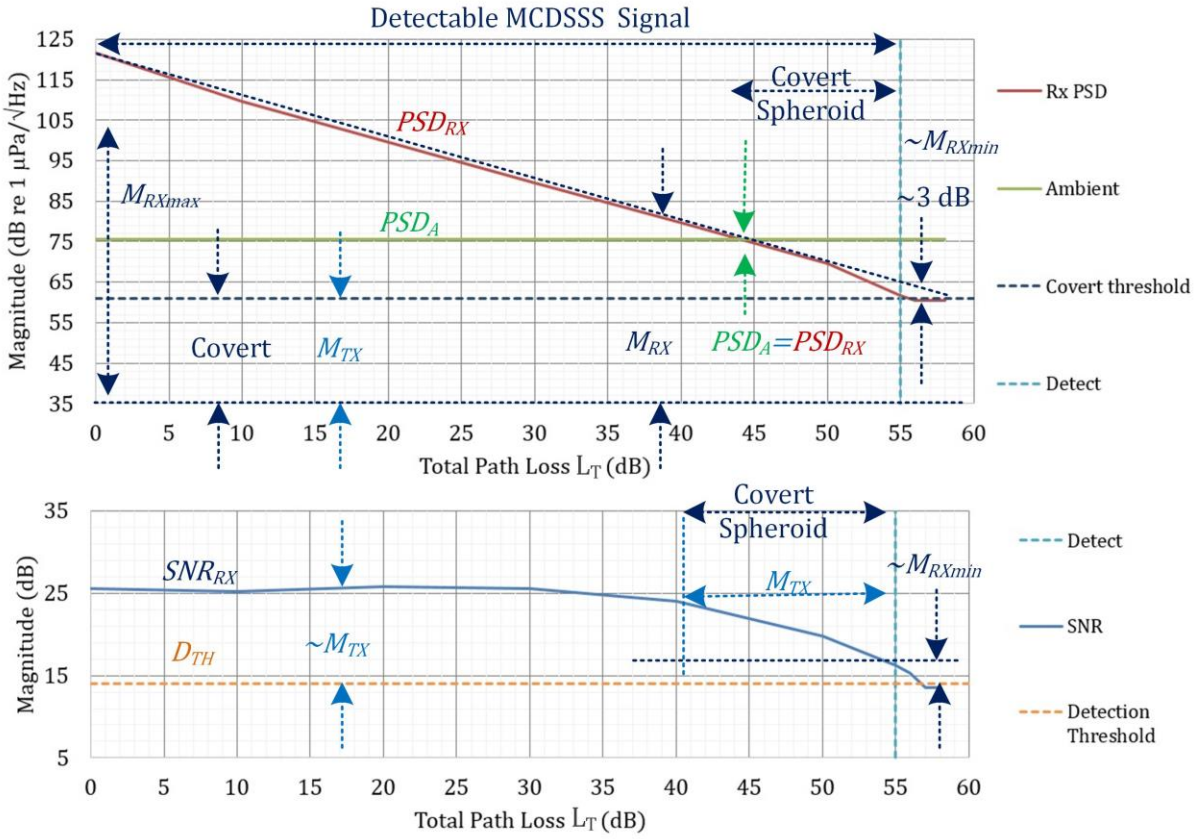

Figure 90 MCDSSS receiver reference (*I*) SNR versus PSD

PSD_{ABS} is used to measure the quality of the communication link (M_{RX} or FOM). PSD_{ABS} is a linear measure of receive power and is inversely proportional the slant range. PSD_{ABS} is used to:

1. Optimise the hydro-acoustic communication link maximum baud rate (Br_{MAX}) and minimum transmit source level (SPL_{TX}).
2. Measure MCDSSS receive margin (M_{RX}).
3. Measure MCDSSS receiver signal power (PSD_{RX}).
4. Measure MCDSSS receiver noise floor in air (PSD_N).
5. Measure isotropic IMO Sea State (SS) number
6. Measure isotropic impulsive biological peak noise and anisotropic boat noise (PSD_A).
7. Predict the maximum communication range (R_{MAX}), (Chapter 4.3.12).
8. Measure covert margin (M_{COVERT}), Eq.(5-36).
9. Predict the minimum covert communication range (R_{COVERT}), Eq.(5-37).

The hydrophone OCV and MCDSSS receiver gain (G_{RX}) are used to convert the relative receiver power (PSD_{REL}) to absolute PSD power (PSD_{RX}) Eq.(5-27).

$$PSD_{REL} = 10\log_{10}\left(\mathrm{RMS}(|\psi_I|)\right)$$
$$PSD_{ABS} = PSD_{REL} + OCV + 20\log_{10}(G_{RX}) \propto -20\log_{10}(R_S) \quad (5\text{-}27)$$

When minimising the MCDSSS receiver fixed point arithmetic noise floor dynamic normalisation of coefficients and algorithms is required to prevent numerical underflow or overflow. Fixed point arithmetic automatic gain control is required for most signal

processing operations to minimise numerical rounding and truncation errors. Receive signal absolute PSD_{ABS} is lost during the normalisation process and requires a parallel signal processing path to preserve receiver gain. The receiver gain (G_{RX}) is the product of the signal processing total dynamic gains Eq.(5-28) (Figure 91).

$$G_{RX} = G_{ADC} \times G_{AGC} \times G_{BBDF} \times G_{FS} \times G_{FFT} \times G_{IFFT} \tag{5-28}$$

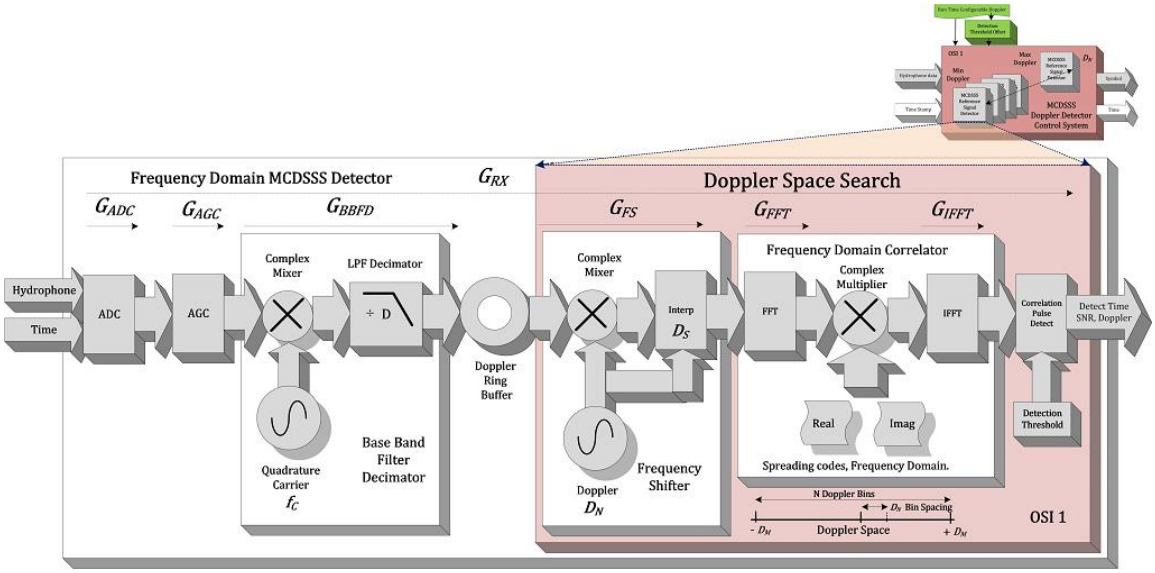

Figure 91 MCDSSS receiver reference (*I*) channel (NO L3 IP)

The MCDSSS receiver in-band power spectral density (PSD_S) is the vector sum of the ambient noise (PSD_A) and the receive signal (PSD_{RX}) Eq.(5-29).

$$\begin{aligned} PSD_A &= 20\log_{10}(V_A) \\ PSD_{RX} &= 20\log_{10}(V_{RX}) \\ PSD_S &\cong 10\log_{10}(V_A^2 + V_{RX}^2) \end{aligned} \tag{5-29}$$

If the MCDSSS receive signal (PSD_{RX}) is the same magnitude as the ambient noise floor (PSD_A) then the MCDSSS receiver in-band power spectral density (PSD_S) is 3 dB above the ambient noise floor Eq.(5-30).

$$\begin{aligned} &\text{If} \quad PSD_A = PSD_{RX} \\ &\text{then} \quad PSD_S = PSD_A + 3\text{ dB} \approx 10\log_{10}(2V_A^2) \end{aligned} \tag{5-30}$$

Figure 92 illustrates the spectrum PSD_S of a MCDSSS 100 baud signal where the receive signal PSD_{RX} is $PSD_\Delta \approx 3$ dB above the ambient noise floor Eq.(5-31).

$$\begin{aligned} PSD_S &= PSD_A + PSD_\Delta = PSD_A + 3\text{ dB} \\ \therefore \quad PSD_A &\approx PSD_{RX} \end{aligned} \tag{5-31}$$

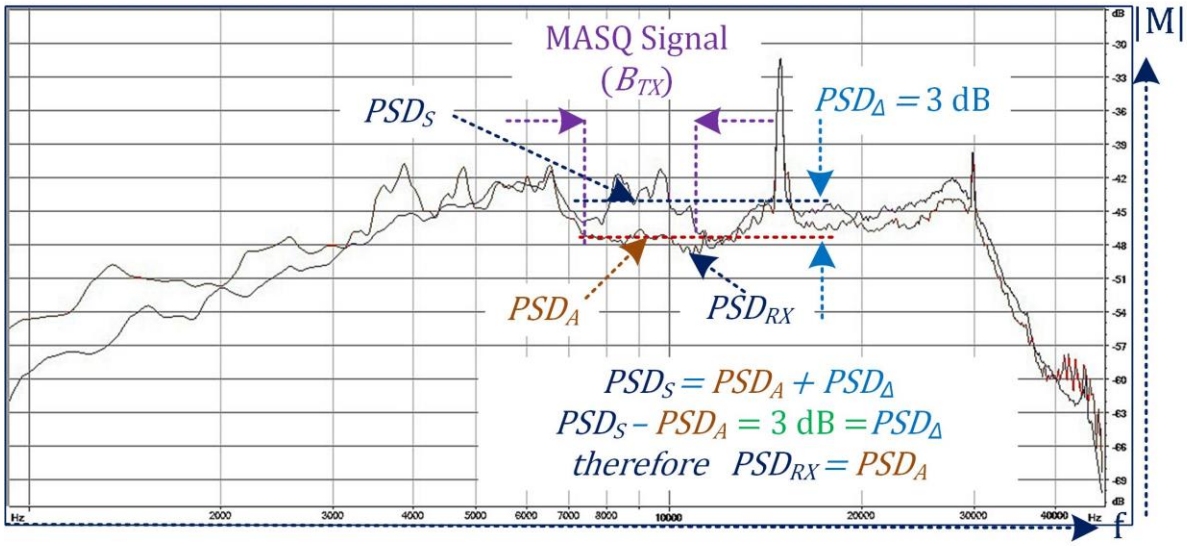

Figure 92 MCDSSS 100 baud 3 dB above ambient (spectrum)

Figure 93 illustrates the firmware version 6.0 time domain aligned spectrogram, PSD (green trace) and SNR (blue trace) of Figure 92 with the MCDSSS 100 baud signal just visible above the ambient noise floor (Figure 93 top faint orange rectangle). The measured receive margin is $M_{RX} = PSD_{RX} - PSD_A \approx 12$ dB. The 100 baud transmit margin is $M_{TX} = 9$ dB and the receiver signal is $PSD_{RX} - D_{TH} = M_{RX} - M_{TX} \approx 3$ dB and consistent with the Eq.(5-31).

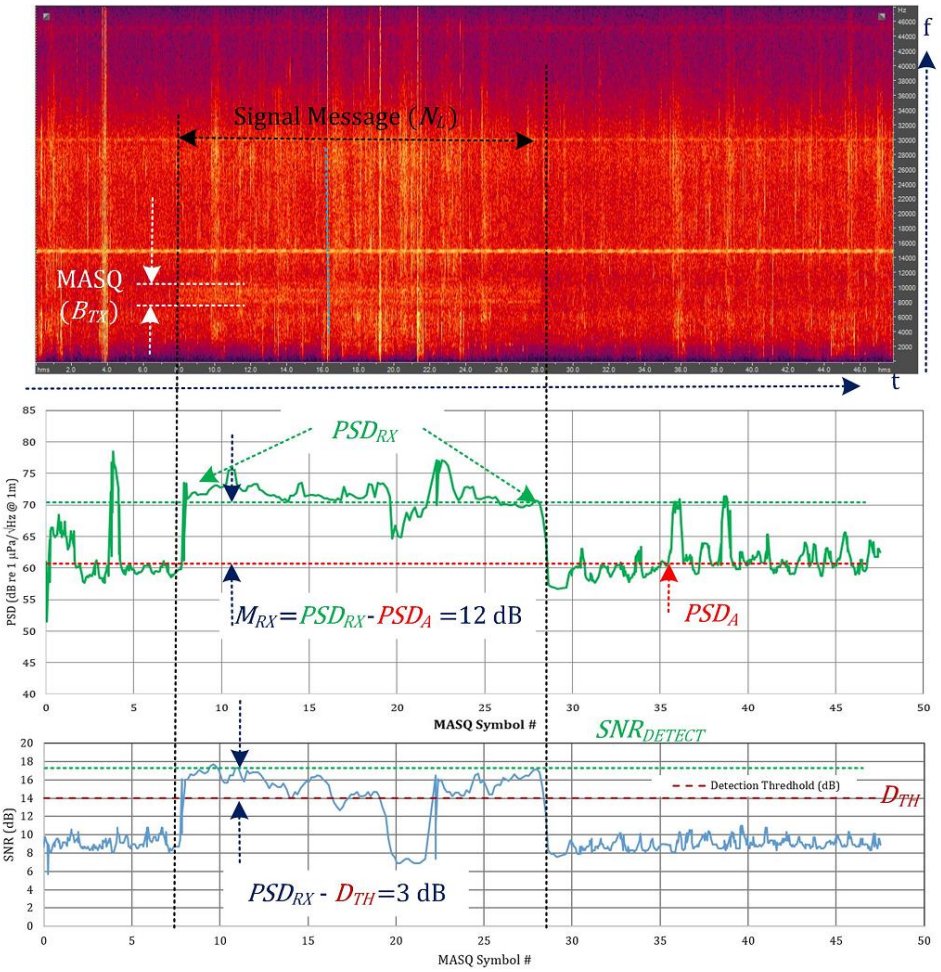

Figure 93 MCDSSS 100 baud 2 dB above ambient (time alligned spectrogram/*PSD*/*SNR*)

Figure 94 illustrates firmware version 6.0 MCDSSS receiver PSD_{ABS} plotted against time and compared to ambient noise for different sea states which provides a real-time measure of the MCDSSS receive signal quality and ambient noise.

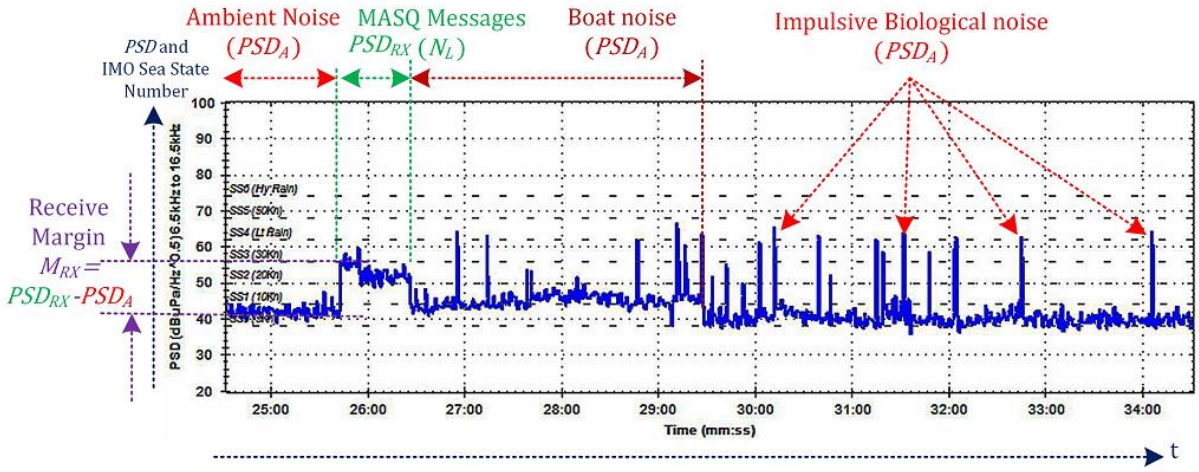

Figure 94 MCDSSS receiver signal (*I*) PSD and ambient PSD verses time

5.7.2.8 Receive Margin Derived Communication Range

The MCDSSS receiver PSD_{ABS} measures the signal detect power ($PSD_{DETECT} = PSD_{RX} + M_{TX}$) when SNR_{RX} is greater than or equal to the detection threshold (D_{TH}) Eq.(5-32).

$$PSD_{DETECT} = PSD_{ABS} = PSD_{RX} + M_{TX} \text{ when } SNR_{RX} \geq D_{TH} \tag{5-32}$$

The MCDSSS receiver PSD_{ABS} measures the ambient noise floor (PSD_A) when SNR_{RX} is less than the detection threshold (D_{TH}) Eq.(5-33).

$$PSD_A = PSD_{ABS} \text{ when } SNR_{RX} < D_{TH} \tag{5-33}$$

The difference between PSD_{DETECT} and the ambient noise floor (PSD_A) provides an estimate of the receive margin (M_{RX}) Eq.(5-33).

$$M_{RX} \approx PSD_{DETECT} - PSD_A \tag{5-34}$$

Reliable ($M_{RELIABLE}$) hydro-acoustic communication occurs when the receive margin (M_{RX}) is greater than 3 dB Eq.(5-35) (i.e. the receive signal power is at least twice the power of the loudest noise source).

$$M_{RELIABLE} > M_{RX} - 3 \text{ dB} \tag{5-35}$$

Covert (M_{COVERT}) hydro-acoustic communication occurs when the receive margin (M_{RX}) is less than the transmit margin (M_{TX}) Eq.(5-36).

$$M_{RX} - M_{TX} > M_{COVERT} \geq 0 \text{ dB} \tag{5-36}$$

For covert communication, MCDSSS transmitters radiate a covert spheroid when the MCDSSS receiver is located inside the spheroid body and outside the covert spheroid hole (Figure 3 left). If the MCDSSS receiver is outside the covert spheroid then no MCDSSS signal is detectable ($M_{RX} \leq M_{TX}$). If the MCDSSS receiver is located inside the covert spheroid hole then communication is not considered to be covert ($M_{COVERT} > M_{TX}$). The maximum covert communication range is equivalent to the maximum range (R_{MAX}). The minimum covert communication range (R_{COVERT}) can be estimated using the covert margin (M_{COVERT}) and the measured range (R_S) Eq.(5-37). The maximum communication range is also equivalent to the maximum covert communication range is useful during deployments as a prediction of at what range communication will be lost.

$$\begin{aligned} R_{MAX} \approx R_{COVERT} \approx R_S \div 10^{\left(\frac{M_{COVERT}}{10}\right)} \text{ for } R_S \leq 5 \text{ km} \quad \text{(for MASQ)} \\ R_{MAX} \approx R_{COVERT} \approx R_S - \frac{1{,}000 M_{COVERT}}{\bar{L}_A} \text{ for } R_S > 5 \text{ km} \quad \text{(for MASQ)} \end{aligned} \tag{5-37}$$

Firmware version 6.0 provides a hydro-acoustic tank calibrated measurement of receiver power (PSD_{RX}) which facilitates the calculation the covert margin (M_{COVERT}) and maximum cover range. For measured range less than $R_S \lesssim 5$ km, the spherical spreading equation (2-12) is used to estimate the minimum covert communication range. For measured range greater than $R_S \gtrsim 5$ km, the environmental absorption equation (2-15) is used to estimate the minimum communication range Eq.(5-37).

5.7.3 MCDSSS Receiver Telemetry Control System Optimisations

5.7.3.1 MCDSSS Shallow Water Telemetry (*Q*) Detector Optimisation

In the presence of in-band interference ($N_M > 0$) the telemetry decoder SNR_Q decays exponentially and can be less than 0.5 dB louder than the second loudest telemetry correlation peak Figure 96 and Figure 95. With SNR_Q as low as 0.5 dB the MCDSSS telemetry detector does not require a detection threshold as is the case with the firmware version 5.x MCDSSS reference channel detector. In firmware version 6.0, the removal of the telemetry detector detection threshold provided an incremental MR improvement for covert signals. False detections of MCDSSS telemetry are now handled by the FEC, however using the second loudest telemetry data as alternative source of FEC data failed to provide the correct telemetry data because the probability of the second loudest telemetry data being correct is small when SNR_Q is less than 0.5 dB. The MCDSSS telemetry detector processing gain is lower than the reference channel detector because the telemetry correlator effectively runs 256 simultaneous and independent MCDSSS detectors per telemetry channel where the probability of a false detection increases by approximately the square root of the number of telemetry receivers because of the 2 dB difference in performance between the reference and telemetry detectors. Chapter 4.3.5.4 MCDSSS receiver performance improvements are best applied to the MCDSSS telemetry detector before the MCDSSS reference detector.

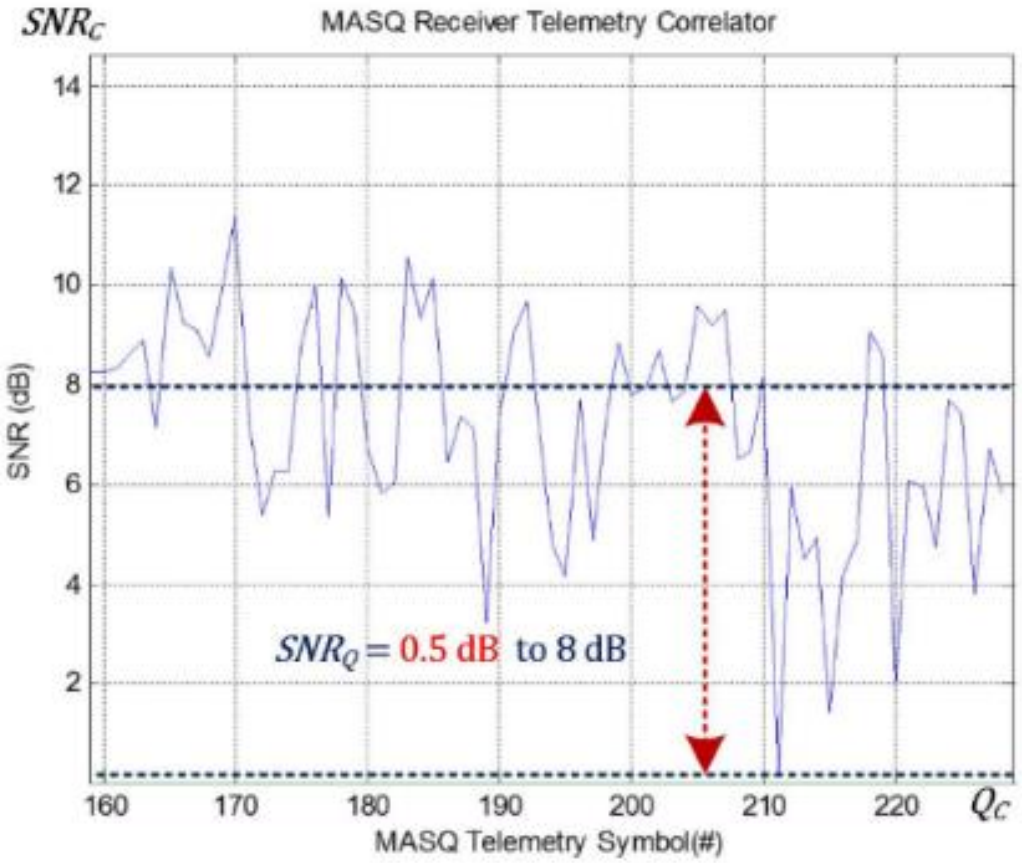

Figure 95 Low SNR MCDSSS telemetry (*Q*) detector SNR

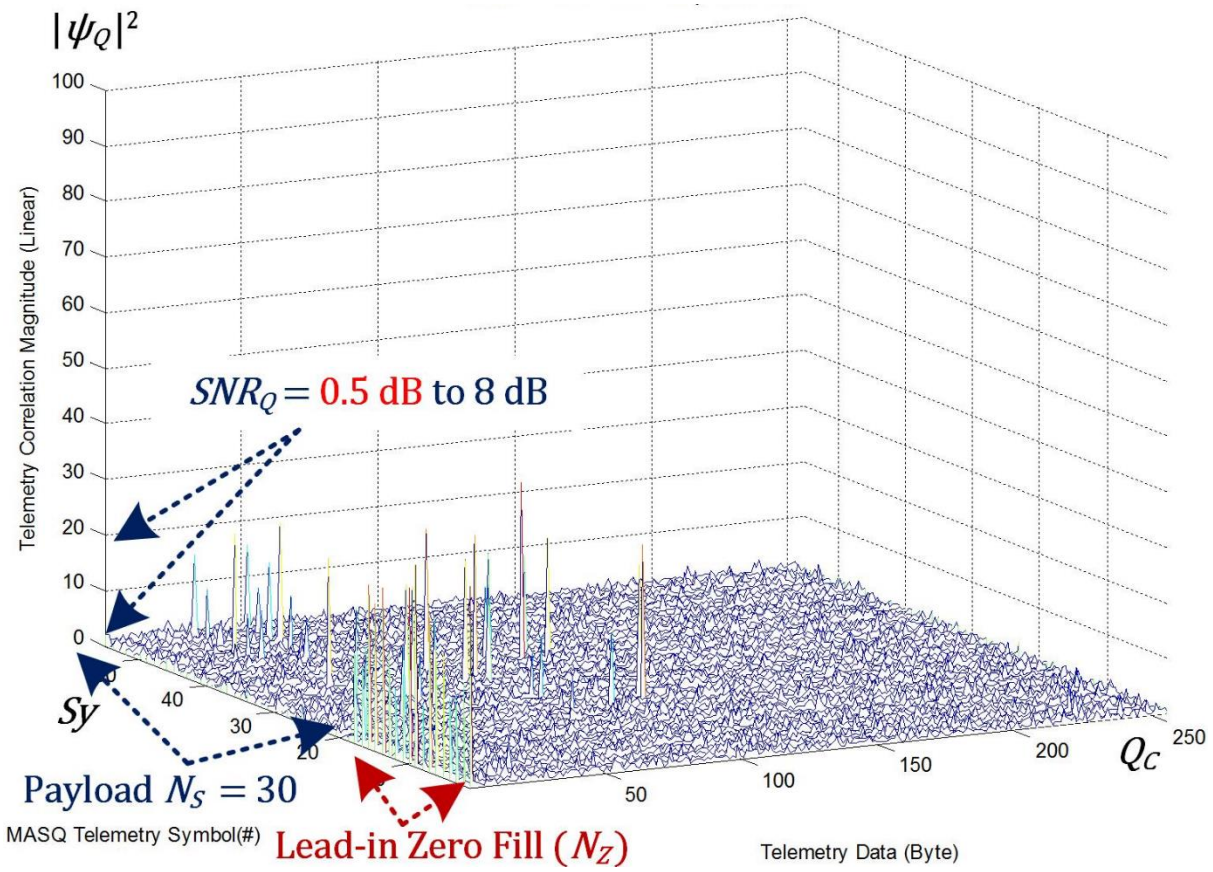

Figure 96 Low SNR MCDSSS telemetry (*Q*) detector waterfall

5.7.3.2 MCDSSS 5 Channel Telemetry Artefact Optimisation

As firmware version 6.0 message reliability was improved towards 99%, analysis of MCDSSS $N_C = 5$ channel covert sea trials data with receive margins less than $M_{RX} <$ 12 dB identified a higher than expected symbol failure rate on the 4th telemetry channel when compared to the 1st, 2nd and 3rd telemetry channels. Figure 97 illustrates the MCDSSS four channel telemetry correlation waterfall plot which exhibits a noise floor artefact for PRN encoded symbols on the fourth telemetry channel. The artefact resulted in false telemetry detection in high ambient noise because the magnitudes of the artefacts were greater than the valid telemetry correlation $(|\Psi_Q|)$. MASQ encodes four channel telemetry using bounded code sets and PRN codes. PRN codes exhibit a 3 dB higher noise floor $(P_{N_I} = 11.7$ dB) Eq.(4-11) compared to bounded code set noise floor $(P_{N_Q} = 13.5$ dB) Eq.(4-12). Demodulating bounded code sets with PRN telemetry codes is not comparing like with like. The firmware version 6.0 MASQ MCDSSS telemetry channel number four symbol PRN encoding has therefore been attenuated by 3 dB to equalise the bounded code sets and PRN code noise floor. Bounded code sets and PRN code noise floor equalisation also has impacts on the selection of multipath optimised spreading codes with good circular cross correlation properties (Chapter 5.5.1).

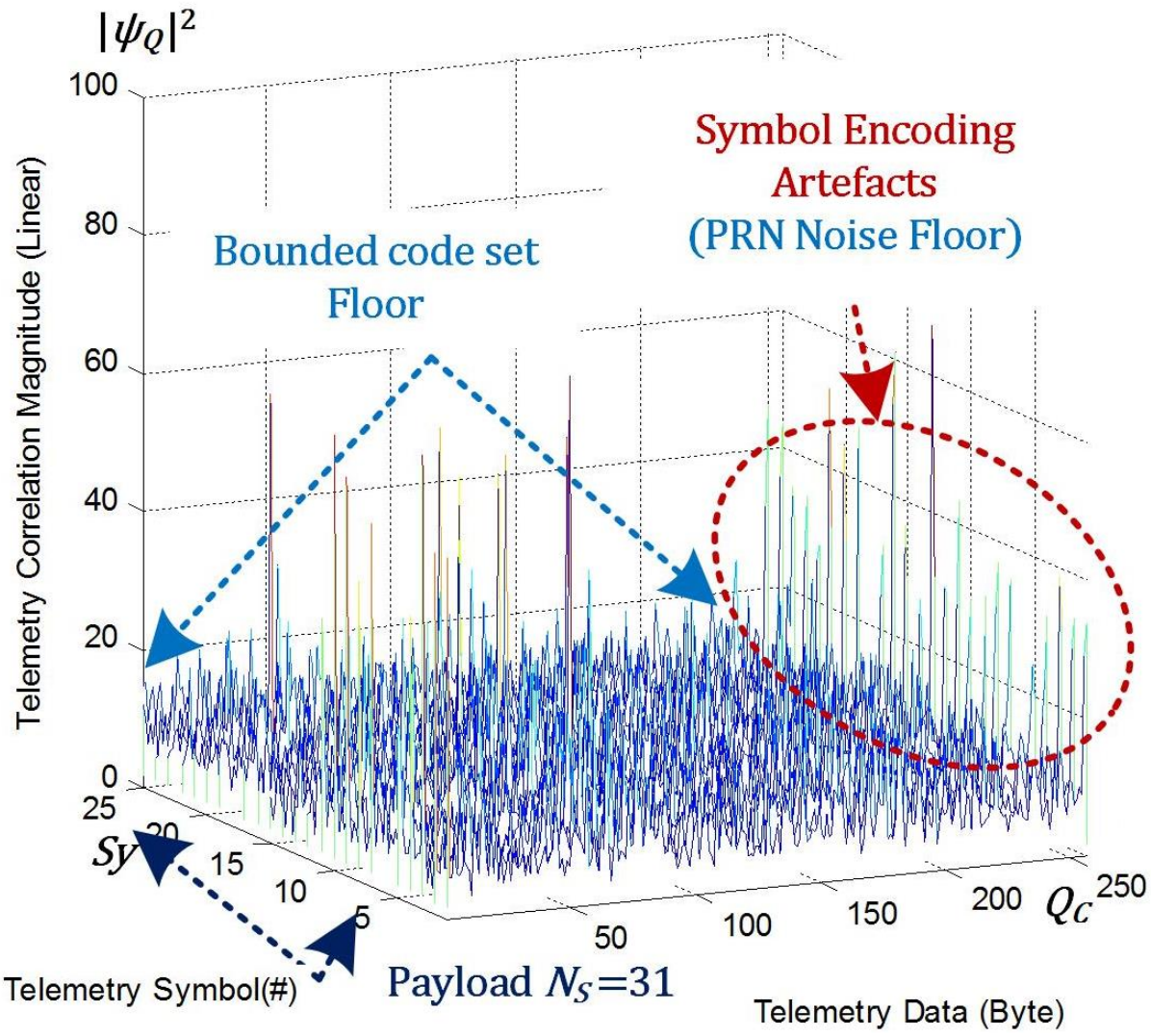

Figure 97 MCDSSS 4 channel telemetry artefacts

5.7.3.3 MCDSSS Telemetry Multipath Deconvolution Optimisation

The MCDSSS receive signal ($V_{RX}(\mathrm{t})$) is the time domain convolution of the MCDSSS transmit signal ($V_{TX}(\mathrm{t})$) and the channel impulse response ($h(\mathrm{t},\tau)$) Eq.(5-38).

$$V_{RX}(\mathrm{t}) = V_{TX}(\mathrm{t}) \otimes h(\mathrm{t},\tau) = \mathcal{F}^{-1}\left(\mathcal{F}\left(V_{TX}(\mathrm{t})\right) \times \overline{\mathcal{F}\left(h(\mathrm{t},\tau)\right)}\right) \tag{5-38}$$

Therefore, the impulse response is the frequency domain deconvolution of the MCDSSS receive and transmit signal conjugate. The MCDSSS reference signal detector $\psi_I(\mathrm{t})$ provides a real time estimate of the in-band channel response ($h(\mathrm{t},\tau)$) Eq.(2-19). MCDSSS multipath interference signals can be used as additional sources of energy to improve the telemetry detector performance. An estimate of the transmit signal (V_{TX}) can be generated by de-convolving the receive signal (V_{RX}) with the in-band channel impulse response, using frequency domain division Eq.(5-39).

$$h(\mathrm{t},\tau) \propto \psi_I(\mathrm{t}) \approx \mathcal{F}^{-1}\left(\frac{\mathcal{F}\left(V_{RX}(\mathrm{t})\right)}{\overline{\mathcal{F}\left(V_{TX}(\mathrm{t})\right)}}\right) \tag{5-39}$$

$$V_{TX}(\mathrm{t}) \approx \mathcal{F}^{-1}\left(\frac{\mathcal{F}\left(V_{RX}(\mathrm{t})\right)}{\overline{\mathcal{F}\left(\psi_I(\mathrm{t})\right)}}\right)$$

Frequency domain deconvolution is a $3N\log_2(N) \approx 31$ K operation where N is the number of spreading code samples multiplied by the frequency domain FFT butterfly operator, which typically requires 8 DSP machine cycles. The in-band channel impulse response is dominated by the multipath signal ($N_M \leq 12$) where the impulse response noise floor does not contain significant information when masked by 16-bit fixed point arithmetic rounding errors. Therefore, a truncated impulse response provides numerically efficient time domain deconvolution which is an $N \times N_M \approx 15$ K operator where the time domain operator is a complex multiply/accumulate requiring one DSP machine cycle. Truncated time domain deconvolution provides at least an order of magnitude performance improvement compared to frequency domain deconvolution. Frequency domain fixed-point deconvolution is a 16-bit in-place operation which is subject to numerical truncation error. Time domain deconvolution is a DSP 40-bit fixed-point accumulator operator which minimises numerical truncation error. The 2016 generation of fixed point DSPs support 70-bit fixed point accumulator arithmetic that can potentially reduce numerical truncation errors, thus supporting $N_M > 12$ with a potential additional improvement in multipath performance by up to 2 dB. Performance comparisons between the 32-bit and 64-bit versions of PC GPM300Windows program detect additional MCDSSS symbols in the failing signal database.

Equation (5-40) describes the time domain deconvolution coherently summing up the three loudest reference channel (I) correlation pulses.

$$\tau[m] = \text{Multipath signal time offset}$$

$$Sy_C[\mathrm{n}] = \mathrm{MAX}\left(\left|\sum_{\mathrm{m}=0}^{N_M<3}\left(\int_0^{\tau_{SY}} Q_{\mathrm{C}}[\mathrm{t},\mathrm{n}].\,\mathrm{e}^{-j(2\pi.f_C.\mathrm{t}+C.\theta_{TX})} * V_{RX}(t_{DETECT}+\tau[\mathrm{m}]-\mathrm{t})\mathrm{dt}\right)\right|_{\mathrm{n}=0}^{256-1}\right) \quad (5\text{-}40)$$

The shallow water multipath processing gain G_M can improve covert performance by approximately 3 dB Eq.(5-41).

$$N_S = 1, \qquad N_M = 0 \rightarrow 2$$
$$G_M = 10\log_{10}(N_S + N_M) = 0\ \mathrm{dB} \rightarrow 5\ \mathrm{dB} \approx 3\ \mathrm{dB} \quad (5\text{-}41)$$

The maximum number of multipath vectors $N_M \leq 3$ is a historical artefact of the NASNet™ predecessor to MASQ which was a technology limitation imposed by the 80 MHz 256 K byte fixed point DSPs available in the 1990s. The MCDSSS transceiver is deployed on a 2000s technology 500 MHz 325 K Byte fixed point DSP which has sufficient excess processing power to support higher order channel impulse response deconvolution ($N_M \geq 3$). Figure 98 illustrates the MCDSSS FEC error rates as a function of multipath impulse and multipath deconvolution. In the presence of any multipath, the MCDSSS signal will not decode if $N_M \geq 3$ regardless of ambient noise. The optimum number of multipath correction samples, that minimise FEC error levels, is approximately $N_M \approx 12$ for high multipath or covert communication.

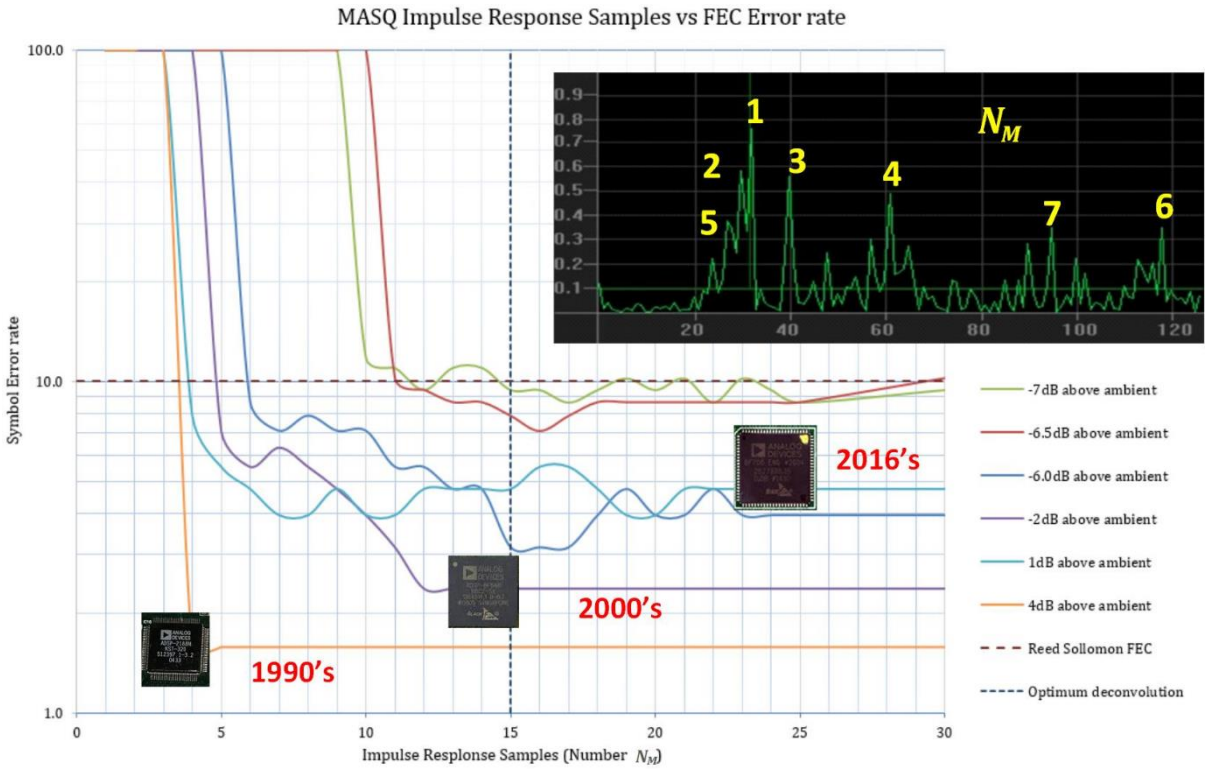

Figure 98 MCDSSS impulse response samples versus FEC error rates

Figure 99 illustrates the MCDSSS receiver telemetry impulse response deconvolution for $N_M \leq 14$. The deconvolution iterations are ordered from the loudest to the 14th loudest multipath magnitude. The initial slant range false detects ($Sy = 150$) decay after the fifth deconvolution iterations. The loud false detect correlation magnitude ($Sy = 241$) remains constant with successive deconvolution iterations. The valid telemetry symbol ($Sy = 48$) rises out of the noise floor after the 10th consecutive deconvolution iteration until the magnitude of the valid MCDSSS symbol exceeds the magnitude of the false detect symbol ($Sy = 241$). Deconvolution beyond $N_M \geq 12$ degrade performance using a 40-bit accumulators.

The optimisation of the number of multipath correction samples of $N_M \leq 12$ increases the processing load by half an order of magnitude, which required the development of a numerically efficient telemetry detector for firmware version 6.0. The MCDSSS telemetry signal can be extracted from the receive signal by removing the carrier, correcting for Doppler and decimating the number of samples to one complex sample per chip (Figure 101 left). The MCDSSS telemetry symbol coding does not contain phase information (i.e. bipolar phase encoded signal Eq.(4-17)). Therefore the complex correlation of receive signal with the telemetry signals can be reduced to a magnitude squared, multiply and accumulate Eq.(5-42) (Figure 101 bottom green).

$$Sy_C = \mathrm{MAX}\left(\left|\sum_{m=0}^{N_M \le 12}\left(\left|\sum_{n=0}^{\tau_{SY}} C_C[n,m] \times \mathrm{Re}(V_{RX}[t_{DETECT} + \tau[m] - n])\right|^2 + \left|\sum_{n=0}^{\tau_{SY}} C_C[n,m] \times \mathrm{Im}(V_{RX}[t_{DETECT} + \tau[m] - n])\right|^2\right)\right|_{c=0}^{256-1}\right) \quad (5\text{-}42)$$

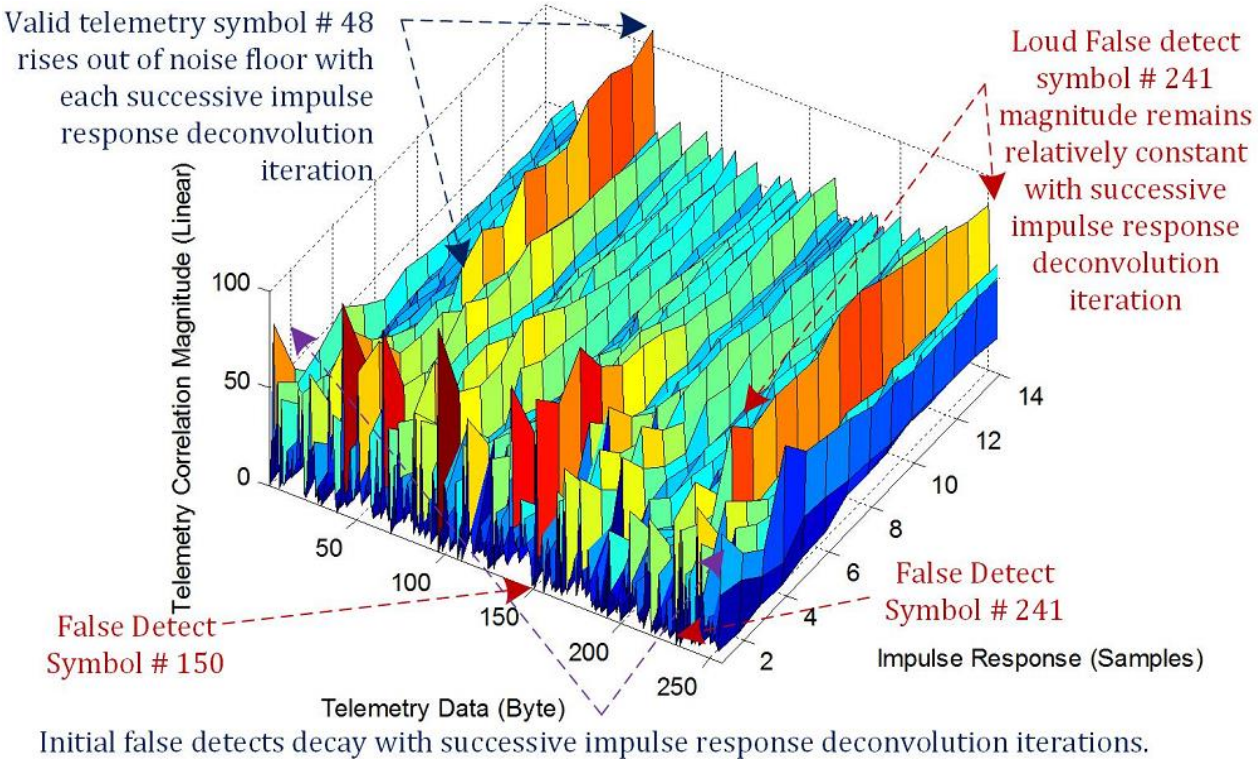

Figure 99 MCDSSS receiver telemetry response deconvolution

The pre-computation of bounded code sets and PRN codes $Q_C(t,n)$ requires approximately 2 M bytes of high speed RAM which exceeds the available DSP 325 K bytes of high speed RAM, therefore the bounded code sets and PRN codes must be dynamically generated. Since bounded code sets are the product of two PRN codes, the receive signal can be pre-multiplied by the first PRN code Eq.(5-43).

$$V_{M1}[n,m] = M_1[n] \times V_{RX}[t_{DETECT} + \tau[m] - n] \quad (5\text{-}43)$$

The telemetry symbol is then detected by correlating against the code rotated second PRN code (M_2) (Figure 100 control system ⑤ green). Detection of the last two symbol PRN codes, for a four telemetry channel MCDSSS signal, does not require the pre-multiplication step Eq.(5-44) and requires separate correlators. Firmware version 6.0 time domain telemetry deconvolution algorithm is numerically intensive however modest Eq.(5-44) algorithm efficiency gains translate to a reduction in DSP processor load and power consumption.

$$Sy_C = \mathrm{MAX}\left(\left|\sum_{m=0}^{N_M \le 15}\left(\left|\sum_{n=0}^{\tau_{SY}} M_2[\mathrm{mod}(n+m,1023)] \times \mathrm{Re}(V_{M1}[n,m])\right|^2 + \left|\sum_{n=0}^{\tau_{SY}} M_2[\mathrm{mod}(n+m,1023)] \times \mathrm{Im}(V_{M1}[n,m])\right|^2\right)\right|_{c=0}^{256-1} \quad (5\text{-}44)$$

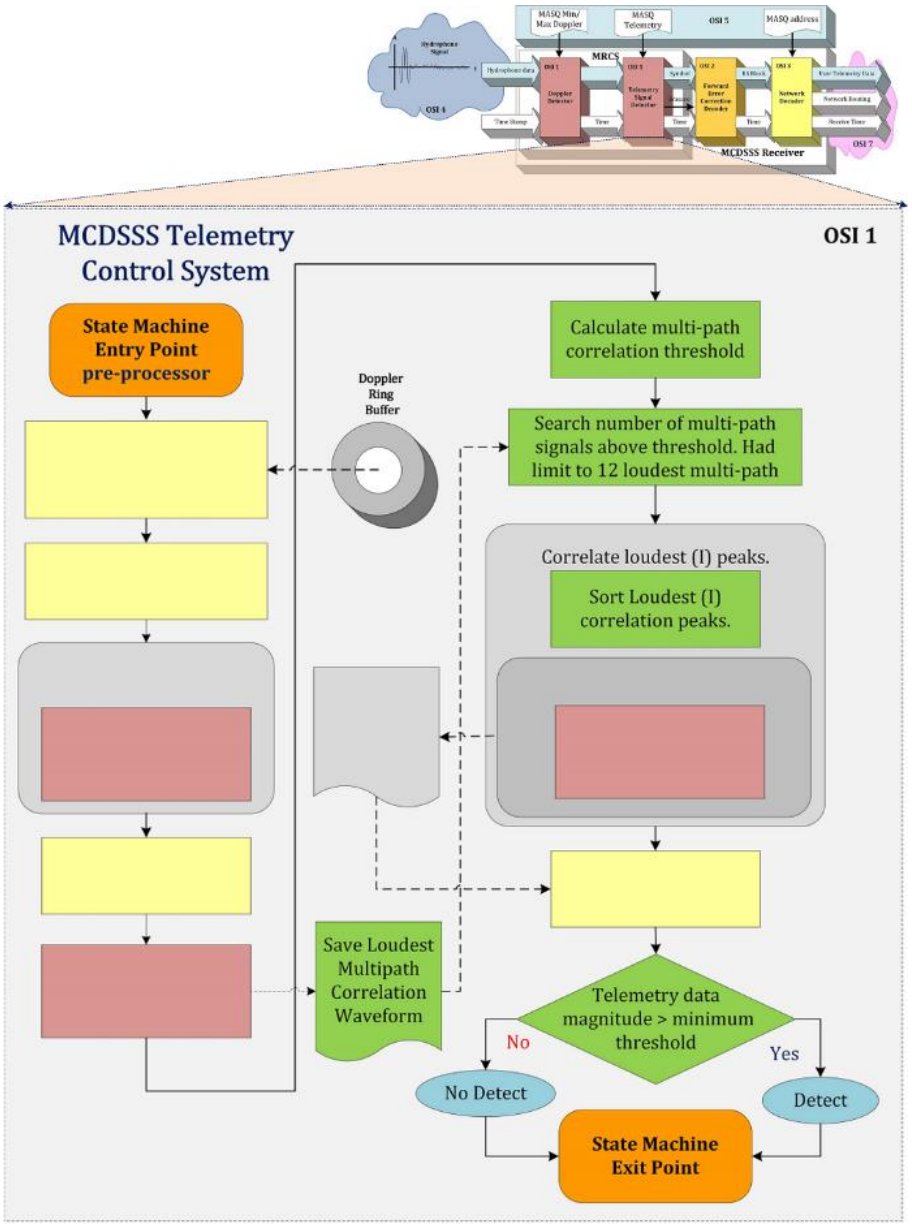

Figure 100 MCDSSS telemetry control system optimisations (NO L3 IP)

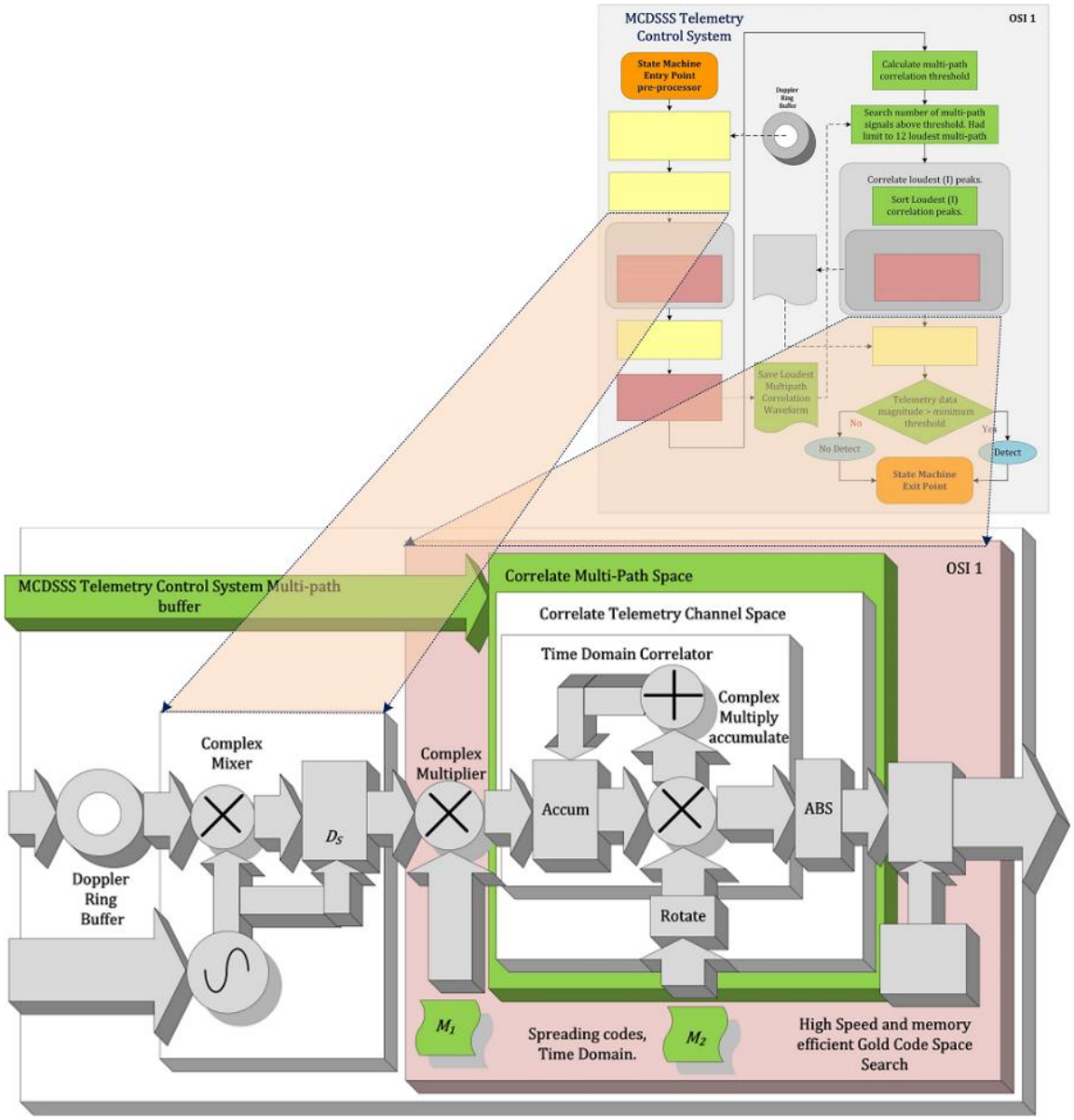

Figure 101 MCDSSS telemetry correlator optimisation (NO L3 IP)

5.7.4 MCDSSS Forward Error Correction Control System Optimisations

The MCDSSS modulation provides reliable communication in the presence of loud impulsive noise when the receive margin is greater than the transmit margin ($M_{RX} > M_{TX}$). When the receive margin is less than the transmit margin ($M_{RX} < M_{TX}$), the MCDSSS symbols are prone to corruption in the presence of loud impulsive noise (Chapter 2.6). The MASQ communication protocol implements Forward Error Correction (FEC) in OSI Data Link Layer 2 to recover corrupted MCDSSS symbols.

Error correction is an unnecessary overhead and not required for non-reverberating non-covert DSSS communication as used on STS and HAIL because the processing gain effectively provides symbol energy redundancy. Error correction is required by MASQ MCDSSS to locate the start and end of the message without requiring a pre-amble or post-amble signal. The forward error correction decoder uses the message symbols to solve the

error correction polynomial even with missing start, middle or end of message symbols. MASQ modulation uses Reed Solomon (RS) [159] FEC which is commercially deployed on CD/DVD/Blue-ray disks, QR codes, DSL/WiMAX/DVT/ATSC data transmission technologies and RAID 6 data storage. Convolution error correction schemes such as Low Density Parity Code (LDPC) [73] were considered but incur more than 50% overhead and require a lower detection threshold [137]. Reed Solomon provides a good compromise of low (+20%) overhead, medium computational load and robust error correction. Unlike convolution error correction, RS supports human readable payloads even if a partial message is received. RS correction is applied to a MCDSSS signal when the end of the message is detected. Very long MCDSSS messages incur a significant delay while the RS algorithm runs through all the start/end of messages locating polynomial permutations, which imposes a minimum inter-message delay, thus reducing the effective data transfer speed. High speed RS implementations provide orders of magnitude performance improvement but require large lookup tables that exceed the available Digital Signal Processor (DSP) high speed memory [159]. Faster RS implementations are available using commodity processor Single Instruction Multiple Data (SIMD) instruction sets but are not portable across different hardware architectures. The MCDSSS generic transceiver implements a memory efficient high-speed RS decoder that runs on multiple platforms however firmware version 6.0 required additional RS performance optimisations to increase the data transfer throughput for long messages.

Sea trial measurements of MCDSSS hydro-acoustic communication in high ambient noise occasionally generate an incorrect RS error correction when the number of erasures is greater than half the number of parity bytes and mandates an extra layer of error checking. MASQ modulation uses Cyclic Redundancy Check (CRC) CCTIT-16 [160] which is commercially deployed on multiple telecommunication protocols such as TCP/IP. CRC is only applied to the user data payload and in the event of a RS decode failure the user message is considered valid if the CRC error check passes. Alternative error checking protocols offer marginal performance improvements.

5.7.4.1 MCDSSS Start/End of Message Synchronisation Optimisation

The MCDSSS receiver locks onto to the start and end of an incoming message by convolving the MCDSSS symbols (Sy_C) with the Reed Solomon (RS) correction (5-45)

$$Decode = Sy_C \otimes RS \tag{5-45}$$

The end of message is detected when a sequence of erasures is detected at the end of the message. A gap in a message may not occur if the ambient noise and/or high multipath environment interference exceed the receive signal level, causing the RS convolver to detect a false end of message. When an end of message is detected and the RS decoder fails, the RS convolver is forced to wait for additional message symbols. Figure 102 (left green) illustrates the firmware version 6.0 RS control system ⑨ which was modified to include an inter message gap detector. User payloads may be less than a two's complement size RS block and zero filled. The leading zero filled symbols may be wiped out in a high ambient noise and/or high multipath environment causing the RS to fail even though the user payload (N_S) may be valid. If the RS decoder fails and a partial zero

filled block is detected, the partial zero filled block is cleared and the RS decoder is run again. Figure 102 (right green) illustrates the firmware version 6.0 RS control system ⑨ which was modified to include leading zero corruption block detector.

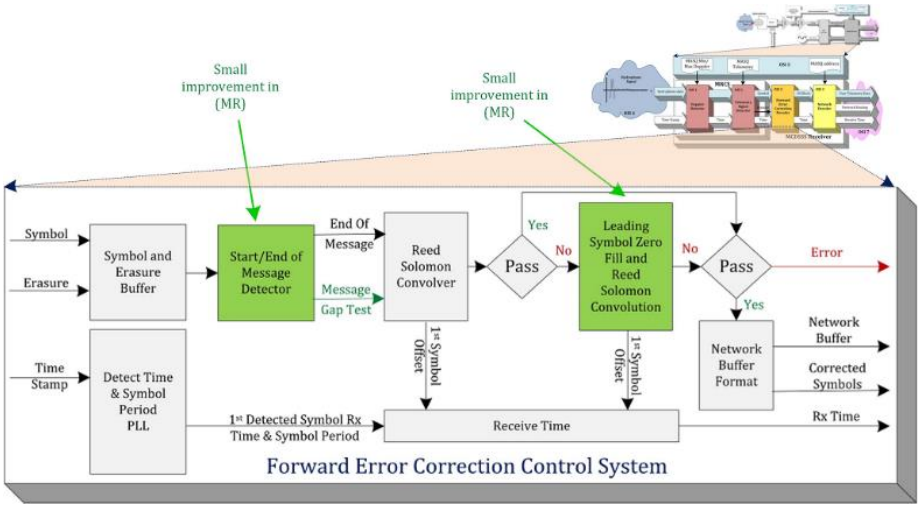

Figure 102 Reed Solomon convolver control system optimisations

When transmitting multiple MCDSSS messages the inter-message gap may be filled with multipath signals casing the MCDSSS receiver to detect the incoming signal as one contiguous message which will fail to decode. Figure 103 (green) illustrates firmware version 6.0 addition of a RS decoder inter message gap detection control system. Post processed sea trial data (Appendix L.7) measured an improvement in the message reliability of less than 0.5% which makes it difficult to estimate the message reliability beyond 99%.

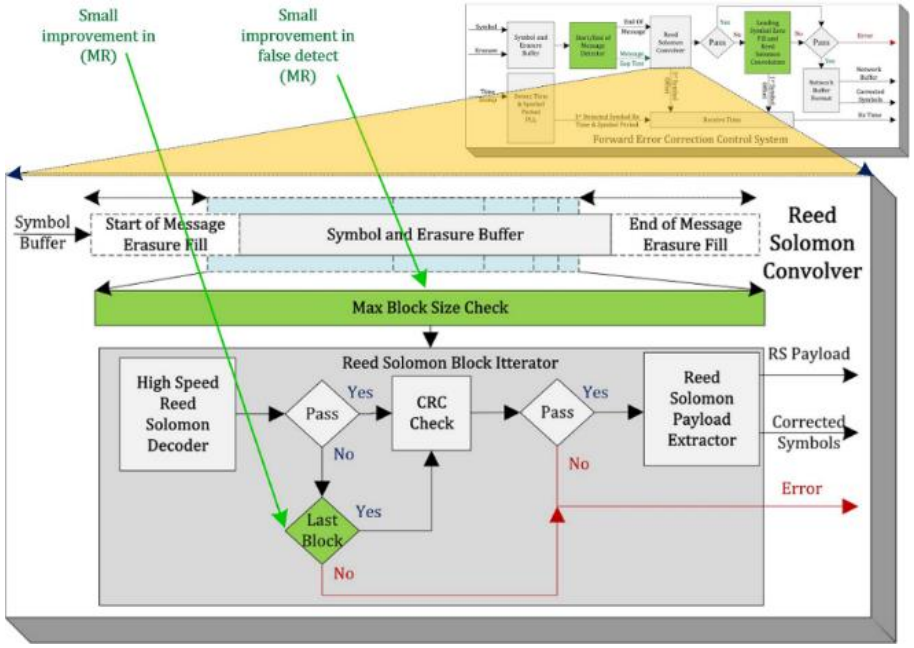

Figure 103 Reed Solomon decoder optimisations

5.7.5 MASQ Telemetry Alert Control System Optimisations

A communication link may fail in the presence of a deteriorating environmental noise floor. Communication can be re-established by lowering the baud rate and/or increasing the transmit source level which requires wireless command and control systems ①, ⑤ for reconfiguring local and remote modems. For low power battery applications MASQ supports sleep mode that uses telemetry alert ⑤ to power up the DSP MCDSSS receiver which can then dynamically reconfigured baud rate and transmit source level. If the telemetry alert receiver is less sensitive than the MCDSSS receiver then re-establishing a marginal communication link is not possible. Therefore the MASQ telemetry alert control system must provide at least 3 dB better detection performance than the 10 dB improved performance of the firmware version 6.0 MCDSSS receiver. Figure 104 illustrates the MASQ telemetry alert receiver block diagram with firmware version 6.0 algorithm and engineering optimisations colour coded green.

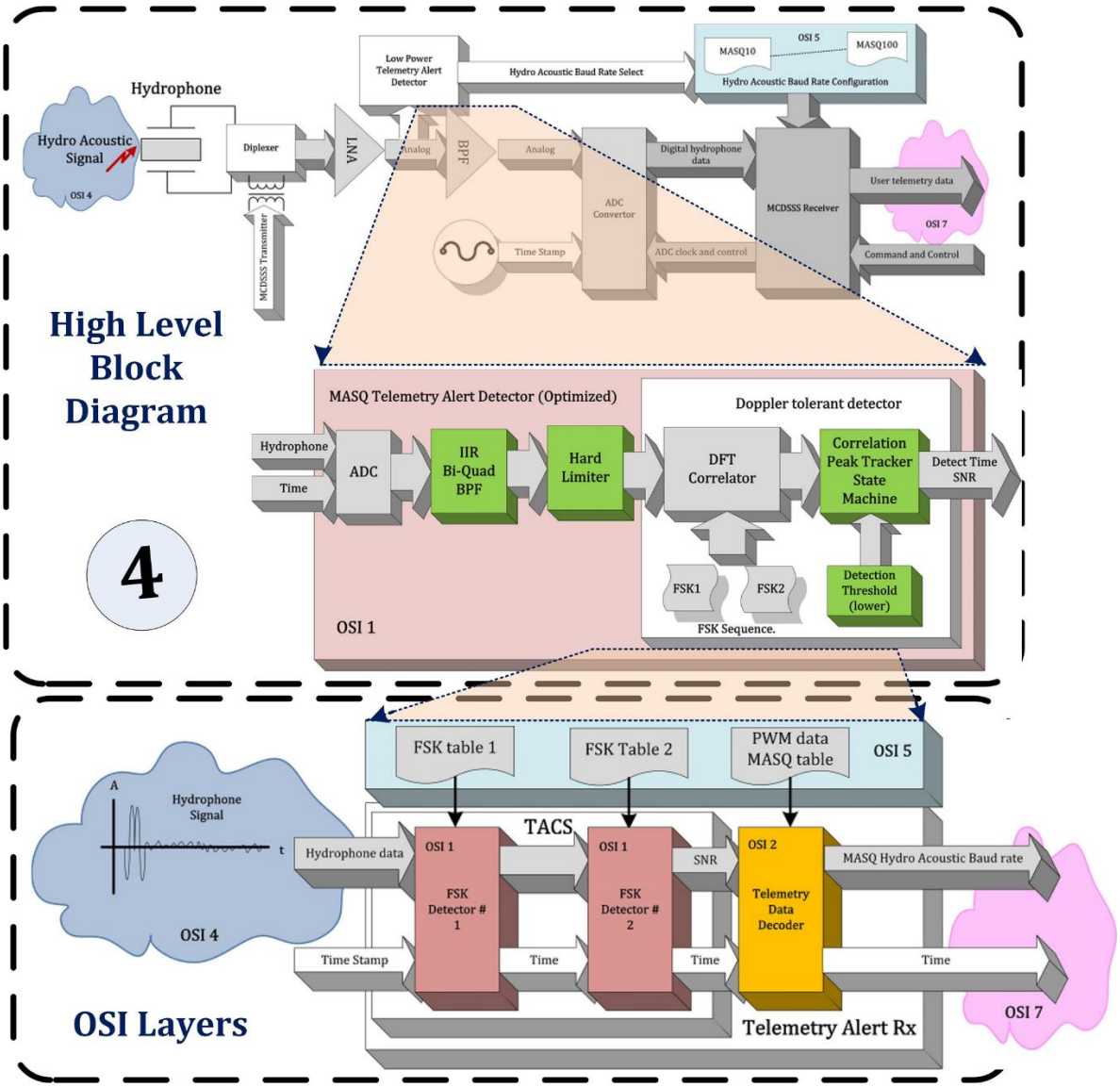

Figure 104 MASQ telemetry control system block diagram (optimisations green)

5.7.5.1 MASQ Transmitter Telemetry Alert Signal

The MASQ communication protocol supports optional dynamic baud rate configuration which is implemented using two Frequency Shift Key (FSK) pulses that precede an incoming MCDSSS message Eq.(5-46) (Figure 105).

$$f_T = 32.758\ \text{kHz}, \qquad TSS_B = 8, \qquad N_F = 2^{TSS_B} = 256$$

$$\tau_{PING} = \frac{N_F}{f_T} = \frac{256}{32.758\ \text{kHz}} = \frac{1}{128\ \text{Hz}} = 7.8125\ \text{ms} \tag{5-46}$$

$$V_{TX_{FSK_N}}(\text{t}) = \sin\left(2\pi . f_{FSK_N}\left[\text{floor}\left(\frac{\text{t}}{\tau_{PING}}\right)\right].\text{t}\right)$$

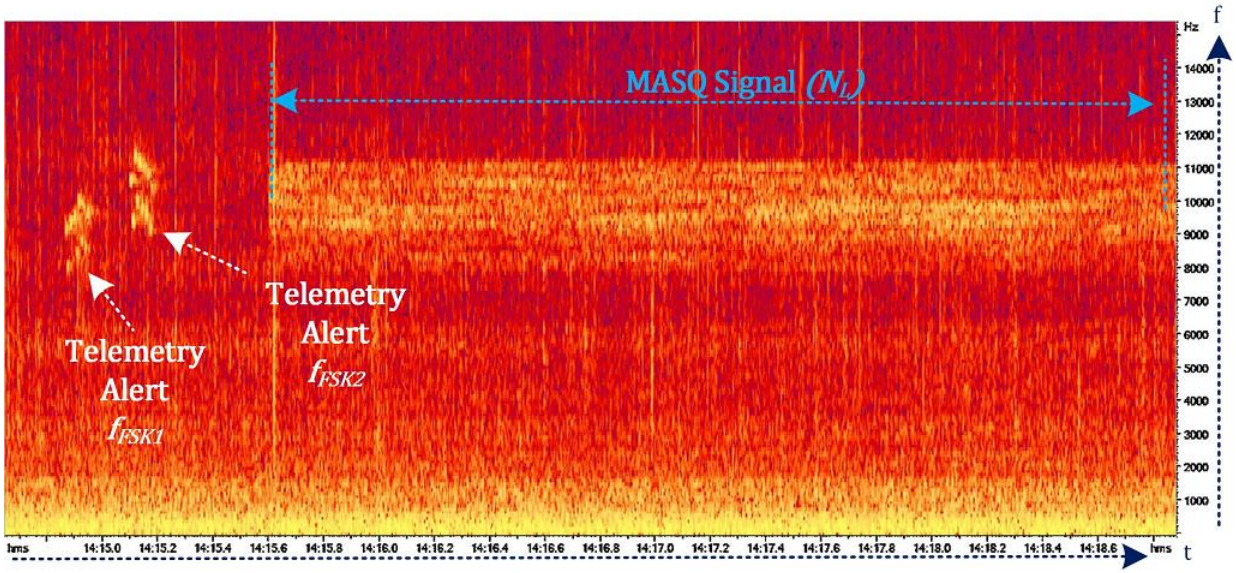

Figure 105 MASQ telemetry alert (100 baud spectrogram)

5.7.5.2 Doppler Tolerant Telemetry Alert Carrier Frequency Spacing

The telemetry alert carrier frequency spacing varies between 140 Hz and 250 Hz which provides tolerance to Doppler because the Doppler shifted carrier frequency is less than $(\Delta(D_S.f_{FSK_2}) \approx 10.040\ \text{kHz} - 9.996\ \text{kHz} < 50\ \text{Hz})$. The ping period $\tau_{PING} = 7.8125$ ms has a bandwidth of $B_{PING} = \frac{1}{\tau_{PING}} = \frac{1}{7.125\ \text{ms}} = 128$ Hz and is approximately equal to the FSK ping carrier spacing. Modulating telemetry data using the time delay between two FSK signals requires the time delay bins to be at least twice the ping bandwidth, as any impulsive ambient noise of sufficient magnitude will falsely trigger neighbouring zoom Discrete Fourier Transform (DFT) detectors. Figure 106 illustrates the spectrogram spectral leakage between neighbouring pings.

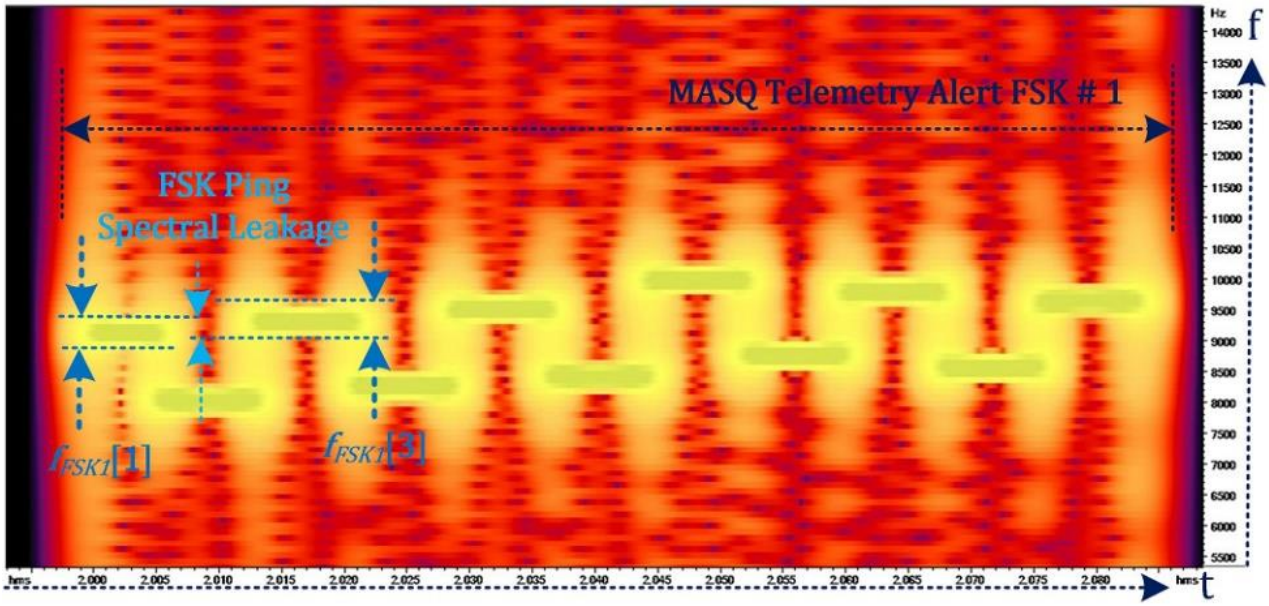

Figure 106 MASQ telemetry alert FSK ping spectral leakage (spectrogram)

5.7.5.3 Telemetry Alert PWM 1 of 16 Data Modulation

Figure 107 illustrates the 1 of 16 FSK telemetry alert data modulation bins. In the presence of noise, the FSK detector time resolution (τ_{FSK}) may be greater than one FSK ping period of $\tau_{PING} = 7.8125$ ms (Figure 110). The data bins are spaced by at least twice the FSK ping period of $2\tau_{PING} = 15.625$ ms to maximise Doppler performance. FSK data modulation is considered valid if the time difference is within ± 7.8125 ms of modulo 15.625 ms delay Eq.(5-47).

$$N_{FSK} = 11$$

$$\tau_{FSK} = N_{FSK} \times \tau_{PING} = 85.9375 \text{ ms}$$

$$\Delta t_{FSK} = t_{FSK2} - t_{FSK1} \tag{5-47}$$

$$Sy_{PWM} = \text{int}\left(\frac{\Delta t_{FSK} - \tau_{PING}}{2\tau_{PING}}\right)$$

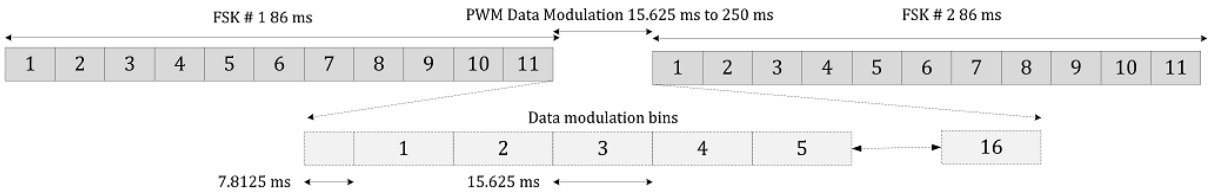

Figure 107 MASQ telemetry alert PWM 1 of 12 data modulation bins

5.7.5.4 Multipath Tolerant Telemetry Alert PWM MASQ20 Optimisation

Figure 108 illustrates the telemetry alert signalling for MASQ20 modulation and the time delay between the f_{FSK_1} and f_{FSK_2} is a long latency $\Delta t_{FSK} = 125$ ms. MASQ20 uses data modulation bin 11 and the total delay between the start of the FSK and MASQ20 is $11 \times 15.6 + 7.8 + 82 \times 2 = 343$ ms. Low MASQ baud rates are used for long-range communication and the FSK signals that are prone to $\tau_M \rightarrow 20$ ms multipath delays

require wider ±7.8125 ms PWM bins. Appendix I sea trial analysis of 10.7 km range and low baud rate communication identified a high false detect rate for the telemetry alert where the decoded incoming MASQ baud rate was slower than the actual MCDSSS baud rate. During long-range and shallow water communication, the telemetry alert FSK#2 signal is subject to long multipath delays greater than $\tau_M > 7.8$ ms and the hard limited telemetry alert detector Figure 106 may report the multipath detect time (τ_M) instead of the slant range time (τ_S). Improvements in the telemetry alert detector shallow water robustness required a change in the MASQ telemetry alert communication protocol where 10 to 50 baud communication occupies two to three $\Delta t_{FSK} = 15.6$ ms time slots (Figure 108 centre green)

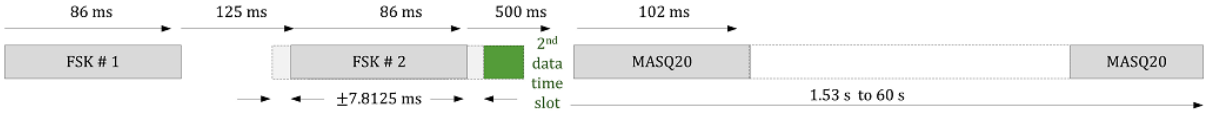

Figure 108 MASQ telemetry alert data modulation (20 baud multipath tolerant)

5.7.5.5 MASQ Telemetry Alert Receiver Replacement

Figure 109 illustrates the MASQ Telemetry Alert Receiver Block diagram.

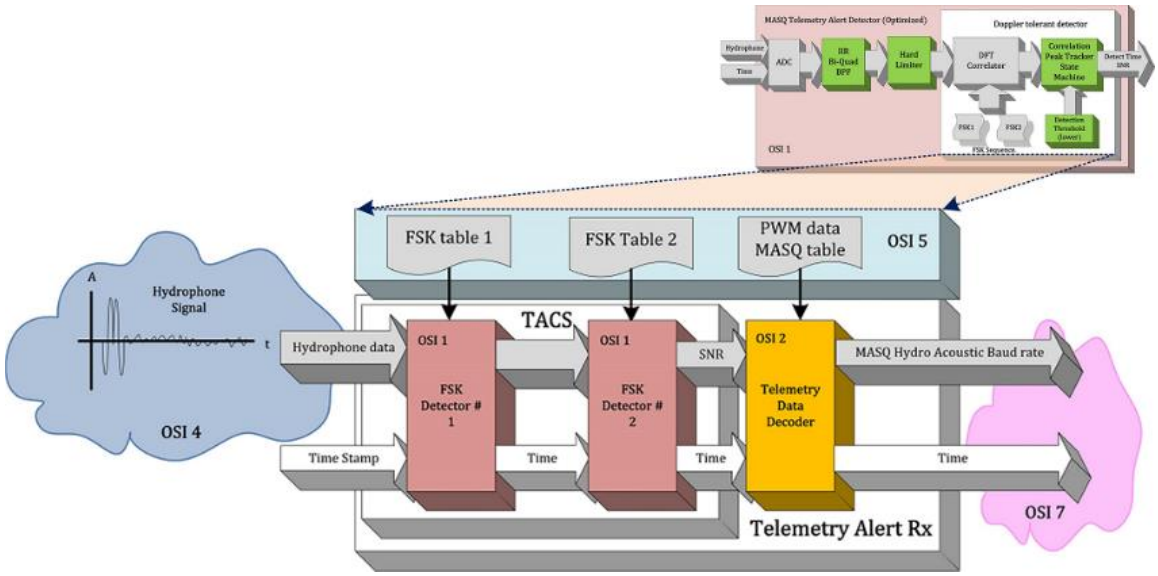

Figure 109 MASQ receiver telemetry alert block diagram (candidate design)

Equation (5-48) describes the time domain detection (ψ_{FSK_N}) of the telemetry alert signal.

$$V_{FSK_N}(\mathrm{t}) = e^{-j2\pi.f_{FSK_N}\left[\mathrm{FLOOR}\left(\frac{\mathrm{t}}{\tau_{PING}}\right)\right].\mathrm{t}}$$

$$\psi^2_{FSK_N} = \left|V_{RX} \otimes V_{FSK_N}\right|^2 \propto \mathrm{P}_{\mathrm{FSK_N}} \text{ (signal receive acoustic power detector)} \tag{5-48}$$

The ($\tau_{FSK} = 85.9$ ms) telemetry alert signal ($V_{TX_{FSK_N}}$) is transmitted at the same power as the MCDSSS signal and must exhibit better detectability than the lowest baud rate MCDSSS ($Br = 10$ baud, $\tau_{MASQ10} = 800$ ms) signal, which is eight time longer and 6.5 dB higher in transmit energy when including the telemetry channel loss ($L_{C2} = 3$ dB) Eq.(5-49).

$$\frac{\epsilon_{MASQ10}}{\epsilon_{FSK}} \propto 10\log_{10}\left(\frac{\tau_S}{\tau_{FSK}}\right) - L_{C2} = 6.5 \text{ dB} \quad (5\text{-}49)$$

Firmware version 6.0 required additional digital signal processing for the FSK detector, to improve the sensitivity by at least 3 dB compared to the MCDSSS 10 baud detector (See Appendix M for sea trial performance validation).

5.7.5.6 Telemetry Alert Detector Baud Rate Dynamic Control System

Figure 110 illustrates the replacement telemetry alert detector and acoustic baud rate configuration sequence which is as follows:

1. Detect FSK #1
2. Power up DSP and initiate DSP boot sequence and configure for the default MCDSSS hydro-acoustic baud rate.
3. Enable telemetry alert FSK #2 detector.
4. If FSK #2 is detected within the PWM period then decode D_{PWM} and reconfigure DSP to detect 1 of 12 baud rate else enable FSK #1 detector.
5. If DSP already detecting valid MCDSSS signal, then ignore FSK #2.
6. Enable telemetry alert FSK #1 detector.

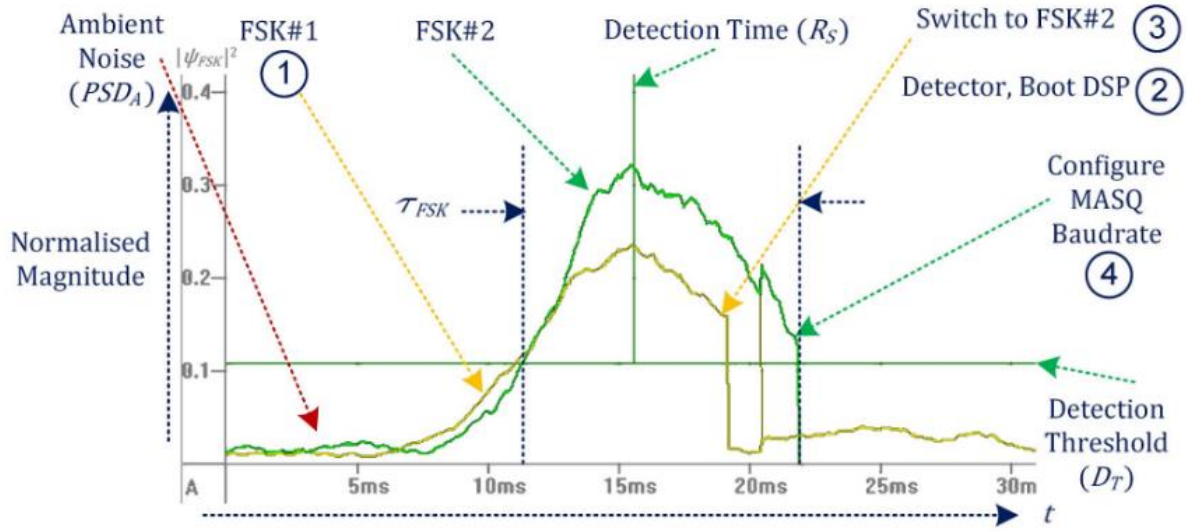

Figure 110 MASQ receiver telemetry alert falling edge detector correlator

5.7.5.7 Telemetry Alert Multipath Control System Optimisation

The MASQ receiver telemetry alert detector provides tolerance to the following sources of interference:

1. High ambient noise floor (PSD_A).
2. Impulsive noise (PSD_A).
3. Multipath reverberation (R_M).
4. Surface ducting interference (R_T).
5. Bottom propagation interference (R_B).
6. Inter-symbol interference ($\Delta t_M > \tau_{FSK}$).
7. Nonlinear channel response ($h(\mathrm{t}, \tau)$).

Tolerance to interference is implemented using a MASQ receiver telemetry alert detector non-linear control system ⑤. For the firmware version 6.0 MCDSSS receiver, a near 10 dB required improvement in the performance required that the telemetry alert detector be at least +3 dB. more sensitive than the MCDSSS telemetry receiver. Lowering the telemetry alert detection threshold by 3 dB generates an unacceptable number of false detections induced by loud impulsive noise and multipath. The addition of a hydrophone signal hard limit normaliser dramatically improved the impulsive noise false detect rate. A hard limited detector is approximately 3 dB less sensitive than an analog detector because the hard limiter only passes the loudest signal. If the out of band noise is louder than the telemetry alert signal then the detector performance will be compromised and required the addition of an IIR high Q band pass filter before the hard limiter, to minimise the in-band signal masking (Figure 111 green)

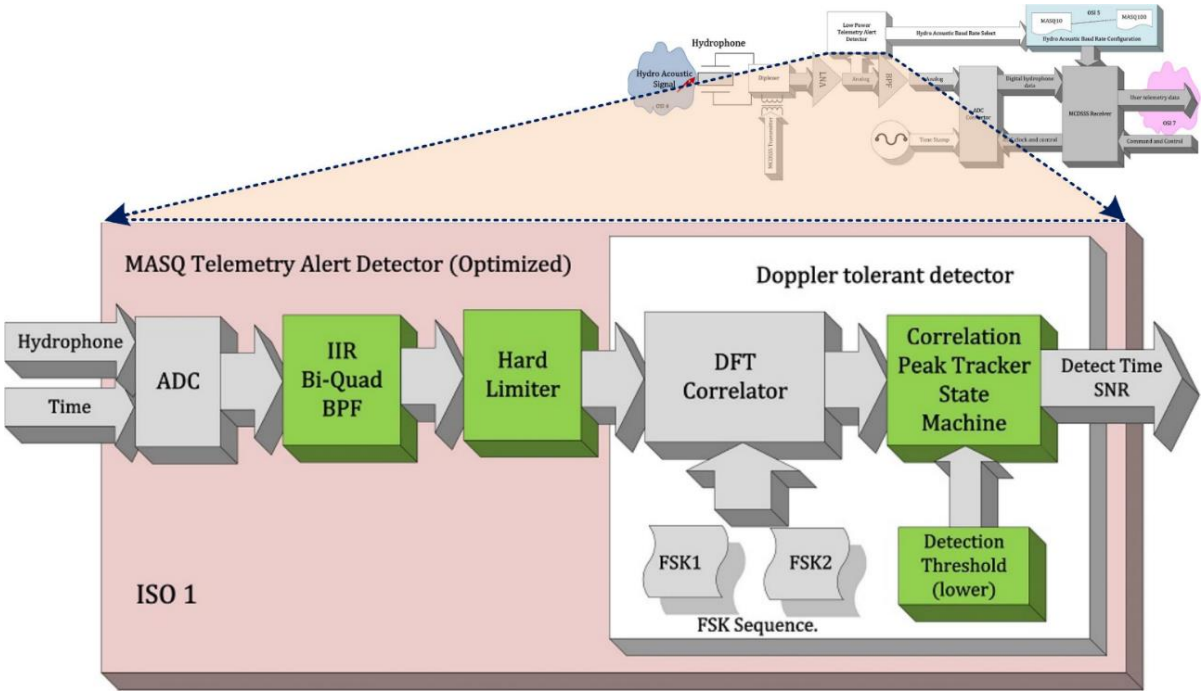

Figure 111 MASQ telemetry alert detector non-linear control system (replacment)

5.7.5.8 MASQ Telemetry Alert Receiver Sensitivity Optimisation

The firmware version 5.x telemetry alert maximum correlation peak detector, or rising edge detector, could not cope with multipath signals and required a robust state machine to track the correlation peak in the presence of loud in-band noise and/or multipath. Multiple control systems were designed and tested but failed when subjected to sea trial data, reverberating air tests or hydro-acoustic tank tests. The control system ④ algorithm that provided the most robust performance was a falling edge correlation peak detector (Figure 110 right vertical lines). The correlation peak must be louder than the detection threshold for a minimum pre-set time and a detection is valid when the correlation peak drops to less than the average of the maximum correlation peak and the detection threshold (Figure 112 green).

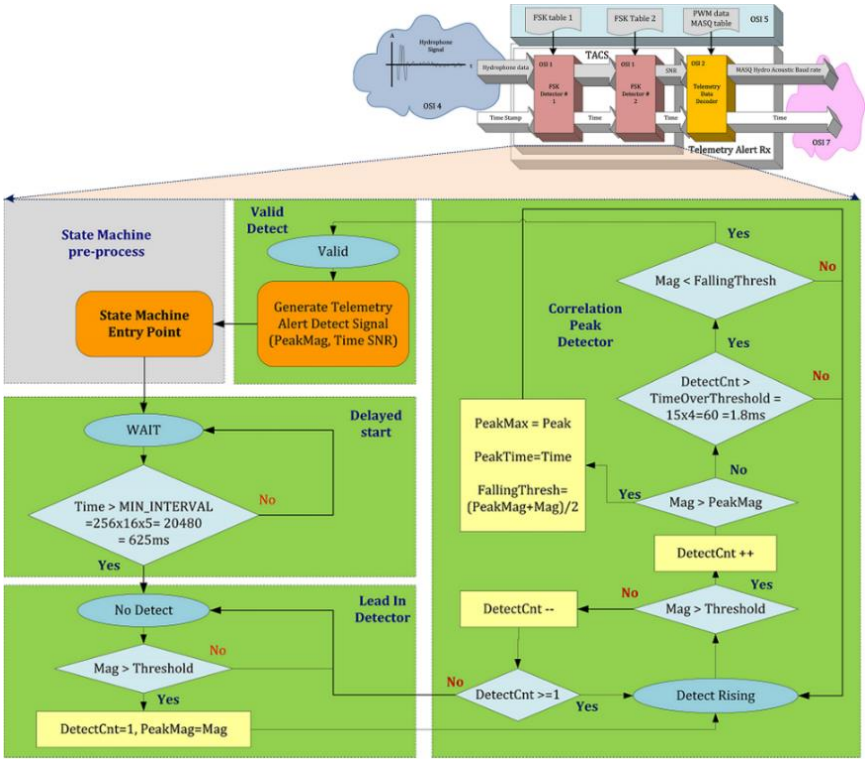

Figure 112 MASQ telemetry alert falling edge correlation peak detector (replacment)

5.7.6 Receiver Maximum Communication Range Optimisation

5.7.6.1 Alternative Differential Low Noise Electronics Options

The low cost PZT transducer requires lower noise electronics to compensate for the PZT transducer's low Open Circuit receive Voltage response (OCV). Differential low noise electronics are a well-established technique used to optimise noise performance [79]. Low noise electrical construction techniques such as differential electronics, differential circuit board traces, and differential electrical cabling are required to provide common mode noise rejection from internal switch mode power supply noise, digital electronics noise and external electrical interference. Analog architectures with improved low noise performance and lower manufacturing cost could not be identified.

5.7.6.2 Receiver Noise Floor Snubbing Networks

For an equivalent MCDSSS receiver input noise less than $SS0$, the radial polarized PZT transducer low $OCV = -180$ dBVrms/1 µPa @ 1 m requires a Low Noise Amplifier (LNA) control system ④ with an equivalent input noise of less than 80 nV/$\sqrt{\text{Hz}}$, which is well within the 10 nV/$\sqrt{\text{Hz}}$ input noise of an ultra-low power 10 mW op-amp Eq.(5-50). Measurements of the hydrophone noise floor identified that the LNA was not the largest source of noise.

$$V_{LNA} = 10^{\frac{(OCV+PSD_{SS0})}{10}} < 80\ \text{nV}/\sqrt{\text{Hz}} \tag{5-50}$$

The LNA is connected to the PZT transducer via a high voltage diplexer. The diplexer was identified as a source of electrically coupled noise which required the addition of a noise

snubbing capacitance (Figure 113 green). Additional electrical and magnetic shielding was required to minimise the noise pickup from internal switch mode power supplies and external electrical noise. Switch mode power supply noise was magnetically picked up by the step-up transformer and noise was reduced by adding a high power load resistor across the step up transformer primary via the power amplifier output (Figure 73 green).

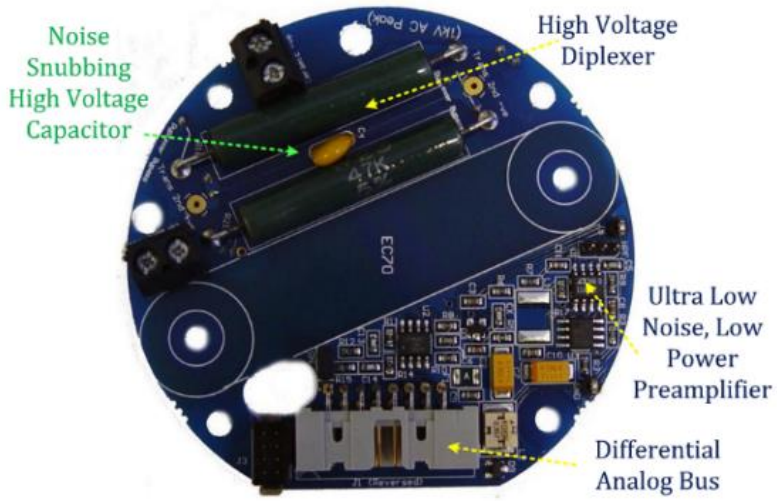

Figure 113 Φ80 mm OD low noise preamplifier and diplexer (candidate design)

5.7.6.3 Low Noise and High Dynamic Range ADC Measurement

A measurement of the MCDSSS receiver dynamic range was required to validated that the analog front end had sufficient dynamic range to detect a long range SS signal in the presence of loud ambient noise. Figure 114 illustrates the φ80 mm OD MCDSSS generic Transceiver Processor Card (TPC). The analog electronics are electrically shielded from the digital electronics located on the other side of the circuit board. The TPC power supplies use variable frequency switch mode convertors with low MCDSSS 6.5 kHz to 16.5 kHz in-band noise. All analog electronics, wiring and circuit board analog traces are differential to minimise electrical noise pickup.

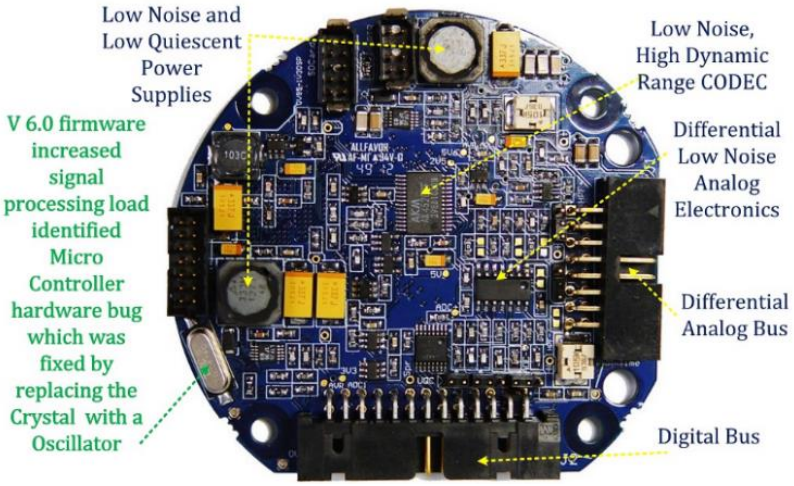

Figure 114 Φ80 mm OD MCDSSS transceiver, analog electronics (candidate design)

The addition of noise snubbing networks improved the TPC ADC dynamic range to be approximately equal to the maximum ambient noise difference $PSD_{\Delta SS} \approx 100$ dB Eq.(7-25), which facilitates simultaneous reception of a long and short range MCDSSS signal in the presence of loud out of band noise (i.e. low frequency vessel propeller or thruster noise). Figure 115 illustrates the TPC ADC dynamic range which was measured at $V_{ADC} \approx 120$ dB and is within the $PSD_{\Delta SS} \approx 100$ dB limit. The TPC ADC noise floor measurement V_{ADC} is required for firmware version 6.0 MCDSSS receiver noise floor calibration Eq.(5-22).

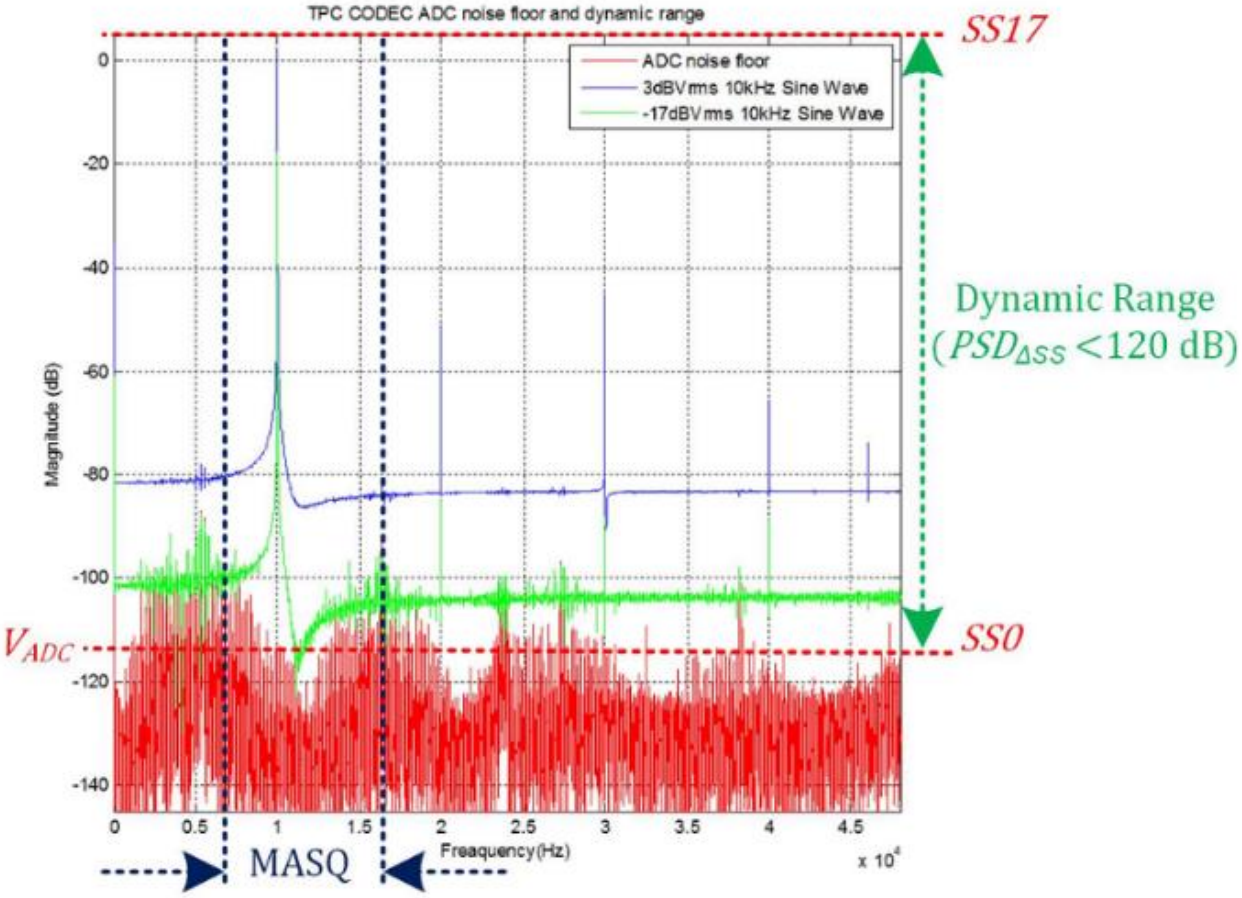

Figure 115 GPM300 TPC CODEC ADC noise floor and dynamic range

5.7.7 MCDSSS Receiver Power Consumption Minimisation

5.7.7.1 Low Quiescent Current Receiver Hardware

The GPM300 low noise preamplifier Figure 113 power consumption is 10 mW which is less than 20% of the MCDSSS generic receiver telemetry alert detector sleep power consumption of 70 mW . Figure 116 illustrates the Φ 80 mm OD MCDSSS Generic Transceiver digital electronics layer. A low power 70 mW microcontroller runs the telemetry alert detector which powers up the DSP when there is an incoming MCDSSS message. The DSP consumes less than 1.7 W when running the MCDSSS receiver. For long-term battery deployments, the transceiver can be acoustically or electrically configured for ultra low power 4 mW deep sleep mode. The capabilities of low power electronics can be harnessed only if numerically efficient software is implemented.

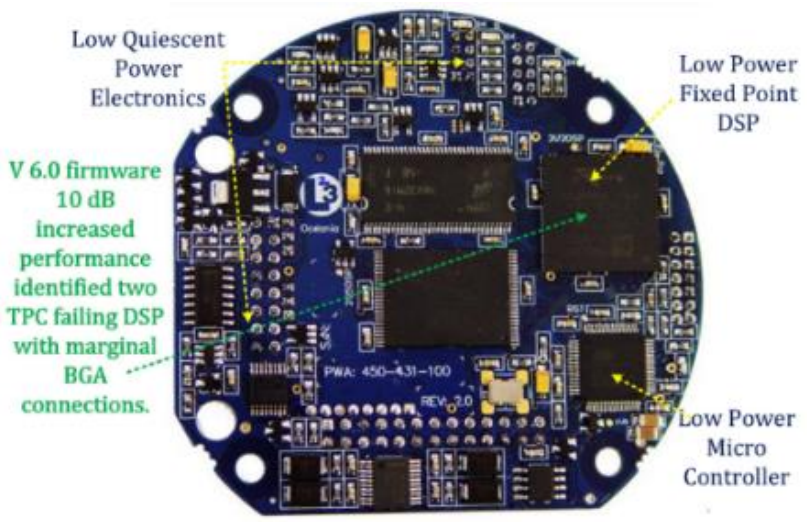

Figure 116 Φ80 mm OD MCDSSS generic transceiver digital electronics (candidate design)

5.7.7.2 Alternative Software Performance Optimisation Options

The MCDSSS generic receiver uses Fast Fourier Transform (FFT) and zoom Discrete Fourier Transform (DFT) high-speed correlators which are well established techniques [92]. Alternative signal processing techniques such as Fast Wavelet Transform and *sinc* interpolation offer marginal performance improvements [97]. The MCDSSS telemetry receiver multipath deconvolution detector uses a time domain correlation algorithm which provides the lowest numerical noise floor but incurs very high (time domain processing) computational load, which almost exceeds the computing capacity of low power DSP's and commercial PC's. Complex arithmetic FFT and DFT correlation algorithms (frequency domain processing) provide the lowest computational load but incur high software complexity and are prone to subtle coding errors which reduce message reliability. The MCDSSS processing gain can provide a reliable communication link even in the presence of faulty algorithms or software bugs. Defective hardware or software may pass functional tests but fail when deployed at long-range or in high ambient noise. The robustness of MCDSSS signalling is highlighted by vessel hull communication and through prop wash communication (Appendix L.6.6).

5.7.7.3 Power Efficient MCDSSS Receiver Software

A time domain correlator ($\psi_I(\mathrm{t})$) can be used to detect a MCDSSS reference signal (V_I) Eq.(5-51). A discrete time domain correlator ($\psi_I[\mathrm{n}]$) with large numerical accumulators has the lowest digital truncation noise floor ($10\log_{10}(\mathrm{V}_D^2) < P_{N_G}$) Eq.(4-13) but incurs a high computational load and high power consumption.

$$\psi_I(\mathrm{t}) = V_I(\mathrm{t}) \otimes V_{RX}(\mathrm{t}) = \int_0^{\tau_S} V_I(\tau) * V_{RX}(\mathrm{t}-\tau)\mathrm{d}\tau$$

$$\psi_I^2[\mathrm{n}] = \sum_{\mathrm{m}=0}^{N_S-1} |V_I[\mathrm{n}] * V_{RX}[\mathrm{n}-\mathrm{m}]|^2 \propto \mathrm{P_I} \text{ (signal receive acoustic power detector)} \tag{5-51}$$

Time domain correlation is an N_{MAC}^2 operation where N_{MAC} is the number of Multiply and Accumulate (MAC) operations. A MCDSSS 10 baud message has a symbol period of $\tau_{MASQ10} = 0.8\,\text{s}$ and the number of hydrophone symbol samples is 76,800 for an $f_S =$ 96,000 sample/s ADC Eq.(5-52).

$$N_{MAC} = \tau_{SY} \times f_S$$
$$N_{MASQ10} = \tau_{MASQ10} \times f_S = 0.8\,\text{s} \times 96{,}000\ \text{samples/s} = 76{,}800\ \text{samples} \tag{5-52}$$

The time domain correlator computational load ($C_{\text{t}_{\text{MASQ10}}}$) for 10 baud is greater than 10^{10} MAC/s Eq.(5-53).

$$C_{\text{t}} = \frac{N_{MAC}^2}{\tau_{SY}}$$
$$C_{\text{t}_{\text{MASQ10}}} = \frac{76{,}800^2}{0.8\,s} > 10^{10}\ \text{MAC/s} \tag{5-53}$$

When the Doppler receiver overhead is included, the numerical processing overhead is greater than $D_N \times Ct > 10^{11}$ MAC/s, which is more than two orders of magnitude higher than the processing power of low power 500 MHz $= 5 \times 10^8$ Hz DSP or industrial 3 GHz $= 3 \times 10^9$ Hz PC.

Correlation in the time domain is equivalent to conjugate multiplication in the frequency domain Eq.(5-54). A frequency domain correlator uses an in place FFT operator which is subject to digital truncation and overflow noise floor ($PSD_N > 0$ dB). Implementation of the frequency domain correlator requires the minimisation of truncation and overflow errors using automatic gain control. Preservation of the FFT gain (G_{FFT}, G_{IFFT}) Figure 91 is required when calculating PSD_{ABS} Eq.(5-28).

$$\psi_I(\text{t}) = V_{RX}(\text{t}) \otimes V_I(\text{t}) \equiv \mathcal{F}^{-1}\left(\mathcal{F}\left(V_{RX}(\text{t})\right) \times \overline{\mathcal{F}\left(V_I(\text{t})\right)}\right)$$
$$\psi_I[\text{n}] = G_{IFFT} \times \text{IFFT}\left[\text{FFT}\left(V_{RX}[\text{n}] \times \overline{\text{FFT}(V_I[\text{n}])} \times G_{FFT}\right)\right] \tag{5-54}$$

The FFT operator is an $N_B \log_2(N_B)$ operation where N_B is the number of FFT butterfly numerical operations. The FFT butterfly requires 8 multiply and 4 accumulate complex numerical operations which is 16 times greater than a time domain correlator multiply-accumulate. Frequency domain correlation requires $C_{\text{f}} < 3 \times 10^6$ MAC/s operations where $\overline{FFT(V_R[t])}$ was optimized as a pre-calculated constant Eq.(5-55).

$$C_{\text{f}} = 2N_B \log_2(N_B) \frac{Br}{B_{PT}}$$
$$C_{\text{f}_{\text{MASQ10}}} = 2 \times 76{,}800 \times \log_2(76{,}800) \times 1.25 < 3 \times 10^6\ \text{MAC/s} \tag{5-55}$$

Frequency domain correlation in conjunction with data decimation can reduce the MCDSSS receiver computational overhead by more than 2 orders of magnitude ($C_{\text{f}_{\text{MASQ10}}} < 2 \times 10^4$ MAC/s) Eq.(5-56) and the MCDSSS receiver block diagram (Figure 91).

$$N_B = S_{CB} + 1 = 1{,}024 \tag{5-56}$$

$$C_{\mathrm{f}} = 2N_B \log_2(N_B).\frac{Br}{B_{PT}}$$

$$C_{\mathrm{f}_{\mathrm{MASQ10}}} = 2 \times 1{,}024 \times \log_2(1{,}024) \times 1.25 < 2 \times 10^4 \text{ MAC/s}$$

Compared to a simple time domain correlator the implementation of a frequency domain MCDSSS receiver is not trivial and accounts for the bulk of the software defined radio infrastructure, which is prone to subtle software bugs masked by the processing gain. As message reliability improved towards 99% stress-testing using hydro-acoustic recordings from multiple communication protocols and air testing of high noise, extreme multipath and/or ultra-long-range communication identified several obscure firmware version 5.x and 6.0 frequency domain correlator software bugs.

5.7.7.4 Power Efficient MASQ Telemetry Alert Receiver Detector

The telemetry alert 70 mW power consumption consumes 24 time less power than the 1.7 W MCDSSS receiver however MASQ modems are typically operated with the MCDSSS receiver running with a 1% duty cycle. Operationally the telemetry alert 70 mW power consumption consumes 4 times more power than the 1% duty cycle 1.7 W MCDSSS. Minimising the telemetry alert receiver power consumption provides a significant improvement in battery powered modem deployment time.

A MASQ telemetry alert detector (ψ_{FSK}) is implemented using the magnitude of a N_{FSK} ping zoom Discrete Fourier Transform (DFT) Eq.(5-57).

$$\psi_{FSK}(\mathrm{t}) = \left| \int_0^{\tau_{PING}} V_{RX}(\mathrm{t}) * V_{FSK_N}(\mathrm{t} - \tau) \mathrm{d}\tau \right| \tag{5-57}$$

The zoom DFT operator is an $N_{FSK} \times N_{PING}^2$ operation where N_{PING} is the number of DFT complex multiply/accumulate and magnitude squared numerical operations. Equation (5-58) describes the computational load (C_{FSK}) of the number of DFT operations required for the detection of a MASQ telemetry alert signal.

$$\begin{gathered} C_{FSK} = 2.N_{FSK}.N_{PING}.f_T \\ C_{FSK} = 2 \times 11 \times 256 \times 32{,}768 < 10^8 \text{ DTF/s} \end{gathered} \tag{5-58}$$

The DFT operator (N_{PING}) is a sinewave complex multiply/accumulate Eq.(5-59).

$$\psi_{FSK}(\mathrm{t}) = \int_0^{\tau_{PING}} V_{RX}(\mathrm{t} - \tau) * e^{-j(2\pi.f_{FSK_N}.\mathrm{t})} \mathrm{d}\tau$$

$$\psi_{FSK}^2 = \sum_{\mathrm{m}=1}^{N_{FSK}} \left(\left| \sum_{\mathrm{n}=0}^{N_{PING}-1} V_{RX}[\mathrm{n} - \mathrm{m}.\tau_{PING}] * e^{-j\theta_L[\mathrm{n}]} \right|^2 \right) \tag{5-59}$$

$$\theta_L[\mathrm{n}] = \frac{f_{\mathrm{L}}.f_{FSK_N}.\mathrm{n}}{f_{\mathrm{T}}}$$

The number of DFT operations can be reduced by N_{PING} using a sliding window correlator with a delay line length of N_{PING} and a cosine/sine lookup table (f_L) Eq.(5-60).

$$\psi_{FSK}^2 = \sum_{\mathrm{m}=1}^{N_{FSK}} \left(\left| \sum_{\mathrm{n}=0}^{N_{PING}-1} V_{RX}[\mathrm{n} - \mathrm{m}.\tau_{PING}] * \mathrm{CosineSineLookup}_{f_\mathrm{L}}[\mathrm{mod}(\theta_L[\mathrm{n}], f_\mathrm{T})] \right|^2 \right) \qquad (5\text{-}60)$$

If the FSK ping samples (N_{PING}) are an integer multiple of $\frac{f_L}{f_T}$, the number of DFT complex multiplications halves because the carrier phase at the start and end of the delay line are identical Eq.(5-61).

$$f_T = 2^{15}, \qquad f_L = 2^{10}, \qquad N_{PING} = 2^8$$

$$\theta_L[\mathrm{n} + N_{PING}] = \frac{f_L.f_{FSK_N}.(\mathrm{n} + N_{PING})}{f_T} = \frac{2^{10}.f_{FSK_N}.(\mathrm{n} + 2^8)}{2^{15}} = \theta_L[\mathrm{n}] + f_{FSK_N}.2^2 \qquad (5\text{-}61)$$

$$\mathrm{mod}(\theta_L[\mathrm{n}], f_\mathrm{L}) = \mathrm{mod}(\theta_L[\mathrm{n} + N_{PING}], f_\mathrm{L}) = \mathrm{mod}(\theta_L[\mathrm{n} + 2^8], 2^{10})$$

The firmware version 6.0 sliding window zoom DFT correlator reduces the computation load (C_{FSK}) by more than two orders of magnitude Eq.(5-62) compared to firmware version 5.x. which was deployed on TPC ultra low power micro controllers that support single clock cycle 16-bit fixed point complex multiply and 64-bit fixed point accumulate. Implementing the telemetry alert detector as an assembler programming language interrupt service routine reduced the power consumption by up to one order of magnitude compared to a high-level C/C++ programming language implementation.

$$C_{FSK} = 4.N_{FSK}.f_T$$
$$C_{FSK} = 4 \times 11 \times 32768 < 10^6 \ \mathrm{DTF/s} \qquad (5\text{-}62)$$

Mobile phone technological advances are continually improving micro controller power consumption, however once the telemetry alert detector power consumption drops below the hardware quiescent power consumption, the law of diminishing returns applies to further algorithm improvements. The GPM300 implements a telemetry alert controller on an ultra-low power micro controller which consumes less than 70 mW, where the majority of the quiescent power is consumed by the micro controller ADC, power supply, hydrophone low noise amplifier and peripheral standby power. A step change in peripheral power consumption would be required before deploying a more numerically efficient telemetry alert detector on a lower power consumption micro controller (i.e. hardware technology change from 3.3 V I/O 1.8 V signal processing core to 1.8 V I/O and 0.5 V signal processing core). The TPC design is currently being upgraded to utilise the state of the art low power micro controller and low voltage peripherals.

5.8 Summary

Message reliability performance was improved via algorithm optimisations which include transmit signal modulation, receive signal demodulation, non-linear multipath tracking control systems, and numerically efficient reliable software defined radios. Engineering optimisations include hydro-acoustic transducer design, broad-band matching networks, energy efficient power amplifier design, low noise floor electronics, low quiescent power

electronics. Sonar equation optimisation required the measurement of the absolute ambient sound pressure level using the measurement of slant range, source level calibrated transmitters and absolute receive power calibrated receivers.

The MCDSSS transceiver comprises multiple interdependent control systems which are inherently unstable in the presence of high ambient noise and multipath. Instabilities in the MCDSSS receiver, Doppler detector and error correction control systems were identified and resolved using failing signal sea trial recordings. Alternative spread spectrum modulation schemes and hardware components were explored. MCDSSS telemetry detector performance was improved via the identification of high ambient noise modulation artefact, optimisation of channel impulse response deconvolution and removal of the telemetry detection threshold. The improvement in the MCDSSS control system stability facilitated the reduction of the receiver detection threshold resulting in an overall 10 dB improvement in performance, however the detection threshold required manual optimisation to within ± 0.25 dB for all baud rates, maximum Doppler and for all DSSS communication protocols.

The 10 dB performance improvement of the MCDSSS receiver required an equivalent 10 dB performance improvement in the telemetry alert detector resulting in the wholesale replacement of the telemetry alert control system. Sea trial measurements identified a long range communication multi-path deficiency in the telemetry alert protocol which required modification. MCDSSS receiver and telemetry alert receiver power consumption was reduced via the implementation of numerically efficient detection algorithms.

The MCDSSS hardware was modified with noise snubbing networks to reduce the receiver noise floor. The MCDSSS transmitter band limiting side band performance was improved. The maximum shallow water source level for oil filled projector was identified. Ocean deployed modems are inherently complex because of power and size constraints and the MCDSSS processing gain masked subtle hardware and software bugs which were identified and resolved during stress testing. Software analysis tools were developed to provide real time and automated testing of alternative algorithm and engineering optimisations. The MCDSSS receiver signal processing was modified to facilitate the measurement of the hydrophone absolute sound pressure level which was calibrated in a hydro acoustic tank. Performance improvements were validated with sea trials in harsh environments using absolute sound pressure measurements to validate that MCDSSS transceiver optimisations had not been over fitted to the failing signal database.

Multiple sea trial measurements identified a non-linear relationship between peak bit energy efficiency (BEE_{PEAK}) of minimum transmit source level (SPL_{BEE}) versus baud rate (Br_{BEE}) which has significant implications for battery and ocean powered covert communication.

Figure 117 illustrates the sonar equation diagram MCDSSS firmware version 6.0 representing a 10 dB performance improvement when compared to firmware version 5.x Figure 7 base line performance:

1. Improvement in MCDSSS Transmitter:
    a. Transmit margin $M_{TX} = 3\text{ dB} \rightarrow 15\text{ dB}$.

b. Hydro-acoustic sideband pollution $LFB > 60$ dB, $UFB > 40$ dB.

2. Improvement in MCDSSS Receiver:
   a. Message decoding with minimum receive margin $M_{RX} > 0$ dB.
   b. Multipath gain $G_M = 0$ dB → 5 dB.
   c. Impulsive noise tolerance 10% → 20% of message length.
   d. Maximum communication range $R_S < 15$ km.
   e. Covert communication $PSD_A \geq PSD_{RX} \geq (PSD_A - 12\text{dB})$.
   f. Receiver noise floor $PSD_N < PSD_{SS0}$.
   g. Ambient noise tolerance $PSD_A > PSD_{SS0} \rightarrow PSD_{SS15}$.

3. MCDSSS Transceiver:
   a. Network routing max communication range $R_S > 15$ km.
   b. Transpond and one-way time of flight measurement accuracy improvement.
   c. Remote ambient noise measurement (PSD_{A_D}).
   d. Remote channel attenuation measurement (L_{T_D}).
   e. Automatic transmit source level and hydro-acoustic baud rate optimisation to $M_{RX} > 4$ dB.

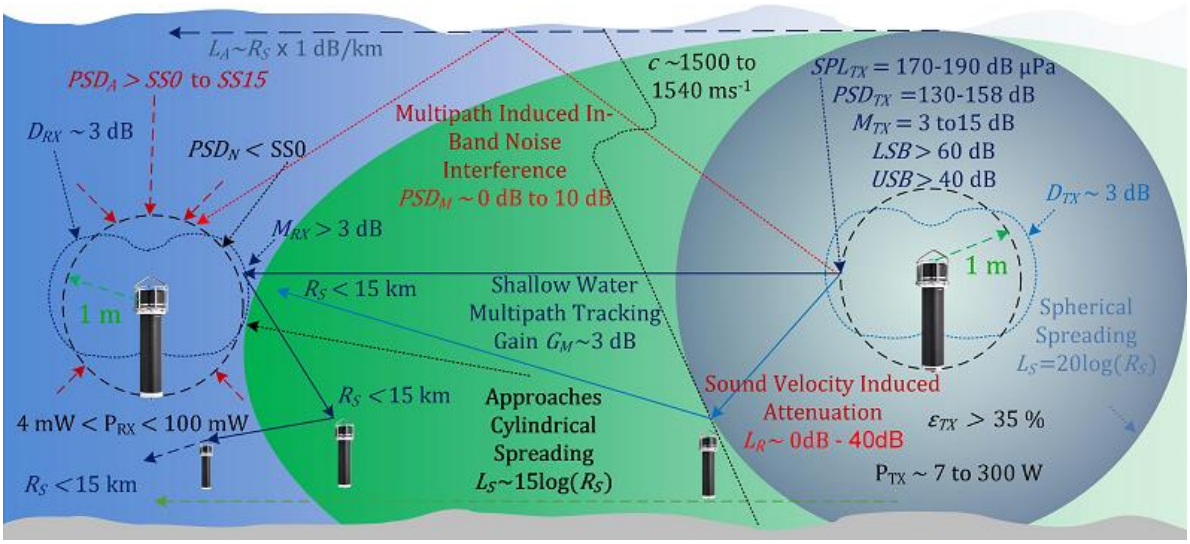

Figure 117 MCDSSS sonar equation diagram optimisations (firmware version 6.0)

6 MCDSSS Communication Performance Improvements

6.1 Introduction

This chapter presents laboratory and sea trial measurements used to validate chapter 5 MCDSSS algorithm and engineering optimisations. The primary performance metric for this thesis is the measurement of message reliability (MR) for high ambient noise, high multi-path and covert communication. Message reliability can be measured using the failing signal database to compare algorithm and engineering optimisations against legacy firmware. The issue of overfitting algorithm and engineering optimisations to the failing signal database is addressed via sea trial measurements in environments with louder ambient noise and higher multi-path. Performance measurements are also presented for improvements in BEE, BER, increase in the maximum baud rate (Br_{MAX}) and decrease in the minimum transmit source level (SPL_{BEE}).

Note: Extracts from this chapter are referenced in [2].

6.2 Message Reliability Improvement Measurements

Figure 118 illustrates that the BALTIC *SS*4 - 6 sea trial (Appendix B) measured improvement in message reliability versus GPM300 firmware. Post processed sea trial recording message reliability increased from 72% to 100% using the firmware version 6.0 deployment of the multipath deconvolution algorithm and telemetry control system (Chapter 5.7.3) optimisations. Resilience to MCDSSS ambient noise floor deterioration also improved following receiver non-linear control system optimisation (Chapter 5.7.1).

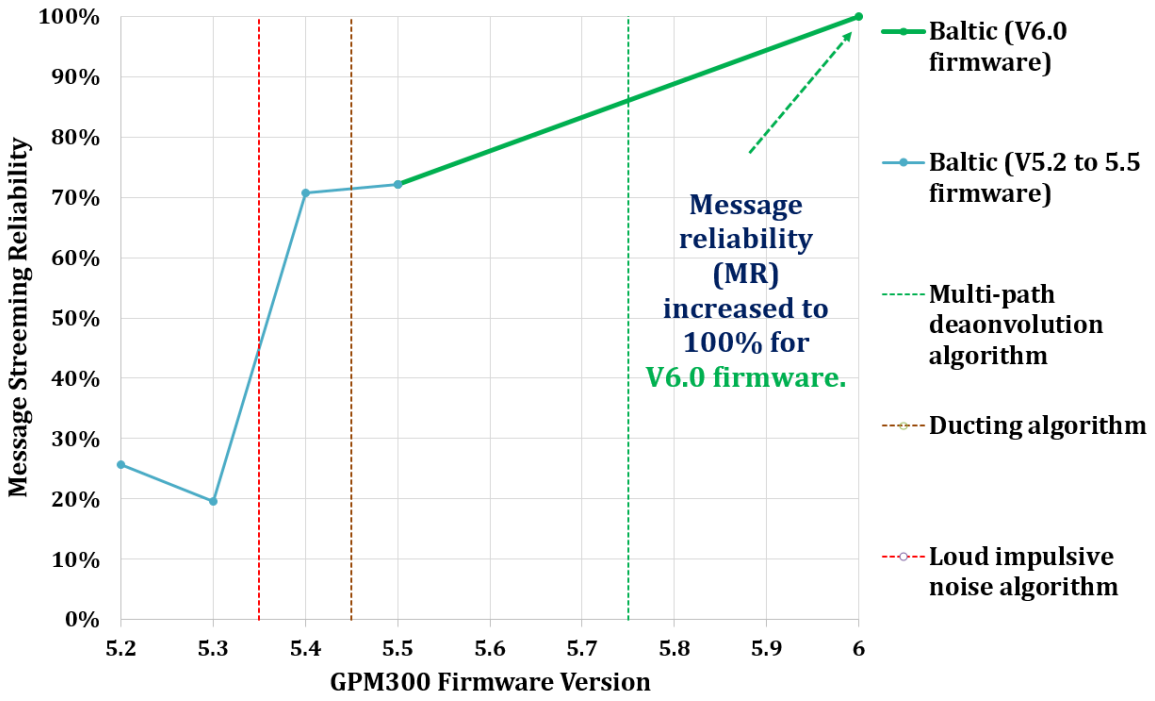

Figure 118 BALTIC, *SS4-6*, message reliability versus firmware version

Figure 119 illustrated the Singapore *SS*4 deployment (Appendix C) message reliability versus the GPM300 firmware version. Post processed sea trial recording message reliability increased from 94% to 100% using firmware version 6.0 with the deployment of the multipath deconvolution algorithm optimisation (Chapter 5.7.2.3). MCDSSS provided reliable operation where conventional short to medium range modems do not operate in the presence of loud bioacoustics noise and loud shipping traffic noise.

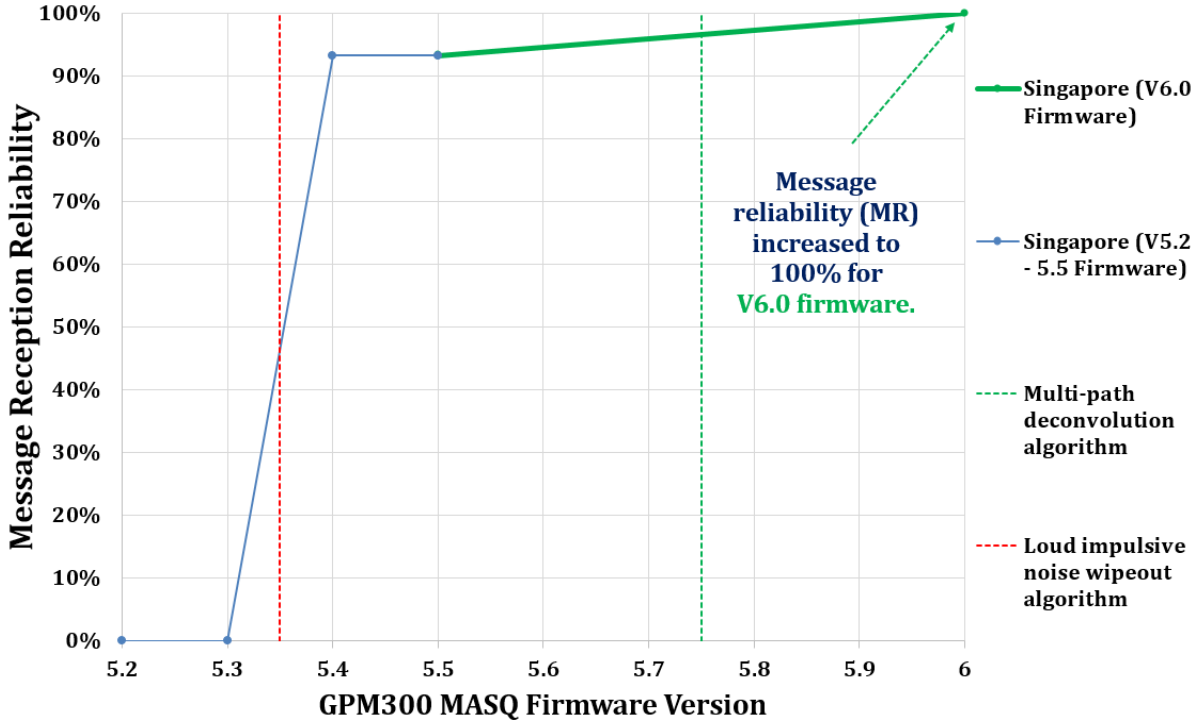

Figure 119 Singapore, *SS4*, 3-40 m message reliability versus firmware version

Figure 120 illustrates the 15 km range *SS*4, 70 m depth sea trial (Appendix L) measured improvement in message reliability versus the GPM300 firmware version. Post processed sea trial recordings message reliability (MR) increased from 92% to less than 99% using the firmware version 6.0 deployment of the extreme multipath tracking algorithms (Figure 81 to Figure 101) and FEC algorithm optimisations (Figure 103 to Figure 102).

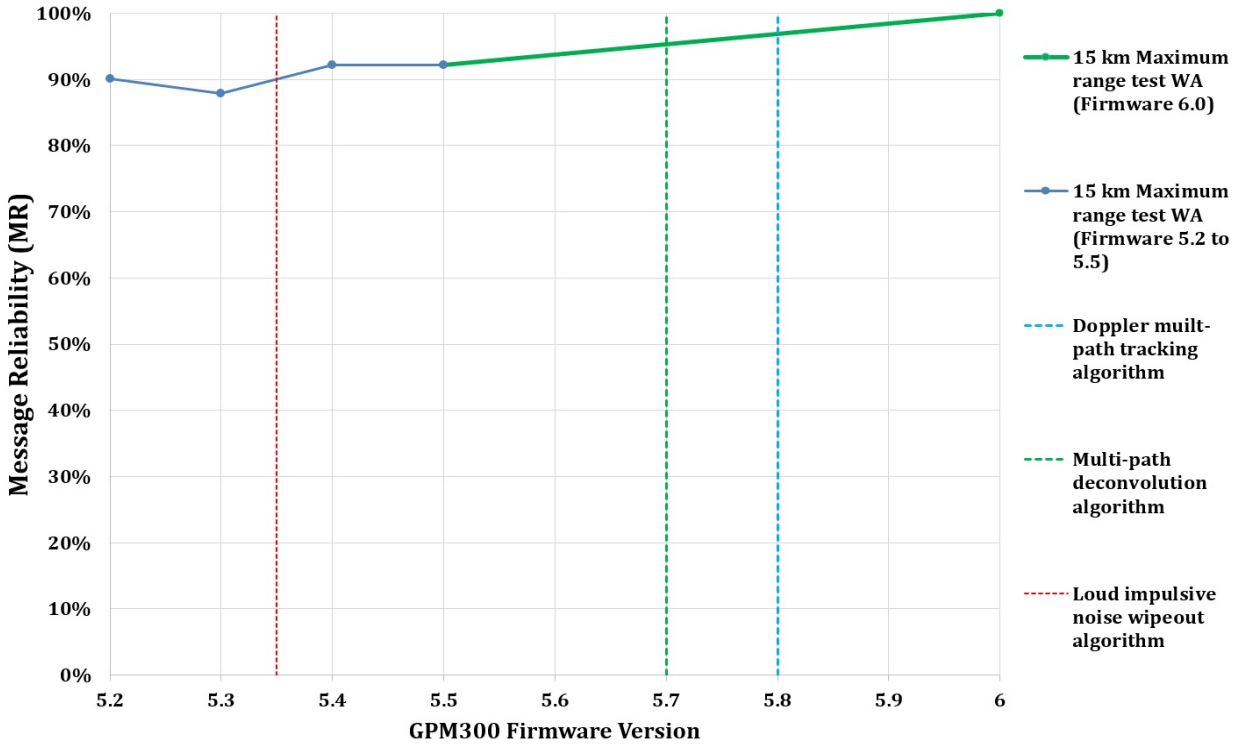

Figure 120 15 km range, *SS4*, 70 m depth message reliability versus firmware version

6.3 Bit Error Rate Improvement Measurements

Figure 121 illustrates the BALTIC *SS*4-6 sea trial (Appendix B) measured bit error rate (BER) as a function of MCDSSS hydro-acoustic baud rate and GPM300 firmware version. The firmware version 6.0 multipath deconvolution algorithm improvements (Chapter 5.7.3.3) decreased the BER by less than one order of magnitude for 50 baud and 100 baud. BER performance improved one order of magnitude for 500 baud. Long range communication typically uses low baud rates such as 50 baud and exhibit higher BER compared to medium range 100 baud rates.

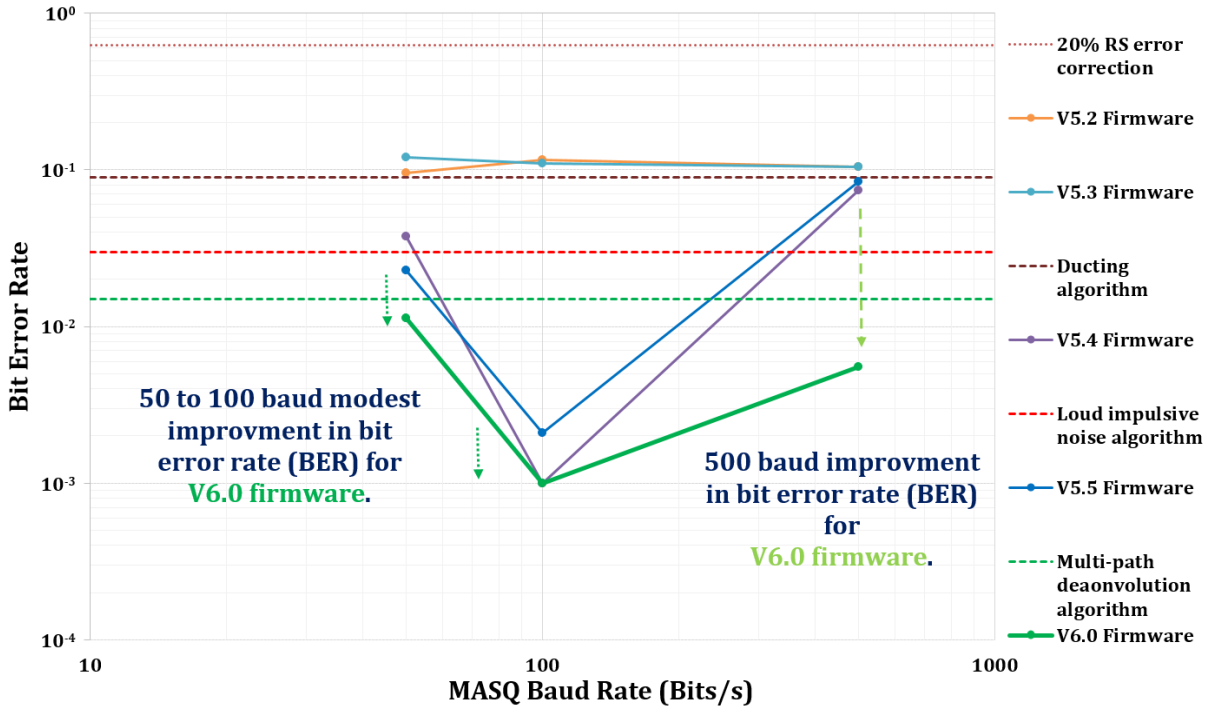

Figure 121 BALTIC, *SS4-6*, bit error rate versus baud rate

Figure 122 illustrates the Singapore *SS4* deployment (Appendix C) measured bit error rate as a function MCDSSS hydro-acoustic baud rate and GPM300 firmware version. The firmware version 6.0 multipath deconvolution algorithm (Chapter 5.7.3.3) degrades the BER by half an order of magnitude and highlights the issue that performance improvements made for a specific environment may degrade performance for an environment with different ambient noise and multi-path. Users of MCDSSS communications are primarily concerned with the reliable reception of user payloads, where the performance metric is message reliability and not BER. For communication in harsh low SNR environments where the BER is worse than 10^{-1} the algorithm and engineering optimisations are focused on reducing the number of corrupted message symbols to less than the error correction threshold of 20%. The optimisations may degrade BER for communication in benign high SNR environments where the BER is better than 10^{-1}. This will not change message reliability MR because the error correction system will always generate a valid user payload.

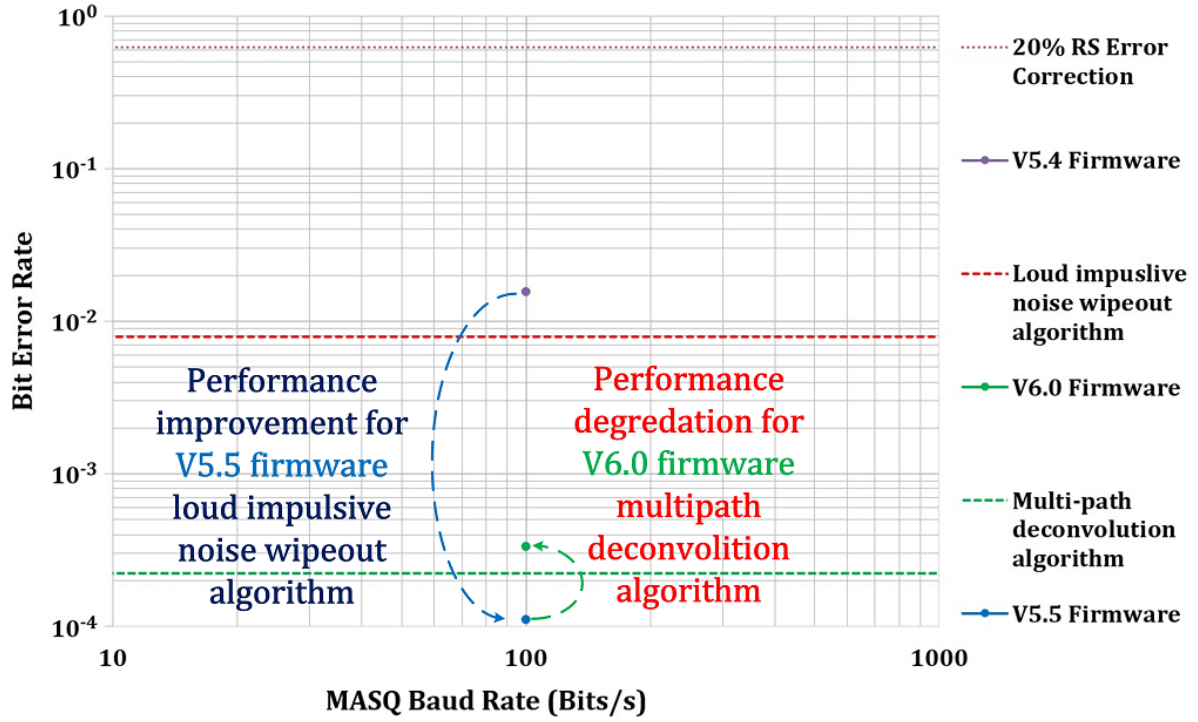

Figure 122 Singapore, *SS4*, bit error rate versus baud rate

6.4 Minimum Transmit Source Level / Maximum Baud Rate

Figure 123 illustrates the 0.2 m range, *SS*4, acoustic baud rate performance (air) measurement of baud rate versus transmit source level which excludes multipath reverberation, and frequency dependant path losses (Appendix D). Chapter 5 algorithm optimisations were applied to firmware version 6.0 and the performance was compared against firmware versions 5.2 to 5.5. Firmware version 6.0 established communication with 100% message reliability from 10 baud to 1,200 baud using 3 dB to 12 dB lower minimum transmit source level when compared against firmware versions 5.2 to 5.5. Firmware version 6.0 established reliable communication at 1,200 baud which could not be replicated using firmware versions 5.2 to 5.5.

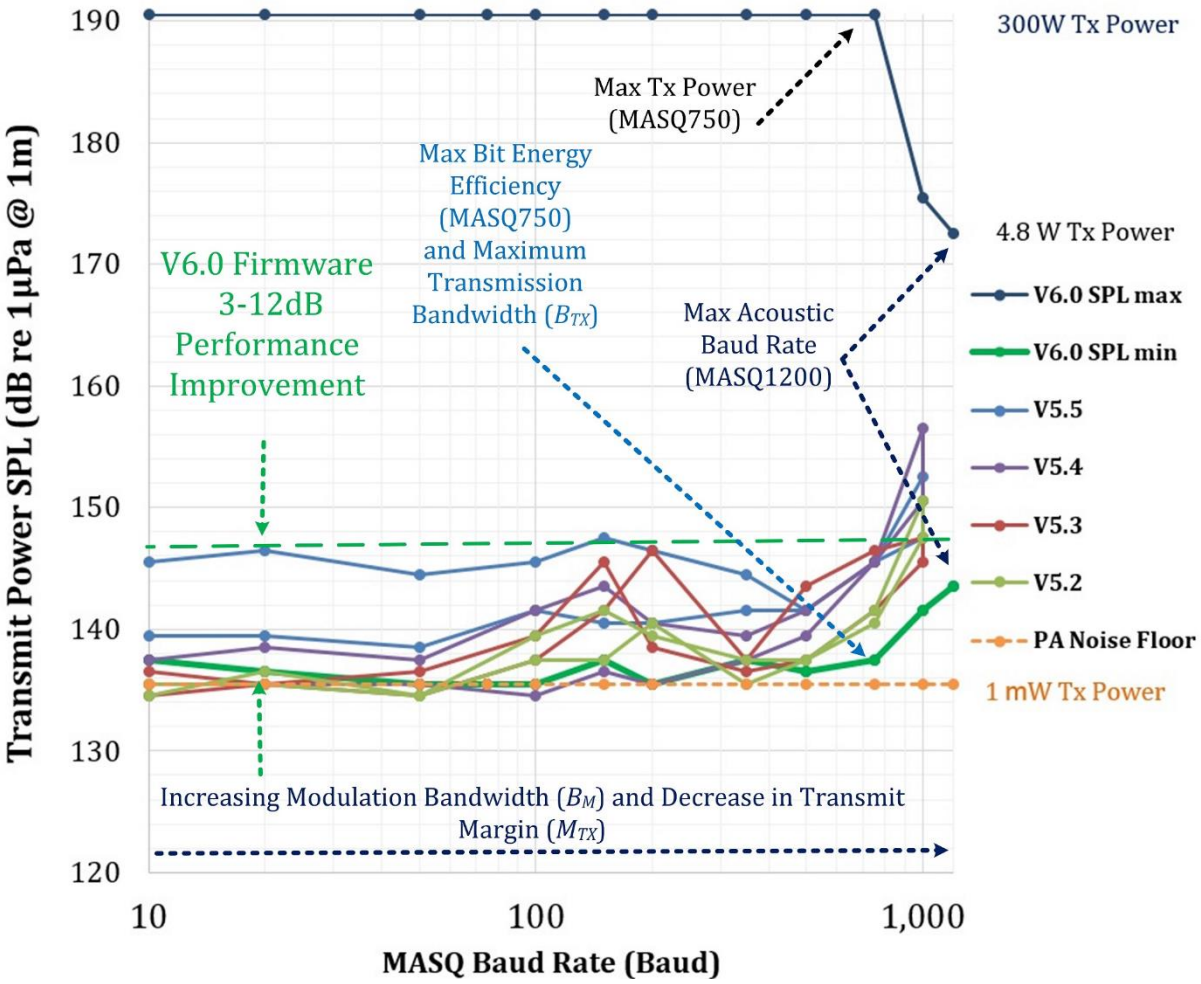

Figure 123 *SS4* minimum transmit power required to obtain reliable communication and maximum available transmit power as a function of baud rate for the 0.2 m range air transmission path transmit source level versus baud rate

Figure 124 illustrates the 22 m range, *SS*0, acoustic baud rate performance (air) measurement of baud rate versus transmit source level which excludes frequency dependant path losses (Appendix E). Firmware version 6.0 resulted in a 3 dB reduction in the minimum transmit source level when compared to firmware version 5.2 to 5.5. Firmware version 6.0 established reliable communication at 500 baud which could not be replicated using firmware versions 5.2 to 5.5. Baud rates higher than 750 baud, with a symbol period of $\tau_{SY} \leq 42$ ms, could not be established for any transmit source level (SPL_{MIN} to SPL_{MAX}) in an environment with a multipath reverberation period of $\tau_{MPE} >$ 25 ms.

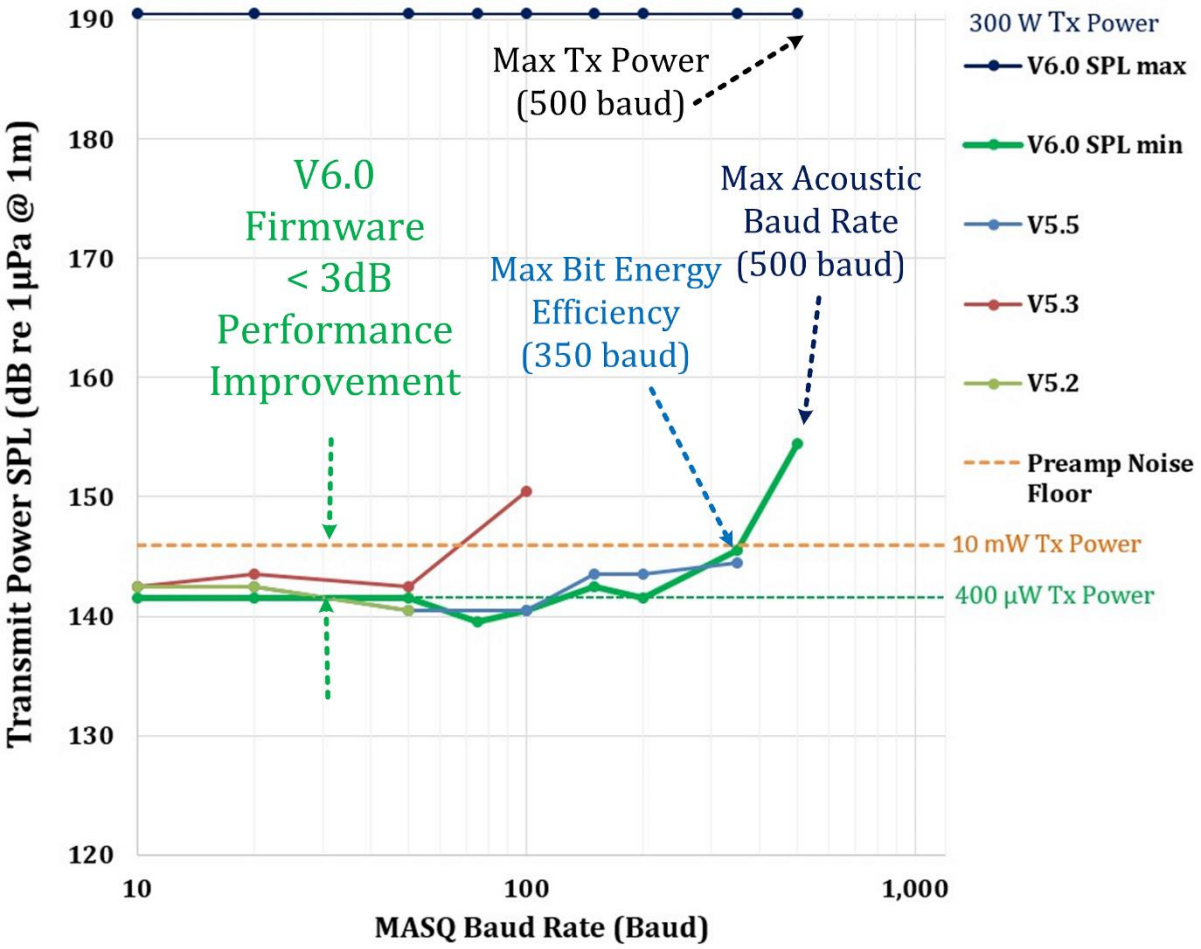

Figure 124 *SS0* minimum transmit power required to obtain reliable communication and maximum available transmit power as a function of baud rate for the 22 m range air transmission path transmit source level versus baud rate

Figure 125 illustrates the 2 m range, *SS*10, hydro-acoustic tank baud rate optimisation performance measurement of baud rate versus transmit source level with the pool pump turned off (Appendix F). Firmware version 6.0 measured approximately 5 dB reduction in the minimum transmit source level when compared to firmware versions 5.2 to 5.5. Firmware version 6.0 established reliable communication at 350 baud which could not be replicated using firmware versions 5.2 to 5.5. Hydro-acoustic baud rates higher than 500 baud, with a symbol period of $\tau_{SY} \leq 32$ ms, could not be established in an environment with a multipath reverberation period of $\tau_{MPE} > 100$ ms (Figure 159).

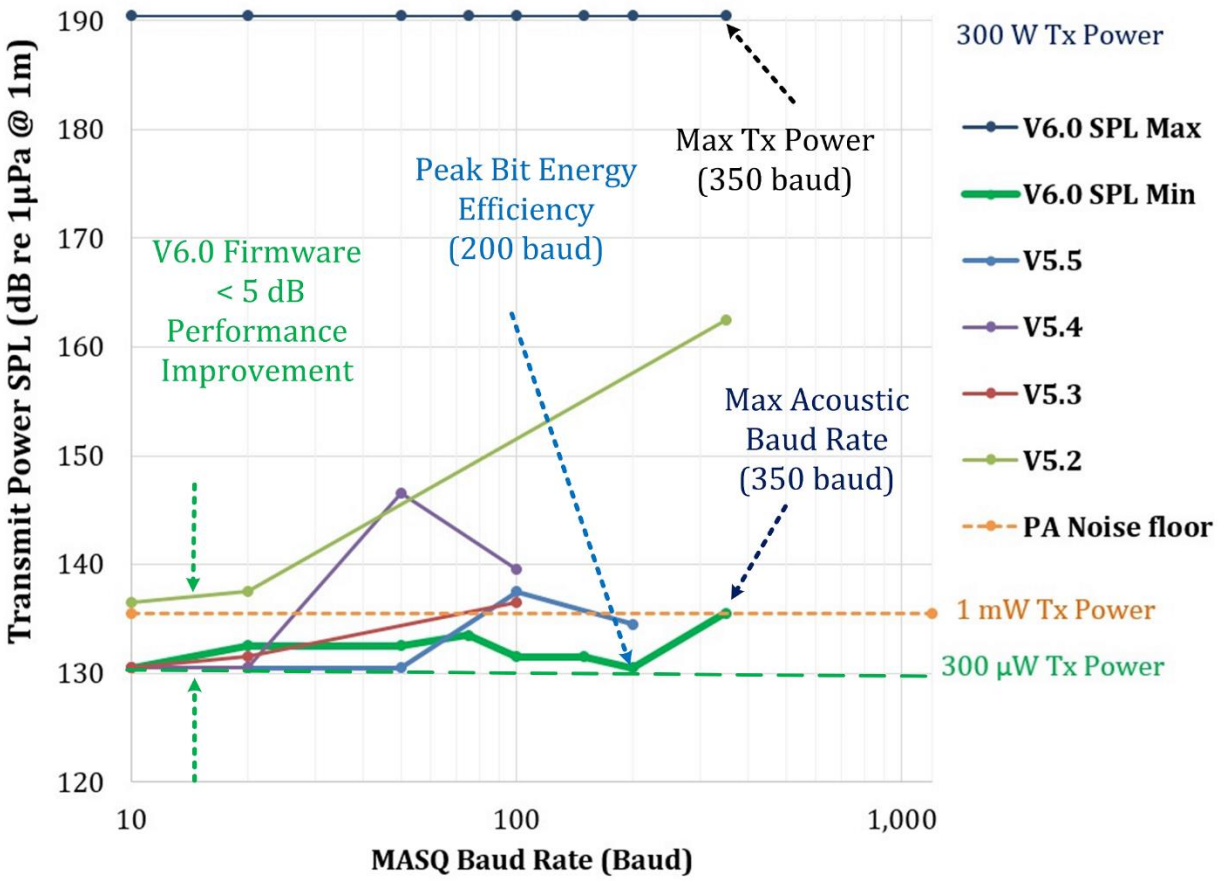

Figure 125 *SS10* minimum transmit power required to obtain reliable communication and maximum available transmit power as a function of baud rate for the 2 m range hydro-acoustic tank transmission path transmit source level versus baud rate (pool pump off)

Figure 126 illustrates the 2 m range, *SS*10, hydro-acoustic tank baud rate optimisation performance measurement of baud rate versus transmit source level with the pool pump operating (Appendix F). Firmware version 6.0 established reliable communication at a higher baud rate of 750 baud with the non-aerating pool pump running compared to 350 baud with the pool pump off. Although the pool pump increased the ambient noise slightly it also roughened the smooth water surface, reducing the effect of multipath induced performance degradation.

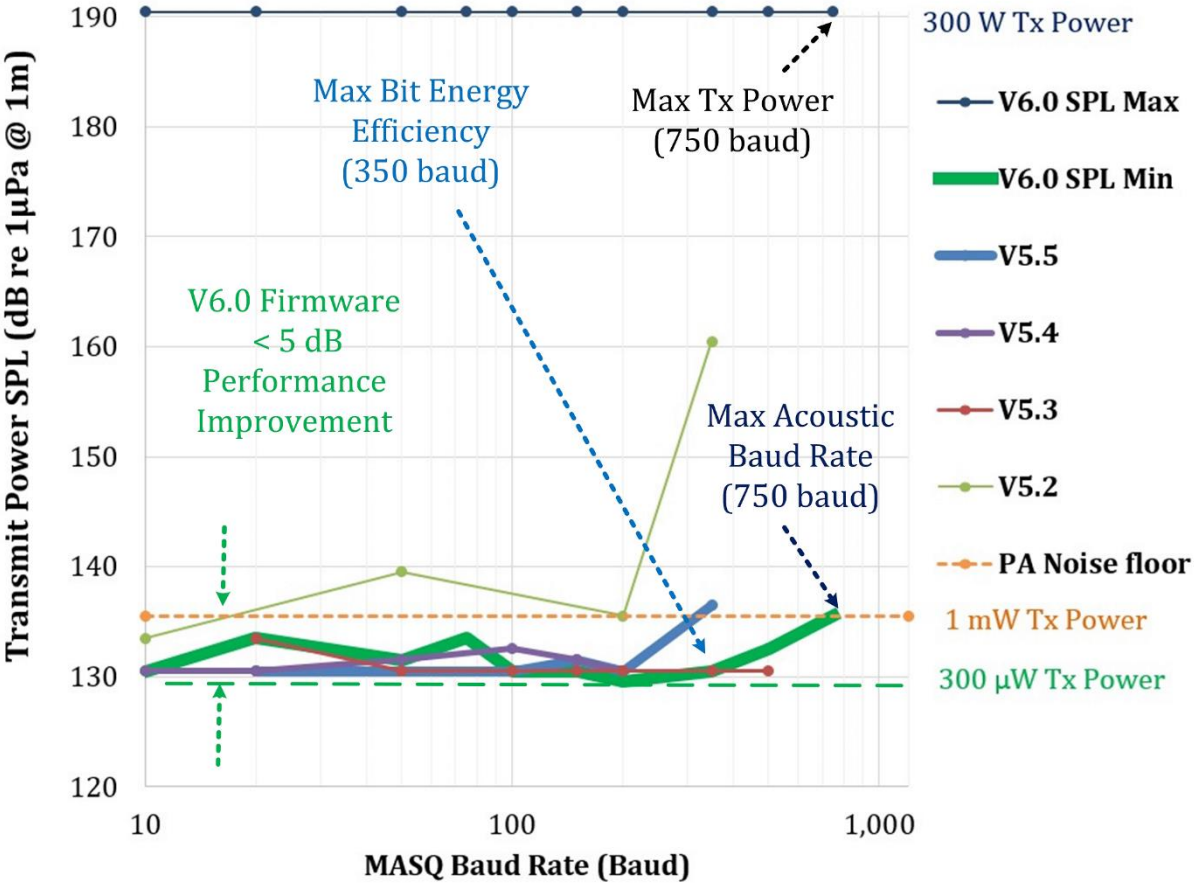

Figure 126 *SS10* minimum transmit power required to obtain reliable communication and maximum available transmit power as a function of baud rate for the 2 m range hydro-acoustic tank transmission path transmit source level versus baud rate (pool pump on)

Figure 127 illustrates the 415 m range, *SS*2, hydro-acoustic baud rate optimisation measurements sea trial (Appendix G). Firmware version 6.0 required 10 dB lower minimum transmit source level when compared to firmware version 5.3. Firmware version 5.3 transmit source level ±5 dB measurement noise was reduced to ±1 dB for firmware version 6.0, which provides a mechanism for accurately probing a hydro acoustic environment's communication channel characteristics.

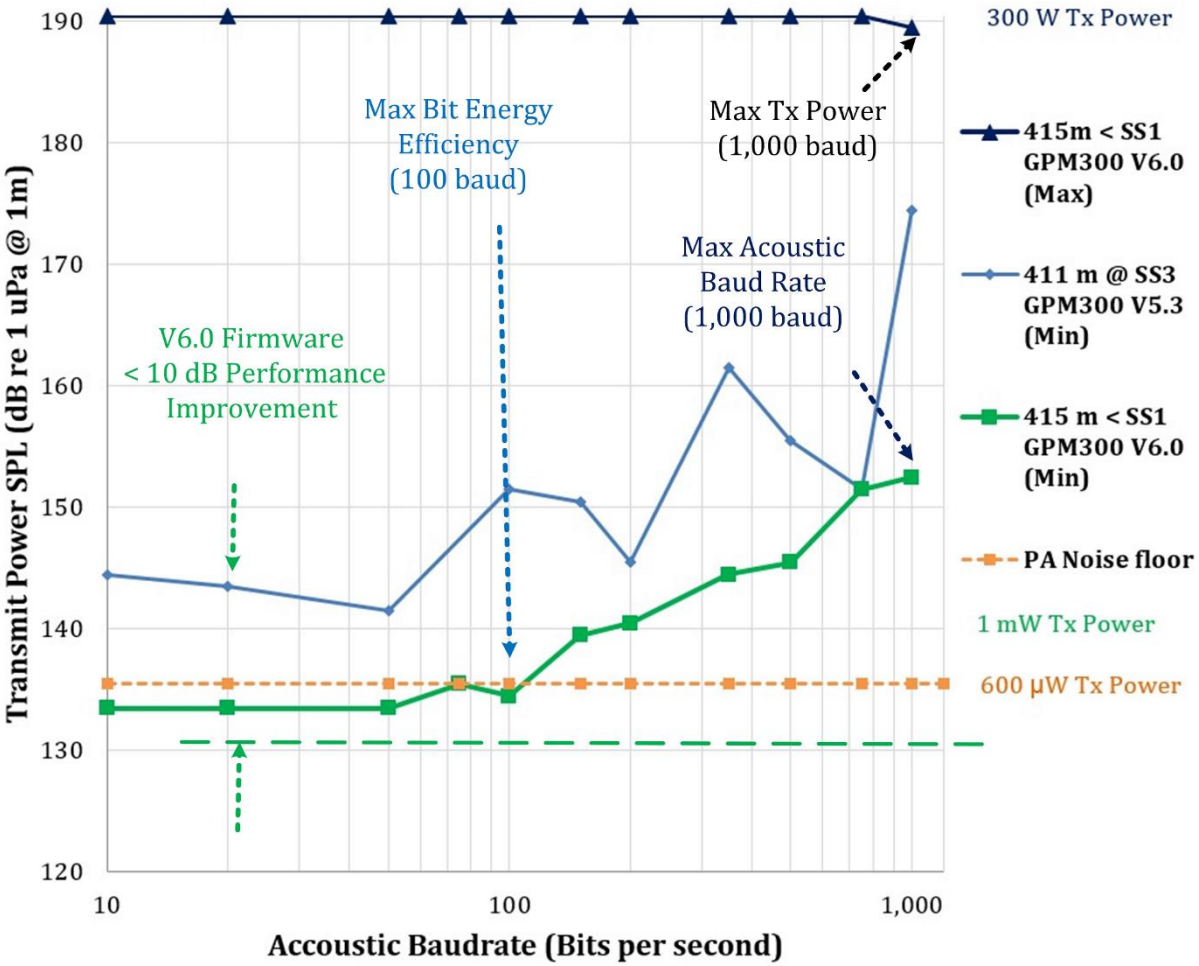

Figure 127 *SS2* minimum transmit power required to obtain reliable communication and maximum available transmit power as a function of baud rate for the 415 m range 3-5 m depth harbour transmission path transmit source level versus baud rate

6.5 Multi-Path Performance Improvement Measurements

The Cockburn Sound GPM300 firmware version 5.5, 6.2 km range, *SS3*, 4-20 m depth, sea trial described in Appendix H established a reliable communication link using 50 baud with a minimum transmit source level of $SPL_{TX} = 176$ dB re 1 µPa @ 1 m.

Figure 128 illustrates the Cockburn Sound GPM300 firmware version 6.0, 8 km range, *SS5-6*, 4-20 m depth sea trial (Appendix J), min/max transmit source level versus hydro-acoustic baud rate. Reliable communication was established from 10 baud to 350 baud. Hydro-acoustic baud rate communication faster than 350 baud could not be established for any transmit source level (SPL_{MIN} to SPL_{MAX}). Minimum transmit source level $SPL_{TX} =$ 174 dB re 1 µPa @ 1 m was required for a 75 baud communication link with Figure 182 spectrogram measuring $SNR \approx -3$ dB covert communication.

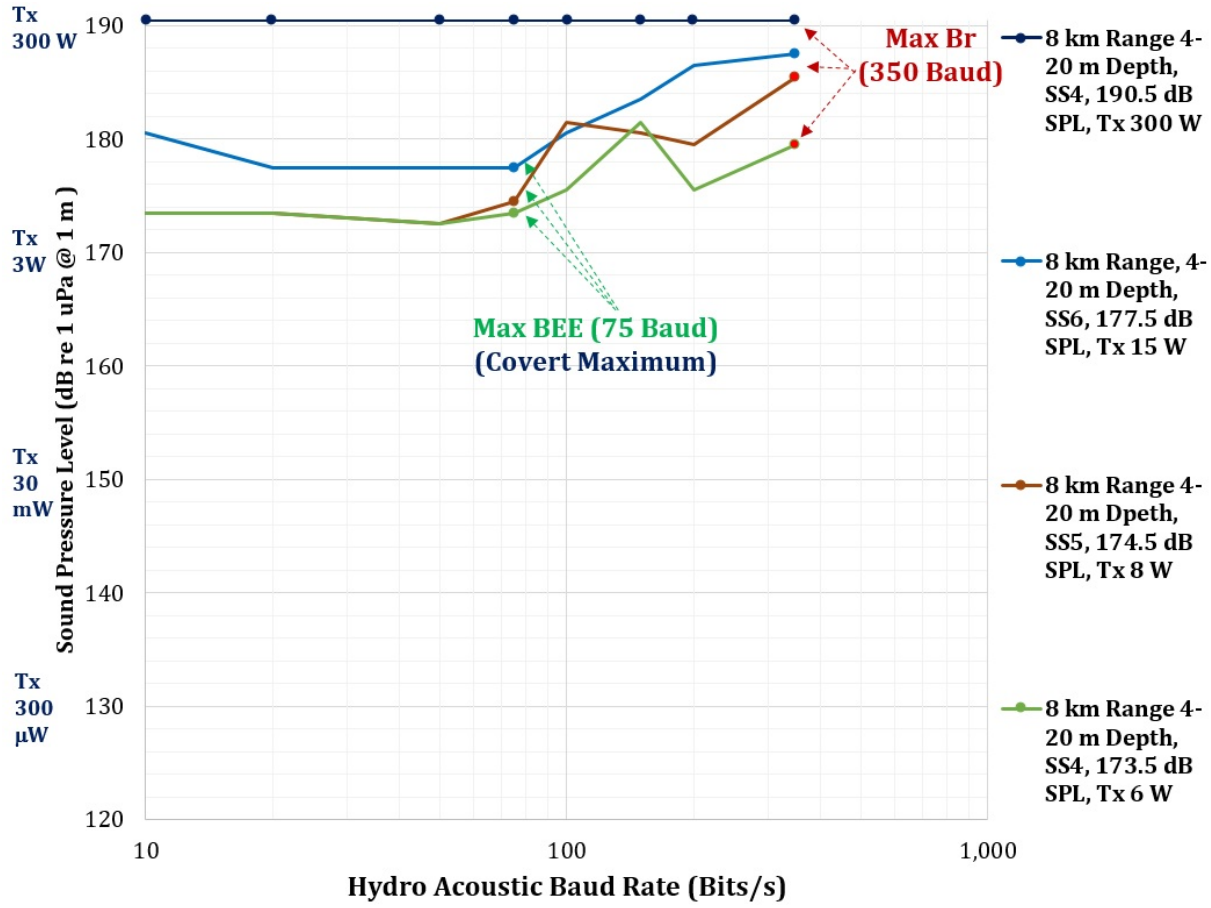

Figure 128 *SS5-6* minimum transmit power required to obtain reliable communication and maximum available transmit power as a function of baud rate for the 8 km range 4-20 m depth Cockburn Sound transmission path transmit source level versus baud rate

Figure 129 illustrates the firmware version 6.0, 1.5 km depth, *SS*2, sea trial (Appendix N) min/max transmit source level versus hydro-acoustic baud rate. Reliable deep water 9.1 km range communication was established at 350 baud using a minimum transmit source level of $\mathrm{SPL_{TX}} = 172$ dB re 1 µPa @ 1 m and is consistent with a $L_S \approx 20\log_{10}(R_S)$ spherical propagation model Eq.(7-24).

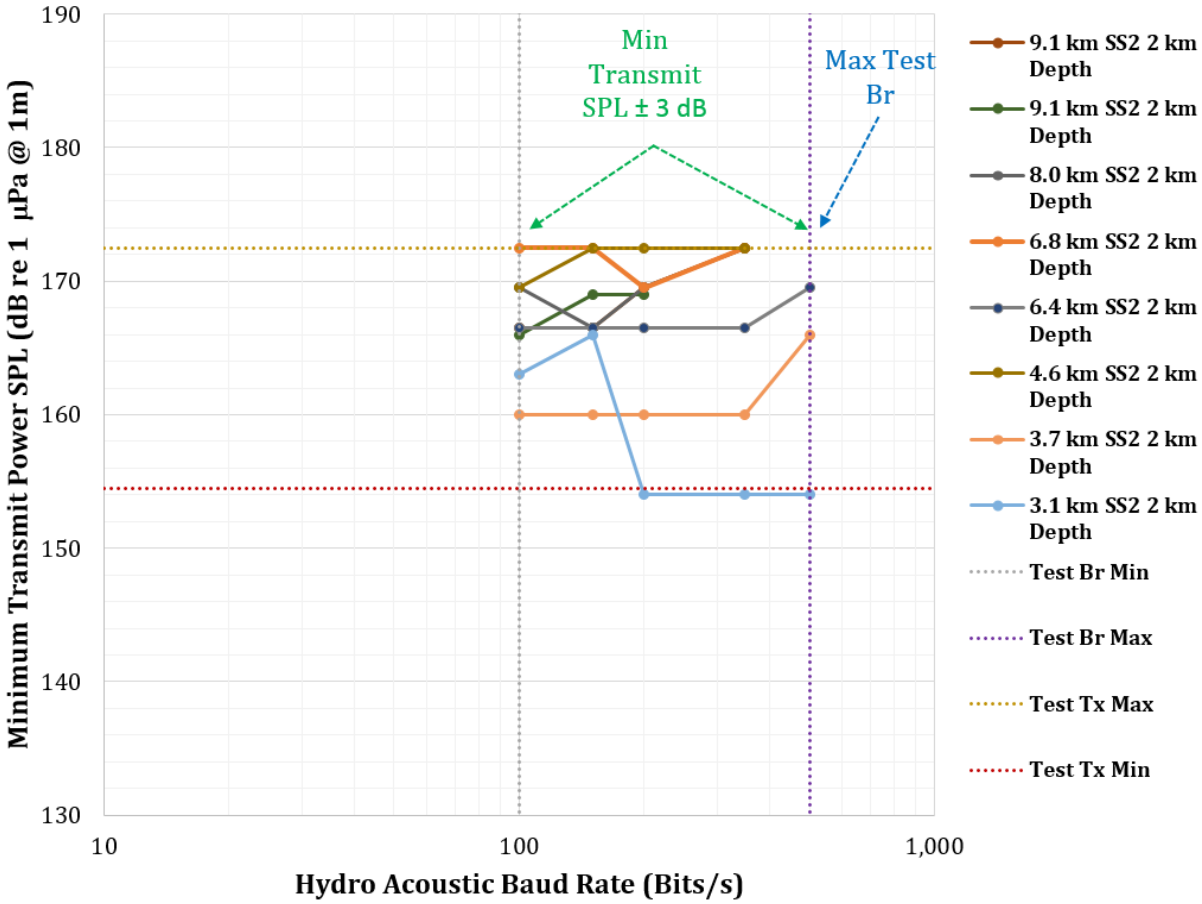

Figure 129 *SS4* minimum transmit power required to obtain reliable communication and maximum available transmit power as a function of baud rate for the 3-9 km range 1.5 km depth ocean transmission path transmit source level versus baud rate

Figure 130 illustrates the firmware version 6.0, 130 m depth, *SS*2, sea trial min/max transmit source level versus hydro-acoustic baud rate (Appendix M). Reliable shallow water 9.7 km range communication was established at 350 baud using a minimum transmit source level of SPL_{TX} = 160 dB re 1 µPa @ 1 m and consistent with the receiver detecting the MCDSSS signal with a $L_S \approx 15\log_{10}(R_S)$ propagation model approaching cylindrical spreading Eq.(7-25).

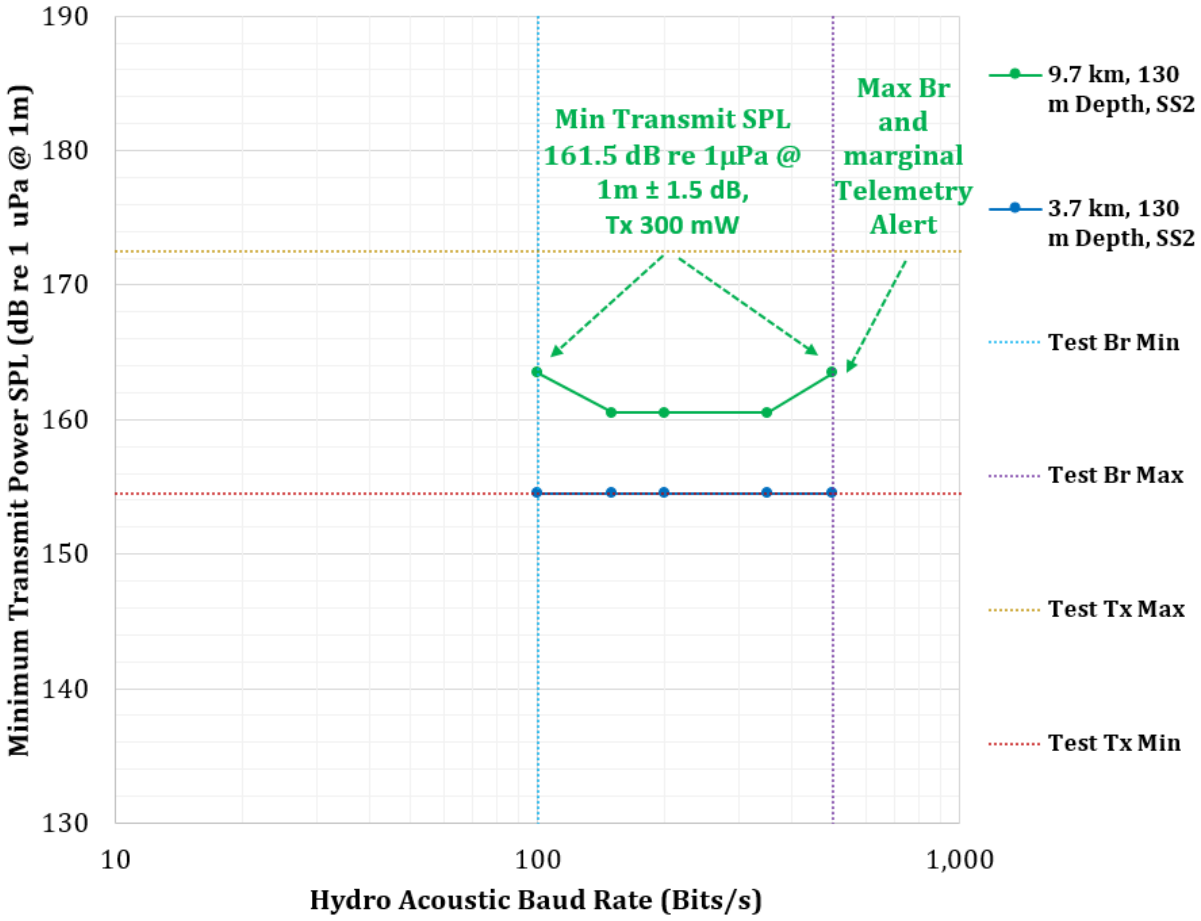

Figure 130 *SS3* minimum transmit power required to obtain reliable communication and maximum available transmit power as a function of baud rate for the 4-10 km range 130 m depth ocean transmission path transmit source level versus baud rate

The Cockburn Sound 8 km range, *SS*6, 4-20 m depth, 75 baud communication link running GPM300 firmware version 6.0 required 2 dB less transmit source level when compared to the Cockburn Sound shorter 6.1 km range, *SS*4, 4 - 20 m depth, and slower 50 baud communication link running GPM300 firmware version 5.5. The 9.7 km range, *SS*2, 130 m shallow water, 350 baud communication link required 12 dB less transmit source level when compared to the 9.1 km range, *SS*2, 1.5 km deep water, 350 baud communication link. These sea trials provide different test environments that demonstrate the reversal of the usual poorer reliability in shallow water. By contrast, in these tests lower transmit source levels were required in shallow water compared to deep water when using performance improvements such as multi-path deconvolution and improved receiver control system stability.

6.6 Peak Bit Energy Efficiency Covert Communication

Improvements in the MCDSSS receiver message reliability enabled a more accurate measurement of minimum transmit source level versus hydro-acoustic baud rate when compared to legacy firmware versions, which has significant power saving implications. The minimum power communication link optimisation control system (Chapter 5.7.7) operated on the assumption that transmit power can be minimised by establishing a communication link using the highest baud rate operated at the lowest transmit source level (Figure 131 red trace), however the 400 m range sea trial described in Appendix G proved this assumption to be false. The blue trace in Figure 131 provides a noisy measurement of bit energy efficiency as a function of baud rate for GPM300 legacy firmware version 5.3. The green trace provides a measurement of bit energy efficiency as a function of baud rate for firmware version 6.0 with a distinctive peak in BEE at baud rates less than the maximum achievable baud rate. Subsequent sea trials in deeper and noisier environments have replicated the peak BEE verse baud rate relationship.

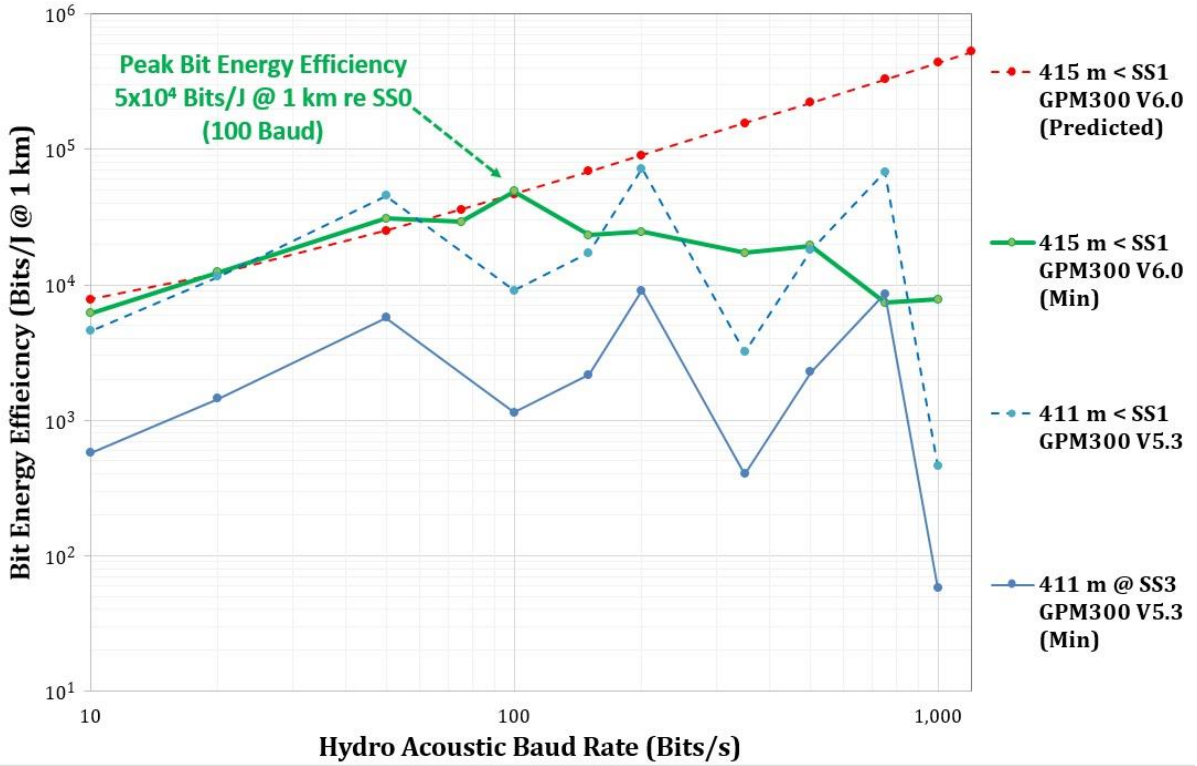

Figure 131 Fremantle Harbour 415 m range bit energy efficiency

6.6.1 Maximum Hydro-acoustic Baud Rate versus Range and Sea State

Precision minimum transmit source level measurements facilitate the generation of an accurate maximum hydro-acoustic baud rate versus communication range, water depth and sea state. Figure 132 summarises sea trial measurements from Appendix G to Appendix N. For example, minimum transmit source level for reliable covert communication, at peak BEE, was established across Fremantle harbour at 100 baud and 135 dB re 1 µPa @ 1 m (Appendix G.5.4), and off the west coast of Australia at 350 baud and 161 dB re 1 µPa @ 1 m (Appendix M.5).

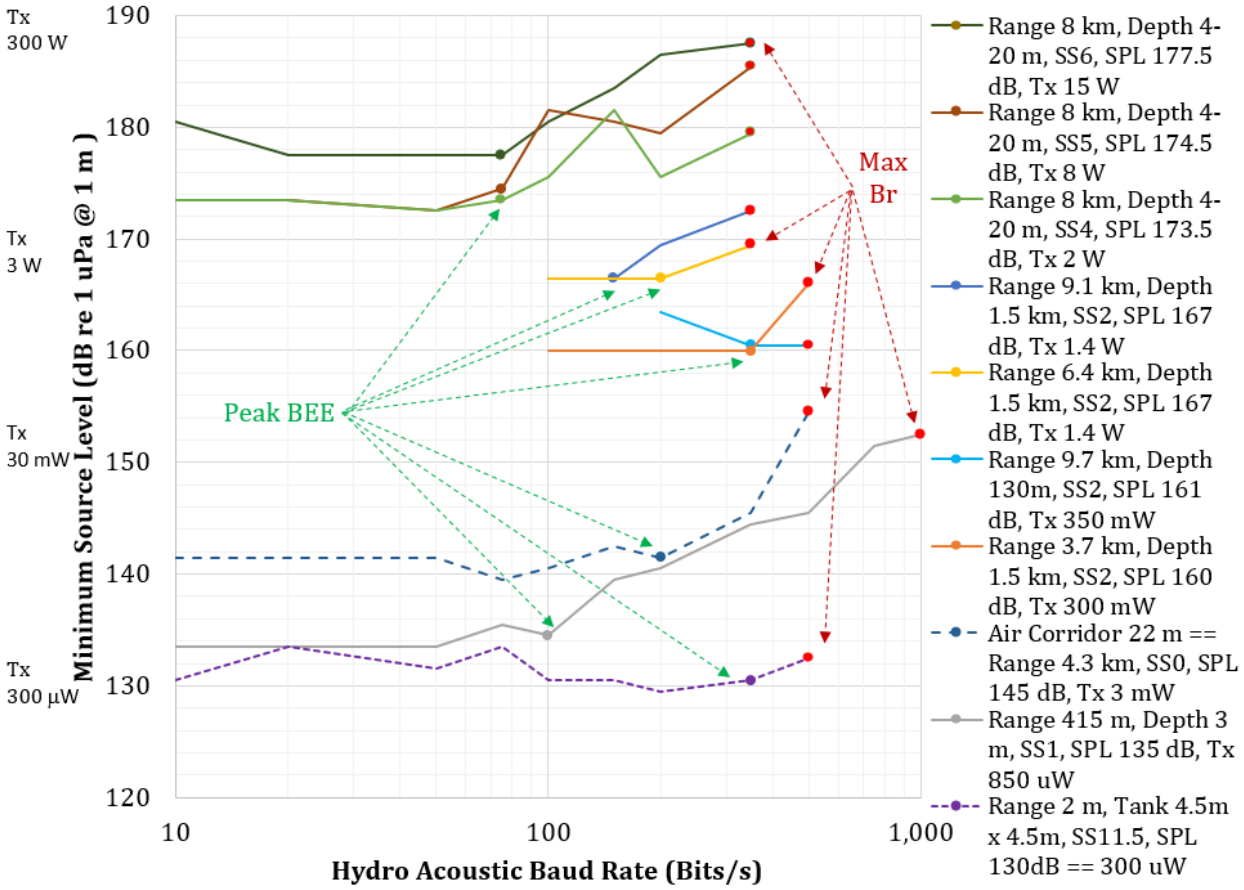

Figure 132 MCDSSS shallow water performance

6.6.2 Peak BEE versus Hydro-acoustic Baud Rate

Precision minimum transmit source level measurements also facilitate the generation of accurate bit energy efficiency versus hydro-acoustic baud rate graphs. Figure 133 provides a summary of the sea trial results shown individually in Figure 147, Figure 152, Figure 160, Figure 169, Figure 184, Figure 218 and Figure 224. The maximum hydro-acoustic baud rate is limited by the multipath reverberation envelope period, however bit energy efficiency is not a linear function of the maximum hydro-acoustic baud rate. BEE peaks as a function of baud rate before the maximum hydro-acoustic baud rate and is limited by the hydro-acoustic ducting channel geometry. Faster baud rates require higher transmit source level to maintain the energy per bit however louder transmit signals increase the self-noise multipath reverberation envelope period and, when operating at peak BEE, will raise multipath signals above the ambient noise ($PSD_A - M_{TX}$) resulting in the multipath signals being detected by the receiver as in-band interference. At 100 km off the west coast of Australia in 1.5 km water depth, 9.1 km range peak BEE = 2×10^3 Bits/J @ 1 km was measured at $Br_{BEE} = 150$ baud (Appendix M) however at 50 km off the west coast of Australia in 130 m water depth and 9.7 km range a peak BEE = 3×10^4 Bits/J @ 1 km was measured at $Br_{BEE} = 350$ baud (Appendix N) which demonstrates the reversal of deep/shallow water reliability. Shallow water MCDSSS covert communication is now more energy efficient than deep water communication where the multipath signals are used as additional sources of MCDSSS receive signal energy. The MCDSSS receiver no longer detects multipath signals as spherical spreading Eq.(2-12) propagating in-band interference. The MCDSSS multi-path deconvolution telemetry receiver detects

multipath signals coherent signals approaching cylindrical spreading Eq.(2-13) propagation.

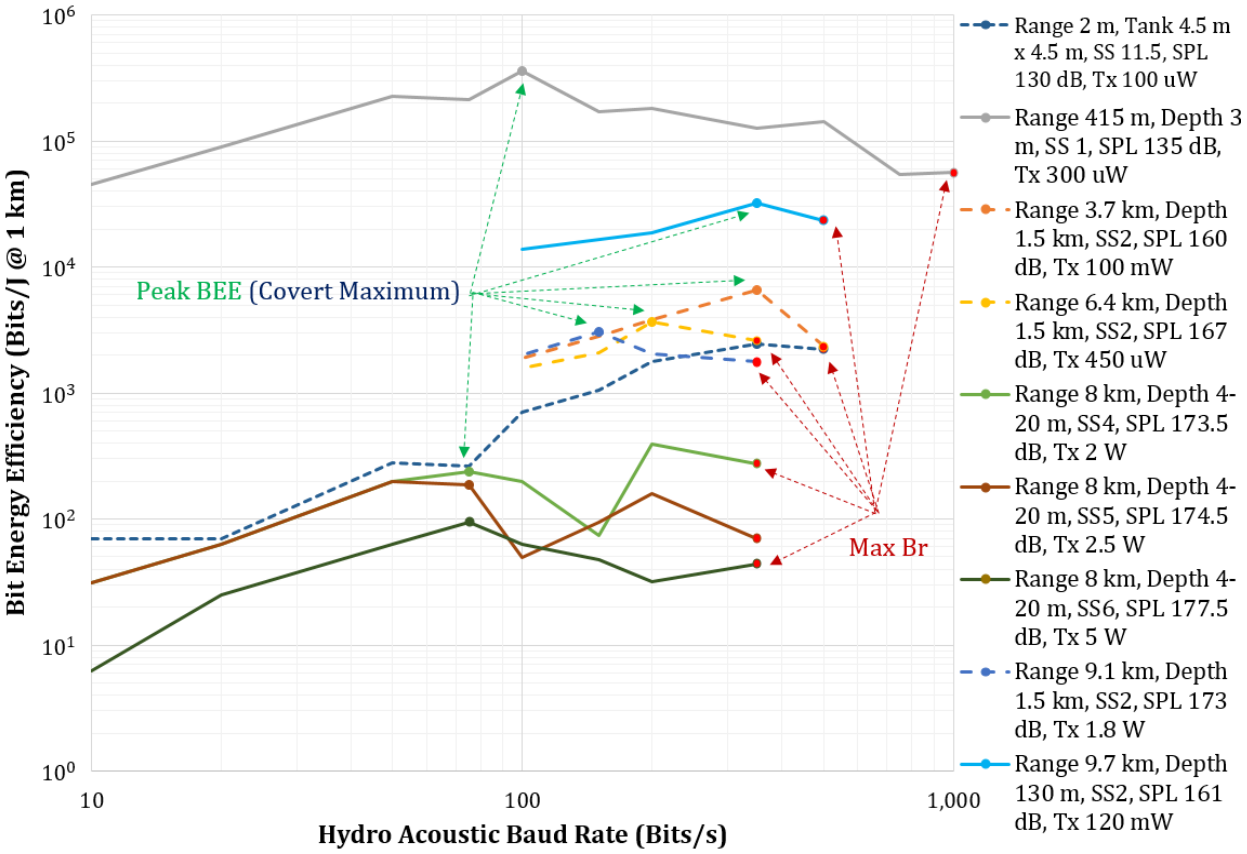

Figure 133 MCDSSS measured bit energy efficiency versus baud rate

6.6.3 Peak BEE versus Communication Range and Sea Sate

Maximum covert performance occurs at peak bit energy efficiency (BEE_{PEAK}) because messages are propagated using the lowest transmit source level for the shortest transmit period which has the lowest probability of intercept (LPI). Sea trial measurements of BEE with different sea states can be compared by using equation (3-6) to normalise measurements to the same sea state zero. Figure 134 illustrates multiple sea trial BEE measurements normalised to $SS0$ where BEE peaks at approximately $BEE_{PEAK} = 10^4$ Bits/J @ 1 km re $SS0$ within ± 1.5 SS or ± 10 dB at a baud rate (Br_{BEE}) lower than the maximum hydro-acoustic baud rate (Br_{MAX}):

1. BEE_{PEAK} Minimum: 3×10^3 Bits/J @ 1 km re $SS0$.
2. BEE_{PEAK} Maximum: 1.5×10^5 Bits/J @ 1 km re $SS0$.
3. BEE_{PEAK} Nominal: $\approx$ **10^4 Bits/J @ 1 km re $SS0$** $\pm$ 1.5 SS.

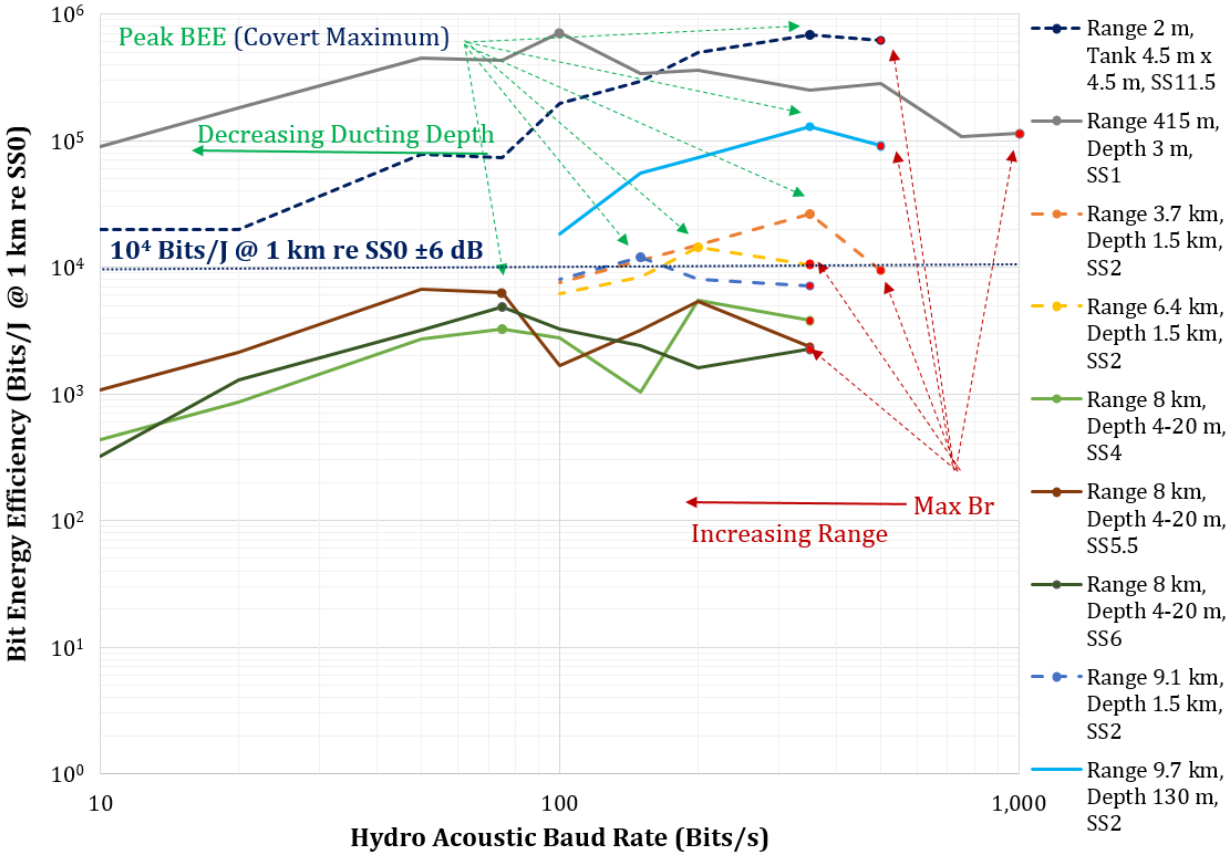

Figure 134 MCDSSS measured bit energy efficiency (normalised for *SS0*)

The hydro-acoustic baud rate (Br_{BEE}), for BEE_{PEAK} as a function of communication range, will be between 50 baud to 500 baud and is dependent on environmental absorption, water depth or surface ducting depth as summarised in Table 3.

Location	Range	Depth	$Ducting_{Depth}$	Aspect Ratio	Sea State	SPL_{BEE}	Br_{Max}	Br_{BEE}	BEE_{PEAK}
	m	m	m		#	dB re 1 µPa @ 1m	baud	baud	bits/J @ 1km re SS0
L3 Oceania tank	2	4.5	0 to 4.5	1:2	0 to +12	130	500	350	7×10^5
Fremantle Harbour	400	3 to 5	0 to 5	1:300	1 to 4	135	1000	100	1×10^5
Cockburn Sound	8,000	4 to 20	0 to 20	1:500	5 to 6	174	350	75	5×10^4
50 km west of WA	10,000	130	0 to 20	1:500	2 to 4	161	500	350	1×10^5
100 km west of WA	10,000	1,500 to 2,500	0 to 100	1:300	2 to 4	167	350	150	1×10^4

Table 3 Western Australia coast mean Br_{BEE} measurement summary

6.6.4 Range versus Sea State for Peak BEE Covert Communication

The BEE_{PEAK} characterisation has a significant implication for battery and ocean energy harvesting powered long-range hydro-acoustic communication links because logarithmic power savings can be realised by measuring the peak BEE as a function of hydro-acoustic baud rate (Br_{BEE}) and minimum source level. There is no power saving when transmitting at source levels that are less than the power amplifier quiescent power. Therefore minimum transmit power (P_{TX}) can be derived from the minimum source level (SPL_{BEE}), power amplifier quiescent power ($P_{Q_{TX}}$) and the electrical to acoustic power efficiency (ϵ_{TX}) which is typically 35% to 40% for a 300 W MCDSSS modem Eq.(6-1).

$$P_{TX} \approx \frac{1}{\epsilon_{TX}} 10^{\left(\frac{SPL_{BEE}-SPL_{1W}}{10}\right)} \text{ for } P_{TX} > P_{Q_{TX}}$$

$$SPL_{1W} \approx 170.5 \text{ dB re 1 µPa @ 1 m / W [129]} \tag{6-1}$$

$$P_{Q_{TX}} \approx 3 \text{ W (for 300 W MCDSSS Modem)}$$

Equation (6-2) derived from equation (2-12) and (2-15), and assuming spherical spreading, describes the difference in transmit source level (ΔSPL_{TX}) required for a communication range (R_S) relative to $R_{REF} = 1$ km as a function of frequency dependant absorption loss ($\bar{L}_A$).

$$\Delta SPL_{TX} \equiv L_T \approx 20\log_{10}\left(\frac{R_S}{R_{REF}}\right) + \frac{\bar{L}_A(R_S - R_{REF})}{R_{REF}} \text{ dB}, \qquad L_R \to 0 \text{ dB}$$

$$R_{REF} = 1{,}000 \text{ m} \tag{6-2}$$

$$\bar{L}_A \approx 1 \text{ dB/km (for MCDSSS 6.5 kHz to 16.5 kHz transmission bandwidth)}$$

The nominal peak $BEE_{PEAK} \approx 10^4$ Bits/J @ 1 km re $SS0 \pm 6$ dB in conjunction with equation (6-2) can be used to predict the maximum operating International Martine Organisation (IMO) Sea State number ($SS\#$) Eq.(7-27) as a function of communication range and hydro-acoustic baud rate (Br_{BEE}) as described by equation (6-3) and illustrated in Figure 135.

$$SS\# \approx \left(10\log_{10}\left(\frac{BEE_{PEAK} \times P_{TX}}{Br_{BEE}}\right) - \Delta SPL_{TX}\right) / SS_{PSD}, \pm 1.5\ SS \tag{6-3}$$

$SS_{PSD} \approx 6$ dB/SS (Approximate rise in ambient noise per IMO sea state number)

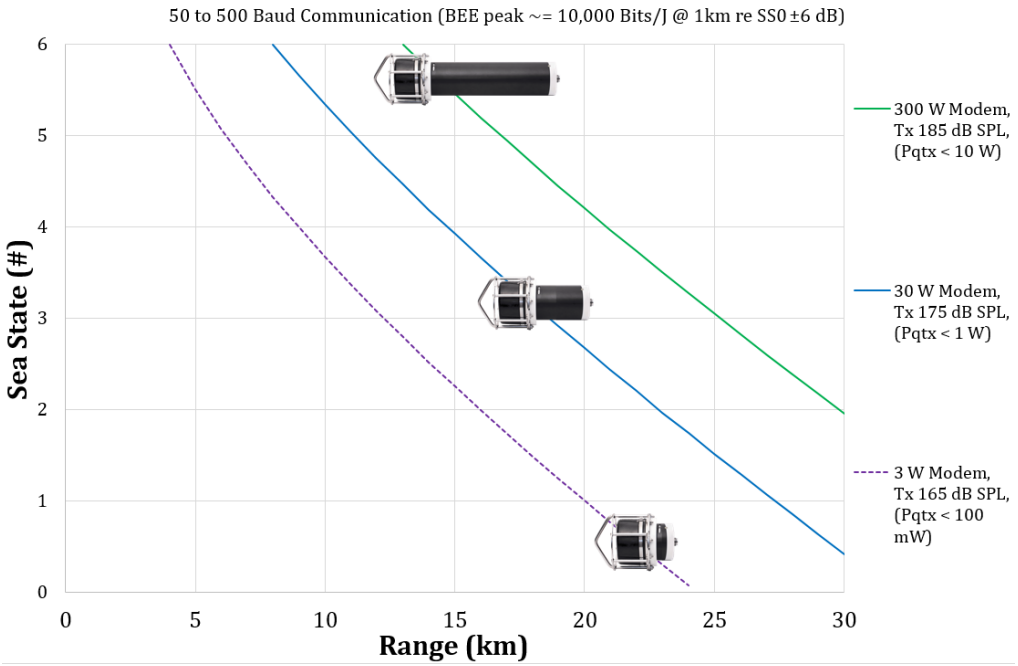

Figure 135 Predicted peak BEE communication range

A 300 W MCDSSS modem generates a maximum SPL_{MAX} = 190 dB re 1 µPa @ 1 m, however the transmitter quiescent power is approximately $P_{Q_{TX}} \approx 3$ W and transmitting signals less than SPL_{TX} = 170 dB re 1 µPa @ 1 m requires less transmitter power than the power amplifier quiescent power and does not save battery power. A 50 km network routed communication link can be established using three 300 W MCDSSS modems transmitting at SPL_{TX} = 185 dB requiring 80 W transmit power but would require a very large 500 Wh battery pack to provide approximately 6 hours of 100% duty cycle transmit time (Figure 136).

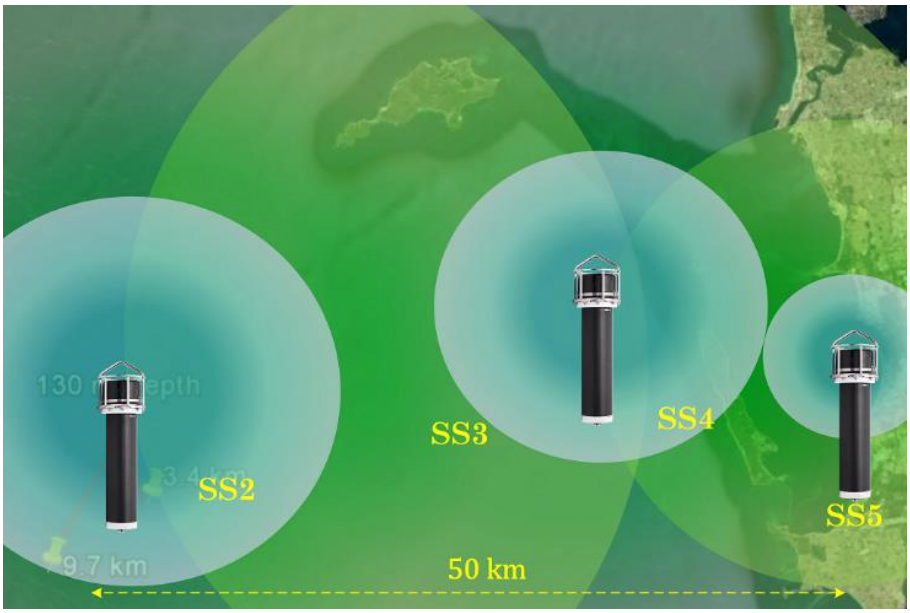

Figure 136 50 km battery powered communication link (300 W Modems)

The transmitter quiescent power can be reduced to less than $P_{Q_{TX}}$ = 300 mW by limiting the source level to SPL_{MAX} = 180 dB re 1 µPa @ 1 m requiring a maximum transmit power of $P_{TX_{MAX}} \approx 30$ W. A $R_S \approx 50$ km network routed communication link using five 30 W MCDSSS modem's operating at SPL_{TX} = 175 dB re 1 µPa @ 1 m requiring 8 W transmit power and 50 Wh battery pack provides 6 hours of 100% duty cycle transmit time. The 300 W modem 1.3 W MCDSSS receiver quiescent power and 0.07 W Telemetry Alert detector quiescent power can be reduced using current technology: ultra low power micro controller and DPS's with a potential 0.5 W MCDSSS receiver quiescent and 0.03 W telemetry alert detector.

If a power efficient 3 W MCDSSS modem can be build then a $R_S \approx 50$ km network routed communication link would require seven 3 W hydro-acoustic modem's operating at SPL_{TX} = 165 dB re 1 µPa @ 1 m and if 1 Wh can be harvested from the ocean then a semi-permanent communication link could be establish (Figure 137). The transmitter maximum SPL_{TX} = 170 dB re 1 µPa @ 1 m , requires 3 W transmit power and a power amplifier with an estimated $P_{Q_{TX}} \approx 50$ mW quiescent however the total quiescent power would be greater than 500 mW which would be dominated by the power required to run MCDSSS software on current micro controller and DSP hardware. The emerging portable device market ultra low power micro controller technology could potentially provide an order of magnitude reduction in total quiescent power. Signal processing would be

distributed across multiple micro controllers and DSP's which would require separate and high electrical efficiency power supplies. Signal processing would be required to dynamically change the DSP core clock speed and voltage to minimise power consumption.

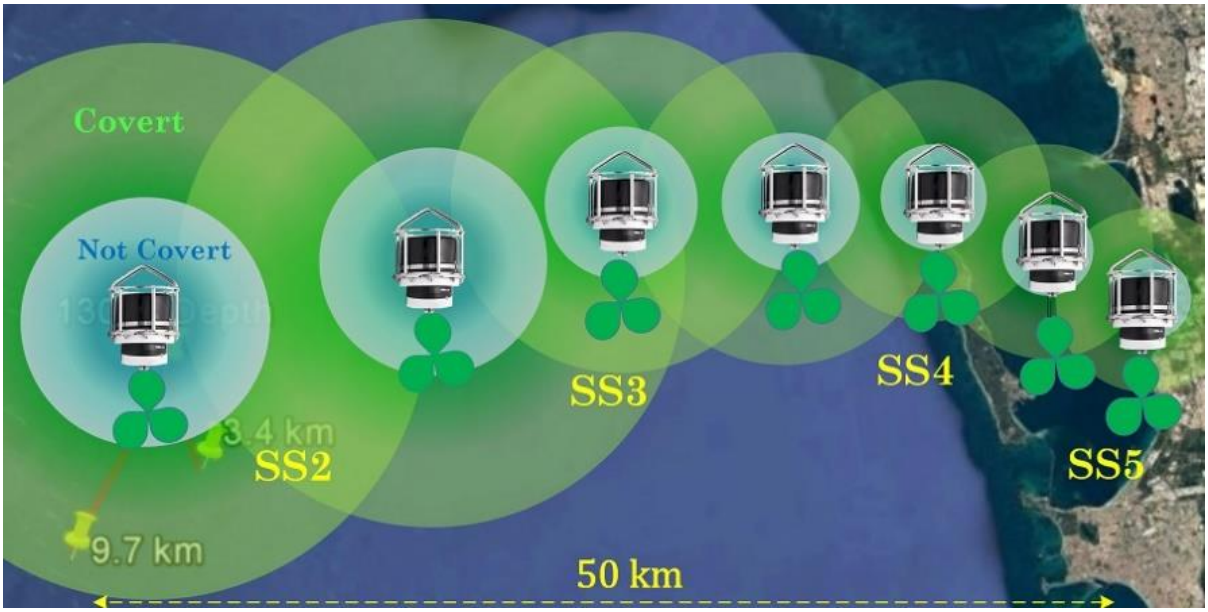

Figure 137 50 km ocean powered communication link (3 W Modems)

The 0.5 kn ocean bottom current, ocean waves or a thermocline could be used to harvest energy to charge a battery as long as the energy harvesting mechanism hydro-acoustic noise is less than the ocean noise floor. The maximum deployment time would be determined by how long it takes for the ocean to consume the energy harvesting mechanism.

6.6.5 Propagation Modelling of Peak BEE versus SPL

The measured performance agrees with predictions using equation (2-17) and equation (3-6) to within $\pm 1\ SS$ (or ± 6 dB), however high precision ± 0.5 dB real time measurements of BEE_{PEAK} are required for optimising communication links. As a general rule BEE_{PEAK} decreases with increasing channel aspect ratio and Br_{MAX} increases with surface roughness and ducting depth. A mathematical relationship between communication range, channel aspect ratio, surface roughness and ambient noise that reliably predicts the sea trial measured Br_{BEE} and SPL_{BEE} listed in Table 3 could not be established. The value of developing a BEE_{PEAK}, Br_{BEE} and SPL_{BEE} numerical model is debatable because the accuracy of a model may be no better than ± 6 dB . The nominal $BEE_{PEAK} \approx 10^4$Bits/J @ 1 km re $SS0, \pm 1.5\ SS$ is useful as a guide however in order to realise significant power savings the transmit source level (SPL_{BEE}) must be optimised to within 30% or 1 dB of the optimal BEE_{PEAK}. Given that the short term ambient noise is highly variable by approximately ± 3 dB then 1 dB BEE_{PEAK} accuracy can only be achieved via periodic precision environmental measurements using mechanisms such as the GPM300 semi-automatic baud rate and transmit source level optimisation control system (Chapter 5.6.7.2.).

6.7 Summary

Post processed failing signal database measured an improvement in message reliability from 80% to approximately 99% however associated measurements registered an improvement and occasionally a degradation in the bit error rate highlighting that a performance improvement for a targeted environment may degrade performance in different environments. The final round of message reliability optimisations resulted in less than 0.1% improvement in performance which makes it difficult to accurately measure message reliability beyond 99% for communication ranges less than 10 km. A reduction in the minimum transmit source level of approximately 10 dB was measured across laboratory and sea trial measurements as well as an improvement in the multi-path reverberation bounded maximum baud rate. Two sets of MCDSSS sea trials measured a reduction in the shallow water minimum transmit source level of approximately 10 dB where the MCDSSS receiver propagation model changes from spherical spreading Eq.(2-12) and approaches cylindrical spreading Eq.(2-13) via the process of channel impulse response deconvolution Eq.(5-40), and improved control system stability. Figure 138 illustrates firmware version 6.0 covert spheroid 10 dB performance improvement compared to firmware version 5.x Figure 3 performance base line. The 10 dB performance improvement extends the communication range from 10 km to approximately 15 km however the nonlinear properties of the processing gain (Figure 90 blue SNR trace) results in an exponential drop in message reliability as you approach the 15 km extended maximum communication range.

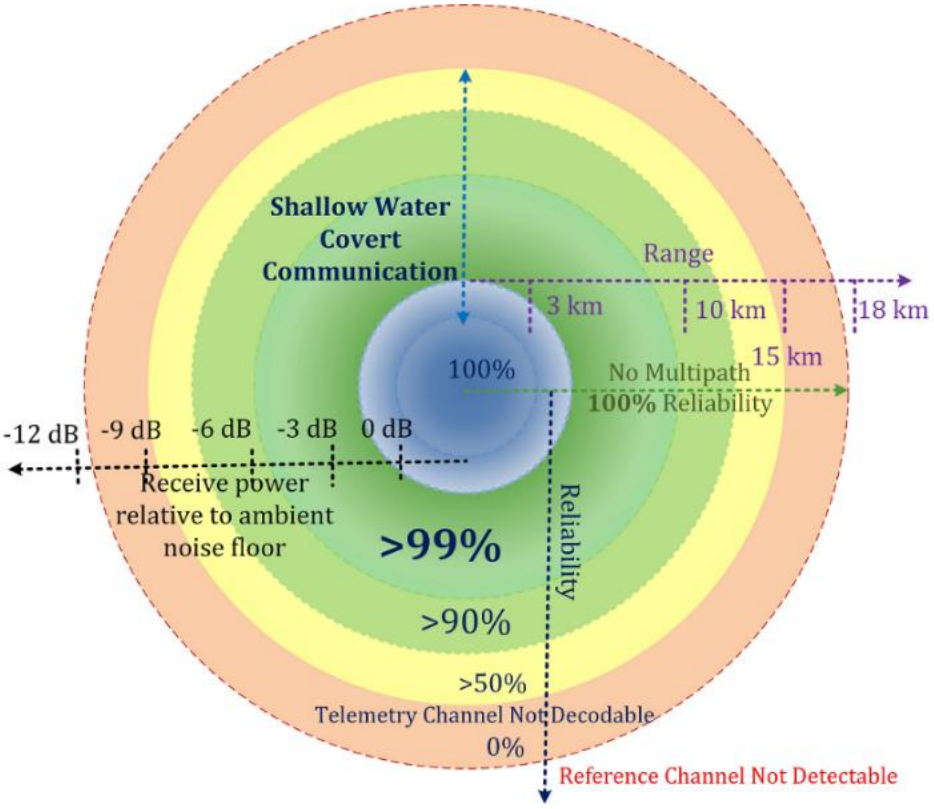

Figure 138 MCDSSS hydro-acoustic reliability covert spheroid (firmware version 6.0)

7 CONCLUSIONS AND RECOMMENDATIONS

7.1 Measured Performance Improvements

For MCDSSS receiver signals operating 0 dB to 12 dB below the ocean ambient noise floor or in harsh environments the primary thesis requirement of increasing the message reliability from +80% to approximately +99% was achieved by optimising tightly coupled control systems. The final round of message reliability optimisations resulted in less than 0.1% improvement in performance which makes it difficult to accurately measure message reliability beyond 99% for communication ranges less than 10 km. The total MCDSSS sea trial performance improvements were measured at approximately 10 dB (Appendix J.6), where the MCDSSS shallow water propagation model changes from spherical spreading Eq.(2-12) to approaching cylindrical spreading Eq.(2-13) via the process of channel impulse response deconvolution Eq.(5-40). The 10 dB improvement in performance can be used to either lower the minimum transmit source level by up to 10 dB, extend communication range by 50% or operate in environments with up to 10 dB louder ambient noise.

7.2 Counter Intuitive Results

Improvements in the MCDSSS receiver message reliability has resulted in an instrument that can be used to accurately probe the hydro-acoustic channel impulse response using variable symbol period , transmit source level and message payload. Precision channel impulse response measurements provide an estimate of the maximum hydro-acoustic baud rate, peak bit energy efficiency and bit error rate. The counter intuitive results are as follows:

1. As expected the maximum hydro-acoustic baud rate (Br_{MAX}) is limited by the multipath reverberation envelope period (τ_{MPE}) however bit energy efficiency (BEE) is not a linear function of the maximum hydro-acoustic baud rate. BEE peaks before the maximum hydro-acoustic baud rate and is also limited by the hydro-acoustic propagation channel geometry and frequency dependent attenuation (L_A) (Chapter 6.6).
2. Operating at the maximum hydro-acoustic baud rate (Br_{MAX}) may not provide the optimum bit energy efficiency for shallow water deployments. Maximum covert performance also occurs at the maximum bit energy efficiency.
3. The peak bit energy efficiency relationship has a significant implication for battery powered and ocean energy harvesting long-range hydro-acoustic communication links because logarithmic power savings can be realised by measuring the peak bit energy efficiency as a function of hydro-acoustic baud rate and minimum transmit source level (SPL_{MIN}).
4. MCDSSS detector false detect rate is not proportional to the number of Doppler receivers (D_N). False detect rate is a nonlinear function of Doppler (D_{MAX}) and bounded by $\log_{10}$ of the number of Doppler receivers. Increasing or decreasing the maximum Doppler imposes a modest change in the maximum communication range (R_{MAX}). Minimising the number of Doppler receivers (D_N) is more significant in reducing the receiver power consumption (P_{RX}). The

logarithmic processing gain (P_G) requires the detection threshold (D_{TH}) to be manual optimisation to within ± 0.25 dB or linear accuracy of $\pm 5\%$.

5. The robustness of MCDSSS processing gain (P_G) provides reliable communication in the presence of open circuit, cracked PZT ceramic, damaged electronic, software bugs or algorithm errors. MCDSSS reliability is a nonlinear function of the processing gain which hinders the identification of communication system message reliability faults.

7.3 Environmental Performance Results

Sea trail and laboratory measurements encounter the following unexpected performance results:

1. Baltic and Singapore deployments:
    a. Reliable MCDSSS communication is an extreme multipath and bottom ducting environment.
2. 11 km depth rated submarines:
    a. Reliable communication in an $+SS15$ anisotropic noise environment.
    b. 22 km voice communication bottom bounce.
3. Western Australian 3 km to 15 km horizontal maximum range trials:
    a. Reversal of shallow/deep water reliability.
    b. Extreme shallow water multipath delay environment ($\tau_{MPE} > 15$ms).
    c. Reliable through vessel hull and turbulent wake communication.
    d. The 3 km to 10 km range, 130 m depth, $SS2$, $SPL_{TX} =$ 164 dB re 1 µPa @ 1 m, requiring 650 mW transmiiter power, 500 baud communication result highlights justification for further power consumption reductions are required in the MCDSSS transmitter power amplifier 3 W and the DSP 1.3 W quiescent power to realise the full battery power savings.
4. Hydro-acoustic tank and air performance verification:
    a. Reliable communication in harsh tank and harsh air test environments translates to reliable shallow water ocean communication.
5. PZT transducer limitation:
    a. De-rating of narrow-band low duty cycle PZT transducer specification by at least 6 dB for broad-band 100% duty cycle operation.
    b. Oil filled PZT transducer cavitation limits shallow water maximum transmit source level (SPL_{MAX}).

7.4 Future Application

The advances made in MCDSSS underwater communication reliability, outlined in this thesis, will be deployed on current and future Australian submarines, AUV's, Wave Gliders and autonomous environmental networked monitoring nodes. MCDSSS performance improvements developed for this thesis have be deployed on the TRITON 36000/2 submarine and landers for the 2018/2019 deep ocean trench expedition. As of 2018 a variant of the MASQ communication protocol has been ratified as a European private communication standard. The MCDSSS covert performance is important for

minimising the health and safely impact of diver identification systems and marine mammals [77] [99]. In particular minimising the acoustic power injected into environment to reduce the hydro-acoustic noise near diver's ears. MCDSSS' robust shallow water and high ambient noise performance may translate to ultra-long-range reliable deep-water communication. Advances in low frequency and low cost hydro-acoustic projectors may provide the potential for affordable ultra-long-range SOFAR channel communication however there are currently no commercial applications. Deployment of MCDSSS transceiver on emerging ultra low power electronics provides the potential of establishing semi-permanent long-range network routed communication powered by ocean energy harvesting.

7.5 Final Remarks

Satellite generated high resolution maps of the Moon and Mars are more detailed than maps of the earth which remains mostly unexplored because two thirds of the earth is covered in water. There have been many advances in underwater sensors, autonomous vehicles and full ocean depth submarines however one of the missing link technologies is long-range, reliable, low power and low cost wireless underwater communication modems. The sea trial results presented in this thesis have made progress in reliable long-range communication and low power consumption modems. The publication of sea trials data may encourage researchers and commercial users to adopt MCDSSS for long-range hydro-acoustic communication as an alternative to cabled and non-real time data logging. Increasing the number of MCDSSS users may advance the technology as communication links are established across longer ranges and in more hostile environments. MCDSSS may evolve or assist in the development of a more robust communication protocols. It is the hope of this candidate that the MCDSSS communication play a part in the continuing exploration of our oceans.

Appendix A References

A.1 Referenced Publications

[1] Alyaoui N., Kachouri A., and Samet M., ***"Automatic Modulation Classification for Underwater Acoustic Communications,"*** The 10th IEEE International Symposium on Signal Processing and Information Technology Pages: 166 - 170, DOI: 10.1109/ISSPIT.2010.5711766, Dec. 2010.

[2] Andronis N., ***"Shallow Water Limits to Hydro-acoustic Baud Rate and Bit Energy Efficiency"*** 19-22 November, Australia Acoustic Society Conference, 2017.

[3] Badiey M., Mu Y., Simmen J., and Forsythe S., ***"Signal variability in shallow-water sound channels."*** *IEEE J. Ocean. Eng.* no. 25 (4):492-500, 2000.

[4] Badiey M., Song A., and Smith K., ***"Coherent reflection from surface gravity water waves during reciprocal acoustic transmissions."*** *The Journal of the Acoustical Society of America* no. 132:EL290. doi: 10.1121/1.4747815, 2012.

[5] Baggeroer A., ***"Acoustic telemetry - An overview."*** *Oceanic Engineering, IEEE Journal of* no. 9 (4):229-235. doi: 10.1109/JOE.1984.1145629, 1984.

[6] Beaujean, P. P., ***"Measurement of the Doppler shift in forward-scattered waves caused by moderate sea surface motion in shallow waters."*** *Acoustics research letters online* no. 6 (4):250, 2005.

[7] Benson C. R., Ryan M. J., and Frater M. R., ***"A tipping point for undersea networks."***, 2012.

[8] Bernault E., "**Array processing techniques for frequency hopping multiple frequency shift keying long-range communications**.". A Thesis Submitted to the Faculty of The College of Engineering in Partial Fulfilment of the Requirements for the Degree of Master of Science, 2002.

[9] Bernstein S., "**Long-range communications at extremely low frequencies**." Proceedings of the IEEE, Vol.62(3), pp.292-312, March 1974.

[10] Brad D. P., and Catipovic J. A., ***"Adaptive multiuser detection for underwater 'acoustical channels,"*** *IEEE* J. *Oceanic Eng.,* vol. 19, pp. 158-165, A r, 1994.

[11] Bragard P., Jourdain G., ***"A fast self-optimized LMS algorithm for nonstationary identification. Application to underwater equalization,"*** in *Proc. ICASSP'90,* Albuquerque, NM, pp. 1425-1428, 1990.

[12] Bobber J. B., **"Underwater Electroacoustics Measurements."** Prentice Hall Signal Processing Series, ISBN 0-13-947607-5, 1984.

[13] Burbis S. W., **"Underwater Acoustic System Analysis."** Peninsula Publishing Los Altos, California USA, ISBN 0-932146-19-8, 1988.

[14] Caiti A., Felisberto P., Husoy T., Jesus S. M., Karasalo I., Massimelli R., Reinen T. A., and Silva A. 2011. ***"Underwater Acoustic Network".*** UAN – Paper read at Oceans, 2011.

[15] Caley M., Duncan A. J., ***"Conceptual development of a dynamic underwater acoustic channel simulator. In Acoustics",*** *Annual Conference of the Australian Acoustical Society*. Gold Coast, Australia: Australian Acoustical Society, *2011.*

[16] Caley M., and Duncan A. J., ***"Transient Doppler and delay spreading in a shallow underwater acoustic channel."*** In *Underwater Communications: Channel Modelling & Validation - hosted by NATO Centre for Maritime Research and Experimentation*. Hotel Due Mari, Sestri Levante, Italy: NATO Centre for Maritime Research and Experimentation, 2012.

[17] Caley M., and Duncan A., ***"Investigation of underwater acoustic multipath Doppler and delay spreading in a shall water marine environment."*** *Acoustics Australia* no. 41 (1):20-28, 2013.

[18] Caley M., Duncan A. J., and Ghiotto A., "***Measurements of Doppler and delay spreading of communication signals in medium depth and shallow underwater acoustic channels.***" In *Acoustics 2012, Annual Conference of the Australian Acoustical Society*. Fremantle, Australia: Australian Acoustical Society, 2012.

[19] Catipovic J., Deffenbaugh M., Freitag L., and Frye D., ***"An acoustic telemetry system for deep ocean mooring data acquisition and control,"*** in *Proc. OCEANS'89,* Seattle, WA, pp. 887-892, Oct 1989.

[20] Catipovic J., Johnson M., and Adams D., ***"Noise cancelling performance of an adaptive receiver for underwater communications,"*** in *Proc. 1994 Symp. AUV Techno!.,* Cambridge, MA, pp. 171-178. , July 1994.

[21] Catipovic J., ***"Performance limitations in underwater acoustic telemetry,"*** *IEEE* J. *Oceanic Eng.,* vol. OE-9, pp. 229-235, Oct. 1984.

[22] Cato D. H., "***Ambient Sea Noise in Australian Waters***", Defence Science and Technology Organisation", Fifth International Congress on sound and vibration Adelaide, South Australia, 1997.

[23] Chappell S., *et al.,* ***"Acoustic communication between two autonomous underwater vehicles,"*** in *Proc. Symp. AUV Techno!.,* Cambridge, MA, pp. 462-469, 1994.

[24] Chitre M., ***"A high-frequency warm shallow water acoustic communications channel model and measurements."*** Vol. 122: ASA, 2007.

[25] Chitre M., Shahabudeen S., and Stojanovic M., ***"Underwater acoustic communications and networking: Recent advances and future challenges,"*** *Marine Tech. Society J.*, vol. 42, pp. 103-116, Spring 2008.

[26] Chitre M., Shahabudeen S., Freitag L., and Stojanovic M., 2008. ***"Recent advances in underwater acoustic communications and networking."*** Paper read at OCEANS 2008, 15-18, Sept 2008.

[27] Claudio D. D., ***"Sustainable Port Development in Singapore (MPA)Sustainable Port Development in Singapore"*** CF3-3-6 (Singapore).pdf 2016.

[28] Coatelan S. and Glavieux A., ***"Design and test of a multicarrier transmission system on the shallow water acoustic channel,"*** in *Proc. OCEANS* '94, Brest, France, pp. III.472-III.477, Sept 1994.

[29] Coates R., ***"Underwater Acoustic Systems."*** New York: Wiley, 1993.

[30] Colin M. E. G. D., and Beerens S. P., ***"False-Alarm Reduction for Low-Frequency Active Sonar With BPSK Pulses: Experimental Results."*** *Oceanic Engineering, IEEE Journal of* no. 36 (1):52-59, 2011.

[31] Collins T., and Atkins P., ***"Doppler-sensitive active sonar pulse designs for reverberation processing."*** *Radar, Sonar and Navigation, IEE Proceedings* - no. 145 (6):347-353. doi: 10.1049/ip-rsn:19982434, 1998.

[32] Constantinou Y., ***"Blind equalization via channel estimation using cyclostationary statistics of signals,"*** M.S. thesis, Northeastern Univ., Boston, MA, 1994.

[33] Cristol X., ***"A Global Model of Fading Channel for Application to Acoustic Communication in Marine Environment."*** NARCISSUS-2005: In *Oceans – Europe, 2005.*

[34] Curtin T., Bellingham J., Catipovic J., and Webb D., ***"Autonomous oceanographic sampling networks,"*** *Oceanogr.,* vol. 6, no. 3, pp. 86-94, 1993.

[35] Dahl P. H., ***"High-frequency forward scattering from the sea surface: the characteristic scales of time and angle spreading."*** *Oceanic Engineering, IEEE Journal of* no. 26 (1):141-151, 2001.

[36] Deane G. B., Preisig J., Tindle C. T., Lavery A., and Stokes M. D., ***"Deterministic forward scatter from surface gravity waves."*** *J. Acoust. Soc. Am.* no. 132 (6):3673-3686. doi: 10.1121/1.4763996, 2012.

[37] Dixon R. C., ***"Spread Spectrum Systems with commercial applications"*** 3rd edition. ISBN 0-471-59342-7, 1994.

[38] Dol H. S., Colin M. E. G. D., Ainslie M. A., van Walree P. A., and Janmaat J., ***"Simulation of an Underwater Acoustic Communication Channel Characterized by Wind-Generated Surface Waves and Bubbles."*** *IEEE J. Ocean. Eng.* no. 38 (4):642-654. doi: 10.1109/JOE.2013.2278931, 2013.

[39] Eggen T. H., Baggeroer A. B., and Preisig J. C., ***"Communication over Doppler spread channels - Part I: Channel and receiver presentation."*** *IEEE journal of oceanic engineering* no. 25 (1):62-71, 2000.

[40] Elfouhaily T. M., and Guérin C. A., ***"A critical survey of approximate scattering wave theories from random rough surfaces.***" *Waves in Random Media* no. 14 (4):R1-R40. doi: 10.1088/0959-7174/14/4/r01, 2004.

[41] Essebbar A., Loubet G., and Vial F., ***"Underwater acoustic channel simulations for communication,"*** in *Proc. OCEANS* '94, Brest, France, pp. 1II.495-1II.500, Sept 1994.

[42] Fischer J., Bennett K., Reible S., Cafarella J., and Yao I., ***"A high rate, underwater acoustic data communications transceiver,"*** in *Proc. OCEANS'92,* Newport, RI, pp. 571-576, Oct 1992.

[43] Freitag L., Stojanovic M., Singh S., and Johnson M., ***"Analysis of channel effects on direct-sequence and frequency-hopped spread-spectrum acoustic communication."*** *IEEE journal of oceanic engineering* no. 26 (4):586-593, 2001.

[44] Gardner A., Collins J., ***"A Second Look at Chip Scale Atomic Clocks for Long Term Precision Timing Four Years in the Field"*** Woods Hole Oceanographic Institution.

[45] Gene H., and Haertling J., ***"Ferroelectric Ceramics History and Technology"***, *American. Ceramic. Society* 82 [4] 797–818, 1999.

[46] Ghiotto A., Andronis N., and Dragojevic M., ***"Reliable Underwater Communication, Proceedings of Acoustics"*** 2012 - Fremantle 21-23 November Fremantle, Australia, 2012.

[47] Goalic A., Labat J., Trubuil J., Saoudi S., and Riouaten D., ***"Toward a digital acoustic underwater phone,"*** in *Proc. OCEANS'94,* Brest, France, pp. III.489-III.494, Sept. 1994.

[48] Gobriel S., ***"Energy Efficiency in Communications and Networks,"*** ISBN 978-953-51-0482-7, April. 2012.

[49] Gray S., and Preisig J., ***"Multiuser detection in dispersive channels using array observations,"*** in *Proc.* 1994 *Con! Inform. Sci. Syst.,* Princeton, NJ, pp. 103-108, Mar. 1994.

[50] Guo Q., and Huang D., ***"GMP-based channel estimation for single-carrier transmissions over doubly selective channels,"*** *IEEE Signal Processing Lett.* vol. 17, pp. 8-11, Jan. 2010.

[51] Guo Q., Ping L., and Huang D., ***"A low-complexity iterative channel estimation and detection technique for doubly selective channels,"*** *IEEE Trans. Wireless Commun.*, vol. 8, pp. 4340-4349, Aug. 2009.

[52] Haykin S., **"Communication Systems"** 4th edition ISBN 1139501453, 2001.

[53] Henderson G. B. *et al.,* ***"Investigation of adaptive beamformer performance and experimental verification of applications in high data rate digital underwater communications,"*** in *Proc. OCEANS'94,* Brest, France, pp. 1.296--1.30 I, Sept. 1994.

[54] Holthuijsen L. H., ***"Waves in oceanic and coastal waters."*** In. Cambridge: Cambridge University Press ISBN 978-0-521-86028-4, 2007.

[55] Hoag D., and Ingle V. K., ***"Underwater video compression using the wavelet transform,"*** in *Proc. OCEANS'95,* San Diego, CA, pp. 1411-1416, Oct. 1995.

[56] Howe G. S., Tarbit P., Hinton O., Sharif B., and Adams A., ***"Sub-sea acoustic remote communications utilising an adaptive receiving beamformer for multipath suppression,"*** in *Proc. OCEANS'94,* Brest, France, pp. 1.313-1.316, Sept. 1994.

[57] Hsu, S. A., Meindl E. A., and Gilhousen D. B., ***"Determining the Power-Law Wind-Profile Exponent under Near-Neutral Stability Conditions at Sea."*** *Journal of Applied Meteorology* no. 33 (6):757-772, 1994.

[58] Hsu F., ***"Square root Kalman filtering for high-speed data received over fading dispersive HF channels,"*** *IEEE Trans. Inform. Theory,* vol. IT-28,pp. 753-763, Sept. 1982.

[59] Huang S. H., Yang T. C., and Huang C. F., ***"Multipath correlations in underwater acoustic communication channels."*** *Journal of the Acoustical Society of America* no. 133 (4), 2013.

[60] Isukapalli Y., Song H. C., and Hodgkiss W. S., ***"Stochastic channel simulator based on local scattering functions."*** *The Journal of the Acoustical Society of America* no. 130 (4):EL200. doi: 10.1121/1.3633688, 2011.

[61] Jarvis S., and Pendergrass N. A., ***"Implementation of a multichannel decision feedback equalizer for shallow water acoustic telemetry using a stabilized fast transversal algorithm,"*** in *Proc. OCEANS'95,* San Diego, CA, pp. 787-796, Oct 1994.

[62] Johnson M., Herold D., and Catipovic J., ***"The design and performance of a compact underwater acoustic network node,"*** in *Proc. OCEANS'94,* Brest, France, pp. II1.467-III.471, Sept 1994.

[63] Karasalo I., ***"Time-domain modelling of turbo-coded underwater communication."*** Paper read at OCEANS, 2011 IEEE - Spain, 6-9 June 2011.

[64] Karjadi E. A., Badiey M., Kirby J. T., and Bayindir C., ***"The Effects of Surface Gravity Waves on High-Frequency Acoustic Propagation in Shallow Water."*** *Oceanic Engineering, IEEE Journal of* no. 37 (1):112-121. doi: 10.1109/JOE.2011.2168670, 2012.

[65] Kaya A., and Yauchi S., ***"An acoustic communication system for subsea robot,"*** in *Proc. OCEANS'89,* Seattle, WA, pp. 765-770, Oct 1989.

[66] Kilfoyle D. B., and Baggeroer A. B., ***"The state of the art in underwater acoustic telemetry."*** *Oceanic Engineering, IEEE Journal of* no. 25 (1):4-27. doi: 10.1109/48.820733, 2000.

[67] Kocic M., Brady D. P., and Stojanovic M., ***"Sparse equalization for real-time digital underwater acoustic communications,"*** in *Proc. OCEANS* '95, San Diego, CA, pp. 1417-1422, Oct. 1995.

[68] Li B., Huang J., Zhou S., Ball K., Stojanovic M., Freitag L., and Willett P., ***"MIMO-OFDM for High-Rate Underwater Acoustic Communications."*** *IEEE journal of oceanic engineering* no. 34 (4):634-644, 2009.

[69] Li W., and Preisig J. C., ***"Estimation of Rapidly Time-Varying Sparse Channels,"*** *Oceanic Engineering, IEEE Journal of,* vol. 32, pp. 927-939, 2007.

[70] Ling F., and Proakis J. G., ***"Adaptive lattice decision-feedback equalizers-Their performance and application to time-variant multipath channels,"*** *IEEE Trans. Commun.,* vol. COM-33, pp. 348-356, Apr. 1985.

[71] Litis R., and Fuxjaeger A., ***"A digital DS spread spectrum receiver with joint channel and Doppler shift estimation,"*** *IEEE Trans. Commun.,* vol. 39, pp. 1255-1265, Aug. 1991.

[72] Marr W. J., ***"Acoustic Based Tactical Control of Underwater Vehicles."*** sNava; Postgraduate School PhD Dissertation, 2003.

[73] MacKay D. J. C., ***"Information Theory, Inference, and Learning Algorithms."*** Cambridge University Press, 2003.

[74] Melodia T., Kulhandjian H., Kuo L. C., and Demirors E., ***"Advances In Underwater Acoustic Networking."*** State University of New York at Buffalo, 2013.

[75] Merriam S., and Porta D., ***"DSP-based acoustic telemetry modems,"*** *Sea Technogy.,* May 1993.

[76] NATO STANAG ***"North Atlantic Treaty Organization (NATO) Standardization Agreement (STANAG), Minimum standard characteristics of underwater telephones for use in submarine, surface ships and helicopters of NATO nations,"*** STANAG No. 1074.

[77] NATO NUARC "***NATO Undersea Research and Marine Mammal Risk Mitigation Rules and Procedures***", NUARC-SP-2008-003, 2008.

[78] Otnes R., Jenserud T., and van Walree P. A., ***"Validation of replay-based underwater acoustic communication channel simulation."*** *IEEE*

Journal of Oceanic Engineering no. 38 (4):689-700. doi: 10.1109/JOE.2013.2262743. 2013.

[79] Ott W. H., ***"Noise Reduction Techniques in Electronic Systems"***, *Bell Telephone Laboratories, Wiley-Interscience Publication* ISBN 0-471-17869-1 *1976*.

[80] Pusey G. M., Duncan A. J., and Smerdon A. M., ***"Analysis of acoustic modem performance for long-range horizontal data transmission."*** OCEANS 2009-EUROPE, pp.1-9, May 2009.

[81] Pelekanakis K., and Baggeroer A. B., ***"Exploiting Space-Time-Frequency Diversity With MIMO-OFDM for Underwater Acoustic Communications."*** *IEEE J. Ocean. Eng.* no. 36 (4):502-513. doi: 10.1109/JOE.2011.2165758. 2011.

[82] Peterson J., and Porter M. B., ***"Ray/Beam Tracing for Modeling the Effects of Ocean and Platform Dynamics."*** *IEEE J. Ocean. Eng.* no. 38 (4):655-665. doi: 10.1109/JOE.2013.2278914. 2013.

[83] Shashi P., Eileen M. P., and Culver R. L., ***"A High-Fidelity Ocean Sampling Mobile Network (SAMON) Simulator Testbed for Evaluating Intelligent Control of Unmanned Underwater Vehicles)."*** IEEE JOURNAL OF OCEANIC ENGINEERING, VOL. 26, NO. 4, OCTOBER 2001.

[84] Pompili D., and Melodia T., ***"An Architecture for Ocean Bottom Under Water Acoustic Sensor Networks (UWASN)."*** Broad-band and Wireless Networking Laboratory Georgia Institute of Technology, Atlanta, GA 30332 2003.

[85] Porter M. B., ***"The BELLHOP Manual and Users Guide - preliminary draft."*** In: HLS Research, La Jolla, CA, USA. 2011.

[86] Porter M. B., ***"Out-of-Plane Effects in Ocean Acoustics."*** edited by Light Heat and C. A. Sound Research Inc La Jolla. 2013.

[87] Porter M. B., Hursky P., and Siderius M., ***"High-frequency propagation for acoustic communications."*** In Impact of Littoral Environmental Variability on Acoustic Predictions and Sonar Performance, edited by Nicholas G. Pace and Finn B. Jensen. Kluwer. 2002.

[88] Potter J. R., Porter M. B., and Preisig J. C., ***"UComms: A Conference and Workshop on Underwater Communications, Channel Modeling, and Validation."*** *Oceanic Engineering, IEEE Journal of* no. 38 (4):603-613. doi: 10.1109/JOE.2013.2283094. 2013.

[89] Preisig J., ***"Acoustic propagation considerations for underwater acoustic communications network development."*** *Mobile computing and communications review* no. 11 (4):2-10. 2007.

[90] Preisig J. C., and Deane G. B., ***"Surface wave focusing and acoustic communications in the surf zone."*** *The Journal of the Acoustical Society of America* no. 116 (4):2067-2080. 2004.

[91] Qarabaqi P., and Stojanovic M., ***"Statistical characterization and computationally efficient modeling of a class of underwater acoustic communication channels."*** *IEEE Journal of Oceanic Engineering* no. 38 (4):701-717. doi: 10.1109/JOE.2013.2278787. 2013.

[92] Rabiner L. R., and Rader M. C., ***"Digital Signal Processing, What is the Fast Fourier Transform"*** *COCHRAN T W. IEEE press*, ISBN 0-87942-018-9, 1972.

[93] Rice J., and Green D., **"Underwater Acoustic Communications and Networks for the US Navy's Seaweb Program."** 2008.

[94] Roberts P., Andronis N., and Ghiotto A., **"Voices from the deep – Acoustic communication with a submarine at the bottom of the Mariana Trench"**, Proceedings of Acoustics - Fremantle Australia 21-23 November 2012.

[95] Rodriguez O. C., Silva A. J., Zabel F., and Jesus S. M., **"The TV-APM interface: a web service for collaborative modeling."** Paper read at 10th European Conference on Underwater Acoustics, at Instanbul, Turkey. 2010.

[96] Priya Banu M., Priya Hari V., Eniya A., and Deepika K., ***"Challenges for Efficient Communication in Underwater Acoustic Sensor Network"*** IJIRSET Volume 4, Special Issue 11, September 2015.

[97] Schanze T., **"Sinc interpolation of discrete periodic signals."** *Signal Processing, IEEE Transactions on* no. 43 (6):1502-1503. doi: 10.1109/78.388863. 1995.

[98] Senne J., Song A., Badiey M., and Smith K., **"Parabolic equation modeling of high frequency acoustic transmission with an evolving sea surface."** *J. Acoust. Soc. Am.* no. 132 (3):1311-1318. doi: 10.1121/1.4742720. 2012.

[99] Siderius M., and Porter M. B., **"Modeling techniques for marine-mammal risk assessment."** *IEEE journal of oceanic engineering* no. 31 (1):49-60. 2006.

[100] Siderius M., and Porter M. B., **"Modeling broad-band ocean acoustic transmissions with time-varying sea surfaces."** *Journal of the Acoustical Society of America* no. 124 (1):14. 2008.

[101] Siderius M., Porter M. B., Hursky P., and McDonald V., ***"Effects of ocean thermocline variability on noncoherent underwater acoustic communications."*** The Journal of the Acoustical Society of America no. 121 (4):1895-1908. 2007.

[102] Silva A., Rodriguez O., Zabel F., Huilery J., and Jesus S. M., ***"Underwater acoustic simulations with a time variable acoustic propagation model."*** In 10th European Conference on Underwater Acoustics. Instanbul, Turkey. 2010.

[103] Slock D. T., Chisci L., Lev-Ari H., and Kailath T., ***"Modular and numerically stable fast transversal filters for multichannel and multiexperiment RLS,"*** *IEEE Trans. Signal Processing,* vol. 40, pp. 784-802, Apr. 1992.

[104] Slock D., and Kailath T., ***"Numerically stable fast transveral filters for recursive least squares adaptive filtering,"*** *IEEE Trans. Acoust., Speech, and Signal Processing,* vol. 39, pp. 92-114, Jan. 1991.

[105] Socheleau F., Laot C., and Passerieux J., ***"Stochastic Replay of Non-WSSUS Underwater Acoustic Communication Channels Recorded at Sea."*** *IEEE Trans. Signal Process.* no. 59 (10):4838-4849. doi: 10.1109/TSP.2011.2160057. 2011.

[106] Soli J., and Hickman G., **"Comparison of Comb and Pulse Train Signal Designs for Active Sonar"** Dept of Electrical and Computer Engineering Duke University Durham, NC 27708, 2012.

[107] Song A., Badiey M., Song H. C., Hodgkiss W. S., Porter M. B., and Group T. K. ***"Impact of ocean variability on coherent underwater acoustic communications during the Kauai experiment"*** *(KauaiEx)*. Vol. 123: ASA. 2008.

[108] Stojanovic M., **"Acoustic (underwater) communications,"** in Encyclope dia of Telecommunications, J. G. Proakis, Ed. John Wiley and Sons, 2003.

[109] Stojanovic M., Proakis J., and Catipovic J., ***"Analysis of the impact of channel estimation errors on the performance of a decision-feedback equalizer in fading multipath channels,"*** *IEEE Trans. Commun.,* vol. 43, pp. 877-886, Feb./Mar'/Apr. 1995.

[110] Stojanovic M., Freitag L., and Johnson M., ***"Channel-estimation-based adaptive equalization of underwater acoustic signals,"*** in *Proc. MTS/ IEEE OCEANS*, vol. 2, pp. 985–990, 1999.

[111] Stojanovic M., "**Efficient acoustic signal processing based on channel estimation for high rate underwater information,"** *J. Acoust. Soc. Amer.*, submitted for publication. June 2008.

[112] Stojanovic M., and Freitag L., ***"Multichannel Detection for Wideband Underwater Acoustic CDMA Communications,"*** Massachusetts Institute of Technology.

[113] Stojanovic M., and Zvonar Z., ***"Multichannel processing of broad-band multiuser communication signals in shallow water acoustic channels,"*** this issue, pp. 156-166, 1996.

[114] Stojanovic M., Catipovic J. A., and Proakis J. G., ***"Performance of high-rate adaptive equalization on a shallow water acoustic channel,"*** submitted to *1. Acoust. Soc. Amer.*

[115] Stojanov M. C., Catipovic J. A., and Proakis J. O., ***"Phase coherent digital communications for underwater acoustic channels,"*** IEEE J. Oceanic Eng., vol. 1, pp. 100-111, Jan. 1994.

[116] Stojanovic M., **"Recent advances in high-speed underwater acoustic communications,"** *IEEE JOURNAL OF OCEANIA ENGINEERING*, VOL. 21, NO 2, Notes: 30 to 40K bits/s QPSK and high order modulation. Networking, submarine and autonomous vehicle communication reference. April. 1996.

[117] Stojanovic M., and Preisig J. C., ***"Underwater acoustic communication channels: propagation models and statistical characterization."*** (Underwater Wireless Communications)(Report). *IEEE communications magazine* no. 47 (1). 2009.

[118] Subramaniam V. L., Rajan S. B., and Bahl R., ***" Trellis Coded Modulation Schemes for Underwater Acoustic Communications,"*** 0-7803-5045-6/98 IEEE 1998.

[119] Suzuki M., and Sasaki T., ***"Digital acoustic image transmission system for deep sea research submersible,"*** in *Proc. OCEANS'92,* Newport, RI, pp. 567-570. , Oct. 1992.

[120] Taehyuk K., Song H. C., Hodgkiss W. S., and Jea Soo K., ***"Long-range multi-carrier acoustic communications in shallow water based on iterative sparse channel estimation."*** *The Journal of the Acoustical Society of America* no. 128:EL372. doi: 10.1121/1.3514157, 2010.

[121] Talavage J., Thiel T., and Brady D., ***"An efficient store-and-forward protocol for a shallow water acoustic local area network,"*** presented at *Proc. OCEANS'94,* Brest, France, Sept. 1994.

[122] Tarbit P. S. D., Howe G., Hinton O., Adams A., and Sharif B., ***"Development of a real-time adaptive equalizer for a high-rate underwater acoustic data communication link,"*** in *Proc. OCEANS'94,* Brest, France, pp. 1.307-1.312. , Sept. 1994.

[123] Tian Chen, Liu Wenyu, Jin Jiang, Wang Yi, and Mo Yijun. ***" Localization and Synchronization for 3D Underwater Acoustic Sensor Networks."*** *Dept. of Electronics and Information Engineering, Huazhong University of Sci & Tech, 430074 Wuhan, Hubei, China 2007.*

[124] Tindle C. T., ***"Wavefronts and waveforms in deep-water sound propagation."*** *J. Acoust. Soc. Am.* no. 112 (2):464-475. doi: 10.1121/1.1489437. 2002.

[125] Trubuil J., Gall Le T., Lapierre G., and Labat J., ***"Development of a Real-Time High Data Rate Acoustic Link."*** G.E.S.M.A. (Groupe d'Etudes Sous-Marines de l'Atlantique), BP 42, 29240 Brest Naval, France. *2002.*

[126] Tomasi B., Zappa G., McCoy K., Casari P., and Zorzi M., ***"Experimental Study of the Space-Time Properties of Acoustic Channels for Underwater Communications."*** In Proceedings of IEEE Oceans 2010 Conference, Sydney Australia. 2010.

[127] Tong L., Xu G., and Kailath T., ***"Blind identification and equalization based on second-order statistics,"*** *IEEE Trans. Inform. Theory,* vol. 40, pp. 340-349, Mar. 1994.

[128] Ungerboeck G., ***"Trellis coded modulation, Parts 1 and 2,"*** IEEE Commun. Mag., pp. 5-21, Feb. 1987.

[129] Urick J. R., ***"Principles of underwater sound"*** 3rd edition ISBN 0932146-62-7, 1983.

[130] van Walree P. A., Jenserud T., and Smedsrud M., ***"A Discrete-Time Channel Simulator Driven by Measured Scattering Functions."*** *IEEE journal on selected areas in communications* no. 26 (9):1628-1637. 2008.

[131] van Walree P. A., ***"Channel sounding for acoustic communications: techniques and shallow-water examples,"*** FFI report /00007. Norwegian Defence Research Establishment. 2011.

[132] van Walree P. A., ***"Propagation and Scattering Effects in Underwater Acoustic Communication Channels."*** *IEEE J. Ocean. Eng.* no. 38 (4):614-631. doi: 10.1109/JOE.2013.2278913. 2013.

[133] van Walree P. A., Jenserud T., and Otnes R., ***"Stretched-exponential Doppler spectra in underwater acoustic communication channels."*** *The Journal of the Acoustical Society of America* no. 128 (5):EL329-EL334. 2010.

[134] van Walree P. A., and Otnes R., ***"Ultrawideband Underwater Acoustic Communication Channels."*** *IEEE J. Ocean. Eng.* no. 38 (4):678-688. doi: 10.1109/JOE.2013.2253391. 2013.

[135] Verdu S., ***"Adaptive multiuser detection,"*** in *Proc. IEEE 3rd Int. Symp.Spread Spectrum Tech. Applicat*, Oulu, Finland, pp. 43-50, July 1994.

[136] Wang Z., ***" Communications and Networking in Underwater Acoustic Networked Systems,"*** Doctoral Dissertations University of Connecticut Graduate School 2013.

[137] Webb W. T. and Steele R., ***"Variable rate QAM for mobile radio,"*** *IEEE Trans. Commun.,* vol. 43, pp. 2223-2230, July 1995.

[138] Williams R. E., and Battestin H. F., ***"Coherent recombination of acoustic multipath signals propagated in the deep ocean,"*** *The Journal of the Acoustical Society of America,* vol. 50, pp. 1433-1442, Page 3 Suchi Barua. 1971.

[139] Wilson B. O., ***"Introduction to Theory and Design of Sonar Transducers,"*** Peninsula Publishing Los Altos, California UAS ISBN 0932146-22-8, 1991.

[140] Yang T. C., ***"Properties of underwater acoustic communication channels in shallow water."*** *The Journal of the Acoustical Society of America* no. 131 (1):129. doi: 10.1121/1.3664053. 2012.

[141] Zaibi G., Nasri N., Kachouri A., Andrieux L. and Samet M., ***"Cross-Layer Design For Energy-Efficient In Wireless Underwater Communication: Acoustic Frequency Identification Case Study,"*** IJCSI International Journal of Computer Science Issues, Vol. 8, Issue 3, No. 2, May 2011.

[142] Ziomek L. J. "***Underwater Acoustics. A Linear Systems Theory Approach"*** Academic Press, Inc, ISBN 0-12-781720-4, 1985.

[143] Ziomek L. J. "***Ray Acoustics."*** In Fundamentals of acoustic field theory and space-time signal processing Florida, USA: CRC Press, Inc, 1995.

[144] Zvonar Z., Brady D., and Catipovic J., ***"An adaptive multiuser receiver for deep water acoustic local area networks,"*** in *Proc. ICAASP'94,* Adelaide, Australia, pp. I1.389-I1.392. , Apr. 1994.

Note: Every reasonable effort has been made to acknowledge the owners of the copyright material. I would be pleased to hear from any copyright owner who has been omitted or incorrectly acknowledged.

A.2 Referenced Internet Links

[145] BENTHOS product information:

http://www.teledynemarine.com/benthos#

[146] L3:

https://www.l3t.com/

[147] L3 Oceania:

http://www2.l3t.com/oceania/

[148] L3 Oceania GPM300:
http://www2.l3t.com/oceania/products/uc_modem.htm
[149] L3 Oceania High Precision Timing Reference:
http://www2.l3t.com/oceania/products/uc_hptr.htm
[150] L3 Oceania AUSSNET:
http://www2.l3t.com/oceania/products/maritime_aussnet.htm
[151] LINQUEST Product information:
http://www.link-quest.com/html/models1.htm
[152] ELAC UT3000 Underwater telephone:
https://www.wartsila.com/products/marine-oil-gas/sonars-naval-acoustics
[153] EVOLOGICS product information:
https://www.evologics.de/en/products/index.html
[154] Deep Sea Challenger:
http://www.deepseachallenge.com/
[155] OSI Model:
https://www.iso.org/ics/35.100.01/x/
[156] Microsemi chip scale caesium atomic clock:
https://www.microsemi.com/product-directory/clocks-frequency-references/3824-chip-scale-atomic-clock-csac
[157] NMEA standards:
https://www.nmea.org/
[158] NATO STANAG:
http://www.nato.int/cps/en/natohq/topics_69269.htm
[159] Reed Solomon:
https://math.berkeley.edu/~mhaiman/math55/reed-solomon.pdf
[160] CRC:
http://www.erg.abdn.ac.uk/users/gorry/course/dl-pages/crc.html
[161] Low frequency source for very long-range communication:
ftp://dns.soest.hawaii.edu/bhowe/outgoing/IEEEOES_2013/papers/130517-010.pdf
[162] Texas Instrument Class D L-C Filter design:
http://www.ti.com/lit/an/sloa119b/sloa119b.pdf
[163] NAUTRONIX (Aberdeen) PROSERV NASNet™:
http://www.proserv.com/related-services/nasnet/
[164] TRITON submarines:
http://tritonsubs.com

Appendix B Baltic *SS4-6* Multipath Deconvolution Measurements

B.1 Introduction

Multiple Baltic (Germany) sea trials have been conducted to select a hydro-acoustic communication protocol suitable for underwater identification. The ELAC UT3000 underwater telephone, configured for MASQ, was trialled with competing systems. The Baltic sea trial database was mined for failing signals which was used to test MR improvements of the MCDSSS receiver multipath tracking non-linear control system.

B.2 MCDSSS Ambient Noise Floor Deterioration Tolerance

Reception of a hydro-acoustic signal may be subject to the deterioration of hydro-acoustic ambient noise floor which degrades the reliability of the communication link (Figure 139). Hydro-acoustic noise floor fluctuations may be due to deteriorating weather, bioacoustics noise or boat traffic. The MCDSSS receiver non-linear control system was redesigned to lock onto a noisy MCDSSS signal and maintain tracking when the signal drops below the detection threshold (Chapter 5.7.1).

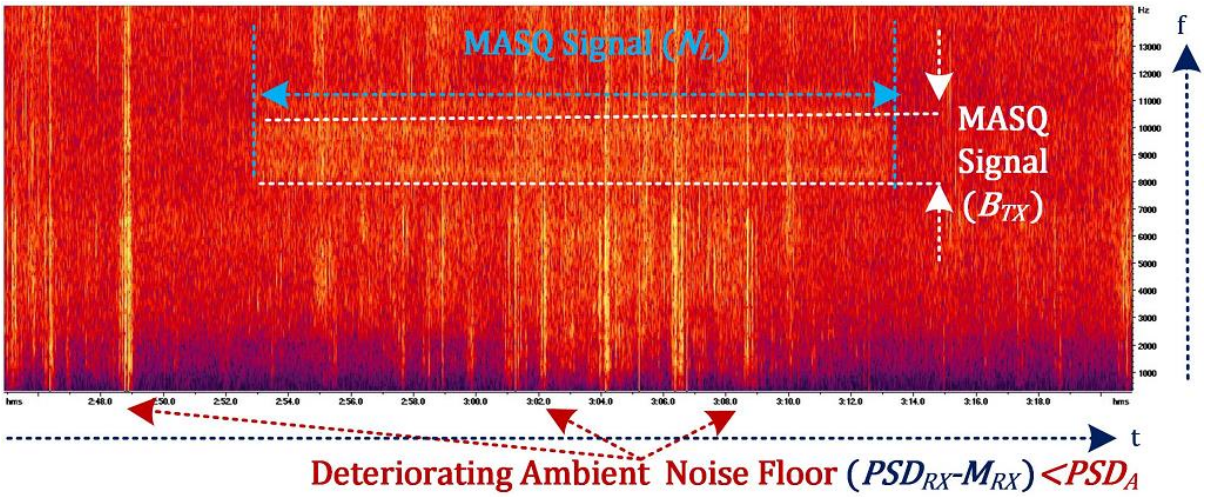

Figure 139 BALTIC hydro-acoustic channel noise floor deterioration (spectrogram)

B.3 Summary

The BALTIC multipath reverberation envelope period was measured at greater than $\tau_{MPE} > 8$ ms and at worst case, the number of multipath signals was greater than $N_M > 10$ (Figure 140). Although the BALTIC selection trials experienced MCDSSS receiver message reliability (MR) issues for a small number of signals the MASQ communication protocol has subsequently been selected as the preferred communication protocol over competing systems. A variant of MASQ has been ratified as a European private communication standard.

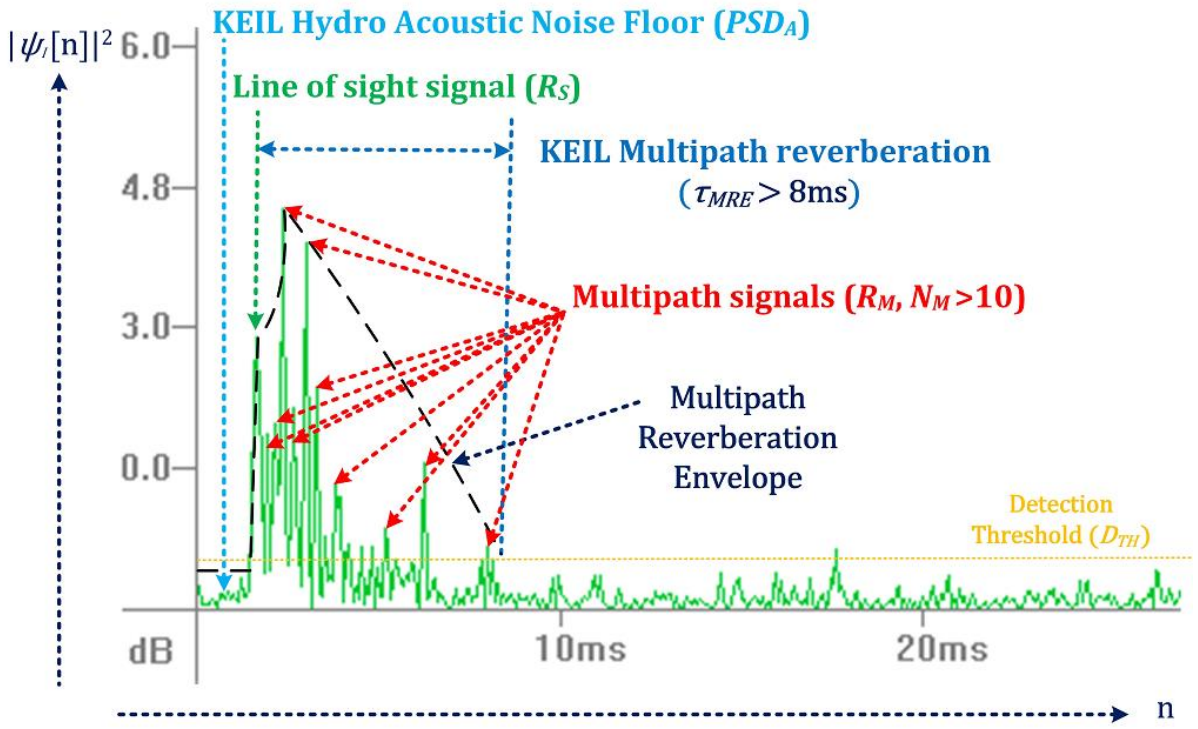

Figure 140 BALTIC multipath reverberation (worst case)

B.3.1 Post-Processed BALTIC Sea Trials Hydro-acoustic Recordings

Chapter 6.2 Figure 118 illustrates the measured improvement in message reliability (MR) versus GPM300 firmware version following the MCDSSS telemetry control system optimisation (Chapter 5.7.3). Message reliability increased from 72% to 100% with the deployment of the multipath deconvolution algorithm.

Chapter 6.6 Figure 131 illustrates the bit error rate as a function MCDSSS hydro-acoustic baud rate and GPM300 firmware version. The multipath deconvolution algorithm improvements (Chapter 5.7.3.3) increased the BER by approximately one order of magnitude for 50 baud and 500 baud but not for 100 baud.

Appendix C Singapore Straits *SS4* Multipath and Bottom Ducting Measurements

C.1 Introduction

Cabled ocean water quality measurement systems have been used to provide real time acoustic backscatter measurements of the water column turbidity. Remote ocean measurements using an anchored buoy provides an RF link to a terrestrial monitoring system. Long range cabled ocean systems are expensive and in some deployments are not practical because of shipping traffic. Hydro-acoustic communication systems provide an alternative to high cost cabled systems [27] (Figure 141). Many commercial hydro-acoustic modems have been tested in the noisy and shallow waters of Singapore but do not provide reliable communication. The L3 Oceania GPM300 3 dB to 15 dB transmit margin provides reliable long-range communication which can be traded off for reliable short range high ambient noise communication.

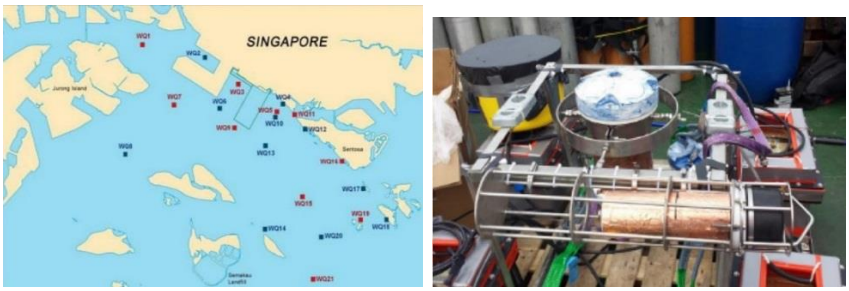

Figure 141 Singapore Strait L3 Oceania GPM300 deployment

C.2 Extreme Multipath Reverberation

Figure 142 illustrates the MCDSSS receiver detection of Singapore shallow water multipath signal which is characterises by a slant range correlation pulse followed by four ($N_M > 4$) multipath signals with τ_{MPE} greater than 10 ms.

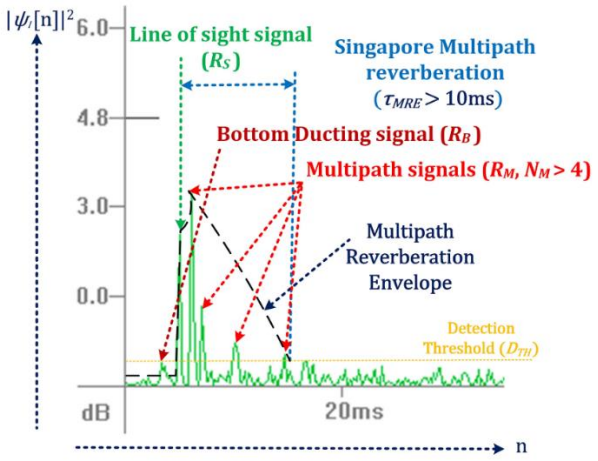

Figure 142 Shallow water multipath (MCDSSS receiver correlator time domain)

C.3 Strong Bottom Ducting

Figure 143 illustrates the MCDSSS receiver correlator waterfall detection plot of the Singapore shallow water multipath signal which is characterised by a slant range

correlation pulse preceded by an intermittent bottom ducting multipath signal. The surface reflections multipath signal magnitudes are occasionally louder than the slant range signal. Even though the Singapore MCDSSS transceivers are statically deployed, the multipath interference changes with time as the water column moves.

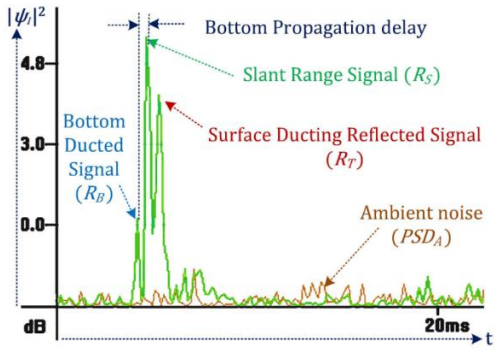

Figure 143 Shallow water multipath (MCDSSS receiver correlator)

C.4 MCDSSS Receiver Multipath Tracking Control System Optimisation

The primary performance requirement was to provide a communication link with a minimum reliability of 90%. The MCDSSS communication protocol provided more than 90% communication reliability except for one deployment which measured a communication reliability of less than 20%. The MCDSSS receiver multipath tracking non-linear control system was optimised to handle the extreme multipath reverberation (Figure 81). Updated GPM300 firmware was remotely uploaded to the GPM300 and the communication reliability increased to greater than 90%.

C.5 Summary

The L3 Oceania GPM300, configured for MCDSSS communication, was successfully deployed around Singapore to provide real time wireless underwater water quality monitoring.

C.5.1 Post-Processed Sea Trials Hydro-acoustic Recordings

The Singapore Striates hydro-acoustic database was mined for failing signals and subsequent analysis identified that the hard ocean bottom induces extreme reverberation in conjunction with loud ambient noise as the interference source. The MCDSSS receiver multipath tracking non-linear control system algorithm (Chapter 5.7.1) was optimised to handle multipath signal ($R_M \geq 4$) and a loud bottom ducting signal ($R_B \leq 1$) that may be louder than the slant range signal (R_S). Chapter 6.2 Figure 119 illustrated the message reliability versus GPM300 firmware version. Message reliability increased from 94% to 100% with the deployment of the impulsive noise wipe-out algorithm (Chapter 5.7.2.3).

Chapter 6.3 Figure 132 illustrates the bit error rate as a function MCDSSS hydro-acoustic baud rate and GPM300 firmware version. The deployment of the multipath deconvolution algorithm degrades the BER by half an order of magnitude and highlights the issue of performance improvements made for Appendix B, BALTIC environment degrades the performance in the Singapore environment.

Appendix D 0.2 m Range *SS4* Air Performance Measurements

D.1 Introduction

The $R_S = 0.2$ m range air communication testing provides a full acoustic baud rates (Br_{MIN} to Br_{MAX}) and full transmit source levels (SPL_{MIN} to SLP_{MAX}) in a controlled environment that simulates:

1. Low $\tau_{MPE} < 2$ ms reverberating multipath communication channel (Figure 144).

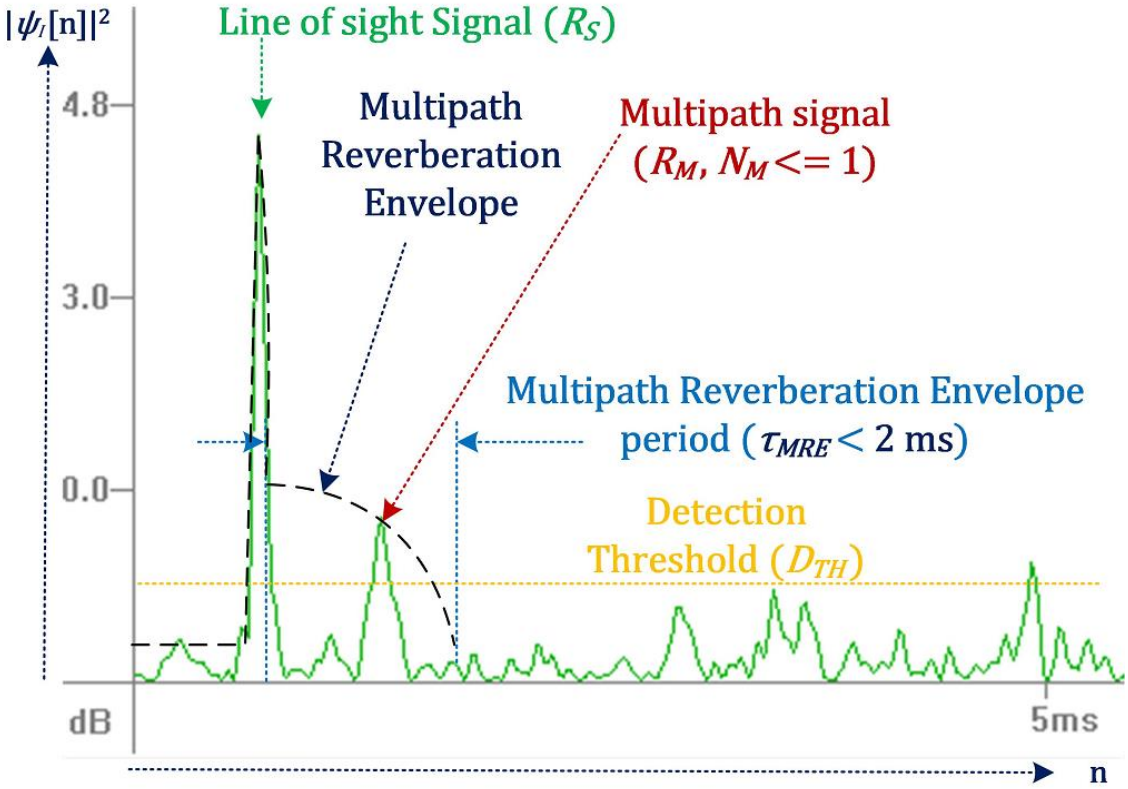

Figure 144 Air 0.2 m range acoustic reverberation envelope < 2 ms

1. The self noise of the transmit GPM300 modem power amplifier is equivalent to shallow water $SS10 < 100$ dB re 1 µPa/$\sqrt{\text{Hz}}$ @ 1 m at the GPM300 receive hydrophone (Figure 146). At a range of 0.2 m the transmitter self noise increases to $SS4 < 164$ dB re 1 µPa/$\sqrt{\text{Hz}}$ @ 0.2 m.
2. Frequency dependent absorption ($L_A = 0$) is insignificant in air at short ranges.
3. Sound velocity induced refraction ($L_R = 0$) is insignificant in air at short ranges.
4. Total path loss (L_T) is dominated by spherical spreading (L_S).
5. PZT to air coupling directivity loss $D_{AIR} = -25\text{ dB} \times 2 = -50$ dB for two modems in the end fire aspect (see Figure 235 blue trace) inducing high path loss.

D.2 0.2 m Range Air Sonar Equation

Figure 145 illustrates the $R_S = 0.2$ m air acoustic baud rate optimisation test sonar equation diagram. An aerated foam cylinder is used to provide low reverberation acoustic

coupling which is required for acoustic baud rates greater than 500 baud. The loudest source of noise was the GPM300 transmitter power amplifier noise floor (PSD_{PA}) which induces the equivalent of $SS4$ at the GPM300 receiver (Chapter 5.6.3).

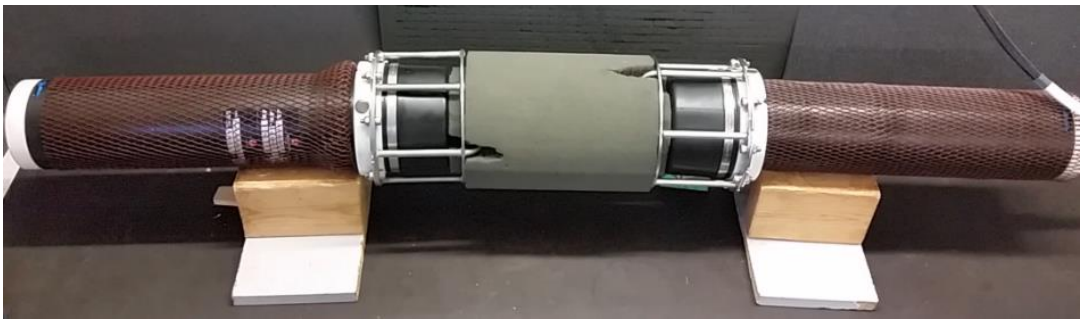

Figure 145 Air 0.2 m range acoustic baud rate optimisation

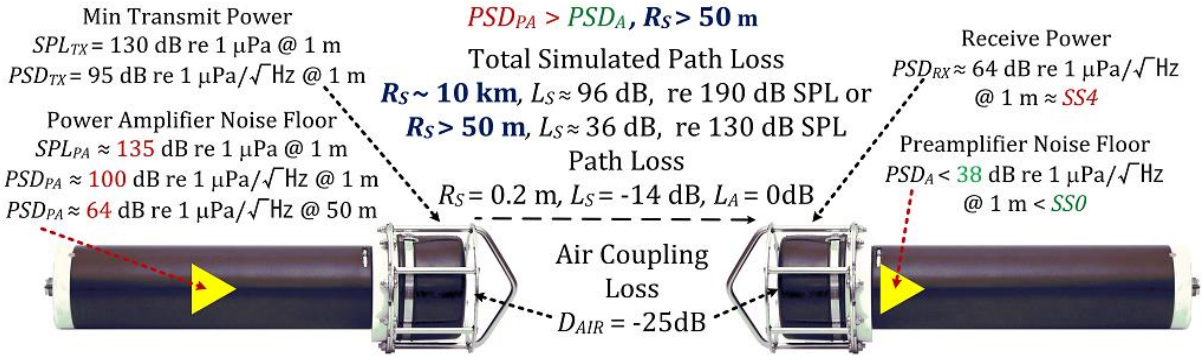

Figure 146 Air 0.2 m range sonar equation diagram

D.3 0.2 m Acoustic Baud Rates Performance Measurement

Figure 116 illustrates the 0.2 m air acoustic baud rate optimisation measurements. Power amplifier noise floor induces $SS12$ noise with a $R_S = 0.2$ m modem separation simulates $L_S = 60$ dB re $SS0$ path loss. Chapter 5 algorithm optimisations were applied to the GPM300 firmware version 6.0 and the performance was compared against firmware versions 5.2 to 5.5:

1. Reliable communication was established from 10 baud to 750 baud hydro-acoustic baud rates using the maximum 190 dB re 1 µPa @ 1 m requiring 300 W transmit power.
2. MCDSSS 1,000 baud to 1,200 baud hydro-acoustic baud rates require 15 dB to 18 dB lower transmit source level to establish a reliable communication link by reducing receiver front end saturation.
3. At maximum transmit source level 190 dB re 1 µPa @ 1 m the air test simulates a $R_S \approx 10$ km $SS4$ hydro-acoustic communication link.
4. Reliable communication was established from 10 baud to 500 baud hydro-acoustic baud rates using less than 140 dB re 1 µPa @ 1 m requiring 1 mW transmit power.
5. At minimum transmit source level 140 dB re 1 µPa @ 1 m the air test simulates a $R_S \approx 50$ m $SS4$ hydro-acoustic communication link.

6. MCDSSS 750 baud to 1,200 baud hydro-acoustic baud rates required 3 dB to 6 dB higher transmit source level and is consistent with the transmit margin reduction induced by the over spreading loss.

D.4 Summary

GPM300 firmware version 6.0 required 3 dB to 15 dB less transmit source level than firmware versions 5.2 to 5.5 to establish a reliable air communication link and demonstrates a measurable improvement in MR.

Figure 147 illustrates the 0.2 m air acoustic baud rate bit energy efficiency. As expected the BEE peaks at highest acoustic baud rate of 750 baud with the highest transmission bandwidth before the over spreading loss for 1,000 and 1,200 baud require an increase in transmit source level.

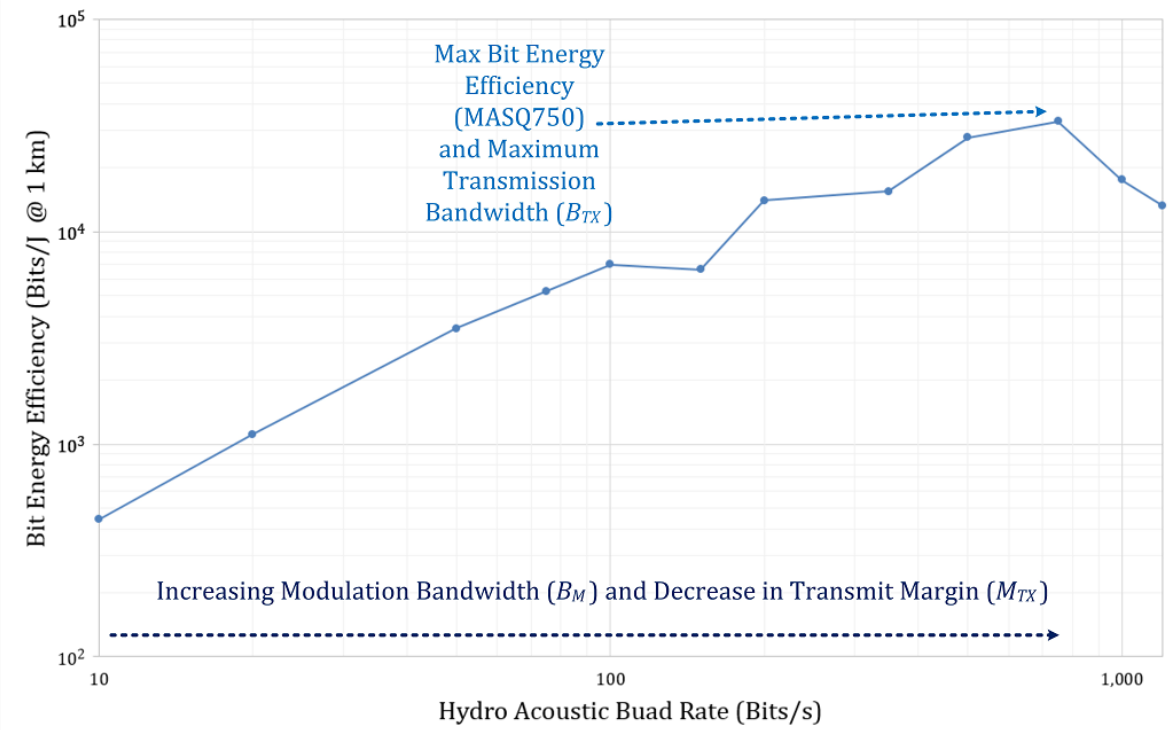

Figure 147 Air bit energy efficiency at 0.2 m range

Appendix E 22 m Range *SS0* Air Performance Measurements

E.1 Introduction

The $R_S = 22$ m range $SS0$ air communication testing provides a high reverberation ($N_M > 8$), low ambient noise and all transmit source levels (SPL_{MIN} to SLP_{MAX}) controlled environment for measuring receiver noise floor performance and range accuracy (ΔR_S). The air communication test is used to validate the GMP300 firmware version 6.0.

E.2 22 m Test Configuration

Figure 148 illustrates the air testing transpond range configuration. Distance between the front face of the acoustic modems was mechanically measured at $R_S = 21.47$ m (i.e. the transpond range test assumes that the acoustic centre of the modem PZT transducer is at the front face of the transducer).

Figure 148 Air testing at 21.47 m range configuration

E.3 22 m Air Acoustic Baud Rate Optimisation

Figure 235 illustrates the sonar equation diagram for the 22 m air acoustic baud rate optimisation measurements:

1. PZT to air coupling loss $D_{AIR} = -25$ dB $\times$ 2 $= -50$ dB (Figure 235 blue trace).
2. The ambient noise was dominated by low frequency building machine noise and the GPM300 receiver noise floor (Figure 149). Ambient $SS0$ noise with at $R_S = 21.47$ m $\equiv L_S = 27$ dB modem separation simulates path $L_T = -D_{AIR} + L_S = 50$ dB $+$ 27 dB $=$ 77 dB re $SS0$.

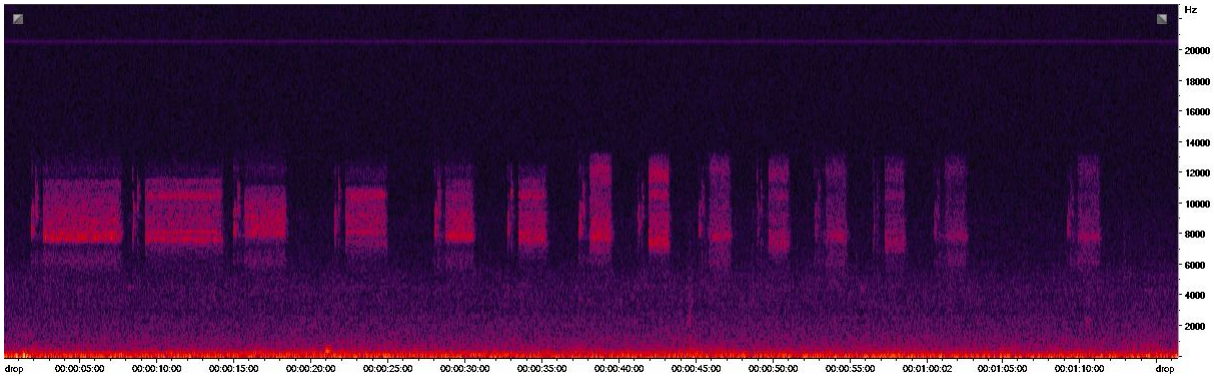

Figure 149 Air 22 m range acoustic baud rate optimisation spectrogram

The total path loss was measured at $L_T = 107$ dB and from Figure 6 the estimated maximum communication range is $R_S = 18$ km → 28 km in $PSD_A = PSD_{SS0}$ in the absence of sound velocity induced refraction ($L_R = 0$ dB) and frequency dependant attenuation ($L_A = 0$ dB).

Figure 150 Air 22 m range testing sonar equation diagram

MCDSSS 10 baud to 500 baud provided a reliable communication. MCDSSS 10 baud and 200 baud provide a covert communication connection.

E.4 Summary

The GPM300 firmware version 6.0 measured a marginal improvement in the minimum transmit source level compared to firmware versions 5.2 to 5.5 except for 500 baud which only establishes a communication link using GPM300 firmware version 6.0. Baud rates higher than 750 baud, with a symbol period of $\tau_{SY} \leq 42$ ms, could not be established for any transmit source level (SPL_{MIN} to SLP_{MAX}), in an environment with a multipath reverberation period of $\tau_{MPE} > 25$ ms (Figure 117).

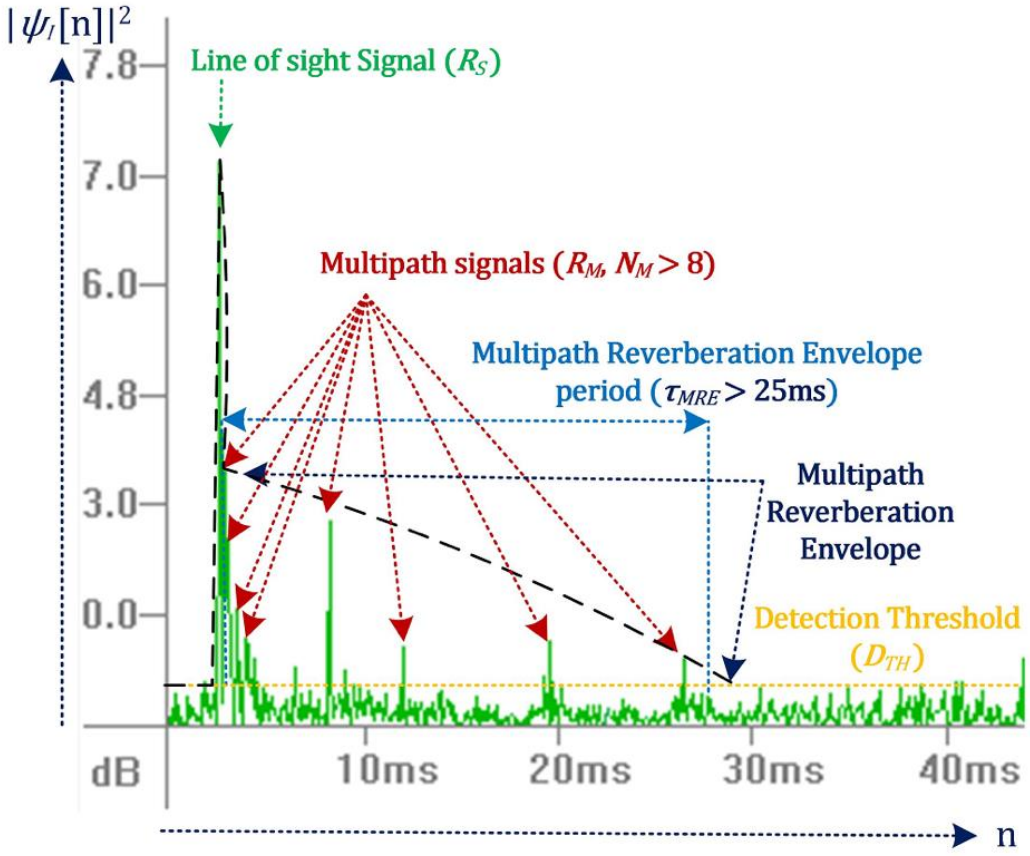

Figure 151 Air 22 m range acoustic reverberation envelope > 25 ms

Figure 152 illustrates the 22 m air acoustic baud rate versus bit energy efficiency. The BEE peaks at the highest acoustic baud rate of 200 baud before a higher transmit source level is required to main a reliable communication link for faster than 500 baud.

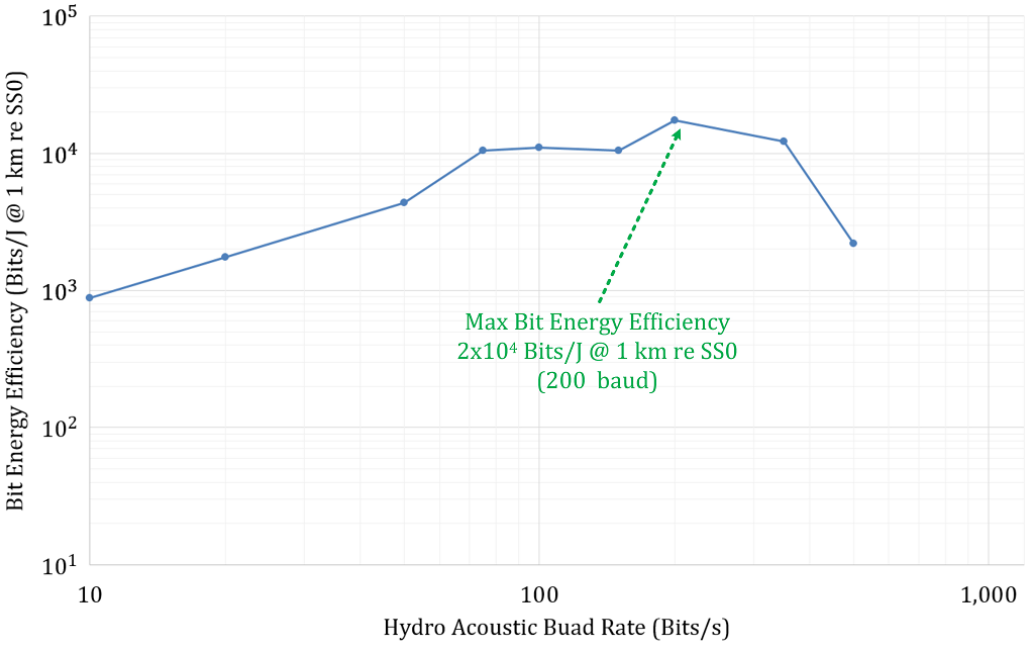

Figure 152 Air 22 m range maximum bit energy efficiency

Appendix F 2 m Range *SS10* Hydro-acoustic Tank Measurements

F.1 Introduction

Sea trials requiring calibrated PSD_A, M_{RX} and R_S measurements are required to provide an estimate of the maximum communication range as a function of SS. Hydro-acoustic tank measurements validate the calibration of MCDSSS receiver absolute ambient power spectral density, tests automatic transmit source level and baud rate optimisation algorithm in an extreme reverberating ($\tau_{MRE} > 250$ ms) inter-symbol interference environment. Measurements of the MCDSSS transceiver absolute slant range accuracy was verified in the absence of sound velocity induced refraction, MCDSSS receiver noise floor and the absence of ocean ambient noise ($PSD_A = 0$ dB).

F.2 L3 Oceania Hydro-acoustic Tank Specifications

The L3 Oceania hydro-acoustic test tank facility (Figure 153 left) specifications are:

1. Sound velocity: $c = 1480$ m/s chlorinated fresh water.
2. Ambient maximum: $PSD_{MAX} \approx 155$ dB re 1 µPa/$\sqrt{\text{Hz}}$ @ 1 m ≡ $SS20$ @ 10 kHz.
3. Ambient minimum: $PSD_A \approx 38$ dB re 1 µPa/$\sqrt{\text{Hz}}$ @ 1 m ≡ $SS0$ @ 10 kHz.
4. Reverberation: $L_S = 4$ dB sidewall and 0 dB surface reflection attenuation.
5. Damping: $\tau_{MRE} \leq 250$ ms ≈ 370 m × c reverberation damping.
6. Depth: $R_D = 4.2$ m.
7. Diameter: 4.5 m.
8. Maximum clear time: $\tau_{SY} \approx 3$ m × $c <$ 2 ms.

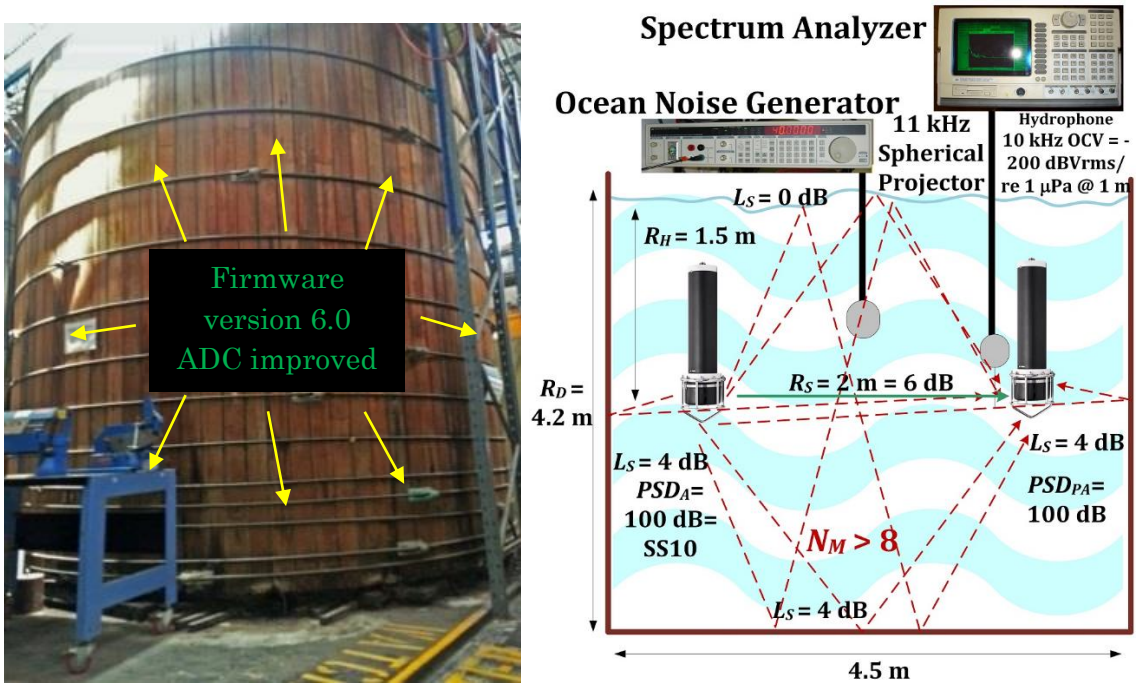

Figure 153 L3 Oceania hydro-acoustic tank sonar equation diagram

F.2.1 Calibration of MCDSSS Receiver Absolute PSD

Figure 153 (right) illustrates a D11 11 kHz 3 kW spherical PZT transducer used to artificially raise the L3 hydro-acoustic tank noise floor. The D11 is suspended in the middle of the tank and the device under test is deployed between the D11 and the tank side walls. A calibrated hydrophone is deployed next to the device being tested to measure the ambient noise.

Figure 154 (right) illustrates the D11 transducer drive voltage versus simulated sea state noise and the L3 hydro-acoustic tank simulated noise as measured by a OCV = −200 dBVrms/µPa @ 1 m hydrophone at $R_S = 1$ m (i.e. $L_T = PSD_A + 200$ dB). Figure 154 (left) illustrates the sinusoidal frequency response artefact induced by the hydro-acoustic tank constructive and destructive interference.

Sea State	PSD	DS360	Wind	Rain	Additional Noise Source
IMO #	dB µPa/Hz√0.5	Vrms	Kn		
0	38	-48	<5		Inshore Biology
1	44	-42	10		
2	50	-36	20		
3	56	-28	30	Light	Shallow Water Biology
4	62	-22	40	Moderate	
5	68	-17	50	Heavy	
6	74	-11	60	Hail	Inboat Motor
7	80	-3			
8	86	3			Outboard motor
9	92	9			
10	98	15			
11	104	21			DP Work Boat
12	110	27			
13	116	33			Loud DP Work Boat

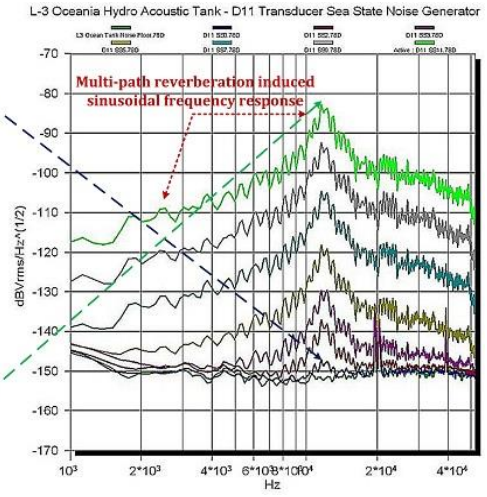

Figure 154 L3 Oceania tank D11 projector sea state noise calibration

Figure 155 illustrates the calibration of GPM300 firmware version 6.0 Through Water Communications (TWC) mail client receive power and *SS* versus time measurement of the L3 hydro-acoustic tank sea state noise generator. The sea state noise generator was stepped from *SS*0 to *SS*10 and back to *SS*0. The GPM300 noise floor was measured at than the L3 Oceania hydro-acoustic tank noise floor ($PSD_N < PSD_{SS0}$).

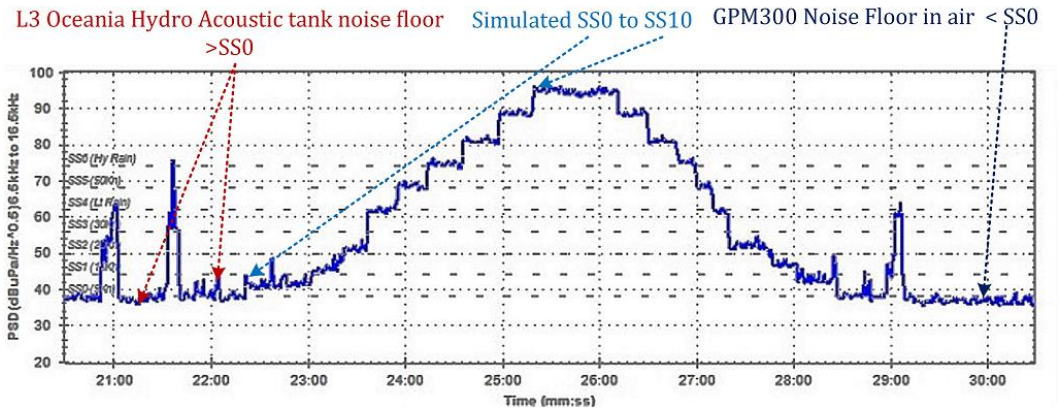

Figure 155 L3 Oceania tank noise generator GPM300 measurement

F.3 2 m Range Hydro-acoustic Tank Deployment

Figure 156 illustrates four GPM300 modems deployed at a depth of $R_H = 1.5$ m in the L3 Oceania hydro-acoustic tank with $R_S = 2.3$ m and $R_S = 0.8$ m base lines.

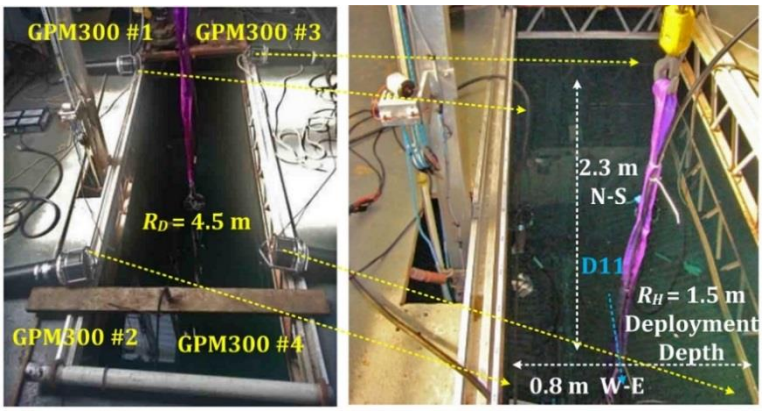

Figure 156 Four by GPM300 modems deployed in L3 Oceania tank

F.3.1 Narrow-band Multipath Reverberation

Figure 157 illustrates an 11 kHz, 200 cycle ping, as measured in the L3 Oceania hydro-acoustic tank with a clear time of approximately 2 ms (i.e. spherical spreading path loss for the first 2 ms of the flight time). Tank reverberation amplifies acoustic signals by 5 dB to 10 dB and the path loss approximates cylindrical spreading [12] [13] Eq.(2-14). Propagating MCDSSS $\tau_S = 32$ ms → 800 ms symbol period signals in a 2 ms clear time hydro-acoustic tank are subject to extreme inter-symbol interference. The number of narrow-band multipath (N_M) signals can be estimated using the increase in SPL_{RX} Eq.(7-1).

$$N_{R_M} \approx 3 \rightarrow 5$$

$$L_M \approx 10\log_{10}\left(N_{R_M}\right) \approx 5 \text{ dB} \rightarrow 10 \text{ dB} \qquad (7\text{-}1)$$

$$SPL_{RX} \approx SPL_{TX} + L_M$$

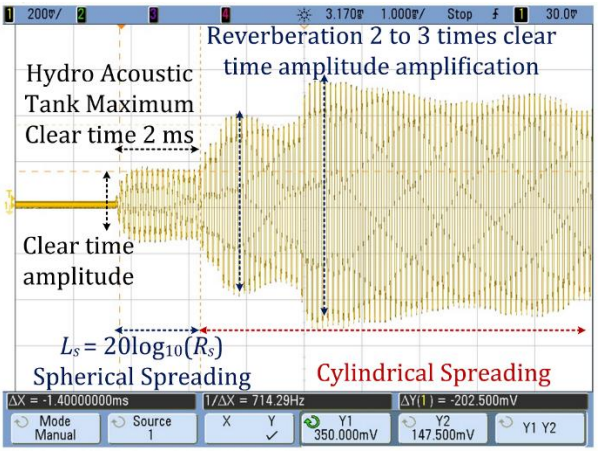

Figure 157 L3 Oceania hydro-acoustic tank clear time

F.3.2 Broad-band Multipath Reverberation

Figure 158 illustrates the MCDSSS receiver waterfall correlation plot of two 350 baud messages measured in the L3 Oceania hydro-acoustic tank and highlights the extreme reverberating environment ($N_M > 8$).

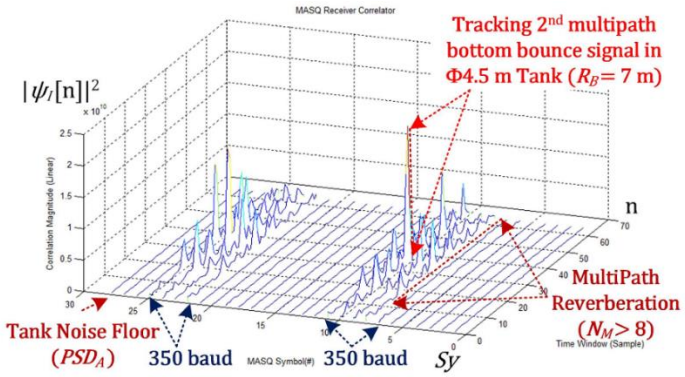

Figure 158 L3 Oceania hydro-acoustic tank MCDSSS receiver waterfall

Figure 159 illustrates the MCDSSS receiver correlation of a 350 baud signal reverberation in the L3 Oceania hydro-acoustic tank as measured by GPM300Windows (Figure 60). The MCDSSS receiver does not track the slant range signal but locks onto the second multipath signal $\tau_{MRE} = 5$ ms, which is $R_M = \tau_{MRE} \times c = 7.4$ m and is twice the distance of the GPM300 to the bottom of the tank. In extreme multipath and inter symbol interference the MCDSSS receiver tracks the hydro-acoustic tank bottom bounce multipath signal in preference to louder slant range or surface reflected signal.

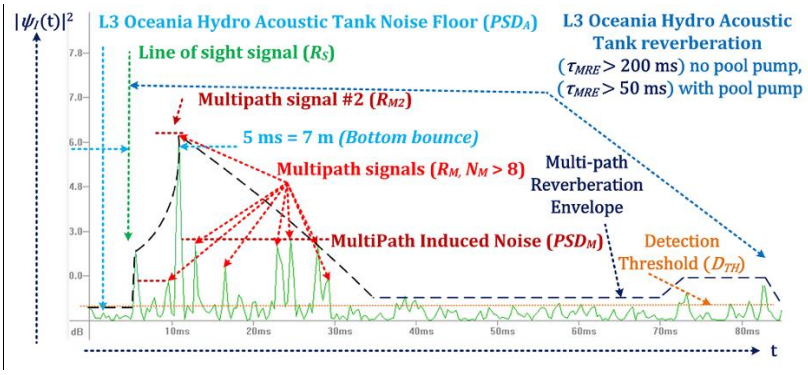

Figure 159 L3 Oceania hydro-acoustic tank MCDSSS receiver correlation

The number of multipath signals (N_M) is approximately 8 which reduces the 14 dB transmit margin (M_{TX}) by 9 dB resulting in a 5 dB receive margin (M_{RX}) Eq.(7-2). The MCDSSS receiver successfully decodes the signal even though the receive margin Figure 159 drops to 0 dB because the MCDSSS telemetry multipath tracking Eq.(5-44) provides up to $G_M = 0$ dB →5 dB additional processing gain.

$$N_M = 6 \rightarrow 10 \approx 8, \qquad M_{TX} = 14 \text{ dB}$$

$$L_M = 10\log_{10}(N_M) \approx 9 \text{ dB} \tag{7-2}$$

$M_{RX} = M_{TX} + G_M - L_M \approx 5 \rightarrow 10$ dB (for 50 baud in the L3 hydro-acoustic tank)

F.4 Summary

MCDSSS receiver absolute ambient power spectral density calibration was validated within the 3 dB accuracy of the L3 Oceania hydro-acoustic tank SPL measurement. The GPM300 MCDSSS receiver noise floor was measured at less than shallow water $SS0$. The loudest source of ambient noise was the GPM300 power amplifier which generated $SS9 \equiv PSD_A = 90$ dB re 1 µPa/$\sqrt{\text{Hz}}$ @ 1 m noise at $R_S = 2$ m $\equiv L_S = 6$ dB modem separation and simulated $L_T = 90$ dB + 6 dB = 96 dB re $SS0$. Semi-automatic transmit source level (SPL_{TX}) and baud rate (Br) optimisation algorithm functioned reliably in an extreme reverberating and inter-symbol interference hydro-acoustic environment ($N_M > 8$). With the pool pump not operating the GPM300 firmware version 6.0 measured approximately 5 dB improvement in transmit source level compared to firmware version 5.2 to firmware version 5.5 (Chapter 6.4 Figure 125 . Hydro-acoustic communication faster than 350 baud rates, with a symbol period of $\tau_{SY} \leq 90$ ms, could not be established for any transmit source level (SPL_{MIN} to SLP_{MAX}) in an environment with a multipath reverberation period of $\tau_{MPE} > 100$ ms Figure 159.

With the pool pump operating the GPM300 firmware version 6.0 measured less than 5 dB improvement in transmit source level compared to firmware version 5.2 to firmware version 5.5 (Figure 125 . Hydro-acoustic baud rates higher than 750 baud, with a symbol period of $\tau_{SY} \leq 32$ ms, could not be established in an environment with a multipath reverberation period of $\tau_{MPE} > 100$ ms Figure 159. Although the pool pump increased the ambient noise, a slightly lower transmit source level was required compared to the pool pump not running with a smooth reflecting surface, which highlights multipath induced performance degradation.

Figure 160 illustrates the $R_S = 2$ m hydro-acoustic tank baud rate bit energy efficiency (BEE). The BEE peaked 10^4 at highest acoustic baud rate of 200 baud before the higher transmit source level was required to maintain a reliable communication link for faster hydro-acoustic baud rates. The maximum 200 baud BEE did not change with change of ambient noise (i.e. with or without the pool pump operating).

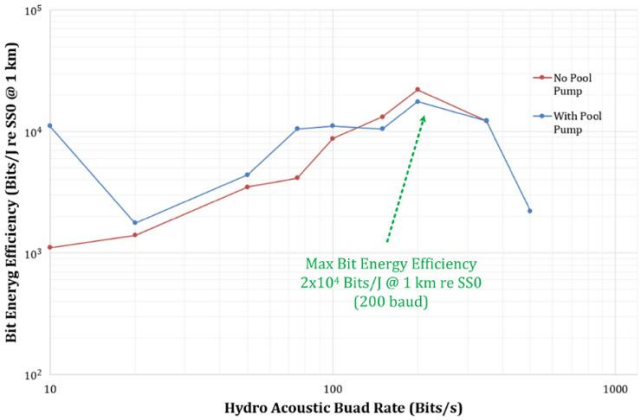

Figure 160 Hydro-acoustic tank 2 m range maximum bit energy efficiency

Appendix G 411/415 m Range *SS2* 3.5 m Depth BEE Measurements

G.1 Introduction

Fremantle harbour provides a fixed range controlled hydro-acoustic stress test environment with $SS0$ to $SS4$ inshore snapping shrimp noise, hard concrete reflecting surfaces, loud fish finder sonar, loud boat traffic, reverberating and multipath channel. The Fremantle Harbour $R_S = 411$ m trial validates the GPM300 firmware version 5.3 automatic transmit source level and acoustic baud rate optimisation network routing algorithm. Voice and digital communication transmit source level difference was measured. Transpond range measurement and network routing transpond measurement was verified. The Fremantle Harbour 415 m trial measured the MCDSSS bit energy efficiency (BEE) to quantify the improvement in performance of GPM300 firmware version 6.0.

G.2 Modem Deployments

The two south-south-west modems (ID #4 and #5) were deployed off a hard concrete stand and were laterally separated by 5.8 m (Figure 161). The southern modem was deployed at a depth of $R_H = 1.8$ m in $R_D = 3.8$ m depth water column. The modem was located 0.1 m from a steel reinforced wall.

The two north-east modems (ID #7 and #8) were deployed off a wooden jetty 2 m from a rock wall and were laterally separated by approximately 5 m. The northern modem #7 was deployed at a depth of $R_H = 2.5$ m in $R_D = 5.2$ m depth water column. The modem was located 4 m from a rock wall. Circular wooden pylons ware located 0.5 m either side of the modem. The modem was cabled to a laptop and a voice interface unit.

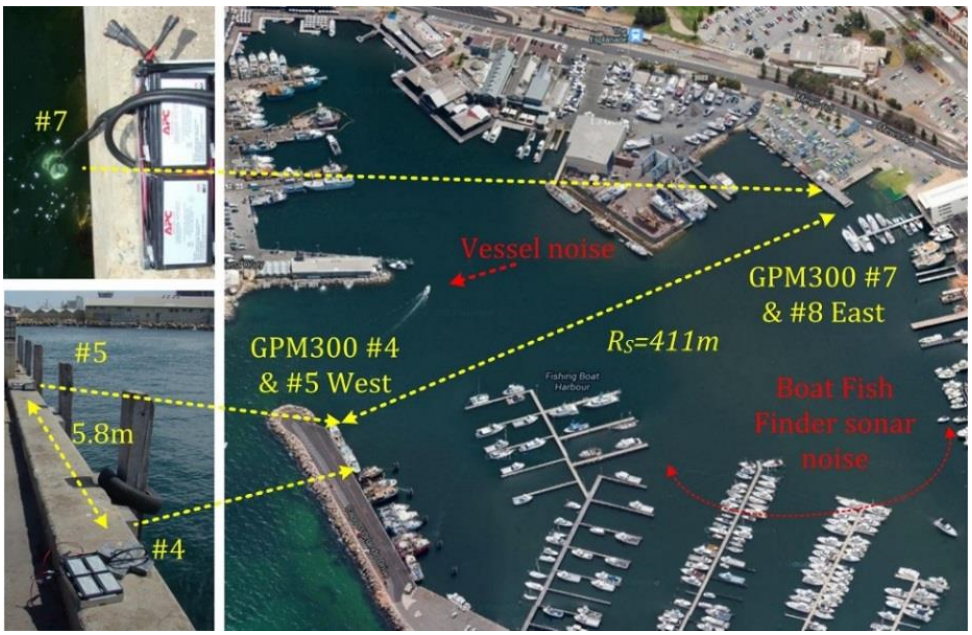

Figure 161 Fremantle fishing boat harbour (411 m hydro-acoustic channel)

G.3 Hydro-acoustic Channel Environment

The short communication channel is not subject to frequency dependent signal absorption ($L_A \rightarrow 0$ dB) which requires at least $R_S > 5$ km before attenuating high acoustic baud rates (i.e. lower acoustic baud rates with lower carrier frequencies do not improve communication reliability by reducing high frequency signal absorption). The relatively shallow water is not subject to sound velocity induced refraction signal attenuation ($L_R \rightarrow 0$ dB).

Fremantle harbour hydro-acoustic channel characteristics are as follows:

1. Channel Length $R_S = 411$ m from NEE to WSS pre eastern jetty demolition and $R_S = 415$ m from NEE to WSS post eastern jetty demolition.
2. Depth $R_D =$ 3.8 m to 5.2 m. Less than 10 m at deepest point. Shallow water and hard concrete structures generated reverberating multipath receptions.
3. Inboard motor boat traffic noise measured at $PSD_A \approx 70$ dB to 75 dB re 1 µPa/$\sqrt{\text{Hz}}$ @ 1 m $\cong PSD_{SS6}$ (equivalent to heavy rain).
4. Outboard motor boat traffic noise measured at $PSD_A >$ 75 dB re 1 µPa/$\sqrt{\text{Hz}}$ @ 1 m $> PSD_{SS6}$ which is louder than heavy rain.
5. The ambient noise was dominated by snapping shrimp and comparable to snapping shrimp noise levels in shallow (up to $R_D \approx 50$ m) warm temperate waters. $PSD_A \approx 55$ dB to 65 dB re 1 µPa/$\sqrt{\text{Hz}}$ @ 1 m $\cong PSD_{SS3} \rightarrow PSD_{SS4}$ and loud 10 kHz to 45 kHz depth sounder and fish finder sonar (Figure 162).

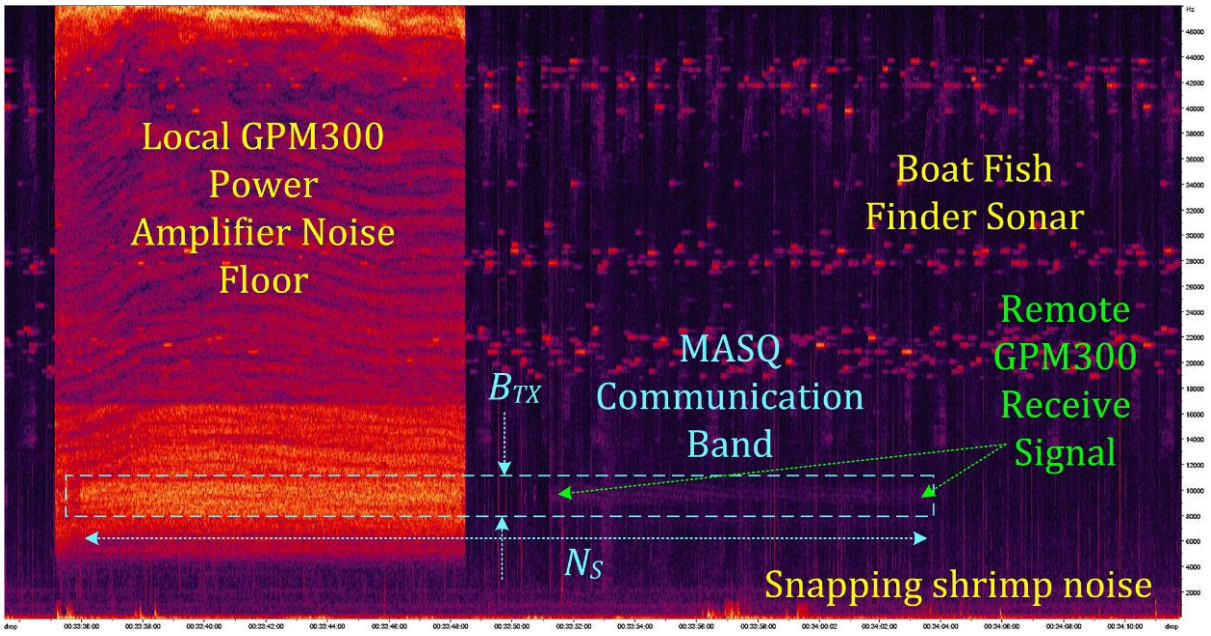

Figure 162 Fremantle fishing boat harbour (L3 Oceania PASOR Spectrogram)

G.4 Harbour Measurements

G.4.1 411 m Range Acoustic Baud Rate Optimisation

A minimum transmit signal power of ($PSD_{TX} =$ 113 dB re 1 µPa/$\sqrt{\text{Hz}}$ @ 1 m) was required in order to arrive at the receiver with < 3 dB receive margin (M_{RX}) Eq.(7-3).

$$A_{TX} = 39 \text{ dB} \equiv SPL_{TX} = 151 \text{ dB re 1 µPa @ 1 m}$$

$$PSD_{TX} = 113 \text{ dB re 1 µPa}/\sqrt{\text{Hz}} \text{ @ 1 m}$$

$$PSD_A = 60 \text{ dB} \pm 2 \text{ dB re 1 µPa µPa}/\sqrt{\text{Hz}} \text{ @ 1 m} \equiv SS4 \quad (7\text{-}3)$$

$$L_T \approx L_S = 20 \log_{10}(411 \text{ m}) = 52 \text{ dB}$$

$$PSD_{MIN} = PSD_A + L_T = 113 \text{ dB re 1 µPa}/\sqrt{\text{Hz}} \text{ @ 1 m}$$

Figure 163 illustrates the predicted $A_{TX} = 39$ dB transmit source level attenuation for $SS3 \rightarrow SS4$, $R_S = 411$ m at $Br = 750$ baud which is within 3 dB of the numerical model.

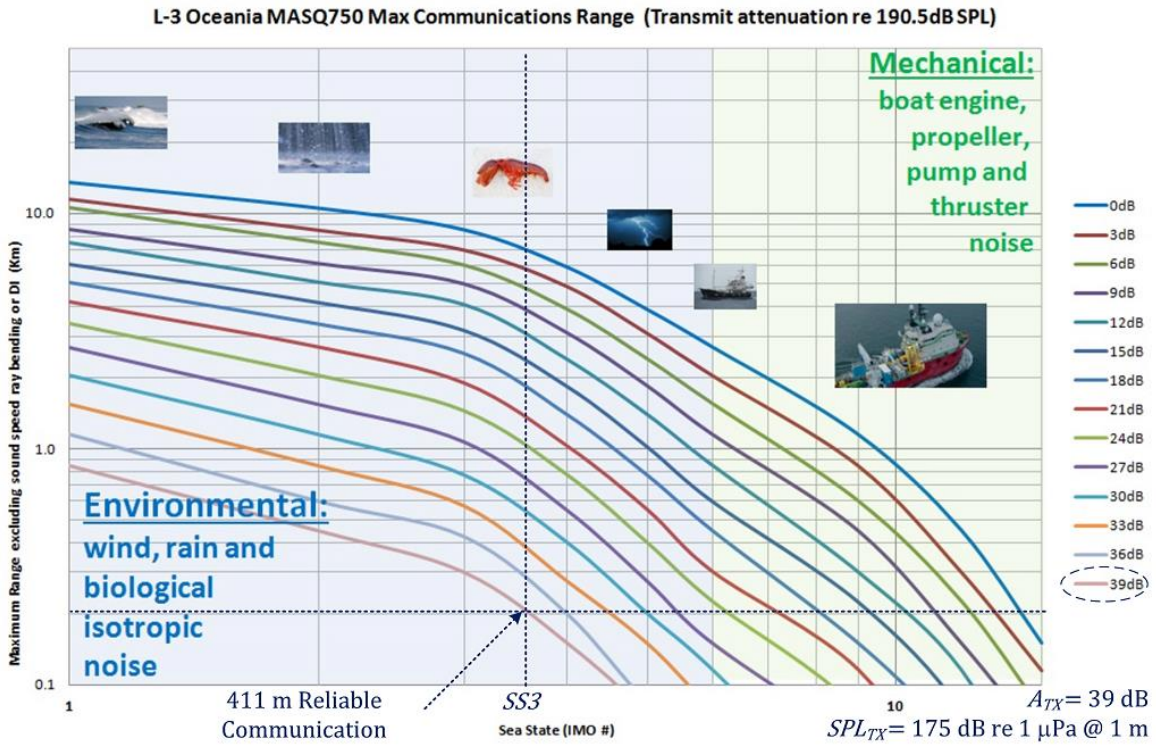

Figure 163 MCDSSS 750 baud versus sea state and attenuation (411 m harbour)

G.4.2 415 m Range Acoustic Baud Rate Optimisation

The firmware version 6.0 acoustic baud rate optimisation algorithm was tested using the GPM300 baud rate optimisation function. The GPM300 configuration tool was used to optimise the transmit source level and baud rate for the hydro-acoustic channel. Figure 163 illustrates the transmit source level attenuation at which each acoustic baud rate could achieve reliable communication and the optimised minimum transmit source level SPL_{MIN} for maximum acoustic baud rate ($Br = 1{,}000$ baud) and minimum transmit source level ($SPL_{TX} = 153$ dB re 1 µPa @ 1 m):

1. MCDSSS 1,000 baud harbour communication was established which was not possible in an 22 m air test or a 4.5 m hydro-acoustic tank.
2. As with hydro-acoustic tank and air testing, the fastest harbour acoustic baud rates required higher transmit source level to overcome multipath and high ambient noise.

3. Harbour communication was established at all acoustic baud rates, except 1,200 baud, which requires a non-reverberating environment for reliable communication.

G.5 Summary

G.5.1 Voice Communication

Measurements validate that narrow-band voice communication requires at least 10 dB higher transmit source level, compared to broad-band digital communication, to establish a legible communication link. Voice communication required 10 dB → 20 dB higher transmit source level ($SPL_{TX} = 170$ dB → 180 dB re 1 µPa @ 1 m) than 750 baud ($SPL_{TX} =$ 160 dB re 1 µPa @ 1 m).

G.5.2 Transpond Range

The 1 m absolute and 0.25 m relative range accuracy performance specification was met. Point to point transpond measured $R_S = 411$ m $\pm$ 1 m with 0.25 m RMS measure repeatability error and network routing transpond measured at $R_S = 412$ m $\pm$ 1 m.

G.5.3 Hydro-acoustic Baud Rate Minimum Transmit Source Level

The GPM300 firmware version 6.0 required 10 dB less transmit source level than firmware version 5.3 to establish a reliable air communication link and demonetarise a measurable improvement in MR (Figure 127 green). Firmware version 5.3 transmit source level ±5 dB measurement noise was reduced to ±1 dB for firmware version 6.0. Maximum transmit $SPL_{TX} = 190$ dB re 1 µPa @ 1 m, for 1,000 baud, required 2 dB attenuation in order to reduce multipath reverberation sufficiently to establish a reliable communication link.

G.5.4 Bit Energy Efficiency Versus Hydro-acoustic Baud Rate

Chapter 6.6 Figure 147 415 m Fremantle harbour identified a significant non-linear relationship between bit energy efficiency and hydro-acoustic baud rate. Bit energy efficiency peaks at highest acoustic baud rate of 100 baud before the over spreading loss requires an increase in transmit source level.

G.5.5 Multipath Reverberation Envelope Versus Hydro-acoustic Baud Rate

Figure 164 illustrates the Fremantle harbour multipath reverberation period of $\tau_{MPE} >$ 5 ms with the worst case number of multipath signals greater than 7.

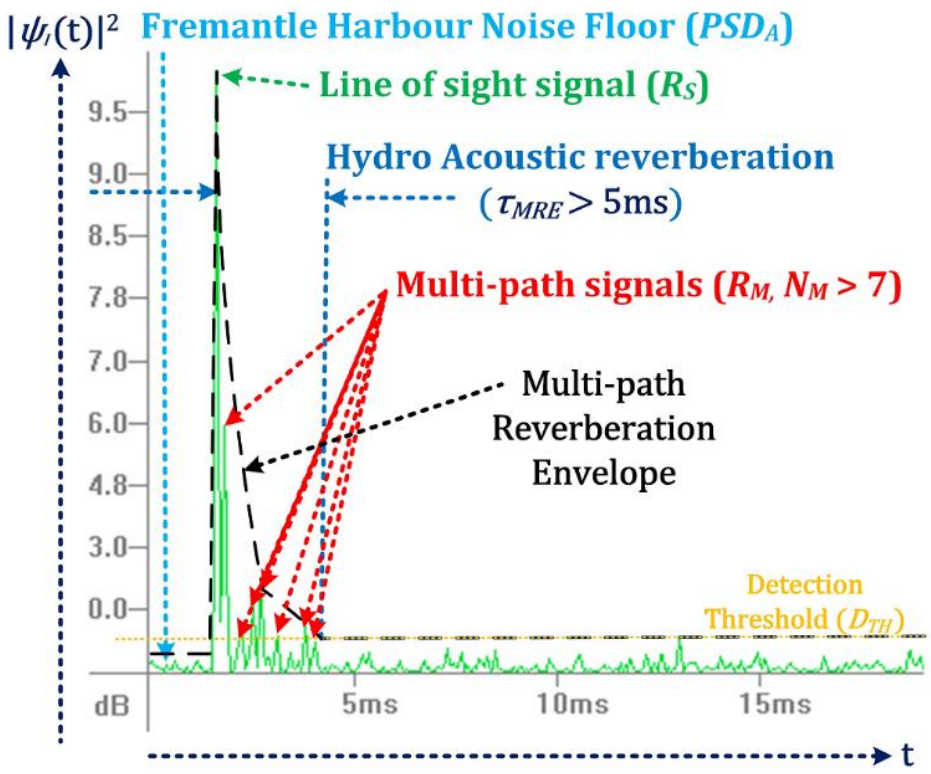

Figure 164 Fremantle Harbour multipath reverberation envelope (worst case)

Figure 165 illustrates a 750 baud message multipath envelope which is dominated by a slant range signal (R_S), very weak bottom ducting signal ($N_B \lesssim 1$), surface reflection(R_{M1}), bottom bounce (R_{M2}), and top/bottom bounce signal (R_{M3}).

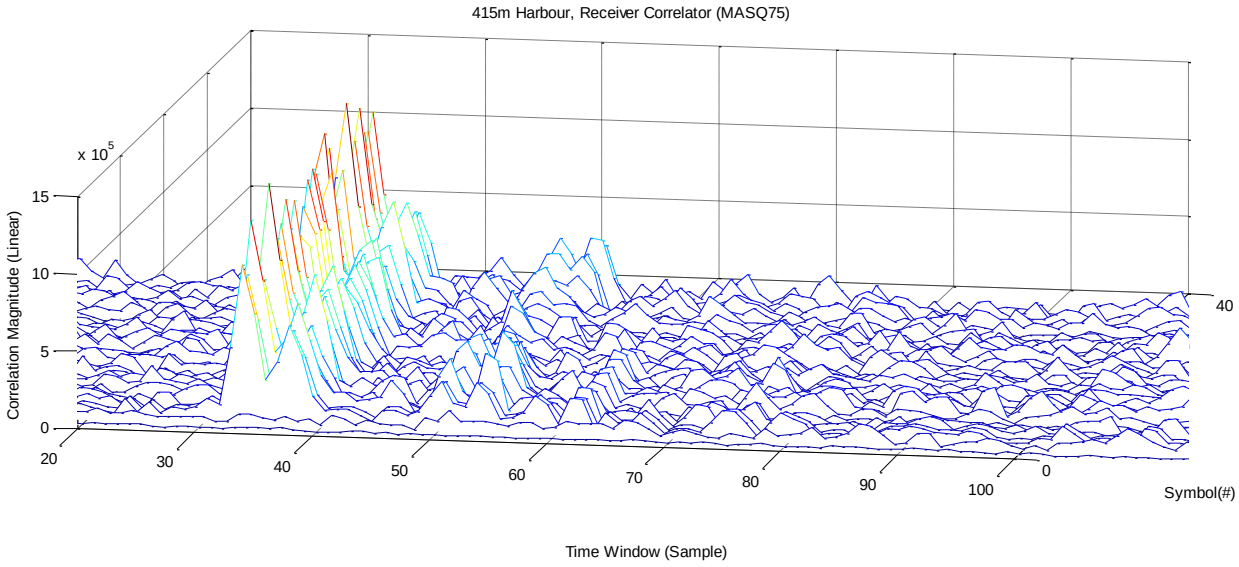

Figure 165 Fremantle Harbour 415 m receiver correlation (750 baud)

Figure 166 illustrates the multipath envelope for 50 baud with two strong $\tau_M >$ 5 ms multipath signals ($N_M \approx 2$).

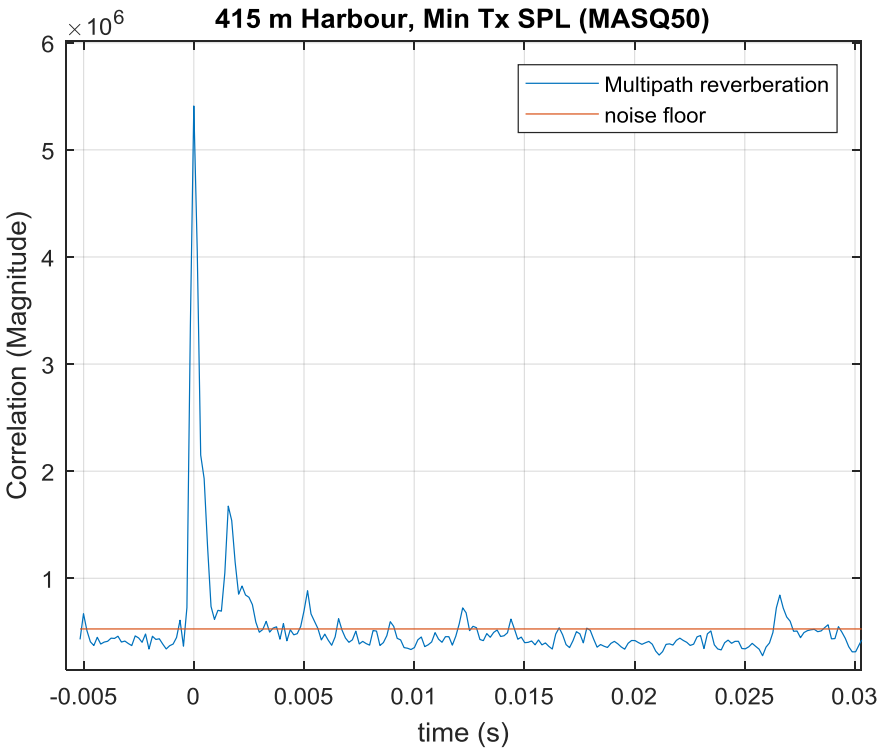

Figure 166 Fremantle Harbour 415 m multipath reverberation envelope (50 baud)

Figure 167 illustrates the multipath envelope for 100 baud with very week $\tau_M < 3$ ms multipath signals ($N_M \lesssim 2$).

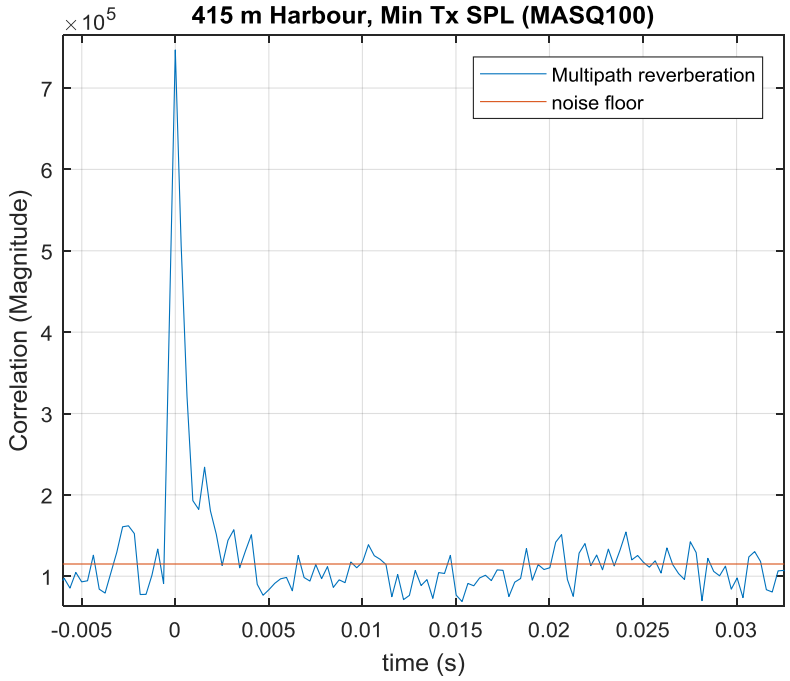

Figure 167 Fremantle Harbour 415 m multipath reverberation envelope (100 baud)

Figure 168 illustrates the multipath envelope for 200 baud with very strong $\tau_M > 7$ ms multipath signal followed by multiple weak $\tau_M > 20$ ms multipath signals ($N_M > 7$).

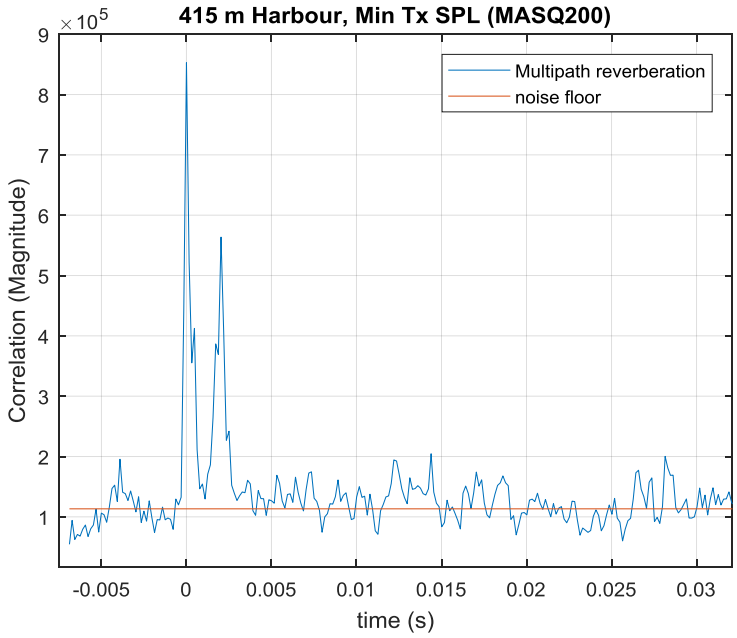

Figure 168 Fremantle Harbour 415 m multipath reverberation envelope (200 baud)

Figure 169 illustrates the Fremantle harbour multipath reverberation envelope (τ_{MRE}) versus MCDSSS hydro-acoustic baud rate. Maximum BEE_{PEAK} occurs when the reliable communication is established using the highest hydro-acoustic baud rate of (Br_{BEE} = 100 baud with the lowest transmit source level SPL_{MIN} = 130 dB re 1 µPa @ 1 m) where the multipath signals are quiet enough to be masked by the ambient noise ($PSD_M < PSD_A \approx PSD_{SS1}$).

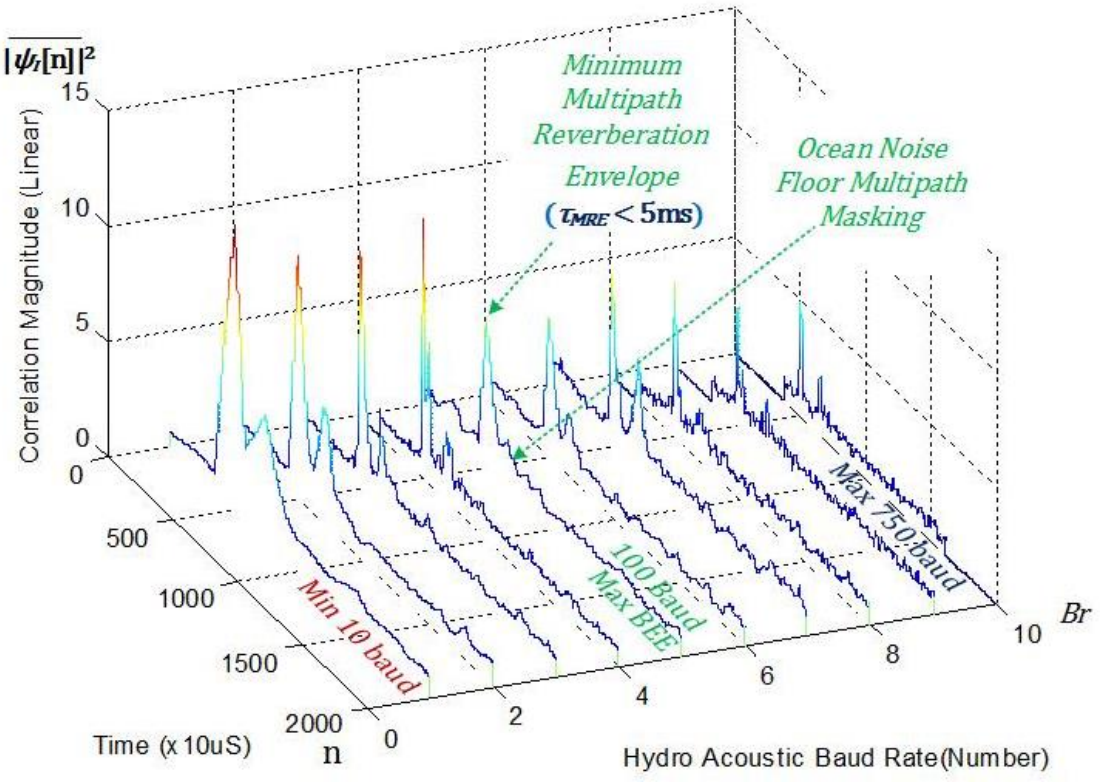

Figure 169 Fremantle Harbour 415 m minimum bit energy efficiency

Appendix H 6.2 km Range *SS2* 4-20 m Depth Measurements

H.1 Introduction

This chapter reprocesses historical GPM300 firmware version 5.5 sea trial data to provide a base line measurement of bit energy efficiency for GPM300 firmware version 6.0. Communication tests were carried out between the Magnetics Wharf and Kwinana Beach jetty (Figure 170). The $R_S = 6.2$ km W to E channel provided a high path loss, noisy, shallow water $R_D < 20$ m depth, reverberating and multipath test environment. The relatively shallow water is not subject to sound velocity induced refraction signal attenuation ($L_R \rightarrow 0$ dB). The ambient noise was dominated by snapping shrimp and was measured at $PSD_A = 60$ dB $\rightarrow$ 70 dB re 1 µPa/$\sqrt{\text{Hz}}$ @ 1 m $\equiv SS4 \rightarrow SS6$.

H.2 Modem Deployments

The north-west modem ID #4 was deployed at a depth of less than $R_H < 1$ m in $R_D = 10$ m depth water column (Figure 170).

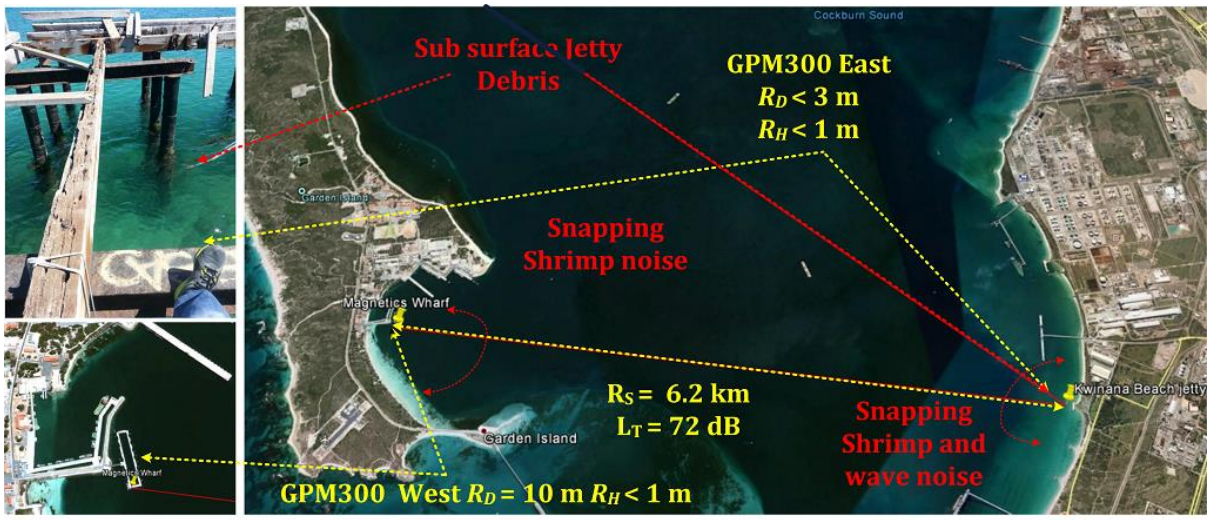

Figure 170 Garden Island magnetics wharf to kwinana beach jetty

The modem was located 0.5 m from an air filled pontoon. The modem was powered from a 48 V lead acid battery allowing full power transmission ($SPL_{MAX} = 190$ dB re 1 µPa @ 1 m). The east modem (ID #5) was deployed off the Kwinana Beach wooden jetty 1 m from metal pylons. Initial link tests between Kwinana Beach and the Magnetics Wharf failed to provide a reliable communication link. Reliable communication was established when the Kwinana Beach modem was re-positioned 0.5 m from behind a row of metal pylons to a location between two pylons and the deployment depth was decreased from 1.5 m to 0.5 m in less than $R_D < 3$ m depth water column. The modem was located 2 m from cylindrical wooden pylons and submerged jetty debris.

H.3 Environmental Conditions

Figure 175 illustrates the Kwinana Beach jetty in-band ambient noise measured at: $PSD_A = 60$ dB $\rightarrow$ 70 dB re 1 µPa/$\sqrt{\text{Hz}}$ @ 1 m $\equiv SS3.5 \rightarrow SS5$ Eq.(7-4).

$$PSD_A = 65 \text{ dB} \pm 5 \text{ dB re 1 µPa}/\sqrt{\text{Hz}} \text{ @ 1 m} = SS3.5 \rightarrow SS5$$

$$L_T = 20\log_{10}(6{,}200 \text{ m}) + 1 \text{ dB/km} \times 6.2 \text{ km} \approx 82 \text{ dB}$$

$$PSD_{TX} = PSD_A + L_T = 65 + 81 = 147 \text{ dB re 1 µPa}/\sqrt{\text{Hz}} \text{ @ 1 m} \quad (7\text{-}4)$$

$$B_{TX} = 6.39 \text{ kHz} \equiv 38 \text{ dB re 1 Hz} \quad \text{(for MCDSSS 50 baud.)}$$

$$SPL_{TX} = PSD_{TX} + B_{TX} = 181 \text{ dB re 1 µPa @ 1 m}$$

A transmit sound pressure level of $SPL_{TX} = 181$ dB re 1 µPa @ 1 m was required at source in order to arrive at the receiver with a margin of $M_{RX} < 6$ dB and is consistent with $L_T = 20\log_{10}(R_S)$ spherical spreading propagation model.

H.4 Summary

GPM300 firmware version 5.5 established a reliable 6.2 km communication link between the Magnetics Wharf and Kwinana beach jetty at 50 baud, transmit source level $A_{TX} = 14$ dB $\equiv SPL_{TX} = 176$ dB re 1 µPa @ 1 m requiring 10 W transmit power. The bit energy efficiency is estimated at BEE = 50 Baud /10W ≈ 50 Bits/J @ 1 km re $SS3 \equiv 5 \times 10^2$ Bits/J @ 1 km re $SS0$. The Magnetics Wharf communication performance was a dramatic improvement compared to the 10.7 km Kwinana Beach jetty to Garden Island N/E Wharf test (Appendix I) indicating that there was most likely jetty debris induced signal attenuation. Figure 171 illustrates the predicted 15 dB transmit source level attenuation for $SS3$ to $SS5$, $R_S = 6.2$ km at 50 baud which is within a few dB's of the numerical model.

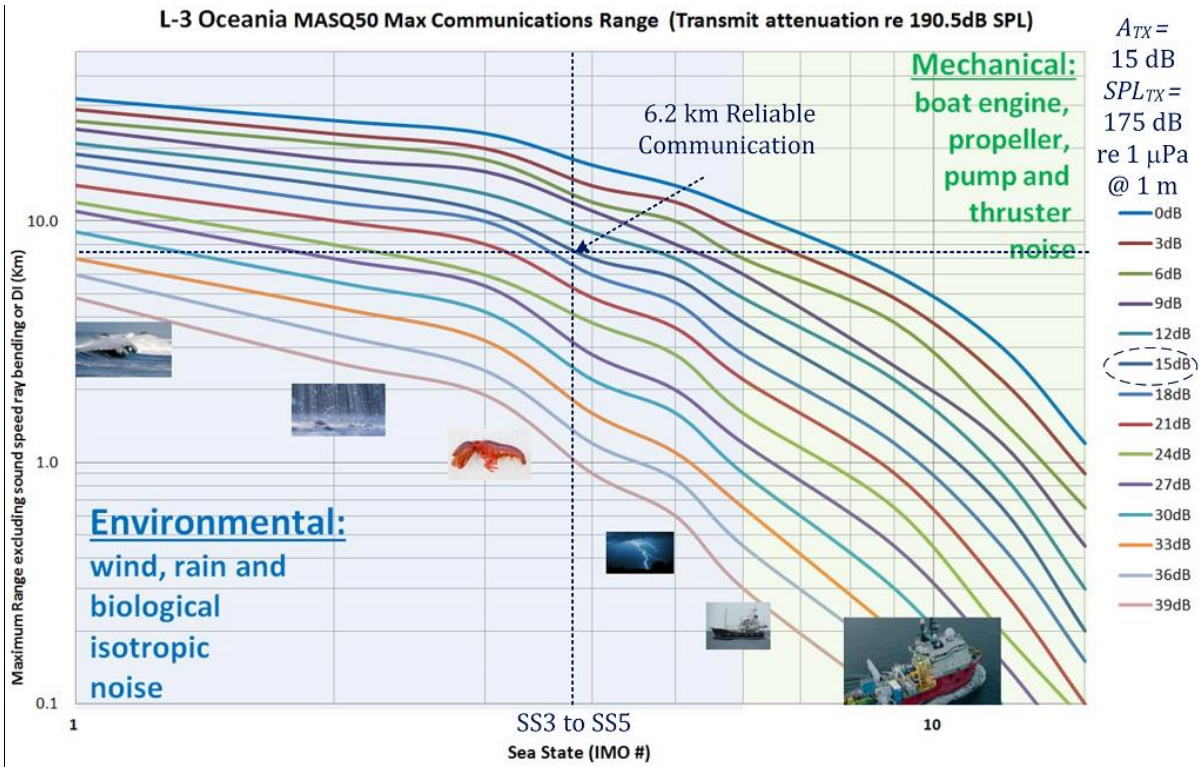

Figure 171 MCDSSS 50 baud versus sea state and attenuation (Magnetics wharf)

Appendix I 10.7 km Range *SS5* 4-20 m Depth Measurements

I.1 Introduction

Long range communication is subject to frequency dependent signal absorption ($L_A > 0$ dB) which comes into effect for ranges greater than $R_S > 5$ km (i.e. lower acoustic baud rates improve communication reliability by reducing high frequency absorption). Shallow water ($R_D < 20$ m) channels are not subject to sound velocity induced refraction signal attenuation ($L_R \rightarrow 0$ dB). The Garden Island N/E Wharf provides a hydro-acoustic stress test environment with loud $SS4$ to $SS6$ inshore snapping shrimp noise and high multipath reverberation. Communication across the $R_S = 10.7$ km Cockburn Sound channel was tested using the GPM300 configuration tool acoustic baud rate optimisation function to optimise the power and data rate for the acoustic channel. MASQ network routing was used to measure a remote modem absolute range, ambient noise and receive power measurements to provide an estimate of the slant range attenuation obstruction. The sensitivity of the FSK alert telemetry ($\tau_{FSK} = 100$ ms) versus MCDSSS 10 baud ($\tau_{MASQ10} = 800$ ms) receive was measured.

I.2 Garden Island Wharf to Kwinana Beach 10.7 km Hydro-acoustic Channel

Figure 172 illustrates the Cockburn Sound 10.7 km Garden Island N/E Wharf to Kwinana beach hydro-acoustic channel which provides a high path loss, noisy and reverberating/multipath stress test environment.

Acoustic channel characteristics:

1. Channel length of $R_S = 10.7$ km NW to SE$L_S = 80.6$ dB, $L_A = 6.5$ dB @ 6.5 kHz, $L_A = 14$ dB @ 16.5 kHz.
2. Depth of $R_D = 10$ m → 3 m less than $R_D < 20$ m at deepest point.
3. Ambient noise measured at $PSD_A > 70$ dB re 1 µPa/$\sqrt{\text{Hz}}$ @ 1 m ≡ PSD_{SS6}.

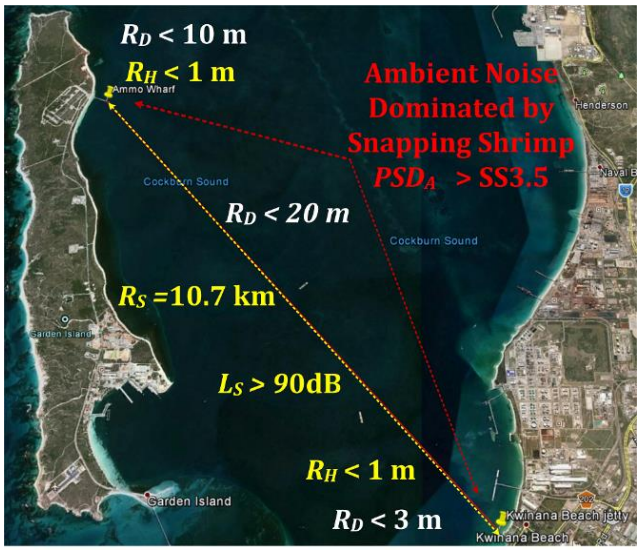

Figure 172 Cockburn Sound (10.7 km hydro-acoustic channel)

I.3 Garden Island North-West Modem Deployment

The north-west modem ID #4 was deployed at a depth of less than $R_H < 1$ m in $R_D < 10$ m depth water column (Figure 173). The modem was located 0.5 m from a cylindrical concrete pylon which reflects acoustic signals.

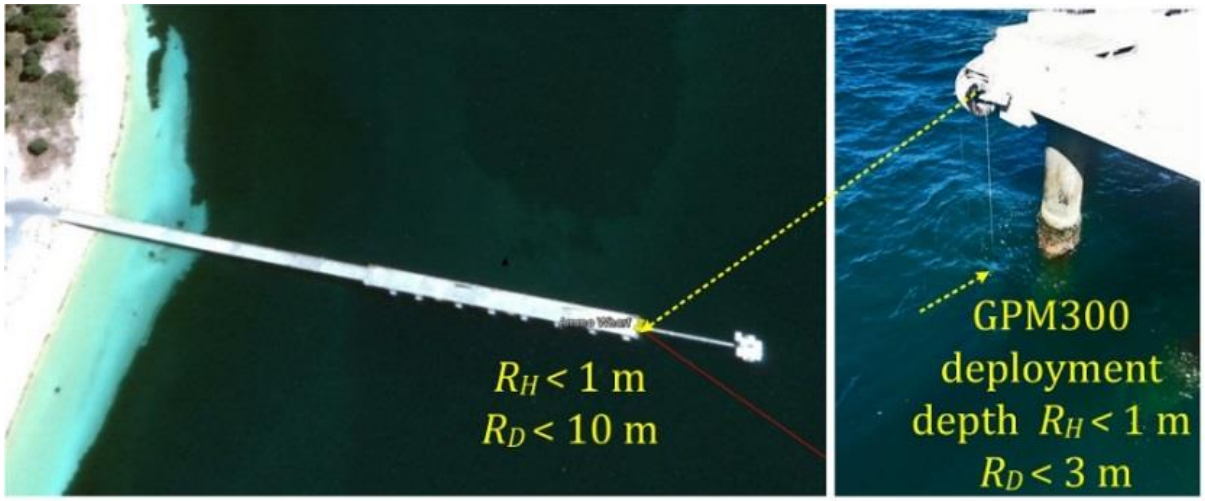

Figure 173 Garden Island N/E wharf

I.4 Kwinana Beach South-East Modem Deployment

The south-east modems (ID #5) was deployed off the Kwinana Beach wooden jetty 1 m from cylindrical pylons and submerged jetty debris (Figure 174). The south-east modem was deployed at a depth of $R_H < 2$ m in less than $R_D < 3$ m depth water column.

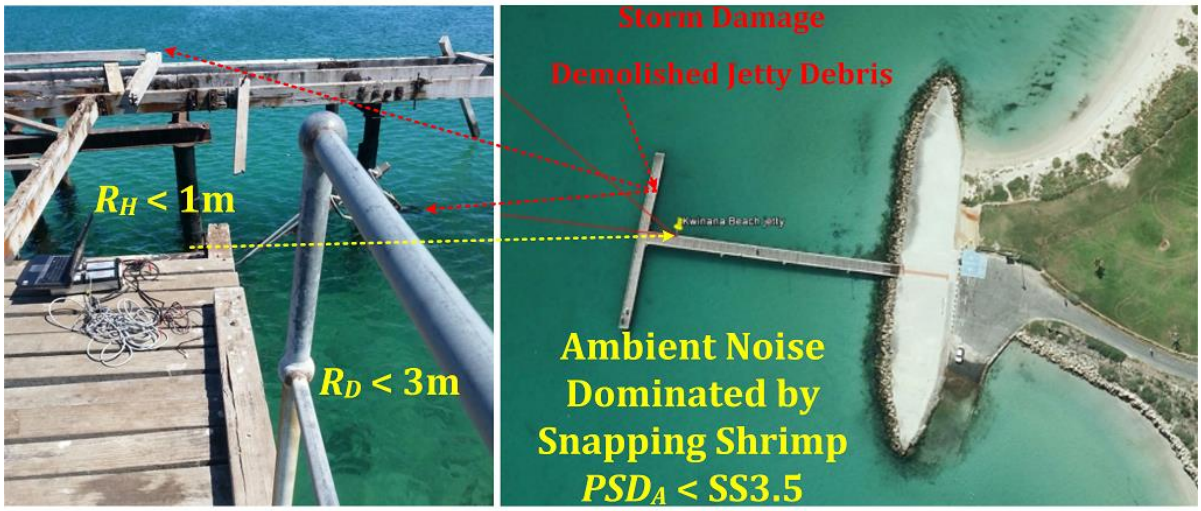

Figure 174 Modem #5 deployment (post storm damage)

I.5 Environmental Conditions

Figure 175 illustrates the Kwinana Beach jetty in-band ambient noise measured at $SS3.5$ to $PSD_A = 60$ dB → 70 dB re 1 µPa/$\sqrt{\text{Hz}}$ @ 1 m ≡ $SS3.5 \rightarrow SS5$.

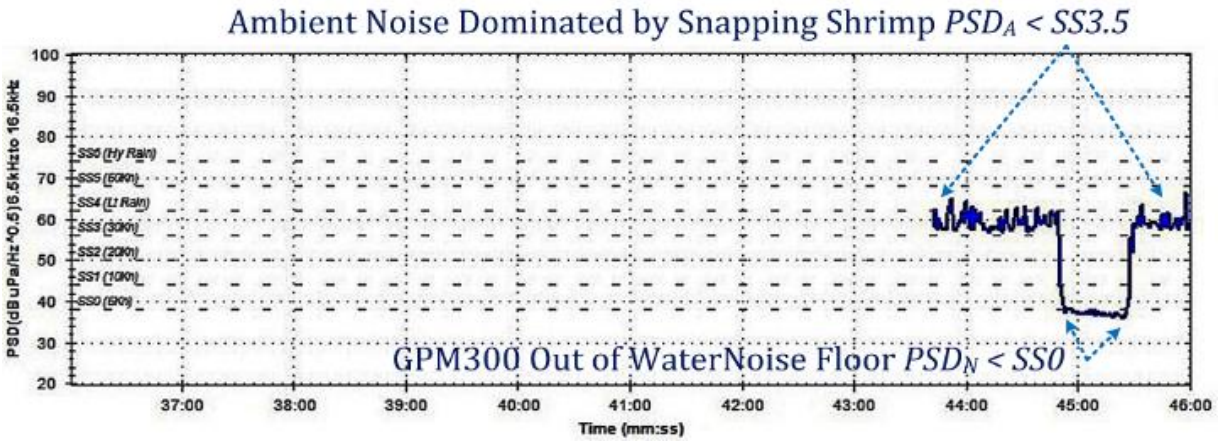

Figure 175 Kwinana beach jetty ambient noise

The noise level and transmission loss are considered here with reference to sea state zero conditions:

1. $PSD_A = 60$ dB → 70 dB re 1 µPa/$\sqrt{\text{Hz}}$ @ 1 m $\equiv SS3.5$.
2. $L_T = 20\log_{10}(10{,}700\text{ m}) + 1\text{ dB/km} \times 10.7\text{ km} \approx 91$ dB.
3. $SPL_{MIN} = PSD_A + L_T = 65 + 91 \equiv 156$ dB re 1 µPa/$\sqrt{\text{Hz}}$ @ 1 m.

A transmit source level of $PSD_{TX} = 156$ dB re 1 µPa/$\sqrt{\text{Hz}}$ @ 1 m $\equiv SPL_{TX} =$ 190 dB re 1 µPa @ 1 m was required at the source for a receiver margin of $M_{RX} < 6$ dB. Cockburn Sound $L_T = 90$ dB path loss is comparable to Appendix F 2 m $SS15$ tank, 2 m $SS6$ Air and air 22 m $SS3$ testing which all simulate a $L_T > 120$ dB path loss.

I.6 Sea Trial Measurements

Optimisations for maximum acoustic baud rate and minimum transmit source level an acoustic baud rate of 10 baud and transmit source level attenuation of $A_{TX} = 0$ dB ≡ 190 dB re 1 µPa @ 1 m was measured for Garden Island N/E Wharf and $A_{TX} = 4$ dB ≡ 186 dB re 1 µPa @ 1 m was measured for Kwinana Beach Jetty.

I.7 Summary

A reliable $R_S = 10.7$ km Kwinana Beach Jetty communication link could only be established using the slowest 10 baud and maximum transmit source level, faster baud rates were expected. The $R_D = 3$ m water depth at Kwinana Beach jetty and the storm damage debris may have contributed to lower communication speed. Transpond measurements from the Garden Island Wharf to Kwinana beach would reply with a telemetry alert but would intermittently fail to detect or decode the 10 baud signal. This test result validates that the telemetry alert signal ($\tau_{FSK} = 100$ ms) is more robust than 10 baud ($\tau_{MASQ10} = 800$ ms) as required by the minimum MCDSSS performance specification. The opposite is the case for 0.2 m air tests where 10 baud is more sensitive than the telemetry alert signal which may be related to the ceramic air coupling loss and air bandwidth.

Communication transpond tests using 50 baud and 20 baud would detect the telemetry alert reply signal but would not decode the MCDSSS signal. Data analysis identified

several instances of 50 baud replay telemetry alert signals being reported as 20 baud and 20 baud replay telemetry alert signals being reported as 10 baud. Subsequent multipath analysis and simulation test identified the telemetry alert detector hard limiter as the source of the false detection which would report the multipath detect time instead of the line of site time for telemetry alert data. This prompted the redesign of the telemetry alert communication protocol to use wide telemetry alert data bins for low baud rate communication (Chapter 5.7.5.4).

Figure 176 illustrates the predicted $A_{TX} = 15$ dB $\equiv$ 175 dB re 1 µPa @ 1 m transmit source level attenuation for $SS4$, $R_S = 10.7$ km at 10 baud. The sea trial transmit source level attenuation was $A_{TX} = 4$ dB $\equiv$ 186 dB re 1 µPa @ 1 m indicating that the jetty rubble obstruction induced an addition $L_O = 15$ dB – 4 dB ≈ 10 dB path loss. The physical obstruction loss can also be calculated using Eq.(5-17). This test demonstrated that a communication link can be establish link using a low baud rate to counter environmental noise increases or obstruction induced acoustic attenuation.

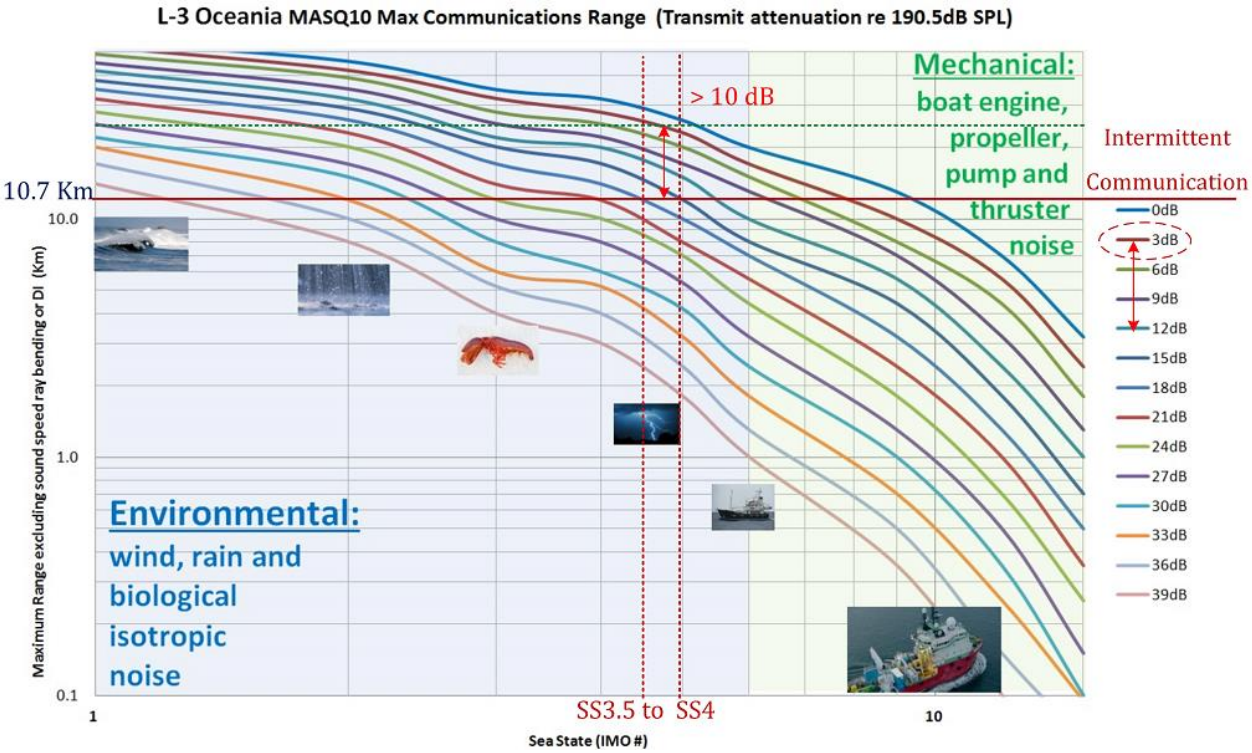

Figure 176 MCDSSS 10 baud versus sea state and attenuation (Garden Island wharf)

Appendix J 8 km Range *SS6* 4-20 m Depth Measurements

J.1 Introduction

A sea trial was carried out on 8 May 2017 between the Garden Island N/E Wharf and the Australian Marine Complex AMC5 Wharf (Figure 170), to validate that the firmware version 6.0 MCDSSS algorithm and engineering optimisations had not been over fitted to the failing signal database. The $R_S = 8$ km W/ E channel provided a high path loss, low sea state induced high multipath, high $SS5$ to $SS6$ ambient noise and shallow water 4 m $< R_D <$ 20 m depth reverberating/multipath test environment. The relatively shallow water is not subject to sound velocity induced refraction signal attenuation ($L_R \rightarrow 0$ dB). The ambient noise was dominated by very loud snapping shrimp and was measured at $PSD_A =$ 60 dB $\rightarrow$ 70 dB re 1 µPa/$\sqrt{\text{Hz}}$ @ 1 m $\equiv SS5 \rightarrow SS6$ which is equivalent to heavy rain.

J.2 Modem Deployments

The east modem ID #28 was deployed at a depth of less than $R_H < 5$ m in $R_D = 7$ m depth water column. The west modem ID #1 was deployed at a depth of less than $R_H < 4$ m in $R_D = 11$ m depth water column.

J.3 Environmental Conditions

The Garden Island N/E Wharf in-band ambient noise was measured at $SS6.5 \rightarrow SS6$ Eq.(7-5).

$$\begin{gathered} PSD_A = 70 \text{ dB} \pm 3 \text{ dB re 1 µPa}/\sqrt{\text{Hz}} \text{ @ 1 m} = SS5.5 \rightarrow SS6 \\ L_T = 20\log_{10}(8{,}000 \text{ m}) + 1 \text{ dB/km} \times 8 \text{ km} \approx 86 \text{ dB} \\ B_{TX} = 10 \text{ kHz} \equiv 40 \text{ dB re 1 Hz for MCDSSS 75 baud} \\ SPL_{MIN} = PSD_A + L_T + B_{TX} - M_{TX} = 70 + 86 + 40 - 14 \\ = 185 \text{ dB re 1 µPa @ 1 m} \end{gathered} \tag{7-5}$$

Assuming a spherical propagation model the estimated minimum transmit sound pressure level, for reliable communication, is $SPL_{TX} \approx$ 185 dB re 1 µPa @ 1 m at source for a receive margin of $M_{RX} > 3$ dB.

J.4 Voice Communication Test

Figure 177 (right) illustrates the UQC Voice $R_S = 8$ km spectrogram that was audible but not legible with a measured receiver $SNR_{RX} \approx 0$ dB.

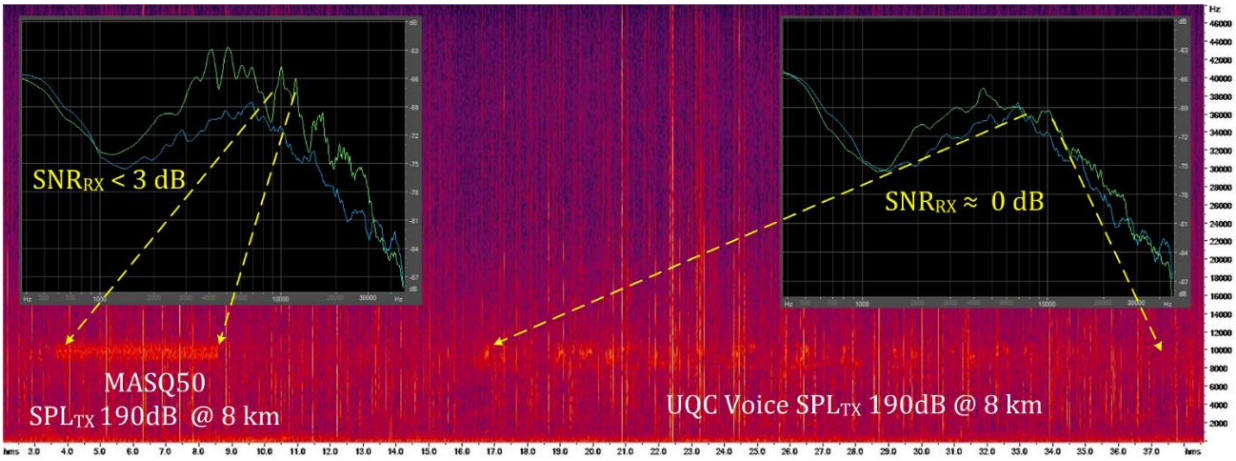

Figure 177 UQC voice comminication spectrogram (0 dB SNR)

The voice communication sonar equation, at a range of $R_S = 8$ km with a transmit source level of $SPL_{TX} = 190$ dB, (requiring 300 W transmit power) predicts a received $SNR_{RX} \approx 0$ dB (Figure 178).

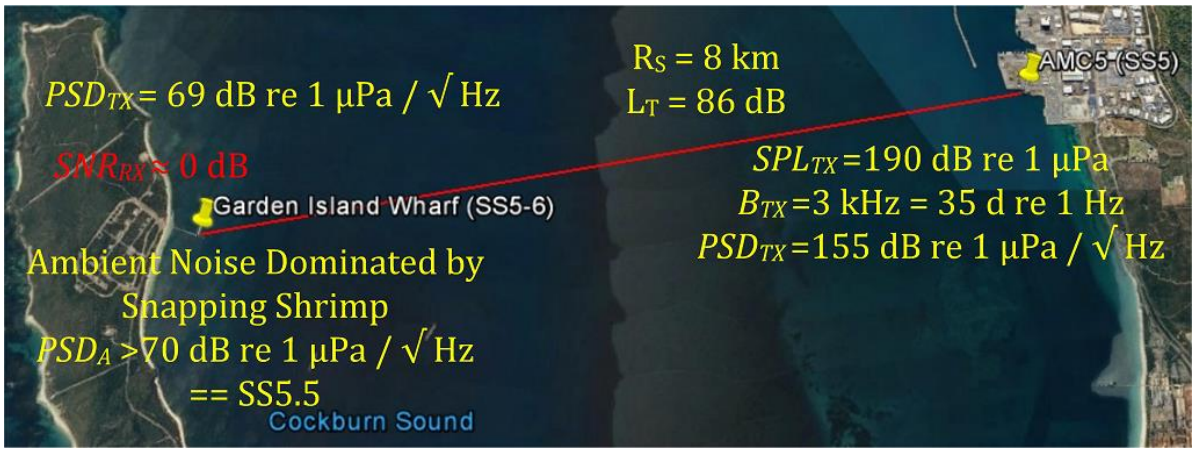

Figure 178 UQC voice comminication sonar equation diagram (0 dB SNR)

Legible voice communication requires at least a $SNR_{RX} > 10$ dB which translates to a transmit source level of $SPL_{TX} > 200$ dB using a 3 kW spherical projector with DI = 0 dB, requiring transmit source level of $SPL_{TX} > 203$ dB requiring 6 kW transmit power which will induce shallow water cavitation (Figure 179).

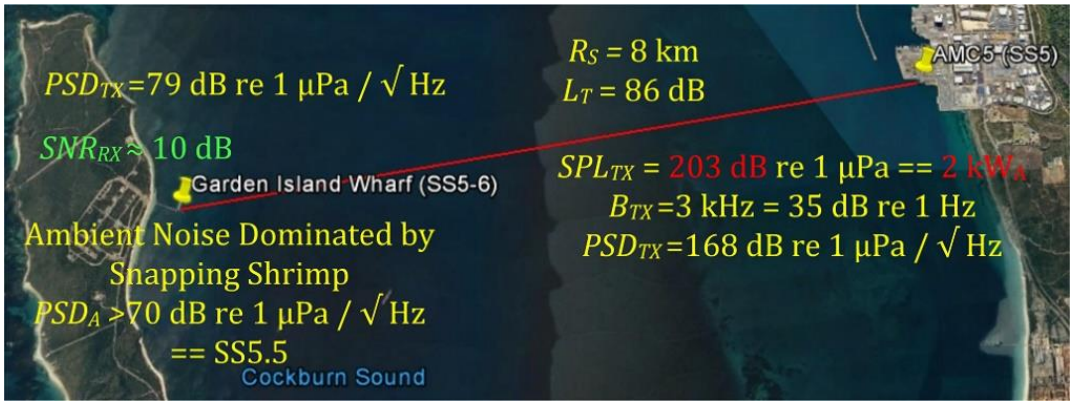

Figure 179 UQC voice comminication sonar equation diagram (10 dB SNR)

The 20 second voice message contains the equivalent of 180 characters by 6 bits which would be more reliably communicated using text messaging at a hydro-acoustic baud rate of 75 baud with a transmit source level as low as $SPL_{TX} \geq 174$ dB, requiring 6 W transmit power (i.e. digital communication requires in the order of 100 time less transmitter electrical power than voice communication).

J.5 Digital Communication Test

Digital communication tests were carried out to measure the channel min/max hydro-acoustic baud rates and min/max transmit source level.

J.5.1 Channel Multipath Characteristics

The $R_S = 8$ km shallow water channel was characterises by a weak slant range signal followed by a weak $R_T = 1.5$ m surface reflection followed by a very weak $R_M = 15$ m bottom reflection (Figure 180).

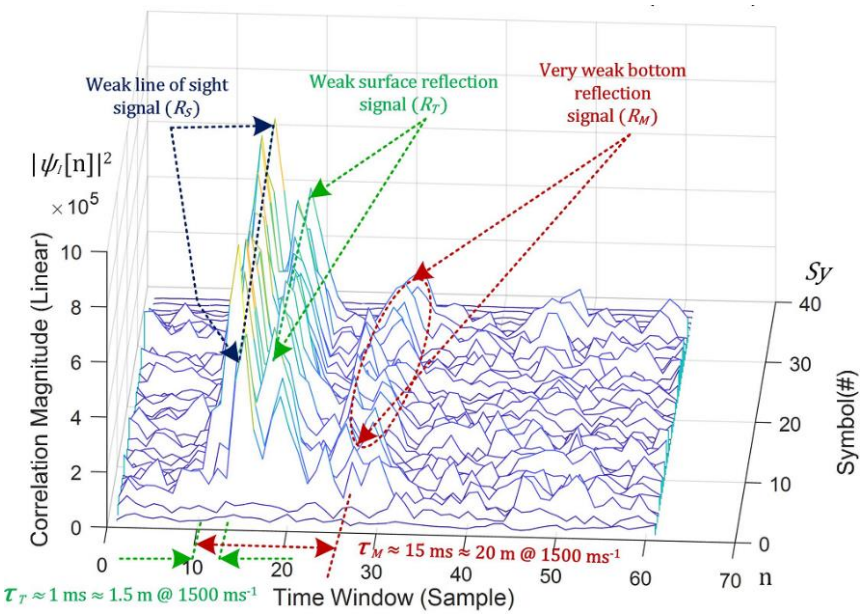

Figure 180 Multipath structure (8 km range 4 m to 20 m depth)

J.5.2 Min/Max Transmit Source Level versus Hydro-acoustic Baud Rate

Figure 128 illustrates the min/max transmit source level versus hydro-acoustic baud rate:

1. Reliable communication was established using 10, 20, 50, 75, 100, 150, 200 and 350 baud. The wind was low and the sea surface was relatively calm. Hydro-acoustic baud rate communication faster than 350 baud could not be established for any transmit source level (SPL_{MIN} to SLP_{MAX}) however with higher winds roughen the surface which reduces multi path and a communication link using 500 baud can be expected as is the case in deeper water.
2. Maximum transmit source level $SPL_{TX} = 190$ dB re 1 µPa @ 1 m requiring 300 W transmit power.
3. Minimum transmit source level $\mathrm{SPL_{TX}} = 174$ dB re 1 µPa @ 1 m requiring 6 W transmit power at 75 baud.

J.5.3 Propagation Model

Figure 181 illustrates the peak BEE sonar equation diagram for a communication link with an estimated receiver $SNR_{RX} \approx -22$ dB which is not consistent with a spherical spreading propagation model Eq.(2-12).

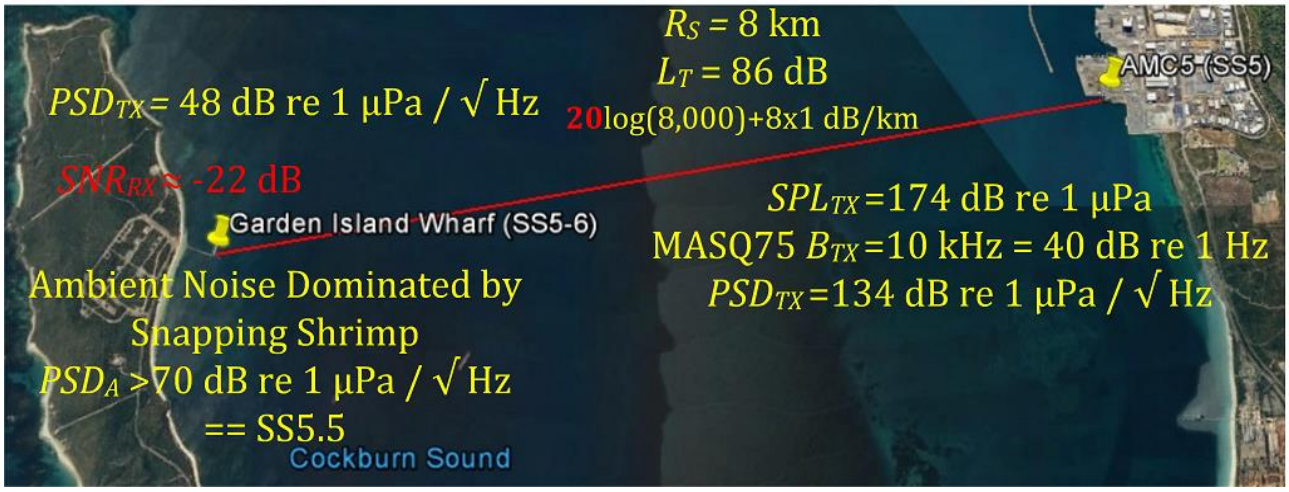

Figure 181 MCDSSS 75 baud sonar equation diagram (spherical spreading)

Figure 182 (right) illustrates the receiver measured peak BEE $SNR_{RX} \approx -3$ dB which was derived using the positive $SNR_{RX} \approx +3$ dB spectrogram (Figure 182 left) and the difference in transmit source level from test logs.

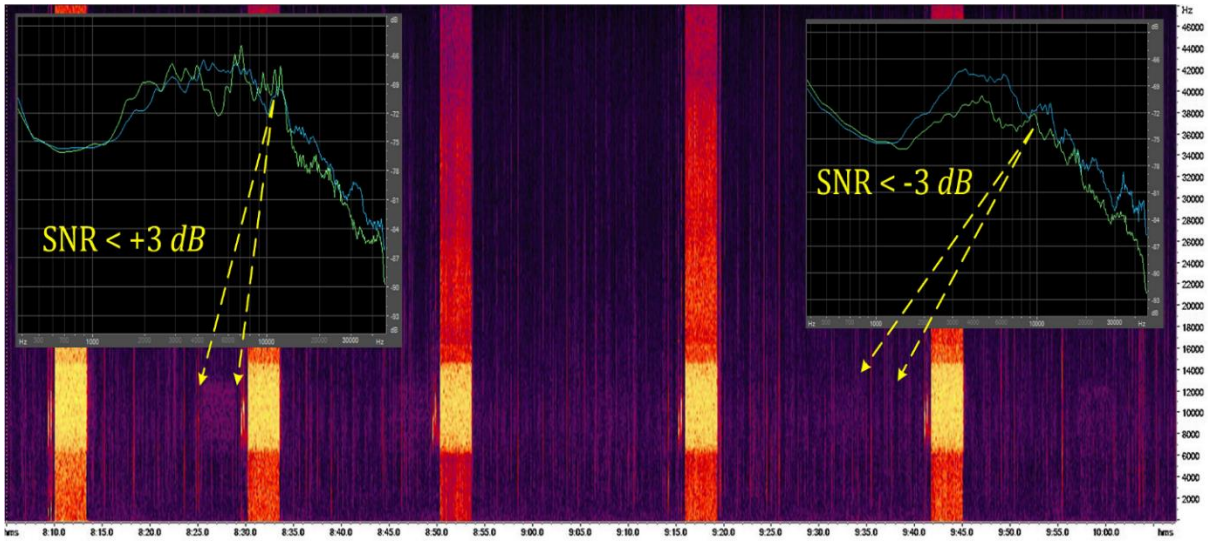

Figure 182 MCDSSS 75 baud comminication spectrogram

Figure 183 illustrates the peak BEE sonar equation diagram for a communication link with an estimated receiver $SNR_{RX} \approx -3$ dB which is consistent with a propagation model approaching cylindrical spreading Eq.(2-13) and is the strongest evidence that the optimised firmware version 6.0 MCDSSS receiver is utilising the multipath signals as additional sources of energy.

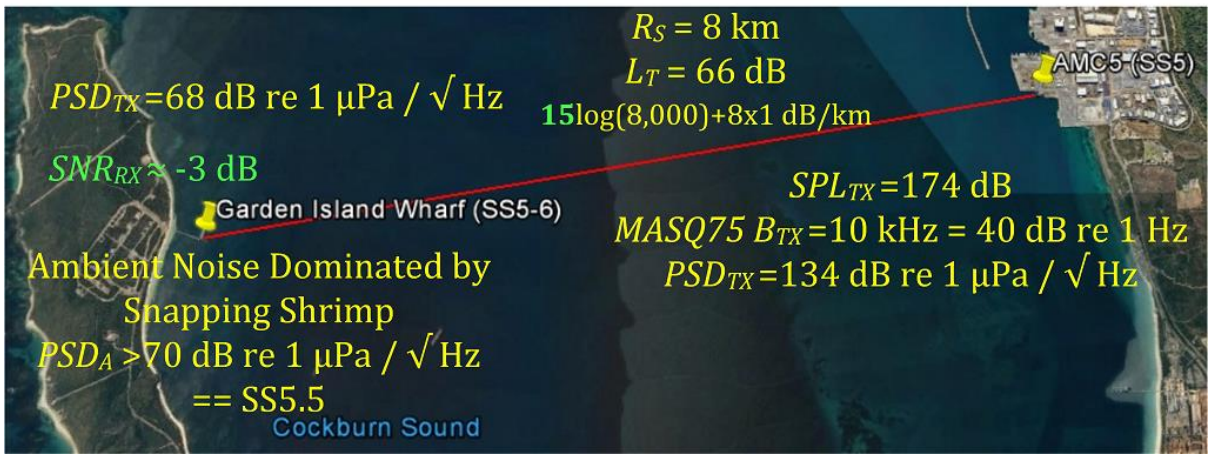

Figure 183 MCDSSS 75 baud sonar equation diagram (≈ cylindrical spreading)

J.5.4 Peak Bit Energy Efficiency

Figure 184 illustrates the peak bit energy efficiency as a function of hydro-acoustic baud rate. Peak BEE was measured at 75 baud and was independent of sea state.

Note: Peak BEE is a function of channel R_S = 8 km range versus R_S = 4m → 20 m depth 1: 500 aspect ratio.

Figure 184 Peak bit energy efficiency (Cokbourn Sound)

Figure 185 illustrates the peak bit energy efficiency normalised for range and sea state using a propagation model approaching cylindrical spreading. The average BEE for the Cockburn sound deployment is estimated at approximately 5×10^3 Bits/J @ 1 km re *SS*0.

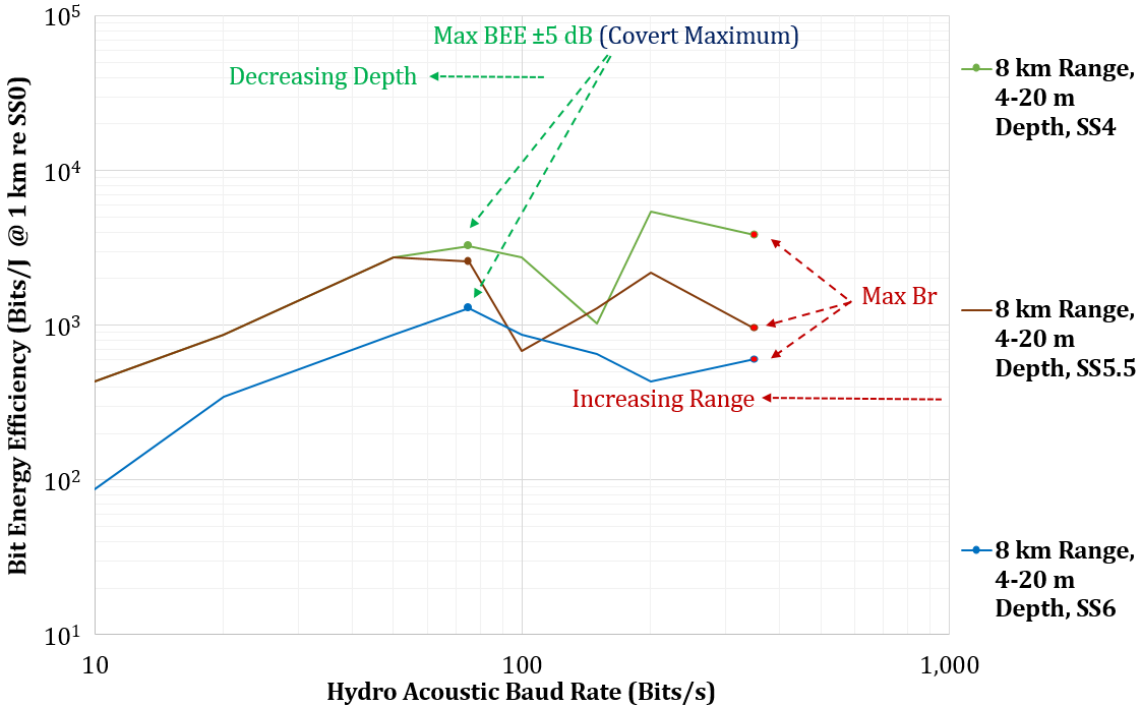

Figure 185 Peak bit energy efficiency (Bits/J @ 1 km re *SS*0)

Figure 186 illustrates the multipath period envelope versus hydro-acoustic baud rate. Although not as pronounced as the Figure 169 Fremantle harbour measurement peak

BEE_{PEAK} occurs when the multipath signals are masked by the ambient noise ($PSD_M < PSD_A - M_{TX}$).

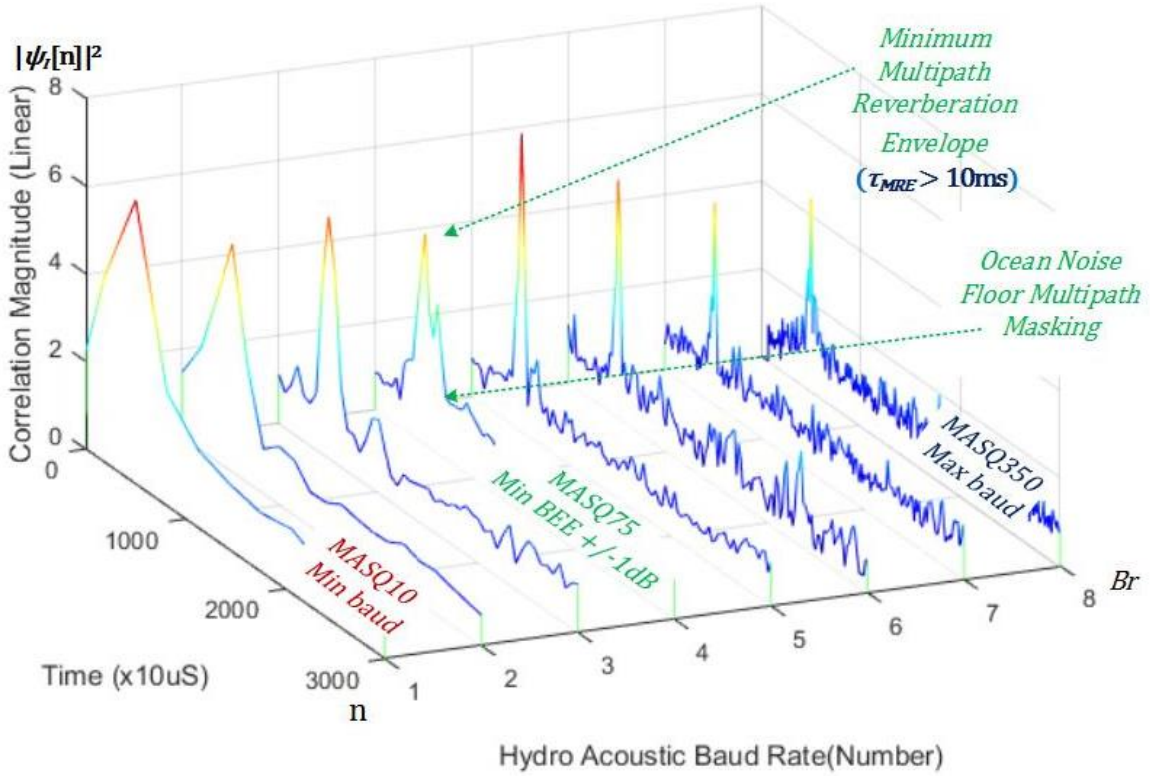

Figure 186 Multipath period envelope versus hydro-acoustic baud rate

J.6 Summary

UQC Voice communication required 10 dB high transmit source level for legible voice communication compared to digital communication. An equivalent 75 baud peak BEE communication link requires 20 dB lower transmit source level than legible UQC voice communication.

A reliable 8 km communication link between the Garden Island Wharf *SS*6 and AMC5 *SS*5 was established using 10, 20, 50, 75, 100, 50, 200 and 350 baud and minimum transmit source level $SPL_{TX} = 174$ dB re 1 µPa @ 1 m requiring 6 W transmit power at 75 baud. The bit energy efficiency is estimated at $\text{BEE} = \frac{75\ \text{Baud}}{6\ \text{W}} \approx 10^1 \frac{\text{Bits}}{\text{J}}$ @ 8 km re *SS*6 $\approx 2 \times 10^3 \frac{\text{Bits}}{\text{J}}$ @ 1 km re *SS*0. The 6.2 km Garden Island Magnetics Wharf to Kwinana beach communication trial (Appendix H.4), using a legacy spherical spreading firmware version 5.x MCDSSS receiver, measured a peak BEE at 5×10^2 Bits/J @ 1 km re *SS*0 which suggests that there is approximately a 10 dB improvement in performance between the firmware version 6.0 MCDSSS optimised receiver and firmware legacy receiver.

Appendix K 8/11 km Depth *SS15* Open Ocean Measurements

K.1 Introduction

The reprocesses sea trail data to provide a performance reference for deep ocean non multipath reverberation and extreme $SS15$ communication. Three of the twelve post processed sea trial communication sonar equations, which exhibit marginal and counter intuitive performance, are presented. Performance measurements from the Deep Sea Challenger deployment were used to guide the design of the acoustic communication system for the TRITON 36000/2 1 km depth type certified submarine.

The 11 km ocean depth Mariana trench submarine dive [154] required wireless voice, text, remote controls and one way time of flight communication (Figure 187). The deployment required full 11 km ocean depth hydro-acoustic modems attached to the submarine and two landers. The surface support vessels were a commercial Dynamic Positioning (DP) workboat and an ocean going Rigid Hulled Inflatable Boat (RHIB). The 11 km depth Mariana Trench submarine dive validates vertical long-range 100 baud performance at full ocean depth ($R_D > 11$ km) in the absence of multipath ($N_M = 0$), MCDSSS receiver reliability in the presence of extremely loud an-isotropic noise ($PSD_A > PSD_{SS15}$), deep water horizontal communication reliability ($R_S > 10$ km) and one-way time of flight and multi-user functions.

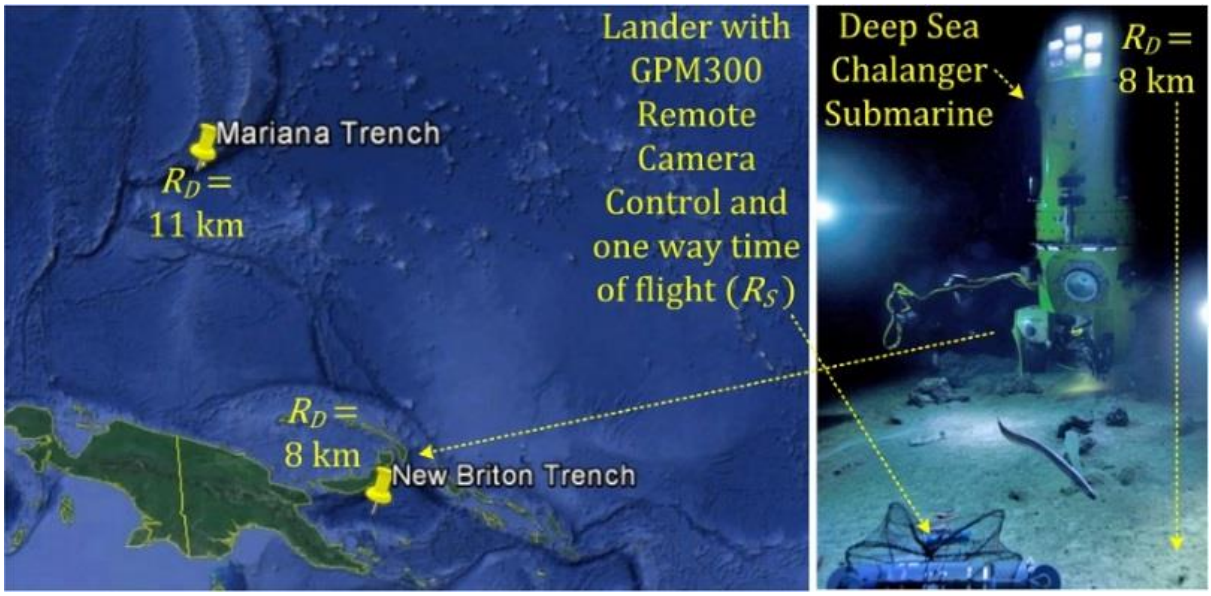

Figure 187 Mariana (11 km depth) and New Britton trench (8 km depth)

Figure 188 illustrates the DP support vessel noise floor $PSD_A > 135$ dB re 1 µPa/$\sqrt{\text{Hz}}$ @ 1 m $> PSD_{SS15}$ which is 70 dB louder than the ocean ambient noise $SS4$.

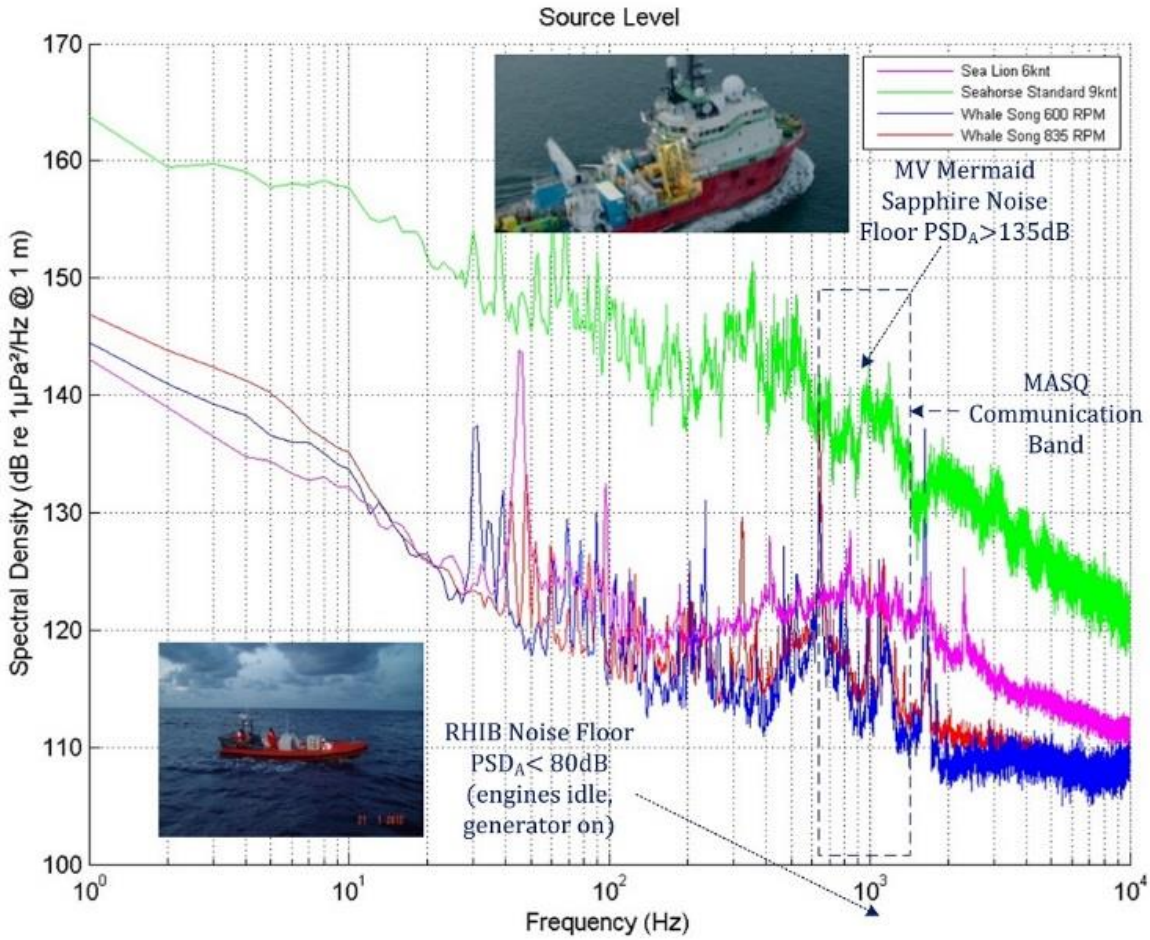

Figure 188 Deep sea challenger support vessel noise floor

Figure 189 illustrates the dual redundant titanium pressure housing L3 Oceania GPM300 modems mounted on the top of the Deep Sea Challenger submarine.

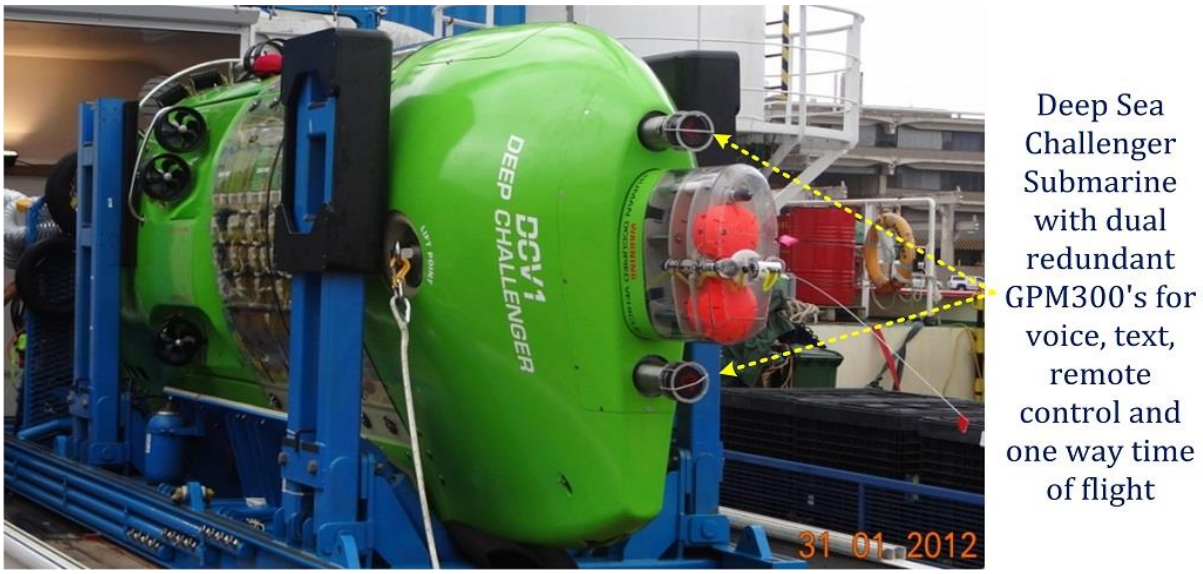

Figure 189 Dual redundant L3 GPM300 (11 km depth submarine)

The Deep Sea Challenger 11 km Mariana trench submarine deployment communication requirements were:

1. 11 km depth bi-directional voice.
2. 11 km depth bi-directional data communication.
3. 11 km depth unmanned bi-directional command and control.
4. Independent periodic submarine vital sign data uplink (CO2, Battery charge, depth, temperature).
5. One-way time of flight.
6. Multi user voice and simultaneous data communication.
7. Two landers with one-way time of flight, data command and control.
8. Horizontal 10 km Omni directional communication when the submarine is near the surface.

In the presence of a loud $PSD_A \approx 135$ dB re 1 µPa/$\sqrt{\text{Hz}}$ @1 m > PSD_{SS15} surface ship requirement number 1 presented the most difficult challenge because voice communication requires a large positive receiver signal to noise ratio compared to digital communication.

K.2 New Briton Trench 8 km Depth Submarine to MV Mermaid Sapphire

Figure 190 illustrates the sonar equation diagram for $R_D = 8$ km depth New Briton Trench submarine to surface Merchant Vestal (MV) Mermaid Sapphire $SS15$ for voice communication.

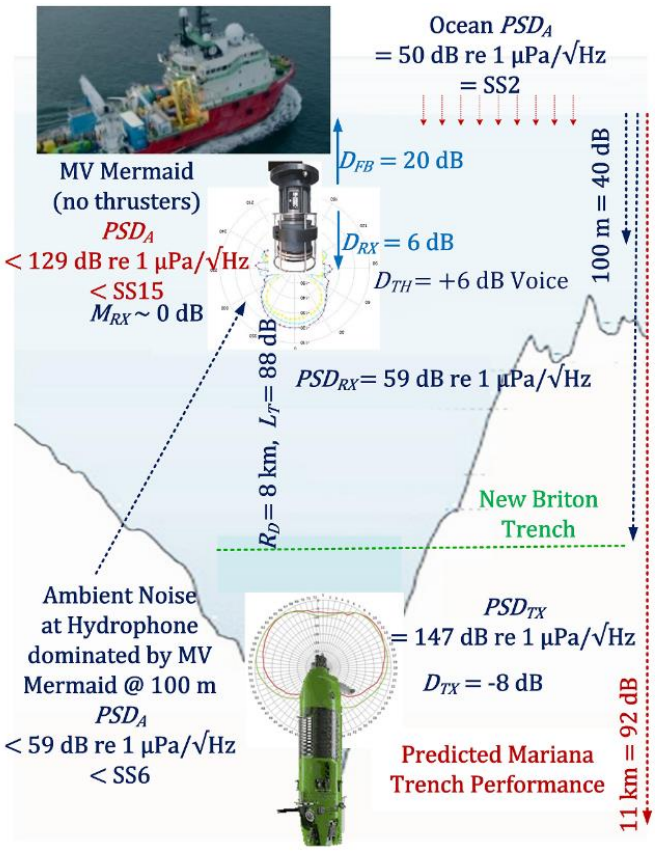

Figure 190 8 km depth New Briton Trench submarine to MV Mermaid (Voice)

A directional hydrophone was deployed 100 m below the hull of MV Mermaid providing $D_{RX} = 6$ dB directivity and 20 dB of front to back ratio surface noise isolation Eq.(7-6).

$$\begin{gathered} R_H = 100 \text{ m} \quad \text{(Direction transducer depth.)} \\ L_H = 20\log_{10}(R_H) = 40 \text{ dB} \quad \text{(Direction transducer path loss.)} \\ D_{FB} = 20 \text{ dB} \quad \text{(Directional transducer front to back ratio.)} \\ D_{RX} = 6 \text{ dB} \quad \text{(Directional transducer directivity.)} \end{gathered} \tag{7-6}$$

The largest source of noise $PSD_{MERMAID} > PSD_{SS15}$ was the MV Mermaid with its thrusters not operating Eq.(7-7).

$$\begin{gathered} PSD_{SS2} = 50 \text{ dB re 1 µPa}/\sqrt{\text{Hz}} \text{ @ 1 m} \equiv SS3 \quad \text{(Isotropic.)} \\ PSD_{MERMAID} > 127 \text{ dB re 1 µPa}/\sqrt{\text{Hz}} \text{ @ 1 m} > PSD_{SS15} \quad \text{(Anisotropic.)} \\ PSD_{MERMAID} > 87 \text{ dB re 1 µPa}/\sqrt{\text{Hz}} \text{ @ 100 m} > PSD_{SS8} \end{gathered} \tag{7-7}$$

The anisotropic MV Mermaid noise was attenuated by the directional hydrophone front to back directivity ($D_{FB} = 20$ dB) reducing the hydrophone input ambient noise to $PSD_A > PSD_{SS5}$ Eq.(7-8).

$$PSD_A = PSD_{MERMAID} + D_{FB} = 67 \text{ dB re 1 µPa}/\sqrt{\text{Hz}} \text{ @ 1 km} > PSD_{SS5} \tag{7-8}$$

The path loss for vertical communication is $L_T = 92$ dB Eq.(7-9).

$$\begin{gathered} R_S = R_D = 8{,}000 \text{ m} \\ L_R = 0 \text{ dB (Vertical)} \\ L_T = L_S + L_A + L_R = 20\log_{10}(R_S) + \frac{R_S}{1{,}000}\bar{L}_A = 86 \text{ dB} \end{gathered} \tag{7-9}$$

The transmit source level is $PSD_{TX} = 147$ dB re 1 µPa/$\sqrt{\text{Hz}}$ @ 1 m Eq.(7-10).

$$\begin{gathered} B_{TX} = 3 \text{ kHz} \\ SPL_{TX} = 190 \text{ dB re 1 µPa @1 m} \\ D_{TX} = 8 \text{ dB} \quad \text{(Vertical Omni transducer.)} \\ PSD_{TX} = SPL_{TX} + D_{TX} - 10\log_{10}(B_{TX}) \\ PSD_{TX} = 190 + 8 - 35 = 147 \text{ dB re 1 µPa}/\sqrt{\text{Hz}} \text{ @ 1 m} \end{gathered} \tag{7-10}$$

For 8 km communication the estimated receive margin is $M_{RX} \approx -6$ dB Eq.(7-11) (Figure 191). Illegible voice communication was reported from the Submarine to MV Mermaid when the sub arrived at the bottom of the 8 km depth New Briton trench. Reliable bi-directional communication was achieved using 100 baud. The New Briton trench

submarine dive demonstrated that voice communication between the submarine and MV Mermaid was not possible for the 11 km Mariana Trench deployment.

$$D_{RX} = 6 \text{ dB} \quad \text{(Vertical directional receiver.)}$$

$$P_G = 0 \text{ dB} \quad \text{(UQC.)}$$

$$D_{TH} = 6 \text{ dB} \quad \text{(Legible voice.)} \tag{7-11}$$

$$M_{RX} = PSD_{TX} - PSD_A + D_{RX} + P_G + D_{TH} - L_T$$

$$M_{RX} = 147 - 67 + 6 + 0 - 6 - 86 \approx -6 \text{ dB}$$

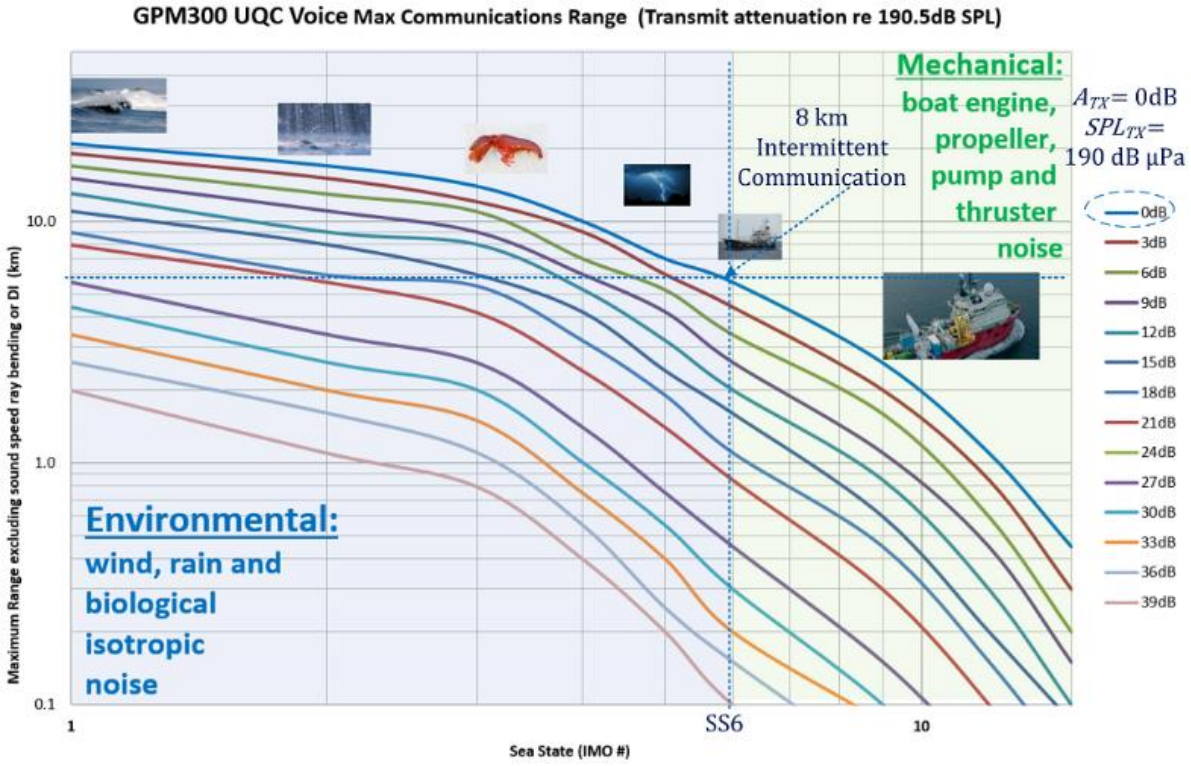

Figure 191 UQC USB voice versus sea state and attenuation (MV Mermaid)

K.3 Mariana Trench 11 km Depth Submarine to RHIB Voice Communication

Figure 192 illustrate the sonar equation diagram for reliable 11 km depth submarine to surface RHIB voice communication.

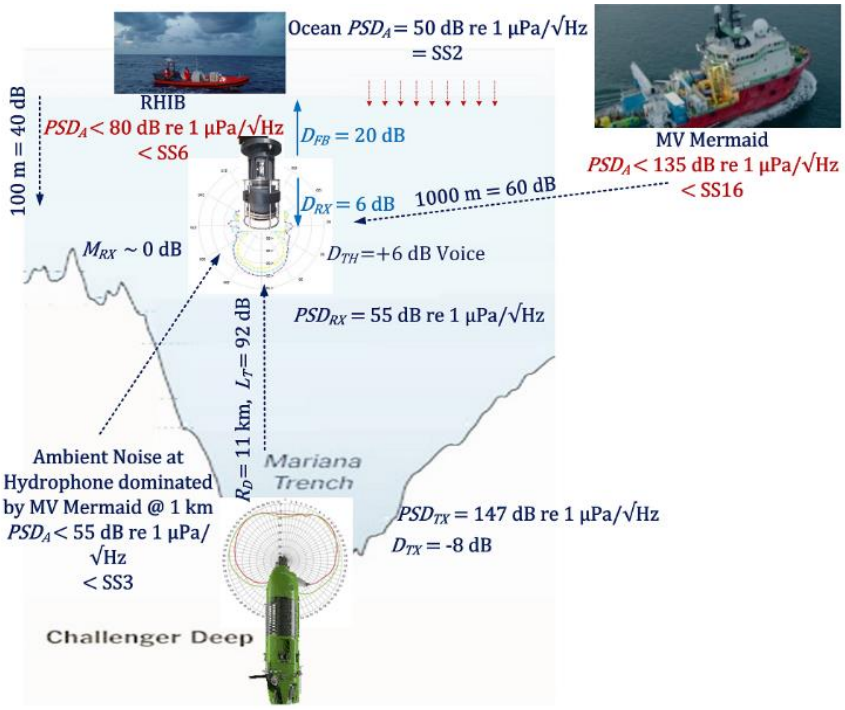

Figure 192 11 km depth submarine to RHIB sonar equation diagram (Voice)

An ocean going RHIB deployed a directional hydrophone 100 m below the hull providing $D_{RX} = 6$ dB directivity and $D_{FB} = 20$ dB front to back ratio surface noise isolation Eq.(7-12).

$$\begin{gathered} R_T = 100 \text{ m} \quad \text{(Direction transducer depth.)} \\ L_T = 20\log_{10}(R_T) = 40 \text{ dB} \quad \text{(Direction transducer path loss.)} \\ D_{FB} = 20 \text{ dB} \quad \text{(Directional transducer front to back ratio.)} \\ D_{RX} = 6 \text{ dB} \quad \text{(Directional transducer Directivity.)} \end{gathered} \tag{7-12}$$

The largest source of noise $PSD_{MERMAID} > PSD_{SS15}$ was the MV Mermaid located 1 km from the directional hydrophone Eq.(7-13).

$$\begin{gathered} PSD_{SS2} = 50 \text{ dB re 1 µPa}/\sqrt{\text{Hz}} \text{ @ 1 m} = PSD_{SS3} \quad \text{(Isotropic noise.)} \\ PSD_{RHIB} = 80 \text{ dB re 1 µPa}/\sqrt{\text{Hz}} \text{ @ 1 m} \\ PSD_{RHIB} = 40 \text{ dB re 1 µPa}/\sqrt{\text{Hz}} \text{ @ 100 m} = PSD_{SS0} \text{ @ 100 m} \\ PSD_{MERMAID} > 135 \text{ dB re 1 µPa}/\sqrt{\text{Hz}} \text{ @ 1 m} > PSD_{SS15} \\ PSD_{MERMAID} > 76 \text{ dB re 1 µPa}/\sqrt{\text{Hz}} \text{ @ 1 km} > PSD_{SS6} \end{gathered} \tag{7-13}$$

The anisotropic MV Mermaid noise was attenuated by the directional hydrophone front to back directivity ($D_{FB} = 20$ dB) reducing the hydrophone input ambient noise to $PSD_A > PSD_{SS3}$ Eq.(7-14).

$$PSD_A = PSD_{MERMAID} - D_{FB} = 55 \text{ dB re 1 µPa}/\sqrt{\text{Hz}} \text{ @ 1 km} > PSD_{SS3} \tag{7-14}$$

The path loss for 11 km vertical communication is $L_T = 92$ dB Eq.(7-15).

$$R_S = R_D = 11{,}000 \text{ m}$$

$$L_R \rightarrow 0 \text{ dB (Vertical)} \tag{7-15}$$

$$L_T = L_S + L_A + L_R = 20\log_{10}(R_S) + \frac{R_S}{1{,}000}\bar{L}_A = 92 \text{ dB}$$

The transmit source level is $PSD_{TX} =$ 147 dB re 1 µPa/$\sqrt{\text{Hz}}$ @ 1 m Eq.(7-16).

$$B_{TX} = 3 \text{ kHz}$$

$$SPL_{TX} = 190 \text{ dB re 1 µPa @ 1 m}$$

$$D_{TX} = 8 \text{ dB} \quad \text{(Vertical Omni transducer.)} \tag{7-16}$$

$$PSD_{TX} = SPL_{TX} + D_{TX} - 10\log_{10}(B_{TX})$$

$$PSD_{TX} = 190 + 8 - 35 = 147 \text{ dB re 1 µPa}/\sqrt{\text{Hz}} \text{ @ 1 m}$$

For 11 km depth communication the estimated receive margin is $M_{RX} \approx 0$ dB Eq.(7-17) and Figure 193. Legible voice communication was only possible when MV Mermaid was not pulsing the DP thrusters.

$$D_{RX} = 6 \text{ dB} \quad \text{(Vertical directional receiver.)}$$

$$P_G = 0 \text{ dB} \quad \text{(UQC.)}$$

$$D_{TH} \geq 6 \text{ dB} \quad \text{(Legible voice.)} \tag{7-17}$$

$$M_{RX} = PSD_{TX} - PSD_A + D_{RX} + P_G + D_{TH} - L_T$$

$$M_{RX} = 147 - 55 + 6 + 0 - 6 - 92 \approx 0 \text{ dB}$$

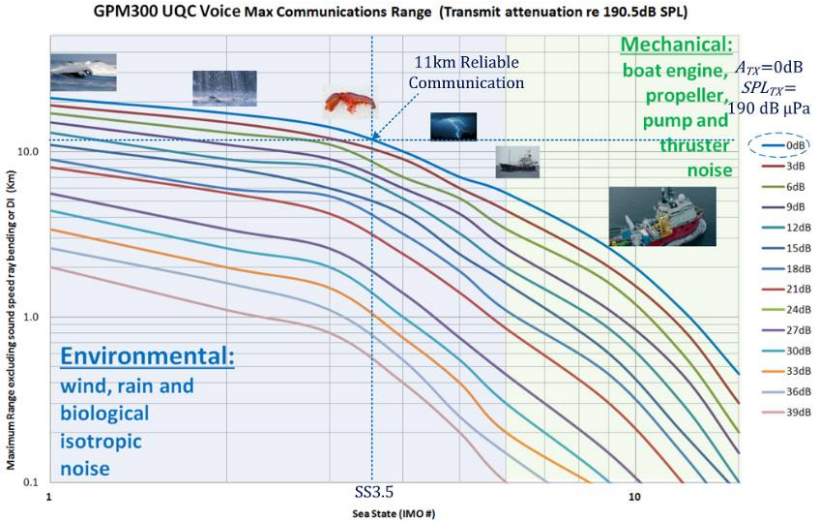

Figure 193 UQC USB voice versus sea state and attenuation (RHIB)

K.4 11 km Depth RHIB to Submarine to RHIB Voice Bottom Bounce

During the Marian Trench submarine dive the RHIB voice communication L3 Oceania operators reported hearing their own voice message with a $t_s = \frac{2R_D}{c} = \frac{22{,}000\text{ m}}{1{,}500\text{ ms}^{-1}} \approx 15$ s delay when the MV Mermaid's DP thrusters were off. Figure 194 illustrates the sonar equation diagram for reliable $R_S = 22$ km bottom bounce RHIB to RHIB voice communication. The $PSD_{TX} = 161$ dB re 1 µPa/$\sqrt{\text{Hz}}$ @ 1 m voice bounce signal is equivalent in performance to a $PSD_{TX} = 200$ dB re 1 µPa/$\sqrt{\text{Hz}}$ @ 1 m source level full ocean depth sounder.

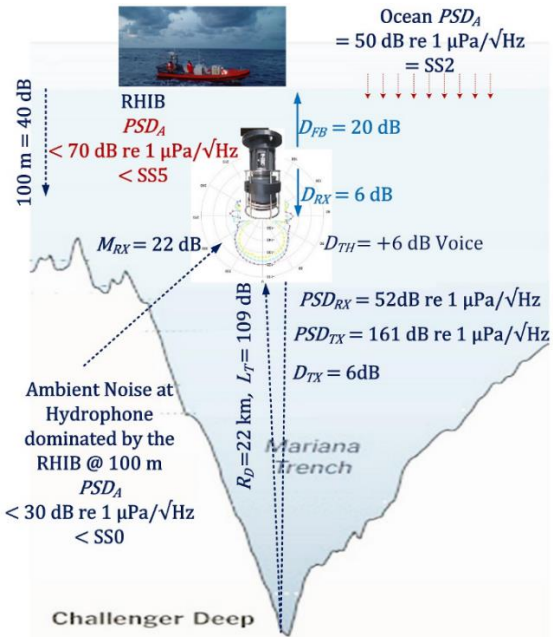

Figure 194 22 km UQC USB voice bottom bounce sonar equation diagram (RHIB)

The largest source of noise $PSD_{RHIB} > PSD_{SS0}$ at the directional hydrophone Eq.(7-18). The MV Mermaid Engines at 1 km was configured for idle and DP thrusters off.

$$PSD_{SS2} = 50 \text{ dB re 1 µPa}/\sqrt{\text{Hz}} \text{ @ 1 m} \equiv SS2 \quad \text{(Isotropic noise.)}$$

$$PSD_{RHIB} < 70 \text{ dB re 1 µPa}/\sqrt{\text{Hz}} \text{ @ 1 m} \tag{7-18}$$

$$PSD_{RHIB} < 30 \text{ dB re 1 µPa}/\sqrt{\text{Hz}} \text{ @ 100 m} \equiv SS0 \text{ @ 100 m} \quad \text{(Engines off.)}$$

The RHIB anisotropic noise was attenuated by the directional hydrophone front to back directivity ($D_{FB} = 20$ dB) reducing the hydrophone input ambient noise to less than the anisotropic deep water noise floor of $PSD_A = PSD_{SS0}$ Eq.(7-19).

$$PSD_A = PSD_{RHIB} - D_{FB} = 10 \text{ dB re 1 µPa}/\sqrt{\text{Hz}} \text{ @ 1 km} = PSD_{SS0} \tag{7-19}$$

The path loss for vertical communication is $L_T = 109$ dB Eq.(7-20).

$$\begin{gathered} R_S = R_D = 22{,}000 \text{ m} \\ L_R = 0 \text{ dB (Vertical)} \end{gathered} \tag{7-20}$$

$$L_T = L_S + L_A + L_R = 20\log_{10}(R_S) + \frac{R_S}{1{,}000}\bar{L}_A = 109 \text{ dB}$$

The transmit source level is $PSD_{TX} = 147$ dB re 1 μPa/$\sqrt{\text{Hz}}$ @ 1 m Eq.(7-21).

$$\begin{gathered} SPL_{TX} = 190 \text{ dB re 1 μPa @1 m} \\ D_{TX} = 6 \text{ dB (vertical Omni-directional transducer)} \\ PSD_{TX} = SPL_{TX} + D_{TX} - 10\log_{10}(B_{TX}) \\ PSD_{TX} = 190 + 6 - 35 = 161 \text{ dB re 1 μPa/}\sqrt{\text{Hz}} \text{ @ 1 m} \end{gathered} \tag{7-21}$$

The estimated receive margin of $M_{RX} > 20$ dB Eq.(7-22). Legible bottom bounce voice communication was audible when MV Mermaid engines were idling and the DP thrusters off. The deployment of an ocean going RHIB to provide 11 km depth voice communication required voice messages to be relayed between the RHIB and MV Mermaid via VHF radio. The bottom bounce reception was used to pre-empt the response from the submarine and go open mic on the VHF radio before the reception of the incoming sub message was received to provide MV Mermaid with real time voice reply.

$$\begin{gathered} D_{RX} = 6 \text{ dB} \quad \text{(Vertical directional receiver.)} \\ P_G = 0 \text{ dB (UQC)} \\ D_{TH} \geq 6 \text{ dB} \quad \text{(For legible voice.)} \\ M_{RX} = PSD_{TX} - PSD_A + D_{RX} + P_G + D_{TH} - L_T \\ M_{RX} = 161 - 30 + 6 + 0 - 6 - 109 > 20 \text{ dB} \end{gathered} \tag{7-22}$$

K.5 Summary

The Marian trench dive imposed an extreme $+SS15$ ambient noise reliable performance requirement on the hydro-acoustic communication system. A combination of $D_{FB} = -20$ dB directional hydrophone deployed vertically $R_H = 100$ m $\equiv L_S = 40$ dB and $R_S = 1$ km $\equiv L_S = 60$ dB horizontal separation from the loudest source of noise were required to provide legible voice communication. When all vessel engines were powered down an unexpected bottom bounce voice reception was audible which was used to time synchronise the VHF radio voice relay from the submarine to the RHIB to MV Mermaid. Voice communication from all surface vessels to the submarine was reliable for all deployments when the submarine thrusters were not operating. The MCDSSS communication $M_{RX} \approx 9$ dB provided reliable digital communication for all deployments. The submarine and landers were one off prototype vehicles that encountered many reliability issues. The New Britton trench, Mariana trench un-manned and Mariana trench manned dives were successful and the most reliable part of the deployment was the hydro-acoustic communications [94].

The Deep Sea Challenger submarine was essentially an experimental vehicle designed for a small number of dives to 11 km depth. Lessons learned from the one man steel hull Deep

Sea Challenger submarine were used to guide the design of the two man titanium hull TRITON 36000/2 submarine [164] which is type certified for 1,000 dives to 11 km depth. The only Deep Sea Challenger sub system that was reused for the TRITON 36000/2 submarine was a network of eight L3 Oceania GPM300 modems including the hardware and software improvements developed for this thesis (Figure 195).

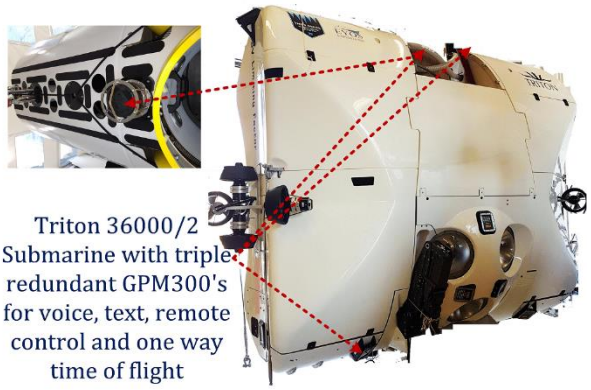

Figure 195 TRITON 36000/2 submanrine with tripple redundant GPM300's

The loudest source of acoustic interference for the Deep Sea Challenger expedition was the +*SS*15 support vessel of opportunity MV Mermaid. The TRITON 2018/2019 expedition, to explore the five deepest ocean tranches, utilises a refurbished ex-submarine hunting vessel DSSV Pressure Drop with a noise floor of *SS*3.5 to *SS*4 which does not require surface directional transducers. The August 2018 Bahama sea trial measured M_{RX} = 10 dB reliable 12.5 km range communication between the 3 m depth +*SS*4 RHIB and 30 m depth +*SS*3 DSSS Pressure Drop GPM300's using 180 dB re 1 µPa @ 1m transmit source level (Figure 196) which is a similar performance to the 8 km range *SS*6 174 dB re 1 µPa @ 1m transmit source level sea trial (Appendix J). When the TRITON 36000/2 submarine was 1 km from DSSV Pressure Drop the submarine thrusters were audible, 10 dB above the ambient noise on the underwater telephone, which provides an estimation of the thruster noise floor at greater than *SS*10. Although the TRITON expedition does not have to deal with support vessel noise the TRITON and Deep Sea Challenger submarines cannot receiver acoustic signals when trusting.

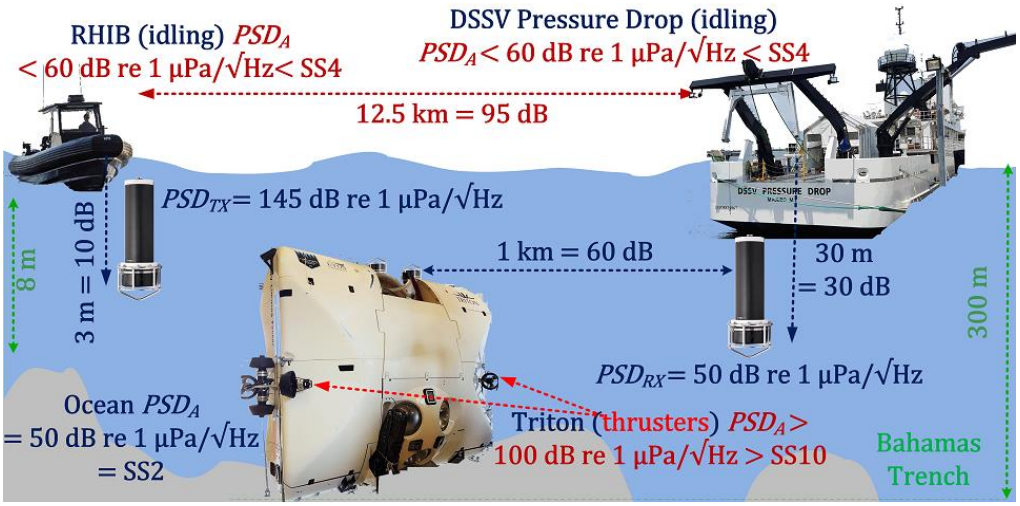

Figure 196 TRITON 36000/2 submarine Bahamas sea trial

Appendix L 15 km Range *SS4* 60 m Depth Measurements

L.1 Introduction

This chapter reprocesses historical sea trial data for +SS4 maximum 15 km range 50 baud, communication which was mined for failing signals used to test message reliability improvement algorithms. On June 2014 a 1½ hour transit window was made available to test the GPM300 long-range communication. The short transit window allowed for five way points stops to 15 km (Figure 197). Due to the limited boat time MCDSSS 50 baud was selected as the long-range communication test candidate. At each waypoint the transmit source level was lowered until communication was lost. The maximum communication range versus transmit source level and ambient noise was plotted against the GPM300 MCDSSS maximum communication prediction graphs. The $R_D < 60$ m ocean depth, 30 km west of Fremantle, provided a hydro-acoustic $SS3.5$ to $SS4.5$ stress test environment which was dominated by offshore snapping shrimp noise. RV Whale Song increased the ambient noise from $SS4$ to $+SS6$ depending on transit speed (v ≈ 10 kn). The 15 km range trial validates horizontal long-range 50 baud performance in +SS4, shallow water ($R_D < 60$ m), multipath ($N_M > 3$) and moderate sound velocity induced surface ducting.

Note: RV Whale Song is an unusually quiet vessel which was purpose built to minimise radiated noise and generates a lower noise field compared to a small outboard motor.

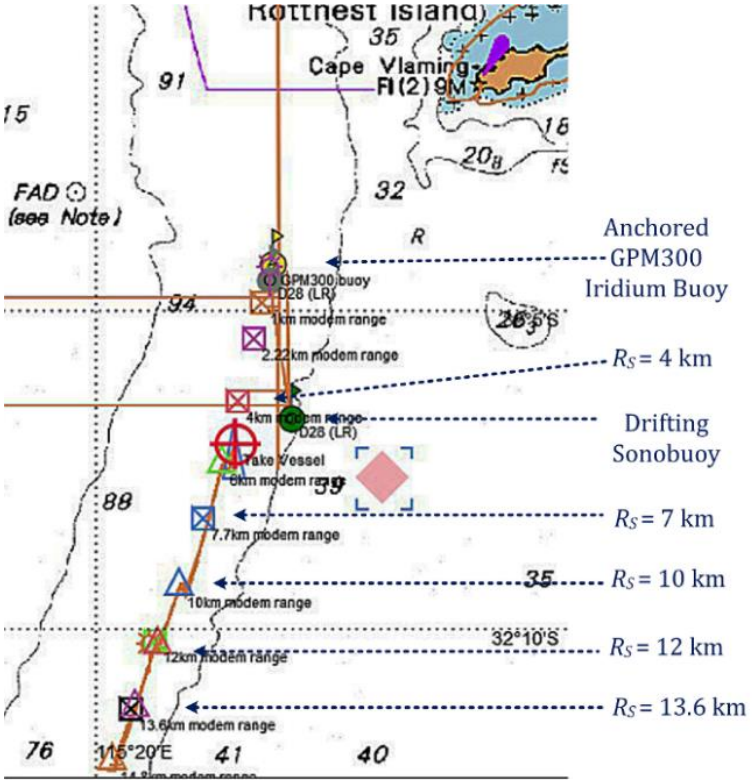

Figure 197 Sea trial way points (L3 Oceania PASOR sonobuoy tracking system)

L.2 Performance Comparison

The L3 Oceania Portable Acoustic Sonobuoy Ranging (PASOR) sonobuoy tracking system was used to measure long-range performance. The PASOR system consists of a quiet ocean going vessel with a +10 m high VHF antenna, multiple SSQ53F sonobuoys and Wave Gliders fitted with L3 Oceania payloads. The RV Whale Song GPM300 was configured to emit MK84 MOD 2 Band K torpedo tracking range pulses which were reliably tracked up to 7.5 km with SSQ53F Sonobuoys and the Wave Glider hydrophone payload. The MK84 MOD 2 Band K range pulse is approximately 45 ms long, encoding 4-bits which is comparable to the 50 baud 150 ms symbol encoding 8-bits. Intermittent MK84 signal tracking was achieved up to range $R_S \approx 10$ km. A SSQ53F hydrophone was deployed at a depth of $R_H \approx 30$ m to record bi-direction MCDSSS communication and measured an ambient noise equivalent to $SS3$ to $SS3.5$.

L.3 GPM300 Through Hull Communication Functional Test

A through hull super structure communication functional test (Figure 198) was carried out on the GPM300/IRIDIUM buoy and the RV Whale Song moon pool retracted GPM300, located 5 m below the deck (Figure 206). The RV Whale Song GPM300 transmit source level of SPL_{TX} = 170 dB re 1 µPa @ 1 m, required 3 W transmit power to provide sufficient SNR_{RX} for a reliable through vessel hull communication link (Refer to through vessel hull super structure communication video "**GPM300 through Hull Communication 5 June 2014.mp4**").

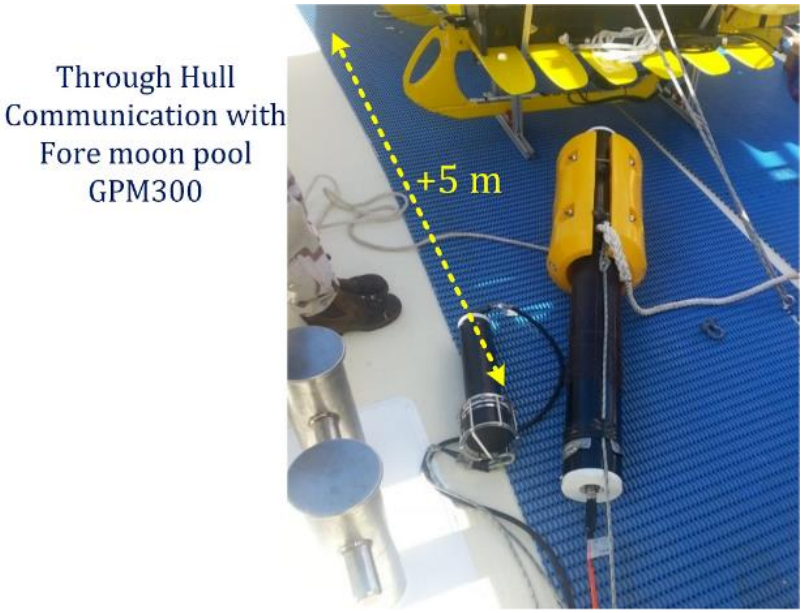

Figure 198 GPM300 through vessel hull super structure communication deck test

L.4 GPM300/IRIDIUM Buoy Deployment

The GPM300/IRIDIUM buoy was deployed in $R_D > 60$ m water depth, 150 m riser rope, 80 kg clump weight, pickup buoy and GPM300 $R_H = 6$ m depth. The GPM300 transmit source level was set to $SPL_{TX} = 186$ dB re 1 µPa @ 1 m requiring 100 W transmit power. The GPM300/IRIDIUM buoy measured an ambient noise $SS3 \rightarrow SS4$.

L.5 Environmental Conditions

L.5.1 Ambient Noise

1. $PSD_A =$ 55 dB to 65 dB re 1 µPa/$\sqrt{\text{Hz}}$ @ 1 m equivalent to $SS3 \rightarrow SS4$.
2. RV Whale Song engines idling when holding station (Figure 199). $PSD_A =$ 60 dB to 70 dB re 1 µPa/$\sqrt{\text{Hz}}$ @ 1 m equivalent to $SS3.5$ to $SS5$ (equivalent to 50 kn wind).

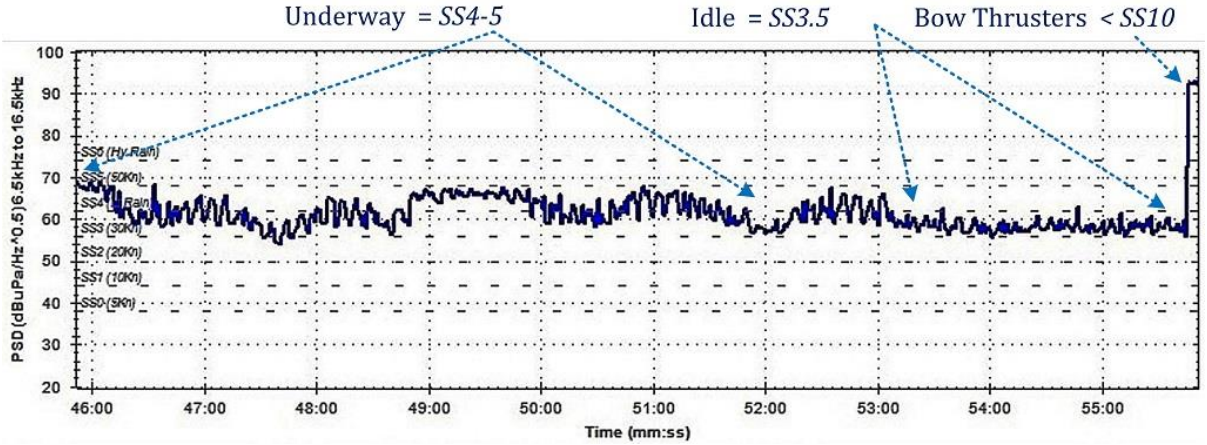

Figure 199 RV Whale Song engines idling and bow thruster (L3 TWC mail client)

L.5.2 RV Whale Song Bow Thruster Noise

The ambient noise was dominated by the RV Whale Song's engine noise which was louder than temperate water off shore snapping shrimp noise levels in up to $R_D \approx 60$ m:

1. Bow thruster noise greater than $PSD_A >$ 90 dB re 1 µPa/$\sqrt{\text{Hz}}$ @ 1 m $> PSD_{SS11}$.
2. Bow thruster noise saturates the GPM300 analog front end.

L.5.3 Sound Velocity Profile

Figure 19 and Figure 200 illustrate the favourable sound velocity profile and multipath ray trace as measured on the 5 June 2014, 30 km west of Fremantle. Acoustic signal attenuation due to sound velocity refraction was moderate.

GPM300/IRIDIUM Buoy deployment:

1. GPM300 deployment depth $R_H = 6$ m.
2. Multipath ray trace well behaved with no big shadow zones or caustics and $R_H =$ 0 m to 2 m surface mixing layer.
3. GPM300 deployed below surface mixing layer $R_D =$ 40 m to 70 m.
4. Southern flowing Leeuwin Current $R_D \approx$ 66 m to 70 m bottom as measured by depth sounder.

RV Whale Song GPM300 deployment:

1. GPM300 deployment depth $R_H =$ 2 m to 3 m.
2. Multipath ray trace (Figure 200) well behaved with no significant shadow zones or caustics 0 m to 2 m

3. GPM300 deployed just below surface mixing layer at $R_D \approx 60$ m.

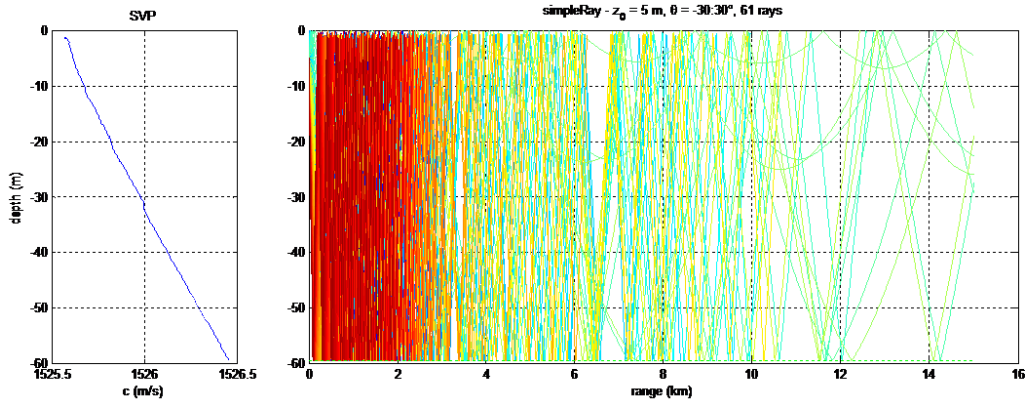

Figure 200 Sound velocity profile / multipath ray trace south of GPM300 buoy

L.6 15 km Maximum Range Sea Trial Measurements

L.6.1 Multipath Interference (In-band)

Figure 201 illustrates the spectrogram of the GPM300 in-band multipath interference as measured by the L3 Oceania PASOR Sonobuoy tracking system using a SSQ53F GPS Sonobuoy drifting south from the GPM300/IRIDIUM Buoy deployment location. Inter symbol interference is a significant problem when operating in depths less than $R_D <$ 200 m. In the absence of multipath interference, the in-band spectrogram should be a uniform white rectangle. The leading 2×80 ms telemetry alert signal and 2.5 s, 50 baud signals are subject to temporal and frequency dependent in-band constructive and destructive interference as illustrated by the spectrogram in-band white stripes.

The MCDSSS receiver, with continuous channel equalisation and inter-symbol tracking, exhibits superior multipath resistance compared to conventional CW, FSK or PSK modems and MK84 MOD2 DSSS signalling.

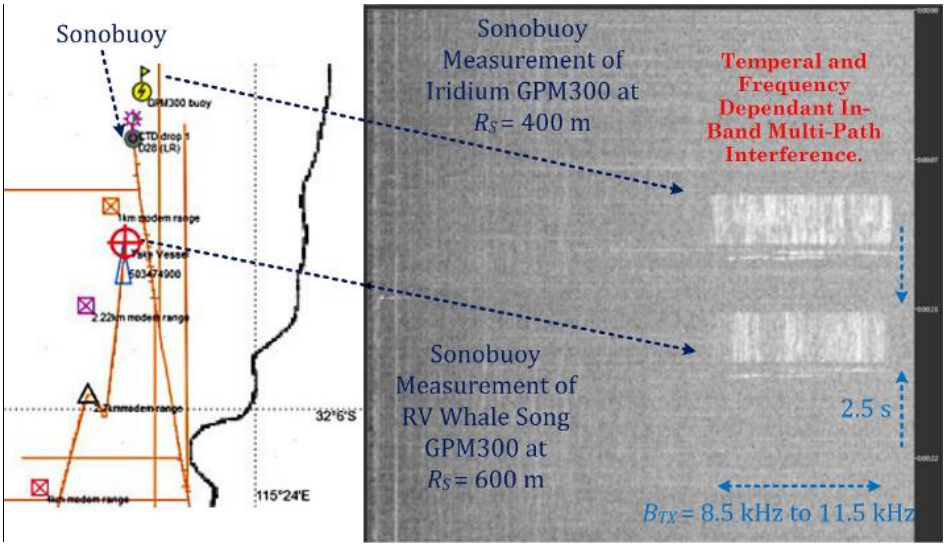

Figure 201 Spectrogram of in-band multipath interference (L3 Oceania PASOR)

L.6.2 Covert 50 Baud Communication

Figure 202 illustrates the spectrogram at $R_S \approx 11$ km range with a transmit source level of $SPL_{TX} = 186$ dB re 1 µPa @ 1 m requiring 100 W transmit power. The spectrogram displays the GPM300 IRIDIUM buoy MCDSSS transmit signal as a non covert (i.e. Sonobuoy is inside the GPM300 IRIDIUM buoy covert spheroid blue zone). The sonobuoy located near the GPM300 IRIDIUM buoy displays the RV Whale Song MCDSSS transmit signal disappearing into the ocean ambient noise floor (i.e. Sonobuoy is drifting into RV Whale Song's covert spheroid green zone).

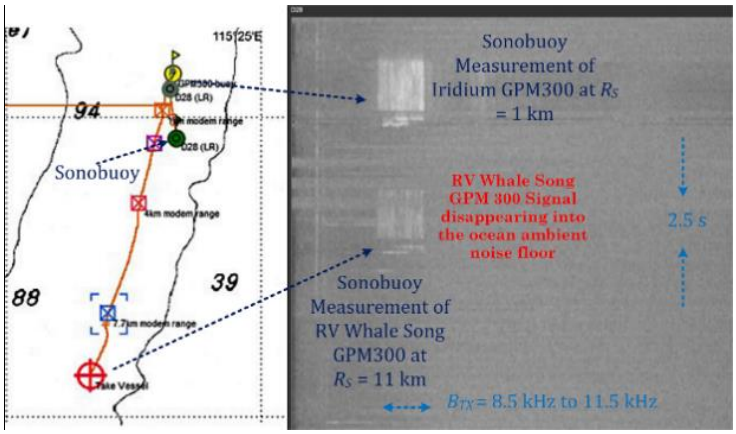

Figure 202 In-band spectrogram at 11 km (L3 Oceania PASOR)

Figure 203 illustrates the spectrogram at $R_S \approx 4$ km range with a transmit source level of $SPL_{TX} = 165$ dB re 1 µPa @ 1 m requiring 1 W transmitter power and providing 100% communication reliability. The spectrogram displays the GPM300/IRIDIUM buoy MCDSSS signal and is not a covert signal when Sonobuoy is inside the GPM300 IRIDIUM buoy covert spheroid blue zone. The sonobuoy located near the GPM300/IRIDIUM buoy does not display a visible spectrogram signal of the RV Whale Song MCDSSS transmit signal as it is below the ocean ambient noise floor (i.e. Sonobuoy is inside RV Whale Song's covert spheroid green zone).

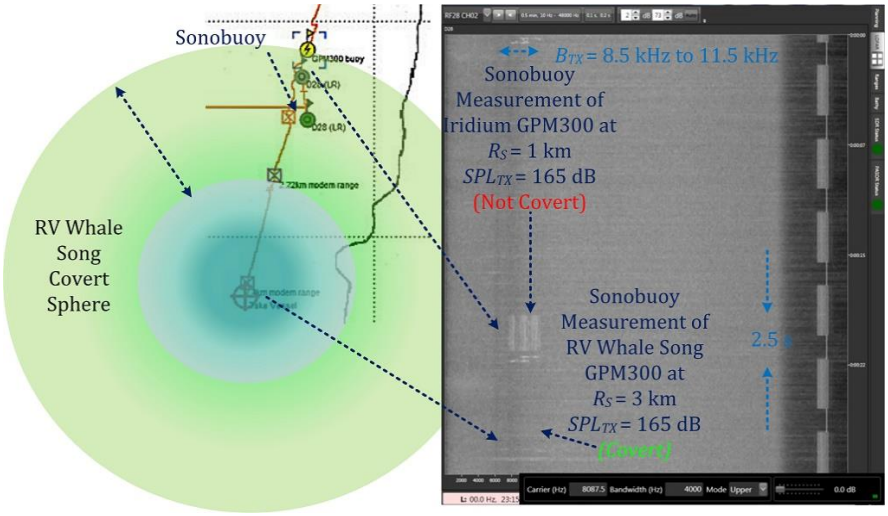

Figure 203 In-band spectrogram at 4 km (L3 Oceania PASOR)

L.6.3 Tracking South with GPM300 Deployed (Slant range)

Figure 204 illustrates the GPM300 deployed through RV Whale Song port side moon pool. The RV Whale Song moon pool hydraulic ram does not have sufficient travel for the GPM300 transducer to clear the keel. Long-range slant range communication may not be available if the remote GPM300 is on the starboard side of RV Whale Song. During waypoint stops the 4 m to 5 m swell rolled RV Whale Song and the keel would occasionally obstruct slant range communication.

Figure 204 GPM300 deployed through RV Whale Song moon pool

L.6.4 Underway at 5.5 Knots

Intermittent through prop wash communication was established with GPM300/IRIDIUM Buoy while RV Whale Song was tracking away from the GPM300 Buoy at v = 5.5 kn. The RV Whale Song superstructure and prop wash obstructs slant range communication (Figure 205).

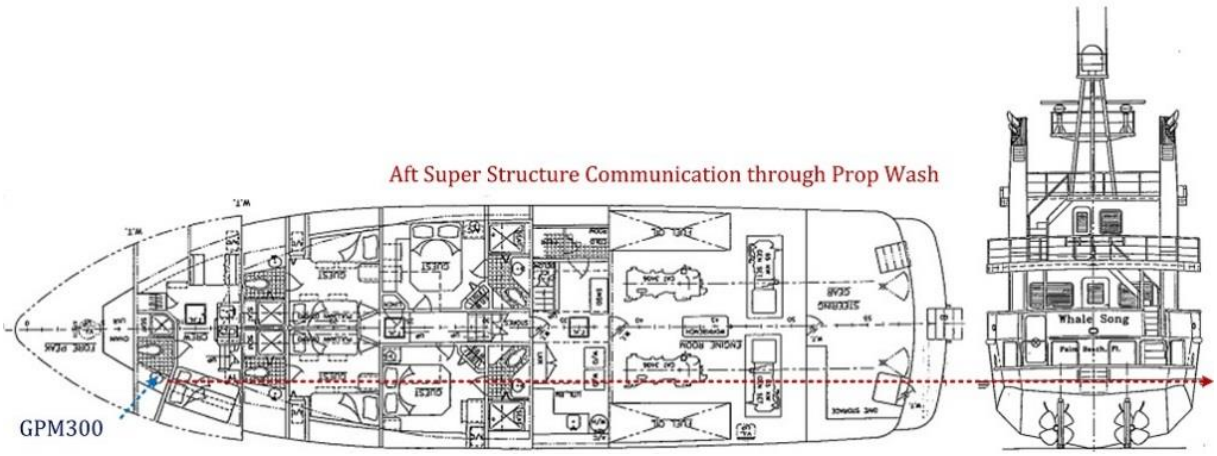

Figure 205 RV Whale Song aft hydro-acoustic communication

L.6.5 Tracking North with GPM300 Retracted (Through Hull)

Figure 206 illustrates the GPM300 retracted up into RV Whale Song port moon pool. The end of the GPM300 transducer boot is level with the top of the moon pool opening. The GPM300 acoustic energy is radiated down using cavity resonance mode and is in excess of 10 dB quieter than broad side acoustic energy radiation.

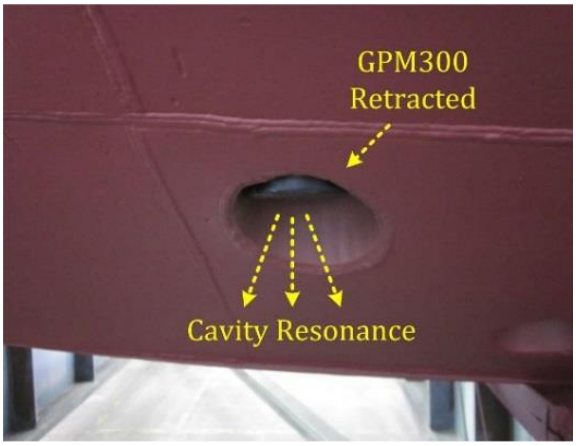

Figure 206 GPM300 retracted inside RV Whale Song moon pool

Figure 207 illustrates the $R_S \approx 3$ km maximum communication distance for RV Whale Song with the GPM300 retracted into the moon pool and with a measured $SS6$ ambient noise and $A_{TX} = 4$ dB $\equiv$ 186 dB re 1 µPa @ 1 m transmit source level attenuation. The maximum communication range coincides with a total transmit source level attenuation of $A_{TX} = 30$ dB $\equiv$ 160 dB re 1 µPa @ 1 m. This measurement suggests that the through vessel hull attenuation, bow wave attenuation and bow thrusters cavity turbulence attenuation contributes an additional 30 dB → 40 dB acoustic signal attenuation.

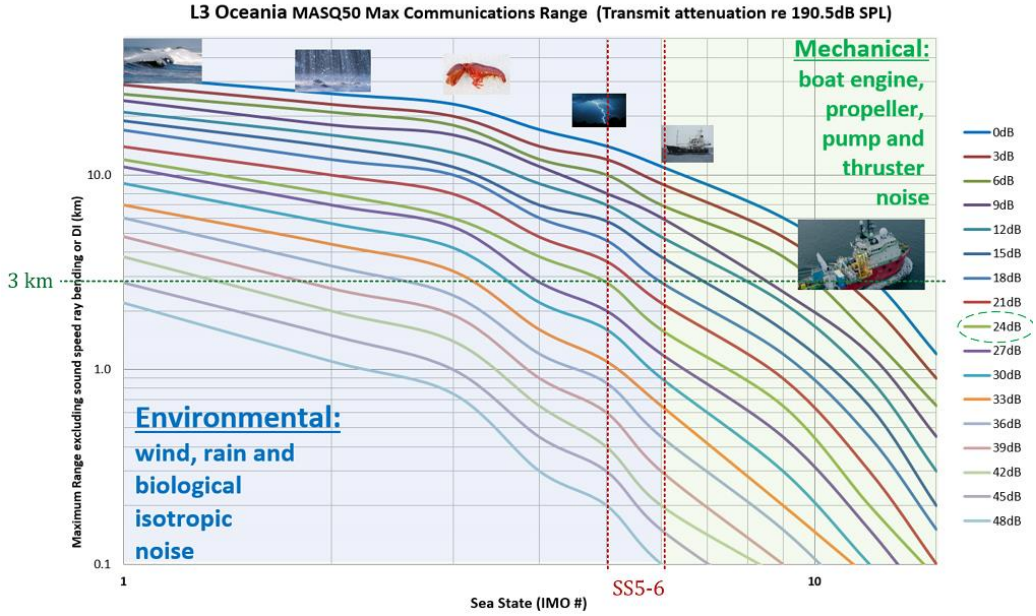

Figure 207 MCDSSS 50 baud maximum communication range (through vessel hull)

L.6.6 Under way Through Hull Communication (GPM300 Retracted)

Figure 208 illustrates the RV Whale Song underway at v = 9.5 kn. The bow wave, bow thrusters and service cavities generate large high ambient noise which reduced the GPM300 receive sensitivity. Reliable underway communication between the RV Whale Song retracted GPM300 and the GPM300/IRIDIUM Buoy was established at a range of less than $R_S < 1$ km while underway.

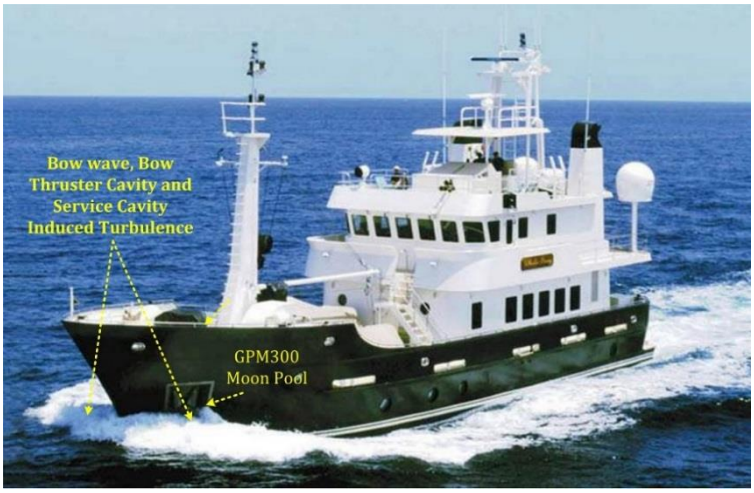

Figure 208 RV Whale Song underway at 9.5 kn

L.7 Summary

Communication was established through the vessel hull and through the bow turbulence which was an unexpected and counter intuitive result. The estimated hull attenuation of +30 dB highlights the robustness of MCDSSS signalling. Figure 209 illustrates the minimum transmit source level required to establish reliable communication at various way points. The measured maximum communication matches the predicted performance to within a few dB.

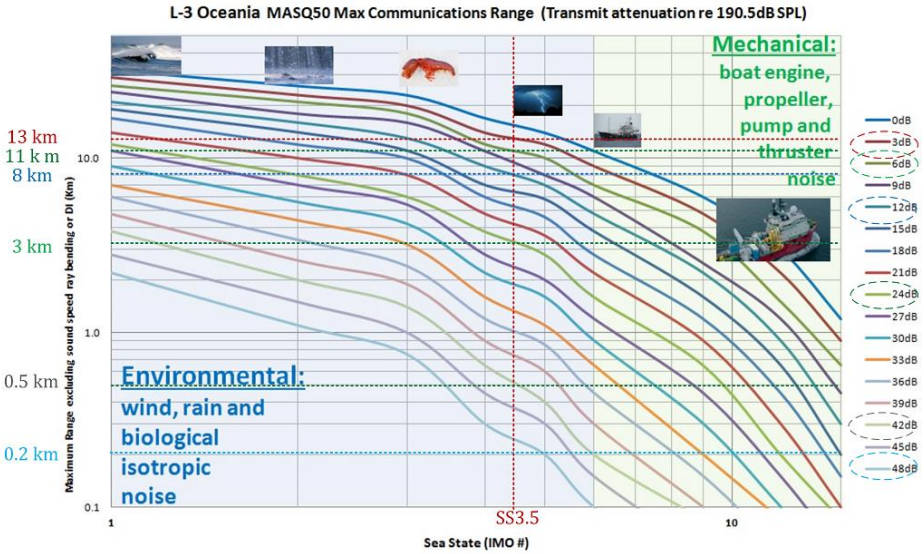

Figure 209 50 baud maximum communication range (slant range)

The L3 Oceania 15 km range hydro-acoustic database was mined to identify failing MCDSSS signals. Figure 210 illustrates the time domain (top green) and spectrogram (bottom orange) recordings of a Sonobuoy recording of the RV Whale Song GPM300 and Iridium Buoy GPM300 bi-directional traffic from 100 m to 15 km. Sonobuoy VHF reception starts to fade beyond a range of $R_S > 10$ km as the sonobuoy antenna drops below the horizon between ocean wave crests (Figure 210 top vertical green lines).

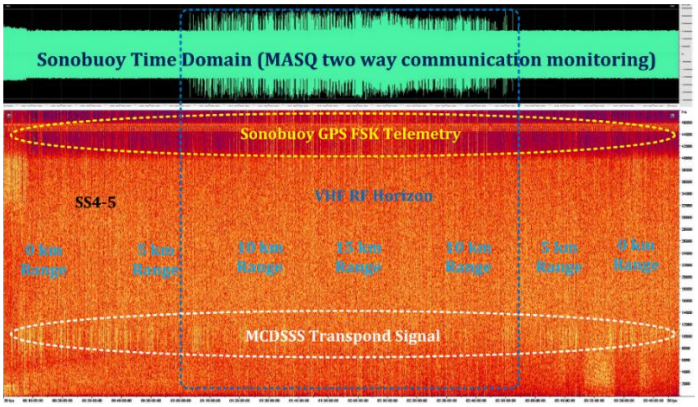

Figure 210 Sonobuoy MCDSSS two way communication monitoring

Figure 211 illustrates the spectrogram of a MCDSSS transpond message (horizontal yellow rectangle) and the VHF RF reception drop outs (vertical orange bands). The intermittent VHF reception for sonobuoy range greater than $R_S > 10$ km provides a robust stress test for the MASQ forward error correction when the RF drop output interference is less than 20%. The Fremantle 30 km west multipath reverberation envelope period was measured a greater than $\tau_{MPE} > 10$ ms and the typical number of multipath signals greater than $N_M > 4$ (Figure 212). The magnitude of almost $\frac{1}{3}$ of the slant range signals (R_S) are less than the first (R_{M1}) or second (R_{M2}) multipath signals.

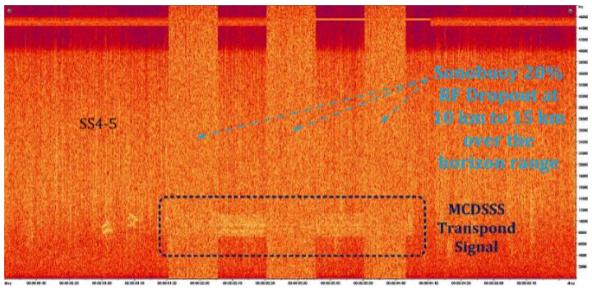

Figure 211 Sonobuoy 20% RF dropout at 10 km to 15 km over the horizon range

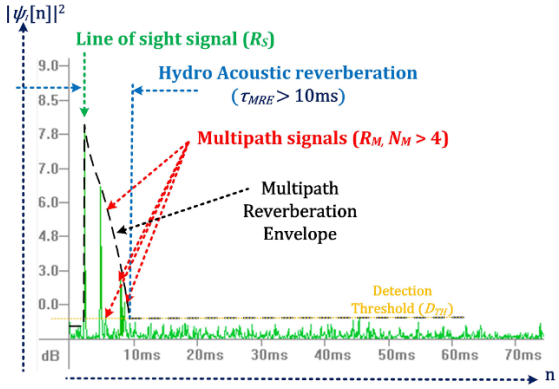

Figure 212 Rottnest Island 20 km SW +10 ms multipath

Figure 120 illustrated the measured improvement in message reliability versus GPM300 firmware version. Post processed sea trial recordings message reliability increased from 92% to > 99% using firmware version 6.0 which implements the extreme multipath tracking algorithms (Figure 81 to Figure 91) and FEC algorithm optimisations Figure 103 to Figure 102.

Appendix M 3.4/9.7 km Range *SS2* 130 m Depth BEE Measurements

M.1 Introduction

On 17th March 2017 a MCDSSS Bit Error Efficiency measurement was conducted ≈ 50 km west of the Australian coast (Figure 226 left) in R_D ≈ 130 m ≅ 90 ms @ 1,500 ms^{-1} depth with the sonobuoy hydrophone deployed R_H = 30 m below the surface. MASQ messages were transmitted from the RV Whale Song at 152.5 to 172.5 dB re 1 µPa @ 1 m source level in 3 dB steps using 100/150/200/350/500 baud. Two sonobuoys were deployed at a range of R_S = 3.4 km and R_S = 9.7 km and measured an ambient noise equivalent to *SS2* (Figure 226 centre right).

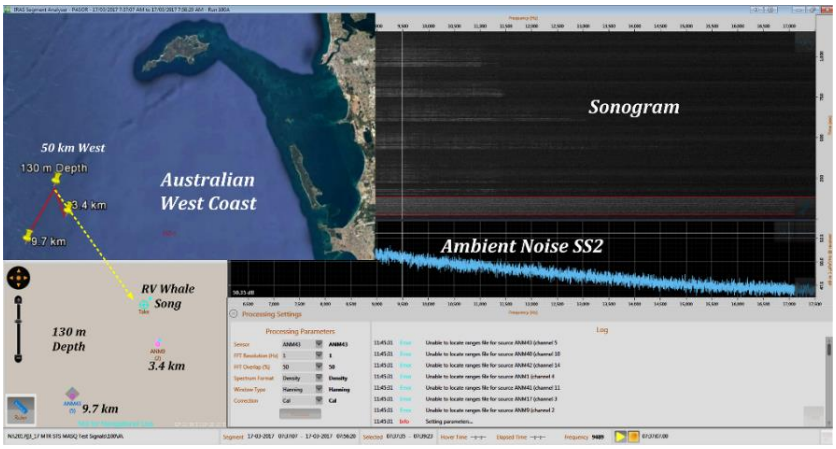

Figure 213 Australian coast, 50 km west (3.4 km / 9.7 km deployment and ambient)

M.2 Sound Velocity Profile

Figure 214 illustrates the measured transmission loss characterised by a uniform sound velocity profile.

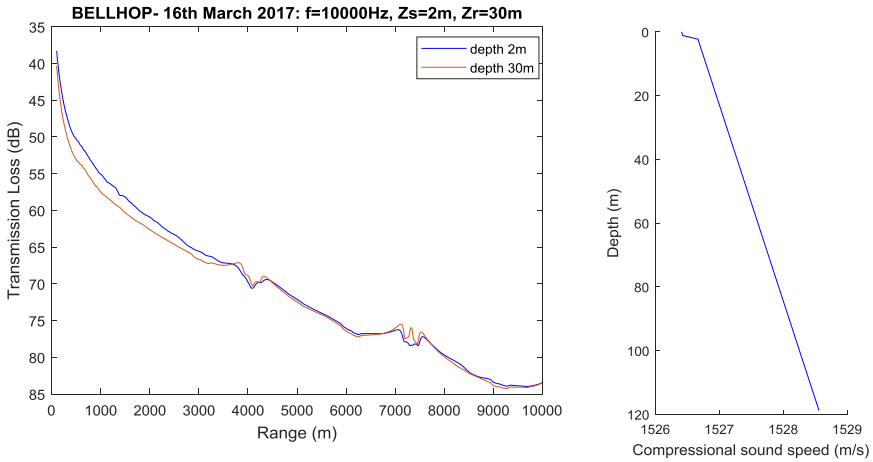

Figure 214 Transmision loss and sound velocity profile for 130 m water depth

Figure 215 illustrates the path loss characterised by a surface ducting channel approximately 10 m below the surface.

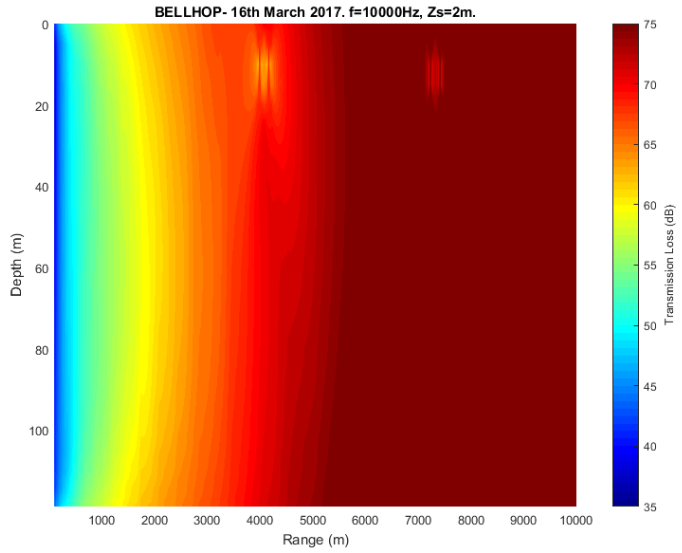

Figure 215 Australian coast, 50 km west (propigation loss)

M.3 Deployment Multipath Characteristics

The $R_S = 3.4$ km range communication link was characterised by a strong slant range signal followed by a surface ducting signal ($R_T \approx 9$ m $\cong 6$ ms @ 1,500 ms^{-1}) and a weak multipath signal ($R_M \approx 20$ m $\cong 14$ ms @ 1,500 ms^{-1}) (Figure 216).

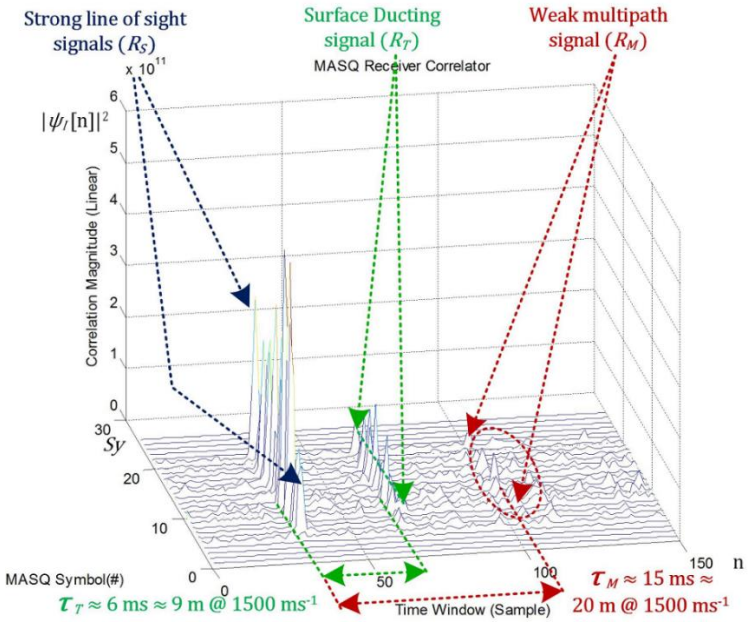

Figure 216 Australian coast, 50 km west (3.4 km range, 200 baud multipath)

The $R_S = 9.7$ km communication link was characterised by a faint bottom ducting signal ($R_B \approx 6$ m $\cong 4$ ms @ 1,500 ms^{-1}), weak slant range signal, strong surface ducting signal ($R_T \approx 2$ m $\cong 1$ ms @ 1,500 ms^{-1}) and a weak multipath signals ($R_M \approx 3 \rightarrow 15$ m $\cong 5$ ms $\rightarrow$ 20 ms @ 1,500 ms^{-1}) (Figure 217). The ($R_D = 130$ m $\cong 87$ ms @ 1,500 ms^{-1}) ocean depth bottom bounce multipath signal is not a significant contributor to inter symbol interference at 200 baud ($\tau_{SY} = 160$ ms).

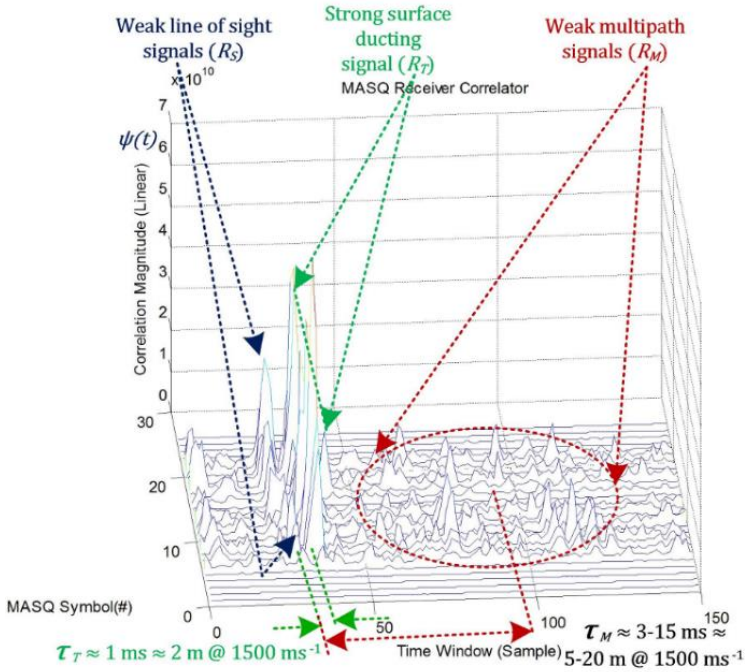

Figure 217 Australian coast, 50 km west (9.7 km range, 200 baud multipath)

M.4 Minimum Transmit Sound Pressure Level

The minimum test transmit source level of 155 dB re 1 µPa @ 1 m requiring 100 mW transmit power was too loud to measure hydro-acoustic baud rate minimum source level at $R_S \approx 3.4$ km. At a range of $R_S \approx 9.7$ km the hydro-acoustic baud rate minimum source level was measured at $SPL_{MIN} = 161.5$ dB re 1 µPa @ 1 m $\pm$ 1.5 dB (requiring 400 mW transmit power) and the maximum hydro-acoustic baud rate was $Br_{MAX} = 500$ baud with intermittent telemetry alert detection (Figure 130) which is consistent with a $L_S \approx 15\log_{10}(R_S)$ propagation model approaching cylindrical spreading Eq.(7-25).

$$\begin{gathered} PSD_A = 50 \text{ dB} \pm 5 \text{ dB re 1 µPa}/\sqrt{\text{Hz}} \text{ @ 1 m} \equiv SS2 \\ L_T \approx 15\log_{10}(9{,}700 \text{ m}) + 1 \text{ dB/km} \times 9.7 \text{ km} \approx 69 \text{ dB} \\ PSD_{TX} = PSD_A + L_T \approx 50 + 69 \approx 119 \text{ dB re 1 µPa}/\sqrt{\text{Hz}} \text{ @ 1 m} \\ B_{TX} = 10 \text{ kHz} \equiv 40 \text{ dB re 1 Hz for MCDSSS 500 baud} \\ SPL_{TX} = PSD_{TX} + B_{TX} \approx 119 + 40 \approx 160 \text{ dB re 1 µPa @ 1 m} \end{gathered} \tag{7-23}$$

M.5 Bit Energy Efficiency (Australian coast 50 km west)

At a range of $R_S \approx 9.7$ km the maximum bit energy efficiency peaked at $Br_{BEE} = 350$ baud and was measured at BEE $\approx 10^4 \pm 3$ dB @ 1 km re $SS2$ or BEE $\approx 10^5 \pm 3$ dB @ 1 km re $SS0$ when corrected for sea state (Figure 218).

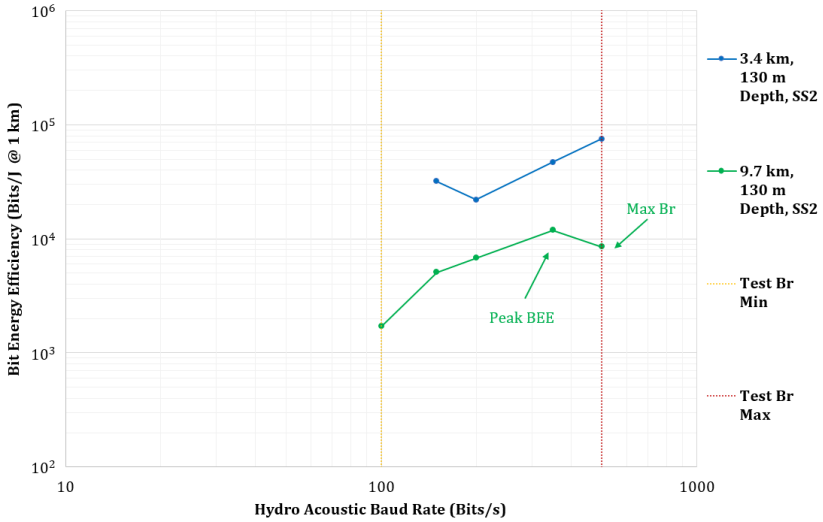

Figure 218 Australian coast, 50 km west (bit energy efficiency)

M.6 Multipath Reverberation Envelope Versus Hydro-acoustic Baud Rate

Figure 219 illustrates the $R_S \approx 3.4$ km multipath reverberation envelope (τ_{MRE}) versus MCDSSS hydro-acoustic baud rate. Maximum BEE peaks when the reliable communication is established using the highest hydro-acoustic baud rate $Br_{BEE} = 350$ baud with the lowest transmit source level $SPL_{MIN} \approx 155$ dB ± 3 dB re 1 µPa @ 1 m and where the multipath signals are quiet enough to be masked by the ambient noise $PSD_A \approx SS2$.

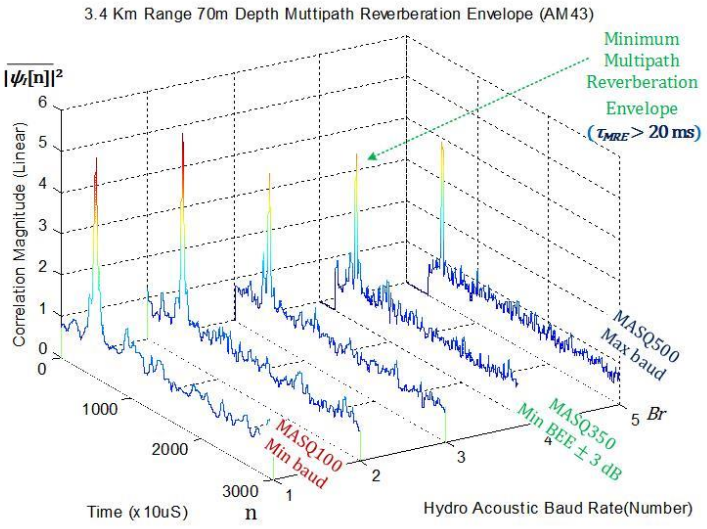

Figure 219 Australian coast, 50 km west (3.4 km range minimum bit energy efficiency)

M.7 Summary

At a range of $R_S = 9.7$ km the peak BEE $\approx 10^4 \pm 3$ dB @ 1 km re $SS2$ occurred at $Br_{BEE} = 350$ baud before the maximum $Br_{MAX} = 500$ baud hydro-acoustic baud rate. The multipath reverberation period limited maximum 500 baud hydro-acoustic baud rate was independent of transmit source level and receive margin. The covert bit error rate was approximately BER $\approx 10^2$ and remained constant as a function of range, hydro-acoustic baud rate and transmit source level.

Appendix N 3.1-9.1 km Range *SS2* 1.5 km Depth BEE Measurements

N.1 Introduction

On 11th April 2017 a MCDSSS bit error efficiency measurement was conducted +100 km west of the Australian coast Figure 220 in $R_D \approx 1.5$ km $\cong 1$ s @ 1,500 ms^{-1} depth water with the sonobuoy hydrophones deployed $R_H = 30$ m below the surface. MASQ messages were transmitted from RV Whale Song $R_H = 0.5$ m depth GPM300 using 152.5 to 172.5 dB re 1 µPa @ 1 m source level in 3 dB steps using 100/150/200/350/500 baud. Eight sonobuoys were deployed at a range of $R_S \approx 3.1$ km to $R_S \approx 9.8$ km and measured an ambient noise equivalent to $PSD_A \approx SS2$.

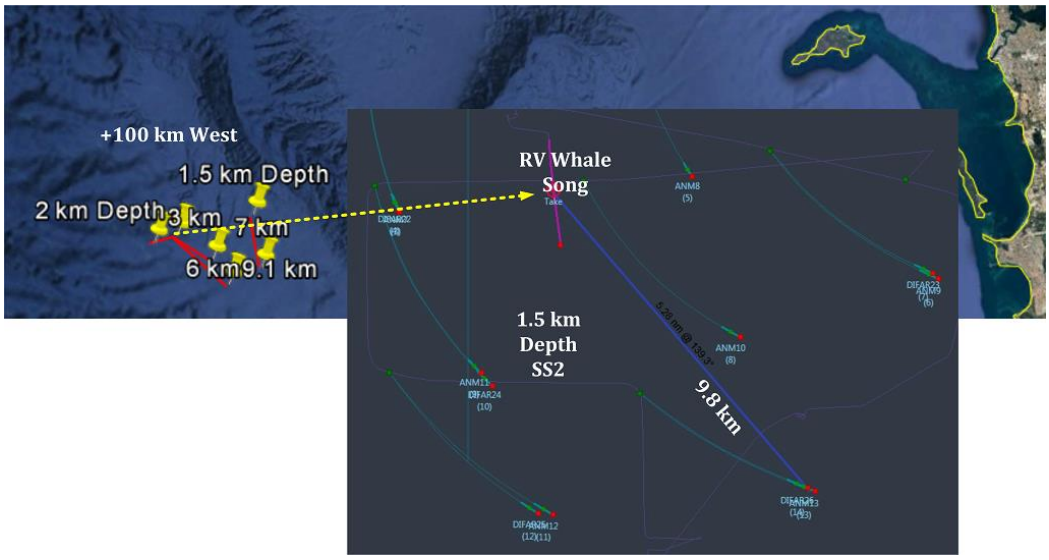

Figure 220 Australian coast, 50 km west (3.1 km to 9.8 km range deployment)

N.2 Sound Velocity Profile

Figure 221 illustrates the measured transmission loss characterised by a uniform sound velocity profile for the first 70 m below the surface.

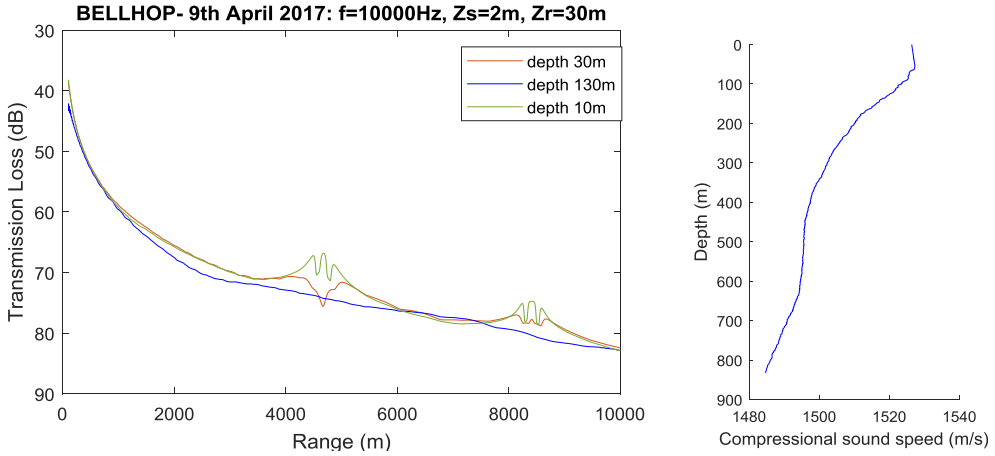

Figure 221 Australian coast, 50 km west (transmision loss and sound velocity profile)

Figure 222 illustrates the path loss characterised by a surface ducting channel approximately 20 m below the surface.

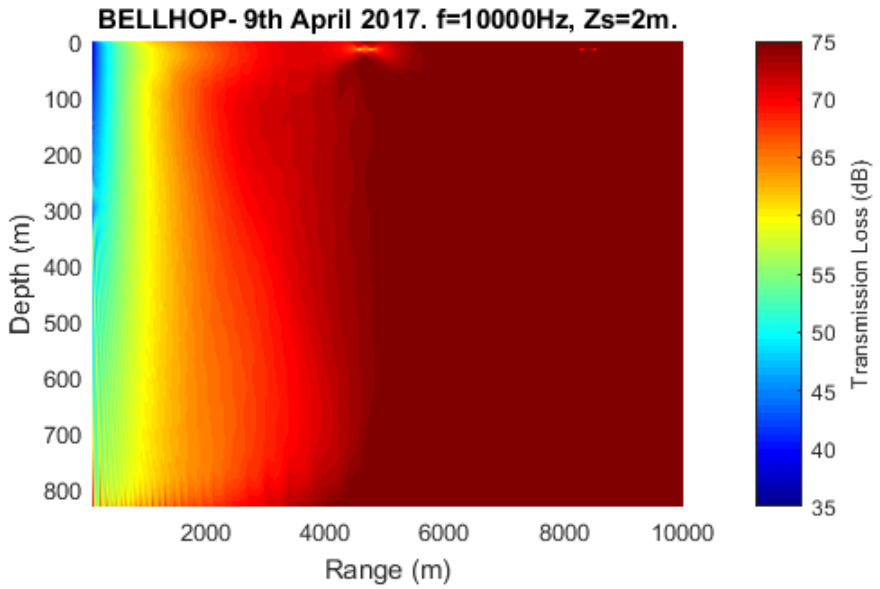

Figure 222 Australian coast, 50 km west (proppigation loss)

N.3 Channel Multipath Characteristics

The $R_S = 9.1$ km communication channel was characterised by a strong slant range signal (R_S), very weak intermittent surface ducting signal ($R_T \approx 2$ m $\cong 1$ ms @ 1,500 ms^{-1}) (Figure 223). The $R_D = 1.5$ km to 2.0 km $\cong 1$ s to 1.3 s @ 1,500 ms^{-1} ocean depth bottom bounce multipath signal does not contribute to the in-band interference.

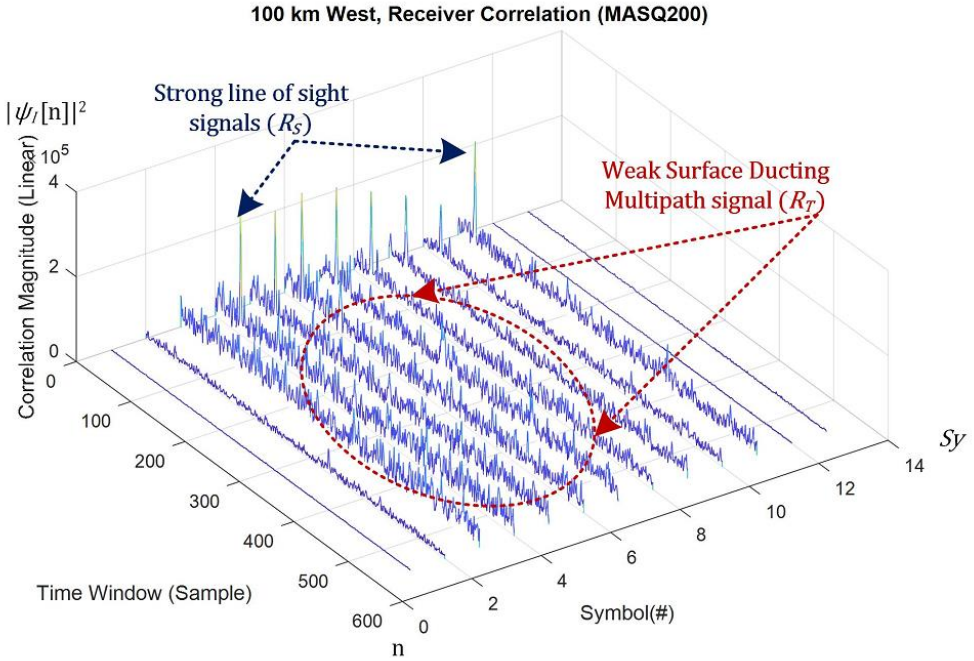

Figure 223 Australian coast, 100 km west (9.1 km range, 200 baud multipath)

N.4 Minimum Transmit Sound Pressure Level

The minimum test transmit source level of 155 dB re 1 µPa @ 1 m was too loud to measure hydro-acoustic baud rate minimum source level at $R_S \approx 3.1$ km. At a range of $R_S \approx 9.1$ km the hydro-acoustic baud rate minimum source level was measured at 173.5 dB re 1 µPa @ 1 m $\pm$ 1.5 dB (requiring 6 W transmit power) and the maximum hydro-acoustic baud rate was $Br_{MAX} = 500$ baud (Chapter 6.5 Figure 129) which is consistent with a $L_S = 20\log_{10}(R_S)$ spherical propagation model Eq.(7-25).

$$
\begin{aligned}
PSD_A &= 50 \text{ dB} \pm 5 \text{ dB re 1 µPa}/\sqrt{\text{Hz}} \text{ @ 1 m} \equiv SS2 \\
L_T &= 20\log_{10}(9{,}100 \text{ m}) + 1 \text{ dB/km} \times 9.1 \text{ km} \approx 88 \text{ dB} \\
PSD_{TX} &= PSD_A + L_T \approx 50 + 88 \approx 138 \text{ dB re 1 µPa}/\sqrt{\text{Hz}} \text{ @ 1 m} \\
B_{TX} &= 10 \text{ kHz} \equiv 40 \text{ dB re 1 Hz for MCDSSS 500 baud} \\
SPL_{TX} &= PSD_{TX} + B_{TX} \approx 138 + 40 \approx 178 \text{ dB re 1 µPa @ 1 m}
\end{aligned}
\tag{7-24}
$$

N.5 Bit Energy Efficiency Versus Hydro-acoustic Baud Rate

At a range of $R_S \approx 3.1$ km the maximum bit energy efficiency peaked at $Br_{MAX} = 500$ baud and was measured at BEE $\approx 10^4 \pm 3$ dB @ 1 km re $SS2$. At a range of $R_S \approx 9.1$ km the maximum bit energy peaked occurred at $Br_{BEE} = 150$ baud and was measured at BEE $\approx 10^4 \pm 3$ dB @ 1 km (Figure 224).

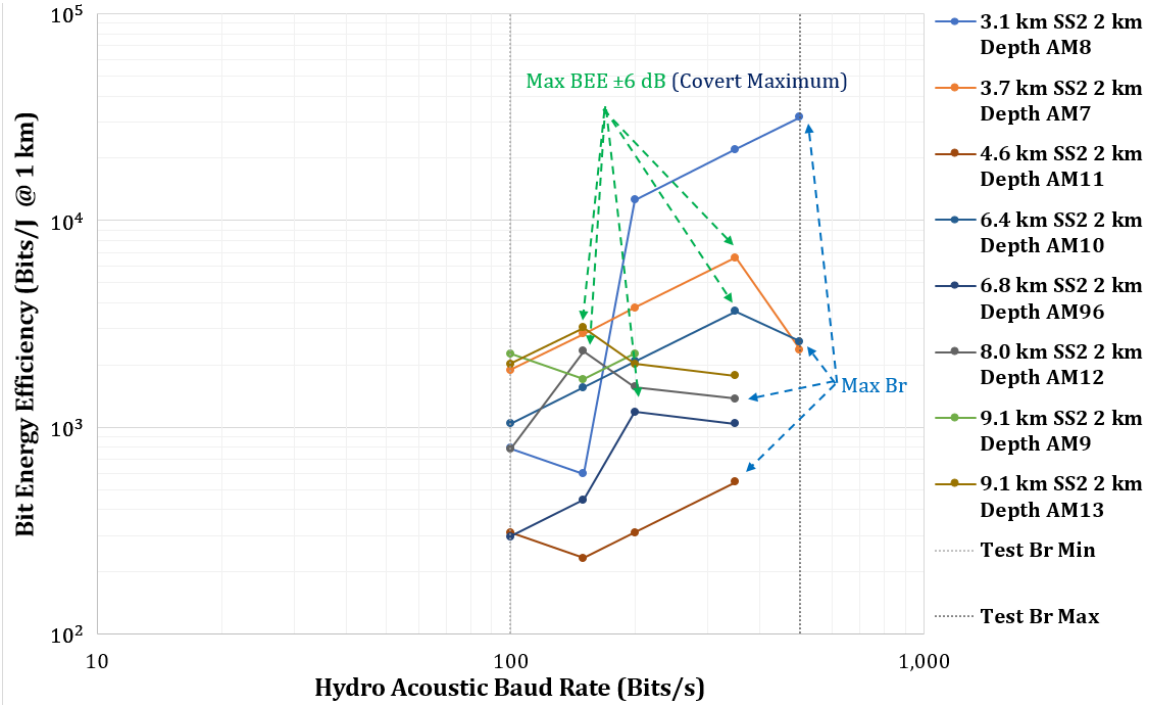

Figure 224 BEE versus hydro-acoustic baud Rate 3.1 km to 9.1 km, 2 km depth, *SS*2

N.6 Multipath Reverberation Envelope Versus Hydro-acoustic Baud Rate

Figure 225 illustrates sonobuoy AM13 $R_S \approx 9.1$ km multipath reverberation envelope (τ_{MRE}) versus MCDSSS hydro-acoustic baud rate. Maximum BEE occurs when the

reliable communication is established using highest hydro-acoustic baud rate $Br_{BEE} = 150$ baud with the lowest transmit source level $SPL_{MIN} \approx 173.5$ dB ± 3 dB re 1 µPa @ 1 m and where the multipath signals a quiet enough to be masked by the ambient noise $PSD_A \approx SS2$.

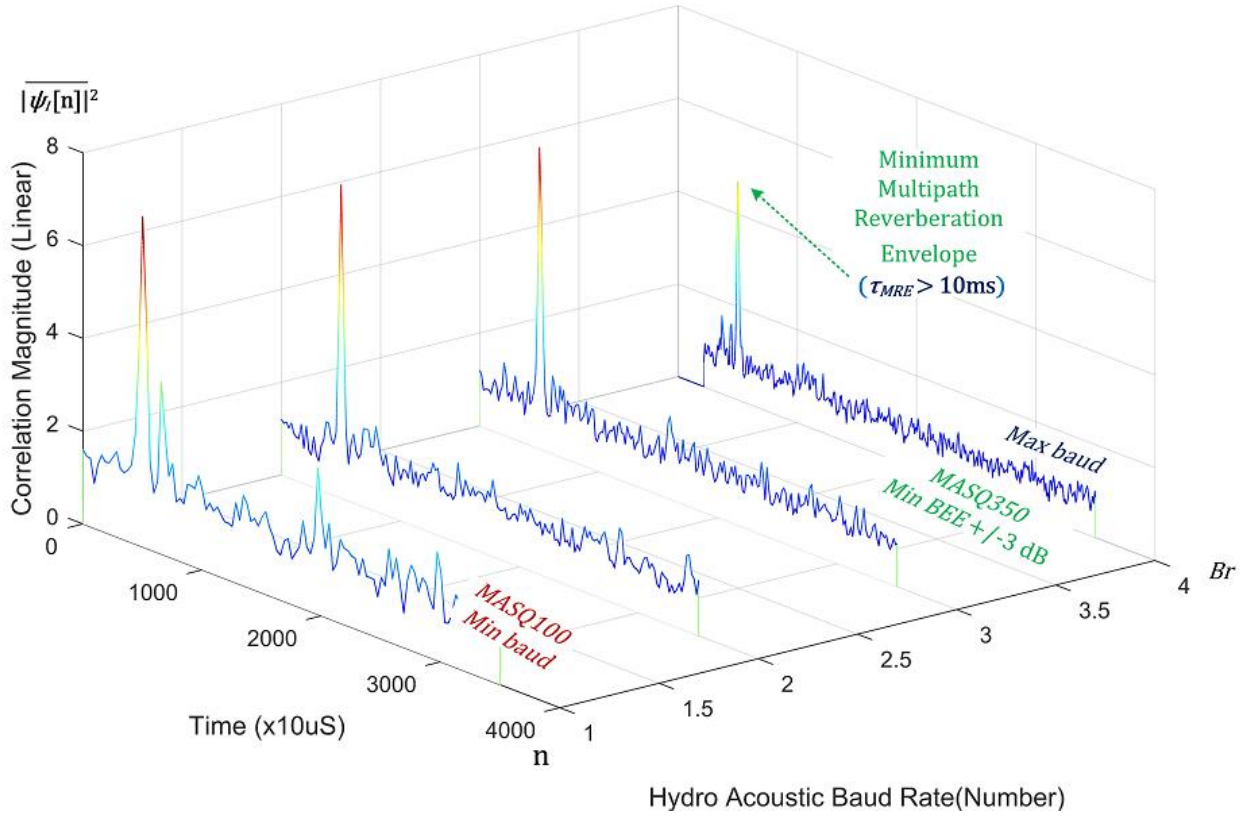

Figure 225 MPE 9.1 km range, 30 m hydrophone 2 m projector depth, *SS*2, (AM13)

N.7 Summary

At a range of $R_S = 3.7$ km the peak BEE $\approx 10^3 \pm 3$ dB @ 1 km re $SS2 \cong 10^5 \pm 3$ dB @ 1 km re $SS0$ occurred at 500 baud however the test transmit source level was too low to measure the peak BEE at $SS2$. At a range of $R_S = 9.1$ km the peak BEE $\approx 5 \times 10^2 \pm 3$ dB @ 1 km re $SS2 \cong 5 \times 10^3 \pm 3$ dB @ 1 km re $SS0$ occurred at $Br_{BEE} = 150$ baud before the maximum $Br_{MAX} = 500$ baud hydro-acoustic baud rate. The peak BEE was dominated by the frequency dependent environmental absorption where communications is more energy efficient to lower the baud rate and carrier frequency. The shallow projector $R_H = 0.5$ m and hydrophone $R_H = 30$ m deployment depths induced weak surface ducting multipath ($R_M = 0.5 \rightarrow 30$ m) reverberation period limited the peak BEE hydro-acoustic baud rate $Br_{BEE} = 150$ baud and was independent of transmit source level and receive margin. The equivalent $R_D = 130$ m shallow water $R_S = 9.7$ km measurement yielded a peak BEE at $Br_{BEE} = 350$ baud highlighting that multipath deconvolution improves MCDSSS shallow water covert performance.

Appendix O 2 km Range *SS4* 500/1,000 Baud Measurements

O.1 Introduction

This chapter reprocesses historical sea trial data to provide lower side band (LSB) interference, 1,000 baud, $SS13$, TCP/IP acoustic handshake protocol and performance baseline measurements required for message reliability improvement validation. Figure 226 illustrates the L3 Oceania Acoustic Underwater Surveillance Network AUSSNet [150] deployment which consists of three hydrophone arrays separated by a 2 km baseline from a surface GPM300/IRIDIUM gateway buoy. The hydrophone array data are pre-processed by the sensor nodes and transferred to the gateway via GPM300 modems at a hydro-acoustic baud rate of 1,000 baud. The gateway beamformed the sensor array data is uplinked to the user via the IRIDIUM satellite network. The remote users control the gateway and sensor nodes via the GPM300 acoustic and satellite network. The gateway and sensor nodes are tested and configured during deployment using a GPM300 deployed over the side of MV Sea Lion at $R_S \approx 500$ m, $R_H < 3$ m using 500 baud.

The L3 Oceania AUSSNet Deployment validates the 500 baud and 1,000 baud performance in $+SS4$ and shallow water multipath ($N_M > 3$), inter-symbol interference, multi-node network routing algorithm, and the LSB acoustic pollution filtering measured at greater than 60 dB/decade. Reliable communication was established for 1,000 baud in $SS3 \rightarrow SS4$ at a range of $R_S \approx 2$ km and 500 baud in $SS13$ at range of $R_S \approx 500$ m.

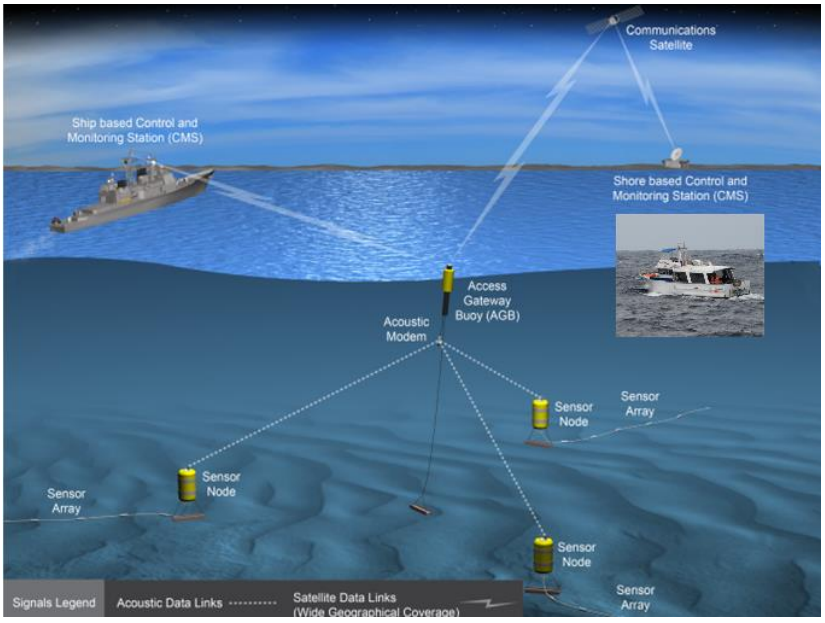

Figure 226 L3 Oceania AUSSNet

O.2 GPM300 TD10 Transducer Spectral Purity (1,000 Baud)

Figure 228 illustrates the GPM300 TD10 transducer spectral purity for 1,000 baud AUSSNet which has a lower side band spectral pollution requirement for acoustic interference to be lower than the ambient noise for frequencies less than 1 kHz (i.e. less than $PSD_A = 60$ dB re 1 μPa/$\sqrt{\text{Hz}}$ @ 1 m for $SS3.5$ to $SS4$ (Figure 227).

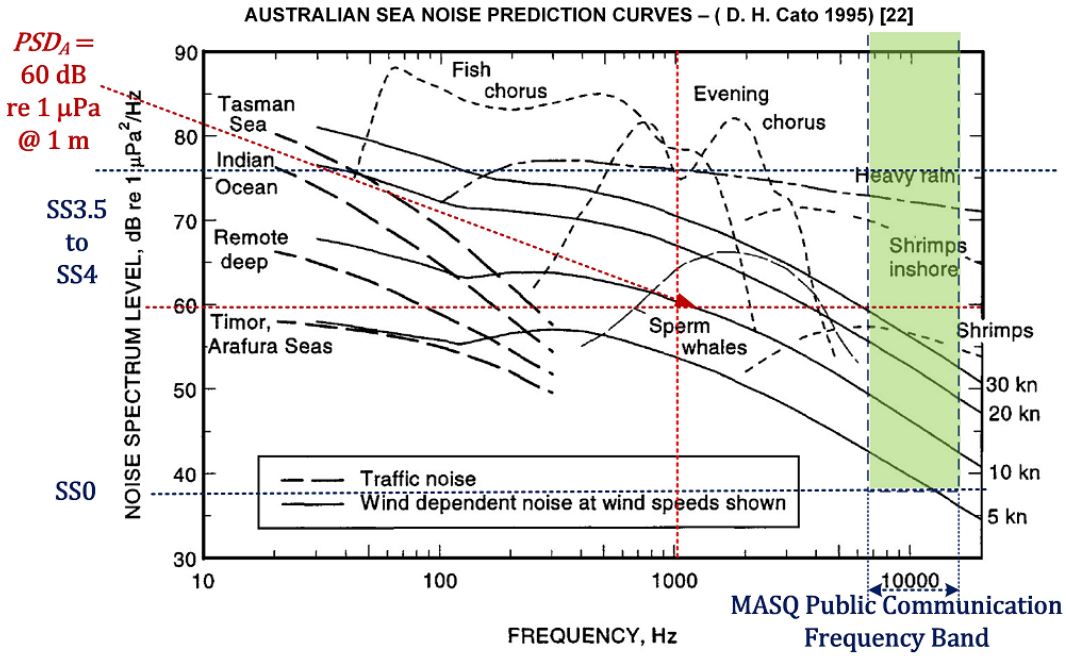

Figure 227 Australian shallow water ambient noise at 1 kHz (NL)

This requires a 1 kHz to 10 kHz MCDSSS low side band attenuation of 80 dB/decade for a transmit source level of $PSD_{TX} = 140$ dB re 1 µPa/$\sqrt{\text{Hz}}$ @ 1 m. Figure 228 illustrates the measured GPM300 TD10 transducer spectral purity for 1,000 baud. The GPM300 $SPL_{TX} = 180$ dB re 1 µPa @ 1 m transmit spectrum (Figure 228 grey trace) illustrates less than 60 dB lower side band (LSB) attenuation at 1 kHz before being masked by the SR785 spectrum analyser 1 Hz to 400 Hz $\frac{1}{f}$ noise.

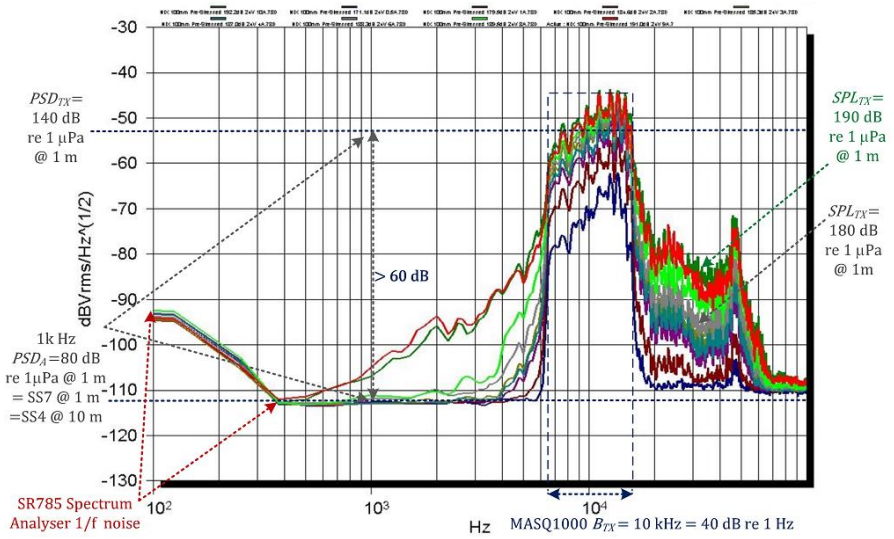

Figure 228 GPM300 TD10 transducer spectral purity (1,000 baud)

The AUSSNet side band attenuation requirement of 80 dB, minus the 60 dB GPM300 LSB performance, results in a 20 dB short fall in attenuation which was provided by the $L_S = 20\log_{10}(10\text{ m}) = 20$ dB horizontal separation between the GPM300 and the closest hydrophone array element.

O.3 Sensor Nodes to GPM300/IRIDIUM Gateway Buoy (1,000 Baud)

Figure 229 illustrates the 1,000 baud maximum communication range for the AUSSNet sensor nodes with a $R_S = 2$ km base line at sea state $SS3.5 \rightarrow SS4$ and a transmit source level of $SPL_{TX} = 180$ dB re 1 µPa @ 1 m.

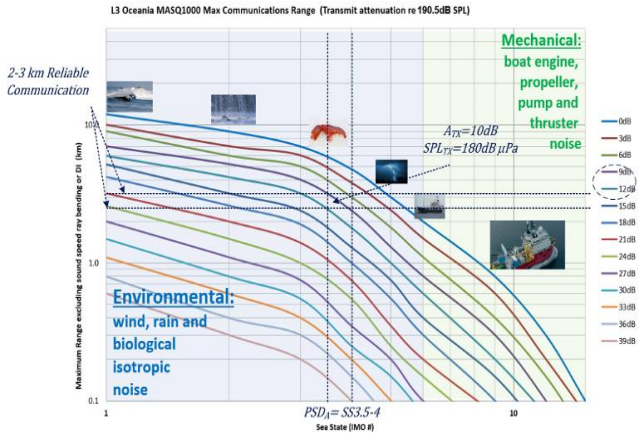

Figure 229 AUSSNet 1,000 baud sensor node to gateway buoy

O.4 MV Sea Lion to GPM300/IRIDIUM Gateway Buoy (500 Baud)

The estimate of the 6 kn MV Sea Lion 6.5 kHz to 16.5 kHz noise floor is approximately $PSD_A \approx 115$ dB re 1 µPa/$\sqrt{\text{Hz}}$ @ 1 m $\approx PSD_{SS13}$. Reliable $R_S \approx 500$ m communication at maximum transmit source level was achieved using 500 baud.

O.5 Summary

All noise floor and communication reliability performance requirements were met. A 20 dB shortfall in LSB attenuation was provided by a $R_S = 10$ m $\equiv L_S = 20$ dB hydrophone array extension cable. The high overhead protocol TCP/IP acoustic network handshaking has been replaced with a variable byte length network header for the latest MASQ communication protocol. The extension of the AUSSNet project Communication Using Ultrasonic Underwater Wireless (CUUUWi) has been funded via Commonwealth of Australia Defence Industry Realisation Fund. For CUUUWi a GPM300 modem is deployed on a wave glider which provides a submarine satellite gateway for voice and text communication. The GPM300 deployed wave glider will also be used to retrieve bottom sensor data such as AUSSNet hydrophone array.

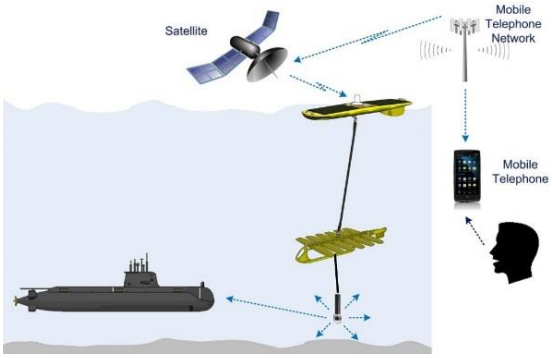

Figure 230 CUUUWi submarine/satellite gateway

Appendix P 0.1-8 km Range *SS5* 10-20 m Depth MCDSSS Coding Order

P.1 Introduction

This chapter reprocesses historical sea trial data to provide MCDSSS modulation, BEE, transducer and power amplifier baseline measurements required for message reliability improvement validation. L3 Oceania conducted a sea trial to measure the performance of 500 baud and 1,000 baud rates which was used to identify the most robust combination of MCDSSS data channels and spread spectrum code order for high speed data transfer. An analysis of suitable acoustic projector was carried out for high speed 1,000 baud PZT transducer. The transducer that was tested was the CTG1330 200 dB maximim souce level, $f_C = 10$ kHz commercial projector with a 6 dB transmission band of $LFB_{6dB} = 7.5$ kHz to $HFB_{6dB} = 20$ kHz, $B_{TX} = 20$ kHz $- 7.5$ kHz $= 12.5$ kHz or $\frac{B_{TX}}{f_C}$=1.25 Octaves.

Table 4 lists the MCDSSS data channel (L_C) and spread spectrum code order (S_{CO}) combinations that were tested for 500 and 1,000 baud.

Table 4 MCDSSS test configurations

MCDSSS	f_C	B_M	LFB_{6dB}	UFB_{6dB}	L_C	S_{CO}	τ_{SY}	Br
#	Hz	Hz	Hz	Hz	#	#	ms	Bits/s
1	13,750	16,000	7,500	20,000	2	8	16	500
2	13,750	32,000	7,500	20,000	2	9	16	500
3	13,750	32,000	7,500	20,000	3	9	16	1,000
4	13,750	16,000	7,500	20,000	3	9	32	500
5	13,750	32,000	7,500	20,000	3	10	32	500
6	13,750	32,000	7,500	20,000	5	10	**32**	1,000
7	13,750	16,000	7,500	20,000	5	10	**64**	500
8	10,937.5	16,000	7,500	14,375	2	8	16	500
9	10,937.5	16,000	7,500	14,375	3	9	32	500
10	10,937.5	16,000	7,500	14,375	5	10	64	500

P.2 CTG1330/ITC1042G Wharf Deployment

The ITC1042G 80 kHz hydrophone and CTG1330 10 kHz transceiver were deployed at the wharf. The ITC1042G passive hydrophone was deployed $R_H = 3$ m from the CTG1330 however due to the excessive ambient noise no MCDSSS message receptions were detected using the Omni directional ITC1042G hydrophone except for the MASQ receiver connected to the $DI = 3$ dB CTG1330 transceiver.

P.3 Environmental Conditions

The test site selected was the Australian Navy Garden Island N/E Wharf which was chosen because of the very high ambient noise and strong multipath reverberation. Figure 231 illustrates the Garden Island Wharf and MV Sea Lion ambient, noise measured at $PSD_A \approx 50$ dB re 1 µPa @ 1 m $\cong SS2$ to peak of $PSD_A = 75$ dB re 1 µPa @ 1 m $\cong SS5$ @ 10 kHz. The wharf ambient noise across the 7.5 kHz to 20 kHz communications band varied from a mean of $PSD_A = 65$ dB re 1 µPa @ 1 m $\cong SS4$ to boat induced peak of $PSD_A \approx$ 90 dB re 1 µPa @ 1 m at 10 kHz $\cong SS9$.

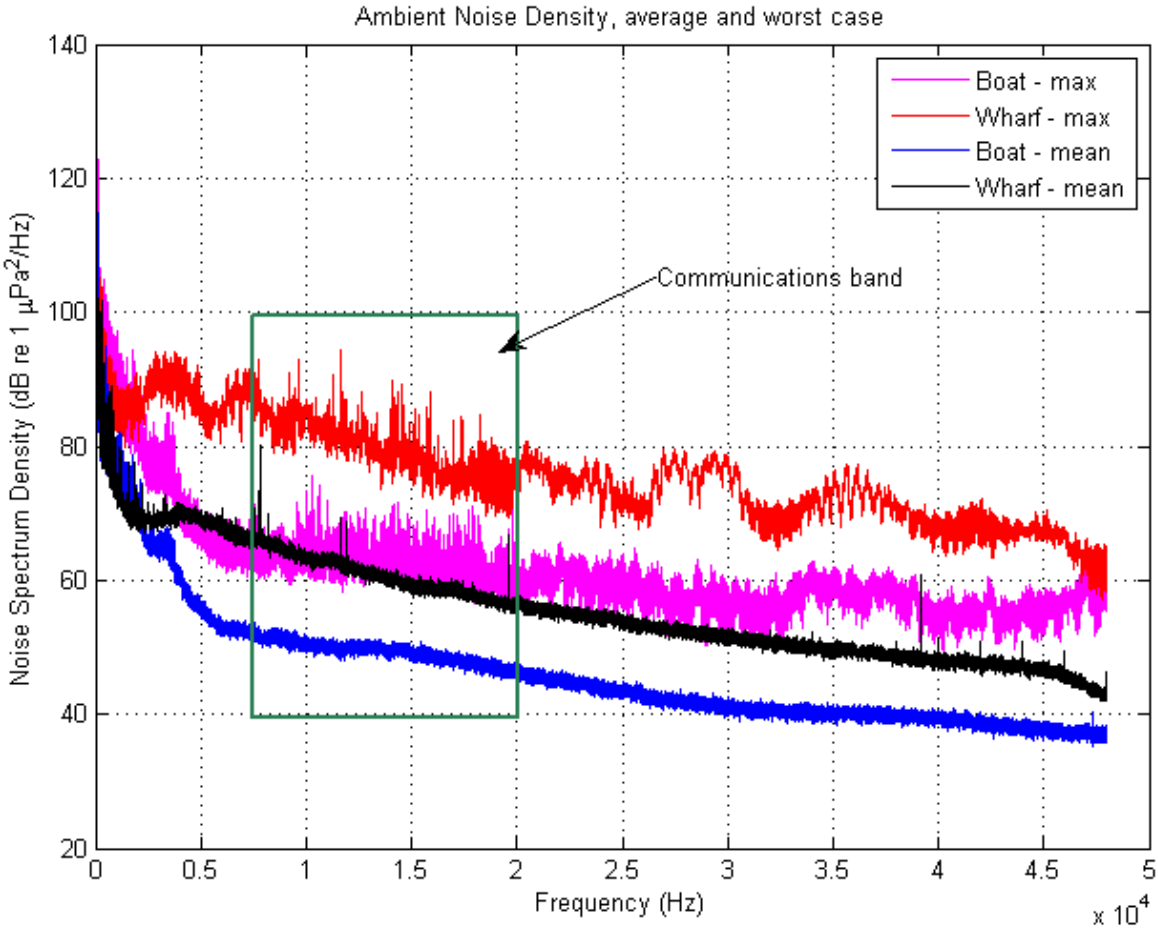

Figure 231 Measured ambient noise floor versus frequency

P.4 Sea Trial Measurements

P.4.1 Short to Medium Range Performance

The wharf deployment depth was $R_H = 3$ m with less than $R_D < 10$ m water depth and MV Sea Loin hydrophone deployment depth was $R_H = 3$ m, $R_D < 20$ m water depth, horizontal rage 100 m to 2 km.

1. Reliable communications was achieved for all modem configuration at a slant range of $R_S \approx 1$ km for transmit source level levels greater than $SPL_{TX} = 170$ dB re 1 µPa @ 1 m requiring 3 W transmit power ≅ BEE 350 @ 1 km re $SS4 \equiv$ BEE 9×10^4 @ 1 km re $SS0$.
2. Reliable communications was only established for $Br = 500$ baud modem configurations at a slant range of $R_S \approx 2$ km for power levels greater than $SPL_{TX} = 180$ dB re 1 µPa @ 1 m requiring 12 W transmit power ≅ BEE 50 @ 2 km re $SS4 \equiv$ BEE 6×10^4 @ 1 km re $SS0$.
3. Wharf to boat $Br = 1{,}000$ baud modem baud was established a slant range of $R_S \approx 2$ km for power levels greater than $SPL_{TX} = 173$ dB re 1 µPa requiring 6 W transmit power ≅ BEE 1.6×10^2@ 2 km re $SS4 \cong$ BEE 2×10^5 @ 1 km re $SS0$

4. Boat to wharf $Br = 500$ baud modem baud was established a slant range of $R_S \approx 2$ km for power levels greater than $SPL_{TX} = 186$ dB re 1 µPa requiring 80 W transmit power ≅ BEE 6.2 @ 2 km re $SS4$ ≅ BEE 8×10^4 @ 1 km re $SS0$
5. Communications was more reliable between the wharf to boat even though the wharf SPL was 10 dB lower than the boat as expected.

The ambient noise level for the wharf and boat was 20 dB higher than expected 10 dB due to bad weather. The ambient noise at the wharf was also high due to the large number of snapping shrimp resident on the pylons. Water line mounted horizontal metal plates and wharf pylons also increased wave induced transients.

P.4.2 Long-Range Performance

The wharf deployment depth was $R_H = 3$ m with less than $R_D < 10$ m water depth and MV Sea Loin deployment was $R_H = 3$ m hydrophone depth, $R_D <$ 20 m water depth, horizontal rage 2 km to 8 km (Figure 232).

1. For long-range communication the wharf ETA 120 W power amplifier was replace with a Crown 2 kW power amplifier which provided 10 dB higher power and allow the power level to be dynamically adjustable for both the wharf and boat.
2. Reliable $Br = 1{,}000$ baud communications was established at a slant range of $R_S \approx 2$ km for power levels greater than $SPL_{TX} = 180$ dB re 1 µPa @ 1 m requiring 12 W transmit power ≅ BEE 60 @ 2 km re $SS4$ ≅ BEE 7×10^4 @ 1 km re $SS0$.
3. Reliable $Br = 500$ baud communications was established at a slant range of $R_S \approx 4$ km for power levels greater than $SPL_{TX} = 186$ dB re 1 µPa @ 1 m requiring 80 W transmit power ≅ BEE 6.2 @ 4 km re SS4 ≅ BEE 5×10^4 @ 1 km re $SS0$.
4. Intermittent $Br = 500$ baud communications was observed at a slant range of $R_S \approx 8$ km for power levels of $SPL_{TX} = 186$ dB re 1 µPa @ 1 m requiring 80 W transmit power ≅ BEE 6.2 @ 8 km re SS4 ≅ BEE 2×10^3 @ 1 km re $SS0$.
5. Communications was unexpectedly more reliable between the boat to wharf even though the wharf ambient was 10 dB higher than the boat.
6. The wharf ambient noise was approximately 10 dB higher during the long-range test compared to the short range test.

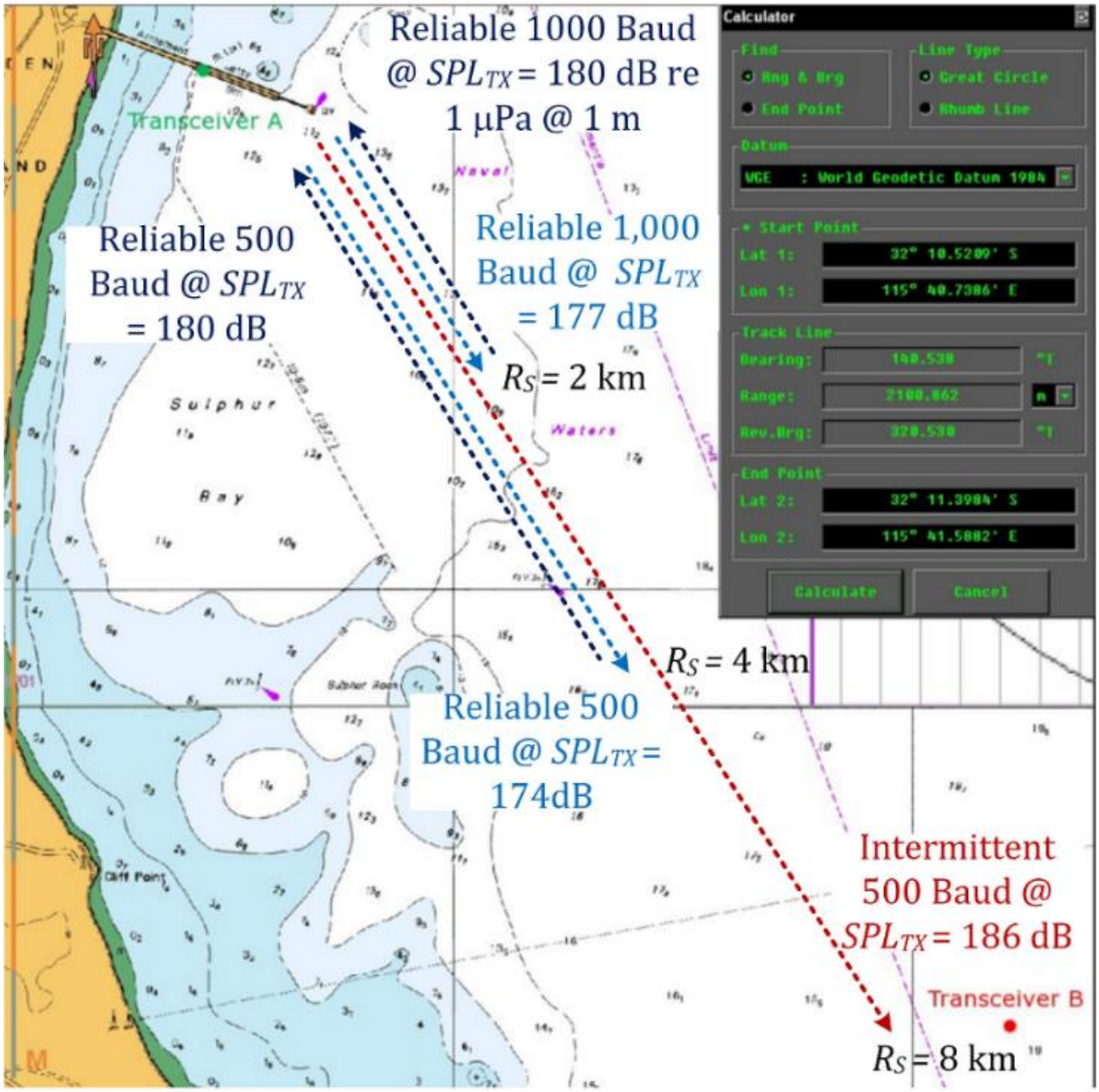

Figure 232 Message reliability versus range sonar equation diagram

P.5 Summary

The predicted performance was that there would be a linear increase in message reliability as the number of channels decreased, spread spectrum code order increased and transmit source level increased. The counter intuitive measured result was that there was an abrupt maximum message reliability improvement when the spectrum code order was maximised which was independent of transmit source level. In the presence of a loud reverberating environment ($N_M > 3$) and loud $+SS4$ ambient noise MCDSSS configuration #6 and #7 provided the most reliable communication link because of the maximum symbol period ($\tau_{SY} = 32$ ms for 1,000 baud and $\tau_{SY} = 64$ ms for 500 baud). Figure 233 illustrates the communication link as a function of receiver SNR_{RX}. Message reliability (MR) of 100% was achieved for MCDSSS configuration #6 and #7. MCDSSS configurations other than #6 and #7 with high receiver SNR did not provide a reliable communication link at any transmit source level *(SPL_{MIN} to SPL_{MIN}).*

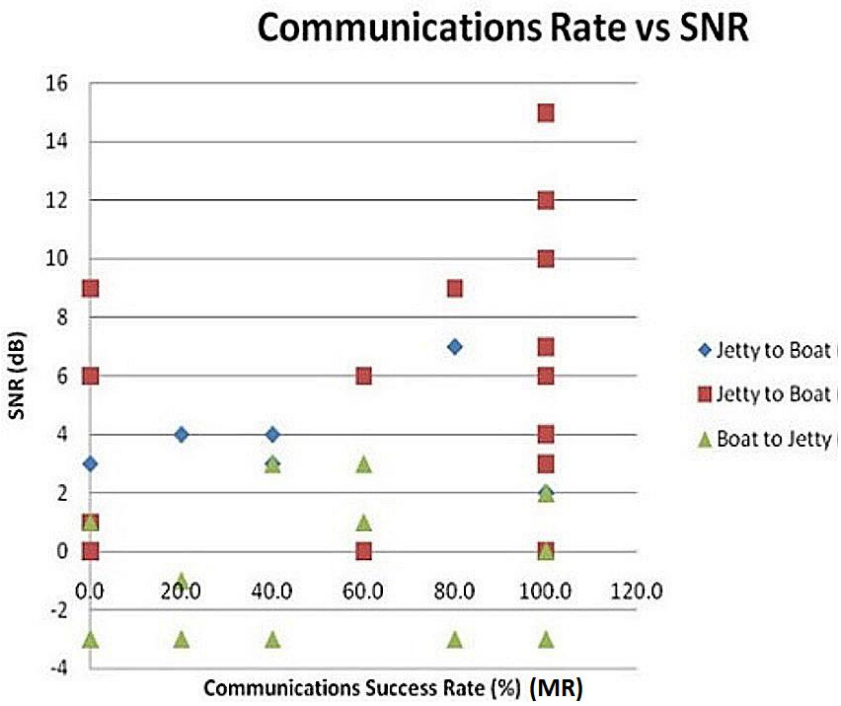

Figure 233 MCDSSS *SS6* wharf trial message reliability versus SNR

The commercial CTG1330 transducer published narrow-band power rating of 200 dB SPL could not be replicated for a broad-band 100% duty cycle signals which resulted in the depolarisation and destruction of the PZT ceramic. As a rule of thumb a narrow-band 200 dB SPL rated transducer, requiring 3 kW transmit power, must be de-rated by at least 6 dB for a broad-band 100% duty cycle signals (194 dB SPL requiring 1 kW transmit power). The commercial CTG1330 published bandwidth of 7.5 kHz to 20 kHz did not deliver significant acoustic energy between 17.5 kHz to 20 kHz. The transducer impedance between 17.5 kHz to 20 kHz presented a short circuit load across the 120 W ETA power amplifier output which overheated and reduce the power amplifier electrical efficiency. Driving the CTG1330 with a 2 kW crown amplifier between 17.5 kHz to 20 kHz overheated the CTG1330 which would eventually de-polarised resulting in the destruction of the ceramic. The effective CTG1330 6 dB transmission bandwidth was measured at $B_{TX} \approx 17.5\text{ kHz} - 7.5\text{ kHz} < 10\text{ kHz}$ or $\frac{B_{TX}}{fc} < 1$ Octave. The CTG1330 7.5 kHz LFB is problematic and does not comply with NATO STANAG 1074 UQC LSB voice communication. The cost of the CTG1330 transducer and commercial power amplifier was more than the build cost target for the GPM300 requiring a cost effective alternative. The start-up and shutdown time for all commercial power amplifiers tested were many orders of magnitude slower than the 10 ms target for the GPM300, which required the power amplifiers to be permanently powered and drained the batteries when not transmitting. The quiescent current of all power amplifiers tested was too high for a battery powered GPM300. A commercially viable GPM300 requires a custom designed +190 dB re 1 µPa @ 1 m SPL ceramic and efficient +300 W power amplifier assuming $\epsilon_{TX} \approx 35\%$ total electrical power to acoustic power conversion efficiency.

Appendix Q IMO Sea State Number Versus Ambient Noise

Table 5 lists the International Martine Organisation (IMO) Sea State (SS) Ambient Power Spectral Density (PSD_A) for the MCDSSS communication channel $LFB = 6.5$ kHz to $UFB = 16.5$ kHz frequency band. Sea states less than 7 are characterised as isotropic weather, environmental and biological noise [56]. Sea states greater than $SS6$ are characterised as anisotropic mechanically induced boat noise. Equation (7-25) describes the conversion of IMO sea state number ($SS\#$) and wind speed (v_{SW}) to an approximate ambient (PSD_A)) across the MASQ frequency band using an estimate for $SS0$ ambient noise floor (PSD_{SS0}) of approximately 38 dB re 1 µPa/$\sqrt{\text{Hz}}$ from Figure 4. **Note:** Sea state is a subjective estimate with an accuracy no better than $\pm 1\ SS$ or $PSD_A \pm 6$ dB.

$$
\begin{gathered}
SS_{\text{dB}} \approx 6\ \text{dB/SS} \quad \text{(Ambient noise or path loss increase per sea state)} \\
PSD_{SS0} = 38\ \text{dB re 1 µPa}/\sqrt{\text{Hz}} \\
PSD_A \approx SS_{\text{dB}} \times SS\# + PSD_{SS0} = 6\ \text{dB} \times \text{SS\#} + 38\ \text{dB re 1 µPa}/\sqrt{\text{Hz}} \\
SS_{WS} = 10\ \text{kn} \quad \text{(Wind speed increase per sea state number.)} \\
PSD_A \approx \frac{SS_{\text{dB}} \times v_{SW}}{SS_{WS}} + PSD_{SS0} = \frac{6\ \text{dB} \times v_{SW}}{10\ \text{kn}} + 38\ \text{dB re 1 µPa}/\sqrt{\text{Hz}} \\
PSD_{\Delta SS} = PSD_{SS17} + PSD_{SS0} \approx 100\ \text{dB}
\end{gathered}
\tag{7-25}
$$

Table 5 IMO sea state number

PSD_A	**Sea State**	**Wind (v_W)**	**Rain**	**Noise**
dB re 1 µPa/$\sqrt{\text{Hz}}$	$SS\#$	kn	Description	Source
$PSD_{SS0} = 38$	0	<5	None	Isotropic
44	1	10	None	
50	2	20	None	
56	3	30	Light	
62	4	40	Moderate	
68	5	50	Heavy	
PSD_{SS6} =74	6	60	Hail	
80	7	Boat mechanical induced noise		Anisotropic
86	8			
92	9			
98	10			
104	11			
110	12			
116	13			
122	14			
128	15			
134	16			
140	17			

Appendix R MASQ MCDSSS Communication Specification

R.1 MASQ Digital and UQC Voice Analog Public Communication Channel

The MASQ communication channel operates in the same hydro-acoustic frequency band as the NATO STANAG 1074 UQC [76] which provides support for concurrent MCDSSS digital and UQC voice analog communication. NATO STANAG 1074 UQC public voice underwater telephone standard is optimised for short to medium range ($R_S < 8$ km) analog voice communications. MASQ communication channel is optimised for short to long-range ($R_S > 10$ km) digital communications.

The NATO STANAG 1074 UQC underwater telephone specifications are:

1. Carrier: $f_{UQC} = 8.087$ kHz
2. Modulation Bandwidth: $B_{UQC} = 3$ kHz
3. Side Band: SB = Upper Side Band ($USB_{6\text{dB}}$)

The UQC carrier and bandwidth impose a 3 dB transmission Upper Frequency Band (UFB_{UQC}) and Lower Frequency Band (LFB_{UQC}) band limit Eq.(7-26). The operating UQC in LSB mode the $LFB_{UQC} = 5.087$ kHz will be band limited by the PZT lower frequency band of 6.5 kHz providing less than $B_{UQC} <$ 2 kHz bandwidth.

$$\begin{aligned} LFB_{UQC} &= B_{UQC} - f_{UQC} \cong 8.087 \text{ kHz} - 3 \text{ kHz} = 5.087 \text{ kHz} \\ UFB_{UQC} &= B_{UQC} + f_{UQC} \cong 8.087 \text{ kHz} + 3 \text{ kHz} = 11.087 \text{ kHz} \end{aligned} \tag{7-26}$$

The MASQ communication channel 6 dB lower and upper frequency bands must be wide than the UQC bandwidth Eq.(7-27).

$$\begin{aligned} LSB_{6dB} &= 5.087 \text{ kHz} < LFB_{UQC} < 8.087 \text{ kHz} \\ USB_{6dB} &= 8.087 \text{ kHz} < UFB_{UQC} < 11.087 \text{ kHz} \end{aligned} \tag{7-27}$$

R.2 MASQ Digital Communication Channel

The MASQ communication channel is configured to transmit and receive on fixed carrier frequencies (f_C), modulation bandwidths (B_M), number of data channels (N_T), and encryption spread spectrum codes which provide a public digital communication channel (i.e. MASQ compatible underwater transceivers can communicate with each other). Many MASQ communication applications are integrated with an underwater telephone for the provision of voice and text communication services. MASQ communication applications that are integrated with NATO STANAG 1074 UQC underwater telephone share the same hydro-acoustic infrastructure.

R.2.1 MASQ Communication Specifications

Table 6 lists the MASQ10 to MASQ1200 hydro-acoustic communication specifications:

MASQ					Modulation Bandwidth (B_M)		Transmit Band Limit (B_{TX})				Over Spreading Loss (L_O)	Processing Gain (P_G - 10log(N_C))	Detection Threshold ($\sim=D_{TH}$)	Transmit Margin (M_{TX})
Baud Rate (Br)	Data Channels (N_C), (N_B), (L_C)			Carrier (f_C)			*LFB*	*UFB*	*BW* $_{6dB}$					
Bits/s	#	Bits	dB	Hz	Hz	dB re 1Hz	Hz	Hz	Hz	dB re 1Hz	dB	dB	dB	dB
10	**2**	8	-3.0	**8800**	**1250**	31.0	**8050**	**9550**	1500	31.8	0.8	27	**13**	**15**
20	**2**	8	-3.0	**9500**	**2557.5**	34.1	**8221**	**10778**	2557	34.1	0.0	27	**13**	**14**
50	**2**	8	-3.0	**9500**	**6394**	38.1	**6303**	**12697**	6394	38.1	0.0	27	**13**	**14**
75	**2**	8	-3.0	**9500**	**9591**	39.8	**6500**	**16500**	10000	40.0	0.2	27	**14**	**14**
100	**5**	32	-7.0	**9500**	**3200**	35.1	**7900**	**11100**	3200	35.1	0.0	23	**14**	**9**
150	**5**	32	-7.0	**9500**	**4795.3125**	36.8	**7102**	**11898**	4795	36.8	0.0	23	**14**	**9**
200	**5**	32	-7.0	**10000**	**6400**	38.1	**6800**	**13200**	6400	38.1	0.0	23	**14**	**9**
350	**5**	32	-7.0	**10000**	**11200**	40.5	**6500**	**16500**	10000	40.0	-0.5	23	**14**	**9**
500	**5**	32	-7.0	**10000**	**16000**	42.0	**6500**	**16500**	10000	40.0	-2.0	23	**14**	**7**
750	**5**	32	-7.0	**12750**	**24000**	43.8	**6500**	**16500**	10000	40.0	-3.8	23	**14**	**5**
1000	**5**	32	-7.0	**12750**	**32000**	45.1	**6500**	**16500**	10000	40.0	-5.1	23	**14**	**4**
1200	**5**	32	-7.0	**12750**	**38400**	45.8	**6500**	**16500**	10000	40.0	-5.8	23	**14**	**3**

Table 6 MASQ communication channel hydro-acoustic baud rates

Table 7 and Table 8 summaries the GPM300 performance [148] and MASQ communication protocol specifications.

Table 7 GPM300 transceiver specifications

Parameter		Min	Typical	Max	Unit
Acoustic					
PZT Ceramic	Transmit hydro-acoustic power	130.5	186	190.5	dB re 1 µPa @ 1 m
	Electrical to acoustic Efficiency		50		%
Power Amplifier	Electrical Power	1		300	Watts
	Efficiency	80	90	95	
	Quiescent (on)		7	10	W
	Quiescent current (off)		6	10	µA
	Power up delay			30	ms
Total Harmonic Distortion	Upper Side band	40	35	20	dB per 3rd Harmonic
	Lower Side band	60	50	40	dB per Decade
Total Efficiency	Total electrical to acoustic	35	40		%
Input Noise	6.5 kHz to 16.5 kHz hydro-acoustic band			38	dB re 1 µPa /√Hz @ 1 m
Hydrophone	Open Circuit Voltage (OCV) response	-180			dB Vrms /1 µPa @ 1 m
Under Water Telephone compatible	Option. Configurable UQC Carrier, Bandwidth, Upper/Lower/Double Sideband 192 dB re 1 µPa @ 1 m				
Analog					
CODEC Band Pass Filter	*HPF* @ 5 kHz	50			dB/Decade
	LPF @ 50 kHz	40			dB/Decade
Analog Dynamic Range	Total electrical.	100	120		dB
Digital					
Dynamic Range	Total ADC dynamic range.	100	120		dB
Doppler	Configurable (Baud rate limited)	0	±8	±80	Knots
False Detect Rate				1	Per Minute
Message Reliability	Positive SNR (Non Covert)		99	100	%
	Negative SNR (Covert)	99			%
Multipath	Track multipath signals	3		12	#
Bit Error Rate	Measured at +*SS*3 (Shallow Water)	10^{-2}	5×10^{-2}	10^{-3}	BER

Table 7 GPM300 transceiver specifications					
Parameter		**Min**	**Typical**	**Max**	**Unit**
Bit Energy Efficiency	Measured at +*SS*3 (Baud rate dependent)	5×10^3	10^4	10^5	Bits /J @ 1 km re *SS*0
LPI (Covert)	Receive signal power below medium to deep water ambient noise.		9		dB
	Receive signal power below shallow water ambient noise.		12		dB
Under Water Telephone	Configurable UQC Carrier, Bandwidth, Upper/Lower/Double Sideband (Optional)				
Transpond and one way Time Of Flight					
Transmit Time Accuracy	Relative to internal clock	10			µS
	Absolute GPS time	100			µS

Table 8 MASQ communication channel performance specifications					
Parameter		**Min**	**Typical**	**Max**	**Unit**
Acoustic					
Transmit	Power	130.5		190.5	SPL
	Frequency Band	6.5		16.5	kHz
	Lower Side Band attenuation	60			dB per Decade
	Upper Side Band attenuation	40			dB @ 3rd harmonic
Receive	Equivalent noise floor < *SS*0			38	PSD
Data Transfer					
Data Symbol	Number of data bits	8			Bits
Payload type	Brevity code	8 Binary			Bits
	SMS ASCII upper case (NMEA)	Pack 6 bit ASCII into 8 bit			Bits
	SMS 7 bit ASCII	8			Bits
	SMS 8 bit binary	8			Bits
	File transfer	8			Bits
Baud Rate Raw	10, 20, 50, 75, 100, 150, 200, 350, 500, 750, 1000, 1200				Baud
Overhead	Error correction including protocol and network overhead	22	30	60	%
Baud Rate Effective	8, 15, 39, 58, 78, 117, 156, 273, 390, 585, 780, 936				Baud
Network					
Header Size		1	2	256	Bytes
Global Address	Code	0			Address
Short Address	8 bits unsigned	1		250	Address
Medium Address	16 bits unsigned	256		65535	Address
Long Address	32 bits unsigned	65526		42949 67295	Address
Routing	Up to 256 network address chaining.				
Key Codes	(Optional)	32	32	64	Bits
Forward Error Correction					
FEC	Reed Solomon				
RS Block Size	15, 31, 63, 127 and 255 symbols				
Parity Symbols	20% of Reed Solomon Block Size rounded up to the next integer.				

Table 8 MASQ communication channel performance specifications					
Parameter		**Min**	**Typical**	**Max**	**Unit**
Erasures	Correct 20% of Reed Solomon user data symbols.				
Random Error	Correct 10% of Reed Solomon user data symbols.				
Control Block	Size		5		Bytes
CRC	CCTIT-16				
Transpond and one way Time of Flight					
Relative Range	Dependent on speed of sound accuracy.	0.25			m
Absolute Range		1			m
Telemetry Alert					
FSK	Number of FSK signal		2		#
	Offset to MASQ signal		1		s
Ping	Pings per FSK		11		#
	Period		7.8125		ms
PWM	Data Bins		16		#
	Period		15.625		ms
	Offset to first bin		7.8125		ms

R.3 GPM300 Communication Range Versus Sea State

Figure 234 illustrates the predicted GPM300 48 V DC power supply communication range versus environmental ambient noise from *SS*0 to *SS*15 generated using the broad-band sonar equation (2-17). The ambient noise can either be estimated using Table 5 or the measured using the GPM300. Quiet survey grade vessels, such as RV Whale Song, generate an equivalent sea state noise of approximately *SS*4 to *SS*7 at 5 kn. Noisy dynamic positioning work boats, such as MV Mermaid, can generate noise in excess of *SS*15. Longer communication range can be established using directional transducers or higher transmit source level in conjunction with an external transducer and power amplifier.

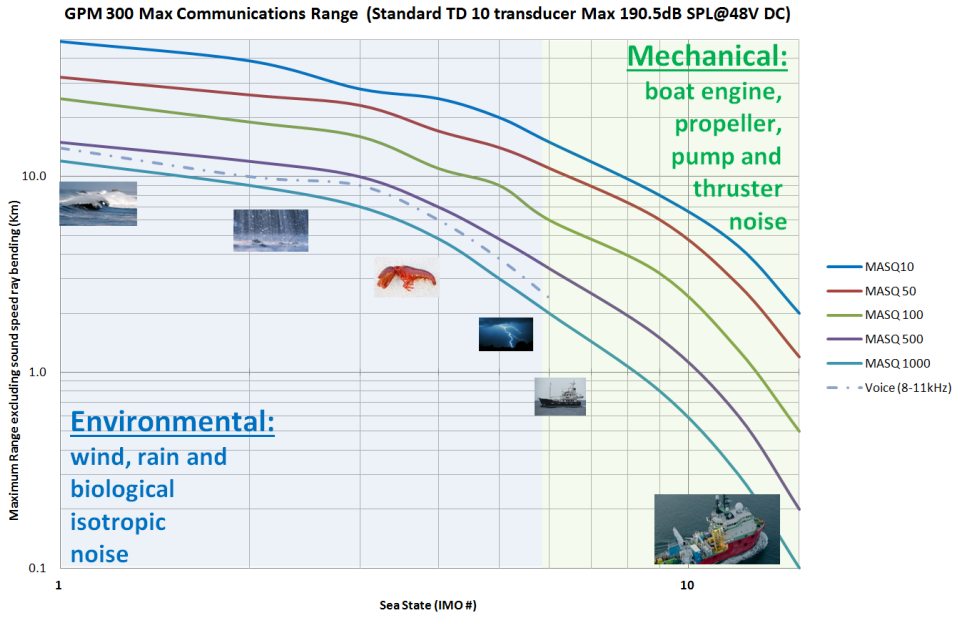

Figure 234 GPM300 communication range versus sea state @ 48 V DC

R.4 GPM300 Hydro-acoustic Beam Pattern and Air Coupling Loss

Figure 235 illustrates the GPM300 TD10 PZT transducer beam pattern for water and air. The standard TD10 water beam pattern provides approximately $DI = 3$ dB at 30° elevation angle. The PZT transducer to air coupling loss is approximately $D_{AIR} \approx -25$ dB in the end-fire aspect (cavity resonance) with a beam width of ±5°. The PZT transducer broadside air coupling loss is approximately $D_{BS} \approx -40$ dB. When operating the GPM300 in air the PZT ceramic operates in cavity resonance mode and behaves similar to an insensitive directional microphone. The GPM300 to GPM300 $DI = 50$ dB air coupling loss, in conjunction with $A_{TX} = 40$ dB transmit source level attenuation and $R_S = 20$ m ≡ $L_S =$ 26 dB range can be used to simulate $L_T = DI + A_{TX} + L_S = 50 + 40 + 26 \approx 115$ dB (Chapter 2.4.3 Maximum Feasible Path Loss) long range communication.

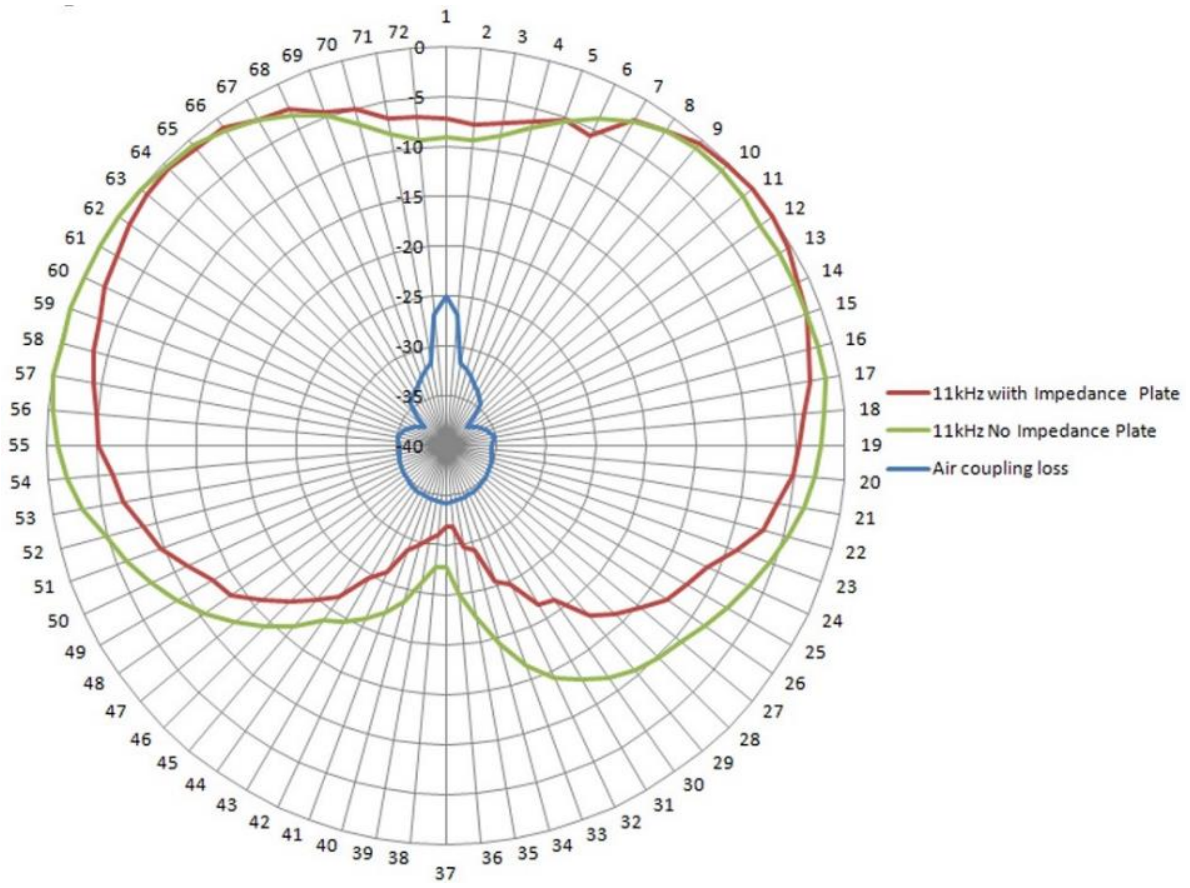

Figure 235 GPM300 TD10 transducer hydro-acoustic beam pattern and air coupling loss

End of Document